

Universitätsklinikum Essen
Institut für Medizinische Strahlenbiologie
Prof. Dr. phil. nat. G. Iliakis

Fachlicher Schlussbericht für das Projekt

**„Biodosimetrie: Ein systembiologischer Ansatz
für die Strahlenbiodosimetrie und der Analyse
der individuellen Strahlensensitivität: ATM/ATR
Signaltransduktionswege und
Strahlenempfindlichkeit in Normal- und Tumor-
Zellen“**

Förderkennzeichen:

02NUK005C

Laufzeit des Vorhabens

01.05.2008 bis 31.10.2013

Das diesem Bericht zugrunde liegende Vorhaben wurde mit Mitteln des Bundesministeriums für Bildung und Forschung unter dem Förderkennzeichen 02NUK005C gefördert. Die Verantwortung für den Inhalt dieser Veröffentlichung liegt beim Autor.

GEFÖRDERT VOM



Bundesministerium
für Bildung
und Forschung

I. Kurze Darstellung zum Vorhaben

1. Aufgabenstellung

Die gesetzten Ziele des Projektes waren es:

Ziel 1: Den Strahlensensibilisierungsmechanismus von Nukleosidanalogen im Hinblick auf die Reparaturmechanismen, die durch diese Substanzen inhibiert werden, zu untersuchen.

Ziel 2: Die Effekte von durch Restriktionsendonukleasen induzierten Doppelstrangbrüchen zu charakterisieren.

Ziel 3: Den Einfluss der Checkpointkinasen Chk1 und Chk2 auf den Zelltod und Chromosomenaberrationen zu untersuchen.

Ziel 4: Die Aktivierung von wichtigen Signalmolekülen der zellulären Antwort auf Strahlenschäden, DNA-Doppelstrangbruch (DSB) -Reparatur, ATM und ATR auf den Zelltod und Chromosomenaberrationen zu studieren.

2. Voraussetzungen, unter denen das Vorhaben durchgeführt wurde

Die intrinsische Strahlenempfindlichkeit von normal und Tumorzellen ist ein Faktor, der maßgeblich den Erfolg der Strahlentherapie mitbestimmt. Die strahlenbiologische Forschung der letzten Jahrzehnte hat gezeigt, dass die zelluläre Strahlenempfindlichkeit wesentlich von der Fähigkeit geschädigter Zellen abhängt, die von ionisierender Strahlung (IR) hervorgerufenen DSB reparieren zu können. Von einigen Nukleosidanalogen, die zum Teil bereits klinische Bedeutung als Chemotherapeutika in der Tumorthherapie innehaben, ist bekannt, dass sie die zelluläre Strahlenempfindlichkeit modulieren können. Die zugrunde liegenden Mechanismen sind jedoch größtenteils unbekannt, weshalb im Rahmen des Projektzieles 1 der Einfluss von Nukleosidanalogen auf die Reparatur von DSB untersucht werden sollte.

Ein weiterer Faktor, der mit hoher Wahrscheinlichkeit einen entscheidenden Einfluss auf Effizienz und Fehlerrate der DSB Reparatur hat, ist die molekulare Komplexität des DNA Schadens. Einen besonders hohen Grad der Komplexität stellt das Auftreten mehrerer DSB in räumlicher Nähe innerhalb einer DNA Sequenz dar. Solche Anhäufungen von DSB könnten zur Destabilisierung des Chromatins und zum Verlust größerer Sequenzbereiche führen. Innerhalb des Projektzieles 2 soll der Einfluss dieser Ebene der Komplexität von DSB auf das Zellüberleben und die Signalgebung infolge von DSB, mithilfe von Endonuklease-erzeugten Brüchen untersucht werden.

Die Entwicklung und Verstärkung einer zellulären Signalantwort auf das Auftreten eines DSB ist ebenfalls essentiell für die erfolgreiche Regulierung der DSB Reparatur. Dies ist deutlich an der hohen Strahlensensitivität von Zellen mit Defekten an den Proteinkinasen ATM und ATR zu erkennen. Diese haben eine bedeutende Rolle bei der Entwicklung des Schadenssignals und phosphorylieren als Antwort auf DSBs eine Vielzahl von Zielproteinen. Die Phosphorylierung von H2AX (γ H2AX) führte zu der Annahme eines Reparatur-spezifischen „Histon-Codes“, welcher möglicherweise die Signalisierung und Reparatur von DNA-Läsionen koordiniert. Aus diesem Grunde sollte im Rahmen des Projektziel 3 der Einfluss von ATM auf die DSB Reparatur, respektive die Phosphorylierung von H2AX und das zelluläre Überleben von Tumor- (Gliom) und Normalgewebiszellen (Fibroblasten) untersucht werden.

Für die Induktion und Prozessierung von DNA-Schäden hat neben der Komplexität des DNA-Schadens auch die Chromatinstruktur einen wesentlichen Einfluss. Bei der Charakterisierung des Chromatins wird in zwei Hauptgruppen unterschieden: transkriptionell aktives Euchromatin (EC) und inaktives Heterochromatin (HC), welches etwa 15-30 % des Chromatinmaterials ausmacht. Hierbei ist die Anordnung des eukaryotischen Genoms in höheren Chromatinstrukturen eng mit der Genexpression verknüpft. Die Struktur des Chromatins wird unter anderem durch post-translationale Modifikationen an Histonproteinen u.a. durch Acetylierung, Methylierung, Phosphorylierung verändert. Diese Modifikationen können entweder zu relaxierten und transkriptionell aktiven Chromatin-Konformationen oder zu kompaktierten transkriptionell

inaktiven Strukturen führen. In humanen Zellen wird die Bildung von EC und HC reichen Regionen unter anderem durch zwei Proteinfamilien, den *trithorax-group*- (TrxG) und *polycomb-group*- (PcG) Proteinen maßgeblich mit beeinflusst. Ein Teilziel dieses Projektes war es (Projektziel 4), ein genetisches System zur Modulation der Chromatinstruktur zu etablieren. Durch knockdown ausgewählter Trithorax- und Polycomb-Proteine sollte Einfluss auf die Bildung von EC und HC genommen und die Auswirkungen auf die Reparatur von DSBs und die Strahlenempfindlichkeit von Gliomzelllinien untersucht werden.

3. Planung und Ablauf des Vorhabens

Ziel 1: Das Strahlensensibilisierungspotential verschiedener Nucleosidanalogue wie ara-A, ara-C und deren fluorinierte Derivate sollte mit Hilfe des Koloniebildungsverfahrens untersucht werden. Pulsfeld- Gelelektrophorese (PFGE) Experimente in verschiedenen Zellwachstumsphasen, wie auch in bestimmten Phasen des Zellzyklus (G1 und G2) sollten durchgeführt werden, um den Effekt auf Doppelstrangbruch (DSB) Reparatur zu bestimmen. Der Effekt von Nucleosidanalogenen auf die Homologe Rekombination (HRR) sollte untersucht werden.

Ziel 2: Um gezielt Restriktionsenzym induzierte DSB in einer Zelle zu erzeugen, wollten wir die I-SceI Endonuclease einsetzen. Mit Hilfe von Zelllinien, die eine vorher bestimmte Anzahl an I-SceI-Erkennungssequenz Integrationsstellen beherbergen, sollte Zellüberleben und Chromosomenaberrationen gemessen werden. Der Effekt von Nucleosidanalogenen auf die Reparatur dieser DSB sollte analysiert werden.

Ziel 3: Die zelluläre Strahlenempfindlichkeit von Tumorlinien (Gliomen) sollte im Klonogenitätstest untersucht werden. Zusätzlich sollten Fibroblasten aus Patienten mit Kopf-Hals- und Lungen-Tumoren mit und ohne Späteffekten in Kultur genommen werden. Die Effektivität der Kombination von fraktionierter Bestrahlung und Inhibitoren der Reparatursignalkaskade (ATM Inhibitoren) um einen synergistischen Effekt bei der Abtötung von Tumorzellen zu erhalten, ist Gegenstand dieses Teilziels. Untersuchungen an selbst etablierten Normalgewebszellen (Fibroblasten) soll zur Abschätzung der therapeutischen Breite der Kombinationstherapien dienen.

Ziel 4: Der Einfluss der Chromatinstruktur auf die Strahlenreaktion von Gliomlinien wird charakterisiert. Durch die gezielte Inhibierung ausgewählter Trithorax- und Polycomb-Proteine mittels spezifischer siRNAs soll Einfluss auf die Bildung von EC und HC genommen und die Auswirkungen auf die Reparatur (mittels γ H2AX), Zellzyklusprogression und Strahlenempfindlichkeit von Gliomzelllinien (Apoptose und Minimonolayer-Überleben) gemessen werden.

4. Angaben zum wissenschaftlichem und technischem Stand

Zwei Hauptprozesse der Reparatur von DSB in eukaryotischen Zellen sind seit längerem bekannt: Die DNA-PK abhängige nicht-homologe Endverknüpfung (D-NHEJ) und die homologe Rekombinationsreparatur (HRR). In jüngerer Zeit wurde jedoch auch ein alternativer Reparaturweg des NHEJ (B-NHEJ) beschrieben, der als backup sowohl für NHEJ als auch für HRR agieren kann. Da die HRR auf eine homologe Sequenz als Matrize für die Reparatur angewiesen ist, ist dieser Prozess auf die Synthese-(S-)Phase und die G2-Phase des Zellzyklus beschränkt. NHEJ hingegen kann während des gesamten Zellzyklus effizient agieren, wobei für B-NHEJ allerdings beobachtet werden konnte, dass dieser Reparaturweg in der G2-Phase eine erhöhte Aktivität aufweist. Diese drei Reparaturwege unterscheiden sich nicht nur anhand der zugrundeliegenden Mechanismen, sondern auch anhand ihres Potentials, eine durch einen DSB unterbrochene Sequenz möglichst originalgetreu wieder zusammen zu fügen. Der einzige Reparaturweg der zuverlässig vermag, durch IR verursachte DSB-geschädigte Sequenzen wieder in ihren Ursprungszustand zurück zu versetzen, ist die HRR. Hierfür ist jedoch wie bereits erwähnt, das Vorliegen einer intakten, homologen Kopie der geschädigten Sequenz erforderlich. Im Laufe der Reparatur eines DSB durch die D-NHEJ werden häufig begrenzte Sequenzveränderungen eingeführt. Trotz dieses Umstandes leistet die D-NHEJ einen entscheidenden Beitrag zum Erhalt der genomischen Stabilität und unterstützt das Zellüberleben. Die B-NHEJ hingegen tendiert

dazu, zu größeren Sequenzverlusten zu führen und wurde vielfach mit der Entstehung von Translokationen und Chromosomenaberrationen in Verbindung gebracht.

Bislang ist größtenteils unklar, wie in der Zelle entschieden wird, durch welchen Reparaturweg ein bestimmter DSB prozessiert wird. Es muss jedoch angenommen werden, dass diese Entscheidung, aufgrund der unterschiedlichen Fehlerwahrscheinlichkeiten der verschiedenen Reparaturmechanismen, einen entscheidenden Einfluss auf das Zellüberleben und die Entstehung von Chromosomenaberrationen hat. Einen wichtigen Faktor für die Auswahl des Reparaturwegs stellt mit großer Sicherheit die Phase des Zellzyklus, in der sich die geschädigte Zelle gerade befindet, dar. Weitere mögliche Faktoren könnten die Komplexität des Schadens (siehe Ziel 2) oder die Lokalisation der Brüche innerhalb des Chromatins sein.

Aktuelle Studien legen nahe, dass die lokalen Veränderungen der Chromatin-Struktur wichtig für eine effiziente Reparatur von DSBs sind. Die Phosphorylierung von H2AX im Bereich von DSBs, führten zu der Annahme eines Reparatur-spezifischen „Histon-Codes“, welcher möglicherweise durch Histon-Modifikation die Signalisierung und Reparatur von DNA-Läsionen koordiniert. Die schlechtere Zugänglichkeit, und der größere Aufwand bezüglich der Chromatinrelaxation, erklären die Tatsache, dass die DSB-Reparatur in kompakten und somit weniger transkriptionsaktiven heterochromatischen Regionen etwas langsamer abläuft, als in stärker transkriptionsaktiven, lockeren, euchromatischen Chromatinregionen (siehe Ziele 3 und 4).

Mittlerweile wird davon ausgegangen, dass die Entscheidung, ob die Enden eines DSB nukleolytisch resektiert werden, ein maßgeblicher, früher Schritt bei der Bestimmung des Reparaturweges ist. Es ist wahrscheinlich, dass die Ausprägung der Signalentwicklung in Folge eines DSB dabei eine wichtige Rolle spielt. In jedem Fall dürfte die Regulation der Entscheidung zwischen verschiedenen Reparaturwegen eine wichtige Rolle bei der Ausbildung der zellulären Strahlenresistenz spielen. Eine Deregulierung dieser Entscheidung könnte somit auch die Grundlage von Strahlensensibilisierung bilden und stellt mit Sicherheit ein interessantes Ziel für die

Modulation der zellulären Strahlensensibilität dar (siehe Ziel 1). Viele dieser Aspekte wurden von den verschiedenen Zielen dieses Projektes adressiert.

5. Zusammenarbeit mit anderen Stellen

Nationale Treffen wie die Jahrestagungen der Gesellschaft für Biologische Strahlenforschung (GBS) wurden zur Diskussion und zum Austausch der Ergebnisse genutzt. Des Weiteren fand während des ganzen Projektzeitraums eine stetige Zusammenarbeit zwischen den beteiligten Forschergruppen in Form von regelmäßigen Treffen statt. Dabei wurden die neuesten Ergebnisse der Projekte in Form von Vorträgen präsentiert und untereinander kritisch diskutiert.

II. Eingehende Darstellung

Aus den bewilligten Mitteln wurden drei Doktoranden über den gesamten Projektzeitraum finanziert. Weitere Doktoranden und Wissenschaftler wurden in definierten Zeiträumen finanziert um das Projekt gezielt voranzutreiben. Mehrere Publikationen resultierten direkt aus der im Rahmen des Projektes geleisteten Forschungsarbeiten und sind diesem Bericht als Anhänge beigefügt: Die Hintergründe der durchgeführten Arbeiten sind detailliert in drei Übersichtsartikeln (Reviews) veröffentlicht (Appendixes 1-3). Die Ergebnisse dieses Projektes sind in zwei bereits fertiggestellten Dissertationen eingehend beschrieben (Appendixes 4 und 5). Eine reife Fassung der dritten, noch nicht abgeschlossenen Doktorarbeit ist dem Bericht ebenfalls beigefügt (Appendix 6). Mit den im Rahmen dieser Doktorarbeiten erhaltenen Daten wurden zudem vier Forschungsartikel (Research articles) zur Veröffentlichung in internationalen wissenschaftlichen Zeitschriften erstellt. Zwei davon wurde bereits bei Journalen eingereicht (Appendices 7 und 8), während zwei weitere zurzeit fertiggestellt werden (werden nachgereicht).

Auflistung der im Appendix enthaltenen Veröffentlichungen:

Appendix 1: Sak A, Stuschke M. (2010) Use of γ H2AX and other biomarkers of double-strand breaks during radiotherapy. Semin Radiat Oncol, 20:223-31. doi: 10.1016/j.semradonc.2010.05.004.

Appendix 2: Mladenov, E., Magin, S., Soni, A., & Iliakis, G. (2013). DNA double-strand break repair as determinant of cellular radiosensitivity to killing and target in radiation therapy. Frontiers in oncology, 3, 113. doi: 10.3389/fonc.2013.00113

Appendix 3: Schieler, A., & Iliakis, G. (2013). DNA double-strand-break complexity levels and their possible contributions to the probability for error-prone processing and repair pathway choice. Nucleic acids research. doi: 10.1093/nar/gkt556

Appendix 4: Promotionsschrift zur Erlangung des Dr. rer. nat.: Schieler, Agnes (2013). Homing endonuclease-based model systems for the study of DNA double strand break induced cell signaling and repair.

Appendix 5: Promotionsschrift zur Erlangung des Dr. rer. nat.: Magin, Simon (2014). A balance shift between error-free and error-prone DNA double-strand break repair pathways as a novel mechanism of radiosensitization by nucleoside analogs.

Appendix 6: Promotionsschrift zur Erlangung des Dr. rer. medic.: Kübler, Dennis (Promotion noch nicht abgeschlossen). Untersuchungen zum Einfluss der Histon-Methylierung auf die Reparaturfähigkeit, Zellzyklusregulation und Strahlensensitivität nach Strahlentherapie in humanen Gliomzelllinien.

Appendix 7: Simon Magin, Maria Papaioannou, Janapriya Saha, Christian Staudt and George Iliakis (submitted). Inhibition of homologous recombination and promotion of mutagenic repair of DNA double-strand breaks underpins arabinoside-nucleoside analog-radiosensitization.

Appendix 8: Ali Sak, Dennis Kübler, Kristina Bannik, Michael Groneberg, Martin Stuschke (submitted). Dependence of radiation induced H2AX phosphorylation on histone methylation: evidence from the chromatin immunoprecipitation assay.

Publikationen in Vorbereitung (werden nachgereicht):

1. **Agnes Schipler, Janapriya Saha, Vladimir Nikolov and George Iliakis.**
Chromosome thripsis by DNA double strand break clusters enhances 53BP1 recruitment and causes translocations by alternative end-joining.
2. **Ali Sak, Dennis Kübler, Kristina Bannik, Michael Groneberg, Martin Stuschke.**
Epigenetic silencing and activation of chromatin: Influence on the radiation sensitivity of glioma cell lines.

Die wichtigsten Befunde des Projekts im Überblick waren:

Ziel 1: Es konnte gezeigt werden, dass Nukleosidanalogue die HRR hemmen und dadurch proliferierende Zellen gegenüber der Abtötung durch IR sensibilisieren. Des Weiteren wurde beobachtet, dass Behandlung mit Nukleosidanalogen zu einer Erhöhung der Aktivität der B-NHEJ führt, sowohl in aktiv wachsenden Zellen, als auch in der Plateau-Phase. Es konnte jedoch gezeigt werden, dass die Gesamteffizienz der DSB-Reparatur in behandelten Zellen unverändert blieb. Dies deutet auf eine Verschiebung in der Balance zwischen verschiedenen Reparaturwegen, anstelle einer allgemeinen Hemmung, als Ursache der Strahlensensibilisierung hin (siehe auch Appendices 5 und 7).

Ziel 2: Die Induktion von DSBs durch I-SceI führte zu einer Reduktion des Zellüberlebens, wobei die Abtötung von Zellen proportional zur Komplexität (im Sinne von gebündelten DSBs) der erzeugten Läsionen war. Es konnte gezeigt werden, dass gebündelte DSBs mit einem höheren Risiko zur Bildung von Chromosomenaberrationen behaftet sind. Außerdem wurde beobachtet, dass Unterschiede in der DNA Schadensantwort hinsichtlich der Signalgenerierung für unterschiedliche Stufen der Schadens-Komplexität existieren (siehe auch Appendix 4).

Ziel 3: Unterschiede in dem Anteil residualer DNA Schäden, als ein möglicher prädiktiver Faktor der Strahlensensitivität, treten nach fraktionierter Bestrahlung von Fibroblasten und auch von Gliomlinien deutlicher hervor. Höhere Anreicherung von DSB nach fraktionierter Bestrahlung ist in strahlensensitiven Gliomlinien deutlicher ausgeprägt als in strahlenresistenten Linien. Inhibition von ATM Signalwegen der DNA-Schadensreparatur verstärkt die Fraktionierungsempfindlichkeit von Gliomlinien (siehe auch Appendices 6 und 8).

Ziel 4: Die Daten zeigen, dass die Modulation von zentralen Trithorax- und Polycombproteinen, respektive EZH2L und ASH2L das Methylierungsmuster von Histonproteinen und somit die Transkriptionsaktivität ändert. Diese beeinflusst wiederum die Aktivierung von DNA-Reparatur, Zellzyklus-Kontrollmechanismen, Apoptose und das Überleben von Zellen. Epigenetische Modulation ist somit eine Möglichkeit die Strahlensensitivität von Gliomzelllinien zu beeinflussen (siehe auch Appendices 6 und 8).

1. Erzielte Ergebnisse

Ziel 1:

Die Kombination von chemotherapeutischen Wirkstoffen mit Strahlentherapie um einen synergistischen Effekt bei der Abtötung von Tumorzellen zu erhalten, ist gegenwärtig einer der vielversprechendsten Ansätze zur Optimierung der Tumortherapie. Im Rahmen von Ziel 1 wurden Mechanismen der Strahlensensibilisierung durch Nukleosidanalogue untersucht, hauptsächlich am Beispiel des Adenosinanalogs 9-beta-D-Arabinofuranosyladenosin (ara-A). Die erzielten Ergebnisse sind hier in einigem Detail zusammengefasst dargestellt. Die vollständige Darstellung aller erzielten Ergebnisse findet sich in Appendices 5 und 7.

Zunächst untersuchten wir, ob die durch ara-A vermittelte Strahlensensibilisierung ausschließlich auf eine durch ara-A hervorgerufene Hemmung der Replikation

zurückzuführen sein könnte. Hierfür wurde zunächst die Stärke der Hemmung von ara-A und anderen Replikationsinhibitoren (Aphidicolin und Hydroxyurea) auf die DNA Synthese in humanen Zellen gemessen. Anhand der erhaltenen Daten wurden Konzentrationen der anderen Replikationsinhibitoren eingesetzt, die der Wirksamkeit der von ara-A eingesetzten Konzentrationen auf die Replikation entsprachen, oder um ein vielfaches wirksamer waren. Keiner der anderen Replikationsinhibitoren rief eine annähernd so starke Strahlensensibilisierung wie ara-A hervor.

Dies deutete darauf hin, dass der Strahlensensibilisierung durch ara-A ein direkter Einfluss auf die Reparatur von DSBs zugrunde liegt. Wir benutzten Immunfluoreszenzfärbungen und konfokale Mikroskopie um die Entstehung von IR induzierten Rad51 foci in einer humanen Tumorzelllinie zu untersuchen, als Indikator für die Effizienz der HRR. Ara-A unterdrückte effektiv die Bildung von IR induzierten Rad51 foci. Dies zeigte einen hemmenden Effekt dieser Substanz auf HRR. Wir nutzten genetisch veränderte Reporterzelllinien, die in Folge der Reparatur eines Endonuklease-induzierten DSB durch HRR ein fluoreszierendes Signalprotein exprimieren. Auch hier konnten wir deutlich beobachten, dass ara-A die Reparatur von DSB durch die homologe Rekombination (HRR) hemmt. Um zu untersuchen, ob diese Hemmung einen entscheidenden Anteil an der Strahlensensibilisierung hat, untersuchten wir das Zellüberleben von durch RNA-Interferenz von Rad51-depletierten humanen Zellen. Diese Zellen konnten durch Behandlung mit ara-A nicht weiter sensibilisiert werden. Dies zeigte, dass die Hemmung der HRR eine wichtige Rolle bei der Strahlensensibilisierung von exponentiell wachsenden, humanen Tumorzellen spielt.

Wir untersuchten auch die Effekte von ara-A auf Reparaturwege der NHEJ. Hierzu wurden zwei weitere Reporterzellsystemen eingesetzt. In einem dieser Systeme (EJ5-GFP) wird die Verknüpfung distaler Enden zweier DSB durch NHEJ gemessen, was im Gegensatz zur Verknüpfung der proximalen Enden zum Verlust der dazwischen gelegenen Sequenzen führt und deshalb ein mutagenes Reparaturereignis darstellt. Die Häufigkeit dieser mutagenen Ereignisse war erhöht, wenn die Zellen mit ara-A behandelt wurden. In einem zweiten Reporterzellsystem (EJ-RFP) wurde die allgemeine Häufigkeit mutagener Reparaturereignisse gemessen. Behandlung mit ara-A führte zu einer deutlichen Erhöhung mutagener Ereignisse auch in diesem System.

Interessanterweise konnte jedoch keine Veränderung der allgemeinen Effizienz der DSB Reparatur in Reparatur-kompetenten Zellen durch ara-A Behandlung in Pulsfeld-Gelelektrophorese-Experimenten (PFGE) festgestellt werden. Da wir bereits gezeigt hatten, dass die HRR von ara-A gehemmt, sowie fehlerhafte Reparatur durch das NHEJ verstärkt wird, deuteten diese Ergebnisse auf eine Verschiebung der Aktivität zwischen verschiedenen Reparaturwegen anstelle einer allgemeinen Hemmung der Reparatur hin.

Wir vermuteten, dass die B-NHEJ von einer solchen Verschiebung profitieren und somit auch für den Anstieg mutagener Reparaturereignisse verantwortlich sein könnte. Die Aktivität der B-NHEJ lässt sich am einfachsten und direkt in Zellen, die nicht kompetent für die D-NHEJ sind, beobachten. Wir wählten embryonale Maus-Fibroblasten (MEF), mit einem knock-out für das Ligase4 Gen (Lig4^{-/-}), als Testsystem aus. Die Reparatur von DSB ist in diesen Zellen während des exponentiellen Wachstums bereits stark beeinträchtigt, findet aber, wenn auch langsamer, statt. Frühere Untersuchungen haben ergeben, dass die stattfindende langsame Reparatur von DSB in diesen Zellen der B-NHEJ zuzuschreiben ist. Erreichen diese Zellen die Plateau-Phase des Wachstums, so wird die B-NHEJ unterdrückt, wodurch die Reparaturfähigkeit der Zellen weiter verschlechtert wird, so dass nahezu keine DSB-Reparatur mehr zu beobachten ist. Wir untersuchten die Reparatur von DSB in Lig4^{-/-} MEF in der Plateau-Phase des Wachstums mit und ohne Behandlung mit ara-A mit Hilfe der PFGE. Behandlung mit ara-A führte zu einem dramatischen Anstieg der Reparaturkapazität unter diesen Bedingungen. Dies zeigte, dass ara-A nicht nur in der Lage war, die Plateau-Phase abhängige Hemmung der B-NHEJ aufzuheben, sondern deren Effizienz noch darüber hinaus zu steigern. So konnten wir erstmalig und eindeutig eine Beförderung der B-NHEJ durch ein Nukleosidanalogs zeigen. Ara-A verstärkte die Reparatur von DSB durch B-NHEJ auch in humanen Tumorzellen mit defekten im D-NHEJ, sowohl in der exponentiellen, als auch der Plateau-phase.

Die Untersuchung von durch IR hervorgerufenen, nukleären gamma-H2AX, ATM und 53BP1-Foci bestätigte die zuvor mit Hilfe der PFGE gemachten Beobachtungen und deutete auf eine Deregulierung der durch DSB ausgelösten Signalwege und eine

möglichen Rolle der Endresektion als Mechanismen, die der Beförderung der B-NHEJ zugrunde liegen, hin.

Wir verglichen die für ara-A gefundenen Ergebnisse mit den Effekten von F-ara-A und ara-C. Beide Nukleosidanalogue konnten A549 Zellen für die Abtötung durch IR sensibilisieren. Für F-ara-A fanden wir ebenfalls eine starke Hemmung der HRR, sowie einen Anstieg mutagener Reparaturereignisse, der etwas schwächer ausgeprägt war als im Falle von ara-A. Ara-C übte einen deutlich schwächeren, hemmenden Einfluss auf die HRR aus, und wir konnten keinen Anstieg mutagener DSB-Reparatur beobachten. Dies deutet darauf hin, dass Hemmung der HRR und Beförderung der B-NHEJ verbreitete Mechanismen der Strahlensensibilisierung durch Nukleosidanalogue sind, aber auch, dass noch weitere Mechanismen existieren.

Wir schlussfolgerten, dass Behandlung mit ara-A in proliferierenden Zellen durch direkte Hemmung der HRR zur Strahlensensibilisierung führt. Gleichzeitig wird die Balance des NHEJ in Richtung des fehlerhafteren B-NHEJ verschoben. Die Überaktivierung der mutagenen B-NHEJ trägt mit hoher Wahrscheinlichkeit ebenfalls zur Strahlensensibilisierung durch ara-A bei, vor allem in der G1- sowie der Plateau-Phase, aber auch in der G2- und S-Phase.

Die Ergebnisse der Arbeiten innerhalb des ersten Projektzieles zeigen einen neuen Mechanismus der Strahlensensibilisierung durch Nukleosidanalogue auf. Diese neuen Erkenntnisse ermöglichen es, neue Wege bei der Untersuchung der Interaktionen dieser Wirkstoffe mit IR zu beschreiten und könnten wichtige Implikationen für die klinische Anwendung von Nukleosidanalogen als Strahlensensibilisierer haben.

Ziel 2:

In Zellen, die ionisierender Strahlung ausgesetzt sind, erfolgt die Energiedeposition nicht einheitlich, sondern entlang der Bahnstruktur der ionisierenden Partikel. Jeder Partikel hat eine einzigartige Bahnstruktur auf Grund des stochastischen Charakters der Wechselwirkung von Partikeln mit den Molekülen der bestrahlten Materie. Dicht ionisierende geladene Partikel mit hohem LET, oder auch Elektronen am Ende ihrer Bahn, induzieren geclusterte DNA-Schäden auf Grund von multiplen Ionisationen in

einem kleinen Volumen. Die Wahrscheinlichkeit der Formation von geclusterten, komplexen DNA Schäden erhöht sich mit Erhöhung des LETs. Es wird angenommen, dass die Prozessierung von komplexen DNA Schäden vermehrt zu Fehlern und so zu genomischer Instabilität und Zelltod führt. Neben dem gemeinsamen Auftreten mehrerer Basenschäden in räumlicher Nähe, sowie der Kombination von Einzel- und Doppelstrangbrüchen (DSB) zusammen mit Basenschäden, stellt das gehäufte Auftreten mehrerer DSB eine Form komplexen DNA-Schadens dar. Die Induktion von zwei oder mehreren DSBs in einem Abstand von einigen hundert Basenpaaren kann die Chromatin Stabilität zerstören und große Deletionen verursachen. Innerhalb von Ziel 2 sollte untersucht werden, inwieweit das clustering von DSBs, in Abständen welche die nukleare Stabilität beeinflussen können, zu Chromosomenabberationen führen kann, die sich letal auf die Zelle auswirken. Die erzielten Ergebnisse sind hier in einigem Detail zusammengefasst dargestellt. Die vollständige Darstellung aller erzielten Ergebnisse findet sich in Appendix 4.

Es wurde ein auf Restriktionsendonukleasen basierendes Modellsystem entwickelt, um DSB mit definierten Abständen und unterschiedlicher Komplexität in der zellulären DNA zu induzieren und anschließend ihr Potential auf biologische Folgen zu untersuchen. Mit Hilfe von Transposontechnologie, die eine hohe Anzahl von Integrationsstellen ermöglicht, wurden genetisch modifizierte Zelllinien mit unterschiedlichen Anzahlen von geclusterten Restriktionsschnittstellen hergestellt. Dies ermöglicht die gleichzeitige Induktion von mehreren DSB mit definierten Abständen in lebenden Zellen, um dadurch komplexe DSB nach Bestrahlung mit ionisierender Strahlung in diesen Zellen zu imitieren. Um gezielt DSB in Zellen zu erzeugen, setzen wir die I-Sce-I Endonuklease ein. Die Erkennungssequenz dieser Restriktionsendonuklease ist in den Genomen höherer Eukaryonten nicht vorhanden. Konstrukte mit einzelnen oder geclusterten induzierbaren DSB wurden an verschiedenen Stellen in das Genom von CHO wt Zellen, als auch in die CHO-Zelllinien XR-C1-3, Xrs6 und irs1SF, welche inaktivierende Mutationen in Proteinen wichtiger Reparaturwege aufweisen, integriert. Die Anzahl der Integrationsstellen, und somit auch die Anzahl der möglichen Doppelstrangbrüche, wurden durch Southern Blotting ermittelt. Mit Hilfe dieser Zelllinien wurden das Zellüberleben und Chromosomenaberrationen nach I-SceI-Expression gemessen.

Überlebensexperimente mit diesen Zelllinien haben gezeigt, dass durch I-SceI induzierte geclusterte DSBs im Gegensatz zu einfachen DSBs, zu einem starken Absterben führen, das mit der Anzahl geclustelter DSBs zunimmt. In Übereinstimmung mit dem hohen Tötungspotential von geclusterten DSBs konnte nachgewiesen werden, dass Metaphasen von Zellen, in denen geclusterte DSBs induziert wurden, neben Chromosomenbrüchen auch dizentrische und Ring-Chromosomen aufwiesen. Dahingegen wiesen Metaphasen von Zellen, in denen nur einfache DSBs induziert worden waren nur seltene Chromosomenbrüche und keine Chromosomenaberrationen auf. Analyse in der Metaphase erlaubt die Detektion von irreversiblen Chromosomenaberrationen, die häufig zum Zelltod führen. Um auch reparable Chromosomenaberrationen beobachten zu können, wurde die Technik der vorzeitigen Chromosomenkondensation (engl. premature chromosome condensation = PCC) eingesetzt. Mit dieser Technik wurden Zellen in der G2-Phase vor dem Eintritt in die Mitose untersucht. G2-PCC Chromosomenbrüche und Chromosomenaustausche wurden separat gemessen. Es zeigte sich, dass Zellen die Konstrukte zur Induktion von komplexen DSBs trugen, eine deutlich größere Anzahl sowohl von Brüchen als auch von Chromosomenaustauschen aufwiesen. Dabei stieg die beobachtete Anzahl der jeweiligen Schäden mit der Anzahl von Brüchen im Cluster an. Daraus folgerten wir, dass komplexe DSBs aufgrund eines höheren Risikos zur Bildung von Chromosomenaberrationen toxischer sind für Zellen als einfache DSBs.

Weiterhin konnte anhand von Lebend-Zell-Mikroskopie-Experimenten gezeigt werden, dass die Foci-Bildung von 53BP1 Unterschiede zwischen simplen und geclusterten DSBs aufweist. In Zellen mit mehrfacher Integration eines Konstrukts zur Induktion eines einfachen DSB konnten lediglich dem Hintergrund entsprechende Zahlen von Foci beobachtet werden. In Zellen, die Konstrukte zur Induktion von zwei DSBs trugen, konnte bereits eine deutliche Neubildung von 53BP1-Foci beobachtet werden, die jedoch noch deutlich unter dem theoretisch zu erwartenden Maximalwert lag. In Zellen die Integrate mit 4 geclusterten DSBs trugen konnten jedoch Foci-Zahlen nahe dem theoretischen Maximalwert beobachtet werden. Dies deutet daraufhin, dass 53BP1

bevorzugt an komplexeren DSBs akkumuliert, möglicherweise um die Resektion an diesen besonders gefährdeten Stellen zu unterdrücken. Interessanterweise wird, wenn die D-NHEJ kompromittiert ist, das theoretische Maximum an 53BP1 foci auch in Zelllinien mit Konstrukten zur Erzeugung von einfachen oder doppelten DSBs erreicht. Dies konnte sowohl unter Verwendung eines DNA-PKcs Inhibitors, als auch in mutanten Zelllinien gezeigt werden. In Zelllinien mit Konstrukten zur Erzeugung von 4 geclusterten DSBs erhöht sich unter diesen Bedingungen die Anzahl beobachteter 53BP1 Foci jedoch nicht weiter, was nahelegt, dass bei Läsionen dieser Komplexität tatsächlich bereits das Maximum der 53BP1 Foci-Bildung erreicht ist. Vergleichbare Ergebnisse wurden auch auf zytogenetischer Ebene erhalten. G2-PCC Chromosomenbrüche nahmen stark in Zelllinien mit Konstrukten zur Erzeugung von doppelten DSB zu, wenn diese mit einem DNA-PKcs Inhibitor behandelt wurden, jedoch nicht weiter in Zelllinien mit Konstrukten zur Erzeugung von 4 geclusterten DSB, so dass nach Behandlung mit dem Inhibitor in beiden Zelllinien gleiche Anzahlen von Chromosomenbrüchen vorlagen. Chromosomenaustausche zeigten ein ähnliches Verhalten. Interessanterweise konnte die Anzahl von Austauschen in Zelllinien mit 4-fachen DSBs durch Behandlung mit einem PARP-Inhibitor halbiert werden, was auf eine wichtige Rolle der B-NHEJ bei der Erzeugung dieser Chromosomenaberrationen aus komplexen DNA Schäden hinweist.

Die Ergebnisse der Arbeiten innerhalb des zweiten Projektzieles zeigen deutlich, dass geclusterte DSBs toxischer sind für Zellen als einzelne DSB, und dass diese Toxizität mit der Anzahl von DSB in einem Cluster zunimmt. Dies spiegelt sich in der erhöhten Anzahl von Chromosomenbrüchen und -aberrationen wieder, die in Zelllinien mit Konstrukten zur Erzeugung von gehäuft auftretenden DSBs gefunden wurden. Die Ergebnisse weisen außerdem auf eine Verbindung zwischen der Komplexität von DSBs und der Entwicklung einer zellulären Signal-Antwort, erkennbar an der unterschiedlichen Ausbildung von 53BP1 Foci, sowie der Auswahl von Reparaturwegen, wie z.B. der B-NHEJ, hin.

Ziel 3:

Ein wichtiger Resistenzmechanismus gegenüber der Strahlen- bzw. Chemotherapie ist die effiziente Reparatur von, durch Strahlen oder Chemotherapeutika induzierten,

Schäden im Erbgut der Tumorzellen. Die induzierten DNA-Schäden können, wenn sie nicht repariert werden, zum Zelltod und somit zur Tumorrückbildung führen. Eine effiziente Reparatur dieser Schäden in bestimmten Tumoren führt jedoch zur Resistenz gegenüber der Strahlen- bzw. Chemotherapie. Mittels Gelelektrophorese, oder auch Focianalyse (γ H2AX, 53BP1), lassen sich Induktion und Reparatur von DSB sowie der Restschaden der nach einer Reparaturinkubation nicht wiederverknüpften DSB bestimmen. Die nach einer Reparaturinkubation von ≥ 6 h nicht wiederverknüpften DSB stellen den Endpunkt einer Reparaturkaskade dar. Bezüglich der Korrelation der Induktion und Reparatur von strahleninduzierten DSB mit dem Zelltod zeigen die verfügbaren Daten einen Trend auf, dass mit zunehmender Prozessierung der DSB von der Induktion über die Reparaturgeschwindigkeit bis zum Restschaden die Korrelation stärker wird. In mehreren Untersuchungen wurde ein positiver Zusammenhang zwischen dem Anteil residualer DSB und der Strahlensensitivität gefunden.

Fraktionierte Bestrahlung, wie sie in der klinischen Tumorthherapie mit etwa 2 Gy täglichen Bestrahlungsdosis üblich ist, kann zur Akkumulation von subletalen Schäden führen, welche dann die Letalität der Zellen steigern können. Das Ziel der Strahlentherapie bösartiger Erkrankungen ist, eine maximale Zerstörung des Tumors bei möglichst geringen bestrahlungsbedingten Nebenwirkungen. Daher wurden auch Normalgewebszellen (Fibroblasten) in die Untersuchungen mit aufgenommen.

Aufgrund veränderter Rahmenbedingungen wurde auf die Charakterisierung der Bedeutung der Checkpointkinasen C0hk1 und Chk2 weitestgehend verzichtet, und stattdessen die Schwerpunkte auf die Charakterisierung der Strahlenreaktion von Normalgewebszellen (Fibroblasten) und Tumorklinien (Gliomen) gelegt.

Die in diesem Projektteil erzielten Ergebnisse sind hier in einigem Detail zusammengefasst dargestellt. Die vollständige Darstellung aller erzielten Ergebnisse findet sich in Appendix 6.

Untersuchungen von Strahlenresistenzmechanismen in Fibroblasten

Zu den Faktoren, die mit einem erhöhten Risiko für schwere radiogene Nebenwirkungen einhergehen, gehören u.a. die Fraktionierung, die Gesamtdosis, sowie die intrinsische Strahlensensitivität. Einer der bestrahlungsbedingten Nebenwirkung ist die Ausbildung einer Fibrose, bei der eine Vermehrung des kollagenen Bindegewebes in den

bestrahlten Organen auftritt. Die unterschiedliche Stärke der Ausbildung einer Fibrose bei Patienten als Antwort des Normalgewebes auf eine ionisierende Bestrahlung erklärt, unabhängig vom Zelltod, einen signifikanten Anteil der dosislimitierenden Komplikationen in der Strahlentherapie. Fibroblasten sind in der Entwicklung der Fibrose nach Bestrahlung maßgeblich beteiligt. So ist die Fibroblasten Zellpopulation in den Gebieten der strahleninduzierten Fibrose erhöht, und es liegt ein hoher Anteil von Fibroblasten mit abnormem Karyotyp vor, was auf die vorangegangene Bestrahlung zurückgeführt werden kann. Grundlage für die Änderungen im Karyotyp von Fibroblasten in fibrösen Regionen sind u.a. Chromosomenaberrationen, die letztlich auf nicht oder- falsch reparierte DSB zurückgeführt werden können.

Im Rahmen von Ziel 3 wurden Mechanismen der Strahlensensibilisierung nach Kombination von fraktionierter Bestrahlung mit Modulatoren der Reparatursignalkaskade in Normalgewebefibroblasten untersucht. Von den 29 selbst etablierten primären Fibroblasten aus Patienten mit Kopf-Hals Tumoren mit unterschiedlichem Grad an Fibrose (Grad 1, 2, 3) wurden 18 bezüglich klonogenes Überleben nach Bestrahlung mit 7.5Gy LD (0.0125Gy/min, low dose rate), und 14 auch nach 3.5Gy HD (1.8Gy/min, high dose rate) bereits charakterisiert. Die mittleren Überlebensdaten variierten von 1.0% bis 4.2% 7.5Gy LD und 7.1% bis 29% nach 3.5Gy HD. Es gab einen signifikanten Zusammenhang zwischen Grad 3 Fibrose und klonogenem Überleben nach Bestrahlung mit 7.5 Gy LD Bestrahlung, sowohl in Oropharynx- als auch in Hypopharynx-Fibroblasten.

In 14 dieser Fibroblasten wurde zudem der residuale Anteil an DSB, als ein möglicher prädiktiver Wert für die Fibrose und die Strahlenempfindlichkeit, sowohl 6 h als auch 24 h nach Bestrahlung mit einer hohen Einzeldosis von 120 Gy ermittelt. Der Anteil residueller DSB mit Werten zwischen 16.8% bis 42.5% nach 6 h und 10.1% bis 32.8% nach 24 h in der Gelelektrophorese ergab keine Korrelation mit dem Überleben nach 7.5 Gy LD oder 3.5 Gy HD. Der Anteil residueller Schäden zeigte ebenfalls keine Korrelation mit dem Fibrosegrad der Fibroblasten. So betrug der mittlere Anteil residueller DSB Schäden nach 6 h und 24 h 32.4±7.9% und 18.7±8.4% in Fibroblasten mit Grad 1 Fibrose (n=5 Fibroblasten) und 25.7±4.1% und 17.5±5.6% in Fibroblasten mit Grad 3 Fibrose (n=5 Fibroblasten).

Die Bestimmung der residualen DSB mittels Gelelektrophorese erfordert relativ hohe Bestrahlungsdosen. Um die mit dieser Methode ermittelten DSB mit den residualen Anteilen nach Bestrahlung mit therapeutischen Dosen von etwa 2 Gy zu korrelieren, wurde zusätzlich die Anzahl von strahleninduzierten γ H2AX Foci bestimmt. Hierzu wurden von den primären Fibroblasten drei (HF1, HF2, HF3) mit unterschiedlicher Überlebensfraktion nach 7.5 Gy LD (3.36%, 1.73% und 1.21%) und unterschiedlichem Anteil an residualen DSB (32.8%, 22.8% und 10.1%) sowie Fibrosegrad (1, 3, 3) für die Analysen zur Bestimmung der γ H2AX Foci ausgewählt. Die mittlere Anzahl initialer Foci 1 h nach Bestrahlung mit 1 Gy war mit Werten von 16.8 ± 1.0 , 17.7 ± 1.3 und 16.4 ± 5.9 Foci bei HF1, HF2 und HF3 nicht signifikant unterschiedlich. Die Anzahl residualer γ H2AX Foci pro Zelle mit Werten von 11.7 ± 2.5 , 8.0 ± 1.5 und 11.3 ± 3.8 24 h nach Bestrahlung mit 4 Gy waren ebenfalls nicht signifikant unterschiedlich, obwohl diesbezüglich die geelektrophoretisch bestimmten DSB Anteile zwischen den Fibroblasten signifikant variierten.

Im Weiteren wurde der Einfluss der ATM-abhängigen Signalkaskade auf die Reparatur von DSB in diesen Fibroblasten untersucht. Behandlung der Zellen mit dem ATM Inhibitor (ATMi) Ku55933 (20 μ M) 1 h vor Bestrahlung führte zu einer signifikanten Reduktion der initialen Foci 1 h nach Bestrahlung mit 1 Gy auf 12.7 ± 5.0 , 13.8 ± 2.0 und 13.5 ± 6.8 bei HF1, HF2 und HF3. Im Gegensatz führte ATMi zu einer signifikanten Erhöhung der Anzahl residualer Foci 24 h nach 10 Gy auf 19.2 ± 4.3 , 16.2 ± 2.1 und 22.5 ± 6.4 in HF1, HF2 und HF3.

Zusätzlich zur Einzeitbestrahlung wurde, wie in der therapeutischen Praxis üblich, die Anzahl residualer γ H2AX Foci nach fraktionierter Bestrahlung untersucht. Fraktionierte Bestrahlung in Abständen von 24 h mit 2 Gy führte zu einem linearen Anstieg der residualer γ H2AX Foci, als Maß für die Akkumulation von DSB. So betragen die Werte nach Bestrahlung mit 4 x 2 Gy Fraktionen 6.4 ± 0.5 , 2.9 ± 0.9 , 4.9 ± 0.1 in HF1, HF2 und HF3. Der relative Anstieg der Anzahl γ H2AX Foci, nach Dosen von 2 x 2 Gy, 3 x 2 Gy und 4 x 2 Gy im Vergleich zu 1 x 2 Gy, als Maß für die Akkumulation der Foci und somit der Fraktionierungsempfindlichkeit, war jedoch bei den Fibroblasten deutlich unterschiedlich ausgeprägt mit einer Steigung von 4% (HF1), 20% (HF2) und 38%

(HF2). Die strahlenresistente Fibroblastenkultur (HF1) zeigt eine eher reduzierte Fraktionierungsempfindlichkeit im γ H2AX Test.

Nach Inhibierung von ATM kehrte sich die Fraktionierungssensitivität der Fibroblasten um. Behandlung mit ATMi führte zu einem signifikanten Anstieg der residualen γ H2AX Foci im Vergleich zu unbehandelten aber bestrahlten Proben. Die Fraktionierungsempfindlichkeit nach ATMi war mit relativen Steigerungen von 123% (HF1), 57% (HF3) und 18% (HF2) genau anders herum. ATM wirkt offensichtlich stärker in Fibroblasten mit einer geringen Fraktionierungssensitivität. Obwohl die Anzahl der Fibroblasten noch zu gering ist, um eine statistisch sichere Aussage bezüglich der Korrelation zwischen Strahlenempfindlichkeit von Fibroblasten und Fraktionierungssensitivität im γ H2AX Assay zu erlauben, zeigt dieser Trend, dass es sich lohnt, weitere Fibroblasten diesbezüglich zu untersuchen.

Die meisten normalen Zelltypen lassen sich in der Zellkultur nicht unbegrenzt vermehren. Mit zunehmender Teilungsaktivität bzw. Passagierung kommt es als Folge zellulärer Differenzierung zu einem schrittweisen Stillstand der Proliferation und wird als replikative Seneszenz bezeichnet. Mit zunehmender Passagierung nimmt auch die Generationszeit in Kultur zu. Je nach Alter der Fibroblasten Spender haben Fibroblasten eine begrenzte Teilungsaktivität von etwa 30-40 Teilungszyklen. Es wurden 3 ausgewählte humane Haut Fibroblasten in frühen und späten Passagierungen (mit mindestens 10 Passagierungen zwischen beiden Gruppen) bezüglich der Bildung von γ H2AX Foci nach Bestrahlung in Abhängigkeit von ATM untersucht. Hierzu wurden die Fibroblasten 1 h vor Bestrahlung mit dem ATM Inhibitor (ATMi) behandelt. Die Focibildung wurde 1 h nach 1 Gy (initial) und 24 h nach 10 Gy (residual) bestimmt. Die Anzahl initialer Foci in replikativ seneszenten (späte Passagen) Fibroblasten war mit Werten von 16.8 ± 1.0 , 17.7 ± 1.3 und 16.4 ± 5.9 Foci pro Zelle in HF1, HF2 und HF3 um etwa 30% niedriger als in frühen Passagen. Die Anzahl residualer Foci mit Werten von 8.4 ± 1.2 , 7.2 ± 1.1 und 8.1 ± 0.6 , respektive in HF1, HF2 und HF3, um etwa 20% geringer in seneszenten Fibroblasten. ATMi verstärkte den Unterschied der Anzahl initialer γ H2AX Foci pro Zelle zwischen frühen und späten Passagen auf etwa 50%.

Untersuchungen von Strahlenresistenzmechanismen in Tumorklinien (Gliomen)

In Vorexperimenten wurden 12 Tumorklinien (Sarkome, Karzinome, Gliome) bezüglich des Anteils residueller DSB 6 h und 120 h nach Bestrahlung mit hohen Dosen von 1 x 120 Gy bzw. 4 x 30 Gy mittels Gelelektrophorese charakterisiert. Die Daten zeigten keine Korrelation mit dem klonogenen Überleben der einzelnen Tumorklinien nach Bestrahlung mit 2 Gy. Erst nach Einteilung in die drei Tumortypen (Sarkome, Karzinome, Gliome) zeigte sich, dass der gemittelte Anteil residueller DSB in den verschiedenen Tumortypen mit den Tumorkontrolldosen (TCD), als ein Maß für die Strahlenempfindlichkeit (Sarkome>Karzinome>Gliome; steigende TCD50 und residuale DSB) im Mausmodell, korreliert. Die weiteren Experimente wurden daher in ausgewählten Gliomlinien mit unterschiedlicher Strahlenempfindlichkeit (A7>HTZ17>U87, U373, MO59K; steigender Überlebensfraktion nach 2 Gy) durchgeführt. Zunächst wurde die initiale (1 h nach IR) als auch die residuale (24 h nach IR) Anzahl von γ H2AX und 53BP1 Foci bestimmt. Hinsichtlich der Ausprägung der Anzahl an Foci (γ H2AX) pro Zelle ergab sich eine signifikante Korrelation mit dem klonogenen Überleben, wobei die Anzahl der Foci mit der Strahlenempfindlichkeit der Linien zunahm (A7> HTZ17>MO59K, U87). Ähnlich verhielt es sich mit der initialen Anzahl 53BP1 Foci. Die Bestimmung der 53BP1 Foci ist bei Tumorklinien zu bevorzugen, weil in replikativen Zellen die Hintergrundsignale der γ H2AX Foci, die strahleninduzierten Signale stark beeinflussen können.

In ausgewählten Gliomlinien (U373, HTZ17, U87, A7, MO59K) wurde zusätzlich der Einfluss der ATM Inhibition auf die Doppelstrangbruch-Reparatur mittels 53BP1 Foci untersucht. Zunächst wurde die Dosisabhängigkeit der initialen (0,5 Gy / 1 h) und der residualen (10 Gy / 4 h) 53BP1 Foci von dem ATM-Inhibitor (0-50 μ M) untersucht. ATM-Inhibition führt in Abhängigkeit von der Konzentration des ATM Inhibitors Ku55933 zu einer Hemmung der initialen und zu einer Anreicherung der residualen Anzahl an Foci. Die strahlenresistenten Linien U87 und M059K zeigten dabei initial wie residual die niedrigsten Focizahlen. Die ATM Wirkung ist bei den Linien ebenfalls unterschiedlich ausgeprägt, mit dem stärksten Effekt bei A7 und U373.

Anschließend wurde der Effekt einer Fraktionierung der Bestrahlungsdosis auf die residualen Foci mit und ohne ATMi untersucht. Die Linien verhalten sich sehr

unterschiedlich bezüglich Restschäden nach fraktionierter Bestrahlung. Während es bei den eher strahlenempfindlichen Linien A7 und HTZ17 zu einer Abnahme der Restschäden kommt, hat die Fraktionierung keinen signifikanten Einfluss auf den Restschaden in U87 und M059K. Inhibition von ATM führt zu einem deutlichen Anstieg des Restschadens nach Fraktionierung in HTZ17, M059K und A7. In U87 ist eher ein moderater Effekt zu beobachten.

Anders als bei Fibroblasten spielen bei den stark replikativen Tumorklinien neben der nicht-homologen Reparatur von DSB (NHEJ), auch die homologe Reparatur (HR), welche maßgeblich in der S/G2-Phase des Zellzyklusses aktiv, ist eine wesentliche Rolle. Daher wurde exemplarisch in drei Gliomlinien (A7, M059K und HTZ17) auch die Anzahl der Rad51 Foci, als ein Maß für die Aktivierung der HR analysiert. Im Gegensatz zu den γ H2AX bzw. 53BP1 Foci mit einem Maximum der Focibildung zwischen 30 - 60 min, welche ein Maß für die Aktivierung der nicht-homologen DSB Reparatur darstellen, haben Rad51 Foci ihr Maximum bei etwa 4 - 6 h. Zu diesem Zeitpunkt ist bereits die erste schnelle Phase der DSB-Reparatur mittels NHEJ abgelaufen. Daher wurde die Anzahl initialer Rad51 Foci erst 4 h und die residualen Foci 24 h nach Bestrahlung mit 10 Gy gemessen. Die Anzahl initialer Rad51 Foci ist in der strahlensensitiven Gliomlinie A7 um den Faktor 10 höher als bei den Linien M059K und HTZ17, mit Werten von 43.0 ± 7.2 , 4.2 ± 0.8 und 7.9 ± 1.4 Foci pro Zelle. Die Anzahl Rad51 Foci 24 h nach Bestrahlung nimmt bei A7 auf 22.1 ± 4.1 ab, ändert sich aber unwesentlich bei HTZ17 (10.4 ± 1.4) und M059K (4.4 ± 0.6). Inhibition der ATM Signalkaskade (mit 20 μ M Ku55933) hat keinen signifikanten Einfluss auf die Anzahl initialer Rad51 Foci bei allen untersuchten Linien. Es führt zu einer deutlichen Steigerung der Anzahl residualer Rad51 Foci in A7 (37.3 ± 5.9) und HTZ17 (33.4 ± 3.6), hat aber keinen signifikanten Einfluss bei M059K (4.7 ± 0.8).

Als weiterer Resistenzmechanismus nach Strahlentherapie wird die Aktivierung der Apoptose diskutiert. Daher wurden die Gliomlinien (HTZ17, U87, A7, M059K, M059J) bezüglich der Apoptose Ausprägung nach Bestrahlung charakterisiert. Es ergaben sich deutliche Unterschiede in der Aktivierung des apoptotischen Zelltodes 72 h nach

Bestrahlung mit 20 Gy zwischen den Zelllinien (M059J>A7>HTZ17>U87>M059K) mit einer apoptotischen Fraktion von $47.2 \pm 4.1\%$, $14.4 \pm 1.3\%$, $5.4 \pm 0.6\%$, $4.4 \pm 0.8\%$ und $0.1 \pm 0.1\%$ bei M059J, A7, HTZ17, U87 und M059K. Die strahleninduzierte Apoptose zeigt zudem eine signifikante Korrelation mit dem klonogenen Überleben nach 2 Gy (SF2) der untersuchten Linien.

Bei der Eradikation von Tumor- und Normalgewebszellen durch die Strahlentherapie spielt neben der Apoptose die irreversible Arretierung der Zellen im Zellzyklus, die Seneszenz, eine wichtige Rolle. Bestrahlung kann die Zellen vorzeitig in die Seneszenz führen. Daher hat die strahleninduzierte Seneszenz, als ein Mechanismus der Erradierung von Zellen, eine wichtige Rolle und wurde daher in die Untersuchungen mit aufgenommen. Die Gliomlinien (HTZ17, U87, A7, M059K) wurden bezüglich der Seneszenzsausprägung nach Bestrahlung mittels β -Galactosidase Aktivität charakterisiert. Es ergaben sich deutliche Unterschiede in der Seneszenzsausprägung 168 h nach Bestrahlung mit 20 Gy zwischen den Zelllinien mit folgender Rangfolge (U87>HTZ17>M059K>A7). Aus diesen Daten lassen sich keine Rückschlüsse auf die Bedeutung der Seneszenz für die Strahlenempfindlichkeit ableiten.

Zusammenfassend zeigen die Ergebnisse der Arbeiten innerhalb des dritten Projektzieles, dass die Induktion und Reparatur von DNA Doppelstrangbrüchen sowie deren Modulation wichtige Mechanismen der Strahlensensibilisierung durch ionisierende Strahlen darstellen. Es besteht aber kein direkter Zusammenhang zwischen der Induktion sowie Reparatur von DSB und der im klonogenen Test gemessenen Strahlenempfindlichkeit. Vielmehr hat die Art der Bestrahlung (Einzeit- oder fraktioniert) einen wesentlichen Einfluss auf die Schadensprozessierung. Berücksichtigt man die Effekte der Modulation mit ATMi nach Einzeitbestrahlung so sind die Effekte mit einem mittleren Steigerungsfaktor von 2.4 ± 0.4 über alle Gliomlinien (5 Linien) und 1.9 ± 0.2 bei Fibroblasten (3 Kulturen) ähnlich stark. Vergleicht man die Effekte einer fraktionierten Bestrahlung (4 x 2 Gy) auf die residualen γ H2AX Foci so betragen die mittleren Steigerungsfaktoren 1.0 ± 0.2 über alle Gliomlinien (4 Linien) und 1.5 ± 0.1 bei Fibroblasten (3 Kulturen). ATMi in Kombination mit der Dosisfraktionierung führt in

Gliomlinien und Fibroblasten zu mittleren Steigerungsfaktoren, entsprechend von 1.9 ± 0.7 und 2.6 ± 1.2 .

Somit sind die Wirkungen der verschiedenen Behandlungsarme auf die Anzahl residualer DSB nach i) Einzeitbestrahlung + ATMi, ii) fraktionierte Bestrahlung und iii) fraktionierte Bestrahlung + ATMi in Gliomlinien und Fibroblasten ähnlich stark. Daher würde weder die Fraktionierung noch die Behandlung mit ATMi die Anreicherung residualer DSB in der Gruppe der Gliomlinien im Vergleich zu der Gruppe der untersuchten Fibroblasten präferentiell fördern. Es gibt jedoch individuelle Unterschiede in der Wirkung der Behandlungsarme bei den einzelnen Gliomlinien und Fibroblasten.

Ziel 4:

Die Chromatinstruktur mit der groben Einteilung in transkriptionsaktivem Euchromatin (EC) und vornehmlich transkriptionsinaktivem Heterochromatin (HC) stellt, mit seinen mannigfaltigen Modifikationen der verschiedenen Histonproteine (u.a. Acetylierung, Methylierung, Phosphorylierung), einen wesentlichen Faktor für die Schadensantwort der Zelle nach Bestrahlung dar. Da EC und HC derart unterschiedliche Umgebungen repräsentieren, liegt die Vermutung nahe, dass sie Unterschiede bezüglich ihrer Anfälligkeit für DNA-Schädigungen und der Reparaturfähigkeit aufweisen. Daher wurde in den Gliomlinien MO59K und A7 die Bedeutung der Histon-Methylierung – insbesondere im Hinblick auf Chromatin-Struktur und Epigenetik – für die Strahlensensitivität der Gliomzelllinien MO59K und A7 untersucht.

Die in diesem Projektteil erzielten Ergebnisse sind hier in einigem Detail zusammengefasst dargestellt. Die vollständige Darstellung aller erzielten Ergebnisse findet sich in Appendix 6.

Etwa 30% des Chromatins in A7 sind H3K9me3 angereicherte Regionen, und somit eher heterochromatisch und daher weniger transkriptionsaktiv. Mikroskopische Analysen der γ H2AX Foci-Verteilung sowohl 1 h als auch 4 h nach Bestrahlung mit 0.5 Gy zeigen,

dass weniger als 15% der H3K9me3 angereicherten Regionen mit γ H2AX Foci assoziiert sind, und somit die γ H2AX Foci in diesen Regionen etwa um den Faktor 2 unterrepräsentiert ist. Mittels ChiP Analysen wurde ebenfalls herausgefunden, dass der initiale Anteil von γ H2AX 1 h nach Bestrahlung mit 60 Gy auf Chromatinfragmenten die vermehrt den Euchromatinmarker H3K4me3 tragen, um etwa 40% signifikant ($p < 0.025$) höher ist als auf Fragmenten, die vornehmlich den Heterochromatinmarker H3K9me3 tragen. Die Analysen mit weiteren Heterochromatinmarker (H3K27me3) und Euchromatinmarker (H3K9me1) zeigten, dass dieser Unterschied sich nicht unbedingt allgemein auf alle Marker übertragen lässt. Diese Daten zeigen, dass es wohl Unterschiede von γ H2AX auf verschiedenen Chromatinkompartimenten 1 h nach Bestrahlung gibt. Dieser Unterschied lässt sich aber nicht unbedingt allgemein auf Hetero- oder Euchromatinmarker zuordnen.

Nachdem wir Unterschiede in der Verteilung von γ H2AX Foci in heterochromatischen und euchromatischen Regionen mittels mikroskopischer als auch proteintechnischer Analysen festgestellt haben, war die Frage nach der Modulierbarkeit dieser Regionen, sowie deren Einfluss auf die Strahlenantwort der Zellen. Hierzu wurde die Transkription zentraler Proteine der Polycomb- (ASH2L) und Trithoraxproteinfamilie (EZH2) mittels siRNA inhibiert. Polycombproteine sind konstitutiver Transkriptionsrepressoren, deren Inhibition sollte das Chromatin in eine transkriptionell aktive Form überführen. Trithoraxproteine sind hingegen Transkriptionsaktivatoren, deren Inhibition sollte die Zellen in eine transkriptionell inaktive Form überführen.

Für die effiziente und aussagekräftige Untersuchung der Einflussnahme auf die Strahlenempfindlichkeit der Gliomzelllinien war es zunächst unumgänglich, den Nachweis für die Effektivität der Proteininhibierung zu erbringen. Dies geschah über den direkten Nachweis der Proteine ASH2L und EZH2 mittels Western-Blot. Beide siRNA für ASH2L (ASH2Li) und EZH2 (EZH2i) führten zu ähnlichen Inhibierungseffizienzen von etwa 70%. Eine deutliche Reduktion der H3K27me3- und H3K9me3-Signalintensität nach EZH2i und ASH2Li Inhibierung mittels Western-Blot und Durchflusszytometrie weisen auf die entsprechende Reduktion von Heterochromatin und Anreicherung von Euchromatin hin. Hierbei machte weder der Zeitpunkt nach der Bestrahlung, noch die Unterscheidung nach G1 bzw. G2/M-Phase-Zellen einen Unterschied.

Die Zellzyklusphase in der die Zellen bestrahlt werden, sowie die Aktivierung der Zellzyklus-Kontrollpunkte nach Bestrahlung, sind wichtige Parameter der Strahlenempfindlichkeit von Zellen. Die Zellzyklus-Kontrollpunkte regulieren Phasenübergänge und kritische Prozesse innerhalb des Zellzyklus und dienen der Integrität des Genoms. Daher wurde mittels Zellzyklusanalyse ermittelt, inwieweit die Inhibierung von ASH2L bzw. EZH2 die Zellzyklusverteilung zum Zeitpunkt und nach der Bestrahlung beeinflussen. Hierdurch konnte eingeschätzt werden, ob die gemessenen Effekte direkt mit der Inhibierung von ASH2L bzw. EZH2 in Verbindung stehen, oder ob es sich um sekundäre Effekte aufgrund von veränderter Zellzyklusverteilung handelt. In MO59K führte die ASH2Li zu einer Reduktion des G2/M-Anteils und zu einer Erhöhung des G1-Anteils 48 h nach Bestrahlung mit 20 Gy. EZH2i hatte einen gegenteiligen aber nicht signifikanten Effekt auf die Zellzyklusverteilung nach Bestrahlung. Die Effekte in A7 nach Bestrahlung mit 10 Gy waren deutlicher ausgeprägt mit einer signifikanten Reduktion des G2/M-Anteils und einer Erhöhung des G1-Anteils nach ASH2Li. EZH2i hatte einen signifikanten gegenteiligen Effekt auf G2/M und G1-Phase.

Im Anschluss wurde mittels spezifischer γ H2AX Foci die Aktivierung von NHEJ Reparatur von DSB analysiert. DSBs wurden mittels γ H2AX-Antikörper, sowohl fluoreszenzmikroskopisch als auch durchflusszytometrisch, nachgewiesen, und die Auswirkungen von ASH2L- bzw. EZH2-Inhibierung auf deren Bildung untersucht. EZH2i begünstigte signifikant die Bildung initialer γ H2AX-Foci in unbestrahlten A7-Zellen. Die Inhibierung von ASH2L hingegen führt zu einer geringfügigen Beeinträchtigung der Bildung von γ H2AX-Foci. Nach Bestrahlung der Zellen mit 0.5 Gy wurde dieser Effekt jedoch hoch signifikant verstärkt. So zeigten sich in bestrahlten A7-Zellen nach ASH2L-Inhibierung etwa 20% weniger Foci als in der untransfizierten Kontrolle. EZH2-Inhibierung wirkte wiederum entgegengesetzt und begünstigte nur geringfügig die Foci-Bildung. Inwieweit ASH2Li und EZH2i die Verteilung der γ H2AX-Signale im EC bzw. HC beeinflusst wurde mittels Western-Blot nach CHIP analysiert. Die Mittelwerte der Messungen ließen keine signifikanten Unterschiede erkennen.

Zusätzlich wurde die Reparatur von DSB auch mit Hilfe von Pulsfeldgelelektrophorese-Experimenten untersucht, weil es im Gegensatz zu dem γ H2AX Assay direkt die DSB wiedergibt. ASH2Li hatte keine nennenswerten

Unterschiede auf die Reparaturkinetik. Wohingegen EZH2i die Reparaturfähigkeit der Zellen, insbesondere die frühe Reparatur, innerhalb der ersten 6 h leicht verzögerte.

Ausgehend von den bisher durchgeführten Untersuchungen bezüglich der Entstehung, Lokalisation und Reparatur von DNA-DSBs, war es von großem Interesse, wie sich die veränderten Faktoren auf das Überleben von Gliomzellen auswirken. Die Bestimmung des Anteils apoptotischer Zellen ist ein schnelles und einfaches Mittel für die Bewertung der spezifischen Strahlensensitivität. Für die Strahlentherapie ist die Apoptoseantwort von Tumorzellen insbesondere in der frühen Interphase von besonderer Bedeutung, da der Tumor durch gezielte Aktivierung von Zelltodmechanismen in geschädigten Zellen verkleinert wird, ohne das umliegende Gewebe zusätzlich zu schädigen. Für diese Untersuchungen wurde die A7 Zelllinie verwendet, weil Sie im Vergleich zu der MO59K Apoptose kompetent ist. Nach Bestrahlung der Zellen mit 20 Gy ließen sich deutliche, hoch signifikante Unterschiede zwischen den Behandlungsgruppen erkennen. So zeigten ASH2L-inhibierte Zellen mit einer Apoptoserate von 4,4 % weniger als halb so viele apoptotische Zellen wie die untransfizierte Kontrolle (11,0 %). Die Inhibierung von EZH2 zeigte erneut den antagonistischen Charakter der beiden Gene. Mit einer Apoptoserate von 19,9 % lagen hier etwa doppelt so viele apoptotische Zellen vor, wie in der untransfizierten Kontrolle.

Da therapeutische Wert von Apoptosen, welche aus der G2/M-Phase resultieren, also eher aus der Mitose und nicht aus der Interphase hervorgehen, als gering einzuordnen ist, wurde überprüft, ob der gesteigerte G2-Anteil nach EZH2-Inhibierung auch für den Anstieg der Apoptoserate verantwortlich ist. Hierzu wurden die Zellen nach der Bestrahlung mittels Genistein (30 μ M und 60 μ M) in der G2 arretiert. Durch Genistein konnte eine annähernde Synchronisation der Zellen 48 h nach Strahleneinwirkung in der G2/M Phase gewährleistet werden. Nach ASH2Li war in allen Fällen ein signifikanter relativer Rückgang der strahleninduzierten Apoptoserate um etwa 15% zu beobachten. Ebenso führte EZH2i in jedem Fall zu einem signifikanten Anstieg der Apoptoserate um etwa 50-70% im Vergleich zu den untransfizierten Kontrollen. Die Proportionen der einzelnen Behandlungsgruppen (Kontrolle, ASH2Li, EZHi) blieben, unabhängig von der Genistein-Behandlung, weitestgehend erhalten.

Diese Daten zeigen, dass die ASH2Li und EZH2i bedingten Änderungen der strahleninduzierten Apoptose zellzyklusunabhängig sind. Möglicherweise führen ASH2Li und EZH2i zu gegenteiligen Änderungen der Expression von Apoptose relevanten Genen führen.

Daher wurden die Effekte der ASH2Li und EZH2i auf die Expressionsrate bestimmter funktioneller Gene untersucht. Hierbei war es von großem Interesse, in wie weit die Genexpression, besonders im Hinblick auf Chromatinmodulation, Zellzyklusregulation, Apoptose und DNA-Reparatur, beeinflusst wird. Einzelne Gene dieser Gruppen wurden gesondert betrachtet. Mit Hilfe der Microarray-Experimente konnten nach ASH2Li bzw. EZH2i insgesamt 1534 signifikant deregulierte Gene identifiziert werden. ASH2Li führte hierbei zu einer erhöhten Genexpression von 289 Genen und zu einer reduzierten Expression von 970 Genen. EZH2i dagegen führte zur erhöhten Expression von 544 Genen und eine reduzierte Expression von 445 Genen festgestellt werden. Bei der Betrachtung der zehn signifikantesten Gene der einzelnen Gruppen fiel auf, dass die meisten Gene bei ASH2Li deutlich geringer exprimiert wurden (Apoptose: 7/10, Zellzyklus: 10/10, Chromatin: 6/10, DNA-Reparatur: 9/10). Im Gegensatz dazu zeigten bei EZH2i etwa die Hälfte der Gene eine erhöhte Expression (Apoptose: 6/10, Zellzyklus: 5/10, Chromatin: 4/10, DNA-Reparatur: 4/10).

Damit der Verlust der Proliferationsfähigkeit, welcher für die Strahlentherapie von noch größerer Bedeutung ist wie die Apoptose, mit in Betracht gezogen werden kann, wurden Langzeitexperimente des Überlebens von Plaquemolayer durchgeführt. Plaquemolayerexperimente, die in der Arbeitsgruppe etabliert worden sind, unterscheiden sich von klonogenem Überlebenstest in der Art, dass nicht das Überleben einer einzelnen Zelle, sondern das von etwa 1500 Zellen im Zellverband ermittelt wird. Daher erfordern Plaquemolayer für die vollständige Kontrolle des Wachstums auch relativ hohe Bestrahlungsdosen. Im Bereich niedriger Dosen bis 12 Gy zeigten sich kaum Änderungen in den Plaquemolayerkontrollraten. Erst ab Strahlendosen von 18 Gy konnte, unabhängig von der jeweiligen Behandlung, das Zellwachstum vollständig kontrolliert werden. Nach ASH2Li konnten keine Unterschiede im Vergleich zur

untransfizierten Kontrolle ausgemacht werden. EZH2i hingegen führte zu einer hochsignifikanten Sensitivierung der Zellen um 1.3 Gy.

Die Ergebnisse der Arbeiten innerhalb des vierten Projektzieles zeigen, dass durch die gezielte Inhibierung ausgewählter TrxG- und PcG-Proteine mittels spezifischen siRNAs Einfluss auf die Aktivität dieser Proteinkomplexe genommen werden kann. Die hierdurch bedingten Änderungen des Methylierungsstatus von Histonproteinen und der Transkriptionsaktivität können direkt oder indirekt bedingten Änderungen der die Antwort der Zellen auf Bestrahlung beeinflussen. Diese sind u.a. die veränderte i) Induktion von γ H2AX Foci, ii) Aktivierung von Zellzykluskontrollpunkten, iii) Aktivierung der Apoptose und iv) Überleben von bestrahlten Plaquemonolayern. Epigenetische Mechanismen sind wichtige Einflußgrößen in der Strahlenantwort von Gliomlinien, deren Modulation bietet daher einen vielversprechenden Ansatz um die Strahlenempfindlichkeit zu steigern.

2. Notwendigkeit der geleisteten Arbeit und Verwertbarkeit der Ergebnisse

Das Projekt hatte zwei Ziele: 1. die wissenschaftlichen Kenntnisse der Strahlenwirkung zu vertiefen und, 2. die gezielte Ausbildung von Studenten um die Kompetenz auf dem Gebiet der Wirkung ionisierender Strahlen zu fördern. Die Reparatur von DNA Schäden spielt eine zentrale Rolle in der Strahlenforschung. Ein genaueres Verständnis der, der DNA-Reparatur zugrundeliegenden, Mechanismen ist Voraussetzung für Fortschritte sowohl im Strahlenschutz, als auch in der Strahlentherapie, wo ionisierende Strahlung genutzt wird um gezielt Tumorzellen auszuschalten. Unter den von ionisierender Strahlung verursachten DNA Schäden habe DNA Doppelstrangbrüche (DSB), wegen ihrer schwerwiegenden Konsequenzen für das Zellüberleben und die Entstehung von Chromosomenaberrationen, besondere Bedeutung. Die hier durchgeführten Arbeiten zur Strahlensensibilisierung durch Nukleosidanaloge, den Einfluss der Schadenskomplexität, der Bedeutung der Chromatinstruktur sowie zur Signalweiterleitung nach der Induktion von DSBs leisten einen wichtigen Beitrag zur Vertiefung unseres Verständnisses der biologischen Effekte ionisierender Strahlung.

Die Hintergründe zu den Projektzielen wurden detailliert in drei bereits veröffentlichten Übersichtsartikeln (Reviews; Appendices 1-3) dargestellt. Zudem wurden zwei Manuskripte mit von in diesen Projektteilen gewonnen Daten und Erkenntnissen zur Publikation in internationalen peer-review Zeitschriften eingereicht (Appendices 7 und 8) während sich zwei weitere in Vorbereitung befinden (werden nachgereicht). Ausserdem wurden innerhalb dieses Projekts bereits 2 Promotionen zum Abschluss gebracht (Appendices 4 und 5) während eine dritte sich kurz vor dem Abschluß befindet (Appendix 6), in denen die aus den Projektzielen 1 und 2 neu gewonnen Erkenntnisse dargelegt sind. Die Ausbildung von 3 Doktoranden gewährleistet die in den Förderpolitischen Zielen formulierte Förderung des wissenschaftlichen Nachwuchses sowie des Kompetenzerhalts in der Biologischen Strahlenforschung.

3. Während der Durchführung des Vorhabens bekannt gewordene Ergebnisse anderer Stellen

Keine.

4. Erfolgte Veröffentlichungen

Magin, Simon Promotionsschrift zur Erlangung des Dr. rer. nat.: A balance shift between error-free and error-prone DNA double-strand break repair pathways as a novel mechanism of radiosensitization by nucleoside analogs. (2014).

Schipler, Agnes Promotionsschrift zur Erlangung des Dr. rer. nat.: Homing endonuclease-based model systems for the study of DNA double strand break induced cell signaling and repair. (2013).

Magin S, Saha J, Wang M, Mladenova V, Coym N, Iliakis G. Lipofection and nucleofection of substrate plasmid can generate widely different readings of DNA end-joining efficiency in different cell lines. DNA Repair 2013, 12: 148-160

Schipler A, Iliakis G. DNA double-strand-break complexity levels and their possible contributions to the probability for error-prone processing and repair pathway choice. Nucleic Acids Res, 2013 Sep;41(16):7589-605. doi: 10.1093/nar/gkt556

Iliakis G, Mladenov E, Magin S, Soni A. DNA Double-Strand Break Repair as determinant of cellular radiosensitivity to killing and target in radiation therapy. Front Oncol 2013, 3: Article 113

Costantino L, Sotiriou SK, Rantala JK, Magin S, E. Mladenov, Helleday T, Haber JE, Iliakis G, Kallioniemi OP, Halazonetis TD. Break-Induced Replication Repair of Damaged Forks Induces Genomic Duplications in Human Cells. *Science*, 2014, 343(6166): 88-91.

Soni A, Siemann M, Grabos M, Murmann T, Pantelias GE, Iliakis G. Requirement for Parp-1 and DNA Ligases 1 or 3 but Not of Xrcc1 in Chromosomal Translocation Formation by Backup End Joining. *Nucleic Acids Res.* 2014;42(10):6380-92.

Dueva R, Iliakis G. Alternative pathways of non-homologous end joining (NHEJ) in genomic instability and cancer. *Transl Cancer Res* 2013, 2, 163-177

Stankowa K, Ivanova K, Mladenov E, Rosidi B, Sharma A, Boteva R, Iliakis G. Conformational transitions of proteins engaged in DNA double-strand break repair, analysed by tryptophan fluorescence emission and FRET. *Biochem J* 2012, 443: 701-709.

Singh SK, Bednar T, Zhang L, Wu W, Mladenov E, Iliakis G. Inhibition of B-NHEJ in Plateau-Phase Cells Is Not a Direct Consequence of Suppressed Growth Factor Signaling. *Int J Radiat Oncol Biol Phys.* 2012, 84: e237-e243.

Manova VI, Singh SK, Iliakis G. Processing of DNA double strands breaks by alternative non-homologous end-joining in hyperacetylated chromatin. *Genome Integrity* 2012, 3:4 doi:10.1186/2041-9414-3-4

Singh SK, Wu W, Stuschke M, Bockisch A, Iliakis G. Reduced Contribution of Thermally-Labile Sugar Lesions to DNA Double-Strand Break Formation after Exposure to Neutrons. *Radiat Res* 2012, 178: 581-590.

Appendix 1

Sak A, Stuschke M.

Use of γ H2AX and other biomarkers of double-strand breaks during radiotherapy.

Semin Radiat Oncol. 2010 Oct;20(4):223-31.

Appendix 1

vertraulich

[aus urheberrechtlichen Gründen]

Appendix 2

Mladenov E, Magin S, Soni A, Iliakis G.

DNA double- strand break repair as determinant of cellular radiosensitivity to killing and target in radiation therapy.

Front Oncol. 2013 May 10;3:113.



DNA double-strand break repair as determinant of cellular radiosensitivity to killing and target in radiation therapy

Emil Mladenov, Simon Magin, Aashish Soni and George Iliakis*

Institute of Medical Radiation Biology, University of Duisburg-Essen Medical School, Essen, Germany

Edited by:

Adam Paul Dicker, Thomas Jefferson University, USA

Reviewed by:

Fatih Uckun, University of Southern California, USA

Aaron Howard Wolfson, University of Miami Miller School of Medicine, USA

*Correspondence:

George Iliakis, Institute of Medical Radiation Biology, University of Duisburg-Essen Medical School, Hufelandstr. 55, 45122 Essen, Germany.
e-mail: georg.iliakis@uk-essen.de

Radiation therapy plays an important role in the management of a wide range of cancers. Besides innovations in the physical application of radiation dose, radiation therapy is likely to benefit from novel approaches exploiting differences in radiation response between normal and tumor cells. While ionizing radiation induces a variety of DNA lesions, including base damages and single-strand breaks, the DNA double-strand break (DSB) is widely considered as the lesion responsible not only for the aimed cell killing of tumor cells, but also for the general genomic instability that leads to the development of secondary cancers among normal cells. Homologous recombination repair (HRR), non-homologous end-joining (NHEJ), and alternative NHEJ, operating as a backup, are the major pathways utilized by cells for the processing of DSBs. Therefore, their function represents a major mechanism of radiation resistance in tumor cells. HRR is also required to overcome replication stress – a potent contributor to genomic instability that fuels cancer development. HRR and alternative NHEJ show strong cell-cycle dependency and are likely to benefit from radiation therapy mediated redistribution of tumor cells throughout the cell-cycle. Moreover, the synthetic lethality phenotype documented between HRR deficiency and PARP inhibition has opened new avenues for targeted therapies. These observations make HRR a particularly intriguing target for treatments aiming to improve the efficacy of radiation therapy. Here, we briefly describe the major pathways of DSB repair and review their possible contribution to cancer cell radioresistance. Finally, we discuss promising alternatives for targeting DSB repair to improve radiation therapy and cancer treatment.

Keywords: DNA double-strand breaks, ionizing radiation, homologous recombination repair, radiosensitization, cancer

INTRODUCTION

During the past few decades extensive efforts have been made to improve cancer therapy both by establishing more successful treatment approaches, as well as by developing effective means for early diagnosis. Despite advances in many fronts, radiation remains one of the most successful treatment modalities for solid cancers that is applied to over 50% of all cancers at one stage of their management (Delaney et al., 2005; Connell and Hellman, 2009; Ahmad et al., 2012; Siegel et al., 2012).

Radiation therapy aims to cure cancer by eradicating tumor cells. The tool of radiation therapy, ionizing radiation (IR), induces a plethora of DNA lesions, including oxidative base damages, single-strand breaks (SSBs), and double-strand breaks (DSBs), which affect the DNA integrity or alter its chemical nature (Ward, 1990). Among these lesions, DSBs have been reported to trigger the most detrimental effects on genome stability, and have been identified as the main contributors to IR induced cell killing through the formation of chromosomal aberrations (Povirk, 2006; Iliakis et al., 2007).

However, while treating tumors, radiation also always reaches normal tissue risking the development of side effects and the

generation of secondary malignancies. As a result, the central challenge of radiation therapy is to maximize tumor cell killing and minimize at the same time the normal tissue side effects. Modern conformal, intensity-modulated radiation therapy approximates this goal by optimizing radiation dose deposition between tumor and the surrounding normal tissue. Further improvements are possible using biological approaches that exploit differences in radiation response between normal and tumor cells and aim at protecting normal cells while maximizing the radiation response of tumor cells. Thus, radiosensitizing agents offer a benefit when radiosensitization occurs rather specifically in cancer cells.

The observation that components of the homologous recombination repair (HRR) pathway are aberrantly expressed in many tumors (Connell et al., 2006; Klein, 2008; Miyagawa, 2008; Tennstedt et al., 2012) and the correlation between tumor radioresistance, poor prognosis, and increased HRR activity make this repair pathway an attractive target with potential for differential responses. This view is further reinforced by the highly selective cell killing exerted by PARP-inhibitors in HRR deficient cells. However, similar conclusions have been also drawn for other DSB repair pathways (see below).

In the present review, we give a brief overview of the current state of knowledge in DSB repair and outline how this information may be harnessed to improve radiation therapy.

All used abbreviations are indicated in **Table A1** in Appendix.

THE DSB REPAIR ARSENAL

Double-strand breaks are generated randomly in the genomic DNA after exposure of cells to IR, or after treatment with radiomimetic drugs, DNA replication inhibitors, or topoisomerase poisons (Povirk, 2012). DSBs also arise randomly throughout the genome from reactive oxygen species generated as byproducts of the cellular metabolism, as well as from errors during DNA replication, the improper elimination of which may contribute to cancer progression (Vilenchik and Knudson, 2003).

Notably, DSBs are also generated in a programmed manner as part of important cellular processes, such as the maturation of lymphoid cells or gametogenesis during meiosis (Keeney et al., 1997; Panizza et al., 2011; Schatz and Swanson, 2011). In both cases specific enzymes are involved in the production of DSBs that are generated under stringent control, mostly at pre-defined locations in the genome.

In cancer therapy, the lethal effects of randomly induced DSBs are exploited to eliminate actively proliferating tumor cells. However, since induction of DSBs by IR appears comparable in normal and tumor cells, specificity of IR-toxicity to cancer cells is likely to rely either on their increased proliferative activity, or on defects in the processing of DSBs. Indeed, tumor cells frequently exhibit defects in various DNA repair pathways, which generate opportunities for enhanced treatment efficacy.

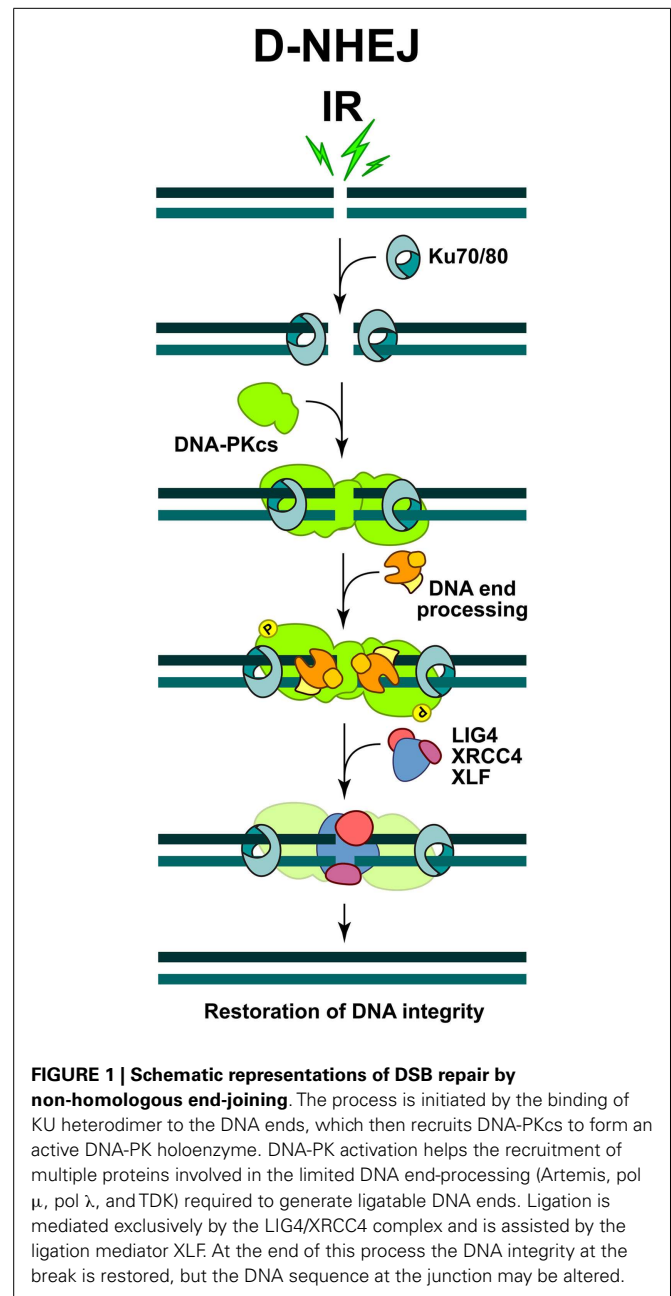
Two mechanistically and genetically distinct pathways contribute to the elimination of DSBs from the genome of higher eukaryotes: non-homologous end-joining (NHEJ), which can be subdivided in DNA-PKcs dependent NHEJ (D-NHEJ) and alternative/backup NHEJ (B-NHEJ) (see below), and HRR.

DSB REPAIR BY D-NHEJ

D-NHEJ catalyzes a simple rejoining reaction between two DNA ends irrespective of their origin (Lieber, 2010) and does not require homology at the ends or elsewhere; these facts render NHEJ operational throughout the cell-cycle. Indeed, D-NHEJ is active in all phases of the cell-cycle, where it removes DSBs from the genome with similar efficiency, but possesses only limited functionality for single-ended DSBs that arise during replication (Metzger and Iliakis, 1991; Rothkamm et al., 2003; Helleday et al., 2007).

The key steps of the classical form of NHEJ are summarized in **Figure 1**. The high affinity of KU heterodimer for free DNA ends ($1-10 \times 10^{-9}$ M, depending on the DNA end-structures), makes it the ultimate initiation factor of this repair pathway (Arosio et al., 2002). Indeed, it has been shown that the two subunits of the KU heterodimer, KU70 and KU80, which form an asymmetric toroid structure, are perfectly designed to bind and thread on free DNA ends (**Figure 1**). The binding of KU to DSBs blocks nucleolytic processing of DNA ends, which is required for the initiation of other DSB repair pathways (see below). However, despite its reported lyase activity (Roberts et al., 2010; Strande et al., 2012), the essential role of KU during NHEJ is to recruit the catalytic subunit of the DNA-PKcs, which dominates and drives the repair of DSBs in cells of higher eukaryotes. Hence, this form of repair has also been termed D-NHEJ (Mladenov and Iliakis, 2011).

The binding and dimerization of DNA-PKcs immobilizes the two DNA ends and thus facilitates the rejoining reaction (Meek et al., 2004). The interactions of DNA-PKcs with KU, as well as the



binding of DNA-PKcs to the DNA result in almost 10-fold increase in DNA-PKcs kinase activity. Accumulating evidence shows that a variety of proteins specifically involved in D-NHEJ, or generally in the DNA damage response (DDR), are phosphorylation targets of DNA-PKcs. However, interference with these phosphorylations is often without effect in DSB repair, and the only modification, which severely affects the end-joining efficiency, is elimination of DNA-PKcs auto-phosphorylation (Meek et al., 2004). Depending on the nature of DNA lesions, DNA-PKcs can be phosphorylated at multiple residues, which is a prerequisite for its dissociation from the damaged sites and the recruitment of other repair factors (**Figure 1**).

Since DSBs generated by IR bear damaged nucleotides at their ends, a limited end-processing by nucleolytic enzymes or DNA polymerases (pol μ and pol λ) is required to generate ligatable ends (Weterings and Chen, 2008) (**Figure 1**). As a result, sequence changes at the junctions generated by NHEJ are possible and therefore mutations likely. Furthermore, since D-NHEJ rejoins DNA ends indiscriminately, it can lead to translocations and other chromosomal rearrangements that are hallmarks of genomic instability. It is therefore quite surprising that despite such limitations, cells of higher eukaryotes extensively utilize D-NHEJ to remove DSBs from their genome.

The final step during D-NHEJ is mediated by a highly specialized ligation complex consisting of DNA Ligase 4 (LIG4) and the X-ray cross complementing 4 (XRCC4) protein (LIG4/XRCC4) (**Figure 1**). Assisted by the auxiliary factor XLF (Cernunos), LIG4/XRCC4 mediates ligation that results in fast and efficient restoration of DNA integrity, albeit often at the cost of sequence information loss.

DSB REPAIR BY B-NHEJ

During the past decade a second pathway for rejoining of broken DNA molecules on the basis of NHEJ was discovered and is presently intensively investigated. As with D-NHEJ this repair pathway also lacks means to restore sequence information at the DSB, and as we will discuss later, it also has a higher probability to join unrelated DNA ends.

Initially, analyses of DSB repair using pulse-field gel electrophoresis (PFGE) in cells deficient in components of D-NHEJ, revealed a robust repair activity that was unrelated to HRR (see below) and reflected a different form of DNA end-joining instead (DiBiase et al., 2000; Singh et al., 2009). This alternative form of DSB repair efficiently substituted for D-NHEJ, but appeared to have backup functions, coming to the fore mainly after failure of D-NHEJ; therefore the term B-NHEJ was proposed for this repair pathway (Iliakis, 2009; Mladenov and Iliakis, 2011). Failures of D-NHEJ, which allow function of B-NHEJ, can also occur locally at a specific DSB, even in repair proficient cells, or globally in cells with mutations in genes encoding for D-NHEJ factors, or after treatment with DNA-PKcs inhibitors. Subsequent work documented the function of such alternative pathways of NHEJ in several processes involving the formation of DSBs, such as V(D)J recombination and class switch recombination (Corneo et al., 2007), and were also implicated in cancer formation (Simsek et al., 2011).

Several enzymatic activities have been implicated in this repair pathway, which is now considered to be distinct from D-NHEJ and which may even be further subdivided into sub-pathways (Wang et al., 2005; Rosidi et al., 2008; Zha et al., 2009; Lee-Theilen et al., 2011; Mladenov and Iliakis, 2011).

A major protein implicated in B-NHEJ is poly (ADP-ribose) polymerase 1 (PARP-1), which plays a main role in the repair of SSBs (see below) and which may effectively compete with KU heterodimer for DNA end-binding (Wang et al., 2006). It has been reported that PARP-1 facilitates the repair of DSBs by B-NHEJ, while another member of the PARP family, PARP-2 strongly suppresses it (Robert et al., 2009) (**Figure 2**). It has also been reported that B-NHEJ benefits from microhomology at the break

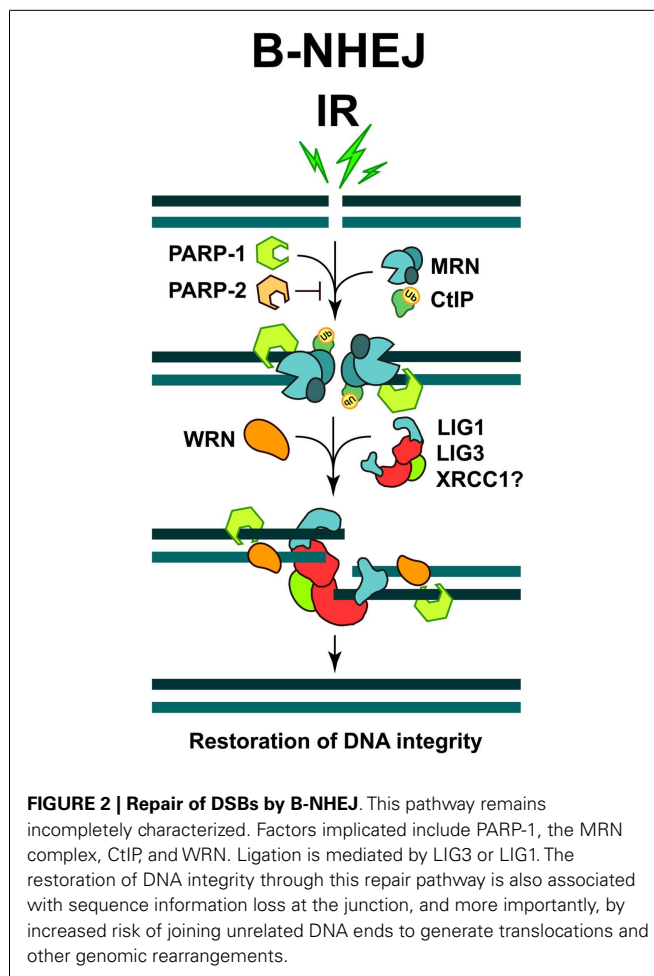


FIGURE 2 | Repair of DSBs by B-NHEJ. This pathway remains incompletely characterized. Factors implicated include PARP-1, the MRN complex, CtIP, and WRN. Ligation is mediated by LIG3 or LIG1. The restoration of DNA integrity through this repair pathway is also associated with sequence information loss at the junction, and more importantly, by increased risk of joining unrelated DNA ends to generate translocations and other genomic rearrangements.

sites, which may be best found if the DNA ends become resected. Indeed, MRE11 and C-terminal binding protein 1 interacting protein (CtIP), both involved in DNA end-resection during HRR (see below), were found to facilitate B-NHEJ (Zha et al., 2009; Lee-Theilen et al., 2011) (**Figure 2**). However, it is important to point out that B-NHEJ does not exhibit a strict requirement for microhomology, therefore, this repair pathway should not be considered as a microhomology dependent (Mansour et al., 2010).

Backup NHEJ, like D-NHEJ, is active in all phases of the cell-cycle, but its activity is significantly potentiated during S and G₂, probably due to the increased activity of DNA end-resection enzymes in these cell-cycle phases. Therefore, it is likely that B-NHEJ also operates as a backup to HRR in the G₂ and S-phases of the cell-cycle (see below). Notably, B-NHEJ is severely compromised when D-NHEJ deficient cells enter a plateau phase of growth or are deprived of serum (Singh et al., 2011, 2012). An intriguing and still unexplained observation is that this effect is not observed in DNA-PKcs deficient cells (Singh et al., 2011).

A ligation activity finalizing B-NHEJ is DNA Ligase 3 (LIG3), a versatile ligase, which in complex with XRCC1 also participates in the repair of SSBs and DNA base damages (Wang et al., 2005; Della-Maria et al., 2011) (**Figure 2**). Assisted by its unique structural

properties, LIG3 ensures the ligation of both DNA strands during DSB repair (Ellenberger and Tomkinson, 2008). However, despite reports to the opposite (Audebert et al., 2004), the role of XRCC1 in LIG3 function during B-NHEJ remains unclear (Della-Maria et al., 2011; Boboila et al., 2012). Recent evidence also implicates DNA Ligase 1 (LIG1) in B-NHEJ (Simsek et al., 2011; Paul et al., 2013). Thus, it appears that while LIG4 is specifically dedicated to D-NHEJ, LIG1, and LIG3 can efficiently support B-NHEJ.

Furthermore, interesting regulatory proteins were implicated in B-NHEJ. The Werner syndrome helicase (WRN), together with LIG3, was found upregulated in chronic myelogenous leukemia (CML), where several D-NHEJ activities are suppressed. Under these conditions WRN and LIG3 form a stable complex, which is recruited to DSBs, thus activating the ligation process (Sallmyr et al., 2008) (Figure 2). Moreover, a form of error-prone repair, with characteristics of single-strand annealing (SSA), was described in many myeloproliferative disorders, which are characterized by the formation of oncogenic fusion tyrosine kinases, including BCR/ABL, TEL/ABL, TEL/JAK2, and TEL/PDGFR (Cramer et al., 2008). This form of repair contributes to the accumulation of intrachromosomal deletions and translocations, a hallmark of the B-NHEJ repair pathway; therefore it has been suggested that it might be a sub-pathway of alternative DSB repair mechanisms (Mladenov and Iliakis, 2011).

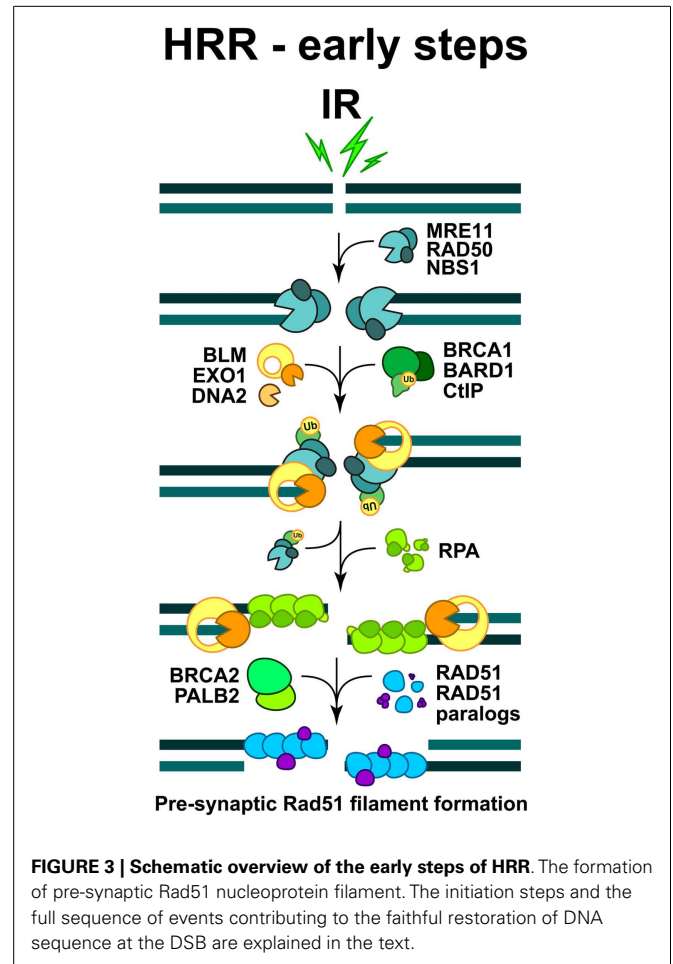
Another factor implicated in B-NHEJ is histone H1, which enhances the rejoining activity of LIG3 presumably by facilitating the synapsing of DNA molecules (Rosidi et al., 2008).

Backup NHEJ is much slower than D-NHEJ and is highly error-prone causing translocations and other genomic rearrangements with high probability. Moreover, a high number of B-NHEJ associated genetic rearrangements have been observed in chromosomal translocations associated with both spontaneous and therapy-related cancers (Greaves and Wiemels, 2003). Thus, B-NHEJ-derived mutations appear to be associated with cancer development and may support tumor progression – particularly when classical NHEJ or HRR are compromised (Bennardo et al., 2008). It is therefore conceivable that activation of B-NHEJ fuels the evolution of cancer, and that it might also serve as target in specialized cancer therapies.

DSB REPAIR BY HRR

The second approach to DSB repair, HRR, requires intact homologous DNA sequences to remove DSBs and to faithfully restore the DNA sequence in their vicinity (San Filippo et al., 2008). One form of HRR (described in Figures 3 and 4) utilizes the sister chromatid as a donor for homologous sequence and is therefore active only in S and G2 phases of the cell-cycle (Onn et al., 2008; San Filippo et al., 2008). In principle, HRR could also be carried out in diploid cells during the G1 phase of the cell-cycle using the homologous chromosome as template. However, the distinct compartmentalization of the nuclear domains of homologous chromosomes make required interactions unfavorable; in fact, it is thought that HRR is actively suppressed in G1 cells in an effort to prevent loss of heterozygosity (LOH) (Paques and Haber, 1999; Aylon and Kupiec, 2004).

DNA end-resection is a necessary requirement for the initiation of HRR, as a long single-stranded 3'-DNA overhang has to be



formed in order to start homology search (West, 2003). Activities implicated in diverse aspects of end-resection include the MRE11-RAD50-NBS1 (MRN complex), the CtIP, as well as Exonuclease 1 (EXO1), DNA2, and the Bloom's syndrome helicase (BLM) (see below) (Figure 3). In order to execute their function during HRR initiation, the MRN complex is quickly recruited to DSB, where it cooperates with CtIP to promote end-resection (Sartori et al., 2007; Kousholt et al., 2012; Leslie, 2013). It is thought that end-resection defines the point of no-return in the decision to process a DSB by HRR. Therefore, the formation of single-stranded DNA regions is frequently used as a surrogate for ongoing HRR. However, as noted above, it is also possible that HRR abrogation after resection will shunt DSBs to B-NHEJ (we will return to this point below).

The combined action of DNA end-resection enzymes results in the formation of single-stranded DNA, decorated by the replication protein A (RPA) (Figure 3). RPA is a heterotrimeric complex, comprising of RPA70, RPA32, and RPA14, which exhibits high affinity for binding to ssDNA regions, such as those formed during DNA replication and occasionally during repair. In the subsequent steps of HRR, RPA is replaced by RAD51 recombinase, which forms a right-handed pre-synaptic RAD51 nucleoprotein filament on the DNA (Figure 3). The replacement of RPA by RAD51

when HRR is disadvantageous (Karpenshif and Bernstein, 2012) (**Figure 4**).

In the subsequent steps of HRR, the RAD51 nucleoprotein filament invades the intact double-stranded DNA molecule to search for homologous sequences and form a structure termed displacement loop (D-loop). When homology is found (synapsis) DNA synthesis will start elongating the 3'-end of the invading strand (**Figure 4**). For elongation to commence, RAD51 in the synaptic complex has to be removed from the very 3' tip of the invading strand to reveal the 3'-OH group for priming; this reaction is facilitated by RAD54 and its interacting partner RAD54B (Li and Heyer, 2009). HRR can take several different routes from this point. Frequently, elongation of the invading 3'-end can continue over a limited distance, followed by displacement of the newly synthesized stretch and re-ligation with the original DNA end resulting in the repair of the DSB (synthesis-dependent strand annealing; SDSA) (**Figure 4**). This is the most frequent event during DSB repair in cells of higher eukaryotes and is equivalent to gene conversion. Alternatively, second end-capture can occur, leading to the formation of a double Holliday junction (dHJ) (DSB repair; DSBR) (**Figure 4**). Depending on the resolution of the dHJ by specialized resolving enzymes, GEN1 and possibly MUS81/EME1, this branch of HRR will result in either crossover or non-crossover (gene conversion) outcomes (Constantinou et al., 2002; Wu and Hickson, 2003; Ip et al., 2008) (**Figure 4**).

First reported in yeast and later in higher eukaryotes, recombination events between areas of homology present in the same DNA molecule could be observed. This process is known as SSA (Ivanov et al., 1996). When this pathway is used to repair a DSB it leads to loss of the DNA segment between the regions of homology and therefore it is considered as mutagenic. The role of SSA in the repair of randomly induced DSBs, such as those generated by IR, remains uncharacterized and is likely to be small. However, there is evidence for a correlation between increased formation of chromosomal aberrations and SSA in cells of myeloproliferative disorders expressing oncogenic fusion tyrosine kinases (Cramer et al., 2008).

Finally, in yeast another mode of HRR – termed break induced replication (BIR) – has been described, that steps into action when one sided DSBs are formed. It is characterized by the initiation of replication through the formation of a replication fork that replicates the entire chromosome past the DSB (Fan et al., 2004). As a result of this peculiarity, BIR can cause extensive LOH (Llorente et al., 2008). However in mammalian cells the action of BIR remains to be demonstrated.

REGULATION OF HRR – WAYS TO MODULATE THE REPAIR PATHWAY CHOICE

Some competition between the DSB repair processes described above is often considered likely (Sonoda et al., 2006; Shrivastav et al., 2008). Although the basis of DSB repair pathway choice in cells of higher eukaryotes remains largely elusive, it is clear that one important determinant is the position of the cell in the cell-cycle – particularly for HRR (see above). In addition to its requirement for a sister chromatid, HRR is also regulated throughout the cell-cycle in at least two ways: (1) Cell-cycle dependent regulation of the expression levels of proteins involved in HRR and (2) through

cyclin dependent kinase (CDK)-dependent phosphorylation of some of its components.

Expression levels of RAD51, Breast cancer susceptibility gene 1 (BRCA1), BRCA2, BLM, and CtIP are all regulated throughout the cell-cycle (Flygare et al., 1996; Yamamoto et al., 1996; Wang et al., 1997; Dutertre et al., 2000; Yu and Chen, 2004; Shrivastav et al., 2008). The respective transcripts and/or proteins are present at low levels in G1 and are hardly detectable or completely absent in non-dividing, G0 cells. Their expression begins with the start of DNA replication and increases further with the progression of cells through S.

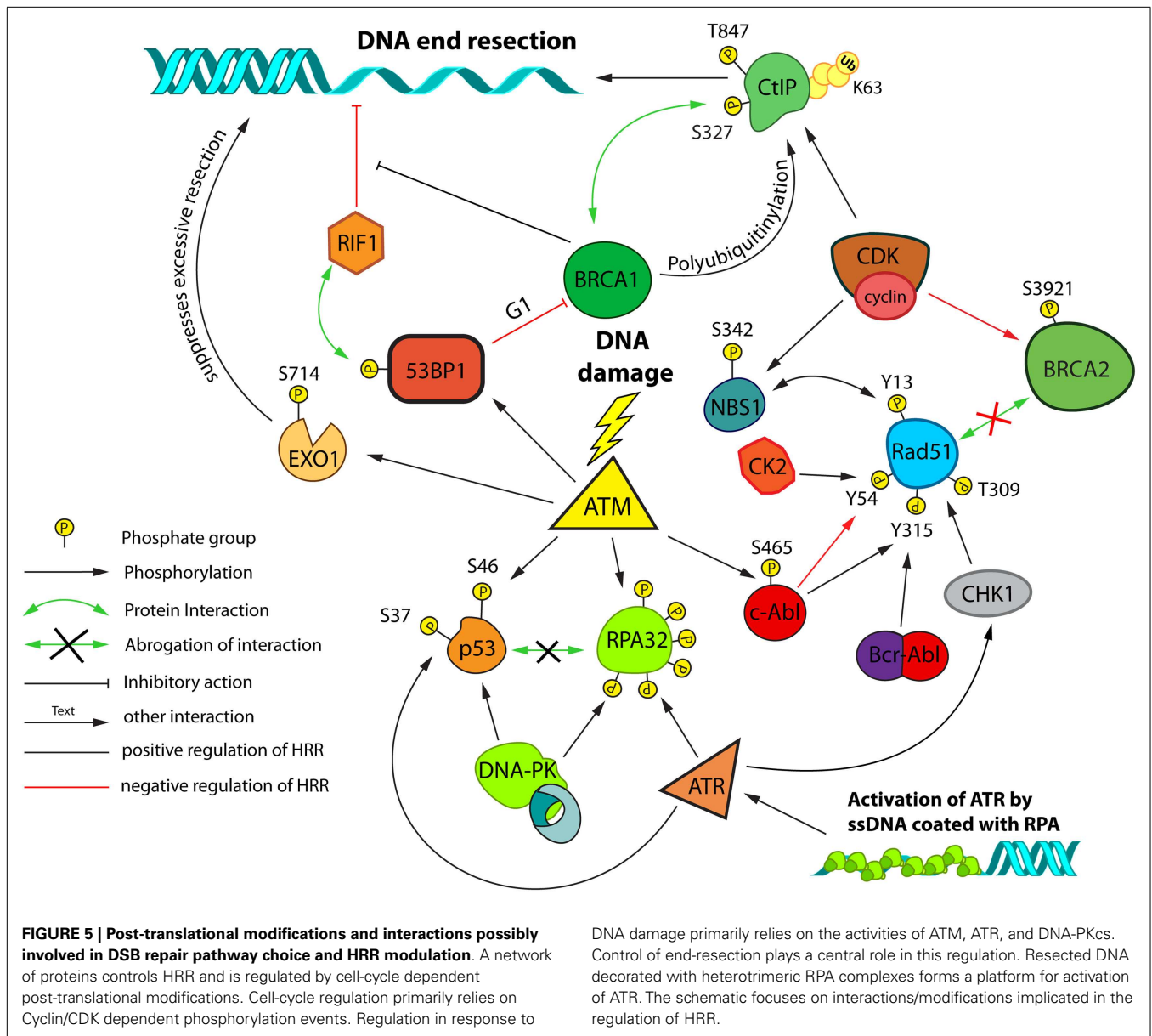
One example of CDK-mediated regulation of HRR is the phosphorylation of Ser-3291 of BRCA2, which counteracts the interaction with RAD51 and thereby negatively regulates HRR activity (Esashi et al., 2005) (**Figure 5**). Another regulatory CDK-mediated phosphorylation occurs at Ser-432 of NBS1 (**Figure 5**), which is believed to act as a primary sensor of DSBs. Phosphorylation of Ser-432 on NBS1 stimulates the conversion of DSBs into substrates for HRR in a MRN-dependent manner (Falck et al., 2012).

Although MRE11, another member of the MRN complex, can act as a nuclease and is involved in facilitating resection of ends at sites of DSBs, the formation of extensive ssDNA regions seems to be carried out by other nucleases like EXO1 and possibly DNA2 (Bolderson et al., 2010; Eid et al., 2010; Grabarz et al., 2012; Tomimatsu et al., 2012) (**Figure 3**) and is facilitated by CtIP and RECQ family members like BLM (Gravel et al., 2008; Mimitou and Symington, 2008; Huertas, 2010).

CtIP not only interacts with the MRN complex, but also with BRCA1 and this interaction is promoted by CDK dependent phosphorylation of CtIP on Ser-327 in S/G2, providing yet another example for cell-cycle regulation of HRR (Yu and Chen, 2004) (**Figure 5**). CtIP is also polyubiquitinated in a BRCA1 dependent manner, without being targeted for proteasomal degradation (Yu et al., 2006). However, these are not the only cell-cycle dependent, regulatory modifications CtIP is subjected to. Phosphorylation of CtIP on Thr-847 by CDKs is required for efficient end-resection, and non-phosphorylatable mutants of this site are defective in end-resection, while phospho-mimicking mutants show resection even in the absence of CDK activity (Huertas and Jackson, 2009).

Moreover, it has been previously reported that CtIP is phosphorylated at Ser-664/745 by the Ataxia telangiectasia mutated (ATM) protein kinase, which plays an important role during DSB repair by homologous recombination (Li et al., 2000). Recently, this observation was extended using Ser-664/745-Ala (phosphomutant) and Ser-664/745-Glu (phospho-mimicking) forms of CtIP fused to GFP; it was thus found that ATM is directly engaged in DNA end-resection by activating CtIP via phosphorylation at Ser-664/745 (Shibata et al., 2011).

Although various models emerge as to how HRR is regulated throughout the cell-cycle, the question of choice for a particular repair pathway for each DSB remains poorly understood. There is however, evidence for crosstalk between HRR and NHEJ and it has been reported that DNA-PKcs, ATM, and ATM and Rad3 related (ATR) (in a CHK1/2 independent manner) collaborate to dissociate a p53/RPA-complex by phosphorylating both of its components (Serrano et al., 2012) (**Figure 5**). Notably, abrogation of these phosphorylations impairs HRR.



A large number of proteins are subjected to post-translational modifications (PTMs) that are elicited by DNA damage or replication stress. We will focus on a small selection of PTMs of proteins that either play a central role in HRR, or exert regulatory functions at key HRR steps.

As mentioned above, CtIP is critical in the regulation of end-resection and is itself post-translationally modified in several ways. Also EXO1, one of the major nucleases implicated in DNA end-resection, has been shown to be phosphorylated at multiple sites. Phosphorylation of EXO1 at Ser-714 by ATM, for example, is required for the recruitment of RAD51 to sites of DSBs (Matsuoka et al., 2007; Bolderson et al., 2010) (Figure 5). Interestingly, this phosphorylation seems to attenuate the nuclease activity of EXO1, suggesting that it might protect from over-resection.

Another level of regulation of end-resection involves p53 binding protein 1 (53BP1) and BRCA1. Interestingly loss of 53BP1 on top of BRCA1 deficiency restores a resistant phenotype in these radiosensitive cells (“synthetic viability”) (Bouwman et al., 2010; Bunting et al., 2010). This has led to a model in which 53BP1 inhibits initiation of DNA end-resection and thus favors the repair by NHEJ. This inhibition is regulated in a negative way by BRCA1 and thus, loss of BRCA1 results in persistent inhibition of end-resection, which can be abolished by removal of 53BP1 (Aly and Ganesan, 2011). A number of very recent publications have now implicated the protein RIF1 as the major downstream effector of the end-protecting function of 53BP1 (Chapman et al., 2013; Di Virgilio et al., 2013; Escribano-Diaz et al., 2013; Zimmermann et al., 2013). One of these studies also found a cell-cycle dependent inhibitory function of 53BP1 on BRCA1 accumulation at DSB in

G1 (Escribano-Diaz et al., 2013), which could account for HRR suppression in G1.

The ssDNA generated during resection is immediately covered with RPA. The middle subunit of RPA (RPA32/RPA2) is a target for multiple PTMs, which may have important roles in the subsequent steps of HRR (Figure 5). It has been shown that hyperphosphorylation of RPA32 is required for RAD51 recruitment in response to replication stress induced by hydroxyurea (HU); however such dependencies were not identified after IR or endonuclease induced DSBs (Shi et al., 2010).

Phosphorylations are not the only form of PTMs induced by DNA damage. Besides the well-known waves of ubiquitylation mediated by the E3-ubiquitin-ligases RNF8 and RNF168, modification with small ubiquitin like modifiers (SUMO) also occurs in response to DNA breaks. RPA70 is sumoylated on at least two sites *in vivo*, but this modification is suppressed by a constitutive interaction of the SUMO-specific protease SENP6 (Dou et al., 2010). In response to replication associated DSBs this interaction is abrogated, which allows sumoylation of RPA70 that promotes HRR (Dou et al., 2010). It has also been reported, that the ubiquitin-ligase activity of BRCA1 depends on its sumoylation (Morris et al., 2009). For the BLM helicase multiple sites of sumoylation have been documented as well and shown to influence its nuclear localization and possibly to act as switches shifting BLM-activity between pro- and anti-recombinogenic functions (Eladad et al., 2005; Ouyang et al., 2009).

Upon formation of a RAD51 coated ssDNA the stability of this nucleoprotein filament is critical for the execution of HRR. In mammalian cells helicases like BLM or RECQ5 have been shown to dismantle RAD51 nucleoprotein filaments (Bugreev et al., 2007; Hu et al., 2007) (Figure 4). Very recently it was shown that the helicase domain containing protein PARI suppresses unscheduled and inappropriate HRR at replication forks in human and chicken cells (Moldovan et al., 2012) (Figure 4). This function is mediated by its interaction with PCNA and might be analogous to the function of Srs2 in yeast.

RAD51 itself can also be post-translationally modified in several ways. Following replication stress, RAD51 is phosphorylated in a CHK1 dependent manner on Thr-309 (Sorensen et al., 2005), and also by the c-ABL tyrosine kinase on Tyr-315, which stabilize association of RAD51 with chromatin (Shimizu et al., 2009) (Figure 5). Two additional phosphorylations of RAD51 that occur in a cell-cycle and DNA damage dependent manner have been recently reported: RAD51 is phosphorylated on Ser-14 by PLK1 which licenses phosphorylation of Thr-13 by CK2 (Yata et al., 2012) (Figure 5). Phosphorylation of Thr-13 leads to direct binding of RAD51 to NBS1, which facilitates its recruitment to sites of DNA damage (Yata et al., 2012).

It is evident from the outline above that the cell-cycle regulation of HRR has different levels and is likely to be complex. Identification of these modifications and characterization of their functional significance is likely to have important implications to our understanding of repair pathway choice.

REGULATION OF HRR BY TYROSINE KINASE SIGNALING

Besides the above described intrinsic cell-cycle dependent regulatory processes, there is evidence for additional regulatory levels

modulating repair of DSBs. An important example is the BCR-ABL fusion tyrosine kinase, a hallmark of CML (Skorski, 2012). The non-mutated c-ABL protein is activated by DNA-PKcs and ATM in response to genotoxic stress (Kharbanda et al., 1995; Baskaran et al., 1997). There are reports suggesting that the constitutively active fusion protein contributes to drug resistance, stimulates HRR, and promotes ectopic recombination events, through either up-regulation of RAD51 levels and/or direct phosphorylation of RAD51 on Tyr-315 (Slupianek et al., 2001, 2002, 2011; Skorski, 2002; Nowicki et al., 2004) (Figure 5).

Up-regulation of mutagenic SSA (see above) by BCR-ABL has also been reported, and BCR-ABL stimulated expression of CtIP and increased DNA end-resection have been suggested as a mechanism (Cramer et al., 2008; Fernandes et al., 2009; Salles et al., 2011). Notably, HRR is negatively regulated by the normal form of c-ABL in irradiated cells by a phosphorylation of RAD51 on Tyr-54 (Yuan et al., 1998) (Figure 5). Another study shows that Rad51 is phosphorylated on both Tyr-315 and Tyr-54 by c-ABL and that these phosphorylations are sequential, with the phosphorylation of Tyr-315 stimulating phosphorylation of Tyr-54 (Popova et al., 2009). Thus, c-ABL may fine-tune recombination repair by balancing activating and inhibitory RAD51 phosphorylations, whereas the constitutively active BCR-ABL protein may cause its hyperactivation with mutagenic consequences. Interestingly, it has been reported, that in ABL-positive CML cells, there is also a shift toward more mutagenic NHEJ repair processes. Sallmyr et al. found LIG4 and Artemis to be down-regulated in these cells, while LIG3 was upregulated. Since in these cells error-prone NHEJ was observed, the authors concluded that the activity of B-NHEJ was enhanced (Brady et al., 2003; Sallmyr et al., 2008).

While the regulatory influence of the ABL kinase on DSB repair has been mainly linked to DDR responses mediated by DNA-PKcs and ATM, there are also examples of modulation of DSB repair through receptor tyrosine kinases activated by their natural extracellular ligands. Over the last 15 years, evidence has accumulated that overexpression and/or mutation of the EGF receptor (EGFR) is associated with resistance to chemo- and radiotherapy (Chen and Nirodi, 2007; Dittmann et al., 2010; Toulany and Rodemann, 2010).

While EGFR is known to exert a cytoprotective action through the activation of cell survival and proliferation pathways, a large body of evidence also implicates EGFR signaling in DSB repair. In glioblastomas, brain tumors characterized by resistance to chemo- and radiotherapy, the EGFR gene is amplified in 50% of the cases and a truncated variant – EGFRvIII – is frequently over expressed. Mukherjee et al. (2009) showed that the expression of this constitutively active EGFR variant confers radioresistance through activation of PI3K-AKT signaling that enhances DSB repair.

In another study the authors showed by scoring γ -H2AX foci that activation of EGFR signaling by its natural ligand EGF enhanced the overall capacity of cells to repair DSBs (Kriegs et al., 2010). Conversely inhibition of EGFR signaling by Erlotinib or Cetuximab reduced DSB repair. The authors found that EGFR activation increased NHEJ, possibly through enhanced MAPK signaling. Another study from the same group showed a positive effect of EGFR activation on HRR (Myllynen et al., 2011). This observation is in agreement with work reported by Golding et al.

(2009) who demonstrated up-regulation of both NHEJ and HRR by EGFRvIII with assays utilizing appropriate, chromosomally integrated reporter constructs.

Several reports also indicate an interference of Imatinib, Erlotinib, and other tyrosine kinase inhibitors (Chinnaiyan et al., 2005; Li et al., 2008; Choudhury et al., 2009; Zhao et al., 2011; Medova et al., 2012; Qiao et al., 2013) with HRR. These results confirm the potential impact of these signaling proteins on DSB repair and highlight their importance as targets for cancer therapy.

DSB REPAIR DEFICIENCY AND CARCINOGENESIS

The observation that in many cancer cells the DDR is impaired emphasizes the connection between DSB repair defects and carcinogenesis and generates opportunities for cancer treatment. Indeed, various forms of cancer present with mutations or show alterations in the expression of genes encoding proteins involved in DNA metabolism (Connell et al., 2006; Klein, 2008; Miyagawa, 2008; Tennstedt et al., 2012). Furthermore, among cancers, the activities of certain repair proteins fluctuate, from complete suppression to strong up-regulation, which necessarily modulates their response to DNA damaging agents. These observations suggest that optimization of cancer therapy will benefit from in-depth analysis of the status of the DDR apparatus in each individual tumor and an adaptation of the treatment strategy to this information.

More specifically, a strong correlation between increased genomic instability, DNA repair defects, and cancer predisposition has been documented in cells isolated from individuals carrying germ line mutations in *BRCA1* or *BRCA2* genes (O'Donovan and Livingston, 2010; Roy et al., 2012). The *BRCA1* and *BRCA2* mutations increase the susceptibility to breast or ovarian cancer, and it has been estimated that the probability of developing these forms of cancer is between 30 and 80% in individuals carrying hetero- or homozygous mutations in these genes (Brody and Biesecker, 1998).

The breast cancer associated gene 1 (*BRCA1*) was identified in 1990 (Walsh and King, 2007) and was cloned a few years later (Miki et al., 1994). Biochemical and structural analyses of human *BRCA1* protein revealed an N-terminal RING domain possessing E3-ubiquitin-ligase activity and a C-terminal BRCT domain, interacting with proteins phosphorylated on serine within the S-X-X-F motif. *BRCA1* consists of 1863 amino acids and plays an important role in maintaining genome integrity through its functions in DNA repair (Rajagopalan et al., 2010; Roy et al., 2012). To become a functional E3-ubiquitin-ligase, the RING domain of *BRCA1* acts in concert with *BRCA1*-associated RING domain 1 protein (*BARD1*), and this complex is involved in the ubiquitylation of CtIP (see above). Despite controversial studies, assigning critical functions for *BRCA1* in NHEJ and nucleotide excision repair (NER), mounting evidence implicates *BRCA1* as a key regulator of HRR (Jasin, 2002; Roy et al., 2012).

The direct recruitment of *BRCA1* to DSBs is mediated by its interaction with Abraxas-RAP80 macro-complex, which binds to ubiquitylated proteins, particularly histones (Wang et al., 2007). Once recruited to DSBs, the main regulatory function of *BRCA1* is to conscript and activate the end-resection promoting factor CtIP (Yun and Hiom, 2009). However, *BRCA1* is not only implicated in

HRR by its role in end-resection, but also due to its indirect interaction with *BRCA2*, which is mediated by the *PALB2* protein (Zhang et al., 2009). Indeed, heterozygous mutations of the latter protein are also associated with predisposition to breast and pancreatic cancers (Popova et al., 2009). This interaction directly connects *BRCA1* to HRR and indeed, deficiency of *BRCA1* is accompanied by abrogated formation of DSB-induced RAD51 foci and severely reduced levels of HRR.

A variety of studies with cultured cell lines has revealed that *BRCA1* deficiency correlates with increased radiosensitivity to killing, which derives from the associated HRR defects (Speit and Trenz, 2004). These observations are further supported by results showing decreased survival of irradiated *BRCA1*^{-/-} mouse embryonic fibroblasts exposed to IR and emphasize the central role of HRR in the maintenance of genomic integrity. Notably, more recent results suggest that inactivation of *BRCA1* ubiquitin-ligase activity up-regulates protein complexes involved in DNA end-resection, causing elevated but aberrant HRR that undermines genomic instability (Drost et al., 2011; Dever et al., 2012). Along these lines, C61G mutation in the *BRCA1* gene is associated with complete loss of *BRCA1* E3-ubiquitin-ligase function, and disruption of the *BRCA1/BARD1* complex, which results in increased formation of RAD51 foci, and abnormal rate of HRR (Drost et al., 2011). Such results explain the observation that many sporadic *BRCA1* deficient tumors develop radioresistance – possibly through enhanced aberrant HRR that triggers the function of the highly mutagenic B-NHEJ repair pathway (see above).

Although the frequency of developing breast and ovarian cancer in individuals harboring mutations in the *BRCA2* gene is lower than in individuals harboring *BRCA1* mutations, *BRCA2*-deficient patients have a 20-fold increased risk of developing prostate cancer and about 10-fold increased risk to pancreatic and other form of tumors like medulloblastomas and gliomas (Roy et al., 2012). This suggests that despite common functions in DNA repair, *BRCA1* and *BRCA2* also have specific functions, which explains the distinct behavior described above.

Breast cancer susceptibility gene 2 (*BRCA2*) is a 3418 amino acids protein, harboring a specific domain consisting of about 30 degenerative BRC repeats that are responsible for the controlled formation of RAD51 and DMC1 nucleoprotein filaments during HRR and meiosis, respectively (Thorslund and West, 2007; Roy et al., 2012). The BRC repeats exhibit subtle sequence variations allowing differential binding of RAD51 and mediating the controlled displacement of RPA from ssDNA regions and the nucleation of RAD51 monomers, which culminates with the formation of a nucleoprotein filament (West, 2003) (Figure 2). The importance of BRC repeats in *BRCA2* function has been demonstrated in patients with point mutations in this domain, which develop breast and ovarian cancer with much higher frequency than patients with mutations in other regions of the gene.

Available biochemical data suggest that the main function of *BRCA2* in DSB repair is to keep RAD51 in monomeric state and to deliver RAD51 monomers to the resected DNA ends. As mentioned above, the potential of *BRCA2* to bind RAD51 is tightly regulated by CDK1 phosphorylation at Ser-3291, in the C-terminal TR2 motif (Esashi et al., 2005, 2007), whose abrogation results

in intolerable HRR and increased genomic instability, but which might be exploited to enhance the killing potential of IR.

However, it is relevant to point out that all these well described functions in DSB repair, are not sufficient to explain initiation and progression of cancer in individuals with mutation in *BRCA* genes. Certainly, it might be speculated that *BRCA1* and *BRCA2* are important for tumor suppression by virtue of their function in HRR. Alternatively, it might be speculated that both proteins suppress error-prone DSB repair pathways. A strong candidate for such effects is B-NHEJ, whose involvement in DSB repair may increase when HRR is abrogated. Moreover, reports that B-NHEJ benefits from the presence of microhomology and the fact that end-resection activities like CtIP and MRN complex facilitate B-NHEJ (Xie et al., 2009; Lee-Theilen et al., 2011), support the idea that B-NHEJ may exploit failures in HRR (see above). This is especially true when limited resection of DNA ends is already accomplished, as this will prevent the recruitment of key factors of classical NHEJ. Another possibility, explaining the tumor susceptibility of *BRCA*-deficient patients is that the common genetic alterations (e.g., *BRCA1* or *BRCA2* mutations) are regularly associated with loss of wild-type p53 (Ramus et al., 1999), ATM (Tommiska et al., 2008), or *CHK2* (Cao et al., 2006). These additional alterations may permit cells to bypass checkpoint controls and evade apoptosis, thereby commencing tumorigenesis.

Multiple studies link mutations in other DSB repair genes with genomic instability and cancer predisposition. Prominent among them, AT, AT like disorder (ATLD), and the NBS display mutations in genes involved in the repair of DSBs by HRR. Thus, in AT patients, ATM activity is abrogated and these individuals primarily develop lymphoid malignancies. The ATLD and NBS syndromes are associated with mutations in *MRE11* and *NBS1* genes, which together with *RAD50* form the MRN complex, involved in initiation of DNA end-resection for HRR (Stracker and Petrini, 2011).

HRR DEFICIENCY AS AN OPPORTUNITY IN CANCER THERAPY: THE CONCEPT OF SYNTHETIC LETHALITY

DNA damaging agents used in cancer treatment induce a spectrum of lesions in the DNA. These lesions are recognized by a variety of cellular lesion-specific DNA repair pathways that operate to remove them from the affected DNA molecules. It is commonly accepted that DSBs are substrates for NHEJ (Lieber, 2010) and HRR (San Filippo et al., 2008). The function of these DNA repair pathways rescues malignant cells from death following exposure to radiation or chemotherapeutic drugs and compromise thus cancer treatment. It follows that inhibition of these repair processes, preferentially in malignant cells, should enhance the efficacy of cancer therapies based on killing cells by the induction of DSBs. Indeed, evidence accumulates that success in cancer treatment often results from DNA repair deficiencies in the cancer cells. Also, it has been observed that when DSB repair deficient tumors develop resistance to radiation or to DSB inducing drugs, they do so by improving their DSB repair potential (Zwet et al., 2002).

Our present understanding of DSB induction and repair allows us to postulate that combination of cytotoxic agents acting by inducing DSBs with inhibitors of DSB repair will enhance tumor cell killing – if this inhibition, or alternatively the induction of

DSBs, could be somehow preferentially targeted to tumor cells. Similar arguments can be developed for other forms of DNA damage and other pathways of DNA repair.

A number of inhibitors of DNA repair have been evaluated, or are undergoing clinical trials, as potential anti-cancer chemicals. Inhibitors of PARP-1 are of particular interest in treating hereditary breast cancers occurring in patients who are carriers of *BRCA1* or *BRCA2* mutations (Bryant et al., 2005; Farmer et al., 2005). As mentioned above, *BRCA2* has been established as an integral component of the HRR machinery, regulating the assembly of *RAD51* filaments and facilitating strand exchange (Thorslund and West, 2007; Carreira and Kowalczykowski, 2009). Also HRR is impaired in *BRCA1* deficient cells.

Poly (ADP-ribose) polymerase 1 is known to be involved in SSB repair, BER, and NER in association with *XRCC1*, *LIG3*, *PNK*, *PCNA*, and *FEN1* (Frouin et al., 2003; Okano et al., 2003). PARP-1 is also involved in DSB repair (Küpper et al., 1995; Tatsumi-Miyajima et al., 1999; Rudat et al., 2001), as well as in the alternative/backup pathways of NHEJ (Wang et al., 2006; Iliakis, 2009). The combination of PARP-inhibitors with *BRCA* deficiency provides a sound paradigm for the power of synthetic lethality as a strategy for improving cancer treatment. Synthetic lethality emerges when the combination of non-lethal mutations in two or more genes operating in different metabolic pathways, or the chemical inhibition of their products, causes cell death.

As expected from the basic premise of synthetic lethality, PARP-1 is also effective in tumors with HRR defects deriving from genes other than *BRCA* – sometimes referred to as “BRCAness” (de Gonzalez et al., 2011). Thus, deficiency in *RAD51*, *RAD54*, *DSS1*, *RPA1*, *NBS1*, *ATR*, *ATM*, *CHK1*, *CHK2*, *FANCD2*, or *FANCC* genes was found to be associated with synthetic lethality to PARP inhibition (McCabe et al., 2006). These results confirm that the critical role of *BRCA1* and *BRCA2* in HRR is the underlying reason for the hyper-sensitivity to PARP-inhibitors of *BRCA*-deficient tumors. Collectively, these results indicate that the approach of synthetic lethality with PARP-1 inhibitors may prove useful for the treatment of a wide range of tumors bearing HRR deficiencies, or displaying properties of “BRCAness.”

An interesting synthetic lethal interaction has been established between *RAD52* and *BRCA2*. Loss of *RAD52* function is synthetically lethal with *BRCA2* deficiency in human cancer cell lines (Feng et al., 2011; Lok et al., 2012). This suggests that *BRCA2* and *RAD52* provide alternative pathways for *RAD51* mediated HRR in mammalian cells. *RAD52* also exerts other synthetic lethal phenotypes: in chicken DT40 cells its inactivation is lethal when it occurs together with inactivation of *XRCC3* (Fujimori et al., 2001). On the other hand, the viability of *BRCA2*-deficient DT40 cells is not compromised by deletion of *RAD52*; rather, an epistatic relationship between *BRCA2* and *RAD52* is suggested in these cells (Qing et al., 2011). Combined defects in the *BRCA2* ortholog *Brh2* and *Rad52* generate a very subtle synthetic lethal phenotype in *U. maydis* (Kojic et al., 2008). These differences between human and other species point to the care required in the generalization of synthetic lethal interactions among species and restrict significantly the spectrum of model organisms that can be used in their study.

Poly (ADP-ribose) polymerase 1 inhibition shows synergistic interactions in combination with *CHK1* inhibition and is thought

to be mediated by the induction of apoptosis. CHK1 induced phosphorylation of ERK1/2 and H2AX is abolished after PARP-1 inhibition (Mitchell et al., 2010). However, the suppression of HRR by CHK1 inhibition makes this kinase an excellent target for synthetic lethality with PARP-1 inhibition also according to the rational framework outlined above.

In agreement with this expectation, Hattori et al. established a BRCA2 synthetic lethal RNAi screen, which identified CHK1 as a potential therapeutic target. Unexpectedly, though, CHK1 inhibitors failed to suppress the growth of BRCA2-deficient cells in the context of KRAS activation and TP53 inactivation found in pancreatic cancers (Hattori et al., 2011). This study extends the above outlined precautions and emphasizes that synthetic lethal interactions identified by *in vitro* screens may fail to show effectiveness in the genetic context of specific cancer forms. Evidently, the identification of synthetic lethal interactions and their exploitation in cancer therapy requires extreme care, appropriate experimentation, and model systems closely resembling the tumor whose cure is envisioned.

IMPACT ON RADIATION THERAPY OF ABNORMAL EXPRESSION OF RAD51

Cancer cell lines show fluctuations in the level of expression of genes involved in cell-cycle control and DDR. The variable expression of genes implicated in HRR, particularly overexpression of *RAD51*, is seen in many tumors and is linked to increased radio- or chemo-resistance. Moreover, a high level of *RAD51* expression is observed in a variety of tumor cell lines (Richardson, 2005) and is associated with a poor outcome in the therapy of lung cancer (Qiao et al., 2005).

In addition, mammalian cells with elevated *RAD51* level show genomic instability (Richardson et al., 2004), increased spontaneous recombination, and resistance to IR or to chemotherapeutic agents (Vispe et al., 1998). All these findings associate increased level of *RAD51* with genomic instability and cancer development. This is surprising considering that the functions of *RAD51* in HRR would predict the opposite, i.e., improved repair capacity. Indeed, it has been shown that many leukemia-related disorders, ovarian and breast carcinomas, as well as colon and rectal adenocarcinomas show, when irradiated, increased formation of *RAD51* foci, which correlates with radioresistance (Raderschall et al., 2002; Klein, 2008). Moreover, the HRR deficiency of cells lacking *RAD51* paralogs or *BRCA1* can be completely or partially rescued by *RAD51* overexpression (Schild and Wiese, 2010). Another report shows that mRNA and protein levels of *RAD51*, *XRCC3*, *RAD52*, and *RAD54* genes are two to fivefold elevated in malignant prostate cancer cell lines (Fan et al., 2004).

Interestingly, the high *RAD51* levels in these tumors are not mediated by *RAD51* gene amplification; rather overexpression is driven by aberrant oncogene related transcriptional activation. This suggests problems with the regulation of DNA metabolism in cancer cells. Major culprit for such behavior is the mutation in the tumor suppressor gene *p53*, which was found to negatively regulate *RAD51* expression (Arias-Lopez et al., 2006; Hannay et al., 2007). As *p53* is the most frequently mutated gene in human cancers (Hansen et al., 2003), a *RAD51*-related radio- and chemo-resistance are likely consequences.

However, fluctuations in *RAD51* level in tumor cells cannot be completely explained by mutations in *p53* gene. There are examples of *RAD51* over expression in a functional *p53* background, suggesting a multilevel control of *RAD51* expression. In these cases high *RAD51* level is associated with *p53*-dependent expression of *p21^{Waf-1}*, which affects the rate of *BRCA1* transcription and the activation of cell-cycle checkpoint response (Walsh et al., 2011). Therefore, a strong G2 cell-cycle arrest is detected in *RAD51*-overexpressing cells, which occurs through *p21* mediated *CDK1* inactivation (Raderschall et al., 2002).

It is relevant to speculate how increased *RAD51* protein levels confer radioresistance in tumor cells, especially when additional mutations are generated in DNA repair genes that should make them radiosensitive.

There are reports suggesting a positive correlation between HRR and high levels of *RAD51*. Thus, *p53* deficient Chinese hamster ovary cells show elevated HRR when transfected with a vector mediating overexpression of the *RAD51* gene (Bertrand et al., 2003). Furthermore, using an I-Sce-I-based reporter system in mouse ES cells (Habrand and Le Pechoux, 2004), it was found that *RAD51* over expression increases HRR. Yet, in the latter case increased HRR was associated with aberrant recombination events including crossovers, chromosome translocations, as well as multiple chromosome rearrangements and aneuploidy, suggesting frequent abrogation of HRR and possibly the engagement of B-NHEJ.

Thus, for successful HRR, *RAD51* levels must be precisely regulated; otherwise chromosomal instability may ensue. The correspondence between *RAD51* over expression, increased HRR, and resistance to chemotherapeutic drugs suggest the possibility for developing treatment strategies based on *RAD51* down regulation – by specific inhibitors or RNAi.

RADIOSENSITIZATION BY CHEMOTHERAPEUTIC AGENTS THROUGH INHIBITION OF HRR

As outlined above, intact or hyperactive HRR often correlates with resistance to therapy, while defects in HRR, when not associated with sensitivity to treatment, offer opportunities for synthetic lethality. It is timely, therefore, to explore means to inhibit HRR in cells proficient in this repair pathway. The potential benefit of this approach is reinforced by the observation that several compounds with antitumor activity and wide application in the clinic also inhibit HRR, and thus generate opportunities for synergistic interactions.

Radiosensitizing effects, in addition to their cytotoxic action, have been demonstrated for many chemotherapeutic drugs. Although the radiosensitizing effects of some of those drugs, e.g., 5-fluorouracil (5-FU), have been known for decades, the underlying mechanisms remain largely unclear. However, the number of radiosensitizers that are found to inhibit HRR is growing. These include nucleoside and base analogs like gemcitabine (Wachters et al., 2003), TAS-106 (Meike et al., 2011), and gimeracil (Takagi et al., 2010) as well as other antimetabolites like pentoxifylline and caffeine (Asaad et al., 2000; Böhm, 2006). Furthermore the ATR inhibitor VE-821 (Prevo et al., 2012) and the CHK1/2 inhibitor AZD7762 (Morgan et al., 2010) have been reported to inhibit HRR.

There is also a growing list of inhibitory substances and therapeutics, which are less directly linked to DNA metabolism and damage response, but which are suggested to radiosensitize tumor cells by inhibiting HRR. These include the tyrosine kinase inhibitors imatinib and erlotinib (Chinnaiyan et al., 2005; Li et al., 2008; Choudhury et al., 2009), the HDAC inhibitor PCI-24781 (Adimoolam et al., 2007), the proteasome inhibitor MG132 (Murakawa et al., 2007), and 17-AAG, an inhibitor of HSP90 (Noguchi et al., 2006). Moreover, mild hyperthermia was found to inhibit HRR and to sensitize cells to PARP-inhibitors (Krawczyk et al., 2011; Bergs et al., 2013). In addition specific inhibitors of HRR are now being identified in specialized screens, like BO2, which inhibits the RAD51 activity in strand exchange (Huang et al., 2012) and RI-1, a specific inhibitor of RAD51 that covalently binds to RAD51 and suppresses RAD51 nucleoprotein filament formation (Budke et al., 2012).

Finally, it should be pointed out that IR, but also many widely used chemotherapeutic compounds induce large amounts of base damage, or generate replication errors that require mismatch repair for correction. As a result, it is possible to significantly improve cancer treatment by developing strategies for the

simultaneous inhibition during treatment of some of these repair pathways, or by exploiting genetic defects in cancer cells in these repair pathways (Kinsella, 2009).

CONCLUSION

It is evident from the above outline that a wealth of information and a variety of approaches are evolving that promise to improve the outcome of radiation therapy beyond the precise and more specific targeting of the radiation dose to the tumor. These approaches are aided and accelerated by rapid advances in synthetic chemistry and in protein structure information. As a result, they are likely to mature quickly and to open a new era of opportunities in radiation therapy. Radiation oncologists are likely to benefit significantly from these developments, if they closely follow them and quickly adapt them to the requirements of treatment of human tumors by IR.

ACKNOWLEDGMENTS

Work supported by Grants from the “Bundesministerium für Bildung und Forschung” (BMBF: 02NUK005C and 03NUK001B) and the “Bundesministerium für Wirtschaft und Technologie” (BMW: ESA-AO-08-IBER, 50WB1229).

REFERENCES

- Adimoolam, S., Sirisawad, M., Chen, J., Thiemann, P., Ford, J. M., and Buggy, J. J. (2007). HDAC inhibitor PCI-24781 decreases RAD51 expression and inhibits homologous recombination. *Proc. Natl. Acad. Sci. U.S.A.* 104, 19482–19487.
- Ahmad, S. S., Duke, S., Jena, R., Williams, M. V., and Burnet, N. G. (2012). Advances in radiotherapy. *BMJ* 345, 33–38.
- Aly, A., and Ganesan, S. (2011). BRCA1, PARP, and 53BP1: conditional synthetic lethality and synthetic viability. *J. Mol. Cell Biol.* 3, 66–74.
- Arias-Lopez, C., Lazaro-Trueba, I., Kerr, P., Lord, C. J., Dexter, T., Iravani, M., et al. (2006). p53 modulates homologous recombination by transcriptional regulation of the RAD51 gene. *EMBO Rep.* 7, 219–224.
- Arosio, D., Cui, S., Ortega, C., Chovanec, M., Di Marco, S., Baldini, G., et al. (2002). Studies on the mode of Ku interaction with DNA. *J. Biol. Chem.* 277, 9741–9748.
- Asaad, N. A., Zeng, Z.-C., Guan, J., Thacker, J., and Iliakis, G. (2000). Homologous recombination as a potential target for caffeine radiosensitization in mammalian cells: reduced caffeine radiosensitization in *XRCC2* and *XRCC3* mutants. *Oncogene* 19, 5788–5800.
- Audebert, M., Salles, B., and Calso, P. (2004). Involvement of poly(ADP-ribose) polymerase-1 and XRCC1/DNA ligase III in an alternative route for DNA double-strand breaks rejoining. *J. Biol. Chem.* 279, 55117–55126.
- Aylon, Y., and Kupiec, M. (2004). New insights into the mechanism of homologous recombination in yeast. *Mutat. Res.* 566, 231–248.
- Badie, S., Liao, C., Thanasoula, M., Barber, P., Hill, M. A., and Tarsounas, M. (2009). RAD51C facilitates checkpoint signaling by promoting CHK2 phosphorylation. *J. Cell Biol.* 185, 587–600.
- Baskaran, R., Wood, L. D., Whitaker, L. L., Canman, C. E., Morgan, S. E., Xu, Y., et al. (1997). Ataxia telangiectasia mutant protein activates c-Abl tyrosine kinase in response to ionizing radiation. *Nature* 387, 516–519.
- Bennardo, N., Cheng, A., Huang, N., and Stark, J. M. (2008). Alternative-NHEJ is a mechanistically distinct pathway of mammalian chromosome break repair. *PLoS Genet.* 4:e1000110. doi:10.1371/journal.pgen.1000110
- Bergs, J. W., Krawczyk, P. M., Borovski, T., Ten Cate, R., Rodermond, H. M., Stap, J., et al. (2013). Inhibition of homologous recombination by hyperthermia shunts early double strand break repair to non-homologous end-joining. *DNA Repair (Amst.)* 12, 38–45.
- Bertrand, P., Lambert, S., Joubert, C., and Lopez, B. S. (2003). Overexpression of mammalian Rad51 does not stimulate tumorigenesis while a dominant-negative Rad51 affects centrosome fragmentation, ploidy and stimulates tumorigenesis, in p53-defective CHO cells. *Oncogene* 22, 7587–7592.
- Boboila, C., Oksenyh, V., Gostissa, M., Wang, J. H., Zha, S., Zhang, Y., et al. (2012). Robust chromosomal DNA repair via alternative end-joining in the absence of X-ray repair cross-complementing protein 1 (XRCC1). *Proc. Natl. Acad. Sci. U.S.A.* 109, 2473–2478.
- Böhm, L. (2006). Inhibition of homologous recombination repair with Pen-toxifylline targets G2 cells generated by radiotherapy and induces major enhancements of the toxicity of cisplatin and melphalan given after irradiation. *Radiat. Oncol.* 1, 12.
- Bolderson, E., Tomimatsu, N., Richard, D. J., Boucher, D., Kumar, R., Pandita, T. K., et al. (2010). Phosphorylation of Exo1 modulates homologous recombination repair of DNA double-strand breaks. *Nucleic Acids Res.* 38, 1821–1831.
- Bouwman, P., Aly, A., Escandell, J. M., Pieterse, M., Bartkova, J., Van Der Gulden, H., et al. (2010). 53BP1 loss rescues BRCA1 deficiency and is associated with triple-negative and BRCA-mutated breast cancers. *Nat. Struct. Mol. Biol.* 17, 688–695.
- Brady, N., Gaymes, T. J., Cheung, M., Mufti, G. J., and Rassool, F. V. (2003). Increased error-prone NHEJ activity in myeloid leukemias is associated with DNA damage at sites that recruit key nonhomologous end-joining proteins. *Cancer Res.* 63, 1798–1805.
- Brody, L. C., and Biesecker, B. B. (1998). Breast cancer susceptibility genes. BRCA1 and BRCA2. *Medicine (Baltimore)* 77, 208–226.
- Bryant, H. E., Schultz, N., Thomas, H. D., Parker, K. M., Flower, D., Lopez, E., et al. (2005). Specific killing of BRCA2-deficient tumours with inhibitors of poly(ADP-ribose) polymerase. *Nature* 434, 913–917.
- Budke, B., Logan, H. L., Kalin, J. H., Zelvianskaia, A. S., Cameron McGuire, W., Miller, L. L., et al. (2012). RI-1: a chemical inhibitor of RAD51 that disrupts homologous recombination in human cells. *Nucleic Acids Res.* 40, 7347–7357.
- Bugreev, D. V., Yu, X., Egelman, E. H., and Mazin, A. V. (2007). Novel pro- and anti-recombination activities of the Bloom’s syndrome helicase. *Genes Dev.* 21, 3085–3094.
- Bunting, S. F., Callén, E., Wong, N., Chen, H.-T., Polato, F., Gunn, A., et al. (2010). 53BP1 inhibits homologous recombination in Brca1-deficient cells by blocking resection of DNA breaks. *Cell* 141, 243–254.
- Cao, L., Kim, S., Xiao, C., Wang, R.-H., Li, W. M., Xu, L. X., et al. (2006). ATM-Chk2-p53 activation prevents tumorigenesis at an expense of organ homeostasis upon Brca1 deficiency. *EMBO J.* 25, 2167–2177.
- Carreira, A., and Kowalczykowski, S. C. (2009). BRCA2 shining light on the regulation of DNA-binding selectivity by RAD51. *Cell Cycle* 8, 3445–3447.

- Chapman, J. R., Barral, P., Vannier, J. B., Borel, V., Steger, M., Tomas-Loba, A., et al. (2013). RIF1 is essential for 53BP1-dependent nonhomologous end joining and suppression of DNA double-strand break resection. *Mol. Cell* 5, 858–871.
- Chen, D. J., and Nirodi, C. S. (2007). The epidermal growth factor receptor: a role in repair of radiation-induced DNA damage. *Clin. Cancer Res.* 13, 6555–6560.
- Chinnaiyan, P., Huang, S., Vallabhaneni, G., Armstrong, E., Varambally, S., Tomlins, S. A., et al. (2005). Mechanisms of enhanced radiation response following epidermal growth factor receptor signaling inhibition by erlotinib (Tarceva). *Cancer Res.* 65, 3328–3335.
- Choudhury, A., Zhao, H., Jalali, F., Al Rashid, S., Ran, J., Supiot, S., et al. (2009). Targeting homologous recombination using imatinib results in enhanced tumor cell chemosensitivity and radiosensitivity. *Mol. Cancer Ther.* 8, 203–213.
- Connell, P. P., and Hellman, S. (2009). Advances in radiotherapy and implications for the next century: a historical perspective. *Cancer Res.* 69, 383–392.
- Connell, P. P., Jayathilaka, K., Haraf, D. J., Weichselbaum, R. R., Vokes, E. E., and Lingen, M. W. (2006). Pilot study examining tumor expression of RAD51 and clinical outcomes in human head cancers. *Int. J. Oncol.* 28, 1113–1119.
- Constantinou, A., Chen, X.-B., McGowan, C. H., and West, S. C. (2002). Holliday junction resolution in human cells: two junction endonucleases with distinct substrate specificities. *EMBO J.* 21, 5577–5585.
- Corneo, B., Wendland, R. L., Deriano, L., Cui, X., Klein, I. A., Wong, S.-Y., et al. (2007). Rag mutations reveal robust alternative end joining. *Nature* 449, 483–486.
- Cramer, K., Nieborowska-Skorska, M., Koptyra, M., Slupianek, A., Penserga, E. T., Eaves, C. J., et al. (2008). BCR/ABL and other kinases from chronic myeloproliferative disorders stimulate single-strand annealing, an unfaithful DNA double-strand break repair. *Cancer Res.* 68, 6884–6888.
- de Gonzalez, A., Curtis, R. E., Kry, S. F., Gilbert, E., Lamart, S., Berg, C. D., et al. (2011). Proportion of second cancers attributable to radiotherapy treatment in adults: a cohort study in the US SEER cancer registries. *Lancet Oncol.* 12, 353–360.
- Delaney, G., Jacob, S., Featherstone, C., and Barton, M. (2005). The role of radiotherapy in cancer treatment. *Cancer* 104, 1129–1137.
- Della-Maria, J., Zhou, Y., Tsai, M.-S., Kuhnlein, J., Carney, J. P., Paull, T. T., et al. (2011). Human Mre11/Human Rad50/Nbs1 and DNA ligase III α /XRCC1 protein complexes act together in an alternative nonhomologous end joining pathway. *J. Biol. Chem.* 286, 33845–33853.
- Dever, S. M., White, E. R., Hartman, M. C. T., and Valerie, K. (2012). BRCA1-directed, enhanced and aberrant homologous recombination: mechanism and potential treatment strategies. *Cell Cycle* 11, 687–694.
- Di Virgilio, M., Callen, E., Yamane, A., Zhang, W., Jankovic, M., Gitlin, A. D., et al. (2013). Rif1 prevents resection of DNA breaks and promotes immunoglobulin class switching. *Science* 339, 711–715.
- DiBiase, S. J., Zeng, Z.-C., Chen, R., Hyslop, T., Curran, W. J. Jr., and Iliakis, G. (2000). DNA-dependent protein kinase stimulates an independently active, nonhomologous, end-joining apparatus. *Cancer Res.* 60, 1245–1253.
- Dittmann, K., Mayer, C., and Rode- mann, H. (2010). Nuclear EGFR as novel therapeutic target. *Strahlenther. Onkol.* 186, 1–6.
- Dou, H., Huang, C., Singh, M., Carpenter, P. B., and Yeh, E. T. H. (2010). Regulation of DNA repair through DeSUMOylation and SUMOylation of replication protein A complex. *Mol. Cell* 39, 333–345.
- Drost, R., Bouwman, P., Rottenberg, S., Boon, U., Schut, E., Klarenbeek, S., et al. (2011). BRCA1 RING function is essential for tumor suppression but dispensable for therapy resistance. *Cancer Cell* 20, 797–809.
- Dutertre, S., Ababou, M., Onclercq, R., Delic, J., Chatton, B., Jaulin, C., et al. (2000). Cell cycle regulation of the endogenous wild type Bloom's syndrome DNA helicase. *Oncogene* 19, 2731–2738.
- Eid, W., Steger, M., El-Shemerly, M., Ferretti, L. P., Pena-Diaz, J., Konig, C., et al. (2010). DNA end resection by CtIP and exonuclease 1 prevents genomic instability. *EMBO Rep.* 11, 897–984.
- Eladad, S., Ye, T.-Z., Hu, P., Leversha, M., Beresten, S., Matunis, M. J., et al. (2005). Intra-nuclear trafficking of the BLM helicase to DNA damage-induced foci is regulated by SUMO modification. *Hum. Mol. Genet.* 14, 1351–1365.
- Ellenberger, T., and Tomkinson, A. E. (2008). Eukaryotic DNA ligases: structural and functional insights. *Annu. Rev. Biochem.* 77, 313–338.
- Esashi, F., Christ, N., Gannon, J., Liu, Y., Hunt, T., Jasin, M., et al. (2005). CDK-dependent phosphorylation of BRCA2 as a regulatory mechanism for recombinational repair. *Nature* 434, 598–604.
- Esashi, F., Galkin, V. E., Yu, X., Egelman, E. H., and West, S. C. (2007). Stabilization of RAD51 nucleoprotein filaments by the C-terminal region of BRCA2. *Nat. Struct. Mol. Biol.* 14, 468–474.
- Escribano-Diaz, C., Orthwein, A., Fradet-Turcotte, A., Xing, M., Young, J. T., Tkac, J., et al. (2013). A cell cycle-dependent regulatory circuit composed of 53BP1-RIF1 and BRCA1-CtIP controls DNA repair pathway choice. *Mol. Cell* 5, 872–883.
- Falck, J., Forment, J. V., Coates, J., Mistrik, M., Lukas, J., Bartek, J., et al. (2012). CDK targeting of NBS1 promotes DNA-end resection, replication restart and homologous recombination. *EMBO Rep.* 13, 561–568.
- Fan, R., Kumaravel, T. S., Jalali, F., Marrano, P., Squire, J. A., and Bristow, R. G. (2004). Defective DNA strand break repair after DNA damage in prostate cancer cells: implications for genetic instability and prostate cancer progression. *Cancer Res.* 64, 8526–8533.
- Farmer, H., McCabe, N., Lord, C. J., Tutt, A. N. J., Johnson, D. A., Richardson, T. B., et al. (2005). Targeting the DNA repair defect in BRCA mutant cells as a therapeutic strategy. *Nature* 434, 917–921.
- Feng, Z., Scott, S. P., Bussen, W., Sharma, G. G., Guo, G., Pandita, T. K., et al. (2011). Rad52 inactivation is synthetically lethal with BRCA2 deficiency. *Proc. Natl. Acad. Sci. U.S.A.* 108, 686–691.
- Fernandes, M. S., Reddy, M. M., Gonneville, J. R., Deroo, S. C., Podar, K., Griffin, J. D., et al. (2009). BCR-ABL promotes the frequency of mutagenic single-strand annealing DNA repair. *Blood* 114, 1813–1819.
- Flygare, J., Benson, F., and Hellgren, D. (1996). Expression of the human RAD51 gene during the cell cycle in primary human peripheral blood lymphocytes. *Biochim. Biophys. Acta* 1312, 231–236.
- Forget, A. L., Bennett, B. T., and Knight, K. L. (2004). Xrcc3 is recruited to DNA double strand breaks early and independent of Rad51. *J. Cell. Biochem.* 93, 429–436.
- Frouin, I., Maga, G., Denegri, M., Riva, F., Savio, M., Spadari, S., et al. (2003). Human proliferating cell nuclear antigen, poly(ADP-ribose) polymerase-1, and p21^{waf1/cip1}. *J. Biol. Chem.* 278, 39265–39268.
- Fujimori, A., Tachiiri, S., Sonoda, E., Thompson, L. H., Kumar Dhar, P., Hiraoka, M., et al. (2001). Rad52 partially substitutes for the Rad51 paralog XRCC3 in maintaining chromosomal integrity in vertebrate cells. *EMBO J.* 20, 5513–5520.
- Golding, S. E., Morgan, R. N., Adams, B. R., Hawkins, A. J., Povirk, L. F., and Valerie, K. (2009). Pro-survival AKT and ERK signaling from EGFR and mutant EGFRvIII enhances DNA double-strand break repair in human glioma cells. *Cancer Biol. Ther.* 8, 730–738.
- Grabarz, A., Barascu, A., Guirouilh-Barbat, J., and Lopez, B. S. (2012). Initiation of DNA double strand break repair: signaling and single-stranded resection dictate the choice between homologous recombination, non-homologous end-joining and alternative end-joining. *Am. J. Cancer Res.* 2, 249–268.
- Gravel, S., Chapman, J. R., Magill, C., and Jackson, S. P. (2008). DNA helicases Sgs1 and BLM promote DNA double-strand break resection. *Genes Dev.* 22, 2767–2772.
- Greaves, M. J., and Wiemels, J. (2003). Origins of chromosome translocations in childhood leukaemia. *Nat. Rev. Cancer* 3, 639–649.
- Haaf, T., Golub, E. I., Reggy, G., Radding, C. M., and Ward, D. C. (1995). Nuclear foci of mammalian Rad51 recombination protein in somatic cells after DNA damage and its localization in synaptonemal complexes. *Proc. Natl. Acad. Sci. U.S.A.* 92, 2298–2302.
- Habrand, J. L., and Le Pechoux, C. (2004). Radiation therapy in the management of adult soft tissue sarcomas. *Ann. Oncol.* 15, iv187–iv191.
- Hannay, J. A. F., Liu, J., Zhu, Q.-S., Bolshakov, S. V., Li, L., Pisters, P. W. T., et al. (2007). Rad51 overexpression contributes to chemoresistance in human soft tissue sarcoma cells: a role for p53/activator protein 2 transcriptional regulation. *Mol. Cancer Ther.* 6, 1650–1660.
- Hansen, L. T., Lundin, C., Spang-Thomsen, M., Petersen, L. N., and Helleday, T. (2003). The role of Rad51 in etoposide (V16) resistance in small cell lung cancer. *Int. J. Cancer* 105, 472–479.

- Hattori, H., Skoulidis, F., Russell, P., and Venkataraman, A. R. (2011). Context dependence of checkpoint kinase 1 as a therapeutic target for pancreatic cancers deficient in the BRCA2 tumor suppressor. *Mol. Cancer Ther.* 10, 670–678.
- Helleday, T., Lo, J., Van Gent, D. C., and Engelward, B. P. (2007). DNA double-strand break repair: from mechanistic understanding to cancer treatment. *DNA Repair (Amst.)* 6, 923–935.
- Hu, Y., Raynard, S., Sehorn, M. G., Lu, X., Bussen, W., Zheng, L., et al. (2007). RECQL5/Recql5 helicase regulates homologous recombination and suppresses tumor formation via disruption of Rad51 presynaptic filaments. *Genes Dev.* 21, 3073–3084.
- Huang, F., Mazina, O. M., Zentner, I. J., Cocklin, S., and Mazin, A. V. (2012). Inhibition of homologous recombination in human cells by targeting RAD51 recombinase. *J. Med. Chem.* 55, 3011–3020.
- Huertas, P. (2010). DNA resection in eukaryotes: deciding how to fix the break. *Nat. Struct. Mol. Biol.* 17, 11–16.
- Huertas, P., and Jackson, S. P. (2009). Human CtIP mediates cell cycle control of DNA end resection and double strand break repair. *J. Biol. Chem.* 284, 9558–9565.
- Iliakis, G. (2009). Backup pathways of NHEJ in cells of higher eukaryotes: cell cycle dependence. *Radiother. Oncol.* 92, 310–315.
- Iliakis, G., Wu, W., Wang, M., Terzoudi, G. I., and Pantelias, G. E. (2007). “Backup pathways of nonhomologous end joining may have a dominant role in the formation of chromosome aberrations,” in *Chromosomal Alterations*, eds G. Obe and Vijayalaxmi (Berlin: Springer Verlag), 67–85.
- Ip, S. C. Y., Rass, U., Blanco, M. G., Flynn, H. R., Skehel, J. M., and West, S. C. (2008). Identification of Holliday junction resolvases from humans and yeast. *Nature* 456, 357–361.
- Ivanov, E. L., Sugawara, N., Fishman-Lobell, J., and Haber, J. E. (1996). Genetic requirements for the single-strand annealing pathway of double-strand break repair in *Saccharomyces cerevisiae*. *Genetics* 142, 693–704.
- Jasin, M. (2002). Homologous repair of DNA damage and tumorigenesis: the BRCA connection. *Oncogene* 21, 8981–8993.
- Karpenshif, Y., and Bernstein, K. A. (2012). From yeast to mammals: recent advances in genetic control of homologous recombination. *DNA Repair (Amst.)* 11, 781–788.
- Keeney, S., Giroux, C. N., and Kleckner, N. (1997). Meiosis-specific DNA double-strand breaks are catalyzed by Spo11, a member of a widely conserved protein family. *Cell* 88, 375–384.
- Kharbanda, S., Ren, R., Pandey, P., Shafman, T. D., Feller, S. M., Weichselbaum, R. R., et al. (1995). Activation of the c-Abl tyrosine kinase in the stress response to DNA-damaging agents. *Nature* 376, 785–788.
- Kinsella, T. J. (2009). Coordination of DNA mismatch repair and base excision repair processing of chemotherapy and radiation damage for targeting resistant cancers. *Clin. Cancer Res.* 15, 1853–1859.
- Klein, H. L. (2008). The consequences of Rad51 overexpression for normal and tumor cells. *DNA Repair (Amst.)* 7, 686–693.
- Kojic, M., Mao, N., Zhou, Q., Lisby, M., and Holloman, W. K. (2008). Compensatory role for Rad52 during recombinational repair in *Ustilago maydis*. *Mol. Microbiol.* 67, 1156–1168.
- Kousholt, A. N., Fugger, K., Hoffmann, S., Larsen, B. D., Menzel, T., Sartori, A. A., et al. (2012). CtIP-dependent DNA resection is required for DNA damage checkpoint maintenance but not initiation. *J. Cell Biol.* 197, 869–876.
- Krawczyk, P. M., Eppink, B., Essers, J., Stap, J., Rodermond, H., Odijk, H., et al. (2011). Mild hyperthermia inhibits homologous recombination, induces BRCA2 degradation, and sensitizes cancer cells to poly(ADP-ribose) polymerase-1 inhibition. *Proc. Natl. Acad. Sci. U.S.A.* 108, 9851–9856.
- Kriegs, M., Kasten-Pisula, U., Rieckmann, T., Holst, K., Saker, J., Dahm-Daphi, J., et al. (2010). The epidermal growth factor receptor modulates DNA double-strand break repair by regulating non-homologous end-joining. *DNA Repair (Amst.)* 9, 889–897.
- Küpper, J. H., Müller, M., Jacobson, M. K., Tatsumi-Miyajima, J., Coyle, D. L., Jacobson, E. L., et al. (1995). *trans*-Dominant inhibition of poly(ADP-Ribosyl)ation sensitizes cells against γ -irradiation and N-methyl-N'-nitrosoguanidine but does not limit DNA replication of a polyomavirus replicon. *Mol. Cell Biol.* 15, 3154–3163.
- Lee-Theilen, M., Matthews, A. J., Kelly, D., Zheng, S., and Chaudhuri, J. (2011). CtIP promotes microhomology-mediated alternative end joining during class-switch recombination. *Nat. Struct. Mol. Biol.* 18, 75–79.
- Leslie, M. (2013). How to live without BRCA1. *J. Cell Biol.* 200, 127.
- Li, L., Wang, H., Yang, E. S., Arteaga, C. L., and Xia, F. (2008). Erlotinib attenuates homologous recombinational repair of chromosomal breaks in human breast cancer cells. *Cancer Res.* 68, 9141–9146.
- Li, S., Ting, N. S. Y., Zheng, L., Chen, P.-L., Ziv, Y., Shiloh, Y., et al. (2000). Functional link of BRCA1 and ataxia telangiectasia gene product in DNA damage response. *Nature* 406, 210–215.
- Li, X., and Heyer, W.-D. (2009). RAD54 controls access to the invading 3'-OH end after RAD51-mediated DNA strand invasion in homologous recombination in *Saccharomyces cerevisiae*. *Nucleic Acids Res.* 37, 638–646.
- Lieber, M. R. (2010). The mechanism of double-strand DNA break repair by the nonhomologous DNA end-joining pathway. *Annu. Rev. Biochem.* 79, 1.1–1.31.
- Llorente, B., Smith, C. E., and Symington, L. S. (2008). Break-induced replication: what is it and what is it for? *Cell Cycle* 7, 859–864.
- Lok, B. H., Carley, A. C., Tchang, B., and Powell, S. N. (2012). RAD52 inactivation is synthetically lethal with deficiencies in BRCA1 and PALB2 in addition to BRCA2 through RAD51-mediated homologous recombination. *Oncogene*. doi:10.1038/onc.2012.391
- Mansour, W. Y., Rhein, T., and Dahm-Daphi, J. (2010). The alternative end-joining pathway for repair of DNA double-strand breaks requires PARP1 but is not dependent upon microhomologies. *Nucleic Acids Res.* 38, 6065–6077.
- Masson, J.-Y., Tarsounas, M. C., Stasiak, A. Z., Stasiak, A., Shah, R., McIlwraith, M. J., et al. (2001). Identification and purification of two distinct complexes containing the five RAD51 paralogs. *Genes Dev.* 15, 3296–3307.
- Matsuoka, S., Ballif, B. A., Smogorzewska, A., McDonald III, E. R., Hurov, K. E., Luo, J., et al. (2007). ATM and ATR substrate analysis reveals extensive protein networks responsive to DNA damage. *Science* 316, 1160–1166.
- McCabe, N., Turner, N. C., Lord, C. J., Kluzek, K., Bialkowska, A., Swift, S., et al. (2006). Deficiency in the repair of DNA damage by homologous recombination and sensitivity to poly(ADP-Ribose) polymerase inhibition. *Cancer Res.* 66, 8109–8115.
- Medova, M., Aebersold, D. M., and Zimmer, Y. (2012). MET inhibition in tumor cells by PHA665752 impairs homologous recombination repair of DNA double strand breaks. *Int. J. Cancer* 130, 728–734.
- Meek, K., Gupta, S., Ramsden, D. A., and Lees-Miller, S. P. (2004). The DNA-dependent protein kinase: the director at the end. *Immunol. Rev.* 200, 132–141.
- Meike, S., Yamamori, T., Yasui, H., Eitaki, M., Matsuda, A., Morimatsu, M., et al. (2011). A nucleoside anticancer drug, 1-(3-C-ethynyl-beta-D-ribo-pentofuranosyl)cytosine (TAS106), sensitizes cells to radiation by suppressing BRCA2 expression. *Mol. Cancer* 10, 92.
- Metzger, L., and Iliakis, G. (1991). Kinetics of DNA double strand breaks throughout the cell cycle as assayed by pulsed field gel electrophoresis in CHO cells. *Int. J. Radiat. Biol.* 59, 1325–1339.
- Miki, Y., Swensen, J., Shattuck-Eidens, D., Futreal, P. A., Harshman, K., Tavtigian, S., et al. (1994). A strong candidate for the breast and ovarian cancer susceptibility gene BRCA1. *Science* 266, 66–71.
- Mimitou, E. P., and Symington, L. S. (2008). Sae2, Exo1 and Sgs1 collaborate in DNA double-strand break processing. *Nature* 455, 770–774.
- Mitchell, J. B., Choudhuri, R., Fabre, K., Sowers, A. L., Citrin, D., Zabludoff, S. D., et al. (2010). In vitro and in vivo radiation sensitization of human tumor cells by a novel checkpoint kinase inhibitor, AZD7762. *Clin. Cancer Res.* 16, 2076–2084.
- Miyagawa, K. (2008). Clinical relevance of the homologous recombination machinery in cancer therapy. *Cancer Sci.* 99, 187–194.
- Mladenov, E., and Iliakis, G. (2011). Induction and repair of DNA double strand breaks: the increasing spectrum of non-homologous end joining pathways. *Mutat. Res.* 711, 61–72.
- Moldovan, G.-L., Dejsuphong, D., Petalcorin, M. I., Hofmann, K., Takeda, S., Boulton, S. J., et al. (2012). Inhibition of homologous recombination by the PCNA-interacting protein PARI. *Mol. Cell* 45, 75–86.
- Morgan, M. A., Parsels, L. A., Zhao, L., Parsels, J. D., Davis, M. A., Hassan, M. C., et al. (2010). Mechanism

- of radiosensitization by the Chk1/2 inhibitor AZD7762 involves abrogation of the G2 checkpoint and inhibition of homologous recombinational DNA repair. *Cancer Res.* 70, 4972–4981.
- Morris, J. R., Boutell, C., Keppler, M., Densham, R., Weekes, D., Alamshah, A., et al. (2009). The SUMO modification pathway is involved in the BRCA1 response to genotoxic stress. *Nature* 462, 886–890.
- Mukherjee, B., McEllin, B., Camacho, C. V., Tomimatsu, N., Sirasana-gandala, S., Nannepaga, S., et al. (2009). EGFRvIII and DNA double-strand break repair: a molecular mechanism for radioresistance in glioblastoma. *Cancer Res.* 69, 4252–4259.
- Murakawa, Y., Sonoda, E., Barber, L. J., Zeng, W., Yokomori, K., Kimura, H., et al. (2007). Inhibitors of the proteasome suppress homologous DNA recombination in mammalian cells. *Cancer Res.* 67, 8536–8543.
- Myllynen, L., Rieckmann, T., Dahm-Daphi, J., Kasten-Pisula, U., Petersen, C., Dikomey, E., et al. (2011). In tumor cells regulation of DNA double strand break repair through EGF receptor involves both NHEJ and HR and is independent of p53 and K-Ras status. *Radiother. Oncol.* 101, 147–151.
- Noguchi, M., Yu, D., Hirayama, R., Ninomiya, Y., Sekine, E., Kubota, N., et al. (2006). Inhibition of homologous recombination repair in irradiated tumor cells pretreated with Hsp90 inhibitor 17-allylamino-17-demethoxygeldanamycin. *Biochem. Biophys. Res. Commun.* 351, 658–663.
- Nowicki, M. O., Falinski, R., Kopytyra, M., Slupianek, A., Stoklosa, T., Gloc, E., et al. (2004). BCR/ABL oncogenic kinase promotes unfaithful repair of the reactive oxygen species-dependent DNA double-strand breaks. *Blood* 104, 3746–3753.
- O'Donovan, P. J., and Livingston, D. M. (2010). BRCA1 and BRCA2: breast/ovarian cancer susceptibility gene products and participants in DNA double-strand break repair. *Carcinogenesis* 31, 961–967.
- Okano, S., Lan, L., Caldecott, K. W., Mori, T., and Yasui, A. (2003). Spatial and temporal cellular responses to single-strand breaks in human cells. *Mol. Cell. Biol.* 23, 3974–3981.
- Onn, I., Heidinger-Pauli, J. M., Guacci, V., Unal, E., and Koshland, D. E. (2008). Sister chromatid cohesion: a simple concept with a complex reality. *Annu. Rev. Cell Dev. Biol.* 24, 105–129.
- Ouyang, K. J., Woo, L. L., Zhu, J., Huo, D., Matunis, M. J., and Ellis, N. A. (2009). SUMO modification regulates BLM and RAD51 interaction at damaged replication forks. *PLoS Biol.* 7:e1000252. doi:10.1371/journal.pbio.1000252
- Panizza, S., Mendoza, M. A., Berlinger, M., Huang, L., Nicolas, A., Shirahige, K., et al. (2011). Spo11-accessory proteins link double-strand break sites to the chromosome axis in early meiotic recombination. *Cell* 146, 372–383.
- Paques, F., and Haber, J. E. (1999). Multiple pathways of recombination induced by double-strand breaks in *Saccharomyces cerevisiae*. *Microbiol. Mol. Biol. Rev.* 63, 349–404.
- Paul, K., Wang, M., Mladenov, E., Bencsik-Theilen, A. A., Bednar, T., Wu, W., et al. (2013). DNA ligases I and III cooperate in alternative non-homologous end-joining in vertebrates. *PLoS ONE* 8:e59505. doi:10.1371/journal.pone.0059505
- Popova, M., Shimizu, H., Yamamoto, K.-I., Lebecqec, M., Takahashi, M., and Fleury, F. (2009). Detection of c-Abl kinase-promoted phosphorylation of Rad51 by specific antibodies reveals that Y54 phosphorylation is dependent on that of Y315. *FEBS Lett.* 583, 1867–1872.
- Povirk, L. F. (2006). Biochemical mechanisms of chromosomal translocations resulting from DNA double-strand breaks. *DNA Repair (Amst.)* 5, 1199–1212.
- Povirk, L. F. (2012). Processing of damaged DNA ends for double-strand break repair in mammalian cells. *ISRN Mol. Biol.* 2012. Article ID 345805.
- Prevo, R., Fokas, E., Reaper, P. M., Charlton, P. A., Pollard, J. R., McKenna, W. G., et al. (2012). The novel ATR inhibitor VE-821 increases sensitivity of pancreatic cancer cells to radiation and chemotherapy. *Cancer Biol. Ther.* 13, 1072–1081.
- Qiao, B., Kerr, M., Groselj, B., Teo, M. T., Knowles, M. A., Bristow, R. G., et al. (2013). Imatinib radiosensitizes bladder cancer by targeting homologous recombination. *Cancer Res.* 73, 1611–1620.
- Qiao, G. B., Wu, Y. L., Yang, X. N., Zhong, W. Z., Xie, D., Guan, X. Y., et al. (2005). High-level expression of Rad51 is an independent prognostic marker of survival in non-small-cell lung cancer patients. *Br. J. Cancer* 93, 137–143.
- Qing, Y., Yamazoe, M., Hirota, K., Dejsuphong, D., Sakai, W., Yamamoto, K. N., et al. (2011). The epistatic relationship between BRCA2 and the other RAD51 mediators in homologous recombination. *PLoS Genet.* 7:e1002148. doi:10.1371/journal.pgen.1002148
- Raderschall, E., Stout, K., Freier, S., Suckow, V., Schweiger, S., and Haaf, T. (2002). Elevated levels of Rad51 recombination protein in tumor cells. *Cancer Res.* 62, 219–225.
- Rajagopalan, S., Andreeva, A., Rutherford, T. J., and Fersht, A. R. (2010). Mapping the physical and functional interactions between the tumor suppressors p53 and BRCA2. *Proc. Natl. Acad. Sci. U.S.A.* 107, 8587–8592.
- Ramus, S. J., Bobrow, L. G., Pharoah, P. D., Finnigan, D. S., Fishman, A., Altaras, M., et al. (1999). Increased frequency of TP53 mutations in BRCA1 and BRCA2 ovarian tumours. *Genes Chromosomes Cancer* 25, 91–96.
- Richardson, C. (2005). RAD51, genomic stability, and tumorigenesis. *Cancer Lett.* 218, 127–139.
- Richardson, C., Horikoshi, N., and Pandita, T. K. (2004). The role of the DNA double-strand break response network in meiosis. *DNA Repair (Amst.)* 3, 1149–1164.
- Robert, I., Dantzer, F., and Reina-San-Martin, B. (2009). Parp1 facilitates alternative NHEJ, whereas Parp2 suppresses IgH/c-myc translocations during immunoglobulin class switch recombination. *J. Exp. Med.* 206, 1047–1056.
- Roberts, S. A., Strande, N., Burkhalter, M. D., Strom, C., Havener, J. M., Hasty, P., et al. (2010). Ku is a 5'-drp/AP lyase that excises nucleotide damage near broken ends. *Nature* 464, 1214–1217.
- Rosidi, B., Wang, M., Wu, W., Sharma, A., Wang, H., and Iliakis, G. (2008). Histone H1 functions as a stimulatory factor in backup pathways of NHEJ. *Nucleic Acids Res.* 36, 1610–1623.
- Rothkamm, K., Krüger, I., Thompson, L. H., and Löbrich, M. (2003). Pathways of DNA double-strand break repair during the mammalian cell cycle. *Mol. Cell. Biol.* 23, 5706–5715.
- Roy, R., Chun, J., and Powell, S. N. (2012). BRCA1 and BRCA2: different roles in a common pathway of genome protection. *Nat. Rev. Cancer* 12, 68–78.
- Rudat, V., Bachmann, N., Küpper, J.-H., and Weber, K.-J. (2001). Overexpression of the DNA-binding domain of poly(ADP-ribose) polymerase inhibits rejoining of ionizing radiation-induced DNA double-strand breaks. *Int. J. Radiat. Biol.* 77, 303–307.
- Salles, D., Mencialha, A. L., Ireno, I. C., Wiesmuller, L., and Abdelhay, E. (2011). BCR-ABL stimulates mutagenic homologous DNA double-strand break repair via the DNA-end-processing factor CtIP. *Carcinogenesis* 32, 27–34.
- Sallmyr, A., Tomkinson, A. E., and Rasool, F. V. (2008). Up-regulation of WRN and DNA ligase III α in chronic myeloid leukemia: consequences for the repair of DNA double-strand breaks. *Blood* 112, 1413–1423.
- San Filippo, J., Sung, P., and Klein, H. (2008). Mechanism of eukaryotic homologous recombination. *Annu. Rev. Biochem.* 77, 229–257.
- Sartori, A. A., Lukas, C., Coates, J., Mistrik, M., Fu, S., Bartek, J., et al. (2007). Human CtIP promotes DNA end resection. *Nature* 450, 509–514.
- Schatz, D. G., and Swanson, P. C. (2011). V(D)J recombination: mechanisms of initiation. *Annu. Rev. Genet.* 45, 167–202.
- Schild, D., and Wiese, C. (2010). Overexpression of RAD51 suppresses recombination defects: a possible mechanism to reverse genomic instability. *Nucleic Acids Res.* 38, 1061–1070.
- Serrano, M. A., Li, Z., Dangeti, M., Musich, P. R., Patrick, S., Roginskaya, M., et al. (2012). DNA-PK, ATM and ATR collaboratively regulate p53-RPA interaction to facilitate homologous recombination DNA repair. *Oncogene*. doi:10.1038/onc.2012.257
- Shi, W., Feng, Z., Zhang, J., Gonzalez-Suarez, I., Vanderwaal, R. P., Wu, X., et al. (2010). The role of RPA2 phosphorylation in homologous recombination in response to replication arrest. *Carcinogenesis* 31, 994–1002.
- Shibata, A., Conrad, S., Birraux, J., Geuting, V., Barton, O., Ismail, A., et al. (2011). Factors determining DNA double-strand break repair pathway choice in G2 phase. *EMBO J.* 30, 1079–1092.
- Shimizu, H., Popova, M., Fleury, F., Kobayashi, M., Hayashi, N., Sakane, I., et al. (2009). c-ABL tyrosine kinase stabilizes RAD51 chromatin association. *Biochem. Biophys. Res. Commun.* 382, 286–291.
- Shrivastav, M., De Haro, L. P., and Nickoloff, J. A. (2008). Regulation of DNA double-strand break

- repair pathway choice. *Cell Res.* 18, 134–147.
- Siegel, R., Desantis, C., Virgo, K., Stein, K., Mariotto, A., Smith, T., et al. (2012). Cancer treatment and survivorship statistics, 2012. *CA Cancer J. Clin.* 62, 220–241.
- Simsek, D., Brunet, E., Wong, S. Y.-W., Katyal, S., Gao, Y., Mckinnon, P. J., et al. (2011). DNA ligase III promotes alternative nonhomologous end-joining during chromosomal translocation formation. *PLoS Genet.* 7:e1002080. doi:10.1371/journal.pgen.1002080
- Singh, S. K., Bednar, T., Zhang, L., Wu, W., Mladenov, E., and Iliakis, G. (2012). Inhibition of B-NHEJ in plateau-phase cells is not a direct consequence of suppressed growth factor signaling. *Int. J. Radiat. Oncol. Biol. Phys.* 84, e237–e243.
- Singh, S. K., Wu, W., Wang, M., and Iliakis, G. (2009). Extensive repair of DNA double-strand breaks in cells deficient in the DNA-PK dependent pathway of NHEJ after exclusion of heat-labile sites. *Radiat. Res.* 172, 152–164.
- Singh, S. K., Wu, W., Zhang, L., Klammer, H., Wang, M., and Iliakis, G. (2011). Widespread dependence of backup NHEJ on growth state: ramifications for the use of DNA-PK inhibitors. *Int. J. Radiat. Oncol. Biol. Phys.* 79, 540–548.
- Skorski, T. (2002). BCR/ABL regulates response to DNA damage: the role in resistance to genotoxic treatment and in genomic instability. *Oncogene* 21, 8591–8604.
- Skorski, T. (2012). Genetic mechanisms of chronic myeloid leukemia blastic transformation. *Curr. Hematol. Malig. Rep.* 7, 87–93.
- Slupianek, A., Dasgupta, Y., Ren, S.-Y., Gurdek, E., Donlin, M., Nieborowska-Skorska, M., et al. (2011). Targeting RAD51 phosphotyrosine-315 to prevent unfaithful recombination repair in BCR-ABL1 leukemia. *Blood* 118, 1062–1068.
- Slupianek, A., Hoser, G., Majsterek, I., Bronisz, A., Malecki, M., Blasiak, J., et al. (2002). Fusion tyrosine kinases induce drug resistance by stimulation of homology-dependent recombination repair, prolongation of G(2)/M phase, and protection from apoptosis. *Mol. Cell Biol.* 22, 4189–4201.
- Slupianek, A., Schmutte, C., Tomblin, G., Nieborowska-Skorska, M., Hoser, G., Nowicki, M. O., et al. (2001). BCR/ABL regulates mammalian RecA homologs, resulting in drug resistance. *Mol. Cell* 8, 795–806.
- Sonoda, E., Hohegger, H., Saberi, A., Taniguchi, Y., and Takeda, S. (2006). Differential usage of non-homologous end-joining and homologous recombination in double strand break repair. *DNA Repair (Amst.)* 5, 1021–1029.
- Sorensen, C. S., Hansen, L. T., Dziegielewska, J., Syljuasen, R. G., Lundin, C., Bartek, J., et al. (2005). The cell-cycle checkpoint kinase Chk1 is required for mammalian homologous recombination repair. *Nat. Cell Biol.* 7, 195–201.
- Speit, G., and Trenz, K. (2004). Chromosomal mutagen sensitivity associated with mutations in BRCA genes. *Cytogenet. Genome Res.* 104, 325–332.
- Stracker, T. H., and Petrini, J. H. J. (2011). The MRE11 complex: starting from the ends. *Nat. Rev. Mol. Cell Biol.* 12, 90–103.
- Strande, N., Roberts, S. A., Oh, S., Hendrickson, E. A., and Ramsden, D. A. (2012). Specificity of the dRP/AP lyase of Ku promotes nonhomologous end joining (NHEJ) fidelity at damaged ends. *J. Biol. Chem.* 287, 13686–13693.
- Suwaki, N., Klare, K., and Tarsounas, M. (2011). RAD51 paralogs: roles in DNA damage signalling, recombinational repair and tumorigenesis. *Semin. Cell Dev. Biol.* 22, 898–905.
- Takagi, M., Sakata, K.-I., Someya, M., Tauchi, H., Iijima, K., Matsumoto, Y., et al. (2010). Gimeracil sensitizes cells to radiation via inhibition of homologous recombination. *Radiother. Oncol.* 96, 259–266.
- Tarsounas, M., Munoz, P., Claas, A., Smiraldi, P. G., Pittman, D. L., Blasco, M. A., et al. (2004). Telomere maintenance requires the RAD51D recombination/repair protein. *Cell* 117, 337–347.
- Tatsumi-Miyajima, J., Küpper, J.-H., Takebe, H., and Bürkle, A. (1999). Trans-dominant inhibition of poly (ADP-ribosyl)ation potentiates alkylation-induced shuttle-vector mutagenesis in Chinese hamster cells. *Mol. Cell. Biochem.* 193, 31–35.
- Tennstedt, P., Fresow, R., Simon, R., Marx, A., Terracciano, L., Petersen, C., et al. (2012). RAD51 overexpression is a negative prognostic marker for colorectal adenocarcinoma. *Int. J. Cancer* 132, 2118–2126.
- Thorslund, T., and West, S. C. (2007). BRCA2: a universal recombinase regulator. *Oncogene* 26, 7720–7730.
- Tomimatsu, N., Mukherjee, B., Deland, K., Kurimasa, A., Bolderson, E., Khanna, K. K., et al. (2012). Exo1 plays a major role in DNA end resection in humans and influences double-strand break repair and damage signaling decisions. *DNA Repair (Amst.)* 11, 441–448.
- Tommiska, J., Bartkova, J., Heinonen, M., Hautala, L., Kilpivaara, O., Eerola, H., et al. (2008). The DNA damage signalling kinase ATM is aberrantly reduced or lost in BRCA1/BRCA2-deficient and ER//PR//ERBB2-triple-negative breast cancer. *Oncogene* 27, 2501–2506.
- Toulany, M., and Rodemann, H. P. (2010). Membrane receptor signaling and control of DNA repair after exposure to ionizing radiation. *Nuklearmedizin* 49, S26–S30.
- Vilenchik, M. M., and Knudson, A. G. (2003). Endogenous DNA double-strand breaks: production, fidelity of repair, and induction of cancer. *Proc. Natl. Acad. Sci. U.S.A.* 100, 12871–12876.
- Vispe, S., Cazaux, C., Lesca, C., and Defais, M. (1998). Overexpression of Rad51 protein stimulates homologous recombination and increases resistance of mammalian cells to ionizing radiation. *Nucleic Acids Res.* 26, 2859–2864.
- Wachters, F. M., Van Putten, J. W. G., Maring, J. G., Zdzienicka, M. Z., Groen, H. J. M., and Kampinga, H. H. (2003). Selective targeting of homologous DNA recombination repair by gemcitabine. *Int. J. Radiat. Oncol. Biol. Phys.* 57, 553–562.
- Walsh, T., Casadei, S., Lee, M. K., Penning, C. C., Nord, A. S., Thornton, A. M., et al. (2011). Mutations in 12 genes for inherited ovarian, fallopian tube, and peritoneal carcinoma identified by massively parallel sequencing. *Proc. Natl. Acad. Sci. U.S.A.* 108, 18032–18037.
- Walsh, T., and King, M.-C. (2007). Ten genes for inherited breast cancer. *Cancer Cell* 11, 103–105.
- Wang, B., Matsuoka, S., Ballif, B. A., Zhang, D., Smogorzewska, A., Gygi, S. P., et al. (2007). Abraxas and RAP80 form a BRCA1 protein complex required for the DNA damage response. *Science* 316, 1194–1198.
- Wang, H., Rosidi, B., Perrault, R., Wang, M., Zhang, L., Windhofer, F., et al. (2005). DNA ligase III as a candidate component of backup pathways of nonhomologous end joining. *Cancer Res.* 65, 4020–4030.
- Wang, M., Wu, W., Wu, W., Rosidi, B., Zhang, L., Wang, H., et al. (2006). PARP-1 and Ku compete for repair of DNA double strand breaks by distinct NHEJ pathways. *Nucleic Acids Res.* 34, 6170–6182.
- Wang, S. C., Lin, S. H., Su, L. K., and Hung, M. C. (1997). Changes in BRCA2 expression during progression of the cell cycle. *Biochem. Biophys. Res. Commun.* 234, 247–251.
- Ward, J. F. (1990). The yield of DNA double-strand breaks produced intracellularly by ionizing radiation: a review. *Int. J. Radiat. Biol.* 57, 1141–1150.
- West, S. C. (2003). Molecular views of recombination proteins and their control. *Nat. Rev. Mol. Cell Biol.* 4, 1–11.
- Weterings, E., and Chen, D. J. (2008). The endless tale of non-homologous end-joining. *Cell Res.* 18, 114–124.
- Wu, L., and Hickson, I. D. (2003). The Bloom's syndrome helicase suppresses crossing over during homologous recombination. *Nature* 426, 870–874.
- Xie, A., Kwok, A., and Scully, R. (2009). Role of mammalian Mre11 in classical and alternative nonhomologous end joining. *Nat. Struct. Mol. Biol.* 16, 814–818.
- Yamamoto, A., Taki, T., Yagi, H., Habu, T., Yoshida, K., Yoshimura, Y., et al. (1996). Cell cycle-dependent expression of the mouse Rad51 gene in proliferating cells. *Mol. Gen. Genet.* 251, 1–12.
- Yata, K., Lloyd, J., Maslen, S., Bleuyard, J.-Y., Skehel, M., Smerdon, S. J., et al. (2012). Plk1 and CK2 act in concert to regulate Rad51 during DNA double strand break repair. *Mol. Cell* 45, 371–383.
- Yu, X., and Chen, J. (2004). DNA damage-induced cell cycle checkpoint control requires CtIP, a phosphorylation-dependent binding partner of BRCA1 C-terminal domains. *Mol. Cell Biol.* 24, 9478–9486.
- Yu, X., Fu, S., Lai, M., Baer, R., and Chen, J. (2006). BRCA1 ubiquitinates its phosphorylation-dependent binding partner CtIP. *Genes Dev.* 20, 1721–1726.
- Yuan, Z.-M., Huang, Y., Ishiko, T., Nakada, S., Utsugisawa, T., Kharbanda, S., et al. (1998). Regulation of Rad51 function by c-Abl in response to DNA damage. *J. Biol. Chem.* 273, 3799–3802.
- Yun, M. H., and Hiom, K. (2009). CtIP-BRCA1 modulates the choice of DNA double-strand-break repair pathway throughout the cell cycle. *Nature* 459, 460–463.
- Zha, S., Boboila, C., and Alt, F. W. (2009). Mre11: roles in DNA

- repair beyond homologous recombination. *Nat. Struct. Mol. Biol.* 16, 798–800.
- Zhang, F., Fan, Q., Ren, K., and Andreassen, P. R. (2009). PALB2 functionally connects the breast cancer susceptibility proteins BRCA1 and BRCA2. *Mol. Cancer Res.* 7, 1110–1118.
- Zhao, H., Luoto, K. R., Meng, A. X., and Bristow, R. G. (2011). The receptor tyrosine kinase inhibitor amuvatinib (MP470) sensitizes tumor cells to radio- and chemo-therapies in part by inhibiting homologous recombination. *Radiother. Oncol.* 101, 59–65.
- Zimmermann, M., Lottersberger, F., Buonomo, S. B., Sfeir, A., and De Lange, T. (2013). 53BP1 regulates DSB repair using Rif1 to control 5' end resection. *Science* 339, 700–704.
- Zwet, M., Overkamp, W. J. I., Van Lange, R. E. E., Essers, J., Van Duijn-Goedhart, A., Wiggers, I., et al. (2002). Brca2 (XRCC11) deficiency results in radioresistant DNA synthesis and a higher frequency of spontaneous deletions. *Mol. Cell. Biol.* 22, 669–679.
- Conflict of Interest Statement:** The authors declare that the research was conducted in the absence of any commercial or financial relationships that could be construed as a potential conflict of interest.
- Received: 30 January 2013; paper pending published: 11 March 2013; accepted: 24 April 2013; published online: 10 May 2013.
- Citation: Mladenov E, Magin S, Soni A and Iliakis G (2013) DNA double-strand break repair as determinant of cellular radiosensitivity to killing and target in radiation therapy. *Front. Oncol.* 3:113. doi: 10.3389/fonc.2013.00113
- This article was submitted to *Frontiers in Radiation Oncology*, a specialty of *Frontiers in Oncology*.
- Copyright © 2013 Mladenov, Magin, Soni and Iliakis. This is an open-access article distributed under the terms of the Creative Commons Attribution License, which permits use, distribution and reproduction in other forums, provided the original authors and source are credited and subject to any copyright notices concerning any third-party graphics etc.

APPENDIX

Table A1 | Used abbreviations.

53BP1	p53 binding protein 1
5-FU	5-fluorouracil
ATM	Ataxia telangiectasia mutated
ATR	ATM and Rad3 related
BARD1	BRCA1-associated RING domain 1 protein
BIR	Break induced replication
BLM	Bloom's syndrome helicase
B-NHEJ	Backup non-homologous end-joining
BRCA1	Breast cancer susceptibility gene 1
BRCA2	Breast cancer susceptibility gene 2
CDKs	Cyclin dependent kinases
CHK1/2	Checkpoint kinase 1/2
CK2	Casein kinase 2
CML	Chronic myelogenous leukemia
CtIP	C-terminal binding protein 1 interacting protein
DDR	DNA damage response
dHJ	Double Holliday junction
D-loop	Displacement loop
DNA-PKcs	DNA dependent protein kinase catalytic subunit
D-NHEJ	DNA-PKcs dependent non-homologous end-joining
DSBs	Double-strand breaks
EXO1	Exonuclease 1
FEN1	Flap endonuclease 1
HDAC	Histone deacetylases
HRR	Homologous recombination repair
HU	Hydroxyurea
IR	Ionizing radiation
LIG1	DNA ligase 1
LIG3	DNA ligase 3
LIG4	DNA ligase 4
LOH	Loss of heterozygosity
MAPK	Mitogen activated protein kinases
MRE11	Meiotic recombination 11
MRN	MRE11/RAD50/NBS1
NBS1	Nijmegen breakage syndrome 1
NHEJ	Non-homologous end-joining
PARI	PCNA-associated recombination inhibitor
PARP-1	Poly (ADP-ribose) polymerase 1
PCNA	Proliferation cell nuclear antigen
PFGE	Pulse-field gel electrophoresis
PI3K	Phosphatidyl inositol 3-OH kinases
PLK1	Polo like kinase 1
PNK	Polynucleotide kinase phosphatase
PTMs	Post-translational modifications
RPA	Replication protein A
RTEL1	Regulator of telomere elongation helicase 1
SDSA	Synthesis-dependent strand annealing
SSA	Single-strand annealing
SSBs	Single-strand breaks
ssDNA	Single-stranded DNA
SUMO	Small ubiquitin like modifiers
WRN	Werner syndrome helicase
XLF	XRCC4 like factor
XRCC1	X-ray cross complemented 1
XRCC4	X-ray cross complemented 4

Appendix 3

Schipler A, Iliakis G.

DNA double-strand-break complexity levels and their possible contributions to the probability for error-prone processing and repair pathway choice.

Nucleic Acids Res. 2013 Sep;41(16):7589-605.

SURVEY AND SUMMARY

DNA double-strand-break complexity levels and their possible contributions to the probability for error-prone processing and repair pathway choice

Agnes Schipler and George Iliakis*

Institute of Medical Radiation Biology, University of Duisburg-Essen Medical School, 45122 Essen, Germany

Received April 22, 2013; Revised May 27, 2013; Accepted May 28, 2013

ABSTRACT

Although the DNA double-strand break (DSB) is defined as a rupture in the double-stranded DNA molecule that can occur without chemical modification in any of the constituent building blocks, it is recognized that this form is restricted to enzyme-induced DSBs. DSBs generated by physical or chemical agents can include at the break site a spectrum of base alterations (lesions). The nature and number of such chemical alterations define the complexity of the DSB and are considered putative determinants for repair pathway choice and the probability that errors will occur during this processing. As the pathways engaged in DSB processing show distinct and frequently inherent propensities for errors, pathway choice also defines the error-levels cells opt to accept. Here, we present a classification of DSBs on the basis of increasing complexity and discuss how complexity may affect processing, as well as how it may cause lethal or carcinogenic processing errors. By critically analyzing the characteristics of DSB repair pathways, we suggest that all repair pathways can in principle remove lesions clustering at the DSB but are likely to fail when they encounter clusters of DSBs that cause a local form of chromothripsis. In the same framework, we also analyze the rationale of DSB repair pathway choice.

INTRODUCTION

The defining feature of a double-strand break (DSB) as DNA lesion is the associated disruption of molecular continuity. The DSB severs in two fragments a linear DNA molecule and linearizes a circular molecule by disrupting the sugar-phosphate backbone on both strands and at

sites located directly opposite each other—or just a few nucleotides apart (up to ~10 bp).

DSBs, by affecting both DNA strands, compromise the fundamental principle used for the repair of lesions confined to one DNA strand: the possibility to use the complementary, undamaged strand as template to restore sequence in the damaged strand. Indeed, excision-based repair pathways, such as base excision repair (BER), nucleotide excision repair and mismatch repair, use the undamaged strand as template to restore the DNA molecule after removal (excision) of the damaged, or mismatched, segment (1).

This feature of the DSB allows the inference that its repair will be difficult, inherently inefficient and slow. However, comparison of the DSB repair kinetics with the kinetics measured for the repair of forms of DNA lesions only affecting one DNA strand provides a surprising outcome. Thus, CHO cells repair DSBs markedly faster than base damage or ultraviolet (UV)-induced lesions (Figure 1). Only the biologically much less consequential single-strand break (SSB) is repaired with slightly faster kinetics. Similar results can be compiled for other experimental systems and demonstrate that cells of higher eukaryotes have evolved an impressive capacity for removing DSBs from their genomes, despite the expected difficulties in performing this task.

The apparently effortless removal notwithstanding, DSBs remain biologically highly dangerous DNA lesions. Indeed, among DNA lesions, DSBs have the highest per lesion probability of causing numerous adverse biological effects including cell death, mutation, as well as transformation to a carcinogenic state.

The severity of the DSB as DNA lesion is evolutionarily ingrained into cellular function. This is convincingly demonstrated by the evolutionarily conserved, highly elaborate and complex network of responses cells mount, when detecting a DSB. The so called ‘DNA damage response (DDR)’ (8), originates, directly or indirectly, from the DSB (and single-stranded DNA regions)

*To whom correspondence should be addressed. Tel: +49 201 723 4152; Fax: +49 201 723 5966; Email: georg.iliakis@uk-essen.de

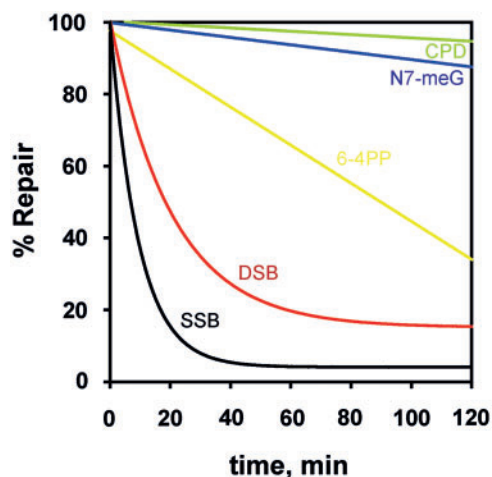


Figure 1. Kinetics of repair of different types of DNA lesions. Shown is the kinetics of removal from CHO-AA8 cells of SSBs, DSBs, 6–4 photoproducts (6–4PP), cyclobutane pyrimidine dimers (CPD) and, for human lymphocytes, of N7-meG. SSB and DSB repair was measured after exposure to 7.5 Gy and 100 Gy of γ -rays, respectively. SSBs were assayed by alkaline filter elution at pH 12.1 and DSBs by non-denaturing filter elution at pH 9.6 (2). Repair of UV-induced CPD and 6–4PP was measured in CHO cells by radioimmunoassay using damage-specific antibodies. Removal of antibody-binding sites after various repair times was determined after 10 J/m² UV-irradiation (3). Repair of N7-meG was measured in human lymphocytes after treatment with alkylating agents (7).

and includes comprehensive intracellular and intercellular regulatory processes that modify nearly every metabolic activity of the cell. The responses integrated in the DDR alert the cell to the DSB presence and set the stage for processing, adaptation or programmed cell death. Indeed, defects in DDR are associated with various developmental, immunological and neurological disorders and are a major driver of cancer (9).

The DDR is triggered not only by accidental DSBs randomly generated in the genome by exogenous agents such as ionizing radiation (IR) and certain chemicals, or during DNA replication stress (4–6), but also by programmed DSBs arising in well defined locations in the genome during meiosis, as well as during V(D)J and immunoglobulin heavy chain class switch recombination (CSR) (10). Thus, DDR integrates the biological responses initiated by DSBs into the cellular life cycle.

DSB PROCESSING CARRIES HIGH RISK FOR MISREPAIR

It may seem surprising why a lesion that can be processed by the cell efficiently and for which the cell devotes extensive resources still remains highly dangerous and linked to severe adverse biological consequences. Extensive work carried out over the past several decades converges to the idea that the adverse consequences of DSBs mainly result from errors or accidents in their processing. Indeed, there is evidence that the probability of processing errors is for DSBs much higher than for lesions confined to one DNA strand (11–14).

Considering the nature of the DSB, three scenarios for errors can be envisioned. First, processing is somehow

interrupted, the DSB remains open and the ends drift apart becoming inaccessible to each other for rejoining. Second, processing of the DSB occurs but after repair the junction is altered—slightly or severely. Associated consequences include here deletions involving several nucleotides; however, numerically conservative alterations in nucleotide sequence, as well as *de novo* additions of nucleotides are also possible (15,16). It should be noted, though, that point mutations are rare after exposure to DSB inducing agents. We discuss later that depending on the pathway engaged to the repair of a DSB, this type of error can be highly unlikely or common.

Third, processing of the DSB occurs, but during repair, incongruent ends are joined together causing thus structural alterations in the genome that can be visualized either as chromosome aberrations (mainly inter and intra chromosomal exchanges) (11–14,17–20), as size alterations in defined genomic restriction fragments after separation by gel electrophoresis (21,22), or finally as genomic alterations detected by next-generation sequencing approaches (23). This is by far the most consequential level of DSB-processing failure, as it generates new sequence combinations in the genome that disrupt or deregulate genes, and which may generate structural chromosome alterations that are incompatible with normal mitotic division. Under certain conditions, this form of error may also follow the events described in the first scenario.

Experimental evidence for all three error scenarios is abundant and typical examples are shown in Figure 2. Thus, unrepaired DSBs can surface as chromatid or chromosome breaks in the subsequent metaphase (Figure 2A); error-prone repair events can lead to large losses of sequence information inactivating a gene, for example, the HPRT gene (Figure 2B). Finally, the joining of wrong ends can cause translocations that can kill cells or can transform them to cancer cells (Figure 2C and the ring chromosome in 2A).

SOURCES OF DSB PROCESSING ERRORS AND PROCESSING ACCIDENTS

The causes of the aforementioned described types of erroneous DSB processing events warrant discussion. Of particular importance and relevance is, without any doubt, the identification and characterization of parameters determining the probability of their occurrence. Available information on the mechanisms underpinning DSB processing allows the definition of three main sources of DSB processing errors:

1. Inherent limitations of repair pathways engaged in DSB processing. As we briefly describe later in the text, multiple pathways process DSBs, and each shows distinct and frequently inherent propensities for errors. Notably, and possibly unexpectedly, the propensity for errors can vary dramatically among repair pathways. It follows that depending on the repair pathway choice made for a particular DSB, the associated risk for errors will vary accordingly. These limitations are compounded by the

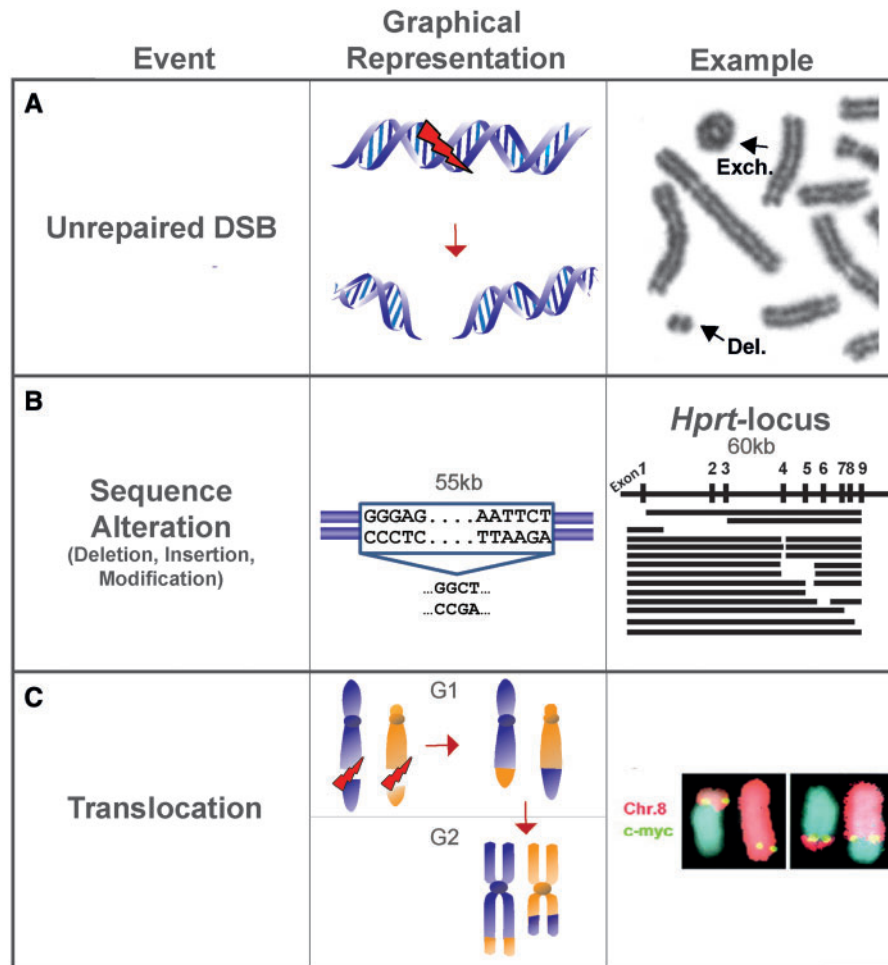


Figure 2. Three scenarios of DSB misrepair. (A) DSB ends drift apart resulting in a chromosomal aberration in the form of an acentric fragment (Del). (B) Rejoining of the DSB occurs but the junction is altered. Examples for large deletions in the *Hprt* locus are shown. The nine exons of *Hprt* are indicated at the top of the right panel. Genomic regions amplified by polymerase chain reaction are shown by solid lines. Spaces between the lines represent DNA sections that are deleted [drawn from results published by (24)]. (C) Joining of incongruent ends can cause chromosomal translocations. Fluorescence *in situ* hybridization analysis shows a c-myc/Ig locus translocation between chromosomes 8 and 14 in a multiple myeloma cell line [image from (25)]. An exchange-type aberration in the form of a ring chromosome is also shown in panel A (Exch).

specifics of the 3D organization of the genome that define the form of possible errors (e.g. translocations) on the basis of proximity between interacting regions and possibly other parameters as well (26–28).

2. The nature of the initiating DSB. Although the DSB is defined as a rupture in the double-stranded DNA molecule that can occur without chemical modification in any of the constituent DNA building blocks, it is recognized that this form of DSB is relatively rare and restricted to certain biologically induced DSBs (see later in the text). DSBs generated by physical or chemical agents can include with the DNA rupture a spectrum of chemical alterations (DNA lesions) in the neighboring bases. It is now widely considered that chemical alterations accompanying the DSB may be determinants of the form of DSB processing chosen by the cell and the probability that errors will occur during this processing. The term complexity is frequently used to describe some of these characteristics of the DSB (29,30).

3. The localization of the DSB in chromatin. The term ‘location’ can refer to the condensation status of chromatin at the site of the DSB, with two extremes: localization in euchromatin or in heterochromatin (31,32). However, location can also refer to sites with DSBs, where DNA replication or transcription occurs; these processes can be affected by a DSB, but they can also interfere with DSB processing and thus cause errors (33). Finally, location can also refer to specific characteristics of the genome including coding, or repetitive regions, intron/exon distribution, induction in active versus inactive genes and so forth.

In the following sections, we discuss possible sources of DSB processing errors and accidents. We first focus on structural aspects of the DSB, define levels of DSB complexity and discuss how DSB complexity may interfere with processing to cause errors. Subsequently, we describe briefly repair pathways engaged in DSB processing and discuss how processing errors such as those summarized in Figure 2 can emerge from their limitations.

The possible role of DSB localization, within chromatin etc., in the erroneous processing of a DSB is not subject of the review.

SYSTEMATIC ANALYSIS OF DSB COMPLEXITY LEVELS

Here, we attempt a classification of DSBs on the basis of increasing complexity and analyze how the specific characteristics of each class affect the processing requirements and the probability of processing errors. To facilitate presentation and subsequent discussion, we will define categories (types) comprising DSBs with progressively increasing complexity.

Type 1 (T1) DSBs: the simplest form

Classic examples of DSBs are those generated by restriction endonucleases (RE) (34,35). This family of proteins binds as a homodimer to specific DNA sequences and disrupts the phosphodiester bonds on both strands of the DNA molecule to generate either blunt or staggered ends (Figure 3A). As disruption of the phosphodiester bond by RE retains the 5'-phosphate and 3'-OH groups at each strand end, rejoining by simple ligation is in principle possible.

RE generates the simplest possible form of DSB, as they disrupt the continuity of the DNA molecule without chemically altering any of its constituent moieties, i.e. lesions in the form of sugar or base modifications are not introduced. We will term here this form of DSB type 1, T1-DSB, to distinguish it from more complex forms that are described later in the text (Figure 3A). Notably, even this 'simple' form of DSB is highly toxic, as indicated by the fact that RE evolved in bacteria as a defense mechanism against invading genomes.

The proposed, one-class grouping of RE-induced DSBs is certainly an oversimplification, as it disregards characteristics that may affect processing. Thus, type (3'- or 5'-) or length of protruding ends have been shown to affect the efficiency of DSB processing *in vitro*, and blunt-ended DSBs are generally more difficult to ligate than DSBs with protruding matching ends (16,38,39).

RE are frequently used as model reagents to generate DSBs at specific sites of a DNA molecule and to analyze the associated cellular responses. This approach has gained ground with the introduction of rare cutting RE and the I-SceI homing endonuclease for which the recognition sequence (18 bp) is not present in mammalian cells but can be introduced according to a pre-conceived design using molecular biology approaches (40–43). These sites can be subsequently cut to generate a DSB by either transfecting into cells vectors expressing I-SceI or by forcing the translocation from the cytoplasm into the nucleus of constitutively expressed I-SceI (44,45). The advantage of this approach is that DSBs are generated at a defined location in the genome, and appropriately constructed reporters allow functional analysis of specific repair pathways.

Type 2 (T2), DSBs: complexity deriving from modified ends

When DSBs are induced by physical or chemical agents, the alterations generated in the DNA are more complex. Among physical agents inducing DSBs, IR takes a prominent place. This is because IR, at low doses, is present in the environment and frequently used in diagnostic medicine. At higher doses, IR is used for the treatment of human diseases like cancer and inflammation (46,47). Recently, IR has gained ground in all fields of biology as a model agent for DSB induction owing to its unique physical characteristics that allow a timely well-defined DSB induction (most DSBs are generated only during the few minutes of exposure) with even distribution within cells (48,49). This goal cannot be achieved with DSB-inducing drugs, which need time to cross cell membrane, be metabolically activated (occasionally) and reach the DNA. In addition, drugs act subsequently for extended and difficult to precisely define periods. Incidentally, similar limitations apply to RE-induced DSBs (see earlier in the text), which require transfection and expression, or at a minimum intracellular translocation, of the I-SceI, or other endonuclease. Moreover, the enzyme remains functional in the cell nucleus for periods that are difficult to accurately define or precisely limit.

But why is IR generating DSBs in the DNA, and how do IR-induced DSBs compare with RE-induced DSBs? Although IR is frequently thought of as a DSB inducing agent, it by no means only generates DSBs in the DNA of irradiated cells. Actually, IR in the form of X-rays or γ -rays frequently used in the laboratory, induces, through oxidation reactions (either direct loss of an electron from DNA constituents or an attack by an \bullet OH produced by the radiolysis of adjacent water), a wide spectrum of lesions including sugar and base damages each of which outnumbers DSBs by \sim 20:1 (50,51). Certain forms of sugar damages disrupt the phosphodiester backbone of the DNA molecule and produce SSBs. It is the coincidence of two SSBs in opposite DNA strands with a maximum displacement of up to 10 bp that is thought to generate DSBs. These DSBs differ from those induced by RE because they frequently comprise a 3'-damaged sugar in the form of phosphoglycolate and a 5'-OH (Figure 3B) (52,53). This form of ends precludes direct DNA ligation and necessitates end processing as a step during repair (54). We will, therefore, term this more complex form of DSB type 2, T2-DSB, to distinguish it from that induced by RE. As IR-induced DSBs are generated by coincidence of two SSBs that can also be displaced by up to 10 bp, blunt ends or ends with protruding single strands similar to those described for RE can be generated.

Oxidation reactions, similar in principle to those initiated by IR, are also initiated by H_2O_2 , an oxidative agent that is also produced intracellularly as byproduct of the cellular metabolism (55). In this case, \bullet OH radicals, generated in the presence of metal ions by Fenton reactions, attack the DNA molecule producing base damages, SSBs and DSBs, more or less, randomly (55–57). Notably, however, after treatment with H_2O_2 , base and sugar

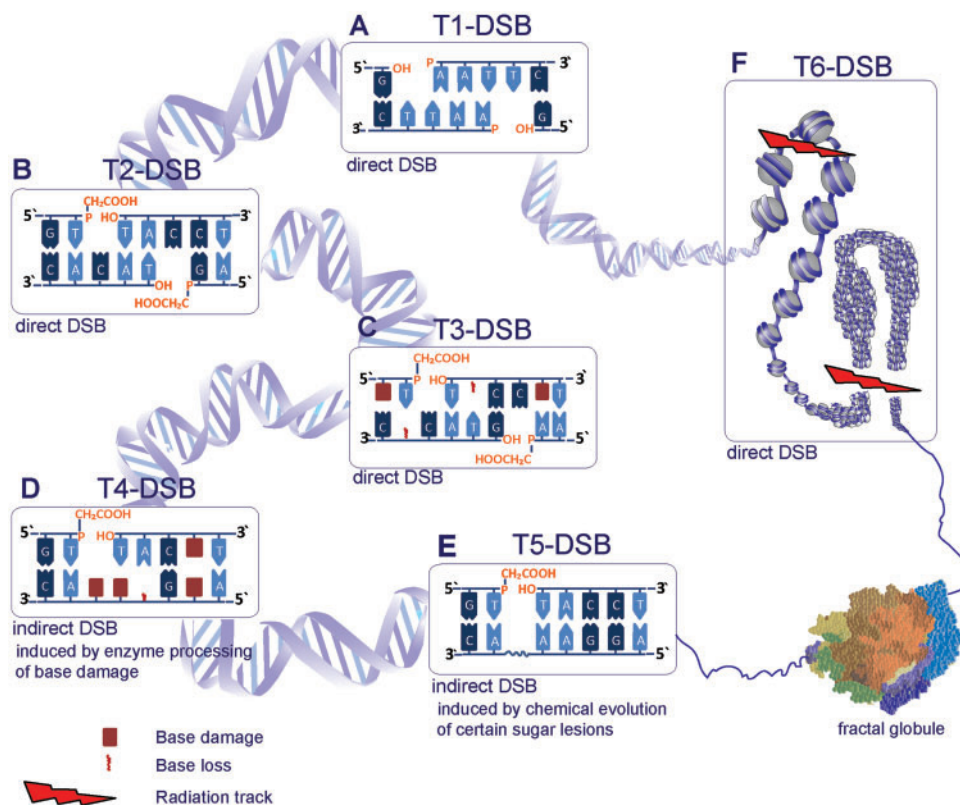


Figure 3. Illustration of the different types of DSBs as defined in the text. (A) T1-DSBs are direct DSBs induced by RE. An example for EcoRI DSB is shown that produces staggered ends with a 5'-phosphate and a 3'-OH group. (B) T2-DSBs are induced by IR and frequently comprise a 3'-phosphoglycolate and a 5'-OH at the DNA ends as shown in this example. (C) IR also induces clustered lesions from ionization clusters, defined as T3-DSBs. In this case, the direct DSB is accompanied by other types of lesions, like base damage or base loss proximal to the DSB. (D) T4-DSBs represent a non-DSB damage cluster that can convert to DSBs (indirect DSB) by enzymatic processing of the constituent base lesions. (E) T5-DSBs are also induced indirectly, up to 1 h after IR, by temperature-sensitive chemical processing of damaged sugar moieties opposing SSBs. (F) T6-DSBs are composed of clustered DSBs that can destabilize chromatin. Two possible scenarios are illustrated: in the first scenario (upper left) radiation induces two DSBs in the linker regions between a nucleosome risking nucleosome loss. The second scenario (lower right) shows higher-order packaging of nucleosomes forming a chromatin loop that is broken as shown by a radiation track. Here, loss of a larger segment of chromatin is possible. In the lower right corner of the drawing the 10-nm chromatin fiber is shown, compacted as a fractal globule (36,37); the opening of a loop from this fractal globule is indicated.

damages outnumber DSBs not only by 20:1 but by >10 000:1 (55). This difference in the relative yields of DSBs hints to specific characteristics of IR that underpin the efficient induction of DSBs. But what are these characteristics?

After exposure to H_2O_2 , and depending on the concentration used, the oxidation events generated by $\cdot\text{OH}$ radicals are relatively evenly distributed within the cell and the DNA and produce large amounts of SSBs (55–57). They produce low yields of DSBs because the probability of simultaneous local induction of two SSBs in opposite DNA strands is very low from a random distribution of oxidation events (Figure 4). However, after exposure to IR, the ionization events causing DNA damage, either directly by occurring in the DNA molecule itself or indirectly through radicals produced by ionization of atoms or molecules in the vicinity of the DNA, are not evenly distributed in space but localize along the tracks of the ionizing particles—secondary electrons in the case of X-rays and γ -rays (59). Using computational approaches based on Monte Carlo track structure codes the stochastic patterns of ionization can be

computed (49,60,61). These calculations show that secondary electrons, at the end of their tracks, generate clusters of ionizations, i.e. multiple ionizations confined in a small volume. When such ionization clusters are generated within the DNA, they can induce damages on both DNA strands and thus give rise to DSBs (Figure 4, see track of the 0.5 keV electron).

It is widely accepted that the adverse biological effects of X-rays or γ -rays derive from DSBs generated within such ionization clusters (62,63), rather than by the coincidence of independently generated ionizations on opposite DNA strands. This is the reason why the dose-yield curves for DSBs increase linearly and not with the square of the applied radiation dose. The simplest DSB that can be generated within such an ionization cluster is a T2-DSB (Figure 3B).

Type 3 (T3), DSBs: complexity deriving from the presence of DNA lesions in the vicinity of the break

Despite the generation of ionization clusters at the ends of low energy electron tracks, X-rays and γ -rays still deposit

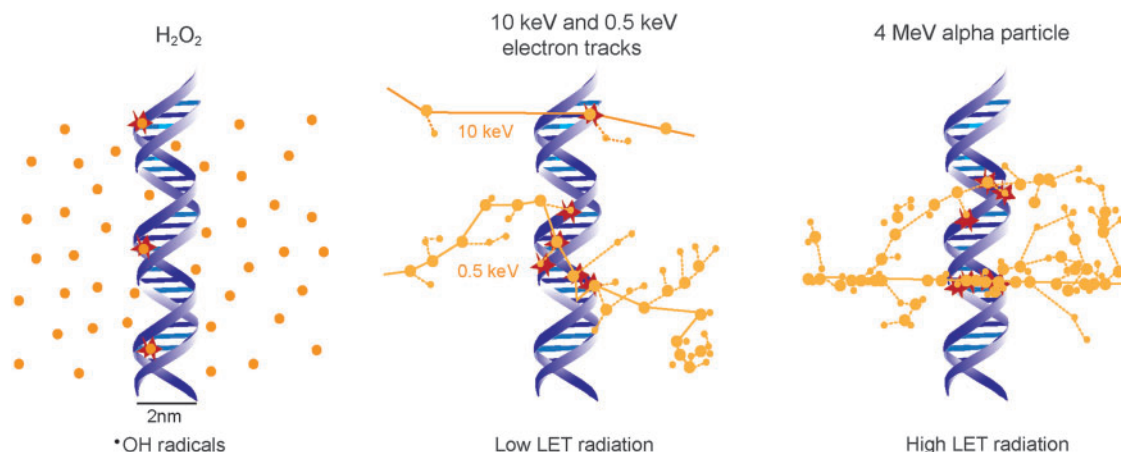


Figure 4. Distribution of DNA damage inducing events after exposure to H_2O_2 and IR of low and high LET. OH radicals from H_2O_2 are evenly distributed in space and induce, therefore, also evenly distributed DNA damage. In the case of IR, ionization events localize along the particle tracks [middle panel 0.5 and 10 keV electrons (e^-), right panel 4 MeV α particle] and can, therefore, induce clustered damage as indicated. Note that with increasing LET (from 10 to 0.5 keV e^- up to the 4 MeV α particle) the damage clustering increases. Large dots represent excitations along the radiation track. Monte Carlo simulated tracks are drawn for the 0.5 keV e^- and the α particle on the same scale as the DNA [redrawn from (58)]. The track for the 10 keV e^- , as well as the events shown after treatment with H_2O_2 are by free drawing and shown only for illustration purposes.

50–70% of their energy in well-separated ionization events from high-energy electrons that ionize sparsely and generate a relatively even ionization pattern within the cell (compare the tracks of high- and low-energy electrons in Figure 4) (62,63). This is why X-rays and γ -rays are considered sparsely ionizing, or low-linear energy transfer (LET), forms of IR. On the other hand, particulate forms of ionizing radiation such as neutrons, α particles, or carbon ions, are considered densely ionizing, or high LET, forms of radiation because they ionize along their tracks at a higher rate than the electrons generated by X-rays (64).

The computed ionization patterns in Figure 4 show the increased ionization density generated by an α particle as compared with an X-ray-generated secondary electron (particularly the high energy one). This increased clustering will also generate frequently DNA damage that is more complex than that induced by low-LET radiations, in the sense that it will comprise more lesions within one or two turns of the DNA helix. It constitutes what is sometimes called clustered damage sites (CDS) or multiply damaged sites (50,65). Although CDS is generated by low-LET radiation, such as X-rays, it occurs more frequently after exposure to high-LET radiations and is implicated in their enhanced biological effects. This is particularly important if one considers that similar numbers of ionizations, and thus presumably also DNA lesions, are generated after exposure to high- and low-LET radiations (51,65–67). Evidently, not only the number of ionizations but also their spatial distribution determines the biological effects of IR (49).

Indeed, although only $\sim 30\%$ of DSBs are expected to contain lesions in addition to the two strand breaks after exposure to low-energy electrons, this fraction increases to 70% after exposure to α -particles. Also, the ratio of the number of SSBs to DSBs is decreased from 22.8 for ^{60}Co

γ -rays to 3.4 for 50 MeV ^{12}C -ions (30,47). As these changes do not increase the yields of DSBs in a manner corresponding to the increased killing after exposure to high- versus low-LET radiation, it can be inferred that increased clustering of DNA damage is an important determinant of the gravity of the resulting biological effect (but see also later in the text) (68).

The simultaneous presence of DSBs and other forms of DNA damage within a clustered damage site generates the next level of complexity, which we term here DSB of type 3, T3-DSB (Figure 3C). The increased complexity of T3-DSBs may compromise cellular repair through the simultaneous recruitment and even engagement of two repair pathways (e.g. DSB repair and BER) to lesions present in close proximity in the DNA molecule. A similar situation is generated by the covalent attachment of proteins at the DSB ends, as it occurs, for example, in DSBs induced by topoisomerase inhibitors (69). Such complications may increase the probability of processing errors as compared with the simpler forms of DSBs described later in the text.

Type 4 (T4) DSBs: indirect form, arising from base damage processing within a non-DSB-CDS

In addition to DNA damage clusters that generate DSBs right at the outset, IR also generates clusters of base damage, possibly including SSBs, which do not form DSBs immediately (non-DSB clusters). DSBs can subsequently form through the processing of a base lesion opposite an unrepaired SSB, or through the parallel processing on both DNA strands of base damage (Figure 3D) (30,70–72). There is evidence that this form of clustered DNA damage outnumbers T2/T3-DSBs after exposure to low-LET radiation by nearly 4:1.

Although the extremely fast processing of SSBs and the particularly slow processing of base damage (Figure 1) reduce the probability for unrepaired SSBs when BER

starts, here again repair by either pathway may be impaired by this clustering of DNA damage and possibly also by the parallel recruitment of components of different repair pathways. Indeed, the repair efficiency of non-DSB clusters processed by BER depends on the nature, the orientation (bi-stranded or tandem) and the distance between lesions (73–76). One or more lesions within a non-DSB cluster can remain unrepaired as a result of reduced or altered glycosylase activity in this context. In the case of bi-stranded clusters containing either two AP sites or an SSB opposing an AP site, a DSB is likely to form through the incision of the AP site during repair (77).

Indirect DSBs forming by the simultaneous disruption of the phosphodiester bond at base damage sites in opposite DNA strands or with the combination of BER activity with a SSB at the opposite strand, form yet another level of complexity that integrates the parameter time post-irradiation in the induction process, and which we will, therefore, term here type 4 DSBs, T4-DSBs. A discriminating characteristic of a T4-DSB is that as it forms, proteins participating in SSB and/or BER may already be engaged at or near the ends of the resulting DSB, which may impair its recognition and processing by the cell.

Type 5 (T5) DSBs: indirect form arising from chemical processing of sugar damage within a CDS

There is evidence that IR induces, in addition to sugar lesions promptly disrupting the sugar–phosphate backbone (prompt DSBs), also lesions doing so after temperature-dependent chemical processing (delayed DSBs) (78). These thermally labile sugar lesions constitute what are considered radiation-induced labile sites (68,78,79). They can include diverse forms of sugar damage, abasic sites and forms of base damage affecting sugar stability. Chemical evolution of such lesions to SSBs within a CDS can generate additional DSBs (62,78,80–83).

Until recently, it was believed that in mammalian cells evolution of such lesions to DSBs only occurs when DNA is incubated after irradiation at high, non-physiological temperatures (e.g. $\sim 50^{\circ}\text{C}$ typically used for cell lysis to analyze DNA breakage) (84–86). However, recent work (87–89) provides evidence that IR induces thermally unstable lesions, which evolve within ~ 1 h under physiological temperatures to SSBs and contribute, when present within a CDS, to the formation of DSBs. These delayed-forming DSBs are thought to be generated continuously during the first post-irradiation hour, and to add to promptly induced DSBs (88).

This process represents yet another way for generating indirectly DSBs within a CDS, which we will term here type 5 DSBs, T5-DSBs, to distinguish them from the other categories described above and also later in the text (Figure 3E). Like T4-DSB, T5-DSBs evolve from non-DSB CDS and belong, therefore, to the indirectly induced DSBs. Several of the complications outlined for the processing of T4-DSBs also apply for the processing of T5-DSBs.

Type 6 (T6) DSBs: complexity deriving from destabilizing chromatin fragmentation via multiple, clustered DSBs

As an additional level of increasing DSB complexity, we consider here clusters of DSBs, where the individual DSBs can in principle belong to any of the aforementioned defined types. This form of DNA damage disrupts the continuity of the DNA in the same general way as simpler forms of DSBs do. However, by involving several DSBs in close proximity (DSB clusters), it severely undermines local chromatin stability and thus overall processing in a location- and composition-dependent manner. On the basis of its constitution, this form of damage can also be considered as a form of highly local chromothripsis—a phenomenon whereby as of yet undefined processes cause extensive local genomic fragmentation (thripsis), which invokes inaccurate rejoining that feeds carcinogenesis (90–93).

DSB clustering as a source of small DNA fragments in irradiated cells and a cause of irreversible radiation effects has been considered by several investigators [see (49) for a review]. Bryant, Johnston and colleagues (94–96) developed a non-ionic neutral filter elution assay to generate histone-depleted nuclear structures retaining higher-order nuclear matrix organization, and used it to measure DNA fragment loss from two or more DSBs within a single-looped chromatin domain. They observed that the spatial distribution of DSBs in higher-order chromatin loops affects their reparability. Fast repair is measured in loops containing a single DSB but slow repair in loops containing multiple DSBs. The latter form of repair is not detectable in cells deficient in Ku80 (see next section). They proposed that higher-order chromatin structure and the spatial distribution of DSBs in topologically independent, looped domains (of ~ 1.6 Mb, as in replicon clusters) plays a crucial role in DSB repair and that misrepair involves DNA fragments loss at such DSB clusters.

Holley and Chatterjee (97) also considered DSB clusters as a particularly consequential form of radiation damage and performed Monte Carlo simulations for the induction in chromatin of such clusters with increasing LET. Their calculations confirm the overall increase in DSB clustering with LET and show the potential of generating in this way relatively small DNA fragments. In these calculations, fragmentation peaks are found at 85 bp and then again at multiples of 1000 bp, independently of LET, possibly representing the revolution period of the DNA about the histone core (~ 85 bp) and the periodicity of nucleosomes packed in a solenoid model of chromatin (see later in the text), respectively. Notably, such small fragments can indeed be detected experimentally using pulsed-field gel electrophoresis in irradiated human fibroblasts (98,99) and can also be inferred by alternative modeling approaches (49,100,101). Atomic force microscopy imaging also shows the induction of clustered DSBs and the associated formation of short DNA fragments— even when irradiating ‘naked’ DNA devoid of any organization as chromatin (102). In the latter experiments, only 35% of the generated fragments are smaller than 147 bp in length

after exposure to low LET radiation, but this proportion increases to 70% after exposure to high-LET radiation.

Small (<70 bp) DNA fragments generated from clustered DSBs have also been implicated by Wang *et al.* (103) in the enhanced killing observed after exposure of cells to high-LET radiation. The authors attribute the enhanced toxicity of such fragments specifically to their inability to accommodate bi-directional binding of the Ku-protein (requires ~30 bp on each side of the DNA fragment, see later in the text and Figure 6D), which is required for the efficient repair of the DSBs within the cluster (103). Notably, additional work shows that the activity of DNA-PK, a complex between the Ku70/80 heterodimer and DNA-PKcs (see later in the text), is also inhibited by short (14–20 bp) DNA fragments (102).

Two essential processes for the maturation of the immune system are mediated by the programmed and highly regulated induction of clusters of DSBs, and in both processes, the intervening DNA segment is lost, albeit in a highly regulated manner (10,104). In V(D)J recombination, taking place in developing B (and T) lymphocytes, the N-terminal variable region of Ig heavy and light chains that bind the antigen is assembled from germ line V, D and J gene segments. This is achieved by the lymphocyte-specific RAG endonuclease, comprising recombination activating gene (RAG) 1 and 2 proteins. The reaction is initiated by the introduction of two DSBs adjacent to target V, D and J sites and proceeds with the removal of the intervening DNA segment and the joining of remaining DNA ends by non-homologous end-joining (NHEJ). Subsequently, and on antigen activation, mature B cells also undergo IgH CSR that replaces one set of IgH constant region exons with another, allowing B cells to secrete different effector antibody classes. CSR is initiated by activation-induced cytidine deaminase that generates DSBs indirectly through clusters of base damage (T4-DSB) in downstream portions of IgH. Such DSBs are joined by NHEJ to complete CSR (105). Notably, this generation of functional antigen receptor loci via clustered-DSB intermediates poses great oncogenic risks (106), which are compounded by the ability of antigen receptor locus regulatory elements to activate expression of the translocated oncogene.

The generation of DSB clusters and their contribution to the adverse effects of IR has also been the subject of extensive mathematical modeling (49). Ostashevsky (107,108) analyzed in this manner the consequences of chromatin fragmentation and ultimately of cell death. The assumption of the developed model is that DSBs generate small and, therefore, unstable DNA fragments (terminal or interstitial) that can be lost from the chromatin context, thus compromising repair of the constituent DSBs (Figures 3 and 5). The probability that such fragments will be lost from their chromatin context is thought to increase with decreasing fragment length. A more specialized induction of DSB clusters within chromatin loops, similar to that considered by Bryant and Johnston, has been used to develop alternative mathematical models by Friedland *et al.* (49,100,101,109), Cucinotta and co-workers (110), as well as by Scholz and co-workers

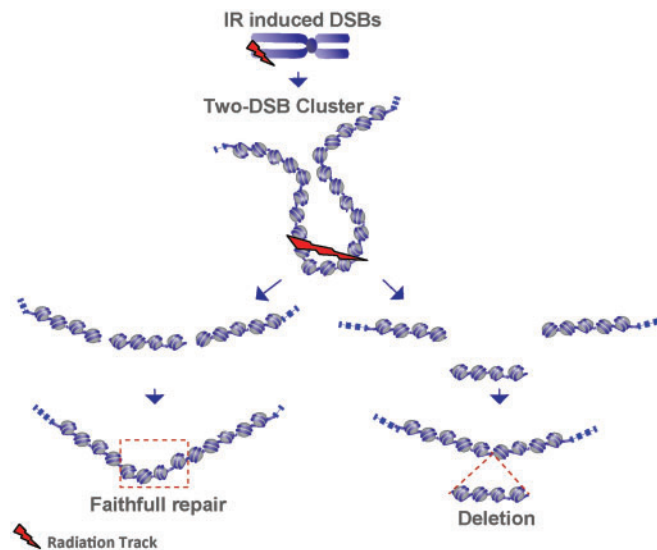


Figure 5. Fragment loss through 2xDSB cluster. An example of clustered DSB: two DSBs in the cluster induced in the linker region between nucleosomes. It can lead to chromatin destabilization through the loss of the DNA segment between the two DSBs. Two possible processing scenarios are illustrated. If the DSB ends stay close, the DNA molecule is restored by simple rejoining. In a second scenario (shown on the right), a small DNA fragment comprising four nucleosomes is lost from the chromatin context causing a deletion and possibly also jeopardizing, or somehow impairing, all forms of processing.

(111–113). The satisfactory fitting achieved under these assumptions of cell survival and DSB repair results suggests that DSB clusters represent a precarious form of DNA damage. Notably, all these models also offer a plausible explanation for the increased biological efficacy of high-LET radiation, as the yields of clustered DSBs are expected to increase, and the length of the associated fragments to decrease with increasing LET (see later in the text). An example of clustered DSBs generating a small (~10 bp) DNA fragment is shown in Figure 4 for the energy deposition pattern calculated for the α particle.

In aggregate, the aforementioned work provides strong albeit indirect support for DSB clustering as yet another level of DSB complexity, which we here term type 6 DSBs—T6-DSBs (Figure 3F). Notably, this form of DNA damage is only rarely studied experimentally despite its potential implications in the adverse effects of IR. Repair complications from DSB clustering will mainly derive from the instability of the generated DNA fragments, whose loss from the higher-order chromatin context is likely to impair the function of all DSB repair pathways (Figure 5) and to cause thus chromosome aberrations (114). Similar complications in repair may incur during chromothripsis and the consequences of the associated chromosome shattering observed may have the same mechanistic underpinnings as those of IR-induced DSB clusters (90–93).

The probability of fragment loss from DSB clusters is likely to depend on the distance between constituent DSBs but will also be strongly determined by the structure of chromatin and its degree of condensation at the cluster site

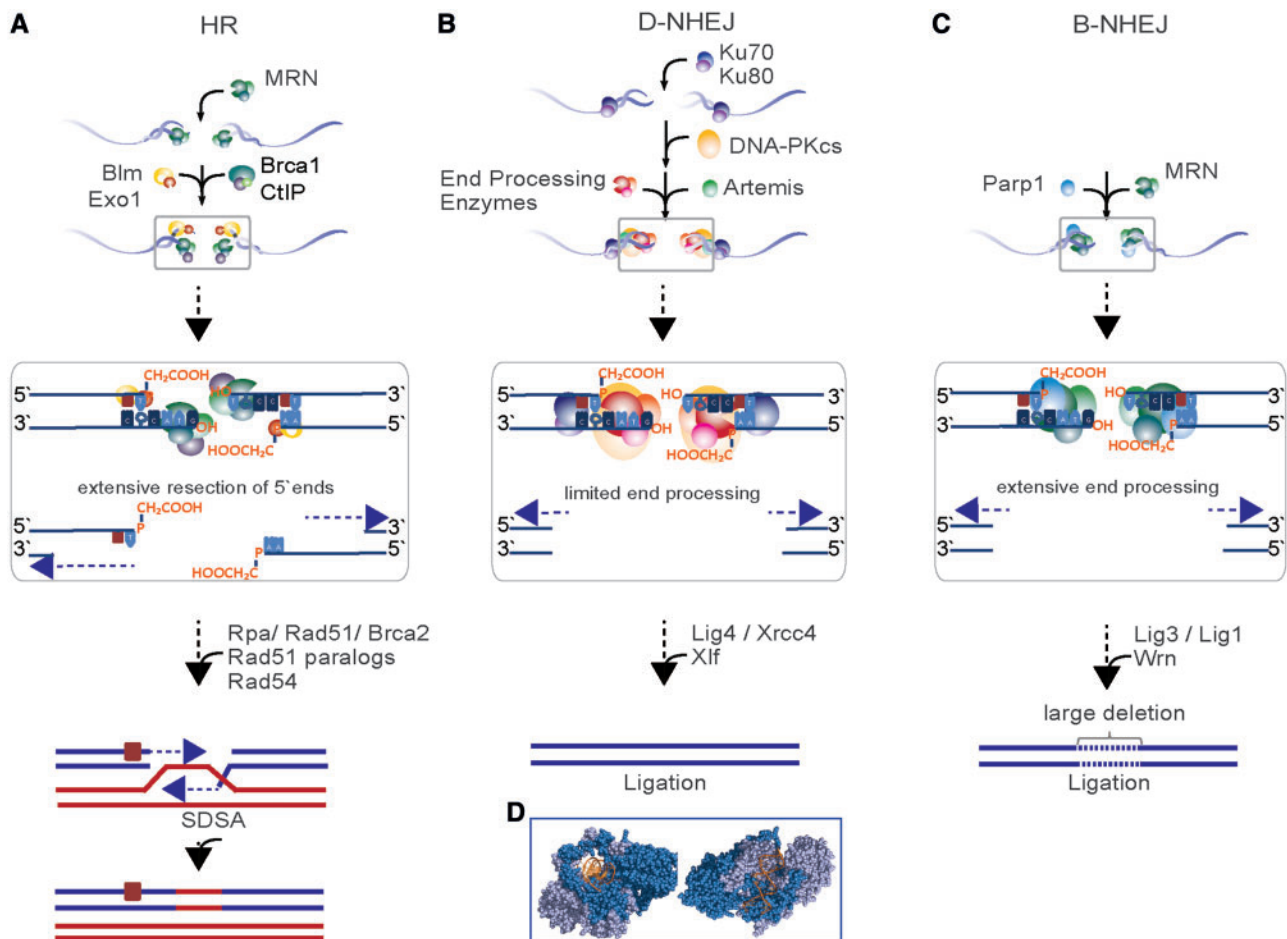


Figure 6. Key steps of DSB repair pathways (HRR, D-NHEJ and B-NHEJ) with examples of end-processing options for T3-DSBs. (A) During HRR, extensive processing of the 5'-ends takes place that can remove lesions in the vicinity of DSB ends. Although base damage remains at the 3'-end after HRR, the DSB is repaired and the remaining single base lesion can be removed by BER at a later time. (B) For D-NHEJ, limited end processing takes place at both DNA strands—5' and 3'. As a result, lesions that span up to 10 bp from the DSB ends could be removed as well, although their presence is likely to delay this processing. (C) During B-NHEJ, even more extensive end processing takes place, and as for D-NHEJ, lesions adjacent to the DSB may be removed. B-NHEJ often results in large deletions—and translocations. (D) Illustration of Ku bound to DNA. This protein–DNA interaction was visualized using the program PyMOL (PyMOL Molecular Graphics System, Version 1.2r3pre, Schrödinger, LLC). The results are from (129). The structure illustrates that each Ku molecule binds roughly two helical turns of DNA.

(see the two examples illustrated in Figure 3F involving only one nucleosome, or a larger chromatin segment). Although the prevailing model for chromatin structure > 10-nm nucleosome filament is that of a 30-nm chromatin fiber including 6–7 nucleosomes per 10-nm length of fiber, recent results question the existence of such structure (115–119). The characterization of human chromatin using novel chromosome conformational capture techniques (23,120–124) favors an alternative structural model of human chromosome with the 10-nm fiber folded in a regulated manner as a long-lived fractal globule—a compact polymer state that emerges during polymer condensation as a result of topological constraints, which prevent one region of the chain from passing across another one (Figure 3, lower right model) (36,37). It will be particularly interesting to examine the stability of DNA fragments generated by DSB clusters in this model of chromatin architecture.

One limitation of the approaches taken hitherto to understand the consequences of T6-DSBs is that they

are indirect, and only mathematical modeling allows connection to biological consequences (49). Vice-versa, approaches documenting the formation of such DNA fragments are in general devoid of directly linked biological effects. As a result the conclusions drawn are tentative and indicative at best.

The nature of DSB induction precludes mechanistic experiments on T6-DSBs using IR as a model agent, as each of the irradiated cells sustains DSBs in a stochastic manner at different numbers and severity, which are randomly distributed throughout the genome; thus, analysis of effects is possible only by theoretical modeling that is tested by fitting to existing data (49). The earlier discussed uncertainty about the 30-nm chromatin fiber that implicitly or explicitly underpins present modeling approaches further complicates the situation. The field will benefit from molecular biology approaches modeling defined combinations of DSB clusters and testing their effects. For example, cell lines can be developed in which simple DSBs, and DSB-clusters are

generated by restriction of I-SceI recognition-sequence-clusters (or the sequences of other site-specific restriction endonucleases) engineered *in vitro* at defined distances (or designed to cut at specific locations in the genome) in a plasmid that is subsequently integrated in multiple copies in the cellular genome. We are presently testing and validating this approach in our laboratory.

PATHWAYS OF DSB REPAIR AND THEIR INHERENT PROPENSITIES FOR PROCESSING ERRORS

Key components of DDR are evolutionarily conserved repair pathways processing DSBs to preserve the integrity of the genome (125,126). DSB repair pathways are broadly classified as homology dependent and homology independent. Homology-independent pathways function throughout the cell cycle and include the DNA-PK-dependent non-homologous end-joining (D-NHEJ; the terms classical or canonical are also frequently used to describe this repair pathway), as well as an alternative end-joining pathway that under certain circumstances operates as back-up to D-NHEJ, and possibly also to homologous recombination repair (HRR), and is, therefore, termed alt-EJ, or B-NHEJ. Homology-dependent pathways, on the other hand, show strong cell cycle dependence and operate only when a sister chromatid becomes available after semi-conservative DNA replication. In the following sections, we describe the key features of each of these DSB repair pathways, outline their inherent propensities for errors and describe the types and sources of errors they can produce.

Homologous recombination repair

HRR is an error-free repair process (127,128) that can be divided into three main stages: pre-synaptic, synaptic and post-synaptic (Figure 6A). After sensing of the DSB by MRN (Mre11-Rad50-Nbs1) in the pre-synaptic stage, the DNA is resected at the DSB site to form an extended region of single-stranded DNA (ssDNA) with 3'-overhangs. Several factors have been implicated in this step including MRN, Exo1, Dna2 and CtIP, as well as the BLM helicase (15). The ssDNA generated in this way is promptly coated by RPA for stabilization from secondary structures and preparation for Rad51 nucleoprotein filament formation. For efficient Rad51 filament formation, different classes of mediator proteins like the Rad51 paralogs (Rad51B, Rad51C, Rad51D, Xrcc2 and Xrcc3), as well as Brca2 are used.

During synapsis, the Rad51 nucleoprotein filament searches for homology and performs strand invasion to form a Holliday junction. Rad54 promotes DNA synthesis associated with branch migration by dissociating Rad51 from the heteroduplex DNA. In the post-synaptic steps associated with a specific sub-pathway (130), synthesis-dependent strand annealing (SDSA), the extended Holliday junction is resolved. This enables the annealing of the newly synthesized strand with the resected strand of the second DNA end and restores the broken DNA

molecule by subsequent DNA synthesis and ligation (Figure 6A).

SDSA is a common DSB repair mechanism in cells of higher eukaryotes. In a different sub-pathway of HRR (not depicted), invasion of both DSB ends into the non-damaged sister chromatid leads to the formation of a double Holliday junction that migrates along the chromatids by DNA synthesis; its subsequent resolution is associated with crossover or non-crossover events depending on which strands are cut by a resolvase (130,131). The outlined complexity of the events involved in HRR and the requirement for homology search makes this repair pathway inherently slow.

The templated nature (through the sister chromatid) of DSB-repair by HRR not only ensures the structural restoration of the DNA molecule but also enables the preservation of the DNA sequence at the DSB. As a result, HRR is an error-free repair pathway on every count.

The events initiating HRR imply that a wide spectrum of structural DNA-end substrate configurations at the DSB, like variations in the overhang length, DNA-end sequence and DNA-end chemistry (e.g. 3'-phosphoglycolate or 5'-OH present in T2 and T3-DSBs) can be accommodated, although they may slow processing (see earlier in the text). This is because many of the altered or missing bases will be removed during resection, and those present in the 3'-ends that are not resected may be either removed by limited resection or may remain in the DNA for processing after completion of the DSB repair (illustrated in Figure 6A). HRR can thus function as a processing integrator for DSB ends with widely different chemistry. We return to this flexibility later in the text.

D-NHEJ

D-NHEJ is widely considered as the prevalent DSB repair pathway in higher eukaryotes (125,126). It mediates the fast ligation of broken DNA ends to ensure chromosome integrity (16) (Figure 6B). It is initiated by the binding of the Ku70/Ku80 heterodimer to DSB termini, which in turn recruits and activates the large protein kinase, DNA-PKcs, to generate a binding scaffold for other NHEJ factors and to mediate their regulation by phosphorylation (132). The process culminates with the ligation of the two DNA ends by the Ligase 4/Xrcc4/Xlf protein complex after displacement of DNA-PKcs from the ends through autophosphorylation. When required, various DNA end-processing functions, including the addition of a 5'-phosphate by Pnk and the removal of 3'-phosphoglycolates by Tdp1, Pnk or Artemis, ensure the generation of ligatable DNA ends (69). Filling of occasionally missing nucleotides is mediated by DNA polymerases λ and μ .

The earlier outlined mechanistic background of D-NHEJ directly points to important strengths but also indicates inherent limitations. D-NHEJ enzymes tolerate a wide spectrum of structural DNA-end substrate configurations, like variations in the overhang length, DNA-end sequence and DNA-end chemistry. It thus can also function as an important integrator funneling for processing ends with widely different chemistry.

The second important feature of this pathway is speed of operation (13). The DSB kinetics shown in Figure 1 actually reflects the function of this repair pathway. Although not formally shown, the key factors of this pathway likely operate in unison and form through sequential interactions a molecular machine at the DSB that ensures fast repair. This unparalleled speed (Figure 1) may be the most defining characteristic of D-NHEJ, as it also maximizes the probability for the joining of the original DNA ends—by reducing the time available for diffusion of DNA-ends away from each other (13). As a result, D-NHEJ suppresses chromosome translocations (13,14,133,134). However, as far as we know at the moment, this pathway has no build-in means (possibly apart from the efficiency of the associated molecular machine) to ensure joining of the original DNA ends- or to suppress joining of incorrect ends. Thus, translocations are in principle possible and do occur through this repair mechanism, albeit infrequently.

Notably, the most salient limitation of the pathway is the absence of build-in mechanisms ensuring the restoration of DNA sequence at the DSB. As a result, changes in nucleotide sequence, or additions and deletions of nucleotides, are likely events (16). Such events become far more likely when end-processing is required to generate ligatable ends, as it is, for example, the case for DSBs of types 2–5. However, here again the high speed of operation ensures that the processing occurring at the ends is more limited than after end joining by the alternative pathway discussed later in the text.

These circumstances render D-NHEJ inherently error prone with high probability for sequence alterations at the junction but low probability for translocations (Figure 7). Indeed, analysis of sequence alterations after RE-induced DSBs at the endogenous thymidine kinase gene (TK) revealed deletion sizes from 1 up to 1201 with

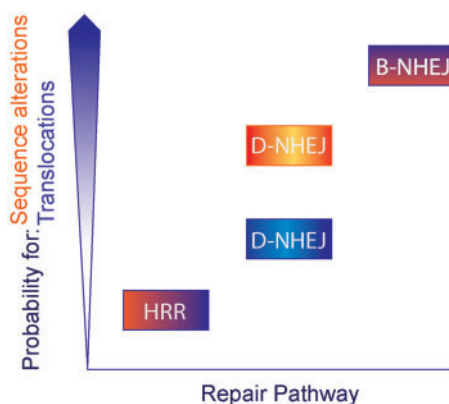


Figure 7. Propensity for errors by HRR, D-NHEJ and B-NHEJ. For each repair pathway, the probability for sequence alterations at the junction is indicated with orange shading, whereas the probability for translocations is indicated with blue shading. The scale is arbitrary and serves only illustration purposes—also when comparing the two sources of errors. HRR has very low probability for both sequence alterations at the junction, as well as for translocations. D-NHEJ has low probability for translocations, but relatively high probability for sequence alterations at the junction. B-NHEJ is, on the other hand, highly error prone on all counts.

a median deletion size of 22 bp (135). Finally, and in line with the arguments raised earlier in the text, damaged-end groups such as damaged bases and sugars, do not affect DNA-PK activation, suggesting that end group chemistry does not have an inhibitory effect on DNA-PK kinase activity (102), although there is evidence for processing impairment *in vitro* assays (73,76).

B-NHEJ

B-NHEJ is an alternative form of DNA end-joining thought to function as back-up to D-NHEJ (13), and possibly also to HRR, hence, the term B-NHEJ (Figure 6C). However, the term alternative end-joining is also frequently used (105,126,136). Although it functions on similar principles, B-NHEJ is slower and less efficient and as a result more error prone than D-NHEJ on two counts (Figure 7). First, deletions and other modifications at the junction are larger than after D-NHEJ. Second, and particularly relevant, the joining probability of unrelated ends is markedly increased. Thus, although the differences in the type of errors generated by D-NHEJ and B-NHEJ are quantitative rather than qualitative (both are unable to restore the junction and can join unrelated DNA ends), B-NHEJ is considered a main source of chromosomal translocations (Figure 7) (13,14,133,134).

Although B-NHEJ can be conveniently studied when D-NHEJ is genetically or chemically compromised, B-NHEJ is thought to get engaged in all cases where D-NHEJ, and possibly HRR, somehow fails. Such failures may include all instances where the assembly of the aforementioned D-NHEJ machine at the DSB is unsuccessful. It seems that B-NHEJ can function in the presence of certain D-NHEJ components (e.g. Lig4, DNA-PKcs etc. in Ku-deficient cells), but it is not clear what role these remaining D-NHEJ components play in the rejoining process. On the other hand, there is evidence that other D-NHEJ components, e.g. Ku, suppress B-NHEJ by preventing one of its putative components, Parp-1, to bind to DNA ends (137).

Although the enzymology and mechanistic details of B-NHEJ are incompletely understood, there is evidence that this pathway can use DNA ligases I and III (Lig1 and Lig3) in the final step (Figure 6C) (138–141). The involvement of Lig3 also explains the involvement of the Parp-1/Lig3/Xrcc1 module that is known to be involved in the repair of SSBs (125,141,142). However, recent work questions the requirement for Xrcc1 in DSB repair by this pathway (138,139,143).

Probably as a result of the slow kinetics but certainly also by virtue of its functional characteristics, B-NHEJ allows more DNA end processing than D-NHEJ. Not surprisingly, therefore, a number of end-processing activities involved in HRR, such as Mre11 (144) and CtIP, as well as Wrn and Bcr/Abl have been implicated in its function (145). This is in line with the possibility that B-NHEJ also backs up failed HRR and explains the frequent presence of microhomologies at B-NHEJ-mediated junctions (136). However, in several experimental systems, microhomology is not a requirement for efficient B-NHEJ.

Finally, B-NHEJ may benefit from the linker histone H1 serving as an alignment factor (146).

Like D-NHEJ, B-NHEJ is also active throughout the cell cycle (147–150). However, unlike D-NHEJ, it shows strong cell cycle-dependent fluctuations with increased activity in G₂, reduced in G₁ and markedly ablated in resting cells (147,148,151,152). Like the other DSB repair pathways, B-NHEJ can accommodate a wide spectrum of DNA-end chemistries (Figure 6C).

Analysis of processing complications for T1-T6-DSBs

The earlier outline indicates that IR-induced DSBs can be present in different ‘flavors’, which in the case of IR strongly depends on the energy deposition events underlying their induction and, thus, the type of radiation used to generate them. DSB complexity, as outlined earlier in the text, is likely to confound DSB processing and may increase the risk of generating processing failures as outlined in Figure 2.

T1-DSBs can be shunted to all known DSB repair pathways, and there are no complications associated with the repair by anyone of them beyond the destabilization of the molecule generated by the DSB and which is a common characteristic of all DSBs.

T2-DSBs have non-ligatable ends and will require end processing before the final ligation. This end processing should be straightforward when repair is started by HRR because of the extensive end processing integrated in this repair pathway (Figure 6A). End processing is also an integral part of D-NHEJ and should also be efficient in B-NHEJ as indicated by the high speed it processes a relatively large proportion of DSBs in D-NHEJ-deficient cells (Figure 6B and C).

Investigation of the processing of T3 and T4 DSBs is a highly active area focusing on the consequences of damage clustering on the functions of enzymes involved in base damage and strand break repair (30,70,153).

But, is the increased level of complexity of T3 and T4 DSBs expected to compromise DSB processing by the known repair pathways? DSB processing by D-NHEJ starts with the binding of Ku to the generated DNA ends, an interaction that occurs extremely fast (10^{-9} M) and involves >15 bp of sequence on each side of the break (Figure 6D) (129). Ku binding on a T3-DSB will suppress the recruitment of base damage repair factors within a CDS, as it will cover over three helical turns of the DNA—or a 3-fold longer DNA segment than the 10 bp typical extension for a CDS. On the other hand, Ku binding to the DNA ends is not impaired by short single-stranded regions and may not be inhibited by the presence of base damage in the vicinity of the DNA ends ensuring thus normal efficiency for D-NHEJ (132). If the ensuing normal end-processing during D-NHEJ removes the damaged bases of the T3-DSBs, site restoration similar to a T2-DSB will occur—possibly with a slight delay. Alternatively, base damage may be retained and may be removed after the rejoining of the DSB ends. An example of such form of processing is indicated in the insert window of Figure 6B.

Similar arguments can be developed for the processing of T3-DSBs by HRR. Here, resection of the 5'-end for up to 2 kb will remove associated base damage—possibly with only a slight delay. Even base damage present within 10 bp on the 3'-end that is not resected may be removed without grossly impairing subsequent processing steps (see example integrated in Figure 6A). Finally, similar arguments can be developed for the processing of T3-DSBs by B-NHEJ. T4 DSBs are similar to the individual DSBs generated during CSR, and under normal circumstances lymphocytes do not seem to have problems dealing with them. This may also be true to similarly induced DSBs in irradiated cells. There is uncertainty as to how cells will respond to T5-DSBs, but the available evidence suggests that they are detected and processed like any of the previous forms of DSBs (88).

Thus, there are no pathway-specific, urgent reasons rationalizing why T3-T5 DSBs should be much more difficult to repair using HRR, D-NHEJ, or B-NHEJ than T1- or T2-DSBs. This may actually be a reason why the validity of conclusions reached using T1-DSBs as a model has not been so far questioned using more complex forms of DSBs. The question can, therefore, be raised as to whether the most severe form of damage complexity defined here, T6-DSBs, is likely to cause processing problems and thus the adverse effects of IR and their increase with increasing LET. Future work should, therefore, focus on characterizing the consequences of defined T6-DSBs using appropriate systems that allow a conclusive analysis of their biological consequences and test the hypothesis of their increased biological severity.

General considerations for DSB repair pathway choice

The preceding description of the characteristics of the known pathways engaged in the processing of DSBs indicates marked differences in their inherent ability to faithfully repair the DSB and thus to maintain genomic integrity. In a hierarchical categorization of the pathways, B-NHEJ will have the highest propensity for errors and HRR the lowest (Figure 7). Actually, among the available repair pathways, only HRR is designed to restore every aspect of a DNA molecule that has sustained a DSB. Yet, HRR can only function when a sister chromatid is present, and even then it is bound to be slow. D-NHEJ, on the other hand, functions throughout the cell cycle, including S- and G₂-phase and has the potential to quickly remove DSBs from the genome, and thus to structurally stabilize it. However, as pointed out earlier in the text, this speedy stabilization has its price, as D-NHEJ readily accepts sequence information losses at the junction. Also the joining of unrelated ends is possible and can lead, although infrequently, to chromosome translocations (Figure 7).

B-NHEJ surfaces as the most precarious of all DSB repair pathways, as it combines increased level of information loss at the junction with much higher probability for chromosome exchange formation. As in some experimental settings, NHEJ pathways seem to be preferred over HRR in cells of higher eukaryotes (see earlier in the text), one can speculate that cells have developed tolerance for

DNA sequence modifications at the junction. The same tolerance mechanisms likely allow chromosome exchanges, thus causing cell death, and in multicellular organisms cancer (14,133,134).

Thus, we become confronted with the conundrum that documented errors in DSB processing, with severe adverse effects, are inherent to the repair pathways used by the cells. This begs the question why cells chose an error-prone repair pathway when an error-free repair pathway, HRR in this case, is available and functional—at least in G₂ (154). It also directly points to issues that need to be addressed when analyzing the network of processes and the decisions that underlie repair pathway choice (15,130,155–157).

This question is particularly relevant because choice among HRR, D-NHEJ or B-NHEJ cannot be considered as one among equivalent options, all of which will lead to the same outcome, i.e. the restoration of the DNA molecule. Rather, different outcomes are certain depending on the choice made and the risk of errors will also be widely different—possibly by orders of magnitude. It would appear logical, at least for cells in G₂ and S-phase to always first attempt repair by HRR and to opt for alternatives only when this pathway fails to engage. Even then D-NHEJ should be considered the first choice with B-NHEJ remaining as last resort—like all back-ups. Within this rationale, the acceptance of error-prone repair pathways will be a compromise taken only after error-free repair pathways failed. Such sequence of priorities would best satisfy the ultimate goal of preserving genomic integrity and accepting errors only to avert the most severe consequences associated with complete lack of repair.

However, this apparently logical scenario does not seem to form the basis of the detectable cellular response, as the extremely high affinity of Ku for DNA ends is likely to initiate D-NHEJ in the vast majority of DSBs. It also leaves unanswered the question as to whether G₁ cells or S-phase cells sustaining DSBs in unreplicated segments of their genome, completely lack means to faithfully restore their genome. These apparent inconsistencies point perhaps to gaps in our knowledge regarding the parameters determining DSB repair pathway choice and the logic underlying this choice.

CONCLUSIONS

DSBs are removed with extremely fast kinetics from the genome. Therefore, repair difficulty cannot be invoked to explain their devastating consequences for the cells. Rather, DSB repair is associated with a high probability for errors, and actually the probability for errors is for DSBs much higher than for any other DNA lesion. Indeed, the adverse biological effects of DSBs derive in their majority from errors in the processing of only few of them. Three pathways process DSBs using different concepts and being associated with different probabilities for errors. This inherent inequality in features and error-risks generates important questions regarding the logic behind repair pathway choice. Are repair pathways engaging DSBs on a first-come-first-serve basis, i.e. as

winners of a competition? If yes why? Is this the best way to decide? If not what logic underlies the selection? HRR is the only, in principle, error-free repair pathway. NHEJ pathways are likely to cause sequence alterations at the DSB junction and translocations; both risks are highest for B-NHEJ. The spectrum of DSBs with their increasing complexity further complicates the substrate fed into the repair pathways and must be considered as a key determinant of the risk for errors. Analysis of the spectrum of possible DSB types leads to T6-DSB, representing DSB clusters (local chromothripsis), as the potentially more dangerous of all. The development of defined biological systems allowing examination of severity of different types of DSBs is highly desirable.

FUNDING

‘Bundesministerium für Bildung und Forschung’ [BMBF: 02NUK005C and 03NUK001B]; ‘Bundesministerium für Wirtschaft und Technologie’ [BMWi: ESA-AO-08-IBER, 50WB1229]. Funding for open access charge: Bundesministerium für Bildung und Forschung Germany.

Conflict of interest statement. None declared.

REFERENCES

- Friedberg, E.C., Walker, G.C., Siede, W., Wood, R.D., Schultz, R.A. and Ellenberger, T. (2006) *DNA Repair and Mutagenesis*, 2nd edn. ASM Press, Washington, D.C.
- van Ankeren, S.C., Murray, D. and Meyn, R.E. (1988) Induction and rejoining of gamma-ray-induced DNA single- and double-strand breaks in Chinese hamster AA8 cells and in two radiosensitive clones. *Radiat. Res.*, **116**, 511–525.
- Nairn, R.S., Mitchell, D.L., Adair, G.M., Thompson, L.H., Siciliano, M.J. and Humphrey, R.M. (1989) UV mutagenesis, cytotoxicity and split-dose recovery in a human—CHO cell hybrid having intermediate (6–4) photoproduct repair. *Mutat. Res.*, **217**, 193–201.
- Berens, T.J. and Toczyski, D.P. (2012) Keeping it together in times of stress: checkpoint function at stalled replication forks. *Mol. Cell*, **45**, 585–586.
- Burrell, R.A., McClelland, S.E., Endesfelder, D., Groth, P., Weller, M.C., Shaikh, N., Domingo, E., Kanu, N., Dewhurst, S.M., Gronroos, E. *et al.* (2013) Replication stress links structural and numerical cancer chromosomal instability. *Nature*, **494**, 492–496.
- Mortusewicz, O., Herr, P. and Helleday, T. (2013) Early replication fragile sites: where replication-transcription collisions cause genetic instability. *EMBO J.*, **32**, 493–495.
- Sorg, U.R., Kleff, V., Fanaei, S., Schumann, A., Moellmann, M., Opalka, B., Thomale, J. and Moritz, T. (2007) O6-methylguanine-DNA-methyltransferase (MGMT) gene therapy targeting haematopoietic stem cells: Studies addressing safety issues. *DNA Repair*, **6**, 1197–1209.
- Zhou, B.B. and Elledge, S.J. (2000) The DNA damage response: putting checkpoints in perspective. *Nature*, **408**, 433–439.
- Jackson, S.P. and Bartek, J. (2009) The DNA-damage response in human biology and disease. *Nature*, **461**, 1071–1078.
- Dudley, D.D., Chaudhuri, J., Bassing, C.H. and Alt, F.W. (2005) Mechanism and control of V(D)J recombination versus class switch recombination: similarities and differences. *Adv. Immunol.*, **86**, 43–112.
- Pfeiffer, P., Goedecke, W. and Obe, G. (2000) Mechanisms of DNA double-strand break repair and their potential to induce chromosomal aberrations. *Mutagenesis*, **15**, 289–302.

12. Cornforth, M.N. and Bedford, J.S. (1993) Ionizing radiation damage and its early development in chromosomes. *Adv. Radiat. Biol.*, **17**, 423–496.
13. Iliakis, G., Wang, H., Perrault, A.R., Boecker, W., Rosidi, B., Windhofer, F., Wu, W., Guan, J., Terzoudi, G. and Pantelias, G. (2004) Mechanisms of DNA double strand break repair and chromosome aberration formation. *Cytogenet. Genome Res.*, **104**, 14–20.
14. Iliakis, G., Wu, W., Wang, M., Terzoudi, G.I. and Pantelias, G.E. (2007) Backup pathways of non-homologous end-joining may have a dominant role in formation of chromosome aberrations. Chapter 5. In: Obe, Gunter. and Vijayalaxmi. (eds), *Chromosomal Alterations*. Springer Verlag, Berlin, Heidelberg, New York, pp. 67–85.
15. Symington, L.S. and Gautier, J. (2011) Double-strand break end resection and repair pathway choice. *Annu. Rev. Genet.*, **45**, 247–271.
16. Lieber, M.R. (2010) The mechanism of double-strand DNA break repair by the nonhomologous DNA end-joining pathway. *Annu. Rev. Biochem.*, **79**, 181–211.
17. Bedford, J.S. (1991) Sublethal damage, potentially lethal damage, and chromosomal aberrations in mammalian cells exposed to ionizing radiations. *Int. J. Radiat. Oncol. Biol. Phys.*, **21**, 1457–1469.
18. Savage, J.R.K. (1970) Sites of radiation induced chromosome exchanges. *Curr. Top. Radiat. Res.*, **6**, 129–194.
19. Ferguson, D.O. and Alt, F.W. (2001) DNA double strand break repair and chromosomal translocation: lessons from animal models. *Oncogene*, **20**, 5572–5579.
20. Chiarle, R., Zhang, Y., Frock, R.L., Lewis, S.M., Molinie, B., Ho, Y.J., Myers, D.R., Choi, V.W., Compagno, M., Malkin, D.J. *et al.* (2011) Genome-wide translocation sequencing reveals mechanisms of chromosome breaks and rearrangements in B cells. *Cell*, **147**, 107–119.
21. Löbrich, M., Rydberg, B. and Cooper, P.K. (1995) Repair of x-ray-induced DNA double-strand breaks in specific *Not I* restriction fragments in human fibroblasts: joining of correct and incorrect ends. *Proc. Natl Acad. Sci. USA*, **92**, 12050–12054.
22. Kühne, M., Rothkamm, K. and Löbrich, M. (2000) No dose-dependence of DNA double-strand break misrejoining following a-particle irradiation. *Int. J. Radiat. Biol.*, **76**, 891–900.
23. Zhang, Y., McCord, R.P., Ho, Y.J., Lajoie, B.R., Hildebrand, D.G., Simon, A.C., Becker, M.S., Alt, F.W. and Dekker, J. (2012) Spatial organization of the mouse genome and its role in recurrent chromosomal translocations. *Cell*, **148**, 908–921.
24. Tereshchenko, I.V., Chen, Y., McDaniel, L.D., Schultz, R.A., Tischfield, J.A. and Shao, C. (2010) Small scale genetic alterations contribute to increased mutability at the X-linked *Hprt* locus *in vivo* in *Blm* hypomorphic mice. *DNA Repair*, **9**, 551–557.
25. Shou, Y., Martelli, M.L., Gabrea, A., Qi, Y., Brents, L.A., Roschke, A., Dewald, G., Kirsch, I.R., Bergsagel, P.L. and Kuehl, W.M. (2000) Diverse karyotypic abnormalities of the *c-myc* locus associated with *c-myc* dysregulation and tumor progression in multiple myeloma. *Proc. Natl Acad. Sci. USA*, **97**, 228–233.
26. Hakim, O., Resch, W., Yamane, A., Klein, I., Kieffer-Kwon, K.-R., Jankovic, M., Oliveira, T., Bothmer, A., Voss, T.C., Ansarah-Sobrinho, C. *et al.* (2012) DNA damage defines sites of recurrent chromosomal translocations in B lymphocytes. *Nature*, **484**, 69–74.
27. Zhang, J., Ding, L., Holmfeldt, L., Wu, G., Heatley, S.L., Payne-Turner, D., Easton, J., Chen, X., Wang, J., Rusch, M. *et al.* (2012) The genetic basis of early T-cell precursor acute lymphoblastic leukaemia. *Nature*, **481**, 157–163.
28. Almuzni, G. and Probst, A.V. (2011) Heterochromatin maintenance and establishment: lessons from the mouse pericentromere. *Nucleus*, **2**, 332–338.
29. Aziz, K., Nowsheen, S., Pantelias, G., Iliakis, G., Gorgoulis, V.G. and Georgakilas, A.G. (2012) Targeting DNA damage and repair: embracing the pharmacological era for successful cancer therapy. *Pharmacol. Ther.*, **133**, 334–350.
30. Georgakilas, A.G., O'Neill, P. and Stewart, R.D. (2012) Induction and repair of clustered DNA lesions: what do we know so far? *Radiat. Res.*, May 17 (doi:10.1667/RR3041.1; epub ahead of print).
31. Jeggo, P.A., Geuting, V. and Löbrich, M. (2011) The role of homologous recombination in radiation-induced double-strand break repair. *Radiother. Oncol.*, **101**, 7–12.
32. Murray, J.M., Stiff, T. and Jeggo, P.A. (2012) DNA double-strand break repair within heterochromatic regions. *Biochem. Soc. Trans.*, **40**, 173–178.
33. Helmrich, A., Ballarino, M., Nudler, E. and Tora, L. (2013) Transcription-replication encounters, consequences and genomic instability. *Nat. Struct. Mol. Biol.*, **20**, 412–418.
34. Obe, G. and Winkel, E.-U. (1985) The chromosome-breaking activity of the restriction endonuclease *Alu I* in CHO cells is independent of the S-phase of the cell cycle. *Mutat. Res.*, **152**, 25–29.
35. Bryant, P.E. and Johnston, P.J. (1993) Restriction-endonuclease-induced DNA double-strand breaks and chromosomal aberrations in mammalian cells. *Mutat. Res.*, **299**, 289–296.
36. Mirny, L. (2011) The fractal globule as a model of chromatin architecture in the cell. *Chromosome Res.*, **19**, 37–51.
37. Bancaud, A., Lavelle, C., Huet, S. and Ellenberg, J. (2012) A fractal model for nuclear organization: current evidence and biological implications. *Nucleic Acids Res.*, **40**, 8783–8792.
38. Pfeiffer, P., Feldmann, E., Odersky, A., Kuhfittig-Kulle, S. and Goedecke, W. (2005) Analysis of double-strand break repair by non-homologous DNA end joining in cell-free extracts from mammalian cells. *Methods Mol. Biol.*, **291**, 351–371.
39. van Gent, D.C. and van der Burg, M. (2007) Non-homologous end-joining, a sticky affair. *Oncogene*, **26**, 7731–7740.
40. Fenina, M., Simon-Chazottes, D., Vandormael-Pournin, S., Soueid, J., Langa, F., Cohen-Tannoudji, M., Bernard, B.A. and Panthier, J.-J. (2012) *I-SceI*-Mediated double-strand break does not increase the frequency of homologous recombination at the *DCT* locus in mouse embryonic stem cells. *PLoS One*, **7**, e39895.
41. Iacovoni, J.S., Caron, P., Lassadi, I., Nicolas, E., Massip, L., Trouche, D. and Legube, G. (2010) High-resolution profiling of *gH2AX* around DNA double strand breaks in the mammalian genome. *EMBO J.*, **29**, 1446–1457.
42. Jasin, M. (1996) Genetic manipulation of genomes with rare-cutting endonucleases. *Trends Genet.*, **12**, 224–228.
43. Gunn, A. and Stark, J.M. (2012) *I-SceI*-based assays to examine distinct repair outcomes of mammalian chromosomal double strand-breaks. *Methods Mol. Biol.*, **920**, 379–391.
44. Soutoglou, E. and Misteli, T. (2008) Activation of the cellular DNA damage response in the absence of DNA lesions. *Science*, **320**, 1507–1510.
45. Bindra, R.S., Goglia, A.G., Jasin, M. and Powell, S.N. (2013) Development of an assay to measure mutagenic non-homologous end-joining repair activity in mammalian cells. *Nucleic Acids Res.*, **41**, e115.
46. Durante, M. and Cucinotta, F.A. (2008) Heavy ion carcinogenesis and human space exploration. *Nat. Rev. Cancer*, **8**, 465–472.
47. Durante, M. and Loeffler, J.S. (2010) Charged particles in radiation oncology. *Nat. Rev. Clin. Oncol.*, **7**, 37–43.
48. Nikjoo, H., O'Neill, P.O., Terrissol, M. and Goodhead, D.T. (1999) Quantitative modelling of DNA damage using monte carlo track structure method. *Radiat. Environ. Biophys.*, **38**, 31–38.
49. Friedland, W., Dingfelder, M., Kundrát, P. and Jacob, P. (2011) Track structures, DNA targets and radiation effects in the biophysical Monte Carlo simulation code PARTRAC. *Mutat. Res.*, **711**, 28–40.
50. Ward, J.F. (1985) Biochemistry of DNA lesions. *Radiat. Res.*, **104**, S103–S111.
51. Ward, J.F. (1990) The yield of DNA double-strand breaks produced intracellularly by ionizing radiation: a review. *Int. J. Radiat. Biol.*, **57**, 1141–1150.
52. Henner, W.D., Grunberg, S.M. and Haseltine, W.A. (1982) Sites and structure of γ radiation-induced DNA strand breaks. *J. Biol. Chem.*, **257**, 11750–11754.
53. Henner, W.D., Rodriguez, L.O., Hecht, S.M. and Haseltine, W.A. (1983) Gamma-ray induced deoxyribonucleic acid strand breaks. *J. Biol. Chem.*, **258**, 711–713.
54. Weinfeld, M., Mani, R.S., Abdou, I., Aceytuno, R.D. and Glover, J.N.M. (2011) Tidying up loose ends: the role of polynucleotide kinase/phosphatase in DNA strand break repair. *Trends Biochem. Sci.*, **36**, 262–271.

55. Ward, J.F., Blakely, W.F. and Jone, E.I. (1985) Mammalian cells are not killed by DNA single-strand breaks caused by hydroxyl radicals from hydrogen peroxide. *Radiat. Res.*, **103**, 383–392.
56. Iliakis, G.E., Pantelias, G.E., Okayasu, R. and Blakely, W.F. (1992) Induction by H₂O₂ of DNA and interphase chromosome damage in plateau phase CHO cells. *Radiat. Res.*, **131**, 193–203.
57. Dahm-Daphi, J., Sass, C. and Alberti, W. (2000) Comparison of biological effects of DNA damage induced by ionizing radiation and hydrogen peroxide in CHO cells. *Int. J. Radiat. Biol.*, **76**, 67–75.
58. Goodhead, D.T. (1995) Molecular and cell models of biological effects of heavy ion radiation. *Radiat. Environ. Biophys.*, **34**, 67–72.
59. Hall, E.J. and Giaccia, A.J. (2006) *Radiobiology for the Radiologist*, 6th Edn. Lippincott Williams & Wilkins, Philadelphia, Baltimore, New York, London, Buenos Aires, Hong Kong, Sydney, Tokyo.
60. Paretzke, H.G. (1987) Radiation track structure theory. Chapter 2. In: Freeman, G.R. (ed.), *Kinetics of Nonhomogeneous Processes*. John Wiley & Sons, Inc., pp. 89–170.
61. Friedland, W., Jacob, P. and Kundrát, P. (2010) Stochastic simulation of DNA double-strand break repair by non-homologous end joining based on track structure calculations. *Radiat. Res.*, **173**, 677–688.
62. Ward, J.F. (1988) DNA damage produced by ionizing radiation in mammalian cells: identities, mechanisms of formation, and reparability. *Prog. Nucleic Acid Res. Mol. Biol.*, **35**, 95–125.
63. Goodhead, D.T. and Nikjoo, H. (1989) Track structure analysis of ultrasoft X-rays compared to high- and low-LET radiations. *Int. J. Radiat. Biol.*, **55**, 513–529.
64. Allen, C., Borak, T.B., Tsujii, H. and Nickoloff, J.A. (2011) Heavy charged particle radiobiology: using enhanced biological effectiveness and improved beam focusing to advance cancer therapy. *Mutat. Res.*, **711**, 150–157.
65. Ward, J.F., Evans, J.W., Limoli, C.L. and Calabro-Jones, P.M. (1987) Radiation and hydrogen peroxide induced free radical damage to DNA. *Br. J. Cancer*, **55**, 105–112.
66. Sutherland, B.M., Bennett, P.V., Sidorkina, O. and Laval, J. (2000) Clustered DNA damages induced in isolated DNA and in human cells by low doses of ionizing radiation. *Proc. Natl Acad. Sci. USA*, **97**, 103–108.
67. Sutherland, R.M., Bennett, P.V., Sutherland, J.C. and Laval, J. (2002) Clustered DNA damages induced by x rays in human cells. *Radiat. Res.*, **157**, 611–616.
68. Goodhead, D.T. (1994) Initial events in the cellular effects of ionizing radiations: clustered damage in DNA. *Int. J. Radiat. Biol.*, **65**, 7–17.
69. Povirk, L.F. (2012) Processing of damaged DNA ends for double-strand break repair in mammalian cells. *ISRN Mol. Biol.*, **2012**, Article: ID 345805.
70. Sage, E. and Harrison, L. (2011) Clustered DNA lesion repair in eukaryotes: relevance to mutagenesis and cell survival. *Mutat. Res.*, **711**, 123–133.
71. Wilson, D.M. III, Kim, D., Berquist, B.R. and Sigurdson, A.J. (2011) Variation in base excision repair capacity. *Mutat. Res.*, **711**, 100–112.
72. Eccles, L.J., O'Neill, P. and Lomax, M.E. (2011) Delayed repair of radiation induced clustered DNA damage: friend or foe? *Mutat. Res.*, **711**, 134–141.
73. Dobbs, T.A., Palmer, P., Maniou, Z., Lomax, M.E. and O'Neill, P. (2008) Interplay of two major repair pathways in the processing of complex double-strand DNA breaks. *DNA Repair*, **7**, 1372–1383.
74. Eccles, L.J., Lomax, M.E. and O'Neill, P. (2010) Hierarchy of lesion processing governs the repair, double-strand break formation and mutability of three-lesion clustered DNA damage. *Nucleic Acids Res.*, **38**, 1123–1134.
75. Mourgues, S., Lomax, M.E. and O'Neill, P. (2007) Base excision repair processing of abasic site/single-strand break lesions within clustered damage sites associated with XRCC1 deficiency. *Nucleic Acids Res.*, **35**, 7676–7687.
76. Covo, S., de Villartay, J.P., Jeggo, P.A. and Livneh, Z. (2009) Translesion DNA synthesis-assisted non-homologous end-joining of complex double-strand breaks prevents loss of DNA sequences in mammalian cells. *Nucleic Acids Res.*, **37**, 6737–6745.
77. Malyarchuk, S., Castore, R. and Harrison, L. (2008) DNA repair of clustered lesions in mammalian cells: involvement of non-homologous end-joining. *Nucleic Acids Res.*, **36**, 4872–4882.
78. Jones, G.D., Boswell, T.V. and Ward, J.F. (1994) Effects of postirradiation temperature on the yields of radiation-induced single- and double-strand breakage in SV40 DNA. *Radiat. Res.*, **138**, 291–296.
79. Brenner, D.J. and Ward, J.F. (1992) Constraints on energy deposition and target size of multiply damaged sites associated with DNA double-strand breaks. *Int. J. Radiat. Biol.*, **61**, 737–748.
80. Lafleur, M.V.M., Woldhuis, J. and Loman, H. (1979) Alkali-labile sites and post-irradiation effects in gamma-irradiated biologically active double-stranded DNA in aqueous solution. *Int. J. Radiat. Biol.*, **36**, 241–247.
81. Henle, E.S., Roots, R., Holley, W.R. and Chatterjee, A. (1995) DNA strand breakage is correlated with unaltered base release after gamma irradiation. *Radiat. Res.*, **143**, 144–150.
82. von Sonntag, C. (2006) *Free-Radical-Induced DNA Damage and Its Repair*. Springer, Berlin-Heidelberg.
83. Fung, H. and Demple, B. (2011) Distinct roles of ap1 protein in the repair of DNA damage induced by ionizing radiation or bleomycin. *J. Biol. Chem.*, **286**, 4968–4977.
84. Rydberg, B. (2000) Radiation-induced heat-labile sites that convert into DNA double-strand breaks. *Radiat. Res.*, **153**, 805–812.
85. Stenerlöv, B., Karlsson, K.H., Cooper, B. and Rydberg, B. (2003) Measurement of prompt DNA double-strand breaks in mammalian cells without including heat-labile sites: results for cells deficient in nonhomologous end joining. *Radiat. Res.*, **159**, 502–510.
86. Karlsson, K.H. and Stenerlöv, B. (2007) Extensive ssDNA end formation at DNA double-strand breaks in non-homologous end-joining deficient cells during the S phase *BMC Mol. Biol.*, **8**, 97.
87. Singh, S.K., Wu, W., Wang, M. and Iliakis, G. (2009) Extensive repair of DNA double-strand breaks in cells deficient in the DNA-PK dependent pathway of NHEJ after exclusion of heat-labile sites. *Radiat. Res.*, **172**, 152–164.
88. Singh, S.K., Wang, M., Staudt, C. and Iliakis, G. (2011) Post-irradiation chemical processing of DNA damage generates double-strand breaks in cells already engaged in repair. *Nucleic Acids Res.*, **39**, 8416–8429.
89. Singh, S.K., Bencsik-Theilen, A., Mladenov, E., Jakob, B., Taucher-Scholz, G. and Iliakis, G. (2013) Reduced contribution of thermally labile sugar lesions to DNA double strand break formation after exposure to heavy ions. *Radiat. Oncol.*, **8**, 77.
90. Stephens, P.J., Greenman, C.D., Fu, B., Yang, F., Rignell, G.R., Mudie, L.J., Pleasance, E.D., Lau, K.W., Beare, D., Stebbings, L.A. *et al.* (2011) Massive genomic rearrangement acquired in a single catastrophic event during cancer development. *Cell*, **144**, 27–40.
91. Forment, J.V., Kaidi, A. and Jackson, S.P. (2012) Chromothripsis and cancer: causes and consequences of chromosome shattering. *Nat. Rev. Cancer*, **12**, 663–670.
92. Kloosterman, W.P., Tavakoli-Yaraki, M., van Roosmalen, M.J., van Binsbergen, E., Renkens, I., Duran, K., Ballarati, L., Vergult, S., Giardino, D., Hansson, K. *et al.* (2012) Constitutional chromothripsis rearrangements involve clustered double-stranded DNA breaks and nonhomologous repair mechanisms. *Cell Rep.*, **1**, 648–655.
93. Molenaar, J.J., Koster, J., Zwijnenburg, D.A., van Sluis, P., Valentijn, L.J., van der Ploeg, I., Hamdi, M., van Nes, J., Westerman, B.A., van Arkel, J. *et al.* (2012) Sequencing of neuroblastoma identifies chromothripsis and defects in neurogenesis genes. *Nature*, **483**, 589–593.
94. Johnston, P.J., Olive, P.L. and Bryant, P.E. (1997) Higher-order chromatin structure-dependent repair of DNA double-strand breaks: modeling the elution of DNA from nucleoids. *Radiat. Res.*, **148**, 561–567.
95. Johnston, P.J. and Bryant, P.E. (1994) A component of DNA double-strand break repair is dependent on the spatial orientation of the lesions within the higher-order structures of chromatin. *Int. J. Radiat. Biol.*, **66**, 531–536.

96. Johnston,P.J., MacPhail,S.H., Banáth,J.P. and Olive,P.L. (1998) Higher-order chromatin structure-dependent repair of DNA double-strand breaks: factors affecting elution of DNA from nucleoids. *Radiat. Res.*, **149**, 533–542.
97. Holley,W.R. and Chatterjee,A. (1996) Clusters of DNA damage induced by ionizing radiation: formation of short DNA fragments. I. theoretical modeling. *Radiat. Res.*, **145**, 188–199.
98. Rydberg,B. (1996) Clusters of DNA damage induced by ionizing radiation: formation of short DNA fragments. II. experimental detection. *Radiat. Res.*, **145**, 200–209.
99. Löbrich,M., Cooper,P.K. and Rydberg,B. (1996) Non-random distribution of DNA double-strand breaks induced by particle irradiation. *Int. J. Radiat. Biol.*, **70**, 493–503.
100. Friedland,W., Dingfelder,M., Jacob,P. and Paretzke,H.G. (2005) Calculated DNA double-strand break and fragmentation yields after irradiation with He ions. *Radiat. Phys. Chem.*, **72**, 279–286.
101. Friedland,W., Jacob,P., Paretzke,H.G. and Stork,T. (1998) Monte carlo simulation of the production of short DNA fragments by low-linear energy transfer radiation using higher-order DNA models. *Radiat. Res.*, **150**, 170–182.
102. Pang,D., Winters,T.A., Jung,M., Purkayastha,S., Cavalli,L.R., Chasovkikh,S., Haddad,B.R. and Dritschilo,A. (2011) Radiation-generated short DNA fragments may perturb non-homologous end-joining and induce genomic instability. *J. Radiat. Res.*, **52**, 309–319.
103. Wang,H., Zhang,X., Wang,P., Yu,X., Essers,J., Chen,D., Kanaar,R., Takeda,S. and Wang,Y. (2010) Characteristics of DNA-binding proteins determine the biological sensitivity to high-linear energy transfer radiation. *Nucleic Acids Res.*, **38**, 3245–3251.
104. Alt,F.W., Zhang,Y., Meng,F.-L., Guo,C. and Schwer,B. (2013) Mechanisms of programmed DNA lesions and genomic instability in the immune system. *Cell*, **152**, 417–429.
105. Boboila,C., Alt,F.W. and Schwer,B. (2012) Chapter one - classical and alternative end-joining pathways for repair of lymphocyte-specific and general DNA double-strand breaks. In: Frederick,W.A. (ed.), *Advances in Immunology*, Vol. 116. Academic Press, New York, pp. 1–49.
106. Zhang,Y., Gostissa,M., Hildebrand,D.G., Becker,M.S., Boboila,C., Chiarle,R., Lewis,S. and Alt,F.W. (2010) The role of mechanistic factors in promoting chromosomal translocations found in lymphoid and other cancers. *Adv. Immunol.*, **106**, 93–111.
107. Ostashevsky,J.Y. (1989) A model relating cell survival to DNA fragment loss and unrepaired double-strand breaks. *Radiat. Res.*, **118**, 437–466.
108. Ostashevsky,J.Y. (2000) Higher-order structure of interphase chromosomes and radiation-induced chromosomal exchange aberrations. *Int. J. Radiat. Biol.*, **76**, 1179–1187.
109. Friedland,W., Jacob,P., Bernhardt,P., Paretzke,H.G. and Dingfelder,M. (2003) Simulation of DNA damage after proton irradiation. *Radiat. Res.*, **159**, 401–410.
110. Ponomarev,A.L. and Cucinotta,F.A. (2006) Chromatin loops are responsible for higher counts of small DNA fragments induced by high-LET radiation, while chromosomal domains do not affect the fragment sizes. *Int. J. Radiat. Biol.*, **82**, 293–305.
111. Friedrich,T., Durante,M. and Scholz,M. (2012) Modeling cell survival after photon irradiation based on double-strand break clustering in megabase pair chromatin loops. *Radiat. Res.*, **178**, 385–394.
112. Friedrich,T., Scholz,U., Elsässer,T., Durante,M. and Scholz,M. (2011) Calculation of the biological effects of ion beams based on the microscopic spatial damage distribution pattern. *Int. J. Radiat. Biol.*, **88**, 103–107.
113. Elsässer,T., Brons,S., Psonka,K., Scholz,M., Gudowska-Nowak,E. and Taucher-Scholz,G. (2008) Biophysical modeling of fragment length distributions of DNA plasmids after X and heavy-ion irradiation analyzed by atomic force microscopy. *Radiat. Res.*, **169**, 649–659.
114. Terzoudi,G.I., Hatzi,V.I., Donta-Bakoyianni,C. and Pantelias,G.E. (2011) Chromatin dynamics during cell cycle mediate conversion of DNA damage into chromatid breaks and affect formation of chromosomal aberrations: biological and clinical significance. *Mutat. Res.*, **711**, 174–186.
115. Fussner,E., Strauss,M., Djuric,U., Li,R., Ahmed,K., Hart,M., Ellis,J. and Bazett-Jones,D.P. (2012) Open and closed domains in the mouse genome are configured as 10-nm chromatin fibres. *EMBO Rep.*, **13**, 992–996.
116. Dekker,J. (2008) Mapping *in vivo* chromatin interactions in yeast suggests an extended chromatin fiber with regional variation in compaction. *J. Biol. Chem.*, **283**, 34532–34540.
117. Eltsov,M., MacLellan,K.M., Maeshima,K., Frangakis,A.S. and Dubochet,J. (2008) Analysis of cryo-electron microscopy images does not support the existence of 30-nm chromatin fibers in mitotic chromosomes *in situ*. *Proc. Natl Acad. Sci. USA*, **105**, 19732–19737.
118. Nishino,Y., Eltsov,M., Joti,Y., Ito,K., Takata,H., Takahashi,Y., Hihara,S., Frangakis,A.S., Imamoto,N., Ishikawa,T. *et al.* (2012) Human mitotic chromosomes consist predominantly of irregularly folded nucleosome fibres without a 30-nm chromatin structure. *EMBO J.*, **31**, 1644–1653.
119. van Holde,K. and Zlatanova,J. (2007) Chromatin fiber structure: where is the problem now? *Semin. Cell Dev. Biol.*, **18**, 651–658.
120. van Berkum,N.L. and Dekker,J. (2009) Determining spatial chromatin organization of large genomic regions using 5C technology. *Methods Mol. Biol.*, **567**, 189–213.
121. Imakaev,M., Fudenberg,G., McCord,R.P., Naumova,N., Goloborodko,A., Lajoie,B.R., Dekker,J. and Mirny,L.A. (2012) Iterative correction of Hi-C data reveals hallmarks of chromosome organization. *Nat. Meth.*, **9**, 999–1003.
122. van Loenhout,M.T.J., de Grunt,M.V. and Dekker,C. (2012) Dynamics of DNA supercoils. *Science*, **338**, 94–97.
123. Thurman,R.E., Rynes,E., Humbert,R., Vierstra,J., Maurano,M.T., Haugen,E., Sheffield,N.C., Stergachis,A.B., Wang,H., Vernot,B. *et al.* (2012) The accessible chromatin landscape of the human genome. *Nature*, **489**, 75–82.
124. Lieberman-Aiden,E., van Berkum,N.L., Williams,L., Imakaev,M., Ragoczy,T., Telling,A., Amit,I., Lajoie,B.R., Sabo,P.J., Dorschner,M.O. *et al.* (2009) Comprehensive mapping of long-range interactions reveals folding principles of the human genome. *Science*, **326**, 289–293.
125. Mladenov,E. and Iliakis,G. (2011) Induction and repair of DNA double strand breaks: the increasing spectrum of non-homologous end joining pathways. *Mutat. Res.*, **711**, 61–72.
126. Kinner,A., Wu,W., Staudt,C. and Iliakis,G. (2008) g-H2AX in recognition and signaling of DNA double-strand breaks in the context of chromatin. *Nucleic Acids Res.*, **36**, 5678–5694.
127. Heyer,W.-D., Ehmsen,K.T. and Liu,J. (2010) Regulation of homologous recombination in eukaryotes. *Annu. Rev. Genet.*, **44**, 113–139.
128. San Filippo,J., Sung,P. and Klein,H. (2008) Mechanism of eukaryotic homologous recombination. *Annu. Rev. Biochem.*, **77**, 229–257.
129. Walker,J.R., Corpina,R.A. and Goldberg,J. (2001) Structure of the Ku heterodimer bound to DNA and its implications for double-strand break repair. *Nature*, **412**, 607–614.
130. Chapman,J.R., Taylor,M.R.G. and Boulton,S.J. (2012) Playing the end game: DNA double-strand break repair pathway choice. *Mol. Cell*, **47**, 497–510.
131. Bzymek,M., Thayer,N.H., Oh,S.D., Kleckner,N. and Hunter,N. (2010) Double Holliday junctions are intermediates of DNA break repair. *Nature*, **464**, 937–941.
132. Weterings,E. and Chen,D.J. (2008) The endless tale of non-homologous end-joining. *Cell Res.*, **18**, 114–124.
133. Lieber,M.R. (2010) NHEJ and its backup pathways in chromosomal translocations. *Nat. Struct. Mol. Biol.*, **17**, 393–395.
134. Gostissa,M., Alt,F.W. and Chiarle,R. (2011) Mechanisms that promote and suppress chromosomal translocations in lymphocytes. *Annu. Rev. Immunol.*, **29**, 319–350.
135. Honma,M., Sakuraba,M., Koizumi,T., Takashima,Y., Sakamoto,H. and Hayashi,M. (2007) Non-homologous end-joining for repairing I-SceI-induced DNA double strand breaks in human cells. *DNA Repair*, **6**, 781–788.
136. McVey,M. and Lee,S.E. (2008) MMEJ repair of double-strand breaks (director's cut): deleted sequences and alternative endings. *Trends Genet.*, **24**, 529–538.

137. Wang, M., Wu, W., Wu, W., Rosidi, B., Zhang, L., Wang, H. and Iliakis, G. (2006) PARP-1 and Ku compete for repair of DNA double strand breaks by distinct NHEJ pathways. *Nucleic Acids Res.*, **34**, 6170–6182.
138. Gao, Y., Katyal, S., Lee, Y., Zhao, J., Rehg, J.E., Russell, H.R. and McKinnon, P.J. (2011) DNA ligase III is critical for mtDNA integrity but not Xrcc1-mediated nuclear DNA repair. *Nature*, **471**, 240–244.
139. Simsek, D., Furda, A., Gao, Y., Artus, J., Brunet, E., Hadjantonakis, A.-K., Van Houten, B., Shuman, S., McKinnon, P.J. and Jasin, M. (2011) Crucial role for DNA ligase III in mitochondria but not in Xrcc1-dependent repair. *Nature*, **471**, 245–248.
140. Simsek, D., Brunet, E., Wong, S.Y.-W., Katyal, S., Gao, Y., McKinnon, P.J., Lou, J., Zhang, L., Li, J., Rebar, E.J. *et al.* (2011) DNA ligase III promotes alternative nonhomologous end-joining during chromosomal translocation formation. *PLoS Genet.*, **7**, e1002080.
141. Paul, K., Wang, M., Mladenov, E., Bencsik-Theilen, A.A., Bednar, T., Wu, W., Arakawa, H. and Iliakis, G. (2013) DNA ligases I and III cooperate in alternative non-homologous end-joining in vertebrates. *PLoS One*, **8**, e59505.
142. Wang, H., Rosidi, B., Perrault, R., Wang, M., Zhang, L., Windhofer, F. and Iliakis, G. (2005) DNA Ligase III as a candidate component of backup pathways of nonhomologous end joining. *Cancer Res.*, **65**, 4020–4030.
143. Boboila, C., Oksenyich, V., Gostissa, M., Wang, J.H., Zha, S., Zhang, Y., Chai, H., Lee, C.-S., Jankovic, M., Saez, L.-M.A. *et al.* (2012) Robust chromosomal DNA repair via alternative end-joining in the absence of X-ray repair cross-complementing protein 1 (XRCC1). *Proc. Natl Acad. Sci. USA*, **109**, 2473–2478.
144. Rass, E., Grabarz, A., Plo, I., Gautier, J., Bertrand, P. and Lopez, B.S. (2009) Role of Mre11 in chromosomal nonhomologous end joining in mammalian cells. *Nat. Struct. Mol. Biol.*, **16**, 819–825.
145. Sallmyr, A., Tomkinson, A.E. and Rassool, F.V. (2008) Up-regulation of WRN and DNA ligase IIIa in chronic myeloid leukemia: consequences for the repair of DNA double-strand breaks. *Blood*, **112**, 1413–1423.
146. Rosidi, B., Wang, M., Wu, W., Sharma, A., Wang, H. and Iliakis, G. (2008) Histone H1 functions as a stimulatory factor in backup pathways of NHEJ. *Nucleic Acids Res.*, **36**, 1610–1623.
147. Singh, S.K., Bednar, T., Zhang, L., Wu, W., Mladenov, E. and Iliakis, G. (2012) Inhibition of B-NHEJ in plateau-phase cells is not a direct consequence of suppressed growth factor signaling. *Int. J. Radiat. Oncol. Biol. Phys.*, **84**, e237–e243.
148. Iliakis, G. (2009) Backup pathways of NHEJ in cells of higher eukaryotes: cell cycle dependence. *Radiother. Oncol.*, **92**, 310–315.
149. Wu, W., Wang, M., Wu, W., Singh, S.K., Mussfeldt, T. and Iliakis, G. (2008) Repair of radiation induced DNA double strand breaks by backup NHEJ is enhanced in G2. *DNA Repair*, **7**, 329–338.
150. Wu, W., Wang, M., Mussfeldt, T. and Iliakis, G. (2008) Enhanced use of backup pathways of NHEJ in G₂ in chinese hamster mutant cells with defects in the classical pathway of NHEJ. *Radiat. Res.*, **170**, 512–520.
151. Singh, S.K., Wu, W., Zhang, L., Klammer, H., Wang, M. and Iliakis, G. (2011) Widespread dependence of backup NHEJ on growth state: ramifications for the use of DNA-PK inhibitors. *Int. J. Radiat. Oncol. Biol. Phys.*, **79**, 540–548.
152. Windhofer, F., Wu, W., Wang, M., Singh, S.K., Saha, J., Rosidi, B. and Iliakis, G. (2007) Marked dependence on growth state of backup pathways of NHEJ. *Int. J. Radiat. Oncol. Biol. Phys.*, **68**, 1462–1470.
153. Georgakilas, A.G. (2008) Processing of DNA damage clusters in human cells: current status of knowledge. *Mol. Biosyst.*, **4**, 30–35.
154. Beucher, A., Birraux, J., Tchouandong, L., Barton, O., Shibata, A., Conrad, S., Goodarzi, A.A., Krempler, A., Jeggo, P.A. and Löbrich, M. (2009) ATM and artemis promote homologous recombination of radiation-induced DNA double-strand breaks in G₂. *EMBO J.*, **28**, 3413–3427.
155. Brandsma, I. and Gent, D.C. (2012) Pathway choice in DNA double strand break repair: observations of a balancing act. *Genome Integrity*, **3**, 9.
156. Shibata, A., Conrad, S., Birraux, J., Geuting, V., Barton, O., Ismail, A., Kakarougkas, A., Meek, K., Taucher-Scholz, G., Löbrich, M. *et al.* (2011) Factors determining DNA double-strand break repair pathway choice in G₂ phase. *EMBO J.*, **30**, 1079–1092.
157. Shrivastav, M., De Haro, L.P. and Nickoloff, J.A. (2008) Regulation of DNA double-strand break repair pathway choice. *Cell Res.*, **18**, 134–147.

Appendix 4

Homing endonuclease-based model systems for the study of DNA double strand break induced cell signaling and repair

Inaugural-Dissertation
zur
Erlangung des Doktorgrades
Dr. rer. nat.

der Fakultät für Biologie
an der
Universität Duisburg-Essen
Standort Essen

vorgelegt von
Agnes Schipler
aus Neumarkt

Juni, 2013

Zusammenfassung

In Zellen, die ionisierender Strahlung ausgesetzt sind, werden aufgrund der speziellen Energiedeposition entlang der Bahnstruktur der ionisierenden Partikel, welche häufig zu multiplen Ionizationen in einem kleinen Volumen führen, geclusterte DNA-Schäden induziert. Es wird angenommen, dass die Prozessierung von geclusterten DNA-Schäden, welche sowohl chemische Basenveränderungen als auch DNA-Strangbrüche umfassen, die sich auf beiden Strängen einer DNA-Windung erstrecken, fehlerhaft abläuft und zur genomischen Instabilität und dem damit verbundenen Zelltod führen kann. Im Gegensatz dazu werden DNA-Schäden, welche isoliert auftreten, von speziellen Reparaturmechanismen fehlerfrei repariert. Eine spezielle Form von geclusterten DNA-Schäden auf Chromatin-Ebene stellen DSB da, die nah beieinander in der DNA induziert werden. Durch das Clustern von DSBs in Abständen von einigen hundert bis einigen tausend bp können instabile Chromosomen-Fragmente generiert werden, die Deletionen verursachen und somit zum Verlust der genomischen Integrität führen. Es existieren theoretische Berechnungen, welche die Induktion von geclusterten DSBs modellieren. Die biologische Relevanz von geclustereten DSBs kann aber nicht getestet werden, da die kontrollierte Induktion von DSBs mittels IR nicht möglich ist.

Im Rahmen dieser Arbeit wurde ein auf der Homing Endonuclease I-SceI basierendes Modellsystem entwickelt, um geclusterte DSBs mit definierten Abständen in der zellulären DNA zu induzieren und anschließend deren biologischen Folgen zu untersuchen. Mithilfe der Transposontechnologie wurden die I-SceI Konstrukte sowohl an verschiedenen Stellen in das Genom von CHO wt Zellen, als auch in den Zelllinien XR-C1-3, Xrs6 und irs1SF, welche inaktivierende Mutationen in Proteinen wichtiger Reparaturwege aufweisen, integriert, um den Einfluss der unterschiedlichen Reparaturwege auf geclusterte DSBs untersuchen zu können. Die Anzahl der Integrationsstellen und somit auch die Anzahl der möglichen Doppelstrangbrüche wurde anhand von Southern Blotting ermittelt.

Mit Hilfe dieser Model-Systeme ist die gleichzeitige Induktion von geclusterten DSBs durch die Transfektion von I-SceI exprimierenden Plasmiden möglich, welche die

Ereignisse nach Bestrahlung mit ionisierender Strahlung in einer Zelle imitieren. Überlebensexperimente mit diesen Zelllinien haben gezeigt, dass durch I-SceI induzierte geclusterte DSBs im Gegensatz zu simplen DSBs, zu einem starken Absterben führen. In Übereinstimmung mit dem hohen Tötungspotential von geclusterten DSBs konnte anhand von Chromosomen-Aberrationen fehlerhafte Reparatur nachgewiesen werden. Weiterhin konnte anhand von Lebend-Zell-Experimenten gezeigt werden, dass die Foci-Bildung von 53BP1 Unterschiede zwischen simplen und geclusterten DSBs aufweist. Diese Ergebnisse weisen auf eine Verbindungen zwischen der Komplexität des DSBs und der Entwicklung einer zellulären Antwort auf DNA Schäden hin.

Das dieser Dissertation zugrunde liegende Vorhaben wurde mit Mitteln des Bundesministeriums für Bildung und Forschung (BMBF) unter dem Förderkennzeichen 02NUK005C gefördert. Die Verantwortung für den Inhalt dieser Veröffentlichung liegt beim Autor.

Table of contents

Table of contents	I
Acknowledgements	v
List of abbreviations	vi
Abstract	xi
1. Introduction	1
1.1. Cellular mechanisms for signaling and repair of DNA double strand breaks (DSBs)	1
1.1.1. DSBs - a threat for genomic stability	1
1.1.2. DNA damage response (DDR)	2
1.1.2.1. Activation of cell cycle checkpoints or apoptosis	2
1.1.2.2. Multistep signaling of DSBs	4
1.1.3. Repair pathways	8
1.1.3.1. HR	8
1.1.3.2. D-NHEJ	10
1.1.3.3. B-NHEJ	11
1.2. Possible sources of DSB induction	13
1.2.1. Ionizing Radiation (IR).....	13
1.2.1.1. Physical and chemical aspects of IR interaction with matter	13
1.2.1.2. Biological consequences of clustered DNA damage induced by IR	15
1.2.1.3. VDJ/CSR	16
1.2.1.4. Endonucleases	17
1.2.1.5. I-SceI as a tool to study DSB repair	18
1.3. Not all DSBs are created equal: Levels of DSB complexity	20
1.3.1. T1-DSB: simple DSBs with clean ends.....	20
1.3.2. T2-DSB: simple DSBs with modified ends.....	22
1.3.3. T3-DSB: Locally multiply damaged sites	22
1.3.4. T4-DSB: Indirect DSB induced by enzymatic processing	23
1.3.5. T5-DSB: Indirect DSB induced by chemical processing	23
1.3.6. T6-DSB: Clustered DSBs	24

2. Aim of the work	27
3. Previous investigations with the I-SceI model system	30
4. Materials and methods	31
4.1. Materials	31
4.1.1. Laboratory apparatus	31
4.1.2. Disposable elements	33
4.1.3. Chemical reagents	33
4.1.4. Commercial kits	35
4.1.5. Cell lines	36
4.1.6. Antibodies	36
4.1.7. Software	37
4.1.8. Plasmids	37
4.1.9. Oligonucleotides	38
4.2. Methods	39
4.2.1. Cell culture	39
4.2.2. Cryopreservation of cells	39
4.2.3. Drug treatments	39
4.2.4. Transfection by electroporation	40
4.2.5. Ionizing Radiation (IR) exposure	40
4.2.6. PCR	40
4.2.7. Agarose gel electrophoresis	42
4.2.8. Restriction enzyme digestion	42
4.2.9. Ligation	42
4.2.10. Transformation	42
4.2.11. Generation of competent <i>E. coli</i>	43
4.2.12. Plasmid preparation	43
4.2.13. Preparation of whole cell lysate	44
4.2.14. Protocol for REAP nuclear/cytoplasmic fractionation	44
4.2.15. Clonogenic survival assay	44
4.2.16. Cell cycle analysis by FACS	45
4.2.17. G2-premature chromosome condensation (G2-PCCs)	45
4.2.18. Southern blotting	47
4.2.18.1. Preparation and digestion of genomic DNA	47

4.2.18.2. Ethanol precipitation of digested DNA.....	48
4.2.18.3. Depurination and denaturation.....	48
4.2.18.4. Transfer to a nylon membrane.....	49
4.2.18.5. Generating radioactive probes for hybridization reactions.....	49
4.2.18.6. Hybridization.....	51
4.2.19. SDS Page.....	52
4.2.20. Immunoblotting.....	52
4.2.21. Immunofluorescence staining.....	53
4.2.22. Live cell imaging.....	53
4.2.23. Foci analysis by Imaris.....	55
5. Results.....	56
5.1. Model Systems for clustered DSBs.....	56
5.1.1. Design of DSB clusters of varying complexities.....	56
5.1.2. Transposition as a tool for achieving multiple random integrations of I-SceI constructs in the mammalian genome.....	60
5.1.3. Cloning of I-SceI constructs into the Sleeping Beauty (SB) transposon vector.....	62
5.1.4. Selected cell lines for transposition.....	64
5.1.5. SB-transposition-based integration of I-SceI constructs in multiple copies in wt CHO cells and DSB repair deficient mutants.....	65
5.1.6. Nomenclature.....	66
5.1.7. Characterization of the derived clones in the different genetic backgrounds.....	67
5.2. Which kind of lesion dominates the strong killing effect of IR?.....	75
5.2.1. Clustered DSBs have a markedly stronger killing capacity than simple DSBs.....	76
5.2.2. Clustered DSBs induce lethal Chromosomal Aberrations.....	80
5.2.3. G2-PCC breaks and exchanges are elevated in cells with clustered as compared to simple DSBs.....	81
5.3. Analysis of DNA damage signaling elicited by simple and clustered DSBs.....	83
5.3.1. Theoretical foci-maximum upon DSB induction by I-SceI.....	83
5.3.2. I-SceI induced DSBs trigger γ -H2AX foci formation at DSB sites.....	84
5.3.3. I-SceI induced DSBs trigger MDC1 foci formation.....	86
5.3.4. Marked differences in 53BP1 foci formation at simple and clustered DSBs.....	89
5.3.5. The number of 53BP1 foci is increased in G2 cells.....	92
5.4. Increasing the complexity of DSBs by various means compromises repair.....	94

5.4.1. Increasing the complexity of I-SceI DSBs by treatment with H ₂ O ₂	94
5.4.2. Increasing the complexity of I-SceI induced DSB ends by compromising D-NHEJ using small molecule inhibitors, or D-NHEJ defective mutants.....	96
5.4.3. Incidence of G2-PCC breaks and exchanges after increasing complexity at DSB sites.....	102
5.5. An inducible I-SceI system overcomes some limitations of the transient I-SceI transfection	105
6. Discussion	108
6.1. Generation and characterization of model systems for simple (T1-) and clustered (T6-) DSBs.....	108
6.2. Clustered DSBs have a higher killing potential compared to simple DSBs.....	109
6.3. The probability for misrepair of clustered DSBs is clearly elevated compared to simple-DSBs	109
6.4. I-SceI-induced simple- and clustered DSBs activate the DDR.....	112
6.5. 53BP1 recruitment differs between simple and complex DSBs.....	113
6.6. The number of 53BP1 foci is doubled in G2 cells (contribution of HR).....	114
6.7. Inhibiting PARP reduces the number of exchanges for T6-DSBs - A hint to the contribution of B-NHEJ for the repair of clustered lesions.....	115
7. Summary and outlook	116
8. References	118
9. Curriculum vitae.....	131
10. Erklärung.....	Error! Bookmark not defined.

Acknowledgements

First I would like to thank my supervisor Prof. Dr. George Iliakis for encouraging and supporting me constantly. I would like to particularly thank him for always giving me a second chance, especially in difficult phases of my thesis. I am very grateful that he shared his unique way of scientific thinking with me during intensive discussions. It helped me a lot in learning how to tackle scientific challenges and see things from different perspectives. It has been a pleasure to be part of your team.

I would like to thank Prof. Dr. Wolfgang-Ulrich Müller for being always helpful and Mrs Müller for her fast administrative assistance.

I would like to also thank JP for teaching me various techniques and sharing his profound knowledge and enthusiasm towards science with me.

My thanks go to Vladimir for the very efficient help in life cell experiments, the proofreading of my thesis and his scientific and great mental support.

I would like to thank Maria, Katja, Theresa and Swetlana for not only being great colleagues but also friends who contributed to have a pleasant time with a great atmosphere at this institute. Of course I would also like to thank all other lab members for always being very friendly and helpful.

My special thanks go to Max, Laura, Agnes and Melanie for going with me through nice and difficult phases, giving me strength and making me enjoy my life. Max I would like to also thank for correcting my thesis.

I am deeply grateful to my parents, who always believe in me and without whose motivation and support this thesis would not have been possible. Thank you for being such a strong foundation in my life.

Finally I would like to gratefully acknowledge the financial support by a grant (03NUK005C) from the BMBF awarded as part of the initiative for the preservation of radiation biology expertise in Germany (KVSF).

List of abbreviations

%	percent
°C	Degree Celsius
4HT	Hydroxytamoxifen
53BP1	p53 binding protein
Ab	Antibody
ADP	Adenosinediphosphate
Approx.	Approximately
ATM	Ataxia-telangiectasia-mutated
ATR	Ataxia-telangiectasia and rad3 related
BER	Base excision repair
B-NHEJ	Backup pathway of nonhomologous end-joining
bp	Base pair
Bq	Bequerel
BRCA1	Breast cancer susceptibility protein 1
BRCA2	Breast cancer susceptibility protein 2
BRCT	Breast cancer C-terminal
BSA	Bovine serum albumin
CE	Cytoplasmic extract
CHO	Chinese hamster ovary
Cpm	Counts per minute
CSR	Class switch recombination
CtIP	C-terminal binding protein interacting protein
DAPI	4',6-diamidino-2-phenylindole
dd	Double distilled
DDR	DNA damage response
DIC	Differential interference contrast
D-MEM	Dulbecco's modified eagle's medium
DMSO	Dimethyl sulfoxide
DNA	Deoxyribonucleic acid

DNA-PK	DNA dependent protein kinase
DNA-PKcs	Catalytic subunit of the protein DNA-PK
D-NHEJ	DNA-PK-dependent non-homologous end joining
ds	Double stranded
DSB	DNA double strand break
e.g.	exempli gratia
ECL	Enhanced chemiluminescence
EDTA	Ethylene diamine tetraacetic acid
EGFP	Enhanced green fluorescent protein
et al.	et alii (and others)
EtBr	Ethidium bromide
eV	Electron volt
Exo1	Exonuclease 1
FACS	Fluorescence activated cell sorting
FBS	Fetal bovine serum
FHA	Fork head-associated
FITC	Fluorescein isothiocyanate
FPLC	Fast protein liquid chromatography
G1	Cell cycle phase gap 1
G2	Cell cycle phase gap 2
Gy	Gray
H	Histidine
h	Hour
HE	Homing endonuclease
HEPES	4-(2-Hydroxyl)-1-piperazineethanesulfonic acid
HR	Homologous recombination repair
HST	Histogram
IR	Ionizing radiation
IR/DR	Inverted/directed repeat
IRIF	Ionizing radiation induced foci
K	Lysine

kDa	Kilodalton
keV	Kilo electron volt
KO	Kusabira orange
LET	Linear energy transfer
LIF	Leica image format
Lig	Ligase
LMDS	Locally multiply damaged site
LSB	Low salt buffer
m	Mouse
Mab	Monoclonal antibody
MDC1	Mediator of the mammalian DNA damage checkpoint 1
MEM	Minimal essential medium
MI	Mitotic index
Min	Minute
MMEJ	Microhomology-mediated end joining
MMR	DNA mismatch repair
M-phase	Cell cycle phase mitosis
MQ	Milli-Q
MRE11	Meiotic recombination 11
MRN complex	Mre11-Rad50-Nbs1 complex
MW	Molecular weight
NBS1	Nijmegen breakage syndrome1
NE	Nuclear extract
ng	Nanogram
NHEJ	Non-homologous end joining
NLS	Nuclear localization signal
Pab	Polyclonal antibody
PAGE	Polyacrylamide gel electrophoresis
PARP	Poly (ADP-ribose) polymerase
PBS	Phosphate buffer saline

PBST	PBS with Tween 20
PCC	Premature chromosome condensation
PFGE	Pulsed field gel electrophoresis
PI	Propidium iodide
PIKK	Phosphoinositide-3-kinase-related protein kinase
PMSF	Phenylmethylsulfonylfluoride
PMT	Photomultipliers
r	Rabbit
RAP80	Receptor-associated protein 80
RBE	Relative biological effectiveness
RE	Restriction endonuclease
RNAse	Ribonuclease
RNF8/168	Ring finger protein 8/168
ROS	Reactive oxygen species
RPA	Replication protein factor A
rpm	Revolution per minute
RS	Recombination signal
RT	Room temperature
SB	Sleeping beauty
SDS	Sodium dodecyl sulfate
SDSA	Synthesis dependent strand annealing
Sec	Second
Ser	Serine
SMC	Structural maintenance of chromosome
S-Phase	Cell cycle synthesis phase
ss	Single stranded
SSA	Single strand annealing
SSB	Single strand break
SUMO	Small ubiquitin-like modifier
TEMED	<i>N</i> '-Tetramethylethylenediamine
Thr	Threonine

Tris	Tris-(hydroxymethyl)-aminomethane
Tyr	Tyrosine
Ub	Ubiquitylation
UIM	Ubiquitin interacting motive
UV	Ultraviolet light
V(D)J	Variable (diversity) joining
WCE	Whole cell extract
wt	Wild type
XRCC	X-ray cross complementation group
γ -H2AX	Phosphorylated form of histone H2AX at Ser-139

Abstract

In cells exposed to ionizing radiation (IR) energy deposition events in the form of ionization clusters induce clustered damages in the DNA. The processing of clustered DNA damage is likely to be different from that of the constituent lesions when induced in isolation, and possibly error-prone. The prevalent view in the field is that base lesions and breaks clustered within one or two DNA helical turns impair processing, not only of the secondarily induced DSBs, but also of themselves causing mutations or cell death.

A special form of clustered DNA damage, which received attention in the past but is presently only rarely studied, is two DSBs induced in close proximity on the DNA molecule. Such clustering of DSBs at distances between a few hundred to a few thousand base pairs is likely to generate unstable chromatin fragments highly prone to loss, which may locally destabilize the genome and initiate adverse biological consequences. Although IR is known to generate this potentially highly-dangerous form of DNA damage, study of its biological relevance is hampered by difficulties to induce it in a controlled manner. This leaves theoretical modeling as the only approach for estimating its induction, but still without offering means for analyzing its effects. In an attempt to close this gap we used advanced biological approaches to model DSB clustering and test its biological consequences.

Therefore cell lines in which simple DSBs and DSB-clusters can be induced in the genome by restriction of I-SceI sites engineered at defined distances in the DNA were developed. For this purpose, constructs carrying one, two or four I-SceI sites, placed at precisely defined distances to model increased clustering of DSBs, were randomly integrated in the genome using the Sleeping Beauty transposon technology. This thesis presents results obtained with clonal cell lines generated from wild type CHO cells, as well as from CHO mutants which are deficient in HR (irs1SF) or NHEJ (Xrs6, XR-C1-3). Before use for experiments, each clone is characterized for the number of construct integrations by Southern blotting, which provides the maximum number of complex DSBs that can be induced upon transfection with I-SceI.

Performing cell survival experiments by colony formation, we could show that CHO clones with high number of integrations undergo extensive killing after induction of DSBs by I-SceI that is proportional to lesion complexity. In accordance with the strong killing observed in survival experiments the probability for misrepair measured by G2-PCC is clearly elevated for DSB clusters, showing that clustered DSBs have a high risk for the formation of chromosomal aberrations. Furthermore life cell imaging of 53BP1 foci revealed differences in signaling characteristics for different levels of DSB complexity unraveling unexpected activation characteristics of the DNA damage response that require further investigations.

1. Introduction

1.1. Cellular mechanisms for signaling and repair of DNA double strand breaks (DSBs)

1.1.1. DSBs - a threat for genomic stability

Maintaining genomic integrity is crucial for cell growth and survival. One of the most dangerous DNA lesions leading to adverse biological consequences are DSBs. They interrupt the continuity of the DNA molecule as both strands of the DNA duplex are severed by a break in the phosphodiester backbone at opposite sites within 10 bps. Unrepaired DSBs may lead to the loss of genomic stability by triggering the formation of translocations, deletions, mutations and by destabilizing chromatin. These repair failures can constitute key driving forces for the development of various human syndromes, neurological disorders, immunodeficiency and cancer (Jackson and Bartek 2009; Bohgaki, Bohgaki *et al.* 2010).

There are different ways how DNA-DSBs can arise, either by exogenous DNA-damaging agents like ionizing radiation (IR) and chemical compounds (radiomimetic drugs, topoisomerase inhibitors) or by endogenous cellular processes, such as generation of reactive oxygen species (ROS), V(D)J recombination and class switch recombination (CSR) during maturation of B- and T-lymphocytes, as well as during DNA replication. A highly regulated signaling network activated upon DSB induction is crucial for cells to orchestrate the DNA repair pathways and maintain genomic integrity. Two main DSB repair pathways have evolved: Homologous recombination (HR) and non-homologous end joining (NHEJ). HR mainly operates in the G2 phase of the cell cycle using a sister chromatid or a homologous chromosome as a template, faithfully restoring the sequence. NHEJ is an error prone pathway that operates in all phases of the cell cycle and promotes direct ligation of the DSB ends thus restoring the DNA structure. In addition, when NHEJ is impeded an alternative end joining pathway termed Backup NHEJ (B-NHEJ) operates (Mladenov and Iliakis 2011).

This work focuses on investigating the possible sources of repair failures of these highly effective repair machineries. We want to test the hypothesis that clustered DSBs are much more prone to repair accidents compared to simple DSBs. The following sections describe cellular responses to DSBs and give examples for various genotoxic agents and endogenous intracellular processes that lead to the formation of DSBs with different levels of complexity.

1.1.2. DNA damage response (DDR)

The signaling process known as DNA damage response is activated after DSB induction to counteract adverse consequences for the cell like translocations and chromosomal aberrations. It triggers a coordinate series of events that regulate cell cycle progression and repair of DNA lesions.

1.1.2.1. Activation of cell cycle checkpoints or apoptosis

In response to DNA damage DDR activates cell cycle checkpoints and pauses cell cycle progression, thus granting time for damaged cells to repair in order to prevent duplication and segregation of the damaged DNA. The DDR is organized into an elaborate network of interacting pathways that have a well-defined hierarchy of their components comprising sensors, transducers, mediators and effectors (Fig. 1). Three members of the phosphatidylinositol-3 kinase-related kinases (PIKK) family namely ATM, ATR and DNA-PKcs play important roles in the signaling network of DDR proteins. These effector proteins consist of serine/threonine protein kinases and have the ability to phosphorylate a number of mediators leading to the propagation of DSB signaling (Shiloh 2003).

Active PIKK kinases phosphorylate the effector kinases CHK1 and CHK2 that can activate different cell cycle checkpoints. Activated ATM, ATR and CHK2 phosphorylate p53 that transactivates p21 leading to the inhibition of cyclin-dependent-kinases and a G1 arrest to stop the cell before replication. In the case that DNA damage is too extensive and cannot be repaired, p53 activates its transcriptional targets including Bax, Puma and Noxa to promote apoptosis.

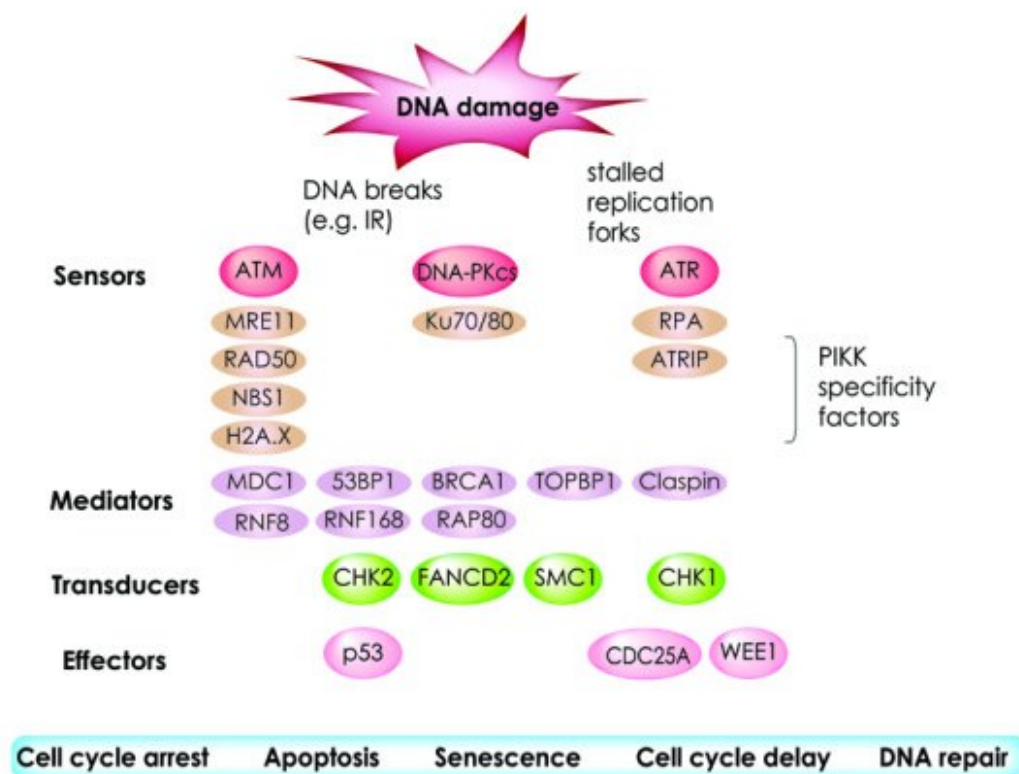


Fig. 1: Schematic representation of DNA damage-signaling and the proteins involved in the different steps (Bohgaki, Bohgaki et al. 2010). DNA lesions are recognized by sensor proteins. Mediators serve to amplify the signaling of DNA damage. Next, proteins including CHK1 and CHK2 serve to transduce the generated DNA damage signals to effector molecules. Finally, the effectors trigger the appropriate, DNA damage-associated cellular responses including apoptosis, senescence, cell-cycle arrest or delay that give time to cells to repair their damaged DNA.

CHK1 mediates intra S and G2 checkpoint activation to prevent cell division. It inactivates CDC25C and activates WEE1 through their phosphorylation resulting in inhibition of CDC2/cyclinB activity, and thus in a G2/M arrest. The CHK1 phosphorylation of CDC25A leads to CDK2 inactivation and a delayed intra S-Phase checkpoint (Sanchez, Wong *et al.* 1997).

1.1.2.2. Multistep signaling of DSBs

The highly ordered assembly of proteins at the DSB-flanking chromatin is mainly mediated by post translational modifications like phosphorylation, ubiquitylation, methylation, SUMOylation and acetylation that regulate protein-protein interactions. While most of the DDR proteins are always synthesized in the cell, activation of the DDR triggers a dramatic increase in their availability, activity and intracellular distribution. The increased local concentration of DDR proteins at DSB sites in distinct nuclear compartments forms the so called Ionizing Radiation Induced Foci (IRIF), a highly regulated and at the same time dynamic process with a tight spatiotemporal coordination of assembly and disassembly of protein complexes (Bekker-Jensen and Mailand 2010).

Immediately after DSB induction the DSB ends are sensed by the MRN (Carson, Schwartz et al. 2003) and the Ku70/80 complexes. The Ku heterodimer has a toroidal structure with a hole through which it loads onto DSB ends (Ciccia and Elledge 2010) within seconds. PARP1/2 also sense DSBs and catalyzes the rapid formation of poly (ADP-ribose) (PAR) chains. PARP1 competes with Ku and promotes B-NHEJ (Wang, Wu et al. 2006). The MRN complex that is also involved in DSB end processing comprises the components Mre11, Rad50 and NBS1. Mre11 has a single strand endonuclease activity and a 3'-5' DNA exonuclease activity. Rad50 belongs to the structural maintenance of chromosome (SMC) protein family. The third component of the MRN complex, NBS1 (Nijmegen breakage syndrome 1) upregulates the endonuclease activity of Mre11 whereas Rad50 upregulates its endo- and exonuclease activity. MRN mediates the recruitment of ATM whereas Ku70/80 recruits DNA-PKcs to DSB ends. MRN interacts with the N-terminal domain of ATM and is also required for ATM activation. In its inactive state ATM forms dimers or multimers, whereas upon activation, ATM is autophosphorylated on Ser 1981 and dissociates into active monomers. ATM mediates H2AX phosphorylation on Ser 139 to form γ -H2AX which serves as a key regulator of checkpoint signaling and repair (Rogakou, Pilch *et al.* 1998; Fernandez-Capetillo, Chen *et al.* 2002; Chapman, Taylor *et al.* 2012).

MDC1 recognizes and binds to γ -H2AX via its tandem BRCA1-C-terminal (BRCT) domains (Stucki, Clapperton *et al.* 2005). MDC1 serves as a key recruitment factor for downstream IRIF associated proteins and protects γ -H2AX from de-phosphorylation.

The MDC1 recruitment to γ -H2AX promotes further accumulation and retention of active ATM and MRN complexes (Lukas, Melander *et al.* 2004) and a subsequent extension of H2AX phosphorylation to flanking nucleosomes (Fig. 2). During this step a positive feedback loop can be created that extends the γ -H2AX domain up to a 2 Mbp region of chromatin (Kinner, Wu *et al.* 2008). MDC1 and ATM recruit additional DDR factors on γ -H2AX marked chromatin, like RNF8, RNF168, BRCA1 and 53BP1.

DDR dependent MDC1 phosphorylation and recruitment to γ -H2AX initiates an ubiquitination cascade at DSB sites. RNF8 belongs to the U3 ubiquitin ligases containing an FHA domain at its N-terminus that recognizes distinct phosphorylation sites in the N-terminal half of MDC1. It signals accumulation of DDR factors downstream of the γ -H2AX-MDC1 interaction (Mailand, Bekker-Jensen *et al.* 2007). RNF168 regulates RNF8-mediated ubiquitylation of histones and maintains this modification at DSBs causing chromatin remodeling. RNF168 contains a RING finger domain and two motifs that interact with ubiquitin (UIM). It ubiquitylates H2A and H2AX generating ubiquitin chains on H2A that are required for the recruitment of 53BP1 and BRCA1 (van Attikum and Gasser 2009). To distinguish the ubiquitylated H2A in IRIF from the ubiquitylated H2A throughout the whole nucleus, RNF8 and RNF168 together with an E2 ubiquitin ligase, UBC13 generate K63-linked non proteolytic ubiquitin chains on histones.

In addition to ubiquitylation and phosphorylation SUMOylation is also required for DSB signaling. The SUMO E3 ligases PIAS1 and PIAS4 are recruited to DSBs and mediate DSB induced ubiquitylation of RNF8 and RNF168. Furthermore, PIAS4 mediates SUMO1 modification of 53BP1 and BRCA1, while SUMO2/3 modification of BRCA1 is also mediated by PIAS4.

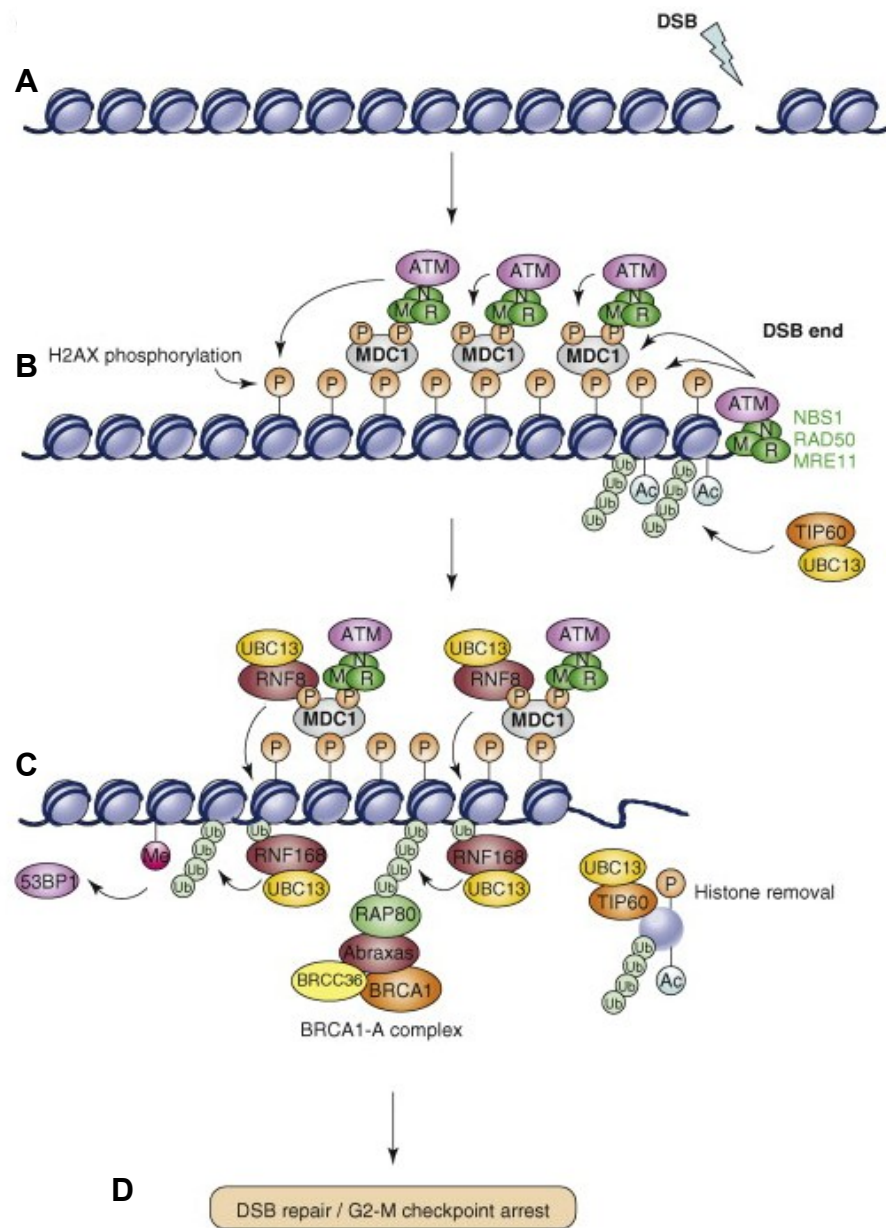


Fig. 2: Model for the function of γ -H2AX at DSB in mammals (van Attikum and Gasser 2009) **A:** A DSB is induced by IR. **B:** The MRN complex binds to the ends of the DSB and recruits ATM, which phosphorylates H2AX. MDC1 is recruited and binds to γ -H2AX. Phosphorylation of MDC1 recruits more MRN-ATM that phosphorylates more H2AX. TIP60 acetylates (Ac) γ -H2AX. Subsequently it associates with the E2 ubiquitin-conjugating enzyme UBC13 to regulate polyubiquitylation (Ub) of acetylated γ -H2AX. **C:** Polyubiquitylated and acetylated γ -H2AX is removed from chromatin. ATM phosphorylates MDC1 to recruit an RNF8-UBC13 complex that regulates ubiquitylation of histone H2AX and H2A. RNF168 binds to these ubiquitylated histones and promotes the formation of ubiquitin conjugates. Polyubiquitylated histones recruit the BRCA1-A complex and 53BP1. The BRCA1-A complex directly binds Ub-histones through the RAP80 subunit. 53BP1 binds to methylated (Me) histones after RNF8-RNF168-UBC13-mediated polyubiquitylation. **D:** Finally, these events facilitate DSB checkpoint arrest and repair.

The recruitment kinetics of MRN, γ -H2AX, MDC1 and RNF8 foci following DSB induction is rapid, reaching maximum accumulation within a few minutes. After 1-2 min a second wave of protein accumulation follows including 53BP1 and BRCA1.

RNF8 facilitates this accumulation of the two checkpoint mediator proteins 53BP1 and BRCA1 to the damaged chromatin through the phospho-dependent FHA domain-mediated binding of RNF8 to MDC1, as well as through its role in ubiquitylating H2AX (Huen, Grant et al. 2007).

The BRCA1-A complex bridges the interaction between BRCA1 and ubiquitylated histones. The ubiquitin BRCA1 response is controlled by chromatin remodeling events mediated by p400 ATPase together with TIP60 acetyltransferase that are recruited by MDC1 to destabilize nucleosomes for efficient ubiquitylation (Luijsterburg and van Attikum 2012). RAP80, which is the central component of the BRCA1-A complex, contains two ubiquitin interaction motifs (UIM) that bind ubiquitylated histones. Together with Abraxas, BRCC36, BRE and NBA1, RAP80 forms the so called MERIT40 complex. Abraxas is a coiled coil domain protein that forms the structural core for protein assembly and binds to the tandem BRCT domains of BRCA1.

The RNF8/RNF168 pathway regulates the efficient association of 53BP1 with H4K20 (histone 4 methylated at Lys 20) by recruiting the ubiquitin selective ATPase VCP (p97) and its cofactor NPL4 to chromatin. VCP mediates the extraction of the polycomb protein L3MBTL1 from chromatin unmasking 53BP1 binding sites. In addition the MMSET methyltransferase promotes 53BP1 recruitment by mediating di-methylation of H4K20 after recruited to the DSB by MDC1 (Luijsterburg and van Attikum 2012).

1.1.3. Repair pathways

The highly efficient DSB repair pathways that function as a part of the DDR are described in the following section.

1.1.3.1. HR

Homologous recombination is an error free process that can be divided into the following three main stages: presynapsis, synapsis and postsynapsis. (Heyer, Ehmsen *et al.* 2010). In the presynaptic stage the DNA DSB is sensed by MRN (Fig. 3A). Subsequently the DNA ends are resected to form extended regions of single stranded DNA (ssDNA) with 3' overhangs. The nucleases Exo1, Dna2 and CtIP are involved in this process together with MRN and the BLM helicase. The ssDNA is coated by RPA (replication protein A) to eliminate secondary structures and stabilize the ssDNA for the formation of the Rad51 nucleoprotein filament. The Rad51 filament formation requires different classes of mediator proteins like the group of Rad51 paralogs (Rad51B, Rad51C, Rad51D, XRCC2, and XRCC3) and BRCA2.

During synapsis the nucleoprotein filament searches for homology and performs strand invasion to form a Holliday junction. Rad54 promotes DNA synthesis associated with branch migration by dissociating Rad51 from the heteroduplex DNA.

During the postsynapsis, predominantly synthesis-dependent strand annealing (SDSA) occurs, where the extended Holliday junction is resolved enabling the annealing of the newly synthesized strand with the resected strand of the second end. Finally after subsequent DNA synthesis and ligation the DNA sequence is restored. In a scenario where the second DNA end is absent, which can occur at telomeres or replication forks, BIR (break induced replication) takes place that restores the integrity of the chromosome but can lead to loss of heterozygosity (San Filippo, Sung *et al.* 2008). Another possibility is the formation of double Holliday Junctions that migrate towards each other, while priming DNA synthesis. In this case the final resolution of the Holliday junctions may lead to the formation of crossover or non-crossover events (Bzymek, Thayer *et al.* 2010). If strand invasion does not occur, a further pathway called single

strand annealing SSA can be utilized by the cell. SSA proceeds by annealing of longer than 30 nt homologous sequences after resection resulting in large deletions.

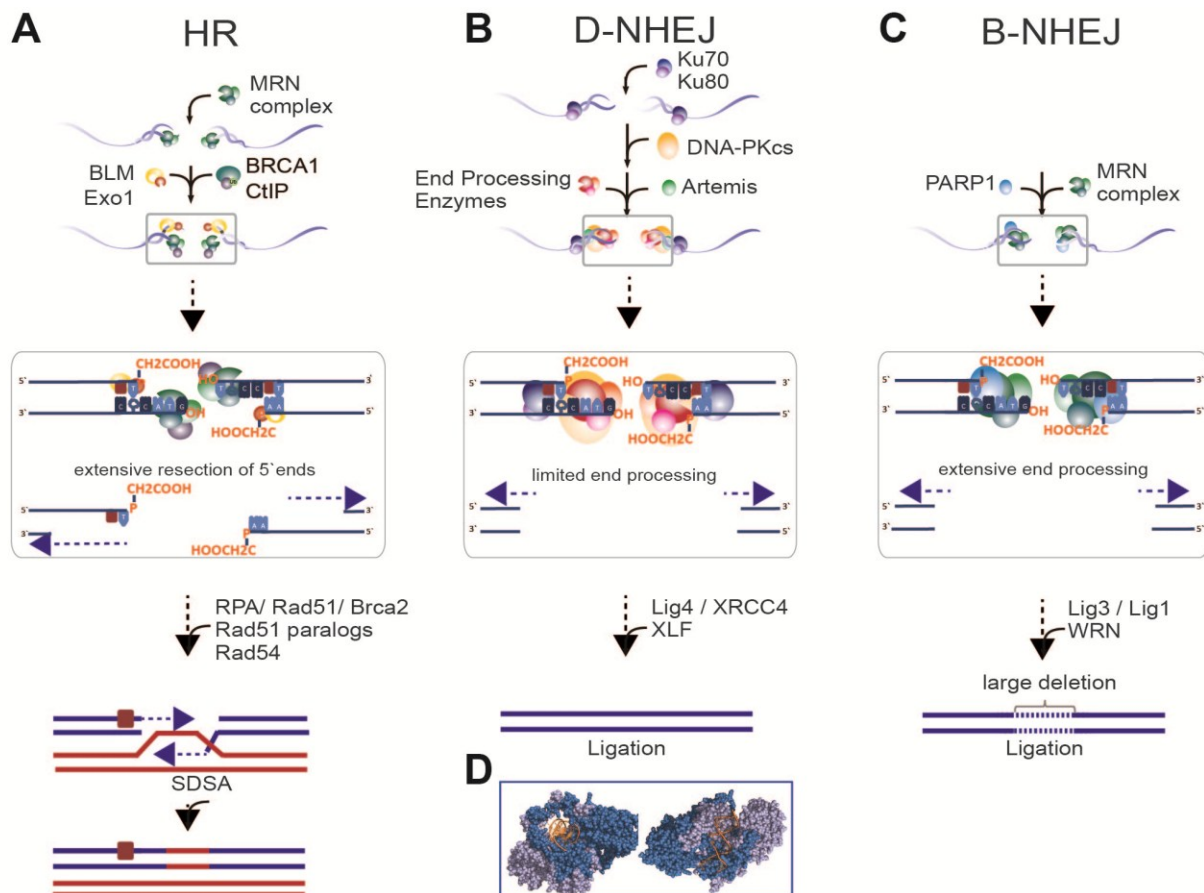


Fig. 3: Schematic representation of the three DSB repair pathways HR, D-NHEJ and B-NHEJ. (Schipler and Iliakis 2013). **A:** During HR, extensive processing of the 5'-ends takes place that can remove lesions in the vicinity of DSB ends. **B:** For D-NHEJ, limited end processing takes place at both DNA strands. **C:** For B-NHEJ extensive end processing takes place. B-NHEJ often results in large deletions and translocations. **D:** The ring shaped Ku proteins binds to 15 bp DNA at the DSB ends

1.1.3.2. D-NHEJ

D-NHEJ is considered as the prevalent DSB repair pathway in higher eukaryotes that essentially mediates the fast (direct) ligation of broken DNA ends to maintain chromosome integrity. (Iliakis, Wang *et al.* 2004). It is initiated by the binding of the Ku70/Ku80 heterodimer to DSB termini generating a scaffold that can associate with all other NHEJ factors (Fig. 3B). The Ku heterodimer has a ring-shaped structure allowing the protein to slide over the ends of the DNA molecule (Walker, Corpina *et al.* 2001). After forming the Ku-DNA complex, Ku recruits (Chappell, Hanakahi *et al.* 2002) and activates the DNA-dependent protein kinase catalytic subunit (DNA-PKcs) that protects the DNA termini against degradation and premature ligation. Furthermore DNA-PKcs tethers the DNA ends and forms a synaptic complex that juxtaposes the broken DNA ends for processing upon a conformational change induced by DNA-PKcs autophosphorylation (Weterings and Chen 2007).

End processing of the DNA termini is required for almost all DSB types except blunt ended DSBs that can be simply religated without further processing. NHEJ enzymes tolerate wide spectra of structural DNA end substrate configurations like variations in the overhang length, DNA end sequence and/or chemistry (Weterings and Chen 2008). Non-compatible single stranded DNA overhangs can be either removed by resection or a new complementary strand is synthesized using the nucleotide sequence overhang as template. In the second case DNA synthesis is performed by proteins like the DNA polymerases λ , μ , and Artemis (that can have a DNA-PKcs-independent exonuclease activity or a DNA-PKCS-dependent endonuclease activity). These end processing steps can lead to different repair outcomes like deletions, insertions or sequence alterations, some of the reasons why NHEJ is considered to be an error prone pathway. End processing can also require the addition of a 5`phosphate group mediated by the mammalian polynucleotide kinase (PNK) in an XRCC4-and DNA-PKcs-dependent manner (Chappell, Hanakahi *et al.* 2002), or the removal of a 3`phosphoglycolate by different enzymes like the tyrosyl-DNA phosphodiesterase TDP1, the polynucleotide kinase PNK and Artemis (Lieber 2010).

In the final step the processed DNA ends are ligated by the Ligase4/XRCC4 protein complex that is attracted to the synaptic repair complex by the Ku-DNA scaffold after releasing DNA-PKcs. Alternatively the XLF/Cernunnos interacts with the XRCC4/Ligase4 complex by stimulating ligation of non-compatible single strand ends followed by synthesis of the complementary strand to prevent nucleotide loss during end resection (Tsai, Kim *et al.* 2007).

1.1.3.3. B-NHEJ

An alternative end-joining pathway termed B-NHEJ (Backup Pathway) or alternative end-joining (alt-NHEJ) operates particularly when classical NHEJ and possibly also HR are impeded (Fig. 3C). This pathway utilizes proteins like PARP-1 and DNA Ligase 3/XRCC1 (Wang, Rosidi *et al.* 2005) that are also known to be involved in the repair of single strand breaks (SSB). Competition for DNA end binding between PARP and Ku is considered as a possible scenario for the initial step after DSB formation, whereas Ku has a significantly increased affinity for binding, underlining the backup character of B-NHEJ (Wang, Wu *et al.* 2006). DNA end processing by Mre11 is implicated as a further step in B-NHEJ, as inhibition of Mre11 in NHEJ compromised CHO cells suppresses end joining (Rass, Grabarz *et al.* 2009). Furthermore the linker Histone H1 has been identified to be involved in the backup pathway probably aligning DNA ends prior to ligation (Rosidi, Wang *et al.* 2008). The finding of abundant regions of microhomology at B-NHEJ mediated repair junctions leads to the assumption that stabilization of the DNA prior to ligation may be promoted by microhomologies. During the final step of the pathway, Ligase 3 functions in a complex with XRCC1 to ligate the DNA ends, a process that is regulated by PARP1 (Audebert, Salles *et al.* 2004). Recent evidence suggests other proteins like the Werner Syndrome Proteins (WRN) and BCR/Abl to be involved in this pathway, whereas WRN forms a complex with Lig3 prior to ligation (Sallmyr, Tomkinson *et al.* 2008).

The activity of B-NHEJ shows strong cell cycle fluctuations. It increases in G2 and is reduced in G1 and is significantly abrogated in resting cells.

This change in activity levels hints to a backup role of B-NHEJ not only for classical NHEJ (D-NHEJ) but also for aberrant HRR, an observation that requires further investigation (Wu, Wang *et al.* 2008).

Although B-NHEJ is facilitated by fortuitously present micro-homologies exposed after resection at the DNA ends (therefore also termed microhomology-mediated end-joining, MMEJ (McVey and Lee 2008), this is not a requirement for its function. DSB processing pathways with absolute requirement for extensive homology, like homologous recombination (HR) and single strand annealing (SSA) operate after DNA replication when a sister chromatid becomes available; they include gene conversion and deletion.

1.2. Possible sources of DSB induction

1.2.1. Ionizing Radiation (IR)

Ionizing radiation (IR) is unique in the broad spectrum of various DNA damage types it can induce as a result of the special characteristics of the initial local energy deposition events (Goodhead, Thacker *et al.* 1993).

IR deposits its energy along the radiation track it traverses producing ionization clusters and is therefore up to 1000 times more effective at cell killing compared to other types of DNA damaging agents that give rise to randomly distributed radicals. The dose of radiation to biological material is defined in terms of the amount of energy absorbed per unit mass. 1 Gy is equivalent to 1 J/kg. DNA damage by IR is formed either as direct action by the local properties of radiation tracks within the DNA, or as an indirect action in the surrounding cellular environment within a radical diffusion distance of around 4 nm. Indirect action is mainly mediated by the radiolysis of water.

The biological effects of IR are the end product of the initial physical events comprising ionizations and excitations of atoms and molecules along the tracks of the ionizing particles. Therefore the interaction of IR with matter can be described by the following consecutive processes: Physicochemical reactions, chemical reactions and finally the biological effect.

1.2.1.1. Physical and chemical aspects of IR interaction with matter

IR is classified as electromagnetic or particulate, whereas the electromagnetic radiation, comprising X-rays and γ -rays is indirectly ionizing as it deposits the majority of its energy through the production of secondary electrons. Particulate radiation including electrons, protons, α -particles, neutrons and heavy charged particles is directly ionizing as its charged particles have sufficient kinetic energy to disrupt the atomic structure of the absorber through which they pass directly producing chemical and biological changes (Hall and Giaccia 2006).

Various computational approaches, named Monte Carlo track structure codes, have been developed to simulate the stochastic effect of ionizing radiation of different

qualities. Monte Carlo computer simulations of radiation tracks include each ionization or excitation of the primary charged particles and all their secondary particles until they come to rest (Paretzke 1987).

The features for the highly structured radiation tracks clearly vary between densely ionizing high linear energy transfer (LET) radiation like neutrons and alpha particles and sparsely ionizing, low LET X-rays or γ -rays (Fig. 4). LET is defined as the average energy that an ionizing particle deposits per unit length of track ($\text{KeV}/\mu\text{m}$) as it traverses matter. In case of low LET radiation most of the energy is deposited as single isolated sparse ionizations whereas localized ionization clusters are formed by low energy secondary electrons at the end of the track comprising 30-50% of the local energy deposition of low LET radiation (Goodhead and Nikjoo 1989). High LET radiation deposits most of its energy within a small volume in the target. Compared to low LET, high LET radiation has a higher number of primary radicals close together in the radiation track therefore, the yield of molecular products from pairs of radicals increases, whereas the single radical products decrease.

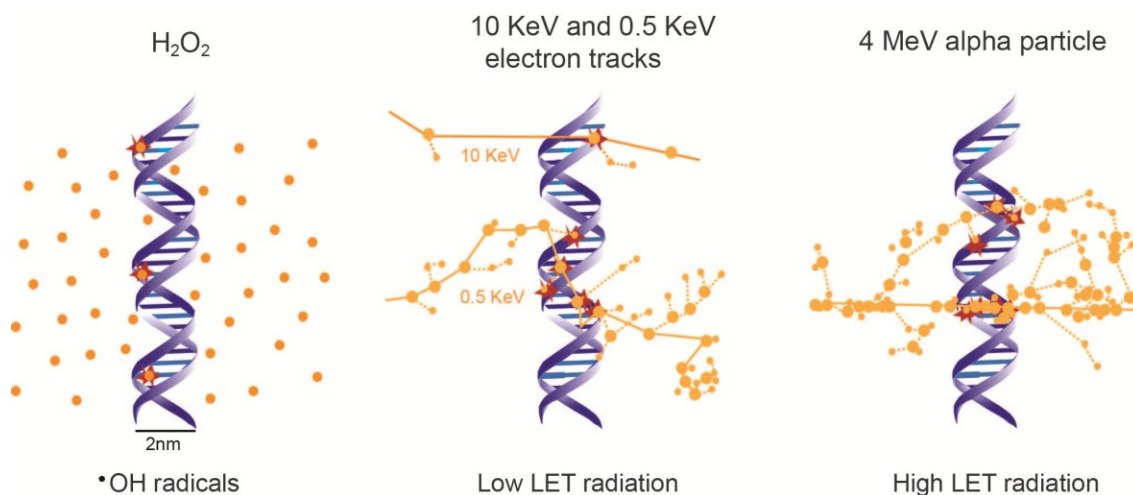


Fig. 4: Random DNA damage induction by H_2O_2 compared to DNA damage induction by low and high LET radiation tracks. $\cdot\text{OH}$ radicals are evenly distributed in space and induce DNA damage randomly. In the case of IR, ionization events localize along the radiation tracks and therefore induce clustered damage. With increasing LET the damage clustering increases. Large dots represent ionizations and small dots represent excitations along the radiation track. The Monte Carlo simulated tracks are drawn on the same scale as the DNA (Goodhead 1995; Schipler and Iliakis 2013)

1.2.1.2. Biological consequences of clustered DNA damage induced by IR

It is assumed that the clustering of DNA damage induced by ionization clusters within single tracks determines the effectiveness of radiation.

Furthermore, differences have been observed in DSB repair efficiency, as well as in the yield of DSBs causing lethal events - by densely or sparsely ionizing radiation. Isolated DNA damages including SSBs as well as DSBs correlate poorly with biological effectiveness for cellular effects. Only slight LET dependence is observed in the general yield of DSBs for different radiation qualities due to the balance between the number of particles and the increased local ionization density. In contrast, the formation of clustered complex DSBs shows a strong LET dependence. Whereas for low energy electrons around 30% of DSBs contain more than two strand breaks, clustering is observed for 70% of DSBs induced by alpha-particles by alpha-particles (Durante and Loeffler 2010; Georgakilas, O'Neill et al. 2012).

All types of IR can induce severe, clustered DNA damage due to its unique characteristics of depositing energy along the tracks of the constituent ionizing particles. Monte Carlo simulations for mammalian cells for low and high LET radiation revealed an increase in cluster complexity with increasing LET, and an associated increase in the ratio of DSBs to SSBs (Nikjoo, O'Neill et al. 1999). Per unit absorbed dose approx. the same number of DNA lesions are created for low and high LET radiation; they comprise around 1000 SSBs and base damages and 20-40 DSBs per Gy of radiation (Ward 1990). But the distribution of the lesions with high LET radiation occurs within smaller regions of the target, causing an increase in cluster complexity. The increased ionization clustering along the tracks of densely ionizing forms of IR generates DNA damage that is more complex, in the sense that it comprises more lesions within the same DNA segment (one or two helical turns), than that induced by low LET radiations. Yet, per unit absorbed dose approx. the same number of DNA lesions are created for low and high LET radiation (Ward 1990). Since high LET forms of IR have greater relative biological effectiveness (RBE) per unit dose than those exposed to low LET radiation, it can be concluded that not the total number of ionizations alone, but also their spatial distribution determine the gravity of the resulting biological effect.

(Goodhead 1994). The RBE of a radiation is defined as the dose of reference radiation divided by the dose of the test radiation to give the same biological effect. The reference radiation has historically been 250 kV X-rays.

1.2.1.3. VDJ/CSR

V(D)J recombination is an essential process in generating a high diversity of B-cell and T-cell receptors during the maturation of B- and T-lymphocytes in order to recognize a wide range of pathogen epitopes. Both processes involve a highly regulated induction of DSB clusters and the loss of intervening sequences.

V(D)J recombination is a specialized somatic DNA rearrangement mechanism that randomly combines variable (V), diversity (D) and joining (J) encoding gene segments of the immunoglobulin heavy chains (IgH) and VJ segments of the immunoglobulin light chains (IgL). The process is initiated by the lymphoid specific factors of the V(D)J recombinases, RAG1 and RAG2 (recombination activating genes), that recognize recombination signal sequences (RSS) flanking each V, D and J gene segment and induce blunt ended DSBs adjacent to them (Dudley, Chaudhuri *et al.* 2005). RSS are composed of conserved heptamer and nonamer sequences and an intervening spacer sequence of 12 or 23 bp. For DSB induction RAG1 and RAG2 form a protein complex and align two RSS to induce two SSBs at the 5' end of each RSS. The resulting 3'OH groups attack the phosphodiester bond on the other strand and produce a 5' phosphorylated double-stranded break at the RSS and a covalently closed hairpin at the coding end that has to be processed prior to rejoining. The induced DSBs are resolved by the DSB repair pathway NHEJ forming signal end joints (SJs) and coding end joints (CJs) finally resulting in recombination of V, D, and J gene segments.

CSR (class switch recombination) occurs exclusively in immunoglobulin genes of mature B-cells. This process allows the expression of an antibody with the same antigen-binding specificity but with an altered effector function, thus enabling the production of different isotypes. During CSR the constant region of the IgH is changed by rejoining the variable domain exon of the heavy chain locus (C_{μ}) with a downstream constant domain exon (C_H) after deleting the intervening sequence. For this recombination process DSBs are generated by the AID enzymes (activation induced

cytidine deaminases) at conserved nucleotide motifs called switch regions (S) located upstream of all C_H genes except C_δ.

In contrast to V(D)J recombination where DSBs are induced at short conserved signal sequences (RS), the S DSB target regions for CSR comprise 1-12 kbp repetitive DNA sequences. AID deaminates cytosine residues at S regions to generate uracil, which is processed by base excision repair (BER) and/or mismatch repair (MMR) pathways into DSBs (Di Noia and Neuberger 2007). Rejoining of DSBs in the last step of CSR is mediated either by NHEJ or by B-NHEJ.

1.2.1.4. Endonucleases

Restriction endonucleases (RE) are prokaryotic enzymes that have the role to protect host cells from invasion of foreign DNA i.e. bacteriophage infection. RE disrupt the phosphodiester bonds on both strands of the DNA molecule to generate either blunt or staggered DSB-ends while retaining the 5' phosphate and 3' OH groups at each strand. Depending on the enzymatic properties, different types of RE are distinguished. The most frequently applied RE in molecular biology are type II RE that are homodimers which recognize a 4-8 bp palindromic DNA sequence. Cleavage of these sites is symmetric about the dyad axis of the restriction site and may result in blunt ends, 5' overhanging fragments, or 3' overhanging fragments, depending on the particular enzyme (Gruen, Chang et al. 2002). Homing endonucleases (HEs) are double stranded DNases that have large, asymmetric recognition sites and coding sequences that are usually embedded in either introns or inteins (Belfort and Roberts 1997). Homing is the lateral transfer of an intervening sequence, either the intron or the intein to a homologous allele that lacks the sequence. The homing endonuclease is encoded by an ORF within the mobile intervening sequence and has evolved to catalyze highly specific DSBs in cognate alleles. In contrast to REs they tolerate some minor sequence degeneracy and bind long DNA target sites (14-40 bp) despite their small size (<40 kDa). The large recognition sequence ensures high specificity and low toxicity associated with excessive cleavage of a host genome (Chevalier and Stoddard 2001). HE recognition sites are extremely rare, with an 18 bp recognition sequence occurring once in every 7×10^{10} bp of a random sequence (Jasin 1996).

1.2.1.5. I-SceI as a tool to study DSB repair

The homing endonuclease I-SceI originates from the mitochondria of *Saccharomyces cerevisiae* with an 18 bp non-palindromic recognition sequence (Fig. 5). I-SceI is a monomer composed of two pseudosymmetric subdomains that recognize asymmetric substrates. It is widely used to study DSB repair pathways in mammalian cell lines as the 18bp recognition sequence is not inherent in mammalian cells (Honma, Sakuraba *et al.* 2007). Therefore cutting of intrachromosomally inserted I-SceI recognition sites result in double-strand DNA cleavage exclusively at the inserted site.

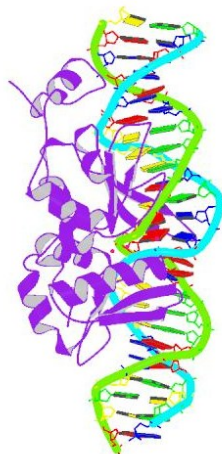


Fig. 5: I-SceI bound to DNA (1R7M protein data bank).

Various fluorescence based assays have been developed allowing functional analysis of specific repair pathways after site specific induction of DSBs by I-SceI. DSBs are either generated by transient transfection of I-SceI expressing vectors, or by a controlled translocation from the cytoplasm into the nucleus of constitutively expressed I-SceI. A widely used recombinational reporter system to measure HR in living cells is the direct repeat green fluorescent protein (DR-GFP) assay. In this system a chromosomally integrated construct harbors the I-SceI recognition site that has been integrated into the GFP gene disrupting the ORF. A truncated GFP gene fragment with the correct ORF sequence has been placed downstream in the construct. Repair of the cleaved I-SceI site by HR using the downstream fragment gives rise to a functional GFP gene, and GFP fluorescence then can be measured by flow cytometry. Using this

assay, the authors could show that error free HR repair of DSBs is decreased 25-fold in XRCC3 deficient CHO cells (Pierce, Johnson *et al.* 1999).

GFP-based chromosomal reporters have been developed to measure D-NHEJ with two I-SceI sites flanking an intervening sequence that separates the promoter from the GFP coding cassette. Simultaneous cleavage of both sites leads to the loss of the intervening sequence resulting in GFP expression upon successful rejoining of the two nearby I-SceI-induced DSBs. Using this assay Mansour *et al.* showed that mammalian cells require Ku for rapid NHEJ for complementary and non-complementary DSB ends. In the absence of Ku, B-NHEJ is employed that is completely dependent on PARP1 but does not need extensive microhomologies (Mansour, Rhein *et al.* 2010).

A further study showed that Mre11 promotes efficient NHEJ in both wild-type and Xrcc4^{-/-} mouse embryonic stem cells. End resection is suppressed in Xrcc4^{-/-} cells after depletion of Mre11, revealing specific roles for Mre11 in both D- and B-NHEJ (Hartlerode, Odate *et al.* 2011).

Bindra *et al.* have developed an assay to measure mutagenic nonhomologous end-joining (B-NHEJ, termed here mut-NHEJ) repair combined with a homologous recombination (HR) assay enabling the simultaneous monitoring of both pathways in living cells (Bindra, Goglia *et al.* 2013). They could show that B-NHEJ repair is suppressed in growth-arrested and serum deprived cells. These results are in accordance with previous observations from our lab (Windhofer, Wu *et al.* 2007; Singh, Wu *et al.* 2011; Singh, Bednar *et al.* 2012) suggesting that end-joining activity in proliferating cells is more likely to be mutagenic.

1.3. Not all DSBs are created equal: Levels of DSB complexity

The cellular responses described in the previous sections (1.1) are based on the assumption that all DSBs are created equal. But depending on the type of the DSB inducing agent, different levels of DSB complexity can be generated (Fig. 6). With increasing complexity also the possibility for processing errors may increase. The following section describes various categories of DSBs, Type 1-6 (T1-6) on the basis of increasing complexity (Schipler and Iliakis 2013).

1.3.1. T1-DSB: simple DSBs with clean ends

T1-DSBs generated by RE or HE are considered as the simplest form as they retain a 5' phosphate and the 3' OH group at each strand break after disrupting the phosphodiester bond (Obe and Natarajan 1985; Bryant and Johnston 1993). Endonuclease induced DSBs have clean ends as the disruption of the continuity of the DNA molecule occurs without chemically altering any of its constituent moieties, i.e. sugar or base modifications do not occur (Fig. 6A). Although T1-DSBs can be rejoined by simple ligation, subtle differences like type, 3' or 5', or length of protruding ends will affect DSB processing. Blunt ended DSBs are, at least *in vitro*, more difficult to ligate than DSBs with overlapping ends (Pfeiffer, Feldmann et al. 2005; van Gent and van der Burg 2007).

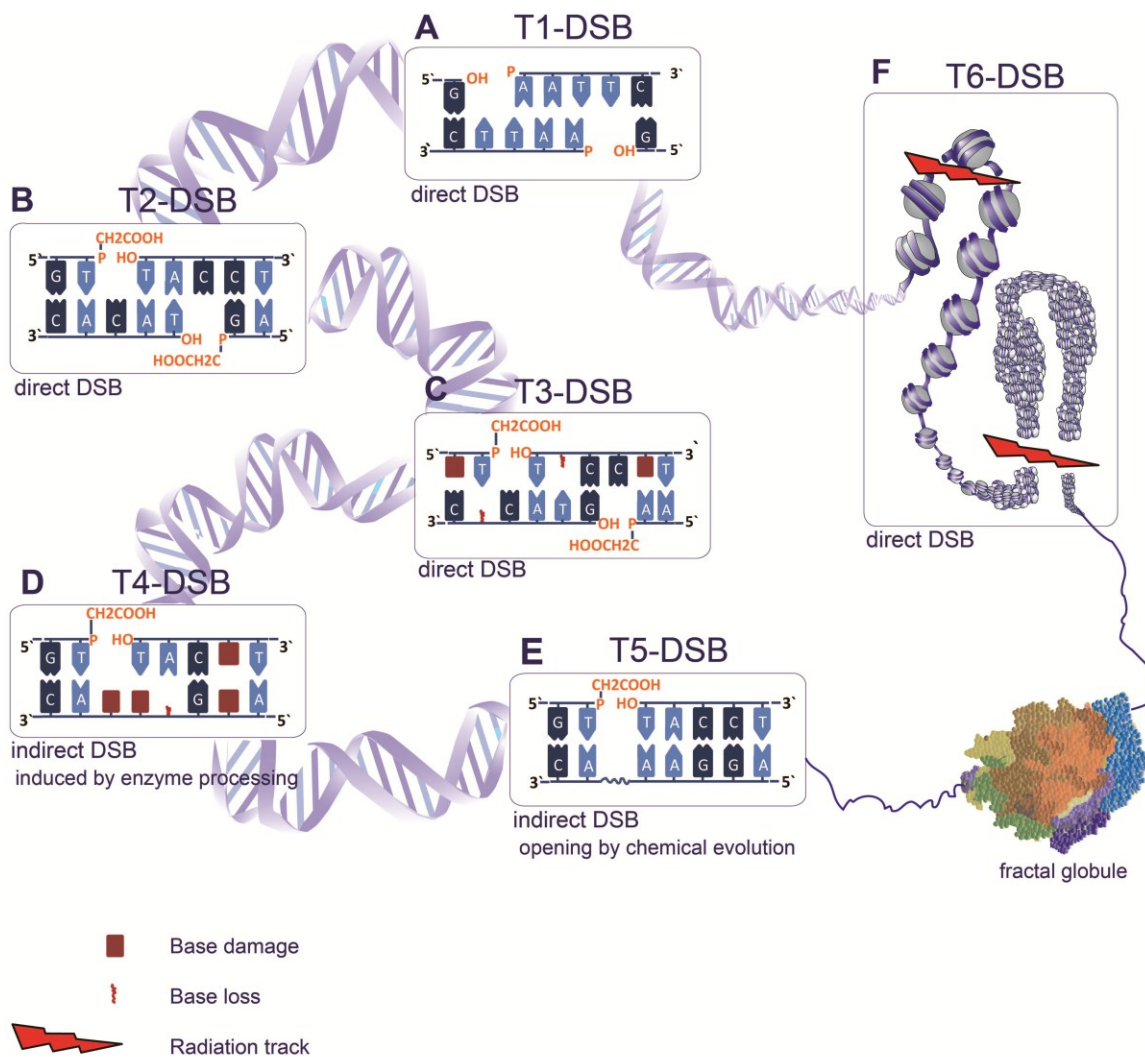


Fig.6: Schematic illustration of DSB Types 1-6. **A:** T1-DSBs are direct DSBs induced by RE with a 5' phosphate and a 3' OH group. **B:** T2-DSBs are induced by IR and frequently comprise a 3' phosphoglycolate and a 5'-OH. **C:** T3-DSB comprises also other types of lesions like base damages or base loss in close proximity to the DSB. **D:** T4-DSB represents a non-DSB cluster that can convert to DSBs by subsequent enzyme processing. **E:** T5-DSBs represent a non-DSB cluster that can convert to DSBs by chemical processing. **F:** T6-DSBs are composed of clustered DSBs. Two examples are shown. A single radiation track induces two DSBs in the linker regions of a nucleosome leading to nucleosomal loss, shown on the left. On the right higher order packaging of nucleosomes is illustrated forming a loop that is also hit by a single radiation track that can lead to chromatin destabilization (Schipler and Iliakis 2013). In the right lower corner the chromatin compacted as a fractal globule is illustrated (Mirny 2011; Bancaud, Lavelle et al. 2012).

1.3.2. T2-DSB: simple DSBs with modified ends

IR generated DSBs differ from those induced by RE because they frequently comprise a 3' damaged sugar in the form of phosphoglycolate and a 5' OH. Therefore the T2-DSBs are categorized as simple DSBs where the complexity derives from modified ends (Fig. 6B). This form of ends precludes direct ligation and necessitates end-processing as a step during repair. In contrast to RE and HE, IR in the form of X-rays or γ -rays, induces, a wide spectrum of lesions through the formation of free radicals resulting in oxidative damage, including sugar and base damages each of which outnumbers DSBs by approx. 20:1 (Ward 1985; Ward 1990). Certain forms of sugar damage disrupt the phosphodiester backbone of the DNA molecule and generate SSBs. Since IR-induced DSBs are generated by coincidence of two SSBs, blunt ends, or ends with protruding single strands similar to those described for RE can be generated.

1.3.3. T3-DSB: Locally multiply damaged sites

The presence of two or more DNA lesions comprising base damages or strand breakages on opposing strands within one helical turn of the DNA constitutes clustered DNA damage that potentially will have more severe biological consequences than the T2-DSBs described above. This possibility was pointed out by John Ward who proposed the term locally multiply damaged sites (LMDS-later simplified as MDS) (Ward 1985). Formations of MDS occur through multiple direct ionizations of the DNA, as well as from combinations of free radical attack and direct ionization events. A single energy deposition is able to produce 2-5 ionizations in a region of 1-4 nm (up to one helical turn) of the DNA-strand.

T3-DSB describes the simultaneous presence of base damages and DSBs within an MDS and generates the next level of complexity (Fig. 6C). The increased complexity of T3-DSB may impair cellular repair systems by simultaneous recruitment and even engagement of two or more repair pathways (DSB repair and base damage repair); thus it may impair the function of both pathways. In addition, base damages in close proximity to DSBs may inhibit enzymes involved in DSB repair. Therefore it is likely that

the probability for accidental misrepair is highly increased compared to the simpler forms of DSBs described above (Schipler and Iliakis 2013).

1.3.4. T4-DSB: Indirect DSB induced by enzymatic processing

In addition to the above described DNA damage clusters comprising DSBs that are induced immediately after radiation exposure, damage clusters can also be generated by IR that partly develop to DSBs at different times after irradiation by enzymatic processing of the initial lesions (non-DSB clusters) (Fig. 6D). DSBs forming by the simultaneous disruption of the phosphodiester bond at base damage sites in opposite strands, or with the combination of BER opposing an SSB, form yet another level of complexity that integrates the parameter time in the induction process and is termed therefore T4-DSB (Schipler and Iliakis 2013). Experimental evidence exists that this form of clustered DNA damage outnumbers T3-DSBs by nearly 4:1. Although BER and SSB repair pathways may remove individual lesions within non-DSB clusters restoring thus the DNA molecule, repair attempts may also fail.

It was shown that the reparability of non-DSB clusters is determined by the composition, spacing and polarity of the lesions comprising the cluster (Hada and Sutherland 2006). One or more lesions within a non DSB cluster can remain unrepaired due to reduced activity of glycosylase or altered nuclease activity. Furthermore a delayed formation of DSB can result as a consequence of attempted post irradiation repair of sugar and base residues (Gulston, de Lara *et al.* 2004). In the case of a bistranded cluster that contains either two AP sites or a SSB opposing an AP site most probably a DSB will be formed through the incision of the AP site during repair (Georgakilas 2008).

1.3.5. T5-DSB: Indirect DSB induced by chemical processing

Recent evidence suggests that IR also generates sugar damage within clustered damage sites that fail to directly break the DNA backbone, but do so after chemical processing within about 1 h after IR (Singh, Wang *et al.* 2011). This way of generating DSBs within a clustered damage site is termed T5-DSB (Fig. 6E).

1.3.6. T6-DSB: Clustered DSBs

Multiple DSBs at close proximity may affect nucleosomal stability and lead to processing failures like deletions and exchange-type aberrations (Fig. 6F). Notably, in this case the outcome in terms of damage probability will depend not only on the stochastic nature of the track structure, but also on the compactness of the targeted chromatin site.

Nucleosomes represent the lowest level of chromatin organization with a nucleosome core particle consisting of approx. 147 bps wrapped 1.67 left handed superhelical turns around the octameric histone core. Two strands of DNA within the nucleosome width of 3 nm are presented on the nucleosomal surface. The histone core contains a modular complex of two H2A–H2B dimers and a (H3–H4) tetramer that are connected by a 0-80 bp linker DNA. It is considered that the nucleosome filament is packed into the secondary structure of an approx. 30 nm chromatin fiber including 6-7 nucleosomes per 10 nm length of fiber. Recent results using novel chromosome conformational capture techniques question the existence of such structure (Dekker 2008; Eltsov, MacLellan et al. 2008; Fussner, Strauss et al. 2012; Nishino, Eltsov et al. 2012) and favour an alternative structural model of human chromosome with the 10-nm fiber folded in a regulated manner as a long-lived fractalGlobule (lower right corner of Fig. 6) (Lieberman-Aiden, van Berkum et al. 2009; van Berkum and Dekker 2009; Thurman, Rynes et al. 2012).

The clustering of DSBs at distances from about hundred bp to few hundred thousand bp will destabilize chromatin and may lead to fragment loss. The process of destabilization will strongly depend upon the actual chromatin structure in the region that sustained this form of DNA damage. Chromatin structure may also affect the linear distance of interacting DSBs. Thus while under some circumstances interaction distances of a few hundreds of bp are envisioned, interactions may also be possible between DSBs separated by Mbp (Fig. 7). Forms of such interactions are actually naturally occurring in a cell during the process of V(D)J and class-switch recombination.(Boboila, Alt et al. 2012). T6-DSB can also be considered as a form of highly local chromothripsis, a

phenomenon by which tens to hundreds of chromosomal rearrangements occur in a single event of cellular crisis.(Stephens, Greenman et al. 2011; Forment, Kaidi et al. 2012; Molenaar, Koster et al. 2012).

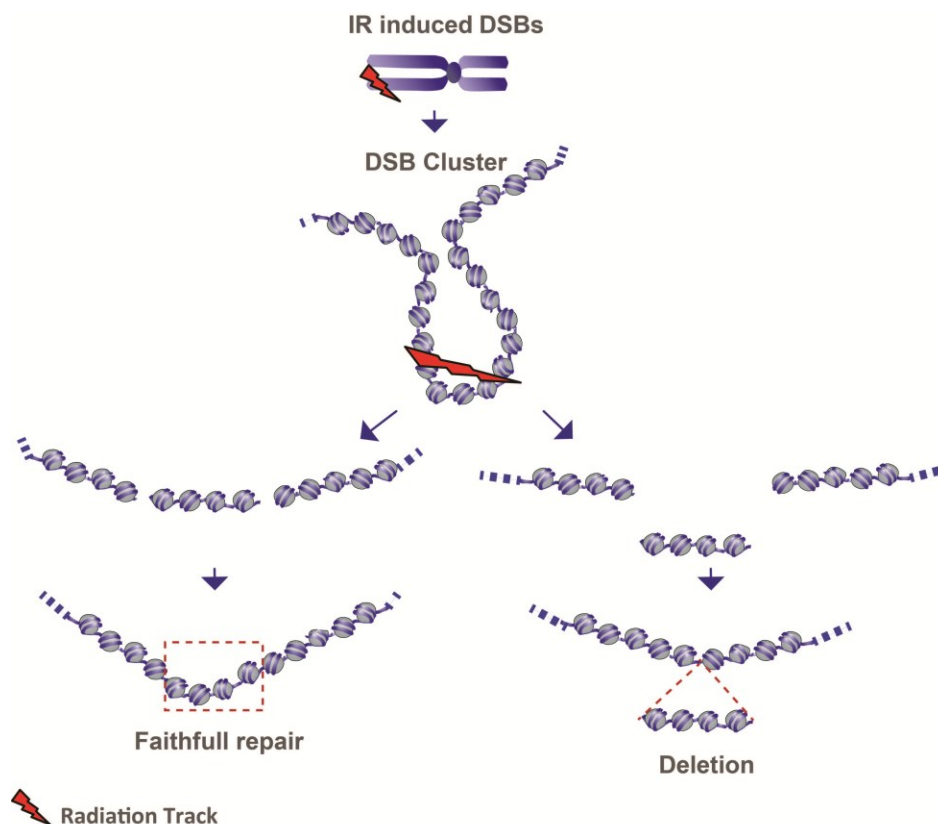


Fig.7: Nucleosomal loss induced by DSB clusters. Two scenarios of repair outcomes for clustered DSBs are shown. In the first scenario (left) the sequence is restored. In the second scenario a deletion occurs due to nucleosomal loss (right) (Schipler and Iliakis 2013).

Several investigations applying theoretical modeling by Monte Carlo Calculations, PFGE and atomic force microscopy (AFM) after high and low LET irradiation describe the potential of clustered DSBs to fragment the genome (reviewed in Schipler and Iliakis 2013). Monte Carlo simulations for DSB induction on higher order structure by radiations of different LET showed regional DSB clustering with the potential of generating DNA fragments (Friedland, Jacob et al. 1998; Friedland, Jacob et al. 2003; Friedland, Dingfelder et al. 2005; Ponomarev and Cucinotta 2006; Friedrich, Scholz et al. 2011). Fragmentation peaks were found at 85bp and multiples of 1000bp

independently of LET (Holley and Chatterjee 1996). This fragmentation pattern represents the revolution period about the nucleosome (~85 bp). In support to this theoretical modeling approach, PFGE showed the generation in human fibroblasts exposed to X-rays and iron ions of DNA fragments in the predicted size range (0.1-2 kbp) (Rydberg 1996). Results obtained using atomic force microscopy imaging (AFM) provide further support for the induction of clustered DSBs forming short DNA fragments - even when irradiating “naked” DNA devoid of any organization in form of chromatin (Pang, Winters *et al.* 2011). Thus, low LET irradiation of pUC19 plasmid DNA (2864 bp) shows that 35% of the generated fragments are 0-50 nm in size (<147 bp), and this proportion increases to 70% after exposure to high LET argon irradiation.

In conclusion, the generation of short DNA fragments by T6-DSBs point to their high risk potential to induce severe biological consequences, but to this date a biological system enabling the investigation of clustered DSBs does not exist.

2. Aim of the work

To assess whether clustered DSBs (T6-DSBs) are a relevant source for adverse biological consequences generated after the induction of DNA damage by IR, we developed an I-SceI homing-endonuclease-based model system. Until now the possible consequences of DSB clustering were modeled by Monte Carlo simulations; a biological system for *in vivo* validation of the expected biological effects was missing, because the stochastic nature of DNA-lesion-induction by IR does not allow the controlled generation of appropriate forms of DNA damage.

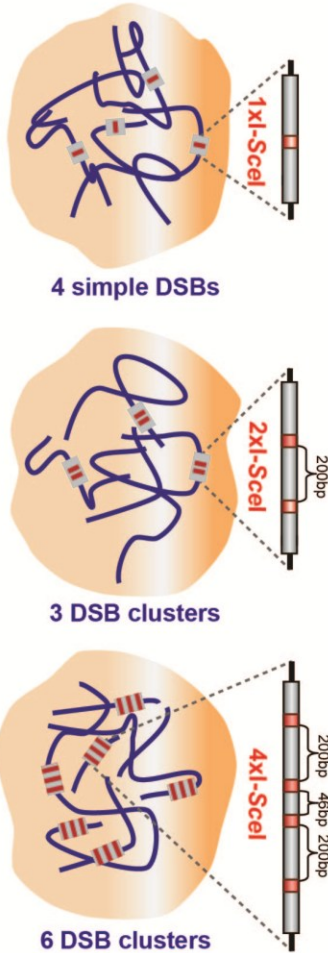
For our model systems we constructed plasmids harboring different numbers of I-SceI restriction sites, ranging from one to four, located at defined distances. The distance of two hundred bps between consecutive I-SceI sites was chosen at first since it reflects the length of DNA that winds around a nucleosome plus the associated linker region. We are hypothesizing that such distances will affect nucleosomal stability, may lead to nucleosome loss and thus to repair failures causing chromosomal aberrations or large deletions. To increase the level of complexity, the I-SceI restriction sites were engineered in the same and in opposite orientation, generating thus either compatible or incompatible ends after the loss of the intervening sequence. Compatible ends can be simply ligated by the repair machinery whereas incompatible ends require end processing before ligation. Constructs harboring different assemblies of I-SceI restriction sites were integrated at multiple locations in the genome of wt and mutant CHO cells. This generated model systems that can mimic events caused by IR, where DSBs are induced simultaneously along the particle tracks at various locations throughout the genome.

To achieve multiple random integrations we introduced the highly efficient Sleeping Beauty transposon technology (SB). The various I-SceI constructs were cloned into the transposon plasmid carrying a neomycin resistance gene for selection and co-transfected with the transposase expressing plasmid that catalyzes the cut and paste transposition event. In order to investigate the contribution of the different repair pathways for simple and clustered DSBs we utilized in addition to wt CHO cells the

following HR and D-NHEJ mutants: Irs1SF with defect in XRCC3, Xrs6 defective in Ku80, and XR-C1-3 defective in DNA-PKcs. After generating a large set of genetically modified cells we characterized them by Southern blotting for the number of integrations, which reflects the number of possible clustered DSBs that can be induced upon transfection and expression of I-SceI. A schematic showing cells with integrations of constructs harboring different combinations of I-SceI sites is shown in Fig. 8.

Experiments were performed using clonal cell lines generated from wt cells and the above outlined CHO mutants and harboring different numbers of the different forms of I-SceI recognition site clusters. From these I-SceI recognition site clusters, DSB clusters can be generated by transient expression of I-SceI and the mediated responses can be investigated at different relevant biological endpoints (Fig. 8). The killing potential of clustered DSBs was examined by the clonogenic survival assay and repair failures that cause chromosome aberration were measured by premature chromosome condensation (PCC) in G2-phase cells. Furthermore, consequences of DSB clustering on cell signaling were investigated by life-cell imaging with reporter plasmid expressing fluorescently tagged (EGFP) MDC1, or 53BP1 fusion proteins.

Biologically tractable forms of clustered DSBs



Biological consequences

Tools and Methods

DSB induction by I-SceI



Signalling	Inhibitors
DSB Repair	Mutants + Inhibitors
Chromosomal Aberration Formation	Cytogenetics
Cell Survival	Colony Formation

Fig. 8: Schematic illustration of the experimental design. On the left three vertebrate cells are shown with different numbers of genomic integrations. For each of the cells one integration is magnified showing the constructs with 1-, 2- and 4xI-SceI recognition sites modeling potential simple and clustered DSBs, respectively. After DSB induction by I-SceI several biological endpoints (indicated at the right) can be evaluated in vivo with this model system using the indicated approaches and methods.

3. Previous investigations with the I-SceI model system

In the first attempt to elucidate the cellular effects of DSB clustering, experiments with the I-SceI model system established in the human A549 cell line were performed in collaboration with J. Saha (Saha 2010). Survival experiments with A549 clones showed strong cell killing after I-SceI induced two-DSB clusters in contrast to simple DSBs. The observed killing effect was dependent on DSB clustering, as well as on the number of I-SceI construct-integrations in the genome. The conclusion was drawn that closely located DSBs are prone to DNA fragment loss and are therefore biologically more effective than simple DSBs. The PCR analysis of the repair junctions revealed that deletions occur around the break junctions in the case of clustered DSBs. Furthermore the DSB end configuration also played a role for cell survival. DSBs forming incompatible ends after the loss of the intervening sequence lead more often to cell death than DSBs with directly ligatable, compatible ends.

To investigate the effect of clustered lesions on chromosome level the formation of chromosomal aberrations was analyzed. But the results were puzzling as the low number of chromosome breaks did not correlate with the strong killing observed in the survival experiments. A possible explanation for this discrepancy was found by live cell imaging of an A549 clone bearing clustered DSBs after co-transfection with I-SceI and a 53BP1-EGFP- expressing plasmid. Observations lead to the suggestion that a large fraction of the cells underwent apoptosis after transfection. The conclusion was drawn that transfected cells may activate apoptotic signals resulting in cell death. Apoptotic cells evade the analysis performed for the evaluation of chromosomal aberrations.

Taken together the results obtained with the A549 model system partially confirm the hypothesis that clustering of DSBs at distances affecting nucleosomal stability may be highly lethal for the cell, but the model system has to be refined to overcome limitations that hamper analysis. In an attempt to find a solution, we established the system in the p53 deficient cell line CHO10B4 that is less prone to apoptosis, as part of this thesis. Furthermore the cell line is advantageous as it has different mutants of the HRR and NHEJ pathway that were additionally applied for the generation of clones.

4. Materials and methods

4.1. Materials

4.1.1. Laboratory apparatus

Beckman Tabletop GS-6R centrifuge	Beckman Coulter, USA
BioFuge (Fresco)	Thermo Scientific, Germany
Cell culture “Herasafe” hood	Thermo Scientific, Germany
CO ₂ Incubator	Sanyo, Japan
Confocal laser scanning microscope	Leica Microsystems, Germany
Coulter Counter	Beckman Coulter, USA
Electro-Transfer Unit	Bio-Rad, USA
Express Pipet-Aid	BD Falcon, USA
Flow Cytometer	Beckman Coulter, USA
FluorImager Typhoon 9400	Molecular Dynamics, Germany
Heating unit	Peter Oehman, Germany
Hybridizer HB-1000	UVP LLC, USA
Inverted Microscope	Olympus, Japan
Magnetic Stirrer	Heidolph, Germany
Molecular Imager VersaDoc	Bio-Rad, USA
Nanodrop	Thermo Scientific, Germany
Nucleofector	Lonza Cologne GmbH, Germany

Odyssey [®] infrared imaging system	LI-COR Biosciences, Germany
Overnight Culture Shaker	Infors, Germany
Pasteur pipette	BD Falcon, USA
Peristaltic pump	Ismatec, Switzerland
pH Meter	InoLab, Germany
Pipettes	Eppendorf, Germany
Rocky Shaker	Peter Oehmen, Germany
Roller drum	Bellco Biotechnology, USA
Scintillation Counter	Beckman Coulter, USA
SDS PAGE mini gels	Mini PROTEAN, Bio-Rad, USA
Temperature control system for Microscopes, environmental chamber for live cell imaging experiments, “Cube & Box”	Live Imaging Services, Switzerland
Thermo-mixer	Eppendorf
Typhoon Scanner	GE Healthcare, USA
Ultracentrifuge	Beckman Coulter, USA
UV Spectrophotometer	Shimadzu Corp., Japan
Vortexer (Vortex-Genie 2)	Scientific Industries, USA
Water Bath	GFL Instruments, Germany
Weighing Balance	Sartorius (BP110 S)
X-ray machine	GE Pantak, Germany

4.1.2. Disposable elements

0.2 µm filter	Millipore, USA
1.5 and 2 ml tubes	Eppendorf, Germany
15 & 50 ml Centrifuge Tubes	BD Falcon, USA
Cell Culture Dishes	Cell Star, USA
Dounce homogenizer	KonTes, Kimble Chase, USA
Flasks and beakers	Schott Duran, Germany
Nitrocellulose membrane	Schleicher Schuell, Germany
Nylon membrane	Roche, Germany
Parafilm	Lab Depot Inc. USA
PVDF membrane	GE Health care, USA
Rainin Pipettes	Mettler Toledo, Germany
Spinner Flask	Bellco, USA
UV Cuvettes	Hellma, Germany

4.1.3. Chemical reagents

Acrylamide-Bis-acrylamide	Roth, Germany
Albumin Bovine	Sigma-Aldrich, USA
Bromophenol Blue	Sigma-Aldrich, USA
Commassie brilliant blue G-250	Serva, USA
DMEM	Sigma-Aldrich, USA
dNTPs	Promega, USA

DTT	Roth, Germany
EDTA	Roth, Germany
Ethanol	Roth, Germany
FCS/FBS	Gibco Life Sciences, USA
Glycerol	Roth, Germany
Glycine	Roth, Germany
Isopropanol	Roth, Germany
KCl	Roth, Germany
Lactalbumin hydrolysate	Sigma-Aldrich, USA
Luria Agar	USB Corp, USA
Luria Broth	USB Corp, USA
McCoy's 5A	Sigma-Aldrich, USA
MEM	Gibco Life Sciences, USA
Methanol	Sigma-Aldrich, USA
NaCl	Roth, Germany
Non-Fat dry milk	Roth, Germany
Nonidet P40	Roche, Germany
Phusion Hot-Start High Fidelity Polymerase	Finnzymes-NEB, USA
Poly L-Lysine	Biochrom AG, Germany
ProLong Gold Antifade solution	Invitrogen, USA.
Propidium Iodide	Sigma-Aldrich, USA

RNase	Sigma-Aldrich, USA
TEMED	Roth, Germany
TRIS Base	Roth, Germany
Tris-HCL	Sigma-Aldrich, USA
Triton X-100	Roth, Germany
Trypsin	Biochrom, Germany
Tween 20	Roth, Germany

4.1.4. Commercial kits

Calf Thymus DNA	Invitrogen
DNA cellulose resins	Sigma-Aldrich, Germany
DNA Maxi-prep Kit	Qiagen, USA
ECL Western Blotting Reagent	GE Healthcare, USA
FlexiGene DNA Kit	Qiagen, USA
Hi Load (26/60) SuperDex 200	GE Healthcare, USA
HiTrap™ Heparin prepacked column	GE Healthcare, USA
Label IT CX Rhodamine Labeling kit	Mirus Bio, USA
Prime-It II Random Primer Labeling kit	Stratagene, USA.
ProbeQuant G-50 Columns	GE Healthcare, USA
QIAquick Nucleotide removal Kit	Qiagen, Germany
QuikHyb Hybridization Solution	Stratagene, USA
α - ³² P CTP	Perkin Elmer, USA

4.1.5. Cell lines

Species	Name	Cell type	Description
Chinese hamster	CHO-10B4	Fibroblast	Repair proficient
Chinese hamster	Irs1SF	Fibroblast	mutation in XRCC3
Chinese hamster	XR-C1-3	Fibroblast	mutation in DNA-PKcs
Chinese hamster	Xrs6	Fibroblast	mutation in Ku 80
Human	U2OS-HA-ER-AsiSI	Osteosarcoma	Cell line stably transfected with the pBABE vector HA-ER-AsiSI
Human	U2OS	Osteosarcoma	-

4.1.6. Antibodies

Name	Provider
Alexa Fluor 488 (mPab, rPab)	Invitrogen, Germany
GAPDH (mMab)	Millipore, Germany
IRDye 680 (mPab, rPab)	LI-COR Biosciences, Germany
I-SceI (rPab)	Santa Cruz Biotechnology, Germany
Lamin A/C (mMab)	Santa Cruz Biotechnology, Germany
Myc Tag (mMab)	Gene Tex, USA
γ -H2AX (mMab)	Abcam, UK

4.1.7. Software

Name	Provider
Adobe Creative Suite® 5.5	Adobe Systems, USA
Image Quant	Adobe Systems Inc. USA
ImarisXT® 6.0	Bitplane AG, Switzerland
Kaluza®	Beckman Coulter, USA
Las AF®	Leica Microsystems, Germany
Metafer®	MetaSystems, Germany
Quantity One®	Bio-Rad, USA
SigmaPlot® 11	Systat Software Inc. USA
Wincycle™	Phoenix Flow Systems, USA

4.1.8. Plasmids

Name	Description
pcDNA3B-puro-mycNLSERT I-Sce-ERT	Expresses a controllable I-SceI protein ((Hartlerode, Odate et al. 2011))
pCMV3xnlslScel	I-SceI expressing Plasmid (M. Jasin)
pCMVT7-SB100x	Transposase expressing plasmid (Ivics, Hackett et al. 1997)
pIRESNeo2-53BP1-EGFP	Expresses a 53BP1-EGFP fusion protein
pEGFP-C2-MDC1	Expresses a MDC1-EGFP fusion protein

pmaxGFP	GFP expressing plasmid
pPCRScrip 1SB-1NS	Cloning vector with one I-SceI site
pPCRScrip 200A	Cloning vector with two I-SceI sites in direct orientation
pPCRScrip 200B	Cloning vector with two I-SceI sites in reverse orientation
pT2SVNeo	Transposon (Ivics, Hackett et al. 1997)
pT2SVNeo 1SB-1NS	Transposon with one I-SceI site construct
pT2SVNeo 200A	Transposon with two I-SceI site constructs in direct orientation
pT2SVNeo 200B	Transposon with two I-SceI site constructs in reverse orientation

4.1.9. Oligonucleotides

Name	Sequence
Double 200Isce1Agfw5`	CCCGAATTCGGGTCTAGACTCGAGG
Double 200Isce1Agrev5`	CCAGAGCTCTACCCGCGGAGATCT
Double 200Isce1Agfw3`	CCAGAGCTGGGTCTAGACTCGAGGG
Double 200Isce1Agrev5`	CCAGAGCTCGAATTCTACCCGCGC

4.2. Methods

4.2.1. Cell culture

Cells were cultivated in 100 mm tissue culture dishes with 15 ml McCoy's growth media supplemented with 10% fetal bovine (FBS) and kept in incubators (Sanyo) at 37 °C with 5% CO₂. Exponentially growing cells were passaged every two (CHO) or three (U2OS) days keeping them at a maximum confluence of less than 75%. For passaging, media was removed and cells were washed with 1 x PBS. 2 ml of 0.05% trypsin-EDTA was added and incubated for 3 min at 37 °C to detach the adhering cells. Trypsin was inactivated by adding 5 ml growth media and cells were resuspended with a Pasteur pipette to reduce cell clumping. Cells were counted with the Coulter Counter (Multisizer™, Beckman Coulter) and appropriate numbers of cells were plated for subculture. Cells were discarded after approx. 30 passages. When frozen cells were thawed, they were passed two times before performing experiments with them.

4.2.2. Cryopreservation of cells

For long term cell storage the freezing protocol of Borrelli was applied (M.J. Borrelli *et al.* 1987). 5×10^6 cells were centrifuged after trypsinization at 4 °C, the media was removed and the pellet was dissolved in cold 500 µl freezing solution A (80% freezing stock: 5 mM KH₂P₀₄, 25 mM KOH, 30 mM NaCl, 0.5 mM MgCl₂, 20 mM L-lactic acid, 5 mM glucose and 0.2 M sorbitol; with 20% sterile MQ water) and kept on ice. 500 µl of freezing solution B (80% freezing stock with 20% DMSO) was added and finally the cells were frozen at -150 °C in cryo vials. One day after thawing the cells, media was changed to remove DMSO and the cells were passaged twice prior to use for experiments.

4.2.3. Drug treatments

Inhibitors were dissolved in dimethyl sulfoxide (DMSO) and added to the culture medium immediately after transfection. The DNA-PKcs inhibitor NU7441 was applied at a concentration of 5 µmol/l. PJ34 inhibits PARP and was used at a concentration of 10 µmol/l.

50 mg/ml stock of G418 was prepared in 100 mM HEPES. The solution was sterilized by filtering through a 0.22 µm filter. Different concentrations were applied for specific cell lines (ranging from 300-500 µg/ml). All stocks were stored at -20 °C.

4.2.4. Transfection by electroporation

The Amaxa Nucleofector[®] device was used for transfection. 1×10^6 – 8×10^6 exponentially growing cells were transfected with 500-1000 ng plasmid/ 1×10^6 cells. The cells were trypsinized, centrifuged at 900 rpm and dissolved in 100 µl transfection reagent. The solution was mixed with max. 10 µl of plasmid and transferred to the electroporation cuvette. According to manufacturer instructions, transfection programs U32 and X05 were used for CHO and U2OS cells, respectively. After transfection the cells were transferred to prewarmed media. Transfection efficiency, measured by FACS analysis of pmax-GFP transfected cells, varied between 90-95% for CHO cells, and was about 70% for U2OS cells.

4.2.5. Ionizing Radiation (IR) exposure

Cells were irradiated with X-rays using an X-ray machine (“Isovolt 320HS”, Seifert/Pantak, General Electric-Pantak). Tube voltage and current were set to 320 kV and 10 mA respectively and 1.65 mm aluminium filter (GE-Healthcare) was used to absorb “soft” X-rays. The dose rate was estimated to 1.3 Gy/min using in-field ionization monitor, calibrated with a PTB dosimeter (Physikalisch-Technische Bundesanstalt, Braunschweig, Germany). Radiation dose was confirmed with Fricke’s chemical dosimetry. An even irradiation field was ensured by rotating the radiation table. Cells were returned to the incubator immediately after IR and collected at different time points post irradiation.

4.2.6. PCR

PCR (Polymerase chain reaction) was performed to amplify DNA sequences and introduce additional restriction sites for further cloning. The PCR reaction mixture was set up in a total volume of 20 µl containing of 1-10 ng template DNA, 100 mM dNTP Mix, 1 x PCR-Buffer, 2.5 U Phusion[®] Polymerase, 0.2 µm of reverse and forward primer and MQ water. For primer sequences see Table 1. The amplification reactions were

performed in a Mastercycler-ep-gradient-S thermal cycler (Eppendorf) with the program illustrated in Table 1. The PCR fragment was run on an agarose gel and extracted using the Qiagen gel extraction kit.

Table 1: program set in the thermo cycler for PCR

Program	Cycles	Temperature	Time
Denaturation	1	98 °C	30 sec
Denaturation	35	98 °C	15 sec
Annealing		65-68 °C	15 sec
Elongation		72 °C	15 sec
Elongation	1	72 °C	5 min
	∞	4 °C	

4.2.7. Agarose gel electrophoresis

1% Agarose gels were prepared for plasmid DNA and 0.8% gels were prepared for genomic DNA. After mixing the agarose with 100 ml 1xTAE (40 mM Tris-Acetate, 1 mM EDTA) the solution was heated in the microwave until boiling. The warm liquid agarose was poured into a 10 x 7 cm gel tray and left to cool down for 1 h RT in order to polymerize. The gel was loaded and run in a 1 x TAE filled electrophoresis chamber (Life Technologies™) at 1 Volt/cm for 1.5 h in case of plasmid DNA and 6 h with 0.5 Volts/cm in case of genomic DNA. In order to visualize the DNA, the gel was stained for 1 h in 50 ml 1 x TAE containing 1% ethidium bromide (EtBr) under gentle shaking.

4.2.8. Restriction enzyme digestion

The restriction reactions for cloning-fragments were carried out in a total volume of 20 µl. 3 µg vector DNA and 900 ng insert DNA, were mixed with 1 U restriction enzyme, 1 x enzyme buffer and MQ water. The reaction mixture was incubated for 30 min at 37 °C. Prior to ligation the fragments were eluted with the QIAquick Gel Extraction Kit (Qiagen).

4.2.9. Ligation

Ligation of insert and vector were carried out at a 1:4 ratio. The reaction mixture with total volume of 20 µl contained 1 x ligation buffer, 1 U T4 Ligase and MQ water. The reaction mixture was incubated at 22 °C overnight.

4.2.10. Transformation

100 µl competent *E.coli* cells were transformed with 10 ng of plasmid DNA, or 7 µl of ligation reaction, respectively. The reaction was incubated for 40 min on ice before heat shock was performed at 42 °C for 50 sec in a Thermo Mixer (Eppendorf) and immediately incubated on ice for 2 min. 800 µl SOC Media was added to the bacterial culture and incubated for 1.5 h at 37 °C with orbital shaking at 220 rpm. Finally 300 µl of the culture was plated on LB-Agar plates containing the antibiotics (100 µg/mL ampicillin and 50 µg/ml kanamycin) according to the resistance gene of the transformed plasmid. LB-Agar plates were incubated at 37 °C overnight.

4.2.11. Generation of competent *E.coli*

For generation of competent *E.Coli* cells of the BL1-blue strain, 50 µl competent cells were incubated in 2 ml LB overnight at 37 °C under orbital shaking at 220 rpm (Thermo). In the next step 2 ml of the overnight culture were added to 200 ml LB media and grown at 37 °C on the shaker until they reached an OD₆₀₀ of 0.4. The culture was chilled on ice for 5 min and centrifuged at 3300 x g at 4 °C for 10 min. The pellet was resuspended in 30 mL ice cold 0.1 M CaCl₂, incubated on ice for 30 min and centrifuged. The pellet was dissolved in 6 ml 0.1 M CaCl₂ solution supplemented with 15% glycerol. Finally, 500 µl aliquots were frozen at -80 °C.

4.2.12. Plasmid preparation

Supercoiled SB transposon (pt2SVNeo) plasmids with different integrations and SB transposase plasmids (pcMV100x) were prepared using CsCl/EtBr gradients. 1 l of plasmid transformed *E. Coli* culture was grown overnight to an OD₆₀₀ of 1.0. The cells were centrifuged for 30 min at 1300xg at 4 °C. After re-suspending the pellet in 10 ml Sucrose/Tris/EDTA solution, 2 ml lysozyme was added, mixed by swirling and incubated for 30 min at RT. 4 ml Triton lysis mix was added and the culture incubated at 37 °C before centrifuging for 1 h in a Beckman JA 25.50 rotor at 48400 x g. The volume of the decanted supernatant was determined and 0.95 g CsCl per ml was added and dissolved. In the next step 0.1 ml of 10 mg/ml EtBr solution was added per ml supernatant and centrifuged for 20 min in a Beckman JA 25.50 rotor at 7000 rpm. For plasmid banding the solution was transferred to Beckman: 4.2 ml ultracentrifuge tube and centrifuged for 16 hours at 20 °C in an ultracentrifuge (Beckman Optima Max) in a near vertical rotor MLN80 at 240000xg.

The lower band containing the supercoiled plasmid was transferred to another 4.2 ml ultracentrifuge tube and topped with CsCl/TE solution containing 0.2 mg/ml EtBr and centrifuged under the same conditions as before. The lower plasmid band was removed and extracted with 1:1 phenol/chloroform twice. The upper phenol phase was discarded while the lower phase was transferred to a fresh tube and precipitated with final ethanol concentration of 66% overnight at -20 °C. After centrifugation (Beckman JA 25.50 at 40.000xg for 30 min) the pellet was dissolved in 0.5% SDS in TE buffer and extracted

again with phenol/chloroform saving the upper phase that was precipitated with ethanol twice. Finally the pellet was dissolved in TE and dialysed.

4.2.13. Preparation of whole cell lysate

Whole cell lysates were prepared using 2×10^6 cells. After washing in 1 x PBS and pelleting, cells they were dissolved in 200 μ l RIPA buffer. 1 x protease inhibitor cocktail (10 μ l for 1 ml) was added to the reaction mixture and incubated for 30 min on ice. The mixture was centrifuged at 14000 x g for 20 min at 4 °C to finally transfer the whole cell lysate to a new tube. The colorimetric Bradford assay was applied to measure protein concentration using a calibration curve generated with different amounts of BSA.

4.2.14. Protocol for REAP nuclear/cytoplasmic fractionation

For subcellular fractionation the REAP (rapid, efficient and practical) protocol was applied (K. Suzuki et al. 2010). 4×10^6 cells were washed twice with ice cold PBS, the cells were scraped with a cell scraper and collected in a 1.5 ml micro-centrifuge tube. After 1 min centrifugation (1200 rpm at 4 °C) the supernatant was decanted. The following steps were carried out on ice. The cell pellet was triturated five times with 500 μ l cold 0.1% NP40-PBS (Calbiochem, San Diego, CA, USA) and spun down for 1 min. The supernatant, containing the cytoplasmic fraction was removed and centrifuged at 8000xg at 4 °C for 1 min and transferred to a new tube. The cell pellet, containing the nuclear fraction was resuspended in 500 μ l cold 0.1% NP40-PBS and centrifuged for 1 min. After decanting the supernatant the pellet was re-suspended in 200 μ l 0.1% NP40-PBS and sonicated on ice twice for 10 sec.

4.2.15. Clonogenic survival assay

For the clonogenic survival assay, exponentially growing cells were irradiated with 4, 8 and 12 Gy of X-rays, trypsinized immediately and plated in different dilutions according to the dose of radiation delivered. For survival with I-SceI transfected cells, 100 and 200 cells were plated in 60 mm dishes immediately after transfection. Transfection with the GFP expressing plasmid max-GFP served as an additional control. Furthermore, to measure the transfection efficiency, 1×10^6 max-GFP transfected cells were plated and FACS analysis measuring the GFP intensity was performed 24 h after transfection.

Cells plated for survival were grown for 10 days (CHO), or 14 days (U2OS) and then stained with 0.75% crystal violet dissolved in 100% methanol. Colonies were counted either manually using a microscope or with the colony counter.

4.2.16. Cell cycle analysis by FACS

Fluorescence-activated cell sorting (FACS) is a specialized type of flow cytometry that allows cell sorting by assessing fluorescence intensity. Cell cycle distribution was evaluated by measuring the propidium iodide (PI) fluorescence intensity. The stoichiometry of PI binding to DNA is sequence independent, making it a convenient means of quantification. Cells were washed with 1 x PBS, trypsinized at 37 °C for 5 min and resuspended in growth media. 1×10^6 untreated or irradiated cells and 2×10^6 transfected cells were collected and centrifuged with 100 x g at 4 °C for 5 min. The media was removed, the cell pellets dissolved in cold 70% ethanol and stored at -20 °C overnight. In the next step the cells were centrifuged (100 x g, 5 min), the supernatant was removed and the cells were dissolved in 800 μ l PI staining solution (40 μ g/ml PI, 62 μ g/ml RNaseA dissolved in PBS) per 1×10^6 cells for 20 min. at 37 °C. The samples were measured in a flow cytometer (Coulter Epics XL, or Gallios™, Beckman Coulter) according to pre-established protocols that were optimized for each cell line. To obtain standard histograms 15000 events were counted, and gated. LMD data files were analysed using the Kaluza® flow cytometry analysis software. Cell cycle distribution calculations were made by WinCycle® software using the generated HST files.

4.2.17. G2-premature chromosome condensation (G2-PCCs)

For G2-PCC preparation 6×10^6 I-SceI transfected and 2×10^6 untreated or irradiated cells were plated for the 8 h time point and 4×10^6 or 1×10^6 cells for the 24 h time point, respectively. At the indicated times 100 nM Calyculin A was added for 25 min. Due to Calyculin A treatment the cells round up and detach, therefore the cells could be “shaken off” by slightly tapping the dish. The cells were collected and centrifuged at 1300 rpm for 7 min. The media was removed leaving 1 ml behind to dissolve the pellet. 10 ml of hypotonic solution (75 mM of KCl) was added drop wise while slightly tapping the tube and incubated for 5 min at RT. After 5 min. centrifugation the supernatant was removed, cells were dissolved and fixed in 10 ml Fixative (3:1 methanol: glacial acetic

acid) and kept at 4 °C overnight. After washing the cells twice in fixative, metaphase spreads were prepared and stained in 3% Giemsa stain, dissolved in 1 x Sörensen's buffer for 15 min and washed with tap water. The slides were air dried at RT overnight and finally mounted with coverslips using Entellan[®] (Merck). An automated imaging system (MetaSystems) was used to obtain high quality images of metaphase chromosomes.

For searching metaphases the M-Search module of the Metafer software (MetaSystems) was employed, using the 10x objective of the Zeiss microscope. A classifier was used for M-Search that was specifically trained for the selected cell line. After performing M-Search, metaphases with good spreading were selected and captured at a higher magnification (63x oil immersion objective) using the AutoCapt setting of the Metafer software.

Images were analysed using the Ikaros Software. For analysis 100 G2-PCC spreads were scored for each time point in three independent repeats. G2-PCC fragments and inter-chromosomal exchanges were counted separately. The data shows the average of G2-PCC breaks or exchanges of three experiments with the error bars representing the standard deviation; significance values were calculated by the t-test for dependent samples.

4.2.18. Southern blotting

Southern blotting is applied to detect specific sequences of plasmid, bacteriophage or genomic DNA by a radioactive probe. The methodology for Southern blotting is divided into several steps. After digestion of the genomic DNA and separation of the digested fragments by agarose gel electrophoresis the DNA fragments are transferred via upward capillary transfer onto a nylon membrane resulting in immobilization of the DNA fragments and preservation of the same DNA banding pattern that was present on the gel. During the next step the membrane is used as a substrate for hybridization with radioactively labelled DNA probes that recognize a specific DNA sequence.

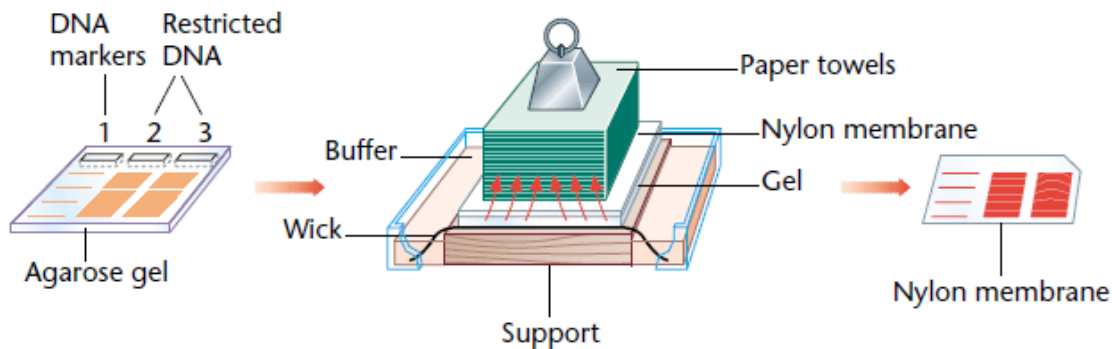


Fig. 9: Schematic representation of Southern blotting (T. A. Brown 2001).

4.2.18.1. Preparation and digestion of genomic DNA

For genomic DNA preparation from CHO cells the DNeasy Blood & Tissue Kit from Qiagen was used with the following modification of the protocol provided by the manufacturer: 12×10^6 CHO cells were spun at 1500 rpm after trypsinization and washing with 1 x PBS. The supernatant was removed and cells were dissolved in 2 ml FG1 solution in a 15 ml falcon tube. In the next step 2 ml FG2 solution mixed with 100 μ l Proteinase K from a 10 ug/ml stock solution was added. The reaction mixture was incubated at 54 °C for 6 h while shaking (400 rpm) in a Thermo-mixer (Eppendorf). After incubation the reaction mixture was transferred to a 50 ml Beckman centrifuge tube,

5 ml isopropanol were added and the tube was shaken until the DNA precipitate was visible. The tubes were centrifuged for 20 min at 4 °C in the Beckman centrifuge. The pellet was washed with 2 ml 70% EtOH and centrifuged again for 15 min. In the last step the pellet was dried at 37 °C and dissolved in 1 ml FG3 while shaking at 64 °C in a water bath. In order to prepare genomic DNA for Southern blotting, 18 µg of genomic DNA were digested with 0.3 Fast Digest Unit (FDU)/µg DNA. After adding the enzyme the reaction was incubated for 12 h at 37 °C and shaken every 15 min at 400 rpm for 15 min in the Thermo-mixer. After digestion the DNA was EtOH precipitated.

Table2: Reaction Mixture for gDNA digestion

DNA	x µL (15 µg)
FD Restriction enzyme buffer (10x)	20 µL
Milli-Q water	x µL
FD Xbal	6 µL (6 x 1 FDU)
Total volume	200 µl

4.2.18.2. Ethanol precipitation of digested DNA

0.1 Vol. of 5 M NaCl and 2.5 Vol. of 100% ethanol were added to 200 µl DNA restriction reaction and incubated at –80 C overnight. The reaction mixture was centrifuged for 30 min at 1300 rpm at 4 °C. After removing the supernatant 200 µl of 70% ethanol was added to the DNA pellet and centrifuged. The pellet was dried for 15 min at 37 °C and dissolved in 25 µl TE buffer. To remove residual ethanol, the dissolved DNA was incubated at 65 °C for 10 min with opened lid of the micro-centrifuge tubes.

4.2.18.3. Depurination and denaturation

Since fragments larger than 15 kb are difficult to transfer to a blotting membrane, the agarose gel was treated with depurination solution (0.2 M HCl) for 7 min on a platform shaker to cleave the DNA strands. During depurination the β-N-glycosidic bond is hydrolytically cleaved leading to the formation of apurinic sites in the DNA. After

depurination the gel was rinsed twice in MQ water and subsequently treated twice for 15 min with denaturation solution (1.5 M NaCl and 0.5 M NaOH) while shaking. This step is required to denature the double stranded DNA to single stranded DNA so that it can be efficiently transferred to the nylon membrane and hybridized to a labelled probe. Furthermore in combination with depurination, denaturation results in the hydrolysis of the phosphodiester backbone at apurinic sites. The gel is again rinsed twice in MQ water and incubated twice on the shaker for 15 min in neutralization solution (1 M Tris (pH 7.4) and 1.5 M NaCl).

4.2.18.4. Transfer to a nylon membrane

A transfer apparatus was built to perform the transfer of the DNA fragments from the agarose gel to the nylon membrane (Fig. 9). After equilibrating the agarose gel for 20 min in 20 x SSPE (3 M NaCl, 0.2 M NaH₂PO₄ · H₂O and 0.02 M EDTA) it was placed on Whatman paper soaked in 20 x SSPE. The Whatman paper is placed on a glass plate on the top of a plastic support and forms a connection between the gel and the container with the reservoir of 20 x SSPE. The wet nylon membrane was placed on the top of the gel and fixed with Para film at the sites before four pieces of 20 x SSPE soaked Whatman paper and a tower of paper towels were placed on the membrane. Additionally four pieces of plastic wrap were fixed on the sides of the nylon membrane and stretched over the sides of the plastic container. This avoids contact between the paper towels and the Whatman paper that would hinder capillary transfer. To stabilize the construct and increase capillary transfer, a 500 g weight was placed on the top of the paper towels. After 24 h of transfer, the transfer apparatus was disassembled and the nylon membrane was rinsed in MQ water and equilibrated in 6 x SSPE for 10 min. In order to crosslink the DNA to the membrane, it was baked at 110 °C for 50 min.

4.2.18.5. Generating radioactive probes for hybridization reactions

A 1.7 kb sequence of the integrated transposon construct served as the probe binding site. 3 µg of the pt2SVNeo transposon plasmid was digested with 1 unit HindIII. The digested plasmid DNA was separated on a 1% agarose gel run at 2 Volts/cm and the DNA fragment needed as a probe was purified with the Qiagen gel purification kit. In

order to prepare and radioactively label the hybridization probe the Prime-It II Random Prime Labeling Kit from Agilent Technologies was used. The procedure is based on the synthesis of complementary DNA strands facilitated by random hexa-nucleotides that serve as primers. The Klenow fragment of DNA polymerase I incorporates nucleotides at the free 3' OH group of the primer. Radioactive nucleotides ($[\alpha\text{-}^{32}\text{P}]\text{-dCTP}$ at 3000 Ci/mmol) are incorporated into the newly synthesized strand. In the first step of the protocol 25 ng probe-DNA dissolved in MQ water and 10 μL of random oligonucleotide primers were prepared in a total volume of 34 μL in a 1.5 ml micro centrifuge tube and incubated for 5 min in a boiling water bath. After brief centrifugation 10 μL of dCTP primer buffer, 5 μL of $[\alpha\text{-}^{32}\text{P}]\text{-dCTP}$ and 1 μL of Klenow enzyme were added and incubated at 37 °C for 30 min. In the last step 2 μL of stop mix were added. Finally the activity of the probe was determined by scintillation counting.

Table 3: Reaction Mixture to generate radioactively labeled probe

Components	Volume
25 ng DNA template	x μL
sterile double-distilled H ₂ O	x μL
5X random primers solution	10 μL
Total Volume	34 μL
5X dCTP buffer	10 μL
$\alpha\text{-}^{32}\text{P}$ dCTP	5 μL
Exo (-) Klenow Enzyme	1 μL
Stop Mix	2 μL

4.2.18.6. Hybridization

For hybridization the QuikHyb Hybridization Solution from Agilent Technologies was used. First, for pre-hybridization, the nylon membrane was soaked in MQ water and incubated while rolling in a roller bottle for 1.5 h in 10 ml prewarmed pre-hybridization solution (for 10 cm² membrane) at 58 °C. The pre-hybridization solution contains 1% calf thymus DNA that was heated prior to use to 96 °C for 5 min and immediately chilled on ice before mixing with the QuikHyb solution.

In the next step 22 µl (2x10⁷ cpm) of the radioactive probe were mixed with 100 µl (10 mg/ml) of calf thymus DNA, incubated 5 min at 96 °C and immediately chilled on ice. 1 ml of the pre-hybridization solution was removed, mixed with the probe and placed back in the roller bottle for hybridization at 58 °C overnight.

The hybridized membrane was washed four times to remove excess radioactivity. The first two washes were performed at RT for 5 min in 200 ml 2 x SSPE with 0.5% SDS and 15 min in 250 ml 2 x SSPE with 0.1% SDS. For the third wash 250 ml of 0.1 x x SSPE with 0.1% SDS were prewarmed and incubated with the membrane for 1-3 h, until counts of 200-300 Bq were measured with a Geiger-Müller counter. At last the membrane was washed in 200 ml 0.1 x SSPE briefly at RT, wrapped in saran wrap, exposed on a storage phosphor screen (GE Healthcare) and placed in a cassette for two days. The film was scanned with the Typhoon™ Variable Mode Imager (GE Healthcare). Before and after scanning the storage phosphor screen was exposed for 15 min to a white light source (ImageEraser) to erase latent images and prepare it for re-use.

4.2.19. SDS Page

Cell lysates were resolved on 10% polyacrylamide gels. For loading 30 µg cell extract were mixed in a 1:1 ratio with 2x Laemmli Buffer, denatured for 5 min at 96 °C and centrifuged briefly at 13000 x g. SDS-PAGE mini gels were prepared using casting stand (Bio-Rad) according to the manufacturer's instructions. For electrophoresis a constant voltage of 130 V was set for 1.5 h.

Table 4: SDS-PAGE

	5 ml Stacking Gel (5%)	5 ml Resolving gel (10%)
Mon. Sol.	840 µl	1.7 ml
4 x SGB (0.125 M)	1.25 ml	-
4 x RGB (0.37 M)	-	1.25 ml
Milli-Q water	2.8 ml	1.9 ml
10% SDS	50 µl	50 µl
10% APS	50 µl	50 µl
TEMED	10 µl	5 µl

4.2.20. Immunoblotting

During Western blotting the proteins are transferred from the SDS-polyacrylamid gel onto a nitrocellulose membrane. Therefore blotting paper (GB004 Whatman), transfer sponge and nitrocellulose membrane of the desired size were prepared and equilibrated in cold 1 x transfer buffer (consisting of 25% 4 x electrode buffer at pH 8.3 (0.1 M Tris-HCl, 0.7 M glycine) and 20% methanol). All components were assembled together with the gel into the electro-transfer unit according to the instructions of the manufacturer (Biorad) and run at 100 V for 60 min. After transfer the membrane was incubated for 2 h in 5% non-fat dry milk in 1 x TBS-T (0.05% Tween20 in 1 x PBS). For immunodetection the membranes were incubated overnight at 4 °C with the primary antibody. After washing three times for 10 min in PBS-T the secondary antibody was incubated for 1.5 h and the membrane was again washed three times in PBS-T prior to detection. The

antibodies were diluted in 5% blocking solution with different dilutions depending on the manufacturer's protocol for the specific antibody. The Odyssey® Infrared Imaging System from LI-COR Biosciences was used for detection and analysis.

4.2.21. Immunofluorescence staining

For γ -H2AX immunofluorescence staining, 0.2×10^6 transfected cells were plated in 35 mm dishes with 2 ml growth medium. 12 h after transfection the growth media was removed, cells were washed with PBS and fixed in 2 ml 2% paraformaldehyde PFA for 15 min. Cells were washed again 3 x for 5 min in PBS and permeabilized in 2 ml P solution (100 mM Tris, (pH 7.4), 50 mM EDTA, 0.5% Triton X-100) for 10 min. After washing, cells were blocked in PBG (0.2% gelatin, 0.5% BSA in PBS) at 4 °C overnight. The primary antibody was diluted 1:400 in PBG and 90 μ l droplets were pipetted on a Parafilm. The cover slips were placed on the antibody solution and incubated for 2 h at RT. After returning the cover slips into the dishes they were washed with PBST (PBS + 0.05% Tween 20) 3 x 10 min at RT. In the next step the cells were incubated for 1.5 h at RT with the secondary antibody diluted 1:400 and finally washed 3 x in PBST. The cells were mounted with 15 μ l ProLong® Gold antifade mounting media (P-7481, Invitrogen) mixed with 1/3 DAPI giving a final DAPI concentration of 50 ng/ml. Before scanning, slides were kept for 24 h at RT and finally stored at 4 °C. Scanning of the slides was carried out on a Confocal Laser Scanning Microscope (CLSM) from Leica Microsystems (DMI 6000 B).

4.2.22. Live cell imaging

Live Cell Imaging was applied to monitor cellular dynamic events, motility and proliferation over a time period of 24 h. The observation of living cells over time was carried out with the Leica TCS SP5 confocal microscope that enables the recording of z-series of optical sections together with time-series (t-dimension). In addition to laser scanning also differential interference contrast (DIC) was applied to observe cell viability and morphology together with foci kinetics. DIC and fluorescence were captured simultaneously in a single image frame.

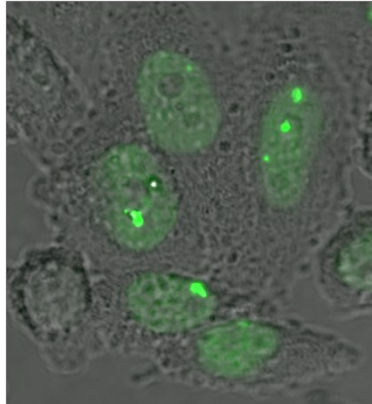


Fig.10: Representative image of cells expressing 53BP1-EGFP visualized by CLSM and merged with the corresponding DIC image.

During live cell imaging optimal environmental conditions have to be provided to the cells to keep them alive and proliferating. In order to substitute for the 5% CO₂ requirement, the cells were cultured in L-15 Leibovitz's Medium containing HEPES. This Medium was specifically designed to grow cells in a CO₂ free atmosphere. Furthermore a temperature controlled system with the microscope inside an environmental chamber, including a stage warmer and an objective heater provides optimum temperature of 37 °C for the cells.

Experiments were carried out with transiently transfected cells that express a EGFP or RFP tagged repair protein that forms foci upon DSB induction. For optimal transfection efficiencies and signal intensities 0.2×10^6 cells were plated three days prior to transfection. After transfection 0.5×10^6 transfected cells were plated in an eight well or 1×10^6 cells were plated in a four well live cell imaging chamber (PAA), respectively. 5 h after plating cells were washed twice with prewarmed PBS and growth media was changed to prewarmed L-15 Leibovitz. Prior to scanning, the chamber was placed in a specifically designed and constructed "chamber holder", as without the special holder optimal focusing at the left and right borders of the chamber was not possible due to a space problem between the objective and the chamber. To avoid disruption of the immersion film due to aberrant focusing that happens with oil objectives during long term experiments at 37 °C, a 63x Leica water objective connected to a Water Immersion Micro Dispenser (Leica) was used for 24 h experiments. The Water Immersion Micro

Dispenser adds MQ water automatically during the whole experiment. The μ -pump mp6 (Bartels mikrotechnik) was set with a pump amplitude of 75 V pumping 279 μ l water every 25 min for 10 sec. EGFP was measured with the 488 nm argon laser and RFP with the 561 nm DPSS (Diode-pumped solid state) laser. The laser power was set to 30% to reduce photo bleaching. Scanning was performed using the following parameters: PMT gain was set at 830 V for the argon laser and 530 V for the DIC detector with the pinhole set at 95 μ m. In total 16 fields were tracked at time intervals of 15 min – 1 h for 24 h.

4.2.23. Foci analysis by Imaris

The analysis of the LIF files (three dimensional data sets) that were generated after scanning was performed using the Imaris[®] software (Imaris 6.0; Bitplane). Movie files were generated with the “Easy 3-D” tool to analyse foci kinetics in a spatio-temporal resolution. For foci scoring, images of 2 h timeframes, starting from 6 h to 24 h were loaded and foci of 100 cells were counted for each time point. Foci were defined as spots of higher intensity than the defined threshold (set at 30-35, varying between different experiments, but constant throughout each experiment) and with minimum size of 0.5 μ m. The data was analysed with Microsoft Excel 2007[®] and graphs were plotted with SigmaPlot[®] 11.0.

5. Results

5.1. Model Systems for clustered DSBs

This section describes the design and the characterization of the model systems developed for the experiments and defines the clones used to evaluate the effect of DSB clustering on various biological endpoints.

5.1.1. Design of DSB clusters of varying complexities

To model simple and complex DSBs, sequences with varying numbers of I-SceI sites at different orientations were designed. We are hypothesizing that the cell will process a single DSB generated at a single I-SceI recognition site as a simple DSB. Complex DSBs are defined in this context as clustered I-SceI recognition sites that model clustered DSBs (T6-DSBs, see Fig. 6) upon their digestion by I-SceI.

Nine different sequences modeling nine forms of lesion complexity were designed (Fig. 11). One sequence contained a single I-SceI site to model the simplest form of RE-induced DSB (T1-DSBs, Fig. 11A). Six further sequences were generated with a pair of I-SceI sites located 200 bp, 500 bp or 1000 bp apart (Fig. 11B). For all of these sequences the I-SceI sites were engineered in two different ways, either in the same or in inverted orientation, designated as direct (D) or reversed (R) orientation. The constructs harboring I-SceI sites in the direct orientation generate upon loss of the intervening DNA segment a DSB with compatible ends, similar to those of the single-site construct (Fig. 11A). The constructs engineered with I-SceI sites in inverted orientation generate upon digestion and intervening fragment loss a DSB with incompatible ends (Fig. 11C).

Furthermore, two sequences were generated harboring clusters of four I-SceI sites with the relative distances in bps as indicated in Fig. 11C. Here again the I-SceI sites were engineered in the direct (D) or in reversed (R) orientation to generate upon loss of all intervening fragments a DSB with either compatible or incompatible ends. The underlying working hypothesis regarding the function of this construct is that the

intervening two DSBs will destabilize DNA and will increase the probability of fragment loss and thus also of the generation of a relatively large deletion.

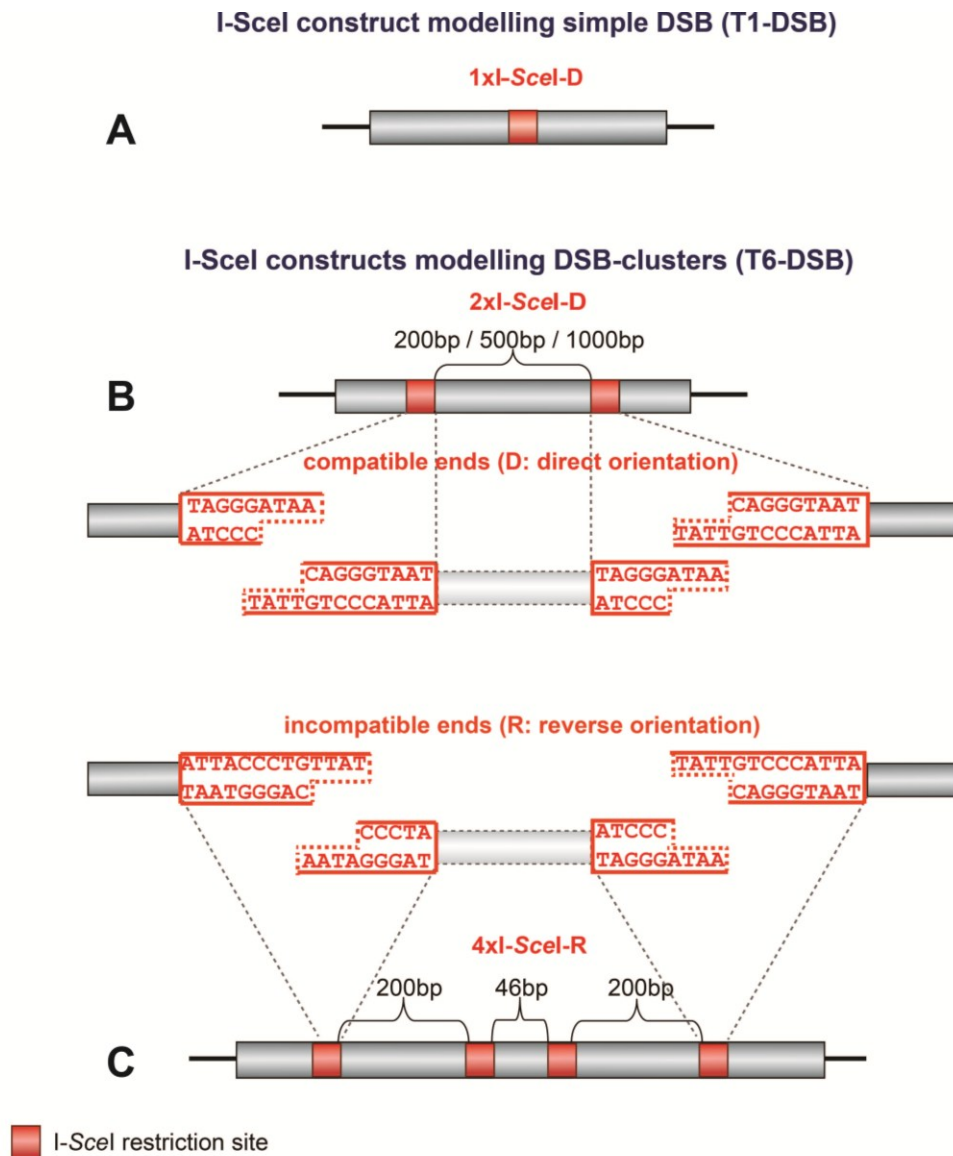


Fig. 11: Models of simple and complex lesions. Constructs carrying different numbers of I-SceI sites engineered at different distances were generated to model different degrees of DSB complexity. The sequences of the I-SceI restriction sites were designed in the direct (D) or reverse (R) orientation in order to generate compatible or incompatible DNA ends after the loss of the intervening sequence. R and D will be used for nomenclature.

The 1xI-SceI and 2xI-SceI site sequences were designed by J. Saha (Saha 2010), commercially procured from Cloning Biotech and delivered in the pPCRScript plasmid, whereas the 4xI-SceI sequences were cloned using the two site sequence as a template as part of the present work. The cloning scheme employed is shown graphically in Fig. 12 and described in detail in the legend of the same figure.

These constructs provide a unique model for testing whether different levels of DSB clustering affect detection and processing by DDR, or whether they destabilize chromatin. The contribution of DSB clustering to DSB detection and signaling can be analyzed by performing live cell imaging. Co-transfection with the I-SceI expression plasmid, or plasmids expressing different fluorescently tagged DDR proteins allow real time detection of DSB processing in the form of protein foci formation and decay. Destabilization of chromatin can be analyzed by performing G2-PCC experiments to analyze chromosome fragmentation and repair.

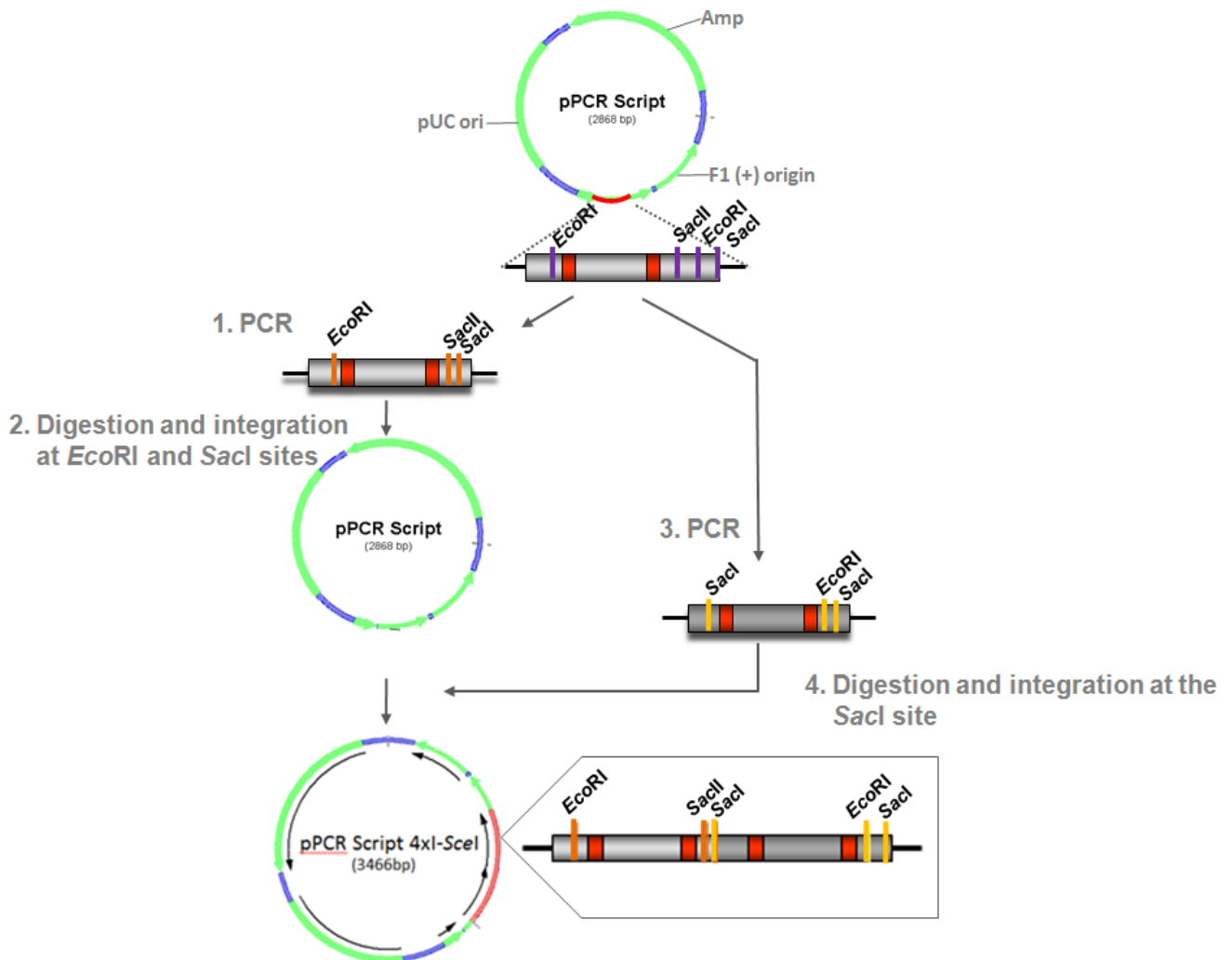


Fig. 12: Cloning strategy of the 4xI-SceI site construct. Four different primers were designed flanking the two site construct with additional RE sites for further cloning (see 4.1.9). In the first step (1.PCR) the 2xI-SceI sequence was amplified and digested at *EcoRI* and *SacI* before ligation into the pPCR script vector in the corresponding sites in the second step (2.). In the third step (3.) the two-site construct was amplified again to generate sequences with a different combination of restriction sites for further cloning (*SacI* at the 5'end and *EcoRI* and *SacI* at the 3'end). The PCR product was digested with *SacI* and cloned in the fourth step (4.) into the vector generated in the second step, already containing the PCR product of the first step. The *SacI* RE site in the final vector (pPCR-4xI-SceI) can be used for further cloning to increase the distance between the second and third I-SceI site or for other types of insertions and further construction strategies. This cloning was performed for I-SceI sites in direct as well as for inverted orientation. The *EcoRI* sites are used for further cloning into the transposon vector pt2SVNeo.

5.1.2. Transposition as a tool for achieving multiple random integrations of I-SceI constructs in the mammalian genome

To achieve high numbers of I-SceI construct integrations we applied the transposon technology. Transposable elements are characteristic segments of DNA which show the distinctive ability to move and replicate within genomes (Izsvak and Ivics 2004). The transposition of DNA transposons is characterized by a “cut and paste mechanism” whereby the transposon is excised from the donor locus and is reinserted randomly somewhere else in the genome. This process is catalyzed by the element-encoded transposase.

Transposons occupy about 45% of the human genome. Despite the fact that they make up such a significant fraction of the genome, there is no indication for DNA-transposon activity in the human genome for the past 50 million years possibly due to their inactivation by mutations.

The “cut and paste” transposition process involves the excision of the DNA Element from its DNA context and its reintegration into a different locus. It can be divided into four major steps.

In the first step the transposase binds as a homodimer to the inverted direct repeats (IR/DRs) of the transposon (Ivics and Izsvak 2004). In the second step the synaptic formation takes place, where the two ends of the transposon element are paired and held together by the transposase. This step serves as a checkpoint for the transposition, controlling whether all molecular requirements are fulfilled. During synaptic complex formation the two IR/DRs with the four transposase binding sites mediate the formation transposase tetramers. The third step, transposon excision, takes place when the synaptic complex formation is completed. The DDE (conserved triad of amino acids) catalytic subdomain of the transposase catalyzes the cleavage at the ends of the SB element and generates overhangs of three nucleotides, GTC, at both ends of the transposon. In the fourth step, reintegration of the transposon takes place, catalyzed by the DDE subunit of the transposase.

Transposable elements generate DSBs due to their mobility. Although HR and NHEJ are involved in the repair of transposon mediated breaks, SB transposition in HR and D-NHEJ deficient cells induces only moderate cell death (Izsvak, Stüwe et al. 2004).

For the goals of this project, we selected the Sleeping Beauty (SB) DNA transposon system developed by Z. Ivics to achieve multiple integrations for the different I-SceI constructs into the chromosomes of cultured cell lines. SB is a highly efficient transposon system that clearly enhances integration events in comparison to the spontaneous integration measured after plasmid transfection (Fig. 13). The SB transposon originates from the TC1/*mariner*-type transposon found in fish genomes and was reconstructed by eliminating different inactivating mutations from the transposase gene. SB shows a random pattern of integration in the human genome (Vigdal, Kaufman et al. 2002). It prefers TA dinucleotides as integration sites, which are found approx. every 20 bp in vertebrate genomes. Palindromic AT-repeats: ATATATAT were found to often surround the integration site. The 3' ends of the excised transposon invade the target DNA molecule after the transposase cleaved the TA dinucleotide target integration site. The TA target site is duplicated upon insertion.

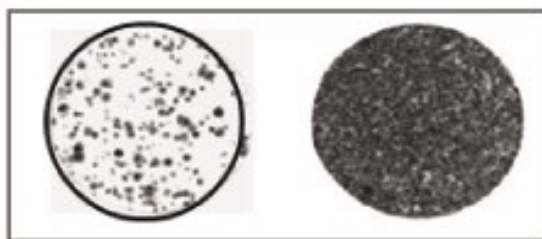


Fig.13: Comparison of spontaneous and SB Transposon mediated integration (Ivics, Hackett et al. 1997). Dishes with colonies of HeLa cells plated after transfection with a plasmid containing a neo resistance gene are shown. Cells are grown under antibiotic selection. Only cells that express the antibiotic resistance gene due to chromosomal integration survive. HeLa cell colonies are obtained in the absence (left dish) or in the presence (right dish) of transposase.

In the implementation used in the present work, SB transposition is mediated by a two component assay, where two non-autonomous transposon elements, the donor plasmid containing a *neo* selectable marker gene flanked by IRs and the helper plasmid expressing the transposase are co-transfected. The number of cell clones resistant to

the neomycin-analog G-418 serves as the indicator for the integration and expression of the *neo* transgene.

5.1.3. Cloning of I-SceI constructs into the Sleeping Beauty (SB) transposon vector

All nine I-SceI constructs were cloned into the SB transposon donor plasmid pT2SVNeo (Fig. 14). The SB transposon consists of the transposon sequence, which is flanked by the inverted/directed repeats (IR/DRs) containing binding sites for the transposase.

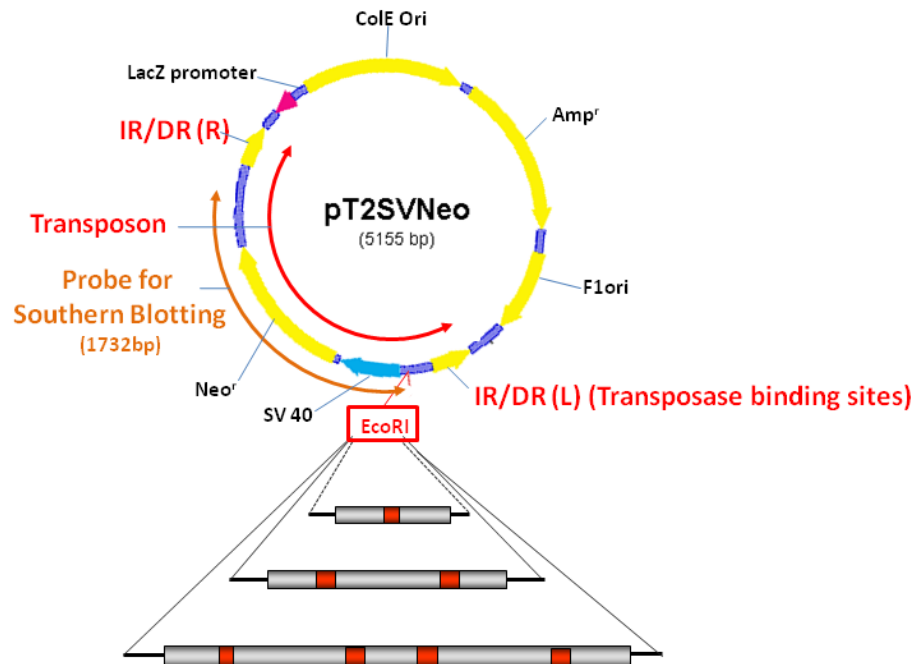


Fig. 14: Cloning of I-SceI constructs into the transposon vector pT2SVNeo. The different I-SceI constructs were cloned into the Sleeping Beauty (SB) transposon vector at the MCS and cotransfected with the SB transposase. Using this type of vectors a high number of random integration events can be achieved in different cell lines.

The SB transposon is non-autonomous and not able to transpose without an appropriate transposase encoding sequence. The transposase binding sites of the SB element show a specific structure. Two binding sites are located at the ends of the 200-250 bp long inverted repeats (IR) and contain short 15-20 bp direct repeats (DRs). Due to this special organization, the entire region is termed IR/DR. Fig. 15 summarizes the function of the two component SB transposition system used here for the selected components.

In pT2SVNeo, the multiple cloning site (MCS) along with the SV40 promoter and the neomycin resistance gene are located between the IR/DR-sequences. The *EcoRI* restriction site at the MCS was selected for non-directional cloning of the I-SceI constructs. Prior to cloning into the pT2SVneo plasmid the I-SceI constructs were excised from the pPCRScripT vector by *EcoRI* digestion.

All nine I-SceI constructs described in 2.1 are cloned between the IR/DRs of the pT2SVNeo plasmids and are thus ready for transfection and genomic integration. The following five pT2SVNeo plasmids were used for further experiments: pT2SVNeo-1xI-SceI-D, pT2SVNeo-2xI-SceI-D, pT2SVNeo-2xI-SceI-R, pT2SVNeo-4xI-SceI-D and pT2SVNeo-4xI-SceI-R.

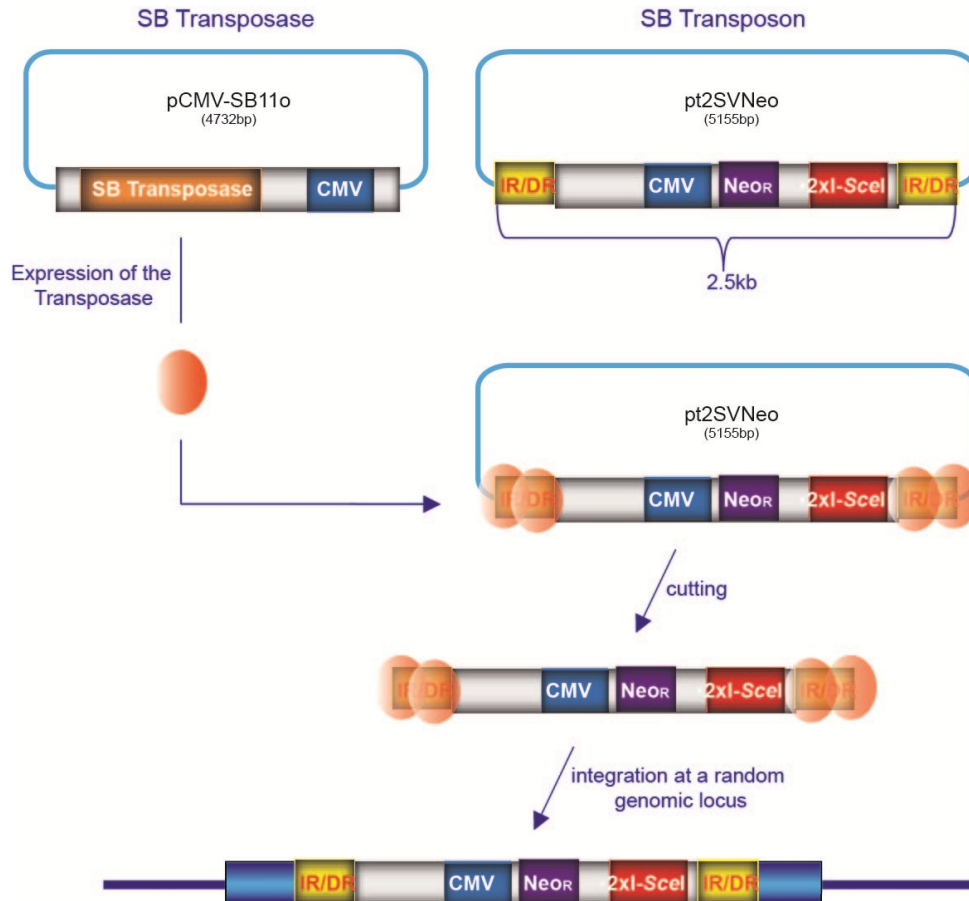


Fig. 15: The Sleeping Beauty Transposon Mechanism. The pCMV-SB11 transposase plasmid is co-transfected with pT2SVNeo at a ratio 1:10. Transposase binds to the IR/DRs of the transposon vector, forms a synaptic complex and excises the sequence from pT2SVNeo. Finally the transposase carries the excised construct to a random genomic locus by binding to a TA site that is duplicated during the integration.

5.1.4. Selected cell lines for transposition

The Chinese hamster ovary (CHO10B4) cells were selected for experiments on the basis of their excellent growth characteristics, good transfection efficiencies, but most importantly due to the availability of derivative mutants with defects in specific pathways of DSB repair. An additional advantage of these cells is their relatively low chromosome number ($2n=22$) that facilitates analysis of the consequences of DSBs using cytogenetic methods. Furthermore, CHO cells are lacking p53 function as a result of a mutation in codon 211 of exon 6. This was perceived as advantage because it was expected to reduce p53-mediated apoptosis. Indeed, we had indications that in the p53 wt human A549 cells, apoptosis compromised analysis of the consequences of lesion complexity using the same model system.

To investigate the contribution of homologous recombination repair (HRR) and of DNA-PK dependent non-homologous end-joining (D-NHEJ) to the processing of complex DSBs, we also selected appropriate CHO mutants for stable integration of I-SceI constructs. Nine complementation groups, with mutations in genes that are involved in DSB repair, have been isolated from radiosensitive rodent cell lines and have been studied for DSB repair defects (Jones, Cox et al. 1988). The *xrs-6* mutant belongs to the X-ray radiation complementation group 5 and carries a mutation in the *XRCC5* gene, encoding the Ku80 subunit of the heterodimeric Ku protein - a component of DNA-PK. *Xrs6* cells completely lack DNA end binding and kinase activities associated with DNA-PK (Finnie, Gottlieb et al. 1995). An additional NHEJ mutant cell line, XR-C1-3, has been assigned to the X-ray radiation complementation group 7 and has a mutation in the *XRCC7* gene encoding the catalytic subunit of DNA-PK (DNA-PKcs); this mutant also lacks DNA-PK catalytic activity. As a result of the corresponding mutations, both cell lines are severely impaired in DSB repair, specifically by D-NHEJ.

The third mutant selected for the present work, *irs1SF*, is defective in HRR as a result of a mutation in the *XRCC3* gene. The *XRCC3* protein is one of the Rad51 paralogs and interacts with Rad51, thus promoting HRR.

5.1.5. SB-transposition-based integration of I-SceI constructs in multiple copies in wt CHO cells and DSB repair deficient mutants

The SB transposon containing donor plasmid vector pT2SVNeo, carrying one of the five I-SceI constructs, is co-transfected with the hyperactive SB transposase expressing helper plasmid pCMV(CAT)SB100x at a 10:1 ratio. Transfections are carried out using the nucleofection technology of Amaxa (see 4.2.4).

Two days post transfection cells were plated in various dilutions and grown in selective media containing the neomycin analog G418. Before inception of these experiments, a G418-toxicity curve was generated to determine the required concentration for tight selection. These experiments revealed that 500µg/ml G418 were required for CHO10B4 and 300µg/ml for Xrs6, XR-C1-3 and irs1SF. Cell clones resistant to G418, due to chromosomal integration and expression of the *neo* transgene, were selected eight days later. Clones were grown in 24 well plates for eight more days, passaged twice and frozen (-150 °C). For a detailed list of generated clones see Tables 5-8.

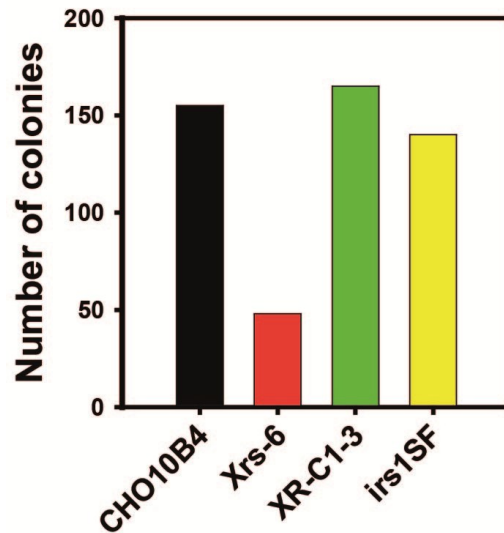


Fig. 16: I-SceI construct integration in CHO wt and Xrs6, XR-C1-3 and irs1SF cells. Two million cells of each of the indicated cell lines were cotransfected with the SB transposon vector carrying 2xI-SceI and the SB transposase. Two days after transfection 1000 cells were plated in G418 selective media. Mutant cell lines were transfected with a four-fold higher plasmid concentration (4 µg pt2SVNeo and 400 ng pcMV SB11 per 10⁶ cells) to enhance the number of integrations (see below) and to compensate for reduced transposition activity that is sometimes associated with the repair defects.

To assess the transposition efficiencies in repair deficient mutants, the number of G418-resistant colonies obtained after the above described transfections were compared between wt cells and mutants. A reduction of approx. 70% in the number of colonies obtained in Xrs6 cells as compared to wt cells can be observed (Fig. 16) underlining that NHEJ has an important but not absolute role for transposition (Izsvak, Stüwe *et al.* 2004).

5.1.6. Nomenclature

The large number of clonal cell lines generated as part of the present work necessitates a rational, informative and clear nomenclature. In this section we describe the basis of the chosen nomenclature. The name of each cell line has four parts. The first part indicates the cell line on the genetic background of which the clones were generated. The second part indicates the construct used for integration. It is this part of the name that informs about the complexity of induced DSB. The third part of the name indicates the number of integrations achieved. The fourth part of the name identifies the specific clone. It should be pointed out, that as a results of the random integration taking place during transposition, two clones obtained after transfection with the same construct and which exhibit the same number of integrations, may show different results as result of differences in the integration sites.

To illustrate, a cell line derived from CHO cells using an I-SceI construct containing two I-SceI sites in reverse orientation to generate incompatible ends (see above) and which was found by Southern blotting to have 7 integrations of the construct will have as clone 4 the name:

CHO-2xISceI-R7.C4

Again, the first letters, illustrated in green, indicate the name of the cell line. Then the description of the I-SceI constructs follows, shown in red, whereas the number 2x stands for the number of I-SceI sites in the integrated construct. After the description of the construct, the integration site number and the reverse (R) or direct (D) orientation of the I-SceI sites (shown in blue) is indicated. The clone number completes the name.

5.1.7. Characterization of the derived clones in the different genetic backgrounds

We used Southern blotting to determine the number of I-SceI construct integrations in the selected clones. In general, a 1.72 kb probe, comprising the neomycin resistance gene, the CMV promoter and 121 bp of the I-SceI construct (Fig. 14), was generated by random priming and used for Southern hybridization. For this purpose, genomic DNA was extracted and digested with XbaI after optimization of the incubation conditions. The Southern Blot in Fig. 17A shows that the addition of XbaI once for twelve hours, is sufficient for complete digestion. Therefore, this condition of genomic DNA digestion was used throughout this clone characterization phase.

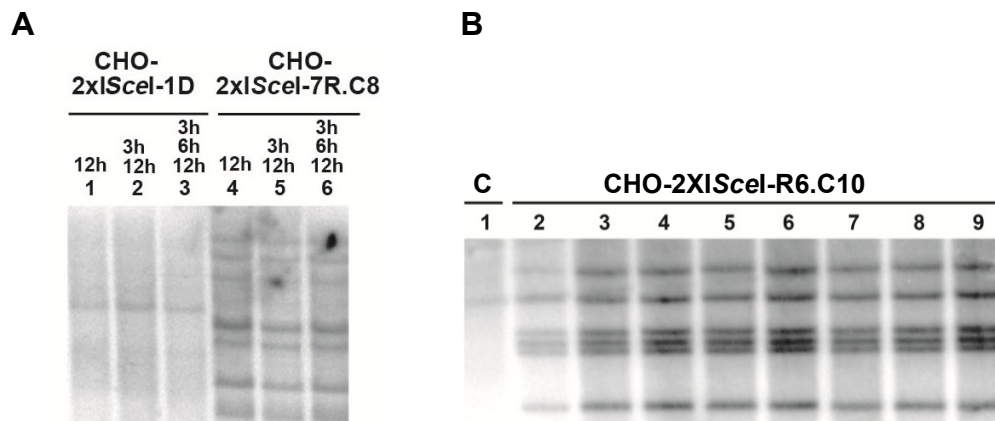


Fig. 17: Southern Blots of CHO-2x.I.SceI-D.1, CHO-1x.I.SceI-R.7 and CHO-2x.I.SceI-R6. **A:** Test for complete digestion of genomic DNA: Genomic DNA (18 μ g) from CHO-2xI.SceI-D.1 and CHO-1xI.SceI-R.7 cells were digested with XbaI (20.000 units per mL) for different time periods. In lanes 1 and 4, the genomic DNA was digested for 12 hours. In lanes 2 and 5, after 12 h an equal amount of enzyme was added for 3h. In lanes 3 and 6 after 12 h an equal amount of enzyme was added for 6 h and then again for 3 h. It is evident that incubation for 12 h is sufficient to complete digestion. **B:** Testing for long term stability of the genomically integrated transposon constructs: Eight clones (lane 2-9) of CHO-2xI.SceI-R6.C10 were passaged approx. 20 times before re-analyzing by Southern blotting. It is evident that integrations remain stable during the tested time interval. **C:** Control: nontransfected cells.

In the first set of CHO cell transfections we used 1 μ g / 10^6 cells of pT2SVNeo-2x-I-SceI and 100 ng / 10^6 cells transposase expressing plasmid. Under these conditions, clones with a maximum of six integrations were obtained. In an effort to increase the number of integrations, we increased fourfold the plasmid concentration in a second set of transfections. With the higher plasmid concentration, clones with up to thirteen integrations could be obtained. Based on this result the higher plasmid concentration

was used from the outset for the generation of clones in the mutant cell lines – also to compensate for possible reductions in transposition efficiency as a result of the repair defects (see above). Fig. 17B also shows that growing one of the selected clones for a few months has no effect on the stability of the integrations.

This form of characterization led to the selection from CHO cells of nine clones harboring 1xl-SceI sites with 2-7 integrations (Fig. 18A). Fig. 17C shows similar results for 18 clones harboring the indicated (2-12) integrations of constructs with 2xl-SceI sites in reverse orientation; twelve clones were also obtained with the construct harboring 2xl-SceI sites in direct orientation (Fig. 18B). Eight CHO10B4 clones bearing 4xl-SceI-site constructs in reverse orientation show 5-11 integrations (Fig. 18D).

Fig. 19 shows a Southern blot for the *irs1SF* mutant. This HR mutant shows in general a lower number of I-SceI-construct integrations, ranging from 1-7. For the *Xrs6* mutant, three types of clones were established and characterized (Fig. 20). Four clones with a 1xl-SceI (Fig. 20A), thirteen clones with 2xl-SceI (Fig. 20B and C) (7-9 integrations for direct orientation and nine clones with 3-11 integrations for reverse orientation); we also generated two clones with 4 integrations harboring 4xl-SceI sites in reverse orientation (Fig. 20D). XR-C1-3 has integrations ranging from 4-9, for direct, and 5-12 for reverse orientation (Fig. 21A).

An overview of all characterized clones for the different cell lines, including nomenclature, type and number of integrated constructs, as well as number of colonies available is given in the Tables 5-8. A total pool of 270 clones was characterized and frozen and is available for use on an “as-needed” basis for the experiments of the present project.

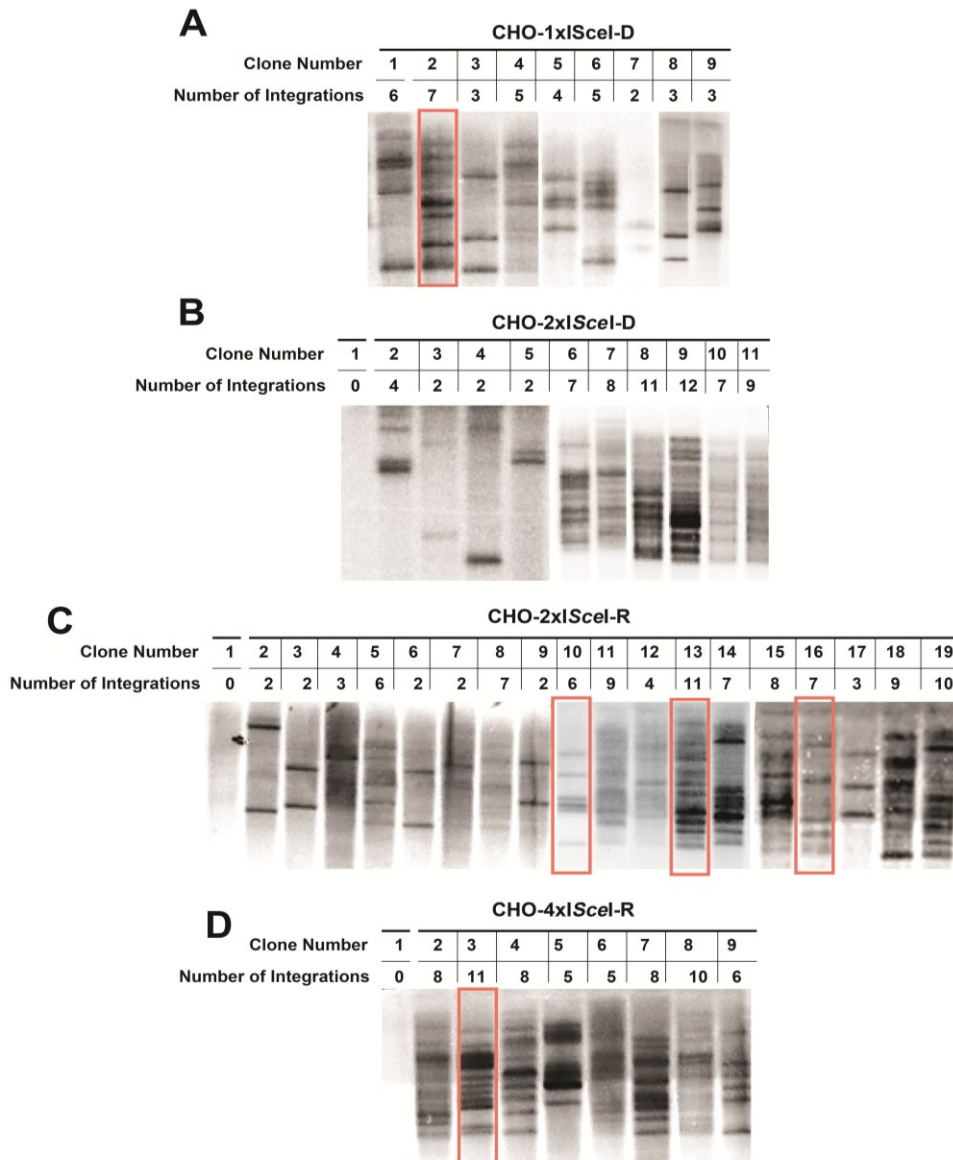


Fig.18: Characterization of CHO clones by Southern blotting harboring the following constructs: A, 1xI-SceI (CHO-1xI-SceI-D); B, 2xI-SceI-D (CHO-2xI-SceI-D) C, 2xI-SceI-R (CHO-2xI-SceI-R) and D, 4xI-SceI-R (CHO-4xI-SceI-R). Genomic DNA of CHO wt cells without integrations serves as control (Lane 1). Lanes 2-5 in Figure B and lanes 2-9 in Figure C represent clones of cells transfected with $1 \mu\text{g}/10^6$ transposon and $100\text{ng}/10^6$ transposase plasmids (7.2×10^{11} molecules Transposon / 2×10^6 cells and 7.8×10^{10} molecules Transposase / 2×10^6 cells). All other lanes represent clones obtained after transfection with $4 \mu\text{g}/10^6$ cells transposon and $400 \text{ng}/10^6$ cells transposase plasmids (1.8×10^{11} molecules transposon / 2×10^6 cells and 2×10^{10} molecules Transposase / 2×10^6 cells). The numbers of integrations range from 2-11. See Table 5 for a detailed list of CHO clones with the different constructs and number of integrations. Clones chosen for further experiments are indicated in red.

Table 5: List of characterized clones with I-SceI construct integrations in CHO10B4 cells

CHO10B4																
Number of I-SceI sites in the construct	Orientation of I-SceI, D: direct, R:reverse	Nomenclature	Number of clones frozen	Number of clones characterized	Number of integrations per cell											
					1	2	3	4	5	6	7	8	9	10	11	12
1	D	CHO-1xI-SceI-D	15	9	-	1	3	1	2	1	1	-	-	-	-	
Clone Number					-	7	3, 8, 9	5	4, 6	1	2	-	-	-	-	
2	D	CHO-2xI-SceI-D	30	10	-	3	-	1	-	-	2	1	1	-	1	
Clone Number					-	3, 4, 5	-	2	-	-	6, 10	7	11	-	8	
2	R	CHO-2xI-SceI-R	30	17	-	5	2	1	-	2	3	1	2	-	1	
Clone Number					-	2, 3, 6, 7, 9	4, 17	12	-	5, 10	8, 14, 16	15	11, 18	19	13	
4	R	CHO-4xI-SceI-R	15	8	-	-	-	-	2	1	-	3	-	1	1	
Clone Number					-	-	-	-	5, 6	9	-	2, 4, 7	-	8	3	

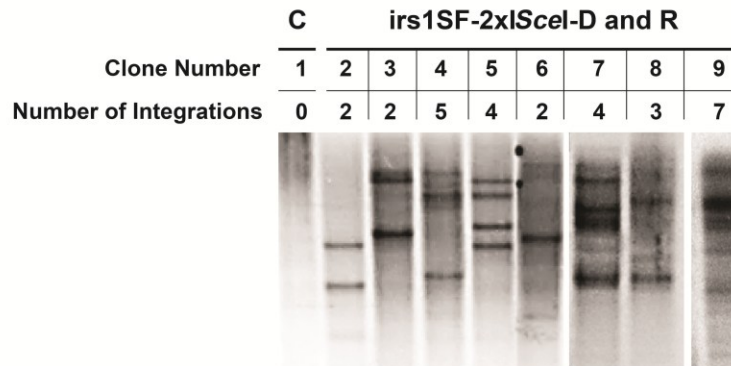


Fig. 19: Characterization of clones obtained from irs1SF cells. Clones of irs1SF cells with integration of constructs harboring 2xI-SceI sites in reverse orientation (irs1SF-2xI-SceI-R). C: Control with genomic DNA of nontransfected irs1SF cells.

Table 6: List of characterized clones with I-SceI construct integrations in irs1SF cells

irs1SF (defect in XRCC3)																
Number of I-SceI sites in the construct	Orientation of I-SceI, D: direct, R: reverse	Nomenclature	Number of clones frozen	Number of clones characterized	Number of integrations per cell											
					1	2	3	4	5	6	7	8	9	10	11	12
1	D	irs1SF-1xI-SceI-D	20	-	-	-	-	-	-	-	-	-	-	-	-	
2	D	irs1SF-2xI-SceI-D	15	2	-	-	-	1	1	-	-	-	-	-	-	
Clone Number								5	4							
2	R	irs1SF-2xI-SceI-R	15	6	-	3	1	2	-	-	1	-	-	-	-	
Clone Number					-	2, 3, 6	8	7	-	-	9	-	-	-	-	
4	R	irs1SF-4xI-SceI-R	20	-	-	-	-	-	-	-	-	-	-	-	-	

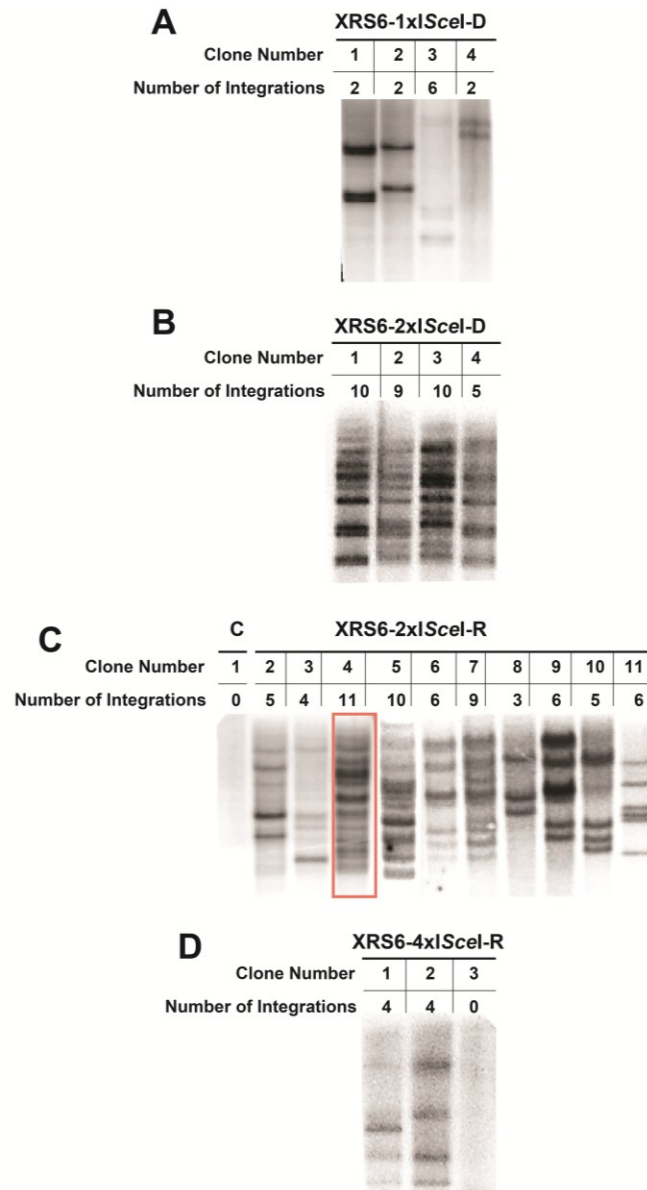


Fig. 20: Characterization of clones obtained from Xrs6 cells. Clones of Xrs6 cells with integrations of the following constructs: **A**, 1xI-Scel-D (XRS6-1xIScel-D); **B**, 2xI-Scel-D (XRS6-2xIScel-D); **C**, 2xI-Scel-R (XRS6-2xIScel-R); and **D**, 4xI-Scel-R (XRS6-4xIScel-R); **C**: Control with genomic DNA of nontransfected Xrs6 cells.

Table 7: List of characterized clones with I-SceI construct integrations in Xrs6 cells

Xrs6 (defect in Ku80)																
Number of I-SceI sites	Orientation of I-SceI, D: direct, R:reverse	Nomenclature	Number of clones frozen	Number of clones characterized	Number of integrations per cell											
					1	2	3	4	5	6	7	8	9	10	11	12
1	D	XRS6-1xISceI	15	4	-	3	-	-	-	1	-	-	-	-	-	
Clone Number					-	1, 2, 4	-	-	-	3	-	-	-	-	-	
2	D	XRS6-2xISceI-D	25	4	-	-	-	-	1	-	-	-	1	2	-	
Clone Number					-	-	-	-	4	-	-	-	2	1, 3	-	
2	R	XRS6-2xISceI-R	25	8	-	-	1	1	2	3	-	-	1	1	1	
Clone Number					-	-	8	3	2, 10	6, 9, 11	-	-	7	5	4	
4	R	XRS6-4xISceI-R	15	2	-	-	-	2	-	-	-	-	-	-	-	
Clone Number					-	-	-	1, 2	-	-	-	-	-	-	-	

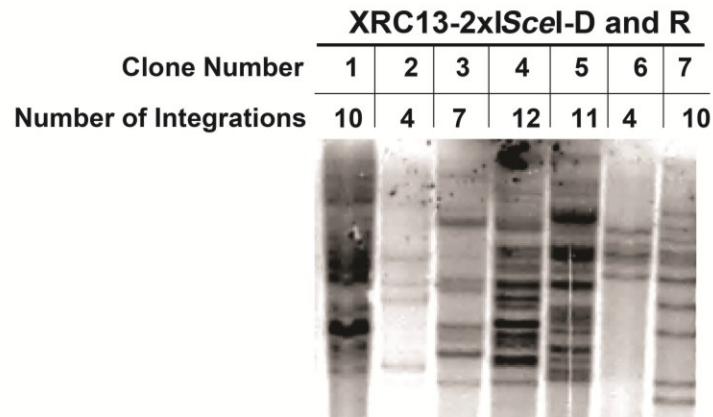


Fig. 21: Characterization of clones obtained from XR-C1-3 cells. Clones of XR-C1-3 cells with integration of constructs harboring 2xI-SceI sites in reverse orientation and direct orientation (XRC13-2xI-SceI-R and D).

Table 8: List of characterized clones with I-SceI construct integrations in XR-C1-3 cells

XR-C1-3 (defect in DNA-PKcs)																
Number of I-SceI sites	Orientation of I-SceI, D: direct, R:reverse	Nomenclature	Number of clones frozen	Number of clones characterized	Number of integrations per cell											
					1	2	3	4	5	6	7	8	9	10	11	12
1	D	XRC13-1xI-SceI	15	-	-	-	-	-	-	-	-	-	-	-		
2	D	XRC13-2xI-SceI-D	10	2	-	-	-	1	-	-	-	-	1	-		
Clone Number					-	-	-	2	-	-	-	-	7	-		
2	R	XRC13-2xI-SceI-R	10	6	-	-	-	-	-	1	1	-	2	1		
Clone Number					-	-	-	-	-	4	3	-	-	1, 7		
4	R	XRC13-4xI-SceI-R	15	-	-	-	-	-	-	-	-	-	-	-		

The selected clones that are used for further experiments described in the following sections are marked with red in the Southern blot figures. In this initial stage of the work, the clones were selected on the basis of their high number of integrations.

The next sections describe experiments that were performed with selected clones harboring various integrations of 1xI-Scel, 2xI-Scel and 4xI-Scel constructs to assess the biological consequences of simple compared to clustered DSBs. A high integration number served as the most important criterion for selection at this stage of the project. The following clones were chosen from the CHO wt- (Table 5, indicated in red) cell line: CHO-1xI-Scel-7D.C2, CHO-2xI-Scel-R11.C13, CHO-4xI-Scel-R11.C3, CHO-2xI-Scel-R6.C10 and CHO-2xI-Scel-R7.16. In addition the D-NHEJ deficient clones XRC13-2xI-Scel-R11.C5 (Table 7) and Xrs6-2xI-Scel-R11.C4 (Table 8) were tested.

5.2. Which kind of lesion dominates the strong killing effect of IR?

Ionizing radiation has a high killing potential. The dose-response curve for cell survival is widely used to describe the loss of reproductive integrity in proliferating cells as a function of radiation dose (Hall and Giaccia 2006). Survival curves for CHO-2xI-Scel-6R.C10 and U2OS cell lines that have been exposed to different doses of X-rays are shown in Fig. 22. Approx. 80% of U2OS and 50% of CHO cells are killed by a radiation dose of 4 Gy.

The relationship between the initial DNA damage, attempted repair and ultimate cell killing by IR are not fully understood (Olive 1998). As described in the Introduction, the biological effects of IR are stochastic in nature. DSBs are considered as the critical lesion for cell killing although the correlation of the initial DSB number, or their repair, to radiosensitivity is still incompletely characterized. Furthermore the increase in DSB yield does not show a strong dependence on radiation quality (Goodhead, Thacker et al. 1993).

Therefore it is likely that the increase in RBE for high LET radiation compared to low LET radiation is not caused by an increase in the number, but by the changed

distribution of the induced DSBs, which in the case of high LET radiation are more frequently generated as clusters (due to the track structure).

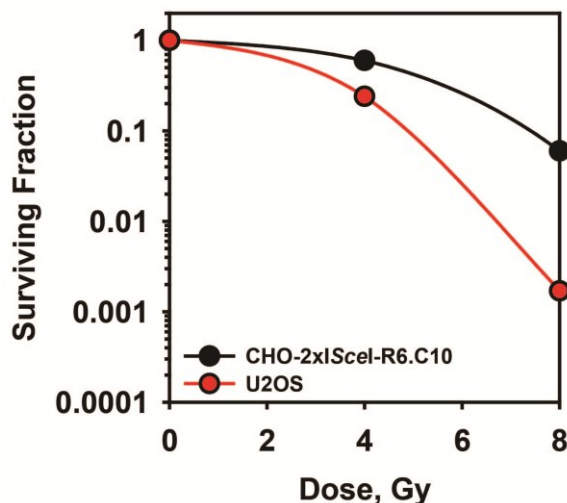


Fig. 22: Survival after irradiation with 4 and 8 Gy X-rays of CHO-2xIscel-R6.C10 and U2OS cells. After IR cells were plated in different dilutions and grown for 10 (CHO) or 14 (U2OS) days to allow colony development.

To test the hypothesis that clustered DSBs have higher probability for adverse biological consequences than simple DSBs, we performed survival experiments with I-Scel-induced simple and clustered DSBs. The I-Scel model system is unique in the sense that it enables the exclusive analysis of the effect of DSBs on cell survival, ruling out potential effects of other types of DNA damage like SSBs or base damages that accompany DSBs in cells exposed to IR.

5.2.1. Clustered DSBs have a markedly stronger killing capacity than simple DSBs

The clonogenic survival assay was performed to assess biological effectiveness of simple compared to clustered DSBs in the I-Scel model system. Immediately after I-Scel transfection of the clones CHO-1xIscel-7D.C2, CHO-2xIscel-11R.C13 and CHO-4xI.Scel-11R.C3 (2×10^6 cells were transfected with $2 \mu\text{g}$ plasmid) cells were plated in different numbers (100, 200 and 500 cells), grown for eight days and stained.

The cells were carefully stored in an incubator avoiding shaking and intensive air current fluctuation as accidentally detached cells form satellite colonies that generate analysis artefacts. Transfection of CHO cells without I-SceI integrations with pmax-GFP served as a control. The transfection efficiency was measured 24h after pmax-GFP transfection by FACS analysis and ranged between 90-98%.

The results (Fig. 23) clearly show that clustered DSBs lead to increased cell killing compared to simple breaks. Whereas the simple DSBs did not show a measurable killing effect, the clustered DSBs showed 35% killing for CHO-2xI-SceI-11R.C13 and with increased clustering killing increased to approx. 50% - in the clone CHO-4xI-SceI-11R.C3.

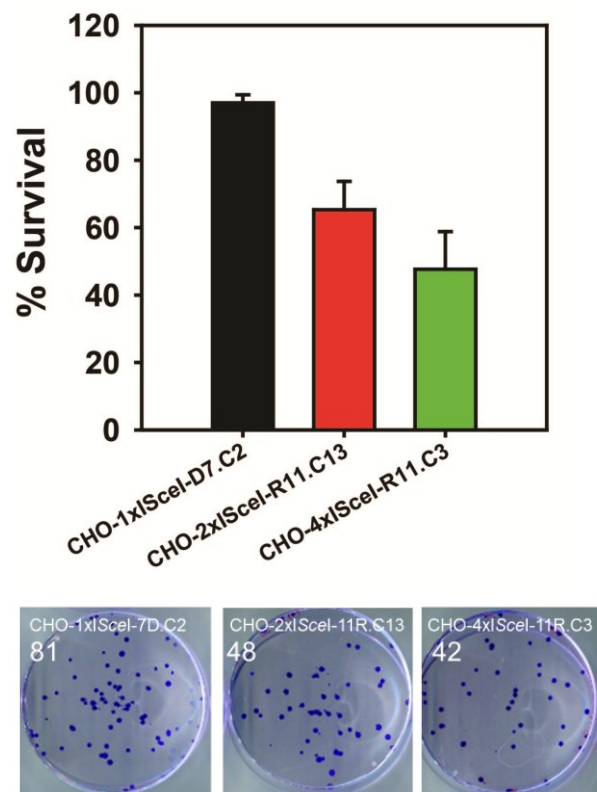


Fig. 23: Survival of cells harboring simple or clustered DSBs in the form of I-SceI recognition sites after transfection with an I-SceI expressing vector. 2×10^6 cells of the cell lines CHO-1xI-SceI-D7.C2, CHO-2xI-SceI-R11.C13 and CHO-4xI-SceI-R11.C3 were transfected with $2 \mu\text{g}$ of pCMV3xnlSI-SceI. 200 cells were plated immediately after transfection and grown for 10 days. The data presented is normalized to CHO10B4 wt cells transfected with pCMV3xnlSI-SceI. The plating efficiency was 78%. Representative dishes with stained colonies are shown.

As an additional control for cellular effects of simple DSBs, survival was measured with the human *AsiSI*-ER-U2OS cells. This cell line is the basis for an experimental system developed by G. Legube in U2OS cells that allows the enzymatic induction of DSBs in cells through the regulated expression of the *AsiSI*-ER RE (Iacovoni, Caron et al. 2010). *AsiSI* recognizes an 8bp sequence (Fig. 24A) that is present in multiple copies in the human genome and therefore generates multiple DSBs at average distances larger than 1 Mbp.

The *AsiSI*-ER-U2OS cells stably express a form of *AsiSI* fused to a modified ligand binding domain of the estrogen receptor. Upon binding of 4HT to this estrogen receptor domain, *AsiSI* translocates to the nucleus and generates sequence specific DSBs. The authors reason that due to CpG methylation only 25% of the approx. 1750 *AsiSI* sites (in G1) are digested.

To follow growth characteristics, growth curves were performed with the parental U2OS cell line and *AsiSI*-ER-U2OS (Fig. 24B). With the exception of the initial slower growth of the *AsiSI*-ER-U2OS cells after the first day, no clear differences in doubling times between the two cell lines could be observed. The slower initial growth may be caused by the leakiness of the system that allows some *AsiSI* molecules to pass the nuclear membrane in the absence of 4HT.

Cell survival was measured with 4HT treated *AsiSI*-ER-U2OS cells (Fig. 24C). The cells were treated for different times (0h, 2h, 4h, and 8h) with 4HT before plating. After treatment 200 cells were plated per dish and were allowed to form colonies in the absence of 4HT. The results show 40% killing after 2 h of treatment that increases to 50% after 8h treatment.

Compared to clustered DSBs where approx. 50% killing is induced for 11 clustered breaks, approx. 150 times more simple-DSBs (according to the *AsiSI* model system) are required to achieve a similar amount of killing. These results clearly imply an increase in adverse biological consequences of clustered compared to simple DSBs.

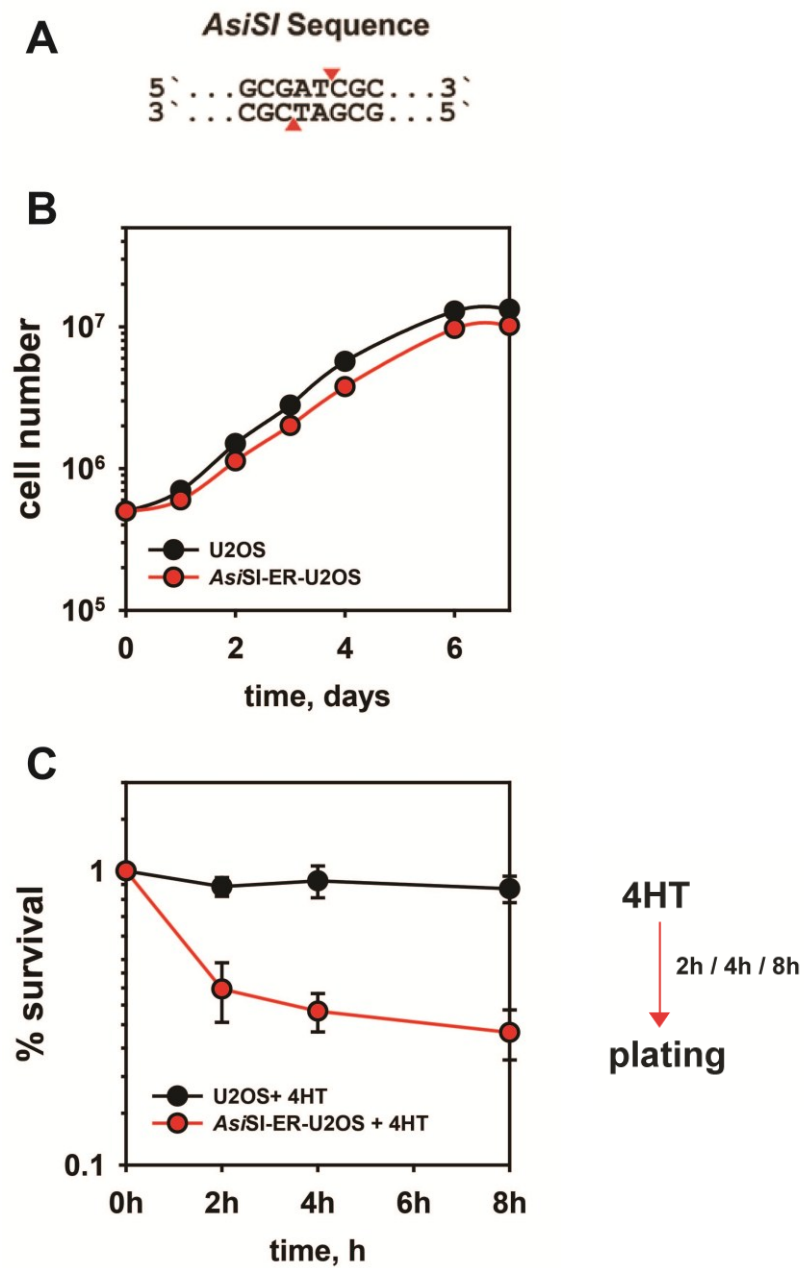


Fig. 24: A: Recognition sequence of the *AsiSI* HE. B: Growth curves of *AsiSI*-ER-U2OS and U2OS cells. 0.5×10^6 cells were plated and counted after 1-7 days. C: Survival curves of *AsiSI*-ER-U2OS cells and the parental U2OS cells after treatment with 4HT for different times. X-axis shows the time cells were treated with 4HT. Plating efficiency was 70%.

5.2.2. Clustered DSBs induce lethal Chromosomal Aberrations

It is widely accepted that unrepaired or misrepaired DNA double strand breaks (DSBs) lead to the formation of chromosome aberrations (Iliakis, Wang *et al.* 2004). To address the question whether clustered DSBs lead with higher probability to chromosome damage than simple DSBs the formation of chromosome aberrations was analyzed. Metaphase spreads were prepared from clones bearing simple DSBs (CHO-1xI-SceI-7D.C2) and clustered DSBs (CHO-2xI-SceI-11R.C13 and CHO-4xI-SceI-11R.C3) 24 h after transfection with I-SceI. Cells were treated with colcemid for 2 h to arrest at mitosis before processing for cytogenetic analysis.

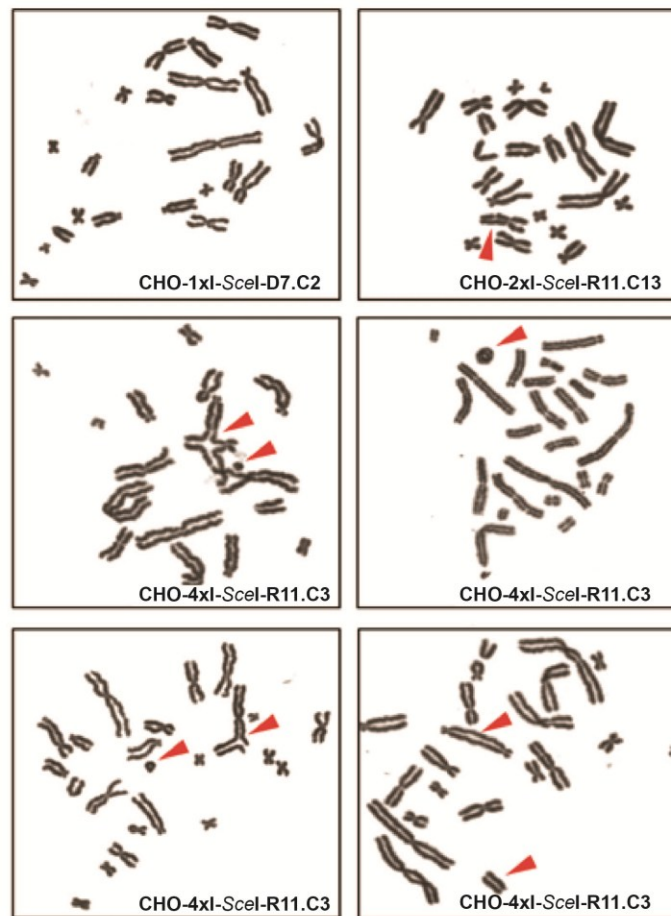


Fig. 25: Representative metaphase spreads of the cell lines CHO1xI-SceI-D7.C2, CHO2xI-SceI-R11.C13 and CHO-4xI-SceI-R11.C3 24h after transfection with pCMV3xnI-SceI. Red arrows indicate chromatid breaks and chromosomal aberrations like dicentrics and rings.

As illustrated in Fig. 25, clustered DSBs generated in CHO-4xI-SceI-11R.C3 cells lead to chromatid breaks, dicentric and rings. In contrast simple DSBs generated in CHO-1xI-SceI-7D.C2 cells only rare chromatid breaks.

Since a good correlation exists between chromosome aberration formation and cell killing, this observation provides an explanation for the increased killing of clustered DSBs measured above. Analysis at metaphase allows detection of irreversible chromosome aberrations that frequently cause cell death. To also detect reparable chromosome aberrations, we performed G2 premature chromosome condensation (G2-PCC). This method allows also the analysis of more cells, as typically only few cells reach metaphase after the treatment employed here.

5.2.3. G2-PCC breaks and exchanges are elevated in cells with clustered as compared to simple DSBs

Calyculin A induced G2 premature chromosome condensation was performed to study chromosome aberrations in the form of chromatid breaks and exchanges in interphase cells. The Serine/Threonine Phosphatase inhibitor calyculin A inhibits the activity of protein phosphatases PP1 and PP2 thus causing a very rapid condensation of chromosomes in G2 phase cells (in CHO cells within 5-10min). In this way analysis of chromosome aberrations is possible at interphase and cells do not need to progress to mitosis.

The clones CHO-1xI-SceI-D7.C2 and CHO-2xI-SceI-R11.C13 and CHO-4xI-SceI-R11.C3 were transfected with I-SceI expressing plasmid (6×10^6 cells with 6 μ g plasmid) and incubated at 37 °C for 8 h and 24 h. 100 nM calyculin A was added for 30 min before collection at these times. Cells with condensed chromosomes were detected with a metaphase finder (Meta-Systems) and analyzed with the Ikaros software (MetaSystems). For every time point 100 cells with condensed chromosomes were scored.

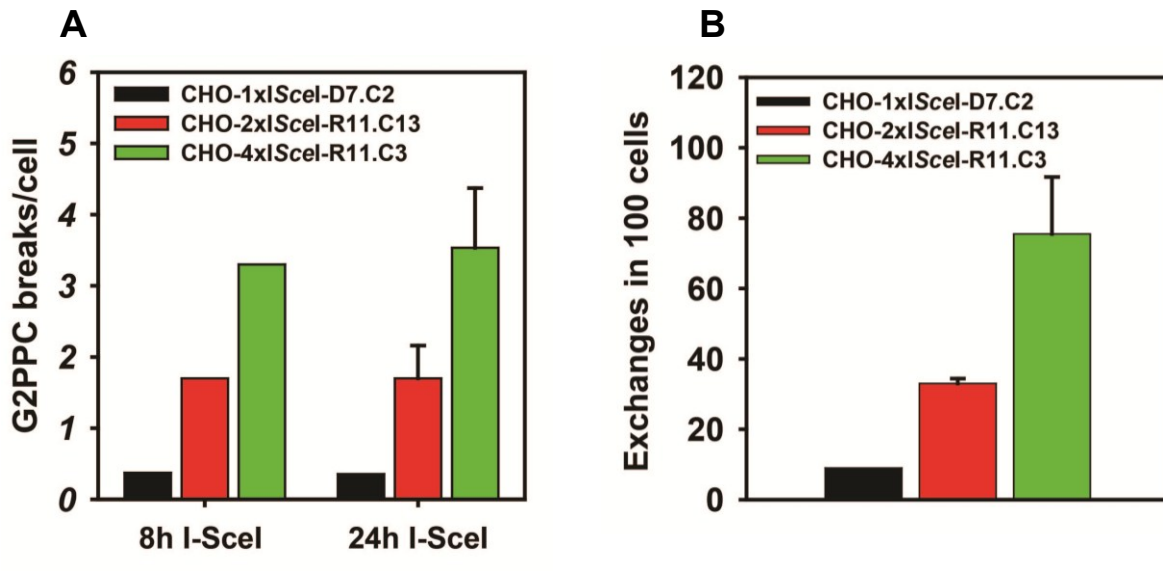


Fig. 26A: G2-PCC breaks per cell in CHO-1xI-SceI-D7.C2, CHO-2xI-SceI-R11.C13 and CHO-4xI-SceI-R11.C3 cells 8 h and 24 h after pCMV3xnlSI-SceI transfection. Graphs represent data after background subtraction measured in non-transfected cells that have approx. 1.2 G2PCC breaks/cell. **B:** Chromosome exchanges in CHO-1xI-SceI-D7.C2, CHO-2xI-SceI-R11.C13 and CHO-4xI-SceI-R11.C3 cells 24h after pCMV3xnlSI-SceI transfection. For each experiment 100 metaphases were analysed. No exchanges could be detected in nontransfected controls.

G2-PCC breaks (Fig. 26A) and exchanges (Fig. 26B) were scored separately. The high number of G2-PCC breaks and chromosomal exchanges measured by G2-PCC, strengthens the above observations that clustered DSBs have a higher killing potential than simple DSBs. Whereas the clustering with two I-SceI sites shows only a slight increase in G2-PCC breaks and exchanges (approx 1.8 G2-PCC/breaks per cell and 30 exchanges in 100 cells), the number of G2-PCC breaks for a higher degree of clustering is clearly elevated (approx. 3.5 G2-PCC breaks/cell and 75 exchanges in 100 cells). We conclude that clustered DSBs are toxic to the cells because they have a high risk for chromosomal aberrations formation.

5.3. Analysis of DNA damage signaling elicited by simple and clustered DSBs

We followed DSB-generated signaling to detect possible differences in signaling characteristics for different levels of DSB complexity. As a first step, we present γ -H2AX foci formation at chromatin. Subsequently foci formations by MDC1 and 53BP1 proteins downstream in the signaling cascade were analyzed. The latter proteins are recruited and are not inherently part of the chromatin like H2AX, therefore they can be observed by live cell imaging to analyze subcellular localization and dynamics in real time over a period of 24 h.

5.3.1. Theoretical foci-maximum upon DSB induction by I-SceI

As the number of I-SceI-construct integrations represents the number of possible DSBs that can be induced by I-SceI, the theoretical maximum of foci for the cell lines used in the experiments was calculated. For this purpose, the percentage of cells in the different phases of the cell cycle, as measured by flow cytometry at different time points after pCMV3xnlsl-SceI transfection, was taken into consideration (Fig. 27). The following formula was applied in the calculation:

$1 \times (\% \text{ G1-cells} : 100) + 1.5 \times (\% \text{ S-cells} : 100) + 2 \times (\% \text{ G2-cells} : 100) \times \text{number of integrations}$

The theoretical maximum calculated in this ways for each cell line is indicated as grey shading in the stacked bar graphs (Fig. 29) or as a dotted line in the graph (Fig. 31 and 34).

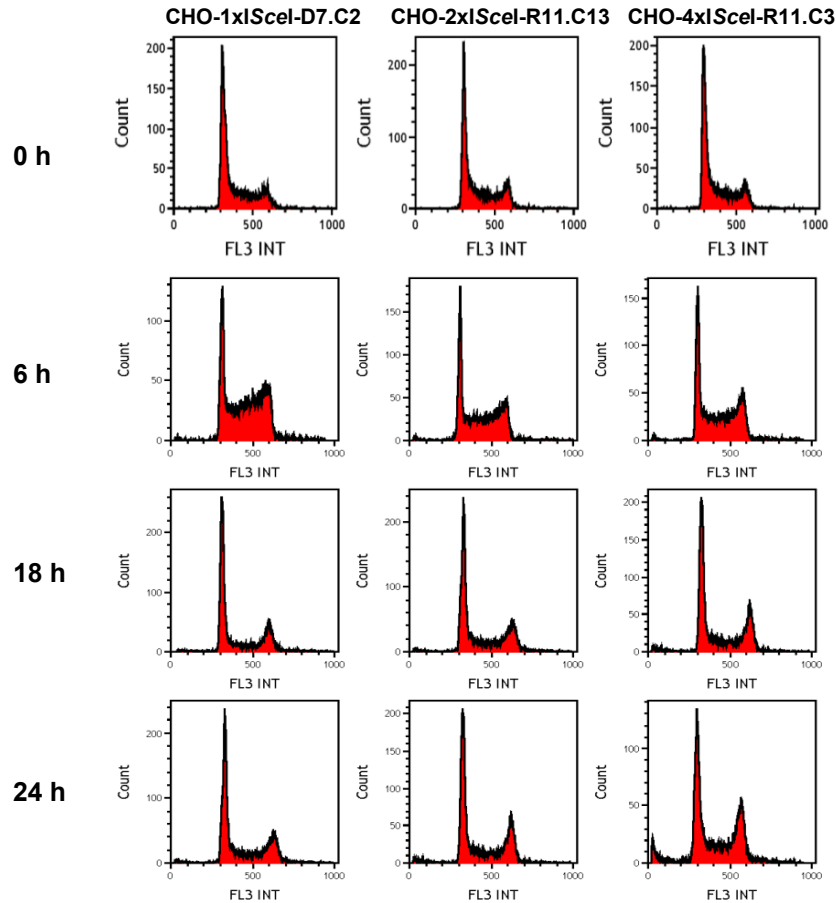


Fig. 27: Flow cytometry analysis of PI stained DNA of I-SceI transfected CHO-1xI-SceI-D7.C2, CHO-2xI-SceI-R11.C13 and CHO-4xI-SceI-R11.C3 cells. Cells were measured 6 h, 18 h and 24 h after transfection.

5.3.2. I-SceI induced DSBs trigger γ -H2AX foci formation at DSB sites

One of the earliest cellular responses to a DSB is the phosphorylation of H2AX at Ser 139 to generate γ -H2AX (Kinner, Wu et al. 2008). As demonstrated in the introduction it occurs through PIKK mediated phosphorylation that triggers a chain of events facilitating eventual repair. After 1Gy X-ray irradiation approx. 27 γ -H2AX foci are induced in the clones CHO-1xI-SceI-D7.C2 and CHO-4xI-SceI-R11.C3 1h, as measured by immunostaining (Fig. 28). This number corresponds to the expected number of γ -H2AX foci in exponentially growing cells after irradiation with 1 Gy X-rays.

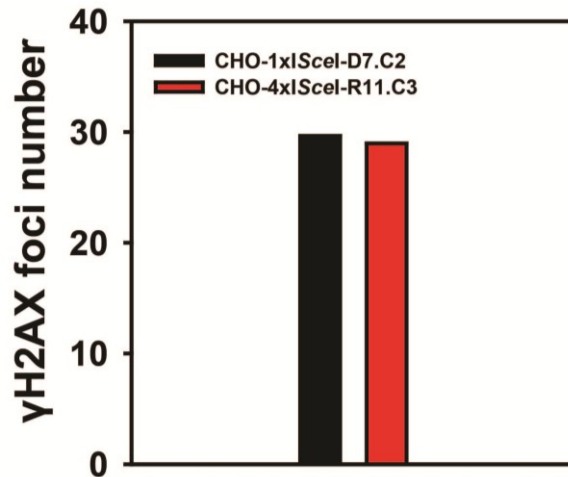


Fig. 28: γ -H2AX foci in CHO-1xI-SceI-D7.C2 and CHO-4xI-SceI-R11.C3 cells 0.5 h after 1 Gy X-ray irradiation. Cells were fixed and immunostained for γ -H2AX 1 h after irradiation. Foci were scored in exponentially growing cells. This experiment was performed in collaboration with V. Nikolov.

To examine whether the degree of DSB clustering affects the degree of signaling emanating from DSBs, we investigated the accumulation of γ -H2AX at I-SceI induced DSBs. γ -H2AX foci were detected in fixed cells 6 h after transfection with a plasmid expressing I-SceI in CHO-1xI-SceI-D7.C2, CHO-2xI-SceI-R11.C13 and CHO-4xI-SceI-R11.C3 cells (Fig. 29).

The foci number measured is close to the theoretical maximum that can be induced in the individual clones according to the number of transposon mediated I-SceI-construct integrations and to the cell cycle phase measured by flow cytometry (see 1.4). This result suggests that practically all I-SceI induced DSBs are recognized by the DDR apparatus.

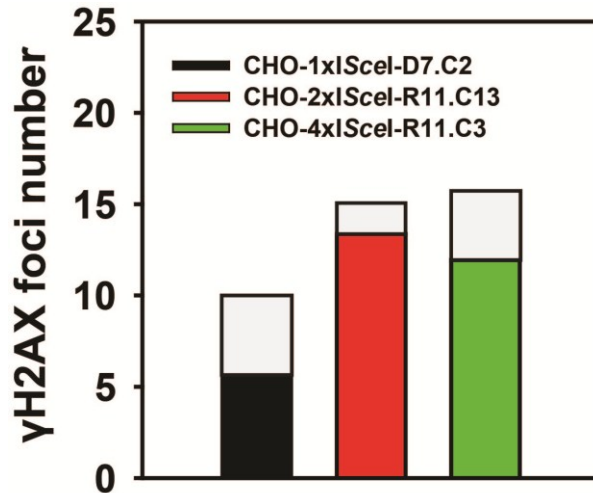


Fig. 29: γ H2AX foci in CHO-1xIScel-D7.C2, CHO-2xIScel-R11.C13 and CHO-4xIScel-R11.C3 cells 12 h after pCMV3xnI-SceI transfection. Cells were fixed and immunostained for γ -H2AX 12 h after transfection. The light grey shaded extensions of each bar show the theoretical maximum of foci that can be reached for each cell line according to the number of I-SceI construct integrations and the cell cycle distribution measured by flow cytometry (See Fig. 27). This experiment was performed in collaboration with V. Nikolov.

5.3.3. I-SceI induced DSBs trigger MDC1 foci formation

MDC1 plays a key role in the assembly of radiation-induced foci and is one of the earliest factors accumulating at DSB sites. MDC1 foci formation depends on the presence of γ -H2AX, as it directly binds to the C-terminal end of γ -H2AX. Kinetics of MDC1 foci were followed by live cell imaging for 24 hours.

For all experiments 10^6 cells were plated two days prior to transfection aiming at approx. 70% confluence. After trypsinization and nucleofection, cells were incubated in Leibovitz Medium supplemented with 10% FBS and were allowed to adhere for 6 h in special live cell microscopy chambers.

After the incubation period, chambers were placed under a Leica confocal microscope at 37 °C and 10-16 fields were defined and tracked every 15 min for a period of 24 h. For each of the indicated time points, 50 cells were analyzed utilizing the Imaris image analysis software. MDC1 foci formation was followed after 1 Gy X-ray irradiation as well

as after DSB induction by I-SceI of CHO clones harboring I-SceI constructs of different complexity and different numbers of integrations.

24 h before irradiation all three clones were transfected with the MDC1-GFP expressing plasmid. The live cell measurement was performed 0.5 h after irradiation. Approx. 22 MDC1-foci were measured for all three clones after 0.5 h that went down to approx. 14 foci after 4 h (Fig. 30).

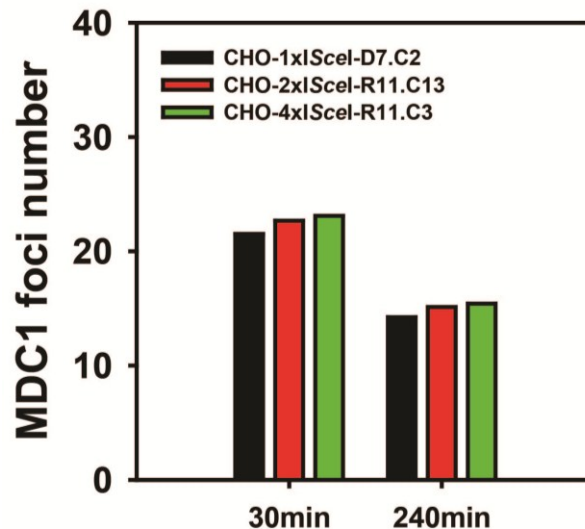


Fig. 30: GFP-MDC1 foci detected by live cell imaging in CHO-1xI-SceI-D7.C2, CHO-2xI-SceI-R11.C13 and CHO-4xI-SceI-R11.C3 cells 30 min and 240 min after 1 Gy X-ray irradiation. This experiment was performed in collaboration with V. Nikolov.

To measure MDC1 foci formation after DSB induction by I-SceI, individual clones were cotransfected with the GFP tagged MDC1 expression construct together with the I-SceI expression construct pCMV3xnlI-SceI (2×10^6 cells were transfected with 2 μ g plasmid). The break in the x Axis of the graphs indicates that the analysis of foci formation started 6 h after transfection.

The numbers of MDC1 foci at the early time points are similar to the number of foci obtained by analysing γ -H2AX and approaches the theoretical maxima for all cell lines with simple and clustered DSBs (Fig. 31B-D). The number of foci decreases only slightly, approx. 1 focus for simple DSBs (Fig. 31B) and approx. 5 foci for clustered DSBs (Fig. 31C and D), as a function of time.

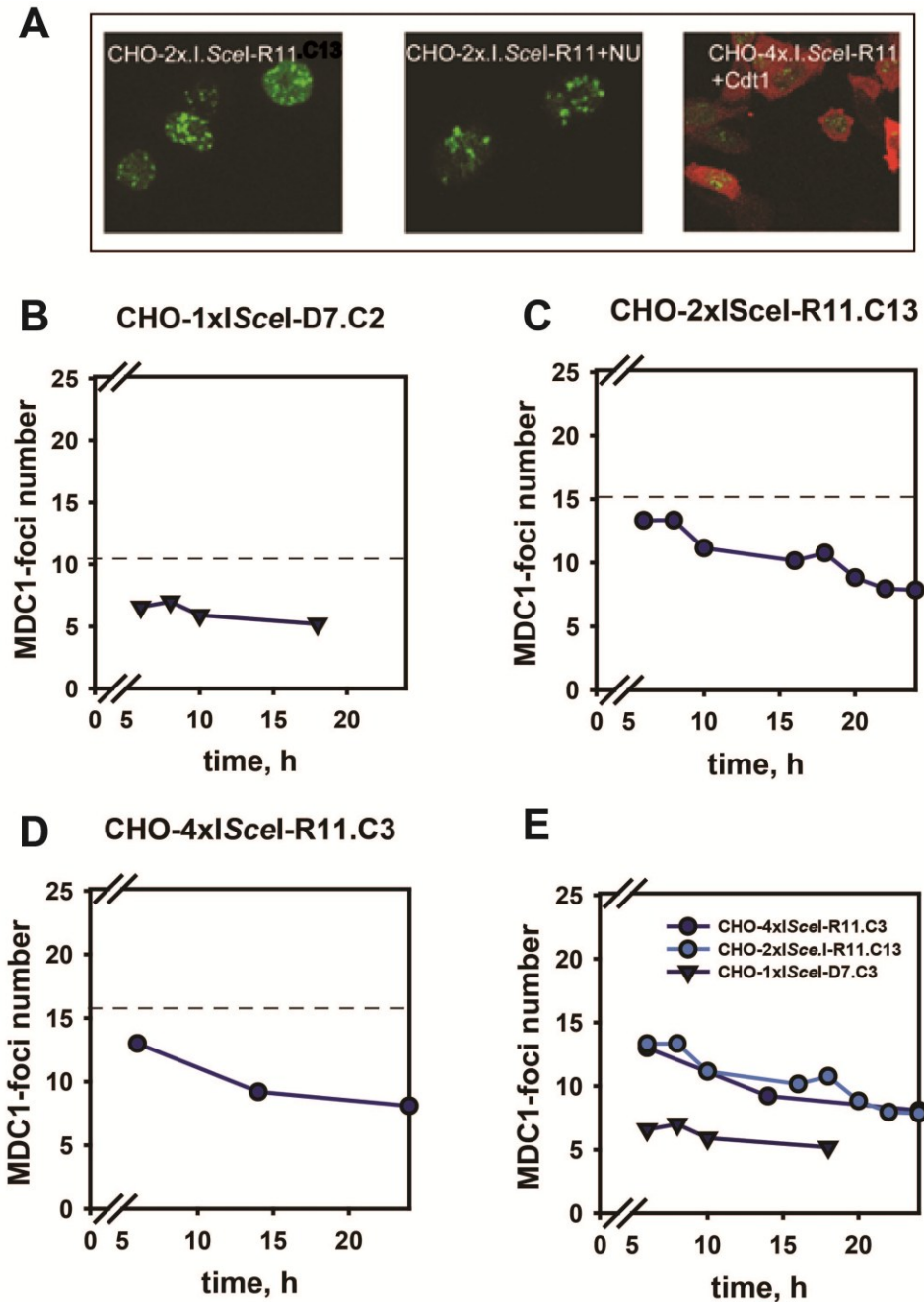


Fig. 31: Representative images and graphs showing GFP-MDC1 foci in pCMV3xnlsl-Scel and GFP-MDC1 cotransfected cells. A: Representative images of MDC1 foci in CHO-2xI.SceI-R11.C13 cells 6 h after transfection. The CHO-4xI.SceI-R11.C3 cells are cotransfected with an I-SceI expressing plasmid tagged with M-Cherry. The even distribution of M-Cherry shows that I-SceI is expressed and is distributed throughout cell. **B:** Foci were followed for 6-24 h after transfection in CHO-1xI.SceI-7D.C2. **C:** CHO-2xI.SceI-R11.C13 and **D:** CHO-4xI.SceI-R11.C3. **E:** Results of all clones are (B-D) plotted together to allow direct comparison. The theoretical maximum for each cell line is indicated with dotted lines. All data are plotted after background subtraction of foci numbers obtained after transfection of only MDC1-GFP (approx. 1-2 foci). These experiments were carried out in collaboration with V. Nikolov.

5.3.4. Marked differences in 53BP1 foci formation at simple and clustered DSBs

53 binding Protein1 (53BP1) is recruited at a late step of the multistep signaling cascade initiated at DSBs. It accumulates at DNA double strand breaks (DSBs) over a 1 Mbp region. 53BP1 foci formation is dependent on PIKK- (ATM/ATR/DNA-PKcs) induced phosphorylation of histone H2AX and can thus be utilized as a marker for DSBs. It has been experimentally determined that in cells exposed to ionizing radiation, the maximum foci number is reached 30 min after irradiation and that foci numbers return to baseline levels after 12-14 h (Schultz, Chehab *et al.* 2000). Human 53BP1 comprises two N-terminal BRCT repeats that bind p53, a tandem Tudor domain, a GAR methylation stretch, two dynein light chain (LC8) binding sites, and numerous PIK kinases and cyclin-dependent (CDK) phosphorylation sites.

The same clones used for MDC1 analysis were transfected with EGFP tagged 53BP1 for live cell imaging experiments under the same conditions as described for MDC1-GFP. The transfection efficiency after nucleofection, as measured using a pmax-GFP plasmid and FACS, ranged from 90-98%. Analysis of the same cells using live cell microscopy gives a transfection efficiency of 80% with optimized conditions (value calculated by dividing GFP-53BP1 positive cells by the total cell number obtained from the DIC image). The difference probably reflects the lower sensitivity of live microscopy as compared to FACS. The background foci level detected in cells only transfected with 53BP1-EGFP ranged between 0 and 2. As a control, CHO cells without I-SceI integrations were transfected with the I-SceI expressing plasmid (Fig. 32).

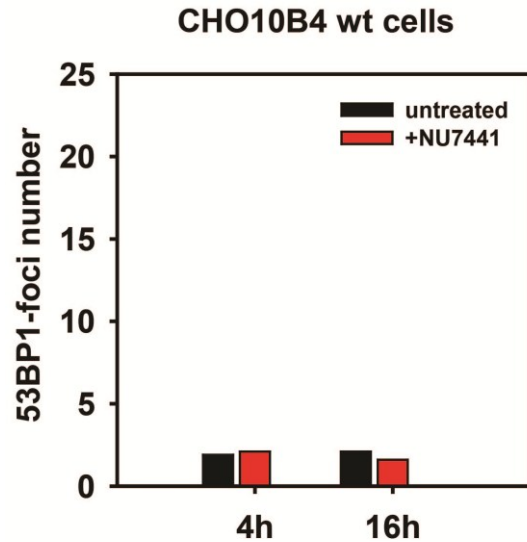


Fig. 32: 53BP1 foci analysis of CHO cells by live cell imaging 4 and 16 h after co-transfection of plasmids expressing EGFP-53BP1 and pCMV3xnlsl-Scel. Shown is the total number of foci detected and corresponds to what we define as background. Quantitatively similar results were obtained with CHO cells transfected only with EGFP-53BP1.

Furthermore wt cells and the clone with CHO-4xIscel-R11.C3 were exposed to 0.5 Gy and foci kinetics were followed for up to 5 h (Fig. 33). The dose of 0.5 Gy was selected to induce about 10 DSBs in (G1) or 20 DSBs in (G2) that approximates the maximum number of I-Scel-construct integrations.

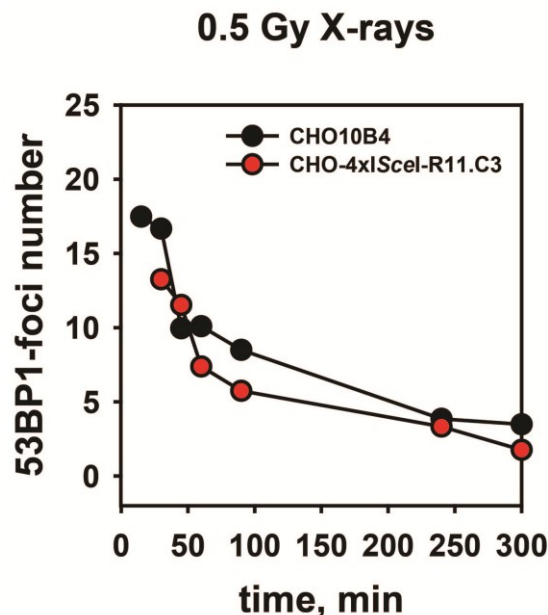


Fig. 33: 53BP1 foci analysis in wt CHO and CHO-4xIscel-R11.C3 cells measured by live cell imaging from 15 min to 5 h after exposure to 0.5 Gy X-rays. Cells were transfected with the EGFP-53BP1 plasmid 24 h before irradiation

The number of foci measured after I-SceI mediated DSB induction in clones modeling different degrees of DSB complexity is shown in Fig. 34. Notably, 53BP1 foci are barely detectable on single I-SceI sites; develop at approx. 50% the expected level with 2xI-SceI sites and at nearly 100% level with 4xI-SceI sites. This is the first evidence that the complexity of the DSB affects the development of the associated signaling.

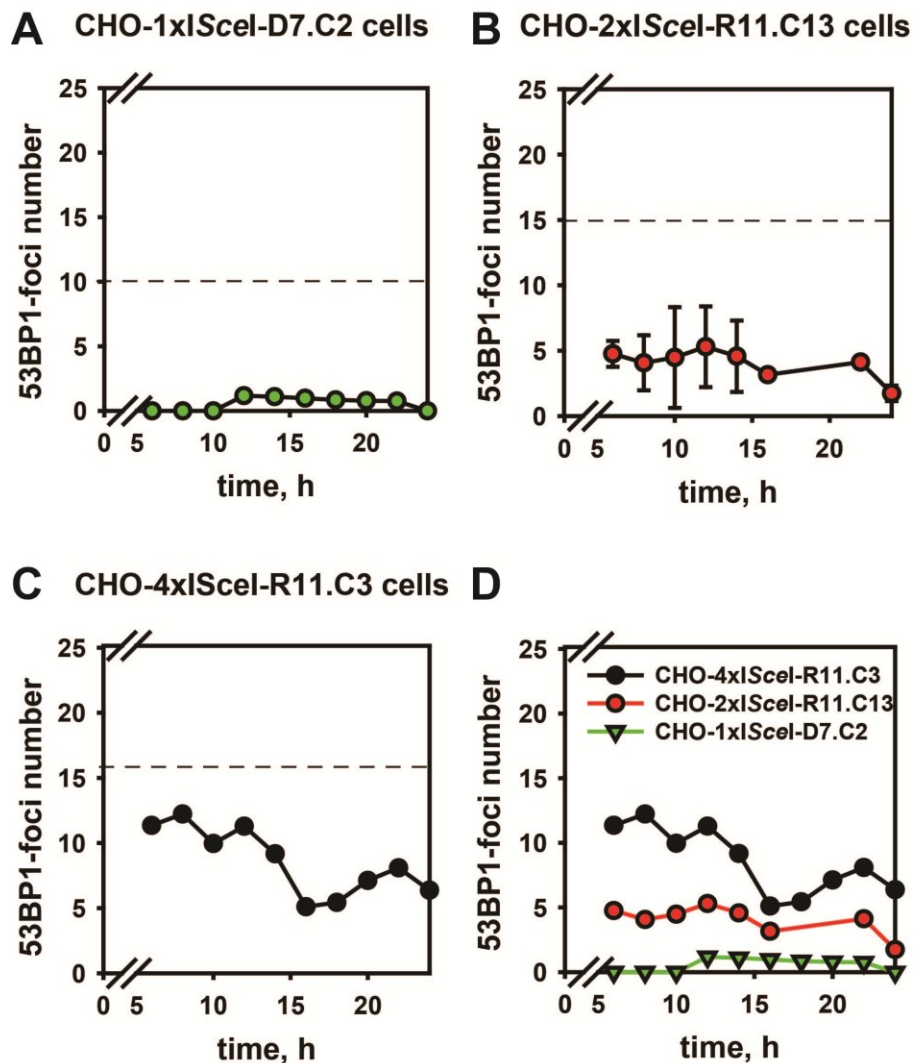


Fig. 34: 53BP1 foci analysis 6-24 hours after cotransfection of CHO-1xI-SceI-D7.C2, CHO-2xI-SceI-R11.C13 and CHO-4xI-SceI-R11.C3 cells with an EGFP-53BP1 and an I-SceI expressing plasmid. The dotted lines indicate the theoretical maximum of I-SceI induced DSBs for the different clones calculated according to cell cycle distribution measured by flow cytometry (see fig. 27).

There are two possible scenarios that may explain the persistence of the foci even after 24 h. First, the growth conditions in Leibovitz media in the 37 °C chamber may not be optimal for cell growth. This may cause some delay in repair. Second, the repeated I-SceI cutting may maintain the signaling at the sites. If this scenario is the case, it is likely that the reduction in the number of 53BP1 foci seen after 12 h reflects loss of the I-SceI site as the enzyme level does not decrease even after 72 h, shown by western blot (Fig. 35).

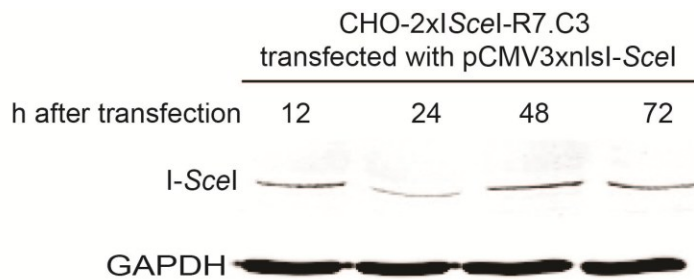


Fig. 35: Western blot results showing expression level of I-SceI in whole cell extracts of I-SceI transfected cells after 12, 24, 48 and 72 h.

This would indicate that different overall responses apply to IR and I-SceI induced DSBs. It is also interesting that the number of 53BP1 foci scored in the clone with the single I-SceI site increases after 12 h. This may suggest that complications associated with repeat-cutting in a subset of the potential cutting sites leads to signaling. Experiments are currently being performed to address these questions.

5.3.5. The number of 53BP1 foci is increased in G2 cells

In order to differentiate cells according to their cell cycle stages, we cotransfected the cells additionally to the I-SceI plasmid with the cell cycle fluorescent reporter vector Cdt1. Expression of the Cdt1 reporter plasmid allows the monitoring of the cell cycle phase in real time. The levels of cell cycle regulating proteins fluctuate throughout the cell cycle with a high expression level of Cdt1 in the G1 phase that decreases during the S phase. Cdt1 is tagged with KO that allows follow up of its expression by live cell

imaging and thus the approximate characterization of the cell cycle phase for each individual cell.

In order to measure 53BP1 foci distribution in different cell cycle phases we cotransfected cells with KO-tagged Cdt1, GFP-tagged 53BP1 and I-SceI expressing plasmid. Fig. 36 shows foci kinetics according to cell cycle phase in CHO-1xI-SceI-7R.C2 cells and CHO-2xI-SceI-11R.C13. The results show a general increase, by approx. a factor of two, in the number of 53BP1 foci in G2 cells as compared to G1 cells for I-SceI transfected clones – particularly for the initial time points. At later times the foci number in G2-phase cells decreases to the level of G1-phase cells.

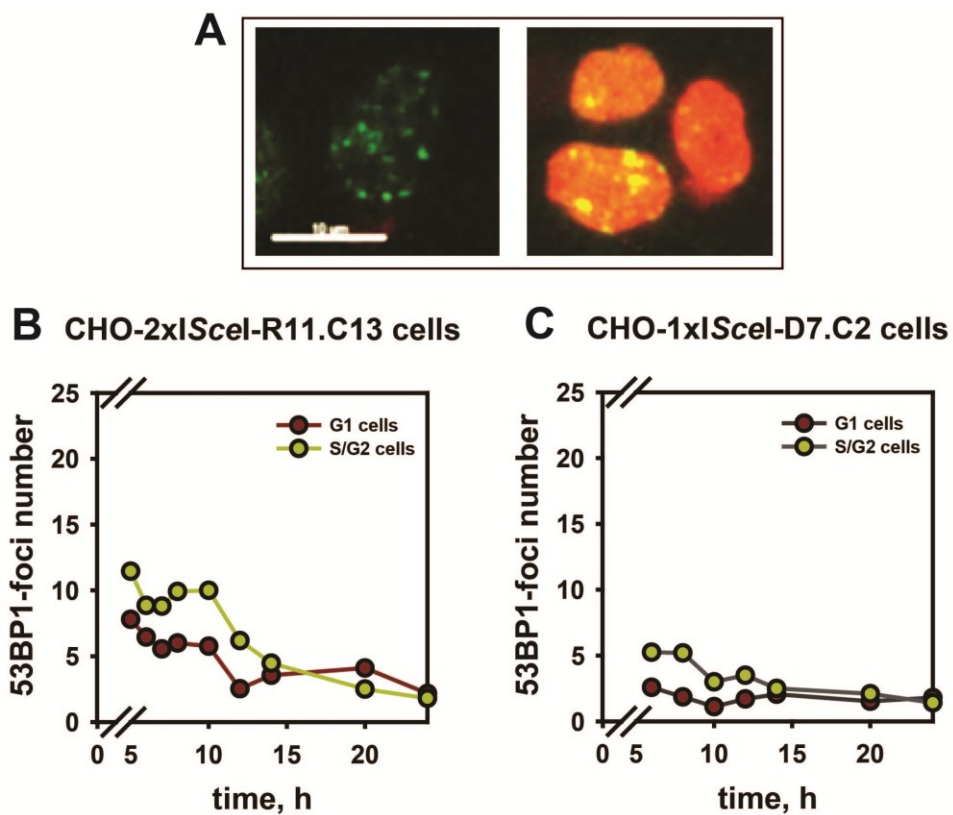


Fig. 36: Representative Images of CHO-2xI-SceI-R11.C3 cells in different cell cycle phases and graphs showing cell cycle distribution of CHO-2xI-SceI-R11.C3 and CHO-1xI-SceI-D7.C2 obtained by live cell imaging. **A:** Cells were co-transfected with KO2-Cdt1, 53BP1-GFP and pCMV3xnlsl-SceI. G1 cells expressing Cdt1 and 53BP1 are yellow whereas S and G2 do not express KO2 tagged Cdt1 and are therefore green. 53BP1 foci were scored separately for G1 and G2 in CHO-2xI-SceI-R11.C3 cells (**B**) and in CHO-1xI-SceI-D7.C2 cells (**C**). 100 cells were analyzed for each time point. This experiment was performed in cooperation with V. Nikolov.

5.4. Increasing the complexity of DSBs by various means compromises repair

To further investigate the effect of DSB complexity on signaling, the following two approaches were followed: Oxidative damage was induced by H₂O₂ in addition to I-SceI induced DSBs to increase the damage complexity at DSB ends. In a further approach the D-NHEJ pathway was inhibited after DSB induction to leave the DSB ends open for longer time, thus increasing the probability of inappropriate end processing and misrepair events.

5.4.1. Increasing the complexity of I-SceI DSBs by treatment with H₂O₂

As illustrated in the Introduction, RE induced DSBs are T1-DSBs, i.e. they can be removed by simple ligation. Radiation induced DSBs on the other hand are more complex and belong to the T2-6 types. To generate information on the possible effect of this form of complexity for the detection and signaling from a DSB, we introduced oxidative damage in cells harboring I-SceI constructs, arguing that this will also reach the DSBs and will increase their complexity. To generate oxidative damage, cells were treated with H₂O₂ after DSB induction by I-SceI.

A concentration of 25 μM that does not significantly increase the number of 53BP1 background foci was chosen for these experiments. H₂O₂ causes a marked increase in the number of 53BP1 foci in CHO-1xI-SceI-D7.C2 and CHO-2xI-SceI-R11.C13 cells when added immediately after I-SceI transfection and measured after 6 h (Fig. 37). These results indicate that increasing the complexity at DSB ends also increases the 53BP1 foci formation to the theoretical maximum for the individual clones. For the higher complexity DSBs in CHO-4xI-SceI-R11.C3 cells, the addition of H₂O₂ did not increase the foci number as the theoretical maximum is reached already without additional treatment.

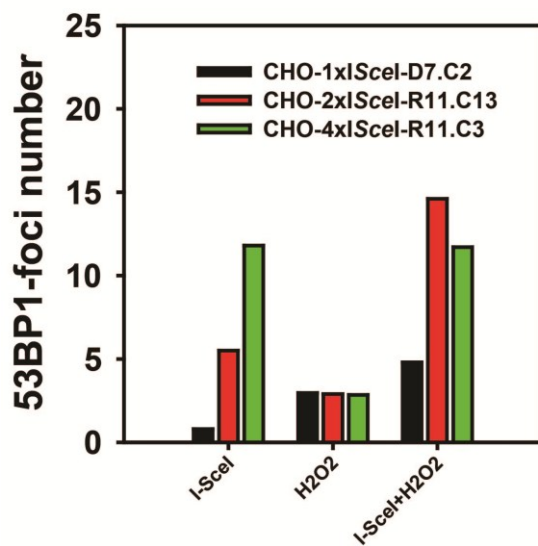


Fig. 37: 53BP1 foci in I-SceI transfected CHO-1xI-SceI-D7.C2, CHO-2xI-SceI-R11.C13 and CHO-1xI-SceI-R11.C3 cells after treatment with H₂O₂, without additional treatment and EGFP-53BP1 transfected cells treated with H₂O₂. 25 μ m H₂O₂ was added immediately after transfection. Results were obtained 6 h after transfection. This experiment was performed in collaboration with V. Nikolov.

5.4.2. Increasing the complexity of I-SceI induced DSB ends by compromising D-NHEJ using small molecule inhibitors, or D-NHEJ defective mutants

The D-NHEJ inhibitor NU7441 that inhibits DNA-PKcs was applied to the cells at a concentration of 2.5 μ M immediately after cotransfection of pCMV3xnI-SceI with EGFP-53BP1. For these experiments the CHO-2xI-SceI-R11.C13 and CHO-4xI-SceI-R11.C3 were employed, as well as CHO-1xI-SceI-D7.C2. A clear difference in 53BP1 foci number with and without NU7441 treatment can be observed for the clones CHO-2xI-SceI-R11.C13 and CHO-1xI-SceI-D7.C2. Interestingly the number of 53BP1 foci does not differ in NU7441 treated CHO-4xI-SceI-R11.C3 from untreated cells (Fig. 38 and 40).

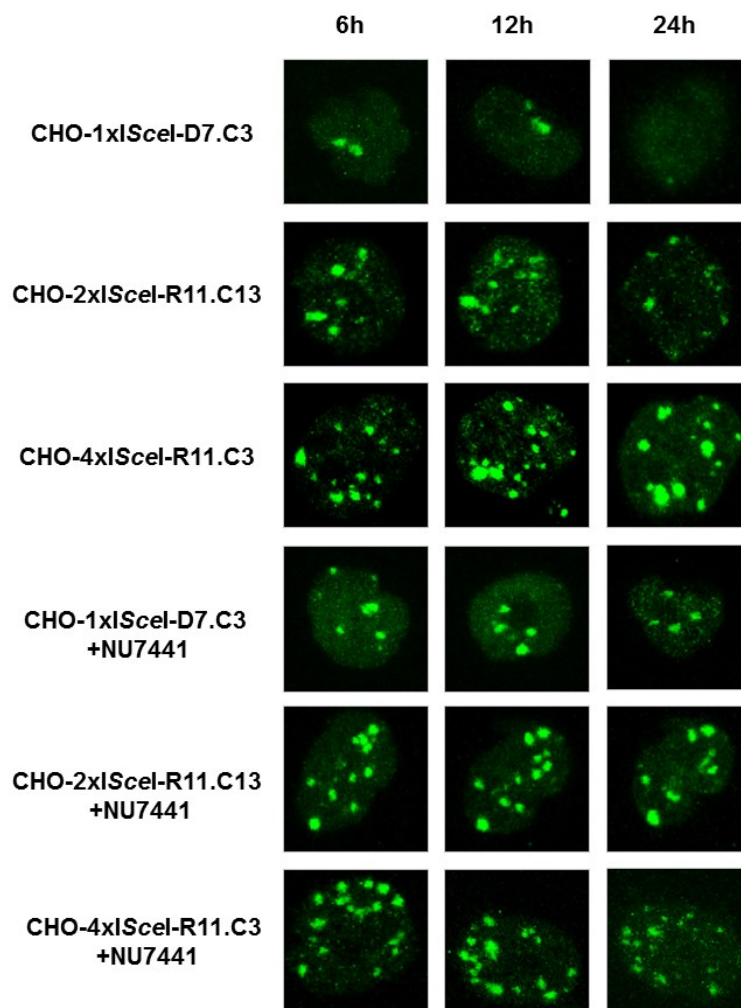


Fig.38: Representative images of pCMV3xnI-SceI and 53BP1-GFP cotransfected cells measured by live cell imaging. CHO-1xI.SceI-D7.C2, CHO-2xI.SceI-R11.C13 and CHO-4xI.SceI-R11.C3 cells are shown 6 h, 12 h and 24 h after transfection. Cells are shown without additional treatment and with addition of the NU7441 inhibitor.

To calculate the theoretical maximum of 53BP1 foci for NU7441 treated cells, the same calculations were performed as described in 5.3.1 based on the flow cytometry measurement from Fig. 39.

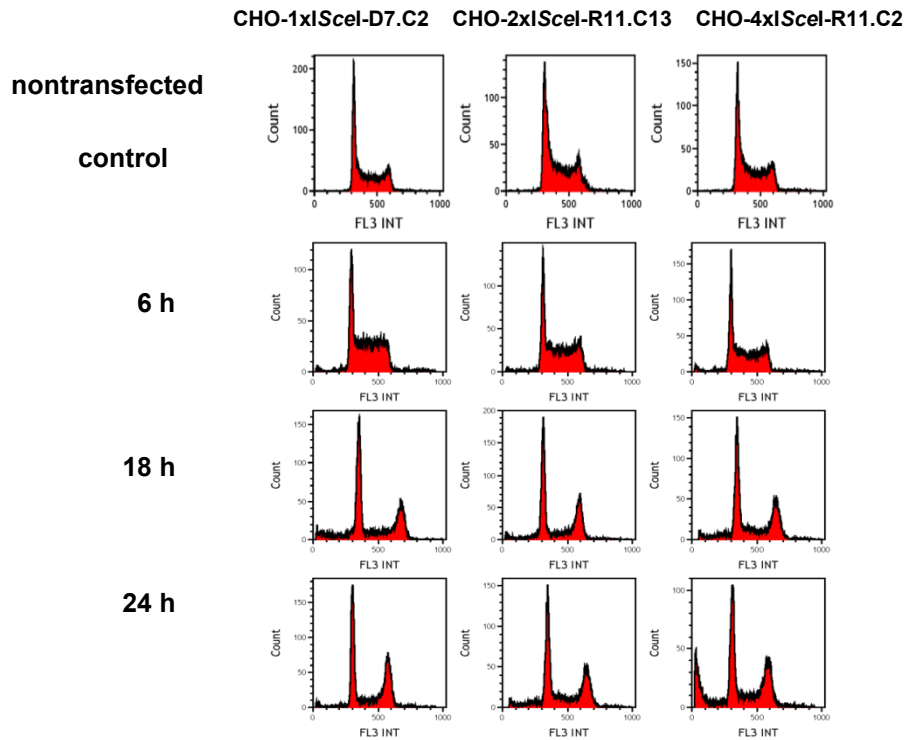


Fig. 39: Flow Cytometry Analysis of PI stained DNA of I-SceI transfected CHO-1xI-SceI-D7.C2, CHO-2xI-SceI-R11.C13 and CHO-4xI-SceI-R11.C2 cells with the addition of the NU7441 Inhibitor. Cells were measured 6 h, 18 h and 24 h after transfection in the presence of NU7441.

Notably, treatment with NU7441 uniformly increased the number of 53BP1 foci detected to the theoretical maximum except in the case of 4xI-SceI where no significant difference can be detected between NU7441 treated and untreated cells (Fig. 40). This result indicates that in the case of highly clustered DSBs, 53BP1 signaling is always required, as without the D-NHEJ inhibitor already the theoretical maximum of foci number is reached.

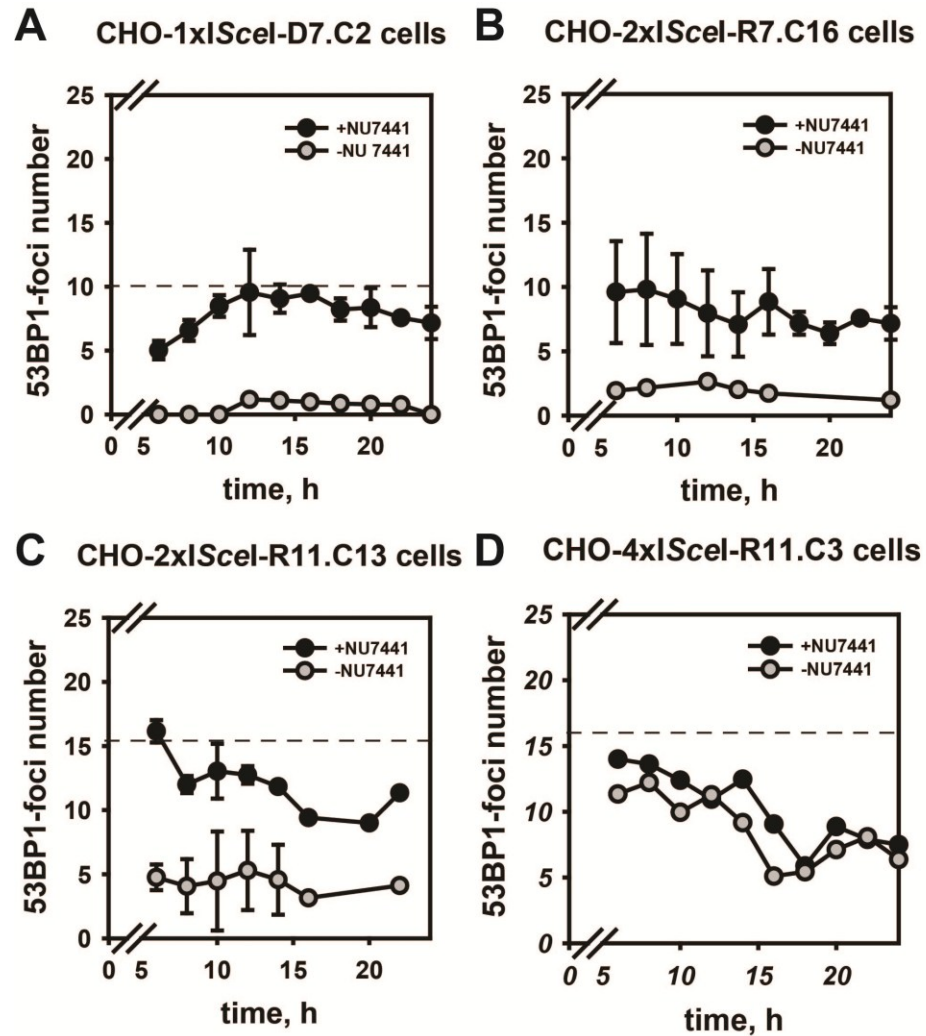


Fig. 40: Analysis of 53BP1 foci kinetics through live cell imaging in CHO clones with the indicated integrations of I-SceI constructs in the presence of NU7441 to inhibit DNA-PKcs. Foci scoring started 6 h after transfection. Dotted lines indicate theoretical maximum of foci-number according to cell cycle distribution measured by flow cytometry (Fig. 39). For illustration purposes the I-SceI transfected cells without NU7441 treatment shown in Fig. 27 are indicated in grey.

To extend the above observations, different NHEJ mutant clones with I-SceI integrations mimicking clustered DSBs were analyzed in a similar set of experiments. Live cell imaging experiments were carried out with the NHEJ mutants XR-C1-3 (defective in DNA-PKcs) (Fig.41 C) and Xrs6 (defective in Ku80) (Fig. 42).

The experimental protocols employed were as described for CHO cells. The number of foci plotted is calculated after background subtraction obtained with the same cells after transfection with the 53BP1 expression vector alone. The clones selected for these experiments are XRC13-2xI-SceI-R11.C5 and XRS6-2xI-SceI-R11.C4. In order to follow 53BP1 foci kinetics in D-NHEJ deficient cells after irradiation, XRC13-2xI-SceI-R11.C5 cells were irradiated with 1 Gy X-rays 24 h post EGFP-53BP1 transfection. The measurement was performed 15 min after irradiation. Starting with 30 foci, after 12 h still approx. 15 foci are present indicating slow repair compared to CHO wt cells, where after 5 h the foci levels decrease to background (Fig. 41 A). The analysis of foci formation after DSBs induction by I-SceI clearly reveal that in a D-NHEJ deficient background, foci form in nearly 100% of the expected I-SceI sites (Fig. 41C). Furthermore a G2 block could be observed by flow cytometry 12 h after transfection (Fig. 41D).

53BP1 has an inhibitory effect on DSB resection and has the ability to tether distally formed DSBs in close proximity (Chapman, Taylor et al. 2012). This could explain the requirement of 53BP1 signaling at clustered or complex DSB ends to hinder end resection that could lead to repair failures.

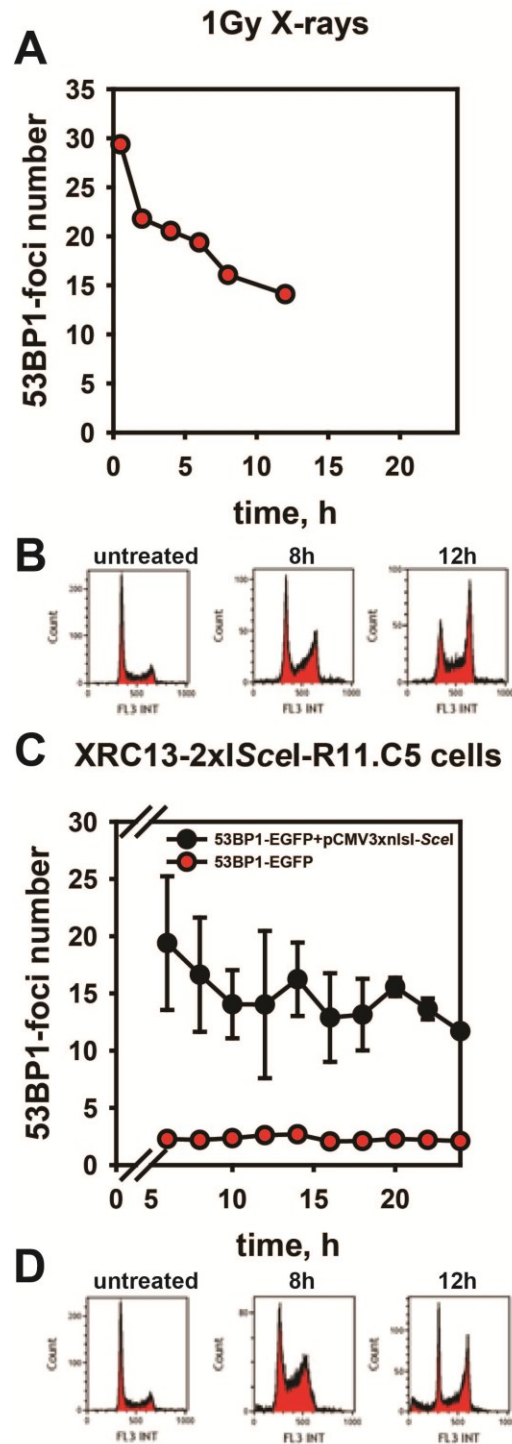


Fig. 41: XRC13-2xISceI-R11.C5 cells were analyzed for 53BP1 foci formation after I-SceI transfection and after exposure to 1 Gy X-rays. A: Irradiated cells (irradiation 6 h after transfection with 53BP1-EGFP) are measured from 0.5-14 h after irradiation. **B:** The flow cytometry analysis of PI stained DNA is shown under the graph for 8 h and 12 h after IR and the unirradiated control. **C:** Accumulation of 53BP1 foci is measured by live cell imaging from 6 to 24 h after transfection of pCMV3xnlsl-SceI. (Vertical bars represent \pm SD). The Experiments were repeated eight times with different types of controls and confirmed repeatedly by V. Nikolov. **D:** The flow cytometry analysis of PI stained DNA 8 h and 12 h after transfection and the nontransfected control are shown.

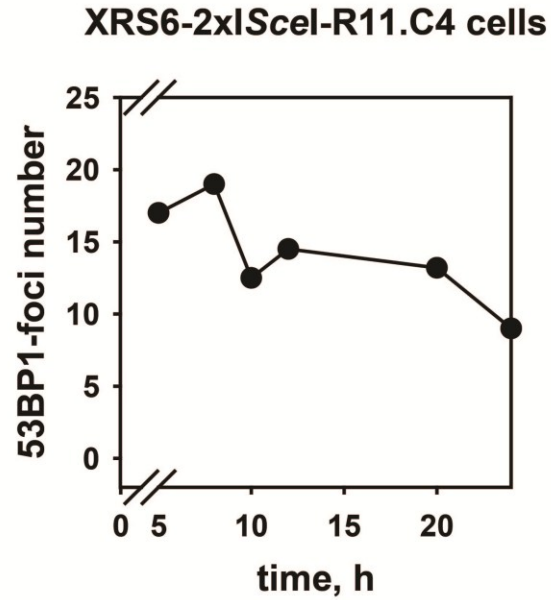


Fig. 42: 53BP1 foci measured by live cell imaging of XRS6-2xIScel-R11.C4 clones after pCMV3xnlsl-Scel co-transfection with 53BP1-EGFP. Foci were scored 5-24 h after transfection and 50 cells were counted for each time point. The experiment was performed two times.

5.4.3. Incidence of G2-PCC breaks and exchanges after increasing complexity at DSB sites

To analyze the incidence of repair failures upon increasing the complexity at DSB ends, G2-PCC was performed in D-NHEJ compromised cells. (Fig. 43 and 44) The results show that G2-PCC breaks and exchanges are increased after NU7441 treatment of I-SceI transfected CHO-1xI-SceI-D7.C2 and CHO-2xI-SceI-R11.C13 cells. In contrast, the number of G2-PCC breaks and exchanges does not increase in the case of highly clustered DSBs (CHO-4xI-SceI-R11.C3) after NU7441 treatment, indicating that the maximum frequency (according to the number of integrations) of misrepair events is generated in this cell line even when the repair pathways are not compromised.

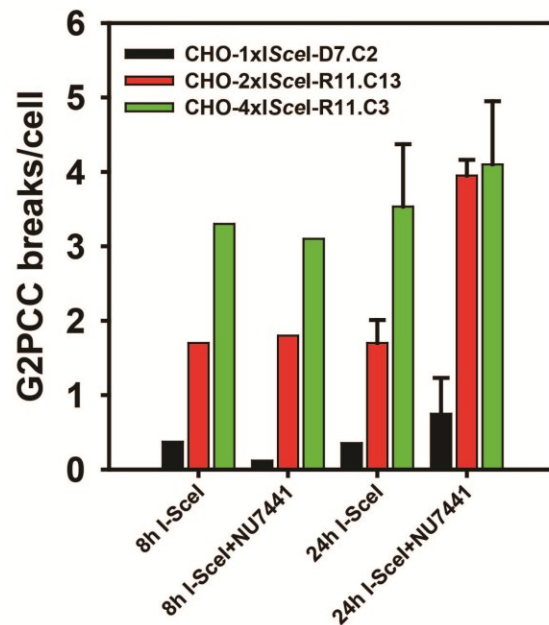


Fig. 43: G2-PCC breaks per cell in CHO-1xI-SceI-D7.C2-, CHO-2xI-SceI-R11.C13-, and CHO-4xI-SceI-R11.C3 cells, 8 h and 24 h after pCMV3xnlsl-SceI transfection, untreated (taken from Fig. 17) and treated with NU7441. Graphs represent data after background subtraction (from nontransfected cells and is approx. 1.2 G2-PCC breaks/cell with and without NU7441 treatment).

The number of G2-PCC breaks in NU7441 treated CHO-2xI-SceI-R11.C13 cells corresponds approx. to the number of G2-PCC breaks observed in the XRC13-2xI-SceI-R11.C5 cells with a D-NHEJ deficient background (Fig. 44). This result suggests that misrepair events occur if HR associated end-resection is carried out but HRR is inhibited, thus directing DSB processing to B-NHEJ.

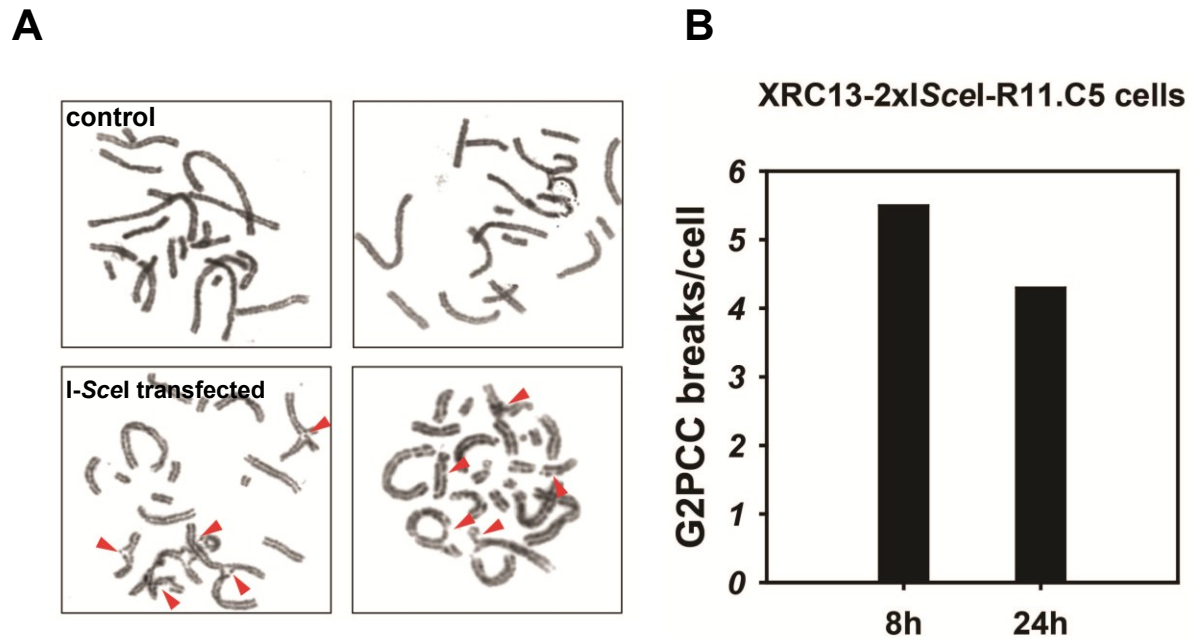


Fig. 44: G2-PCC Graph of XRC13-2xI-SceI-R11.C5 (B) with representative chromosome spreads from cells transfected with pCMV3xnlI-SceI and nontransfected controls (A).

Interestingly the number of exchanges in CHO-4xI-SceI-11R.C3 cells decrease approx. 50% after inhibiting PARP with PJ34 (Fig. 45). The two-site clones do not show any reduction in the exchange number and in the single-site clone the exchanges are reduced from 9 to 5 out of 100 cells.

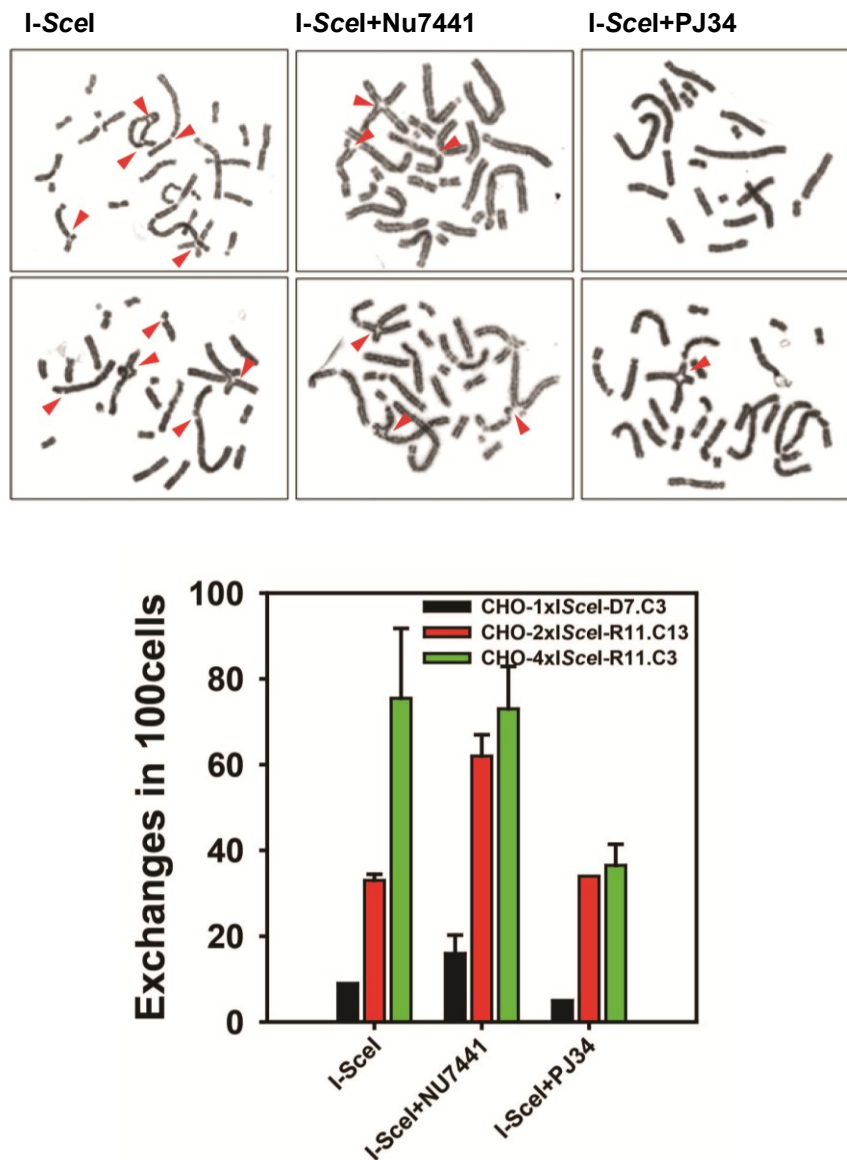


Fig. 45 A: Graph showing total number of exchanges out of 100 pCMV3xnI-SceI transfected, CHO-1xI-SceI-D7.C2, CHO-2xI-SceI-R11.C13 and CHO-4xI-SceI-R11.C3 cells (with representative images of chromosome spreads of CHO-4xI-SceI-R11.C3 cells) and cells with additional NU7441 or PJ34 treatment with representative images. No exchanges could be detected in the nontransfected controls with NU7441 and PJ34 treatment.

5.5. An inducible I-SceI system overcomes some limitations of the transient I-SceI transfection

For the induction of DSBs in the above experiments, the I-SceI expressing plasmid pCMV3xnlsl-SceI was co-transfected with the 53BP1 expressing plasmid. This system allows little control for the induction of DSBs, the cells are stressed by the electroporation and expression of I-SceI that takes at least 2 h. We generated an inducible I-SceI activation system to overcome some of the limitations associated with this approach. This system gives the possibility to analyze early foci kinetics. After stable integration in CHO-2xl-SceI-R6.C10-cells with the NEIE plasmid, a cell line is generated where the localization of I-SceI can be easily regulated. This is because the plasmid expresses a fusion I-SceI protein containing the mutant human estrogen receptor ligand-binding domain that allows 4HT regulated translocation of I-SceI from the cytoplasm where it normally resides to the nucleus. Fig. 46A shows the domain composition of the regulated I-SceI, whereas Fig. 46C shows a western blot demonstrating the expected translocation of I-SceI from the cytoplasm into the nucleus upon addition of 4HT.

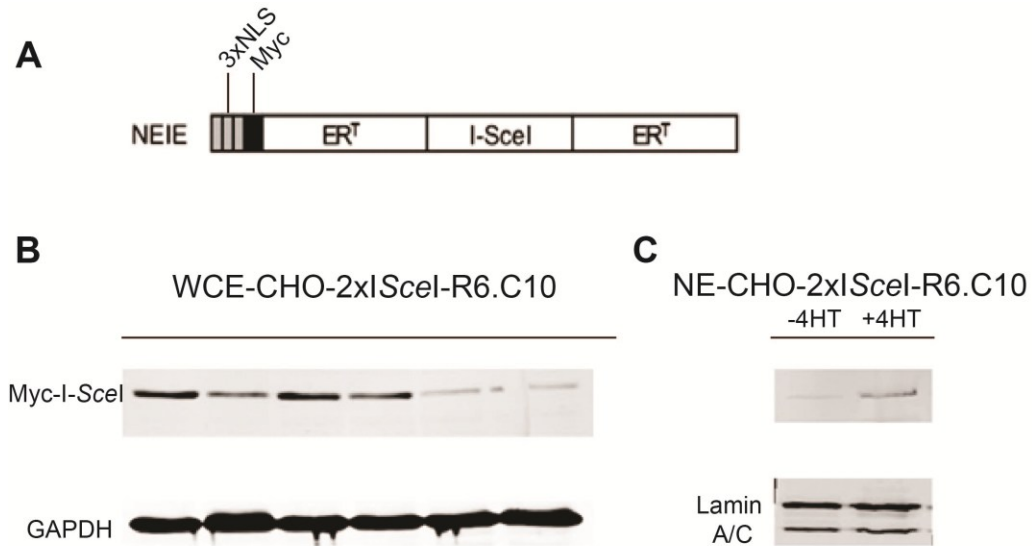
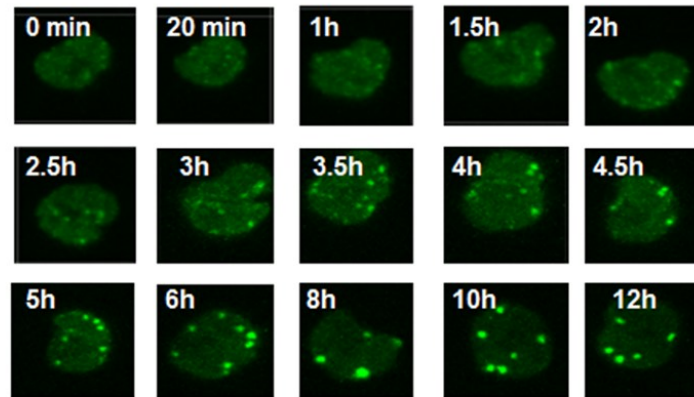


Fig. 46: Characteristics of an I-SceI inducible system. A: Representative scheme of the stably integrated I-SceI-expressing construct. The NEIE plasmid expresses from a pCMV promoter an I-SceI chimera with an N-terminal triple-Myc tag, a nuclear localization signal and the mutant human estrogen receptor ligand-binding domain. It carries puromycin as selection marker. (Description of the nomenclature of **NEIE**: N: NLS, E: modified estrogen receptor, I: I-SceI) **B: Western blot with whole cell extracts of clones that were stably transfected with the NEIE plasmid and grown in phenol red free media.** Six puromycin resistant clones were tested for Myc tagged I-SceI expression. The expression level varies between the different clones. The clone with the highest expression level (lane 3) was chosen for further testing of I-SceI expression and regulation, shown in C. **C: Nuclear extract of the clone from lane 3 (B) was prepared for western blotting, to test for I-SceI translocation from the cytoplasm to the nucleus.** Lane 1 represents the level of Myc tagged I-SceI in the nucleus without 4HT induction, indicating that I-SceI is mainly localized in the cytoplasm. Upon addition of 4HT (1 μ M) (lane 2) I-SceI translocates into the nucleus where it digests the integrated I-SceI recognition sites (Clones were generated in phenol red free media and stripped serum.)

To validate the system, live cell experiments were carried out with the cell line CHO-2xISceI-R6.C10 transfected with EGFP-53BP1. Measurement was started immediately after 4HT induced I-SceI translocation in NU7441 treated and untreated cells (Fig. 47). Foci formation can be detected approx. 1.5 h after addition of 4HT. Further experiments are needed to refine and validate this system.



CHO-2xI-SceI-R6.C10

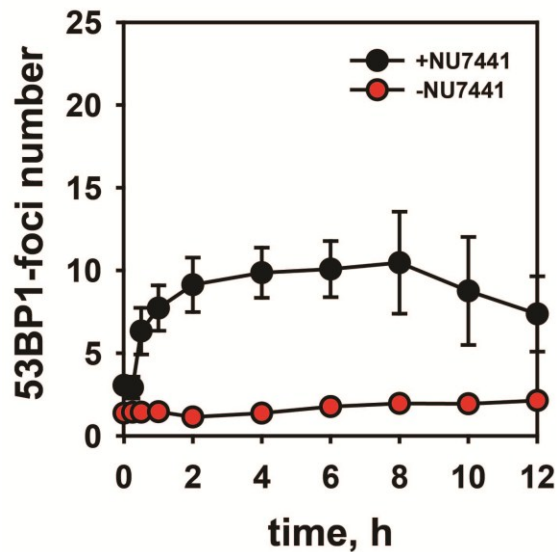


Fig. 47: Live cell imaging of CHO-2xI-SceI-R6.C10 that expresses constitutively a regulable form of I-SceI RE. Nuclear translocation of I-SceI upon addition of 4HT leads to the formation of DSBs that are detectable as 53BP1 foci only in the presence of NU7441. **A:** Typical images obtained at the indicated times after addition of 4HT and NU7441 treatment. **B:** The graph shows the induction kinetics of 53BP1 after 4HT treatment with and without NU7441.

6. Discussion

6.1. Generation and characterization of model systems for simple (T1-) and clustered (T6-) DSBs

In an attempt to elucidate the type of lesion dominating the adverse effects of IR we established I-SceI based model systems in wt, NHEJ and HR deficient CHO cells. One of the major advantages of these systems is that DSBs are exclusively induced in contrast to the plethora of lesion types induced by IR. In addition to the control over the type of lesion the spacing between consecutive DSBs can also be defined. The distances were engineered to resemble the winding around either one or two nucleosomes plus the linker regions in order to elucidate the probability for repair accidents caused by the simultaneous cleavage of two or more linker regions that may lead to chromatin destabilization. Additionally, as a control a model system for simple lesions was also generated.

In contrast to numerous I-SceI based reporter systems that are mostly integrated at a single genomic locus, we applied the transposon technology to generate clones with a high number of integrations at random genomic sites thus achieving integration numbers that correspond to the number of DSBs induced after approx. 0.5 Gy X-rays. Hypothesizing that clustering of DSBs is a key source for repair accidents caused by IR, simple (T1-DSBs) and clustered DSBs (T6-DSBs) were induced upon I-SceI transfection to analyze their biological consequences.

The features of the CHO-4xI-SceI cells also make them a potential candidate as a model system for chromothripsis, an event that is not triggered by IR but can spontaneously arise during cancer development. Chromothripsis describes the formation of tens to hundreds of locally clustered DNA rearrangements interspersed with widespread losses of sequence fragments through a single, cataclysmic event. Rearrangements can occur by chromosome shattering and rejoining of pieces by end-joining DNA repair pathways,

or by aberrant DNA replication-based mechanisms (Forment, Kaidi et al. 2012; Korbel and Campbell 2013).

Similar to chromothripsis, in the 4xI-SceI cells a high number of clustered DSBs are induced in a single event leading to genomic rearrangement. However, further investigations are required to examine similarities between chromothripsis and the 4xI-SceI based system.

6.2. Clustered DSBs have a higher killing potential compared to simple DSBs

The reproductive cell death was measured by loss of colony forming ability for simple and clustered DSBs with different degrees of clustering. A clear killing effect was seen for T6-DSBs compared to T1-DSBs with a correlation between the increase in clustering and the decrease in the colony forming ability. The increase in clustering also leads to a higher probability for the local disruption of chromatin as more nucleosomes are involved and a larger fragment can get lost from the chromatin context. As an additional control for simple lesions the *AsiSI*-ER-U2OS cells were used, generating DSBs upon 4HT induction separated by at least 1 Mb. As the *AsiSI* sites are inherent in the human genome the theoretical maximum of breaks that can be induced is around 1750 in G1 cells. Still the killing effect is similar to the killing observed after only 11 four-DSB-clusters, underlining the high killing potential of clustered DSBs compared to simple DSBs.

6.3. The probability for misrepair of clustered DSBs is clearly elevated compared to simple-DSBs

In order to address the questions how the cellular repair machinery deals with simple and complex DSBs and which DSB type is the cause for misrepair and thus for lethal events, we measured chromatid breaks and inter chromosomal chromatid exchanges using the G2-PCC technique. According to the models of aberration formation, chromosome exchanges result from the interaction of two or more breaks in close

spatial and temporal proximity, where the wrong chromosome ends are joined (Savage 1998; Loucas, Durante et al. 2013), whereas chromatid breaks are caused by the lack of repair.

The results show that the yields of G2-PCC breaks as well as exchanges are clearly increased in clones with complex DSBs (CHO-2xl.SceI-R11.C13 and CHO-4xl.SceI-R11.C3) compared to the clone with simple DSBs (CHO-1xl.SceI-D7.C2) (Fig. 26A and B). These observations imply that complex DSBs lead to repair accidents and therefore could be the main cause for lethal events leading to the high killing observed in survival experiments.

It has to be pointed out that repair failures are clearly increased in CHO-4xl.SceI-R11.C3-cells compared to CHO-2xl.SceI-R11.C13-cells. G2-PCC breaks as well as exchanges are increased at least two-fold. These results suggest that not only the DSB type, (T1-DSB or T6-DSB) determines cellular consequences but also the degree of DSB clustering of T6-DSBs, with a correlation between increased repair accidents and increased DSB clustering.

In cells harboring the 2xl-SceI constructs the following two DSB-induction scenarios are probable; either both I-SceI sites are cleaved simultaneously, or the sites are cleaved one after another and most likely repaired faithfully. The simultaneous cleavage of both sites possibly leads to the loss of a fragment comprising a single nucleosome and results in a deletion of >200 bp or sometimes in the rejoining with wrong ends. For the cells harboring 4xl-SceI site constructs, there are various possibilities for DSB induction; i.e. only two or three sites out of the four possible sites may be cleaved simultaneously in various combinations. The most likely scenario is that the whole intervening fragment of 446 bp between the outer sites gets lost after simultaneous cleavage of all four sites. The simultaneous cleavage of all four sites probably leads to chromatin loss comprising two nucleosomes, as the intervening two DSBs destabilize the DNA in addition to the two outer I-SceI-sites. The remaining DSB ends are then probably misrejoined with higher probability than in the case of 2xl-SceI DSBs as seen by the high number of exchanges for CHO-4xl.SceI-R11.C3-cells (approx. 80 in 100 metaphases, Fig. 26)

compared to the CHO-2xl.SceI-R11.C13-cells that have approx. half the number of exchanges (approx. 35 in 100 metaphases).

It remains to investigate whether the distance between the two I-SceI sites or the increased number of I-SceI sites compared to the two-DSB construct leads to the high frequency of misrepair. This question can be addressed by generating clones with the 500 and 1000 bp spacer I-SceI constructs illustrated in Fig. 11B and measuring exchanges after DSB induction. However, both scenarios may lead to the loss of DNA fragments and destabilize the chromatin structure.

Also the analysis of metaphase chromosomes is in accordance with the G2-PCC data and shows the most severe repair outcomes, i.e. the highest number of chromosome aberrations, for CHO-4xl.SceI-R11.C3 clones. Lethal asymmetric chromosome aberrations like dicentrics, rings and their associated acentric fragments are formed frequently, whereas in CHO-2xl.SceI-R11.C13 cells chromatid breaks are abundant and in CHO-1xl.SceI-D7.C2 cells only very few chromatid breaks could be observed.

In human cells approx. 2.8 dicentricspers 100 cells are formed after 0.5 Gy irradiation (Bauchinger and Gotz 1979). Taking the number of chromosomes in CHO cells into consideration, the frequency of dicentrics in CHO-4xl.SceI-R11.C3 cells after induction of clustered DSBs is clearly elevated. Nevertheless, further quantitative analysis is required to validate this observation. In conclusion, T6-DSBs are clearly more deleterious for the cells than T1-DSBs, and the degree of T6-DSB clustering evidently also plays an important role.

Pioneering research in elucidating restriction enzyme induced chromosomal aberrations in mammalian cells was performed by P. Bryant, G. Obe and W. Morgan (Bryant 1984). They applied (various) PvuII and BamHI for restriction; these enzymes recognize numerous sites in the human genome and in this way cause a high degree of fragmentation, i.e. BamHI leads to 5 kb fragments when cleaving naked human DNA. Site specific endonucleases are widely-used up to date to investigate the formation of translocations after DSB induction, as the precise mechanisms that mediate translocation formation are poorly understood. They are essential events not only after

IR induced DSB misrepair but also in the malignant transformation of several tumor types (Coquelle, Rozier et al. 2002; Weinstock, Elliott et al. 2006; Brunet, Simsek et al. 2009). The results presented in this thesis confirm the formation of chromosomal aberrations by stable chromosomally integrated I-SceI sites at multiple genomic locations. The analysis of translocation frequencies in our I-SceI model-systems by whole genome sequencing or fluorescence in situ hybridization (FISH) would reveal further important information about the formation of translocations in simple compared to clustered DSBs.

6.4. I-SceI-induced simple- and clustered DSBs activate the DDR

To investigate the recruitment of DDR signaling proteins to simple and clustered DSB damage sites, immunostaining of γ -H2AX and live cell imaging of MDC1 and 53BP1 were performed. Foci formation for γ -H2AX and MDC1 was triggered for all I-SceI sites independently of complexity indicating that the DDR signaling cascade is activated for all types of DSBs induced. These results are important as they validate the I-SceI model system as a reliable approach to investigate DDR signaling from simple and complex lesions.

In contrast to radiation induced DSBs, the I-SceI-generated DSBs are not induced simultaneously. In this case, DSB induction is a long process of cutting and religation until a mutation event occurs or chromatin destabilization takes place and the recognition site becomes altered. The simplest form of repairing an I-SceI induced DSB would be by religation, in this way reconstructing the I-SceI restriction site and making it available for renewed cleavage.

In the case of DSB repair involving end resection the I-SceI site would be lost. The MDC1 foci kinetics for all types of DSBs (T1- and T6-DSBs) reach the theoretical maximum 6 h after transfection and slightly decline thereafter. This observation could be an indication for repeated cycles of cleavage and ligation, which would complicate analysis of DSB repair kinetics using this model system. Also, for firm conclusions concerning MDC1 foci kinetics the long term growth conditions utilized in live cell

imaging need to be investigated in greater detail. Furthermore the I-SceI-trex (Bennardo, Cheng et al. 2008), a fusion protein that has in addition to I-SceI cleavage a 3' to 5' exonucleolytic activity, can be used to hinder reconstitution of I-SceI sites after the initial cleavage.

6.5. 53BP1 recruitment differs between simple and complex DSBs

In contrast to γ -H2AX and MDC1 that are present in all types of lesions, our results show that 53BP1 recruitment to DSB sites depends on the type of lesion. 53BP1 foci formation was followed by live cell imaging for 24 h after co-transfection with the 53BP1-GFP and I-SceI expressing plasmids. Whereas for CHO-4xI-SceI.R11.C3 the theoretical maximum of 53BP1-foci was reached after 6 h, only about half of the theoretical maximum was reached for CHO-2xI-SceI.R11.C13 and the number of 53BP1-foci for CHO-1xI-SceI.D7.C2 corresponded to the background foci levels.

53BP1-foci formation is γ -H2AX and H4K20 dimethylation dependent and spans a 1 Mb region surrounding the DSB. 53BP1 is involved in long range intrachromosomal V(D)J recombination and CSR (Difilippantonio, Gapud et al. 2008), as well as in the fusion between dysfunctional telomeres (Dimitrova, Chen et al. 2008). Therefore it is considered that 53BP1 serves as a synapsis factor to mediate long range joining of distant DNA breaks. Recently it has been discovered that 53BP1 plays a role in pathway selection by blocking 5' end resection with the help of Rif1 (Bothmer, Robbiani et al. 2010; Bunting, Callén et al. 2010; Zimmermann, Lottersberger et al. 2013).

A possible explanation for the difference in 53BP1 recruitment triggered by simple and clustered DSBs could be the role of 53BP1 to promote genomic stability by regulating the metabolism of DNA ends. The protection of DNA ends from end resection favors D-NHEJ and prevents B-NHEJ and HR that require extensive end processing (Bothmer, Robbiani et al. 2010). Therefore it is reasonable to protect DNA ends of complex DSBs that are prone to cause chromatin destabilization and mediate fast repair by D-NHEJ.

A further explanation could be a correlation between chromatin remodeling and lesion complexity, where complex DSBs induce a modification of the chromatin structure that

is required for 53BP1 recruitment, whereas simple DSBs are immediately religated. Chromatin architecture in the region surrounding the DSB has a critical impact on the ability of cells to mount an effective DNA damage response. DSBs promote the formation of open, relaxed chromatin domains which are spatially confined to the area surrounding the break. For simple T1-DSBs with compatible ends, it is likely that chromatin remodeling around the DSB is limited and fast and does not reach the 53BP1 recruitment step. To investigate this hypothesis it would be important to analyze foci formation of upstream proteins in the signaling cascade, like RNF8 and RNF168.

The connection between lesion complexity and 53BP1 recruitment is also underlined by the results obtained with different NHEJ mutant cell lines and the application of the NU7441 inhibitor to inhibit DNA-PKcs. In this case, 53BP1 foci form according to the theoretical maximum numbers for all cell lines including CHO-1xI-SceI-D7.C2. Compromising D-NHEJ leads to an increase in complexity at DSB ends, as the ends probably remain open for a longer time period.

A further modification of DSB ends was achieved by the addition of H₂O₂ that converts T1-DSBs to T3-DSBs. The increase of complexity at the DSB ends here also leads to an increase in 53BP1 signaling. A conclusion can be drawn that a synergistic effect exists between 53BP1 foci formation and aspects of DSB repair.

6.6. The number of 53BP1 foci is doubled in G2 cells (contribution of HR)

It will be important for future experiments to investigate the performance of HR in the developed model systems. The I-SceI constructs are stably integrated at random loci in the genome of CHO cells, therefore upon I-SceI mediated DSB induction most probably a DSB will be induced by I-SceI in the homologous sequence as well. This hypothesis is supported by the doubling of 53BP1 foci number in G2- compared to G1-cells observed by live cell imaging after co-transfection with a Cdt1 construct identifying G1 cells.

During HR the resected 3' ssDNA invades an intact homologous duplex, driving the pairing of homologous sequences and strand exchange. In a scenario where the

homologous sequence is not intact due to a DSB at the same location, HR will be compromised. In this case the cells become reliant on D-NHEJ or B-NHEJ that do not require an intact chromatin as a template for repair, but have the propensity to direct joining across the break site which may produce complex chromosomal rearrangements that promote genomic instability and cell death (Iliakis, Wu et al. 2007)

6.7. Inhibiting PARP reduces the number of exchanges for T6-DSBs - A hint to the contribution of B-NHEJ for the repair of clustered lesions

To elucidate the contribution of NHEJ and B-NHEJ to the repair of simple compared to clustered DSBs, pathway-specific proteins were inhibited and the formations of exchanges were analyzed.

Inhibition of DNA-PKcs, a protein involved in the early steps of NHEJ leads to an increase in exchanges and G2-PCC-breaks for CHO-1xIScel-D7.C2 and CHO-2xIScel-R11.C13 cells not only after inhibition with NU7441 but also in the DNA-PKcs deficient cell line XRC13-2xIScel-R11.C5. These results clearly indicate the important role for D-NHEJ in the repair of T1-DSBs and also the 2xIScel-T6-DSB. In contrast, the theoretical maximum of breaks and exchanges for CHO-4xIScel-R11.C3-cells is already reached in NHEJ proficient cells. Two conclusions can be drawn from this observation. First, NHEJ cannot efficiently deal with highly clustered breaks leading to a high frequency of G2-PCC-breaks, misrejoining and asymmetric chromosomal aberrations. Second, it is likely that repair of highly clustered lesions is therefore directed to B-NHEJ.

The involvement of B-NHEJ is also underlined by the decrease in the formation of exchanges after PARP inhibition, where exchanges are reduced by around 50% after treatment with the PARP inhibitor PJ34. B-NHEJ is considered to be the main source for chromosomal translocations (Iliakis, Wang et al. 2004; Iliakis, Wu et al. 2007; Lieber 2010; Gostissa, Alt et al. 2011). Therefore the inhibition of PARP clearly reduces the incidence of chromosomal aberration formation (Boboila, Jankovic et al. 2010; Simsek, Brunet et al. 2011; Wray, Williamson et al. 2013).

7. Summary and outlook

A huge set of clones with different numbers of transposon mediated I-SceI construct integrations, characterized by Southern blot, have been generated in CHO wt, NHEJ and HR deficient CHO cells for the use in various experiments as a model system mimicking the effects of IR. Biological consequences of simple and clustered DSBs in CHO wt and NHEJ deficient cells have been tested with different approaches, clearly proving the toxic effect of clustered DSBs.

In future experiments it would be interesting to measure translocation events induced by clustered DSBs compared to simple DSBs. Translocations could be analyzed by fluorescence in situ hybridization (FISH) or by whole genome sequence analysis. Furthermore the genomic locations of the integrated constructs could be revealed by whole genome sequencing. To determine whether the integrations are located at transcribed or non-transcribed regions is of particular interest. Hi-C analysis (Lieberman-Aiden, van Berkum et al. 2009) would shed light on the three dimensional architecture of the genomes and the spatial proximity of the integrated constructs. It could be investigated whether the spatial proximity in the three-dimensional structure leads to more translocations for simple and clustered lesions than spatially distant integrations.

Live cell imaging experiments showed differences in 53BP1 signaling characteristics between simple and clustered breaks. This result could be strengthened by increasing lesion complexity in clones with simple DSBs by the addition of H₂O₂ and by using repair compromised mutant cell lines. In order to further investigate the functional consequences of complexity dependent 53BP1 signaling, ubiquitylation and signaling by RNF8 and RNF168 should be examined. End resection should also be analyzed by immunostaining of the ssDNA binding protein RPA.

Further approaches with NHEJ (XR-C1-3 and Xrs6) and HR (irs1SF) deficient cells harboring the maximum number of integrations should be performed to evaluate the involvement of the different repair pathways. Especially the performance of HR in these

cell lines should be analyzed as I-SceI induced DSBs are also present in the homologous strand that could pose problems during homology search for the HR-machinery.

An inducible I-SceI system was generated that overcomes some limitations of the transient I-SceI transfection. Still, after the induced translocation of the I-SceI protein to the nucleus, the duration for cleavage cannot be controlled as the protein is expressed for at least 72 h. The stable genomic integration of a construct with a ligand dependent protein destabilization domain as an additional control for an I-SceI inducible system would be helpful to control the time period of DSB induction as the removal of the ligand would stop further cleavage by inducing the degradation of the I-SceI protein. Using this approach could help to elucidate the contribution of the different repair pathways as DSBs could be induced in specific cell cycle phases.

8. References

Audebert, M., B. Salles, et al. (2004). "Involvement of Poly(ADP-ribose) Polymerase-1 and XRCC1/DNA Ligase III in an Alternative Route for DNA Double-strand Breaks Rejoining." Journal of Biological Chemistry 279: 55117-55126.

Bancaud, A., C. Lavelle, et al. (2012). "A fractal model for nuclear organization: current evidence and biological implications." Nucleic Acids Research 40(18): 8783-8792.

Bauchinger, M. and G. Gotz (1979). "Distribution of radiation induced lesions in human chromosomes and dose-effect relation analysed with G-banding." Radiation and Environmental Biophysics 16: 355-366.

Bekker-Jensen, S. and N. Mailand (2010). "Assembly and function of DNA double-strand break repair foci in mammalian cells." DNA Repair 9(12): 1219-1228.

Belfort, M. and R. J. Roberts (1997). "Homing endonucleases: keeping the house in order." Nucleic Acids Research 25(17): 3379-3388.

Bennardo, N., A. Cheng, et al. (2008). "Alternative-NHEJ Is a Mechanistically Distinct Pathway of Mammalian Chromosome Break Repair." PLoS Genetics 4(6): e1000110.

Bindra, R. S., A. G. Goglia, et al. (2013). "Development of an assay to measure mutagenic non-homologous end-joining repair activity in mammalian cells." Nucleic Acids Research in press.

Boboila, C., F. W. Alt, et al. (2012). Chapter One - Classical and Alternative End-Joining Pathways for Repair of Lymphocyte-Specific and General DNA Double-Strand Breaks. Advances in Immunology. W. A. Frederick, Academic Press. Volume 116: 1-49.

Boboila, C., M. Jankovic, et al. (2010). "Alternative end-joining catalyzes robust IgH locus deletions and translocations in the combined absence of ligase 4 and Ku70." Proceedings of the National Academy of Sciences of the United States of America 107(7): 3034-3039.

-
- Bohgaki, T., M. Bohgaki, et al. (2010). "DNA double-strand break signaling and human disorders." Genome Integrity 1: 15.
- Bothmer, A., D. F. Robbiani, et al. (2010). "53BP1 regulates DNA resection and the choice between classical and alternative end joining during class switch recombination." Journal of Experimental Medicine 207(4): 855-865.
- Brunet, E., D. Simsek, et al. (2009). "Chromosomal translocations induced at specified loci in human stem cells." Proceedings of the National Academy of Sciences of the United States of America 106(26): 10620-10625.
- Bryant, P. E. (1984). "Enzymatic restriction of mammalian cell DNA using Pvu II and Bam H1: evidence for the double-strand break origin of chromosomal aberrations." International Journal of Radiation Biology 46: 57-65.
- Bryant, P. E. and P. J. Johnston (1993). "Restriction-endonuclease-induced DNA double-strand breaks and chromosomal aberrations in mammalian cells." Mutation Research 299: 289-296.
- Bunting, S. F., E. Callén, et al. (2010). "53BP1 Inhibits Homologous Recombination in Brca1-Deficient Cells by Blocking Resection of DNA Breaks." Cell 141: 243-254.
- Bzymek, M., N. H. Thayer, et al. (2010). "Double Holliday junctions are intermediates of DNA break repair." Nature 464(7290): 937-941.
- Carson, C. T., R. A. Schwartz, et al. (2003). "The Mre11 complex is required for ATM activation and the G₂/M checkpoint." EMBO Journal 22: 6610-6620.
- Chapman, J. R., Martin R. G. Taylor, et al. (2012). "Playing the End Game: DNA Double-Strand Break Repair Pathway Choice." Molecular Cell 47(4): 497-510.
- Chappell, C., L. A. Hanakahi, et al. (2002). "Involvement of human polynucleotide kinase in double-strand break repair by non-homologous end joining." EMBO Journal 21: 2827-2832.

-
- Chevalier, B. S. and B. L. Stoddard (2001). "Homing endonucleases: structural and functional insight into the catalysts of intron/intein mobility." Nucleic Acids Research 29(18): 3757-3774.
- Ciccia, A. and S. J. Elledge (2010). "The DNA Damage Response: Making It Safe to Play with Knives." Molecular Cell 40(2): 179-204.
- Coquelle, A., L. Rozier, et al. (2002). "Induction of multiple double-strand breaks within an hsr by meganuclease I-SceI expression or fragile site activation leads to formation of double minutes and other chromosomal rearrangements." Oncogene 21: 7671-7679.
- Dekker, J. (2008). "Mapping in Vivo Chromatin Interactions in Yeast Suggests an Extended Chromatin Fiber with Regional Variation in Compaction." Journal of Biological Chemistry 283(50): 34532-34540.
- Di Noia, J. M. and M. S. Neuberger (2007). "Molecular Mechanisms of Antibody Somatic Hypermutation." Annual Review of Biochemistry 76(1): 1-22.
- Difilippantonio, S., E. Gapud, et al. (2008). "53BP1 facilitates long-range DNA end-joining during V(D)J recombination." Nature 456: 529-533.
- Dimitrova, N., Y.-C. M. Chen, et al. (2008). "53BP1 promotes non-homologous end joining of telomeres by increasing chromatin mobility." Nature 456: 524-528.
- Dudley, D. D., J. Chaudhuri, et al. (2005). "Mechanism and Control of V(D)J Recombination versus Class Switch Recombination: Similarities and Differences." Advances in Immunology 86: 43-112.
- Durante, M. and J. S. Loeffler (2010). "Charged particles in radiation oncology." Nature Reviews. Clinical Oncology 7(1): 37-43.
- Eltsov, M., K. M. MacLellan, et al. (2008). "Analysis of cryo-electron microscopy images does not support the existence of 30-nm chromatin fibers in mitotic chromosomes in situ." Proceedings of the National Academy of Sciences 105(50): 19732-19737.

-
- Fernandez-Capetillo, O., H.-T. Chen, et al. (2002). "DNA damage-induced G₂-M checkpoint activation by histone H2Ax and 53BP1." Nature Cell Biology 4: 993-997.
- Finnie, N. J., T. M. Gottlieb, et al. (1995). "DNA-dependent protein kinase activity is absent in xrs-6 cells: implications for site-specific recombination and DNA double-strand break repair." Proceedings of the National Academy of Sciences of the United States of America 92: 320-324.
- Forment, J. V., A. Kaidi, et al. (2012). "Chromothripsis and cancer: causes and consequences of chromosome shattering." Nature Reviews. Cancer 12(10): 663-670.
- Friedland, W., M. Dingfelder, et al. (2005). "Calculated DNA double-strand break and fragmentation yields after irradiation with He ions." Radiation Physics and Chemistry 72(2-3): 279-286.
- Friedland, W., P. Jacob, et al. (2003). "Simulation of DNA Damage after Proton Irradiation." Radiation Research 159(3): 401-410.
- Friedland, W., P. Jacob, et al. (1998). "Monte Carlo Simulation of the Production of Short DNA Fragments by Low-Linear Energy Transfer Radiation Using Higher-Order DNA Models." Radiation Research 150: 170-182.
- Friedrich, T., U. Scholz, et al. (2011). "Calculation of the biological effects of ion beams based on the microscopic spatial damage distribution pattern." International Journal of Radiation Biology 88(1-2): 103-107.
- Fussner, E., M. Strauss, et al. (2012). "Open and closed domains in the mouse genome are configured as 10-nm chromatin fibres." EMBO Reports 13(11): 992-996.
- Georgakilas, A. G. (2008). "Processing of DNA damage clusters in human cells: current status of knowledge." Molecular BioSystems 4(1): 30-35.
- Georgakilas, A. G., P. O'Neill, et al. (2012). "Induction and Repair of Clustered DNA Lesions: What do we know so far?" Radiation Research in press.

-
- Goodhead, D. T. (1994). "Initial events in the cellular effects of ionizing radiations: clustered damage in DNA." International Journal of Radiation Biology 65(1): 7-17.
- Goodhead, D. T. (1995). "Molecular and cell models of biological effects of heavy ion radiation." Radiation and Environmental Biophysics 34: 67-72.
- Goodhead, D. T. and H. Nikjoo (1989). "Track structure analysis of ultrasoft X-rays compared to high- and low-LET radiations." International Journal of Radiation Biology 55(4): 513-529.
- Goodhead, D. T., J. Thacker, et al. (1993). "Effects of radiations of different qualities on cells: molecular mechanisms of damage and repair." International Journal of Radiation Biology 63(5): 543-556.
- Gostissa, M., F. W. Alt, et al. (2011). "Mechanisms that Promote and Suppress Chromosomal Translocations in Lymphocytes." Annual Review of Immunology 29(1): 319-350.
- Gruen, M., K. Chang, et al. (2002). "An in vivo selection system for homing endonuclease activity." Nucleic Acids Research 30(7): e29.
- Gulston, M., C. de Lara, et al. (2004). "Processing of clustered DNA damage generates additional double-strand breaks in mammalian cells post-irradiation." Nucleic Acids Research 32(4): 1602-1609.
- Hada, M. and B. M. Sutherland (2006). "Spectrum of Complex DNA Damages Depends on the Incident Radiation." Radiation Research 165: 223-230.
- Hall, E. J. and A. J. Giaccia (2006). Radiobiology for the Radiologist. Philadelphia, Baltimore, New York, London, Buenos Aires, Hong Kong, Sydney, Tokyo, Lippincott Williams & Wilkins.
- Hartlerode, A., S. Odate, et al. (2011). "Cell Cycle-Dependent Induction of Homologous Recombination by a Tightly Regulated I-SceI Fusion Protein." PLoS ONE 6(3): e16501.

-
- Heyer, W.-D., K. T. Ehmsen, et al. (2010). "Regulation of Homologous Recombination in Eukaryotes." Annual Review of Genetics 44: 113-139.
- Holley, W. R. and A. Chatterjee (1996). "Clusters of DNA damage induced by ionizing radiation: Formation of short DNA fragments. 1. Theoretical modeling." Radiation Research 145: 188-199.
- Honma, M., M. Sakuraba, et al. (2007). "Non-homologous end-joining for repairing I-SceI-induced DNA double strand breaks in human cells." DNA Repair 6(6): 781-788.
- Huen, M. S. Y., R. Grant, et al. (2007). "RNF8 transduces the DNA-damage signal via histone ubiquitylation and checkpoint protein assembly." Cell 131: 901-914.
- Iacovoni, J. S., P. Caron, et al. (2010). "High-resolution profiling of gH2AX around DNA double strand breaks in the mammalian genome." EMBO Journal 29(8): 1446-1457.
- Iliakis, G., H. Wang, et al. (2004). "Mechanisms of DNA double strand break repair and chromosome aberration formation." Cytogenetic and Genome Research 104: 14-20.
- Iliakis, G., W. Wu, et al. (2007). Backup Pathways of Nonhomologous End Joining May Have a Dominant Role in the Formation of Chromosome Aberrations. Chromosomal Alterations. G. Obe, Vijayalaxmi. Berlin, Heidelberg, New York, Springer Verlag: 67-85.
- Ivics, Z., P. B. Hackett, et al. (1997). "Molecular Reconstruction of Sleeping Beauty, a Tc1-like Transposon from Fish, and Its Transposition in Human Cells." Cell 91: 501-510.
- Ivics, Z. and Z. Izsvak (2004). "Transposable Elements for Transgenesis and Insertional Mutagenesis in Vertebrates." Methods in Molecular Biology 260: 255-276.
- Izsvak, Z. and Z. Ivics (2004). "Sleeping Beauty Transposition: Biology and Applications for Molecular Therapy." Molecular Therapy 9: 147-156.
- Izsvak, Z., E. E. Stüwe, et al. (2004). "Healing the Wounds Inflicted by Sleeping Beauty Transposition by Double-Strand Break Repair in Mammalian Somatic Cells." Molecular Cell 13: 279-290.

-
- Jackson, S. P. and J. Bartek (2009). "The DNA-damage response in human biology and disease." Nature 461(7267): 1071-1078.
- Jasin, M. (1996). "Genetic manipulation of genomes with rare-cutting endonucleases." Trends in Genetics 12: 224-228.
- Jones, N. J., R. Cox, et al. (1988). "Six complementation groups for ionising-radiation sensitivity in Chinese hamster cells." Mutation Research 193: 139-144.
- Kinner, A., W. Wu, et al. (2008). "g-H2AX in recognition and signaling of DNA double-strand breaks in the context of chromatin." Nucleic Acids Research 36(17): 5678-5694.
- Korbel, Jan O. and Peter J. Campbell (2013). "Criteria for Inference of Chromothripsis in Cancer Genomes." Cell 152(6): 1226-1236.
- Lieber, M. R. (2010). "The Mechanism of Double-Strand DNA Break Repair by the Nonhomologous DNA End-Joining Pathway." Annual Review of Biochemistry 79: 1.1-1.31.
- Lieber, M. R. (2010). "NHEJ and its backup pathways in chromosomal translocations." Nature Structural & Molecular Biology 17(4): 393-395.
- Lieberman-Aiden, E., N. L. van Berkum, et al. (2009). "Comprehensive Mapping of Long-Range Interactions Reveals Folding Principles of the Human Genome." Science 326(5950): 289-293.
- Loucas, B. D., M. Durante, et al. (2013). "Chromosome Damage in Human Cells by γ Rays, α Particles and Heavy Ions: Track Interactions in Basic Dose-Response Relationships." Radiation Research 179(1): 9-20.
- Luijsterburg, M. S. and H. van Attikum (2012). "Close encounters of the RNF8th kind: when chromatin meets DNA repair." Current Opinion in Cell Biology 24(3): 439-447.
- Lukas, C., F. Melander, et al. (2004). "Mdc1 couples DNA double-strand break recognition by Nbs1 with its H2AX-dependent chromatin retention." EMBO Journal 23: 2674-2683.

- Mailand, N., S. Bekker-Jensen, et al. (2007). "RNF8 ubiquitylates histones at DNA double-strand breaks and promotes assembly of repair proteins." Cell 131: 887-900.
- Mansour, W. Y., T. Rhein, et al. (2010). "The alternative end-joining pathway for repair of DNA double-strand breaks requires PARP1 but is not dependent upon microhomologies." Nucleic Acids Research 38(18): 6065-6077.
- McVey, M. and S. E. Lee (2008). "MMEJ repair of double-strand breaks (director's cut): deleted sequences and alternative endings." Trends in Genetics 24(11): 529-538.
- Mirny, L. (2011). "The fractal globule as a model of chromatin architecture in the cell." Chromosome Research 19(1): 37-51.
- Mladenov, E. and G. Iliakis (2011). "Induction and Repair of DNA Double Strand Breaks: The Increasing Spectrum of Non-homologous End Joining Pathways." Mutation Research/Fundamental and Molecular Mechanisms of Mutagenesis 711: 61-72.
- Molenaar, J. J., J. Koster, et al. (2012). "Sequencing of neuroblastoma identifies chromothripsis and defects in neuritogenesis genes." Nature 483(7391): 589-593.
- Nikjoo, H., P. O. O'Neill, et al. (1999). "Quantitative modelling of DNA damage using Monte Carlo track structure method." Radiation and Environmental Biophysics 38: 31-38.
- Nishino, Y., M. Eltsov, et al. (2012). "Human mitotic chromosomes consist predominantly of irregularly folded nucleosome fibres without a 30-nm chromatin structure." EMBO Journal 31(7): 1644-1653.
- Obe, G. and A. T. Natarajan (1985). "Chromosomal aberrations induced by the restriction endonuclease Alu I in Chinese hamster ovary cells: Influence of duration of treatment and potentiation by cytosine arabinoside." Mutation Research 152: 205-210.
- Olive, P. L. (1998). "The Role of DNA Single- and Double-Strand Breaks in Cell Killing by Ionizing Radiation." Radiation Research 150 (Suppl.): S42-S51.

-
- Pang, D., T. A. Winters, et al. (2011). "Radiation-generated Short DNA Fragments May Perturb Non-homologous End-joining and Induce Genomic Instability." Journal of Radiation Research 52: 309-319.
- Paretzke, H. G. (1987). Radiation track structure theory. Kinetics of Nonhomogeneous Processes. G. R. Freeman, John Wiley & Sons, Inc.: 89-170.
- Pfeiffer, P., E. Feldmann, et al. (2005). "Analysis of double-strand break repair by non-homologous DNA end joining in cell-free extracts from mammalian cells." Methods in Molecular Biology 291: 351-371.
- Pierce, A. J., R. D. Johnson, et al. (1999). "XRCC3 promotes homology-directed repair of DNA damage in mammalian cells." Genes & Development 13: 2633-2638.
- Ponomarev, A. L. and F. A. Cucinotta (2006). "Chromatin loops are responsible for higher counts of small DNA fragments induced by high-LET radiation, while chromosomal domains do not affect the fragment sizes." International Journal of Radiation Biology 82(4): 293-305.
- Rass, E., A. Grabarz, et al. (2009). "Role of Mre11 in chromosomal nonhomologous end joining in mammalian cells." Nature Structural & Molecular Biology 16(8): 819-825.
- Rogakou, E. P., D. R. Pilch, et al. (1998). "DNA double-stranded breaks induce histone H2AX phosphorylation on serine 139." Journal of Biological Chemistry 273: 5858-5868.
- Rosidi, B., M. Wang, et al. (2008). "Histone H1 functions as a stimulatory factor in backup pathways of NHEJ." Nucleic Acids Research 36(5): 1610-1623.
- Rydberg, B. (1996). "Clusters of DNA damage induced by ionizing radiation: Formation of short DNA fragments. 11. Experimental detection." Radiation Research 145: 200-209.
- Saha, J. (2010). "Development of Defined Biological Models for Complex Radiation-Induced DNA Lesions Using Homing Endonucleases and Transposon Technology: Feasibility and Initial Characterization." Ph.D. thesis.

-
- Sallmyr, A., A. E. Tomkinson, et al. (2008). "Up-regulation of WRN and DNA ligase IIIa in chronic myeloid leukemia: consequences for the repair of DNA double-strand breaks." Blood 112(4): 1413-1423.
- San Filippo, J., P. Sung, et al. (2008). "Mechanism of Eukaryotic Homologous Recombination." Annual Review of Biochemistry 77: 229-257.
- Sanchez, Y., C. Wong, et al. (1997). "Conservation of the Chk1 checkpoint pathway in mammals: Linkage of DNA damage to Cdk regulation through Cdc25." Science 277: 1497-1501.
- Savage, J. R. K. (1998). "A brief survey of aberration origin theories." Mutation Research 404: 139-147.
- Schipler, A. and G. Iliakis (2013). "DNA double-strand-break complexity levels and their possible contributions to the probability for error-prone processing and repair pathway choice." Nucleic Acids Research Epub ahead of print.
- Schultz, L. B., N. H. Chehab, et al. (2000). "p53 binding protein 1 (53BP1) is an early participant in the cellular response to DNA double-strand breaks." Journal of Cell Biology 151: 1381-1390.
- Shiloh, Y. (2003). "ATM and related protein kinases: Safeguarding genome integrity." Nature Reviews. Cancer 3: 155-168.
- Simsek, D., E. Brunet, et al. (2011). "DNA Ligase III Promotes Alternative Nonhomologous End-Joining during Chromosomal Translocation Formation." PLoS Genetics 7(6): e1002080.
- Singh, S. K., T. Bednar, et al. (2012). "Inhibition of B-NHEJ in Plateau-Phase Cells Is Not a Direct Consequence of Suppressed Growth Factor Signaling." International Journal of Radiation Oncology Biology Physics 84(2): e237-e243.
- Singh, S. K., M. Wang, et al. (2011). "Post-irradiation chemical processing of DNA damage generates double-strand breaks in cells already engaged in repair." Nucleic Acids Research 39(19): 8416-8429.

-
- Singh, S. K., W. Wu, et al. (2011). "Widespread Dependence of Backup NHEJ on Growth State: Ramifications for the Use of DNA-PK Inhibitors." International Journal of Radiation Oncology Biology Physics 79(2): 540-548.
- Stephens, P. J., C. D. Greenman, et al. (2011). "Massive Genomic Rearrangement Acquired in a Single Catastrophic Event during Cancer Development." Cell 144: 27-40.
- Stucki, M., J. A. Clapperton, et al. (2005). "MDC1 directly binds phosphorylated histone H2AX to regulate cellular responses to DNA double-strand breaks." Cell 123: 1213-1226.
- Thurman, R. E., E. Rynes, et al. (2012). "The accessible chromatin landscape of the human genome." Nature 489(7414): 75-82.
- Tsai, C. J., S. A. Kim, et al. (2007). "Cernunnos/XLF promotes the ligation of mismatched and noncohesive DNA ends." Proceedings of the National Academy of Sciences of the United States of America 104(19): 7851-7856.
- van Attikum, H. and S. M. Gasser (2009). "Crosstalk between histone modifications during the DNA damage response." Trends in Cell Biology 19(5): 207-217.
- van Berkum, N. L. and J. Dekker (2009). "Determining Spatial Chromatin Organization of Large Genomic Regions Using 5C Technology." Methods in Molecular Biology 567: 189-213.
- van Gent, D. C. and M. van der Burg (2007). "Non-homologous end-joining, a sticky affair." Oncogene 26(56): 7731-7740.
- Vigdal, T. J., C. D. Kaufman, et al. (2002). "Common Physical Properties of DNA Affecting Target Site Selection of Sleeping Beauty and other Tc1/mariner Transposable Elements." Journal of Molecular Biology 323(3): 441-452.
- Walker, J. R., R. A. Corpina, et al. (2001). "Structure of the Ku heterodimer bound to DNA and its implications for double-strand break repair." Nature 412: 607-614.

-
- Wang, H., B. Rosidi, et al. (2005). "DNA Ligase III as a Candidate Component of Backup Pathways of Nonhomologous End Joining." Cancer Research 65(10): 4020-4030.
- Wang, M., W. Wu, et al. (2006). "PARP-1 and Ku compete for repair of DNA double strand breaks by distinct NHEJ pathways." Nucleic Acids Research 34(21): 6170-6182.
- Ward, J. F. (1985). "Biochemistry of DNA lesions." Radiation Research 104: S103-S111.
- Ward, J. F. (1990). "The yield of DNA double-strand breaks produced intracellularly by ionizing radiation: a review." International Journal of Radiation Biology 57: 1141-1150.
- Weinstock, D. M., B. Elliott, et al. (2006). "A model of oncogenic rearrangements: differences between chromosomal translocation mechanisms and simple double-strand break repair." Blood 107(2): 777-780.
- Weterings, E. and D. J. Chen (2007). "DNA-dependent protein kinase in nonhomologous end joining: a lock with multiple keys?" Journal of Cell Biology 179(2): 183-186.
- Weterings, E. and D. J. Chen (2008). "The endless tale of non-homologous end-joining." Cell Research 18(1): 114-124.
- Windhofer, F., W. Wu, et al. (2007). "Marked dependence on growth state of backup pathways of NHEJ." International Journal of Radiation Oncology Biology Physics 68(5): 1462-1470.
- Wray, J., E. A. Williamson, et al. (2013). "PARP1 is required for chromosomal translocations." Blood in press.
- Wu, W., M. Wang, et al. (2008). "Enhanced Use of Backup Pathways of NHEJ in G₂ in Chinese Hamster Mutant Cells with Defects in the Classical Pathway of NHEJ." Radiation Research 170: 512-520.

Zimmermann, M., F. Lottersberger, et al. (2013). "53BP1 Regulates DSB Repair Using Rif1 to Control 5' End Resection." Science 339(6120): 700-704.

Curriculum vitae

Der Lebenslauf ist in der veröffentlichten Version aus Gründen des Datenschutzes nicht enthalten.

Appendix 5

A balance shift between error-free and error-prone DNA double-strand break repair pathways as a novel mechanism of radiosensitization by nucleoside analogs

Inaugural-Dissertation
zur
Erlangung des Doktorgrades
Dr. rer. nat.

der Fakultät für Biologie
an der
Universität Duisburg-Essen
Standort Essen

vorgelegt von
Simon Magin
aus Trier

Februar, 2014

Zusammenfassung

Verbesserungen in der Behandlung von Krebsleiden zu erzielen gehört zu den großen Herausforderungen der modernen Medizin. Die Kombination von chemotherapeutischen Wirkstoffen mit Strahlentherapie um einen synergistischen Effekt bei der Abtötung von Tumorzellen zu erhalten, ist hierbei gegenwärtig einer der vielversprechendsten Ansätze. Das Ziel dieser Promotionsarbeit war es Mechanismen der Strahlensensibilisierung durch Nukleosidanalogue am Beispiel von 9-beta-D-Arabinofuranosyladenosin (ara-A) aufzuklären.

Hierzu wurde der Einfluss von ara-A auf die Reparatur von DNA-Doppelstrangbrüchen (DSB) untersucht. Wir konnten beobachten das ara-A Reparatur durch homologe Rekombination (HRR) inhibiert und konnten zeigen das diese Hemmung eine wichtige Rolle bei der Strahlensensibilisierung von exponentiell wachsenden, humanen Tumorzellen spielt.

Wir untersuchten auch die Effekte von ara-A auf Reparaturwege der nicht-homologen-Endverknüpfung (NHEJ). In zwei Reporterzellsystemen konnten wir einen durch ara-A ausgelösten Anstieg der Häufigkeit fehlerhafter DSB-Reparaturereignisse beobachten. Es konnte jedoch keine Veränderung der allgemeinen Effizienz der DSB Reparatur in Reparatur-kompetenten Zellen durch ara-A Behandlung in Pulsfeld-Gelelektrophorese-Experimenten (PFGE) festgestellt werden. Diese Ergebnisse deuteten auf eine Verschiebung der Aktivität zwischen verschiedenen Reparaturwegen anstelle einer allgemeinen Hemmung der Reparatur hin.

Durch Untersuchung der DSB-Reparatur in Reparatur-inkompetenten Zellen mit Hilfe der PFGE konnten wir zum ersten Mal eine Beförderung der besonders fehleranfälligen, alternativen Backup-Mechanismen der NHEJ (B-NHEJ) durch ein Nukleosidanalogue zeigen. Ara-A verstärkte die Reparatur von DSB durch B-NHEJ in aktiv wachsenden humanen Tumorzellen. Des Weiteren konnte in Mauszellen durch Behandlung mit ara-A die Plateauphase-abhängige Unterdrückung des B-NHEJ vollständig aufgehoben werden, was zu einem dramatischen Anstieg der Reparaturkompetenz in diesen Zellen führte. Die Untersuchung von durch ionisierende Strahlung hervorgerufenen, nukleären gamma-H2AX, ATM und 53BP1-Foci bestätigte diese Beobachtungen und deutete auf eine Deregulierung der durch

DSB ausgelösten Signalwege und einer möglichen Rolle der Endresektion als zugrunde liegende Mechanismen hin.

Wir schließen, dass Behandlung mit ara-A in proliferierenden Zellen durch direkte Hemmung der HRR zur Strahlensensibilisierung führt. Gleichzeitig wird die Balance des NHEJ in Richtung des fehlerhafteren B-NHEJ verschoben. Die Überaktivierung der mutagenen B-NHEJ trägt mit hoher Wahrscheinlichkeit ebenfalls zur Strahlensensibilisierung durch ara-A bei, vor allem in der G1- sowie der Plateau-Phase des Wachstums, aber auch in der G2- und S-Phase.

Die Ergebnisse dieser Arbeit zeigen einen neuen Mechanismus der Strahlensensibilisierung durch Nukleosidanaloge auf. Diese neuen Erkenntnisse ermöglichen es neue Wege bei der Untersuchung der Interaktionen dieser Wirkstoffe mit ionisierender Strahlung zu beschreiten und könnten wichtige Implikationen für die klinische Anwendung von Nukleosidanalogen als Strahlensensibilisierer haben.

Das dieser Dissertation zugrunde liegende Vorhaben wurde mit Mitteln des Bundesministeriums für Bildung und Forschung (BMBF) unter dem Förderkennzeichen 02NUK005C gefördert. Die Verantwortung für den Inhalt dieser Veröffentlichung liegt beim Autor.

Contents

Contents	I
List of figures	IV
List of tables	V
List of abbreviations	V
1 Introduction	1
1.1 The role of chemoradiotherapy in the treatment of cancer	1
1.2 Nucleoside analogs and their role in chemotherapy	2
1.2.1 Overview and general considerations	2
1.2.2 Cellular metabolism and modes of action of NAs used in this study.....	5
1.3 Radiotherapy and the effects of ionizing radiation	8
1.3.1 Tumor and normal tissue response to IR	8
1.3.2 Repair of potentially lethal damage	10
1.3.3 Basic physics of the interaction of IR with biological matter.....	13
1.3.4 Mechanisms of DNA damage induction and types of DNA lesions induced	15
1.3.5 Different types of DSB and damage complexity.....	16
1.4 Cellular responses to DSB	19
1.4.1 DSB detection and signaling- The DNA damage response	19
1.4.2 Mechanisms of DSB Repair in Eukaryotes	23
1.5 The role of DSB in cell killing and cancer induction by IR	35
1.5.1 The DSB as cancerogenic lesion	35
1.5.2 The DSB as lethal lesion	35
1.6 Evidence connecting DSB repair to cellular radiosensitivity and PLD	36
1.7 Synergistic interactions between IR and nucleoside analogs	38
2 Aims and scope of this work	39
3 Materials and Methods	40
3.1 Materials	40
3.2 Methods	46
3.2.1 Cell culture.....	46
3.2.2 Flow cytometry.....	49
3.2.3 X-Irradiation	50

3.2.4	Transfection of nucleic acids	51
3.2.5	Repair-outcome-specific chromosomal reporters.....	52
3.2.6	Clonogenic survival assay	54
3.2.7	Pulsed-field gel electrophoresis.....	55
3.2.8	PFGE with sorted cell populations.....	57
3.2.9	Immunofluorescence staining.....	58
3.2.10	SDS-PAGE	60
3.2.11	Confocal laser scanning microscopy (CLSM) and foci quantification	62
3.2.12	In vivo replication assay	64
4	Results.....	65
4.1	Inhibition of DNA replication in A549 cells	65
4.2	Radiosensitization of cycling A549 cells by ara-A	66
4.3	Impact of ara-A treatment on HRR.....	69
4.3.1	Inhibition of IR induced RAD51 foci formation by ara-A.....	69
4.3.2	Proficiency in HRR is a prerequisite for radiosensitization by ara-A.....	73
4.3.3	Effects of ara-A on homology directed repair in reporter gene assays	75
4.4	Impact of ara-A treatment on NHEJ.....	83
4.4.1	Non-homologous rejoining of distal ends in paired DSB.....	83
4.4.2	The effect of ara-A on mutagenic repair in the EJ-RFP system.....	86
4.4.3	Effect of ara-A on DSB repair kinetics in D-NHEJ proficient cells.....	88
4.4.4	Effect of ara-A on DSB repair in D-NHEJ deficient cells.....	91
4.4.5	Relieve of serum deprivation-induced inhibition of B-NHEJ by ara-A.....	93
4.4.6	Analysis of IR induced foci in serum deprived MEF Lig4 ^{-/-}	96
4.5	Effects of other NAs on radiosensitivity and DSB repair.....	102
4.5.1	Effects on the survival of A549 cells.....	102
4.5.2	Effects on ara-C and fludarabine on HRR, SSA and distal NHEJ.....	104
4.5.3	Effects on mutagenic repair in EJ-DR cells	108
5	Discussion.....	109
5.1	Design of this study and general considerations.....	109
5.2	Inhibition of replication and sensitization of cycling cells	110
5.3	Methods for the measurement of DSB repair.....	111
5.3.1	PFGE	111
5.3.2	IRIF	112
5.3.3	The use of I-SceI reporter assays for the assessment of DSB repair pathway activities.....	113

5.4	Effects of ara-A on HRR	115
5.4.1	Effect of ara-A on IR induced Rad51 foci formation	115
5.4.2	Survival with Rad51 silenced cells	116
5.4.3	Effect of ara-A on HRR of the DR-GFP reporter construct.....	117
5.4.4	Effect of ara-A on SSA.....	119
5.5	Effects of ara-A on NHEJ	120
5.5.1	Effect of ara-A on distal end-joining.....	120
5.5.2	Effect of ara-A on mutagenic DSB repair in the EJ-RFP system	120
5.5.3	PFGE of sorted G1 and G2 cells from an exponentially growing culture	121
5.5.4	Ara-A enhances B-NHEJ in D-NHEJ deficient HCT116 cells	123
5.5.5	Relieve of B-NHEJ suppression in plateau phase MEF Lig4 ^{-/-} cells by ara-A	123
5.5.6	Promotion of B-NHEJ is not productive for survival	124
5.5.7	Detection of IRIF in plateau phase MEF cells	125
5.6	Radiosensitization by other NAs	129
5.6.1	Clonogenic survival after exposure to IR.....	129
5.6.2	Effect of other NAs in reporter cell assays	130
6	Summary and Conclusions	133
7	Bibliography	135
8	Appendix	169
8.1	Part A: Supplementary data	169
8.1.1	Effect of earlier start of ara-A treatment in DRaa40 cells	169
8.1.2	Inherent problems with the interpretation of data obtained at later times in I-SceI inducible reporter systems	170
8.1.3	Effects of Nu7441 on DSB repair	174
8.1.4	Enhancement of B-NHEJ by ara-A does not confer radioresistance	175
8.1.5	53BP1 bodies in serum deprived MEF Lig4 ^{-/-}	177
8.1.6	Inhibition of DNA replication by ara-C and gemcitabine.....	178
8.2	Part B: Supplementary information on NAs	179
8.2.1	BrdU and IdU	179
8.2.2	5-FU.....	180
9	Acknowledgements	181
10	Curriculum vitae	184
11	Publications	187
12	Declaration	188

List of figures

FIGURE 1 CHEMICAL STRUCTURES OF SELECTED NUCLEOSIDE ANALOGS.	4
FIGURE 2 REPAIR OF POTENTIALLY LETHAL DAMAGE.	12
FIGURE 3 DNA DAMAGE INDUCTION BY LOW AND HIGH LET RADIATION TRACKS.	14
FIGURE 4 TYPES OF DSB WITH DIFFERENT LEVELS OF COMPLEXITY	16
FIGURE 5 SURVIVAL CURVES FOR CULTURED CELLS OF HUMAN ORIGIN	17
FIGURE 6 REPAIR KINETICS OF DIFFERENT FORMS OF DNA DAMAGE.....	18
FIGURE 7 RECRUITMENT KINETICS OF PROTEINS INVOLVED IN THE DDR	20
FIGURE 8 SIMPLIFIED SCHEMATIC OF THE CELLULAR RESPONSE TO DSB	22
FIGURE 9 SCHEMATIC OVERVIEW OF KEY FACTORS AND STEPS OF D-NHEJ.....	26
FIGURE 10 STEPS AND OUTCOMES OF HOMOLGY DIRECTED REPAIR PATHWAYS.	29
FIGURE 11 SCHEMATIC OVERVIEW OF KEY FACTORS AND STEPS OF B-NHEJ.....	34
FIGURE 12 GROWTH CURVE OF A549 CELLS.	48
FIGURE 13 MEASUREMENT OF DNA REPLICATION BY ³ H-THYMIDINE INCORPORATION IN A549 CELLS.	65
FIGURE 14 EFFECT OF ARA-A ON THE RADIOSENSITIVITY TO KILLING OF A549 CELLS.....	67
FIGURE 15 INHIBITION OF RAD51 FOCI FORMATION IN A549 CELLS BY ARA-A.	71
FIGURE 16 REQUIREMENT OF HRR FOR THE RADIOSENSITIZATION BY ARA-A.	74
FIGURE 17 SUPPRESSION OF HRR IN DRAA40 CELLS HARBORING THE DR-GFP REPORTER.....	77
FIGURE 18 TIME DEPENDENCE OF THE EFFECT OF ARA-A IN DRAA40 CELLS (DR-GFP).	78
FIGURE 19 KNOCKDOWN OF COMPONENTS OF HRR IN U2OS 282C CELLS (DR-GFP).....	79
FIGURE 20 INHIBITION OF HRR BY ARA-A IN U2OS 282C CELLS.....	80
FIGURE 21 EFFECTS OF ARA-A ON SSA MEDIATED REPAIR IN U2OS 283C CELLS (SA-GFP).....	82
FIGURE 22 EFFECT OF ARA-A ON THE JOINING OF DISTAL ENDS IN U2OS 280A (EJ5-GFP).	85
FIGURE 23 EFFECT OF ARA-A ON MUTAGENIC DSB REPAIR PATHWAYS IN U2OS EJ-DR CELLS.....	87
FIGURE 24 DSB REPAIR BY PFGE IN SORTED G1 AND G2 A549 CELLS.	90
FIGURE 25 ENHANCEMENT OF DSB REPAIR IN D-NHEJ DEFICIENT HUMAN CELLS.....	92
FIGURE 26 DSB REPAIR BY PFGE IN EXPONENTIALLY GROWING AND SERUM DEPRIVED MEF.....	94
FIGURE 27 ARA-A TREATMENT REACTIVATES DSB REPAIR IN SERUM DEPRIVED LIG4 ^{-/-} CELLS.....	95
FIGURE 28 QUANTIFICATION OF γ H2AX AND 53BP1 FOCI IN SERUM DEPRIVED LIG4 ^{-/-} MEFs.....	98
FIGURE 29 QUANTIFICATION OF PATM-S1981 FOCI IN SERUM DEPRIVED LIG4 ^{-/-} MEFs.....	101
FIGURE 30 COMPARISON OF RADIOSENSITIZATION BY POST-IRRADIATION TREATMENT WITH DIFFERENT NAS. ...	103
FIGURE 31 EFFECT OF FLUDARABINE AND ARA-C ON HRR IN U2OS 282C CELLS (DR-GFP).....	105
FIGURE 32 EFFECT OF FLUDARABINE AND ARA-C ON SSA IN U2OS 283C CELLS (SA-GFP).....	106
FIGURE 33 EFFECT OF FLUDARABINE AND ARA-C ON THE JOINING OF DISTAL ENDS OF TWO DSB (EJ5-GFP)...	107
FIGURE 34 EFFECT OF FLUDARABINE AND ARA-C IN U2OS EJ-DR CELLS (EJ-RFP).....	108
FIGURE 35 EFFECT OF EARLIER START OF ARA-A TREATMENT IN DRAA40 CELLS	169

FIGURE 36 CONTINUOUS DAMAGE INDUCTION AND SHIFTS IN CELL CYCLE DISTRIBUTION LEAD TO DECEPTIVE SIGNAL GENERATION IN LATE MEASUREMENTS IN I-SCEI REPORTER ASSAYS.....	171
FIGURE 37 KINETICS OF REPORTER GENE EXPRESSION IN EJ-DR CELLS.	173
FIGURE 38 A549 EXPONENTIALLY GROWING WITH OR WITHOUT 5 μ M NU7441.....	174
FIGURE 39 TREATMENT OF U2OS 280A (EJ5-GFP) WITH 5 μ M NU7441 FOR DIFFERENT LENGTH OF TIME.	175
FIGURE 40 ARA-A DOES NOT IMPROVE SURVIVAL IN SERUM DEPRIVED MEF LIG4 ^{-/-} CELLS.....	176
FIGURE 41 53BP1 BODIES IN SERUM DEPRIVED MEF Lig4 ^{-/-}	177
FIGURE 42 INHIBITION OF REPLICATION BY ARA-C AND GEMCITABINE.	178

List of tables

TABLE 3.1: LABORATORY APPARATUSES.....	40
TABLE 3.2: CHEMICALS	42
TABLE 3.3: SOFTWARE.....	45
TABLE 3.4: CELL LINES.....	47
TABLE 3.5: NUCLEOFECTOR PROGRAMS	51
TABLE 3.6: siRNAs	52
TABLE 3.7: ANTIBODIES IMMUNOFLUORESCENCE.....	60
TABLE 3.8: ANTIBODIES WESTERN BLOT	61
TABLE 3.9: MICROSCOPE SETTINGS AND PARAMETERS	63
TABLE 4.1: QUANTIFICATION OF ARA-A MEDIATED RADIOSENSITIZATION.....	68

List of abbreviations

5-FU	5-fluorouracil
Ab	Antibody
ADA	Adenosine deaminase
AFIGE	Asymmetric field inversion gel electrophoresis
ATM	Ataxia telangiectasia mutated kinase
ATR	ATM and Rad3 related kinase
ara-A	9- β -D-arabinofuranosyladenosine

Ara-C	cytosine arabinoside; Ara-C
bp	Base pairs
B-NHEJ	Backup Non-homologous end-joining
BrdU	5-bromo-2'-deoxyuridine
CHO	Chinese hamster ovary cell line
CLL	Chronic lymphoid leukemia
CML	Chronic myeloid leukemia
CLSM	Confocal laser scanning microscopy
dCK	Deoxycytidine kinase
DDR	DNA damage response
dHJ	Double Holliday junction
DNA	Deoxyribonucleic acid
DNA-PK	DNA-dependent protein kinase
DNA-PKcs	DNA-dependent protein kinase catalytic subunit
DEQ	Dose equivalent
dFdC	2',2'-difluoro-2'-deoxycytidine; Gemcitabine
DMEM	Dulbecco's modified Eagle medium
DNA	Deoxyribonucleic acid
DR	Dose response
DSB	Double-strand break/s
dsDNA	Double-stranded DNA

EdU	5-ethynyl-2'-deoxyuridine
FACS	Fluorescence activated cell sorting
FDR	Fraction of DNA released
EGFP	Enhanced green fluorescent protein
Gy	Gray (J/kg)
h	hour
hCNT	Human concentrative nucleoside transporter
hENT	Human equilibrative nucleoside transporter
HU	Hydroxyurea
HRR	Homologous recombination repair
IF	Immunofluorescence
IR	Ionizing radiation
IRIF	Ionizing radiation induced foci
IdU	5-iodo-2'-deoxyuridine
k	Kilo (10^3)
LASER	Light amplification by stimulated emission of radiation
LET	Linear energy transfer
LMA	Low melting agarose
M	Mega (10^6)
MDC1	Mediator of DNA damage checkpoint 1
MEF	Mouse embryonal fibroblasts

MIP	Maximum intensity projection
MMC	Mitomycin C
MRN	Mre11-Rad50-Nbs1 complex
NAHR	Non-allelic homologous recombination
NAs	Nucleoside analogs
NHEJ	Non-homologous end-joining
ORF	Open reading frame
PARP	Poly(ADP-ribose) polymerases
PBS	Phosphate buffered saline
PE	Plating efficiency
PFGE	Pulsed-field gel electrophoresis
PI	Propidium iodide
PIKK	Phosphatidylinositide 3-kinase related kinases
PLD	Potential lethal damage
PMT	Photomultiplier tube
PTM	Post-translational modification
Puro	Puromycin resistance gene
RIPA	Radio-immuno-precipitation buffer
RK	Repair kinetics
RNA	Ribonucleic acid
RNAi	RNA interference

RnR	Ribonucleotide reductase
RPA	Replication protein A
s.d.	Standard deviation
s.e.m.	Standard error of the mean
SER	Sensitizer enhancement ratio
siRNA	Small interfering RNA
SLD	Sub-lethal damage
ssDNA	Single-stranded DNA
SSB	Single-strand breaks

1 Introduction

1.1 The role of chemoradiotherapy in the treatment of cancer

Cancer is the leading cause of death in Western Europe and North America (Ferlay, 2007; Jemal, 2011). Surgery, chemotherapy and radiotherapy (RT) are the three major treatment options for solid cancers. Current estimates state that more than 50% of patients with cancer should receive radiation treatment at least once during their illness (Delaney, 2005) and the U. S. cancer treatment and survivorship statistics 2012 show that RT belongs to the most frequently employed treatments for solid cancers (Siegel, 2012).

Thus, finding ways to improve the efficacy of RT and advancing the understanding of its actions is an important task in oncology. The past 2 decades have seen impressive achievements in delivery and targeting of the radiation dose contributing to this aim (Ahmad, 2012; Thariat, 2013). Despite these advances recurrence after initial eradication of detectable disease remains a major problem (Catton, 2003; Siglin, 2012). Recurrence may be due to radiation resistant sub-populations within the tumor or occult metastases.

An approach that can address both of these issues is the combination of chemotherapy with RT (Seiwert, 2007; Fietkau, 2012). One of the potential benefits of this combination is the gain of systemic action through chemotherapy that can complement the local action of irradiation. Importantly, for a variety of chemotherapeutics a synergistic action with ionizing radiation (IR) has also been observed that results from sensitization of cells to the killing effects of radiation.

Nucleoside analogs (NAs) represent an important family of antimetabolite drugs, several members of which have been demonstrated to possess radiosensitizing potential (Galmarini, 2002; Jordheim, 2013; Lee, 2013). A better understanding of the basic principles of this radiosensitization will help to develop treatments that increase the efficacy of radiotherapy and improve local control. In the present thesis mechanisms of radiosensitization by nucleoside analogs (NAs) are studied at the example of 9- β -D-arabinofuranosyladenosine (ara-A) and compared to the effects of other NAs.

In the following, the roles and effects of nucleoside chemotherapy and radiotherapy as single treatments will be described first to lay the basis for the understanding of their synergistic effects.

1.2 Nucleoside analogs and their role in chemotherapy

1.2.1 Overview and general considerations

NAs represent a class of rationally designed anticancer drugs. They were and are developed based on the knowledge of the chemical structure of nucleic acids and their building blocks. These compounds share high structural similarity with naturally occurring cellular nucleosides. Due to this similarity NAs can interfere with various enzymatic processes and compete with endogenous nucleosides. Prominent among these are processes of the nucleic acid metabolism, namely the synthesis of deoxyribonucleic acid (DNA) and ribonucleic acid (RNA) and nucleoside/nucleotide biosynthesis, where they can be used as fraudulent substrates. Therefore, nucleoside analogs used in anticancer therapy are classified as anti-metabolite drugs. The therapeutic gain of cytotoxic NA treatment derives from the differences in division and replication rates of rapidly proliferating tumor vs. normal somatic cells.

In order to unfold their therapeutic potential, NAs have to pass the cell membrane and become activated by mono-, di- and triphosphorylation by intracellular nucleoside and nucleotide kinases (Parker, 2009). Cellular uptake can occur by passive diffusion or by active transport via membrane proteins of the human concentrative and equilibrative nucleoside transporter families (hCNT and hENT respectively). Human cells possess four principal deoxyribonucleoside kinases that can perform the initial monophosphorylation of nucleosides. These are deoxycytidine kinase (dCK), thymidine kinases 1 & 2 and deoxyguanosine kinase (Arner and Eriksson, 1995). Adenosine kinase can be considered as a fifth deoxyribonucleoside kinase, as it was found to phosphorylate deoxyadenosine and several purine analogs (Hershfield, 1982; Cory and Cory, 1994). The nucleoside kinase which is critical for the initial activation of most NAs in cancer therapy is dCK.

Many purine- and pyrimidine analogs have been tested for or are currently in clinical use in cancer therapy. Purine analogs include 6-mercaptopurine (6-MP), 6-thioguanine, cladribine, clofarabine, deoxycoformicin (pentostatin), nelarabine, 9- β -D-arabinofuranosyladenine (ara-A) and 9- β -D-arabinofuranosyl-2-fluoroadenine (fludarabine or F-ara-A). Pyrimidine analogs include 5-fluorouracil (5-FU), capecitabine (a 5-FU prodrug), 5-aza-2-deoxycytidine (decitabine), 1- β -D-arabinofuranosylcytosine (cytarabine or ara-C), and 2',2'-difluorodeoxycytidine (gemcitabine or dFdC) (Miser, 1992; Galmarini, 2002; Hajdo, 2010). Several other nucleoside analogs like sapacitabine (CNDAC) and troxacitabine are currently in development or being evaluated in clinical trials (Szafraniec, 2004). In their diversity NAs comprise one of the largest classes of cancer therapeutics (Parker, 2009).

NAs often differ from each other or the natural nucleosides they resemble only by small modifications like single substitutions (e.g. a halogenation) or sugar isomery (e.g. arabinoside NAs) (Figure 1). Despite the structural likeness among NAs there is a remarkably high variance in clinical activities between different of these molecules (Ewald, 2008). Ara-C and Fludarabine for example are both extensively used in the treatment of hematological malignancies, but display little action against solid tumors (ara-C against acute lymphoid leukemia [ALL] and acute myeloid leukemia [AML]; fludarabine against chronic lymphoid leukemia [CLL], AML or non-Hodgkin lymphoma [NHL])(Chun, 1991). Gemcitabine on the other hand has been found to be effective (as a single treatment or together with platinum agents) in the treatment of a number of solid malignancies including non-small cell lung cancer, pancreatic cancer, breast and bladder cancer, while also displaying some activity against hematological malignancies (Jordheim, 2013). 5-FU and its pro-drugs (capecitabine, floxuridine) show activity against a number of solid tumor types, including breast, head and neck and most notably colorectal cancers (Longley, 2003), but find seldom use against hematological malignancies (Pardee, 2012).

This surprisingly high selectivity of structurally similar drugs may on one hand be explained by differences in the uptake, concentration and activation of individual drugs in different cellular compartments, and on the other hand by mechanistic differences of

their actions. The former conditions can arise from differences in the expression of transporters and activating or inactivating enzymes between tissues and lineages. Regarding mechanisms of NA cytotoxicity the interference with cellular replication is a common denominator between most NAs, but further activities also play a role. These include inhibition of RNA synthesis, deregulation of nucleotide pools by inhibition of ribonucleotide reductase (RnR), inhibition of nucleotide biosynthesis, induction of apoptosis, reduction of DNA methylation and induction of DNA damage (Consoli, 1998; McGinn and Lawrence, 2001; Galmarini, 2002; Ewald, 2008; Liu, 2012b).

We wanted to focus our study on the effects of ara-A and ara-C and the fluorinated derivatives fludarabine and gemcitabine (Figure 1). In the following section the cellular metabolism and known modes of action of these NAs are summarized.

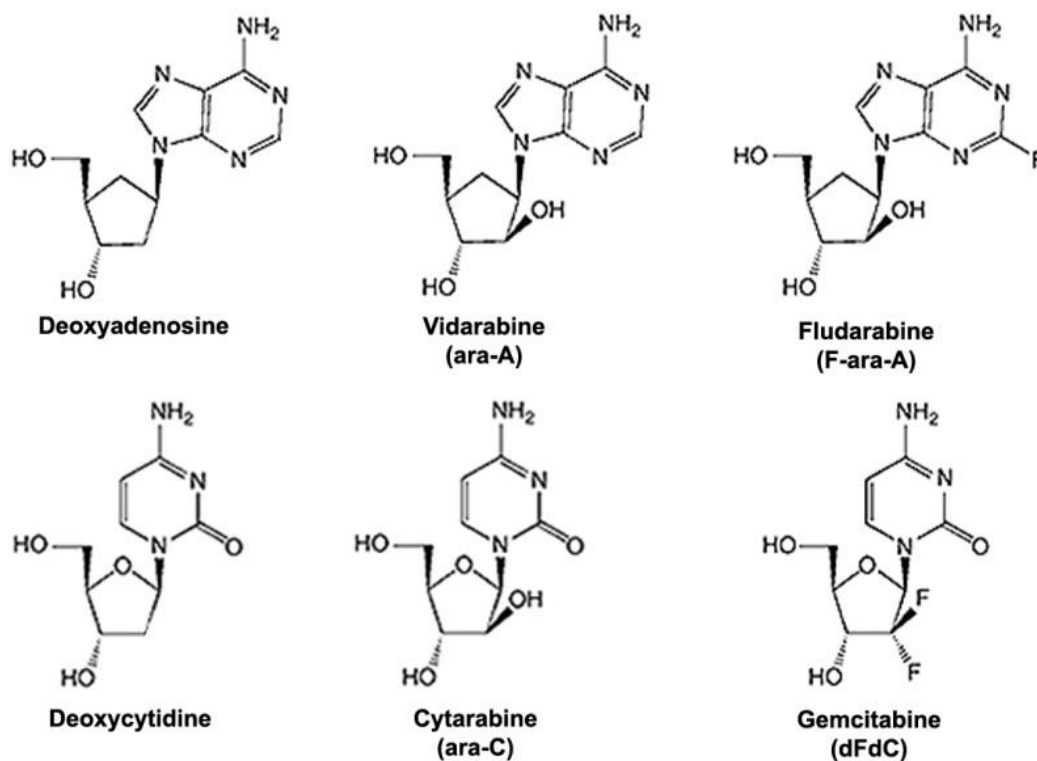


Figure 1 Chemical structures of selected nucleoside analogs. Structures of deoxyadenosine and deoxycytidine and their analogs ara-A, fludarabine, ara-C and gemcitabine.

1.2.2 Cellular metabolism and modes of action of NAs used in this study

1.2.2.1 Ara-A

Ara-A is a functional analog of deoxyadenosine. that is incorporated into DNA, but not RNA (Kufe, 1983). Ara-A differs from deoxyadenosine by having arabinose as sugar moiety instead of deoxyribose. Arabinose is an isomere of ribose in which the 2' hydroxyl group on the furanosyl ring is in β instead α configuration (Hubeek I, 2006).

Adenosine kinase has been implicated as the activating enzyme that performs the initial phosphorylation of ara-A within the cell, which is uncommon for NAs (Chan and Juranka, 1981; Cass, 1983). However, ara-A has also been reported to be a minor substrate for dCK and deoxyguanosine kinase (Arner and Eriksson, 1995). Ara-A is quickly deaminated by adenosine deaminase (ADA) in cells or plasma resulting in fast deactivation (Lepage, 1975; Tanaka, 1984).

Ara-A effectively inhibits DNA, but not RNA synthesis. In DNA synthesis ara-A is not a definitive chain terminator and most ara-A nucleotides are found in internucleotide linkages at lower concentrations, while the proportion of ara-A at terminal positions appears to increase with rising concentrations (Plunkett, 1974; Muller, 1975; Kufe, 1983; Ohno, 1989). It has been demonstrated, that ara-A inhibits the DNA polymerases α and β (Dicioccio and Srivastava, 1977). It is also a very potent inhibitor of DNA primase, which synthesizes RNA primers during replication and forms a complex with polymerase α (Kuchta and Wilhelm, 1991). Additionally, ara-A has been shown to inhibit RnR, whereby it may modify the balance of nucleotide pools in the cells, which is expected to further contribute to inhibition of replication (Moore and Cohen, 1967; Chang and Cheng, 1980).

1.2.2.2 Fludarabine

The development of fludarabine resulted from the search for a deamination resistant derivative of ara-A (Montgomery and Hewson, 1969). Fludarabine is not a substrate for ADA and thus is metabolically more stable (Brockman, 1977). Fludarabine shares a

number of similarities with ara-A regarding its mode of action, but there are also some remarkable differences.

An important difference exists regarding the activation of the two NAs. The initial phosphorylation steps of fludarabine and ara-A seem to be catalyzed by different enzymatic activities as cells deficient for dCK show strongly increased resistance against fludarabine while remaining relatively sensitive to ara-A (Dow, 1980; Cory and Cory, 1994). Thus fludarabine, in contrast to ara-A is mainly activated by dCK.

Like ara-A, fludarabine is incorporated into DNA, but unlike ara-A fludarabine appears to be a veritable chain terminator (Huang, 1990). Also unlike ara-A, fludarabine is incorporated into RNA (Huang and Plunkett, 1991). Similar to ara-A, fludarabine does inhibit the DNA polymerases α and β , as well as DNA primase (White, 1982; Catapano, 1993). Another mechanism that is likely to contribute to the impact of fludarabine on replication is inhibition of Ligase1, which has not been found for ara-A (Yang, 1992). Fludarabine has also been shown to inhibit RnR, but to be at least 10 fold as effective as ara-A in doing so (White, 1982).

1.2.2.3 Ara-C

Ara-C, like ara-A, is an arabinoside NA in which the deoxyribose sugar (deoxyribofuranose) has been replaced by a β -D-furanosylarabinoside ring (Figure 1). It is a structural analog of deoxycytidine. Like other NAs, it needs to be converted to an active metabolite upon cellular uptake.

Transport into the cell is mainly achieved through hENT at plasma concentrations achieved during standard treatment (0.5 -1 μ M), but mainly occurs by passive diffusion at the concentrations of around 100 μ M that are achieved during high dose ara-C treatment (Early, 1982; Liliemark, 1985; Hubeek I, 2006). The initial step in activation of ara-C is phosphorylation by dCK. Through consecutive phosphorylation by mono- and diphosphate kinases, Ara-CMP is ultimately converted to the active metabolite ara-CTP.

Ara-CTP is incorporated into DNA and causes strong inhibition of DNA synthesis. This inhibition is thought to be elicited by a mechanism of relative chain termination, since

most ara-CMP residues are found in internucleotide linkages (Graham and Whitmore, 1970), although higher concentrations of ara-C seem to increase the proportion of ara-CMP nucleotides in terminal positions (Ohno, 1988). Ara-CTP is a weak competitive inhibitor of DNA polymerase α and to a lesser extent of polymerase β (Matsukage, 1978; Miller and Chinault, 1982). Incorporation of ara-CMP into RNA is barely detectable (Kufe, 1980), but there are reports that show inhibition of RNA synthesis by ara-C (de Vries, 2006), which may take place by an inhibition of RNA polymerase without requiring incorporation (Chuang and Chuang, 1976). Unlike the other NAs used in this study, ara-C is not an inhibitor of RnR (Moore and Cohen, 1967).

1.2.2.4 Gemcitabine

Gemcitabine (2'-difluoro-2'-deoxycytidine or dFdC) is a halogenated cytidine analog (Hertel, 1988). It is different from most other halogenated NAs in that the fluorine substitutions are located on the sugar ring instead of the base. Fluorination renders gemcitabine substantially more resistant to deamination than ara-C (Hertel, 1990). Similar to other NAs dFdC has to be converted into active metabolites upon entry into the cell. The first and rate limiting step is phosphorylation performed by dCK. Subsequently gemcitabine is di- and triphosphorylated to dFdCDP and dFdCTP. dFdCTP is incorporated into DNA and to a lesser extent also into RNA by cellular polymerases (Vanhaperen, 1993). dFdCDP is a potent inhibitor of RnR (Heinemann, 1990). The resulting depletion of deoxynucleotide pools contributes to replication inhibition by gemcitabine. It also represents a self-potentiating mechanism of this drug, as reduction of dCTP levels result in increased incorporation of gemcitabine into DNA.

Another self-potentiating mechanism is inhibition of dCMP deaminase by dFdCTP, an enzyme capable of deactivating gemcitabine (Heinemann, 1992). A third self-potentiating mechanism is present at high concentrations of dFdCTP, which lead to inhibition of CTP synthetase. This further contributes to dCTP depletion and the accompanying increase of dFdCTP incorporation. Once a gemcitabine nucleotide is incorporated into DNA only a single further nucleotide is added to the chain, then elongation stops (Huang, 1991). The proofreading function of DNA polymerase ϵ is

essentially unable to remove the incorporated dFdCMP. This mode of disruption of DNA synthesis has been termed “masked chain-termination” (Plunkett, 1995).

The intracellular half-life of Gemcitabine is exceptionally long compared to most other NAs (Plunkett, 1995). Long half-life, the unusual mode of chain termination and the multiple self-potentiating mechanisms of Gemcitabine may partially explain why it is more effective in solid tumors than many other NAs (Shewach DS, 2006).

1.3 Radiotherapy and the effects of Ionizing radiation

1.3.1 Tumor and normal tissue response to IR

Radiotherapy uses IR to efficiently eradicate tumor cells in a localized, non-invasive way that also allows the treatment of growths that are difficult to resect. A critical parameter limiting the use of radiotherapy is the risk for the occurrence of acute or late side effects like erythema and edema or fibrosis in normal tissue. The incidence and severity of such side effects depends on radiation dose and the radiosensitivity of the irradiated normal tissue. There is a strong correlation between the turnover rate of an irradiated tissue and its radiosensitivity (Begonie, 1906). Fast growing tissues like mucosa are very radiosensitive, while tissues with low mitotic rates like the central nervous system or skeletal muscles are less radiosensitive.

Similarly, rapidly dividing tumor cells also show higher susceptibility towards killing by IR than the surrounding healthy tissue which, depending on the location, usually consists mainly of mitotically inactive, terminally differentiated cells (Hall and Giaccia, 2006). This connection between growth rate and radiosensitivity forms one of the fundamentals of radiotherapy.

Despite this growth rate dependent difference in radiosensitivity, the total doses that are required for curative therapy are so high that they would lead to intolerably high normal tissue damage, if administered as a single dose. This was a major problem in the beginnings of radiotherapy, and side effects were often severe. Reduction of these side effects was and is the main reason to break down the total radiation dose into smaller

portions, so called fractions (Connell and Hellman, 2009). Modern external beam radiotherapy is given almost exclusively as fractionated radiotherapy. Indeed, the risk for side effects can be substantially reduced by fractionation. However, even under these conditions side effects are not completely abolished, and the probability of occurrence strongly depend on the type of tissue in the radiation field (West and Barnett, 2011). Decades of extensive radiobiological research and experiences with fractionation have led to the formulation of some key principles, the so called four Rs of radiotherapy (Withers, 1975), which try to rationalize the advantages gained by fractionation with several distinct, but potentially cooperative mechanisms: repair, redistribution, repopulation and reoxygenation.

Repair refers to the capacity of cells to repair so called sub-lethal damage (SLD) between fractions of radiation, which improves their chance of survival. This “R” is the factor that led to the initial development of fractionated irradiation schemes, since they allow delivery of total doses that would intolerably damage surrounding healthy tissue when given as a single dose. It is usually assumed that normal cells repair SLD better than tumor cells, resulting thus in a net benefit for the patient.

Redistribution of irradiated cells in the cell cycle also occurs between fractions. When tumor tissue is irradiated, cells are hit in all phases of the cell cycle. Cells show strong variations in their radiosensitivity depending on the cell cycle phase they are in. Commonly the radioresistance increases during S-Phase and is lowest for cells in M-Phase (Tamulevicius, 2007). There is evidence that these differences are related to cell cycle dependent regulation of the activity of different DSB repair pathways (Rothkamm, 2003; Tamulevicius, 2007). Upon irradiation cells in sensitive phases of the cycle are killed preferentially. Surviving cells in resistant phases progress through the cell cycle and reach more sensitive phases, where they can be eradicated more efficiently by the subsequent dose fraction.

Besides redistribution of tumor cells, the allowed intervals between fractions may give normal tissues and tumors time to refill their ranks. Inactivation of cells during radiotherapy is often compensated by an increase in the mitotic activity of the tumor.

This repopulation has to be taken into account and potentially counteracted to ensure success of radiation therapy.

While position in the cell cycle is a cell intrinsic determinant of radiosensitivity, a well-known cell extrinsic factor for a cell's susceptibility to killing is the oxygenation status. Hypoxic regions of tumors are known to be more resistant to radiation than regions that lie close to blood vessels and are therefore well oxygenated. This phenomenon is known as the oxygen effect. A popular explanation for this effect is the Oxygen fixation hypothesis (Ewing, 1998; Bertout, 2008) that postulates that Oxygen di-radicals can act as a fixating agent for DNA lesions induced by IR. After irradiation, cells in better oxygenated regions of the tumor will be killed preferentially. Cells located more distant from blood vessels can now move in into more oxygen rich regions and become oxygenated - or alternatively new blood vessels can form. This development leads to reoxygenation of formerly hypoxic cells enabling more efficient killing of cells during later fractions.

The correlation of mitotic activity and susceptibility to killing, as well as the four "Rs" can help to explain many of the effects of IR in fractionated radiotherapy – both the beneficial action on tumor cells and the partial protection of normal tissue. However, radiosensitivity does not only differ between tissues types, but there is also variability between the same tissues from different patients and between different tumors of the same or similar type (Deacon, 1984; Tucker and Thames, 1989). In cases where growth rate and architecture of tissues or tumors under study are similar, differences in radiosensitivity have to derive from other factors. These individual differences are referred to as intrinsic radiosensitivity (Roberts, 1999; West and Barnett, 2011). Intrinsic cellular radiosensitivity has been shown to be an important factor underlying cell killing by IR and the radioresponse of tumors (Fertil and Malaise, 1981; Deacon, 1984; Steel, 1989; Tucker and Thames, 1989; Gerweck, 2006).

1.3.2 Repair of potentially lethal damage

In the context of radiobiology cell death refers to the mitotic inactivation of treated cells. The sensitivity of cells to killing by IR can be assessed *in vitro* in clonogenic colony

formation assays (Hall and Giaccia, 2006). In these experiments the reproductive potential of cells is assessed at the single cell level. Loss of this potential can be realized via different routes including mitotic catastrophe, senescence, autophagy, apoptosis or necrosis (Balcer-Kubiczek, 2012). The contribution of these mechanisms or pathways to cell killing differs among cells and depends on factors like cell type and radiation dose (Puck and Marcus, 1956; Held, 1997). Apoptosis as an immediate response to radiation (interphase death) for example plays a decisive role only in a small number of cellular systems, e.g. lymphocytes (Ross, 1999). Mitotic catastrophe is considered to be a main route to cell death after IR in most systems, but may not be a genuine pathway of cell death itself. Instead cells running into mitotic catastrophe may eventually die, i.e. cease to proliferate, by any of the other pathways mentioned above (Galluzzi, 2012).

Analysis of cells exposed to increasing doses of IR yield characteristic survival curves (Figure 2). Various treatments or conditions can result in modification of the radiosensitivity of cells in this assay, e.g. the oxygenation status (see above). Post-treatment conditions that can modify the survival of irradiated cells are assumed to exert their effects through either repair or fixation of damage that is only potentially lethal (Phillips and Tolmach, 1966) (Little, 1969; Iliakis, 1988a).

A classic experiment can be performed with cells in the plateau, or stationary phase, of growth. When these cells are irradiated they can be plated as single cells in fresh growth medium either immediately after irradiation (immediate plating) or at increasing periods of time after irradiation (delayed-plating). Plating in fresh, serum supplemented growth medium results in the re-entrance of cells into the cell cycle and their progression through S-Phase, which is also a prerequisite for colony formation. Delayed plating occasionally has a profound impact on the survival of cells. Cells that are plated immediately after irradiation exhibit the lowest survival levels. If plating is delayed for longer times (e.g. 6-24h) the cells display more radioresistance (Figure 2). This phenomenon is ascribed to the repair of potentially lethal damage (PLD). Incubation of cells in their resting state apparently allows the repair of some PLD which is inhibited when cells are stimulated to reenter the cell cycle by immediate plating.

This experimental setup can be used to test a condition or treatment, e.g. incubation with a drug, for its potential to interfere with the repair of PLD by its ability to prevent the increase in survival normally associated with delayed plating. A variety of treatments has been identified that are able to inhibit repair of PLD. Notably, these include NAs like ara-A (Figure 2). When this approach is used, repair of PLD and its inhibition is measured in non-cycling cells. However, PLD repair also occurs in actively cycling cells and is assumed to contribute to the cell cycle dependent fluctuations in radiosensitivity to killing (Iliakis and Nusse, 1983b; Stamato, 1988). Similarly, differences in the intrinsic radiosensitivity of cells can be interpreted as differences in their capability to repair PLD. The precise molecular nature of the lesion/s underlying PLD remains to be fully characterized.

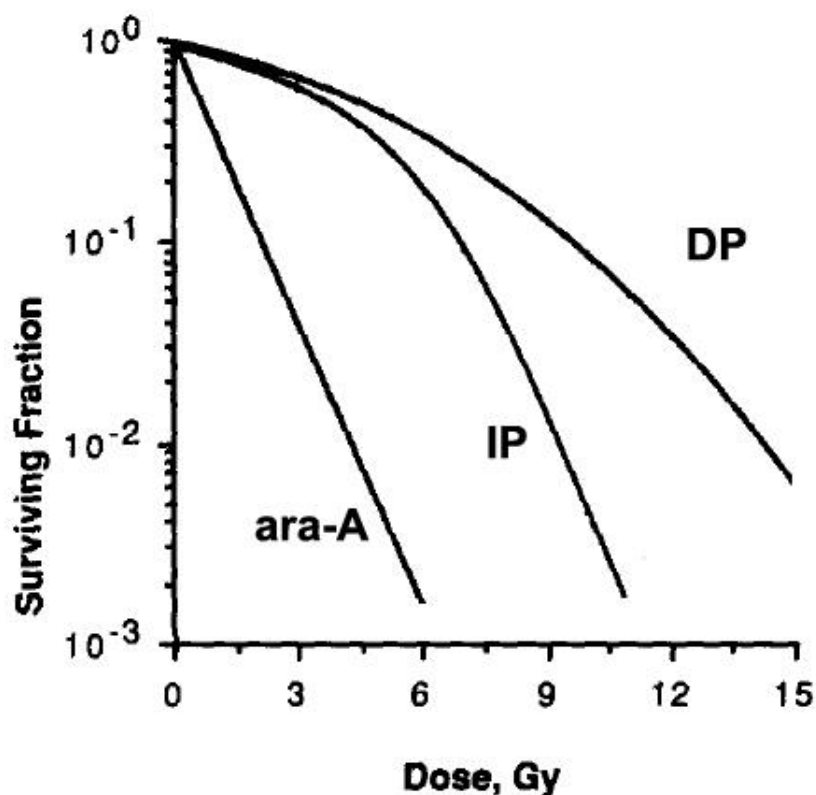


Figure 2 Repair of potentially lethal damage. Survival curves of plateau-phase cells plated either immediately (IP) or after prolonged incubation in the plateau-phase (DP) after irradiation. Also shown is the survival of cells treated with ara-A at concentrations that cause maximum fixation of PLD during incubation in plateau-phase before delayed plating,

In order to understand the repair or fixation of which type of lesion/s may underlie phenomena like the fluctuations of radiosensitivity during the cell cycle, intrinsic cellular radiosensitivity and PLD repair it is necessary to take a look at the physical mechanisms of damage induction by IR and the associated cellular responses on a molecular level.

1.3.3 Basic physics of the interaction of IR with biological matter

Damage to the DNA is the source for the prominent biological effects that can be observed after exposure to IR. These effects include mutation, chromosome aberration, neoplastic transformation, mitotic inactivation and cell death. IR is particularly efficient in inducing lesions that lead to the formation of chromosome aberrations. Excellent correlations have been found for the induction of chromosome aberrations and cell killing as well as the repair of chromosome breaks and PLD repair (Carrano, 1973; Virsik and Harder, 1980; Cornforth and Bedford, 1987).

Ionizing radiation (IR) is highly energetic radiation that is characterized by its potential to expel electrons from atomic shells or chemical bonds. The different types of IR that exist can be categorized into particulate and electromagnetic radiation. Particulate IR includes α (Helium nuclei) and β (electrons) radiation, as well as any other particle that carries sufficient kinetic energy to ionize other atoms (e.g. accelerated neutrons, protons or heavy ions). X-rays and γ -rays represent the electromagnetic forms of IR. Since all experiments in this work were exclusively carried out with X-rays we will focus mostly on this form of radiation.

X-rays consist of high energy photons that can ionize atoms as a consequence of interactions with orbital electrons. At photon energies that are used in radiation therapy (200 keV to 25 MeV) a process called Compton scattering is the predominant interaction process in soft tissue (Hall and Giaccia, 2006). When this type of interaction takes place, only part of the photon's energy is absorbed by the interacting electron, resulting in expulsion of the electron from its shell. The remaining energy is carried away by a scattered photon. Electrons that have been liberated by interaction with a photon travel through the surrounding medium and can cause further ionizations. Those electrons (as

well as those produced by further interactions) are often referred to as secondary electrons, despite the fact that they represent the product of the primary ionization event. Secondary electrons account for the vast majority of ionizations caused by electromagnetic IR, which is thus considered as indirectly ionizing radiation. Since most of the energy is deposited in a disperse pattern, X-rays are also considered to be a sparsely ionizing radiation. This is in contrast to the pattern of energy deposition of radiation types like alpha particles or neutrons, which produce dense ionization tracks (Figure 3).

A measure for the density of ionizations generated by a particular form of radiation is provided by the physical quantity: linear energy transfer (LET [$\text{keV}/\mu\text{M}$]). Thus, sparsely ionizing radiations are often also referred to as low LET and densely ionizing radiations as high LET radiation. However, secondary electrons induced by X- or γ -rays lose energy during the interactions along their track. With decreasing velocity the interaction probability of such electrons increases. This causes an increase in LET associated with clustering of ionizations especially at the ends of their tracks (Goodhead, 1994).

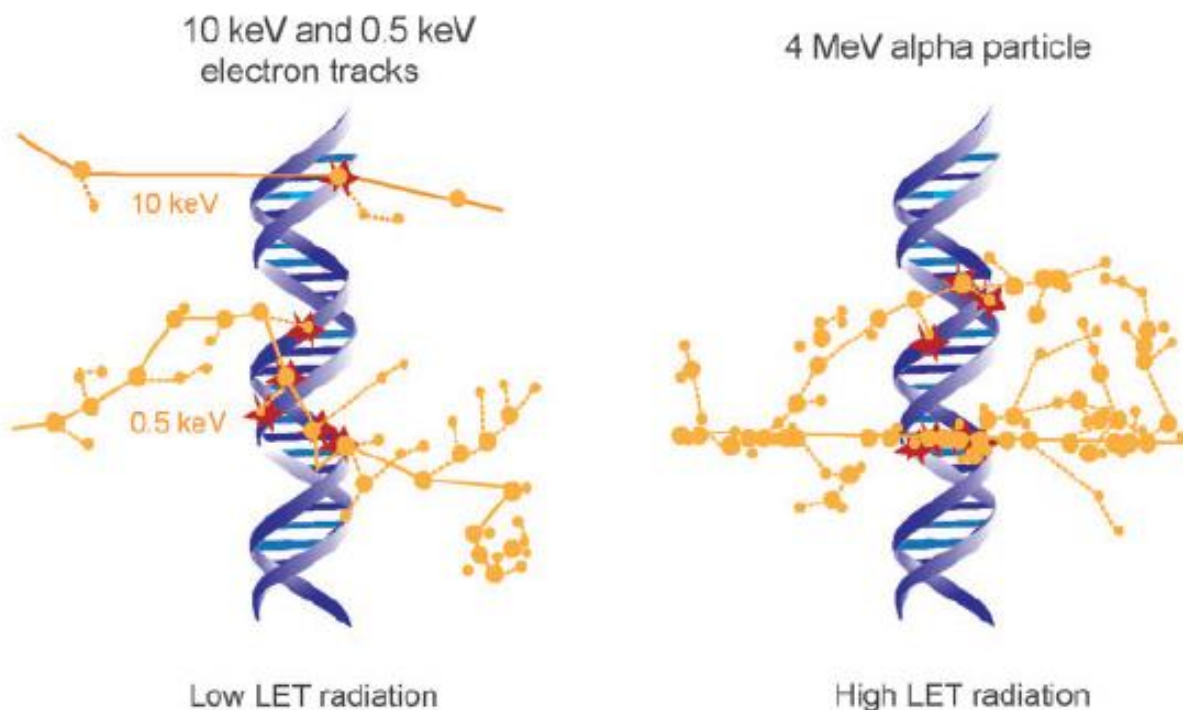


Figure 3 DNA damage induction by low and high LET radiation tracks. Ionization events caused by IR localize along radiation tracks and can induce clustered damage at the DNA. With increasing LET the

probability for DNA damage clustering increases. Large dots represent ionizations and small dots represent excitations along the radiation track. The Monte Carlo simulated tracks are drawn on the same scale as the DNA. (modified from (Schipler and Iliakis, 2013))

1.3.4 Mechanisms of DNA damage induction and types of DNA lesions induced

Ionization of atoms that take part in a molecular bond can result in the formation of free radicals. Radicals are highly reactive, short lived chemical species characterized by an unpaired valence electron. Production of radicals can take place directly in the target molecule (i.e. the DNA), which would be considered as direct effect. However, since a cell is composed of water to approximately 70% (Alberts, 2008) the majority of radicals generated initiate from H₂O (e.g. hydroxyl radicals). Consequently the majority of DNA damage induced by sparsely ionizing radiations is due to the indirect effect exerted by water produced free radicals. Due to the short life time of free radicals the probability of interaction with DNA is only significant when the radical forms in close proximity to the DNA molecule. The spectrum of chemical modifications induced in the DNA by radiation is highly diverse and includes oxidative damage to bases and sugars, cross-links between bases or between DNA and proteins and breaks in the sugar phosphate backbone. Breakage of the sugar phosphate backbone on both strands of the double helix within a couple of nucleotides will lead to the formation of a double-strand break (DSB). Accumulation of ionizations in small volumes, as it occurs at the end of secondary electron tracks, increases the likelihood of the induction of multiple damages in short sequence stretches. Such sites of accumulated damage are being referred to as multiply damage sites or clustered DNA damage. Clustering of ionizations increases the probability of induction of two or more single-strand breaks (SSB) in close proximity, thereby increasing the chances for the generation of a DSB. However, DSB are not a uniform class of damage. Instead the term subsumes a variety of chemically different entities, which will be briefly reviewed in the next paragraphs.

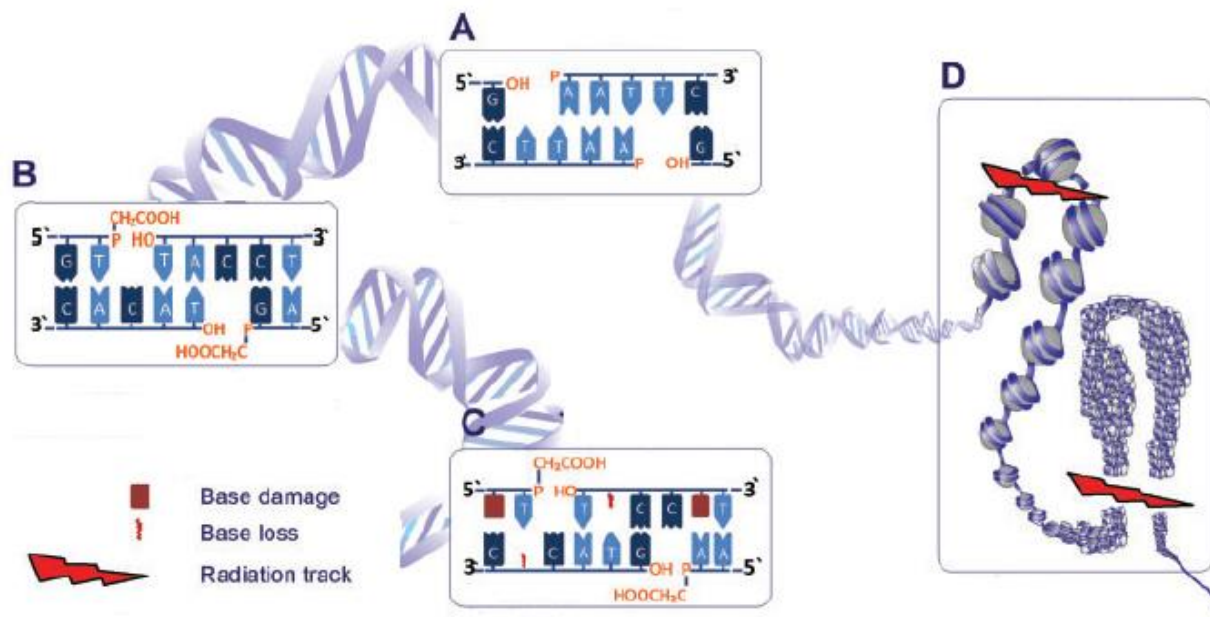


Figure 4 Types of DSB with different levels of complexity **A)** DSB induced by a RE with a 5'-phosphate and a 3'-OH group. **B)** DSB induced by IR frequently comprise a 3' phosphoglycolate and a 5'-OH. **C)** DSB induced by IR that comprises also other types of lesions like base damages or base loss in close proximity to the DSB. **D)** Clusters of multiple DSBs. Two examples are shown: On the left, a single radiation track induces two DSBs in the linker regions of a nucleosome leading to loss of the nucleosome. On the right, a higher order packaging of nucleosomes is illustrated. Chromatin loops can be severed by a single radiation track if hit appropriately. (modified from (Schipler and Iliakis, 2013))

1.3.5 Different types of DSB and damage complexity

The simplest type of DSB that can be envisaged is the one induced by a restriction endonuclease (Figure 4 A). No further damage is involved and the ends of the DSB are equipped with intact 3'-OH and 5'-phosphate groups that can readily be religated. However, this type of clean break cannot be expected to be found after exposure to IR. Instead, DSB induced by IR usually contain modified ends, e.g. 5'-OH and 3'-phosphoglycolate groups, as illustrated in Figure 4 B. In addition, for a proportion of DSB induced by IR further types of damage are to be expected in the vicinity of the break (Figure 4 C). DSB in conjunction with additional DNA lesions are usually referred to as complex DSB. An additional level of complexity can be added by clustering of multiple

DSB, which may lead to loss of nucleosomes or entire chromatin domains (Schipler and Iliakis, 2013). The list of different DSB types presented here is by no means complete and is further complicated by the existence of indirect DSB that can develop from IR-induced non-DSB lesions by enzymatic processing or thermal evolution (Singh, 2009; Singh, 2013). Computational modelling yields distinct ratios for various DSB types as a function of radiation quality. In general, with increasing LET of radiation the complexity of damage induced in the DNA increases (Nikjoo, 1999; Friedland, 2012). Importantly, cellular survival decreases with increasing LET (Figure 5). These observations create a close link between DSB, damage complexity and cell killing.

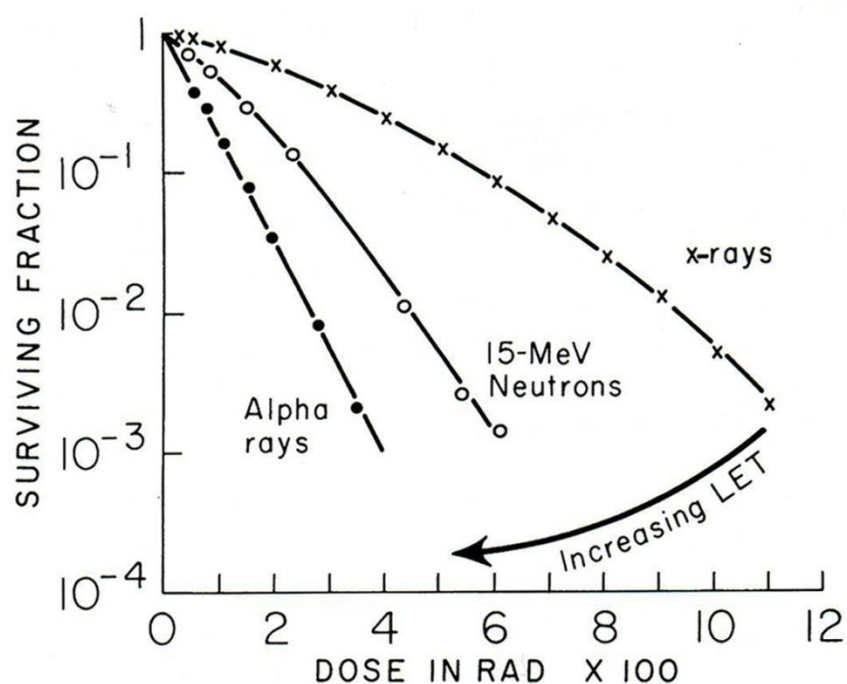


Figure 5 Survival curves for cultured cells of human origin Human cells were exposed to 250 kV X-rays, 15 MeV neutrons and 4 MeV α -particles. Survival curves obtained with neutrons and alpha rays have steeper slopes and a smaller initial shoulder than curves generated with x-rays. (modified from (Hall and Giaccia, 2006))

DSB threaten the integrity of chromosomal DNA and undermine the fundamental principle of DNA repair as both strands of the helix are disconnected and no intact strand is available for repair. In contrast, SSB or base damages don't compromise the continuity of the DNA molecule and the complementary strand of the double helix can serve as repair template. Although conceptually the repair of DSB is particularly difficult,

actually recognition and repair of DSB is in higher eukaryotic cells faster and more efficient than of many other DNA lesions (Eriksson, 2007; Schieler and Iliakis, 2013) (see also Figure 6). Cells have evolved elaborate mechanisms to correct and repair DSB. However, complex DSB consisting of multiple different types of damage pose particularly demanding challenges to the cellular repair machinery. The involvement of several steps of processing and the potential participation of multiple pathways of DNA repair is likely to be associated with a higher risk of accidents. It is now widely believed that the induction of complex DSB is a key aspect of IR, underlying the effective induction of chromosomal aberrations and cell killing (Goodhead, 1994; Schieler and Iliakis, 2013). The chemical nature of a DSB and its complexity may also be factors participating in the determination of repair pathway choice. In the following paragraphs the key events of the cellular response to DSB induction will be described

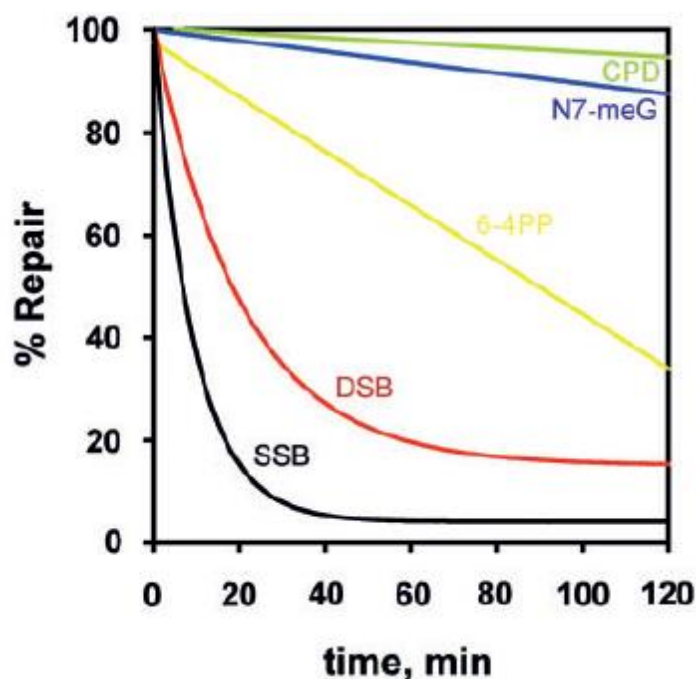


Figure 6 Repair kinetics of different forms of DNA damage Shown is the kinetics of removal of SSBs, DSBs, 6–4 photoproducts (6–4PP), cyclobutane pyrimidine dimers (CPD) from CHO-AA8 cells. Kinetics of N7-meG comes from measurements in human lymphocytes. (from (Schieler and Iliakis, 2013))

1.4 Cellular responses to DSB

1.4.1 DSB detection and signaling- The DNA damage response

Induction of a DSB initiates a cascade of posttranslational protein modifications (PTMs) that signal to the cellular repair and cell cycle control machineries (Grabarz, 2012). The events elicited by this DNA damage response (DDR) include changes in chromatin, in gene expression, the relocation of a large number of proteins, the regulation of DNA repair and the activation of cell cycle checkpoints (Bekker-Jensen and Mailand, 2010). The molecular components of the DDR can be categorized into damage sensors, transducers, mediators and effectors. The recruitment and activation of factors involved in DDR follows a hierarchical order beginning with the recognition of DSB. Candidates for the function of primary damage sensors are the MRE11-RAD50-NBS1 complex (MRN), the KU70/KU80 heterodimer (KU) as well as the Poly(ADP-ribose) polymerases 1 (PARP1) (Wang, 2006b; Polo and Jackson, 2011). All of these proteins and complexes are capable of binding to DSB ends and are among the first proteins that recruited to the breaks (Polo and Jackson, 2011) (Figure 7). The MRN complex can tether DSB ends by binding with its globular domains comprised of the dimerized RAD50 and MRE11 subunits (Lavin, 2007; Williams, 2008). KU is highly abundant in the cell and displays extraordinarily high affinity for dsDNA end. PARP1 becomes directly activated by binding to DNA breaks and start to poly(ADP-ribosylate) substrate proteins (D'Silva, 1999; Kun, 2002). Any of those putative damage sensors is also strongly implicated in other processes related to DNA repair, e.g. DNA end-resection (MRN), non-homologous end-joining (KU) and SSB repair (PARP). Most models in the literature ascribe the role of the major DSB sensor to MRN, although KU and PARP1 arrive earlier at breaks and MRN recruitment is modulated by PARP1 (Haince, 2008; Polo and Jackson, 2011).

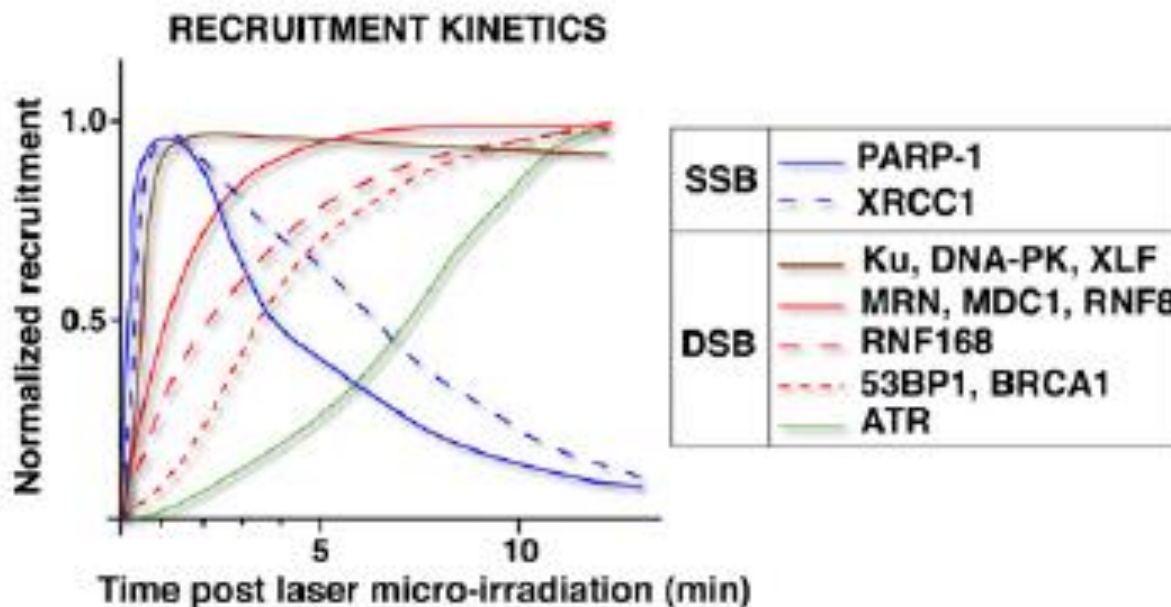


Figure 7 Recruitment kinetics of proteins involved in the DDR Sequential recruitment of DDR factors to SSBs and DSBs generated by laser microirradiation. (from (Polo and Jackson, 2011))

On the next hierarchical level, the role of the signal transducers is taken by three members of the family of phosphatidylinositol 3-kinase related kinases (PIKKs). Among those the ataxia telangiectasia mutated kinase (ATM) has emerged as a master kinase in IR induced DDR signaling. ATM is activated in response to DSB in a MRN dependent manner (Uziel, 2003). In its inactive form ATM persists as a dimer in the cell, which dissociates upon intermolecular autophosphorylation at Serine 1981 (pS1981) in response to DSB (Bakkenist and Kastan, 2003). The DNA-dependent protein kinase catalytic subunit (DNA-PKcs) is another member of the PIKK family that becomes activated in response to DSB. Together with KU it forms the DNA dependent protein kinase (DNA-PK) that plays a central role in the non-homologous end-joining pathway of DSB repair. It is capable of phosphorylating a number of important targets involved in DSB signaling, repair and chromatin structure, but possesses a substantially smaller substrate spectrum than ATM (Stiff, 2004; Tomimatsu, 2009). ATM and Rad3 related kinase (ATR) is a further PIKK involved in the DDR. ATR becomes not directly activated by DSB, but by single-stranded DNA (ssDNA). In conjunction with its partner ATRIP it binds to ssDNA coated with replication protein A (RPA). Thus, ATR activation in

response to DSB requires the resection of 5' strand of the dsDNA at the end of the break. Resection of DSB ends again is tightly regulated and highly depending on the cell cycle phase, as is explained in more detail below (1.4.2.3).

A number of mediator proteins help to maintain and amplify the signaling that is initiated by the transducer kinases. One of the first posttranslational modifications in response to a DSB is phosphorylation of the histone variant H2AX, on Serine 139. This phosphorylation can be mediated by ATM and DNA-PKcs and likely also by ATR (Stiff, 2004; Ward, 2004; Wang, 2005c). In its phosphorylated form the histone variant is termed γ H2AX (Rogakou, 1998). γ H2AX spreads to both sides of the DSB covering the region around the break up to a length of a few megabases (Nakamura, 2010). It provides a binding platform for the mediator of DNA damage checkpoint protein 1 (MDC1) (Stucki, 2005). MDC1 constitutively interacts with the MRN complex (Spycher, 2008) and can also interact with ATM. Thereby, MDC1 binding to γ H2AX leads to accumulation of these factors around DSB and contributes to stabilization and amplification of the damage signal. Phosphorylation of MDC1 by ATM also leads to the recruitment of the E3 Ubiquitin Ligase RNF8, which elicits ubiquitylation of a number of targets, including the histones H2A and H2AX. This in turn leads to the recruitment of RNF168, another E3 Ligase that mediates the polyubiquitylation of H2A (Bohgaki, 2010). Together these ubiquitylations have been implicated in the recruitment of BRCA1 and 53BP1, factors that play important roles in DSB repair pathway choice by regulating the resection of DSB ends (Stewart, 2009; Bunting, 2010; Escribano-Diaz, 2013).

The multiple PTMs and accumulations of proteins at damage sites that are part of the DDR can be visualized by immunofluorescence staining and microscopy. Staining with antibodies against γ H2AX, MDC1, ATM-pS1981, 53BP1 and many other proteins involved in the DDR and DSB repair reveals a pattern of focal protein accumulations in the nuclei of cells after exposure to IR. Measurement of induction and decay of these IR induced foci (IRIF) has been used extensively to investigate mechanisms and kinetics of DSB signaling and repair.

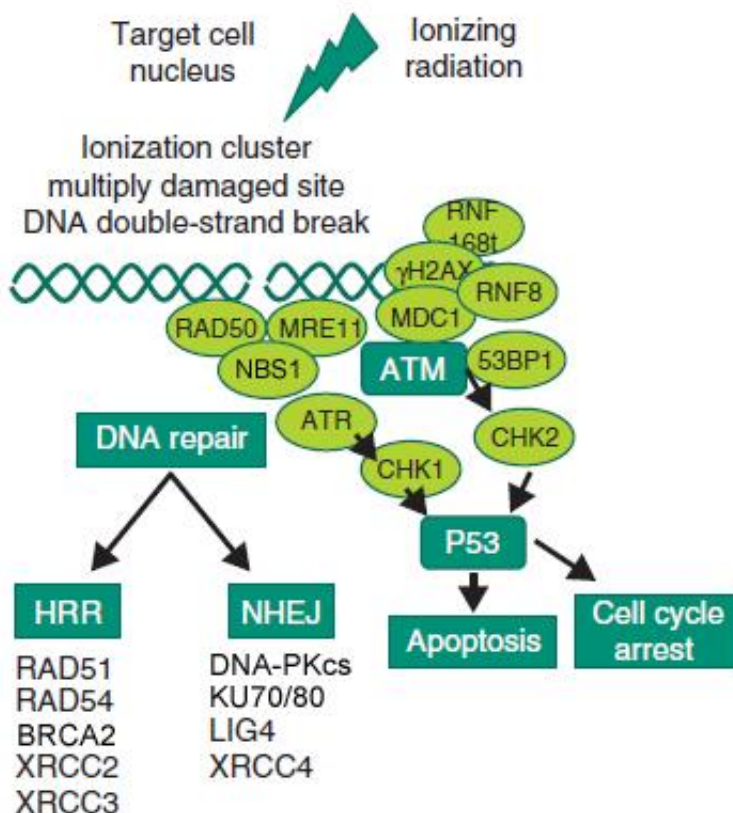


Figure 8 Simplified schematic of the cellular response to DSB Induction of a DSB triggers a complex cascade of events that results in signaling to the cellular DNA repair machinery and cell cycle checkpoint control. (modified from (West and Barnett, 2011))

One of the central functions of DDR is to cause cell cycle arrests that prevent cells with damaged genomes from progressing into subsequent phases. The pathways that elicit these arrests or delays in the progression through the cycle are called checkpoints. The main effectors of cell cycle checkpoints are the checkpoint kinases CHK1 and CHK2. ATM and Chk2, as well as ATR and CHK1 form two signaling modules that primarily coordinate checkpoint activation in response to DNA damage (Reinhardt and Yaffe, 2009). Both pathways converge on members of the CDC25 family of phosphatases. Inactivating phosphorylations placed on CDC25 by CHK1 and CHK2 prevent the removal of inhibitory phosphorylations on CDK/cyclin complexes that are critical for cell cycle progression. In addition, CHK2 phosphorylates p53 in response to DNA damage thereby contributing to the stabilization of this protein and the development of a G1 arrest (Chehab, 2000). Activation of p53 can also trigger the activation of apoptotic

pathways; however apoptosis plays an important role as a response to IR only in some cell systems (see below). The action of CHK1 on the other hand can arrest cells at the G2/M border via phosphorylation of CDC25C. DNA damage checkpoints prevent cells with excessive genetic damage from progressing through the cycle and thereby contributing to genomic stability. By halting cells in the current phase of the cell cycle, checkpoints provide time to the cellular repair machinery to deal with existing DNA lesions. In the following paragraphs the pathways of DSB repair are briefly described.

1.4.2 Mechanisms of DSB Repair in Eukaryotes

1.4.2.1 A short overview of DSB repair pathways

It is important to note that DSB and other DNA damages don't occur only as a product of exogenous insults like IR, radiomimetic drugs or topoisomerase inhibitors. The genome of a cell is in constant need for maintenance and repair due to attack by byproducts of its own metabolism, thermodynamic degradation of DNA or replication accidents. In addition DSB can be induced in a programmed manner by the cell as part of scheduled processes like the generation of antibody diversity (V(D)J recombination) or meiotic recombination. As a consequence eukaryotic cells have developed highly effective mechanisms for the management of DSB. Classically, the spectrum of DSB repair mechanisms is divided into two main categories: non-homologous end-joining (NHEJ) and homologous recombination repair (HRR). NHEJ operates throughout the cell cycle and rejoins the free ends of DSB with fast kinetics (Mao, 2008). NHEJ frequently introduces sequence alterations at the joints it generates. The chemical nature of DSB induced by IR usually necessitates some processing in order to generate ligatable ends (see Figure 4). In the case of repair by NHEJ loss or gain of bases at the molecular junction is the consequence of this processing. HRR on the other hand uses the intact sequence on a sister chromatid as template to faithfully restore the sequence around the break. The requirement of HRR for the availability of already replicated, homologous sequences restrict this repair pathway to the S- and G2- phases of the cell cycle. Since this type of repair involves search for homology, more extensive processing and synthesis, as well as the resolution of intermediary structures it is considered a slow

process in comparison to NHEJ. More recently other repair pathways, with varying fidelity and requirements for homology, have emerged diversifying the simplistic classification outlined above. Most notably, alternative pathways of NHEJ acting as backup (B-NHEJ) for the classical, DNA-dependent protein kinase (DNA-PK) dependent pathway of NHEJ (D-NHEJ), have been described. Next to different modes of HRR an additional homology directed repair process, single-strand annealing, exists as well, which uses intra-molecular homologies to seal DSB.

Although there is common consent that the majority of breaks are handled by D-NHEJ if this pathway is not compromised, an important contribution of HRR to the repair of DSB and the maintenance of genomic stability is undisputed as well. Importantly, there is a large body of evidence that suggests that HRR is the mechanism that underlies the S-Phase dependent radioresistance that can be observed in proficient cell lines (Iliakis and Nusse, 1983a; Wang, 2003b; Wang, 2004a). How the decision is made for a particular DSB to be repaired by one of the available pathways remains largely unknown, but may involve factors like lesion complexity or radiation dose. The most important DSB repair pathways and sub-pathways are described in more detail below.

1.4.2.2 D-NHEJ

D-NHEJ is considered to be the dominant pathway of DSB repair in mammalian cells, in contrast to yeast, where the dominant repair pathway is HRR (Mansour, 2008; Mao, 2008; Weterings and Chen, 2008). As indicated by its designation, it is dependent on the DNA-PK complex. This consists of the KU70/KU80 heterodimer (KU) and the large DNA-PK catalytic subunit (DNA-PK_{cs}). Unlike most other factors involved in D-NHEJ, DNA-PK_{cs} is not found in yeast and many other lower eukaryotes and is also absent in prokaryotes. This makes it tempting to speculate, that the development of the extremely fast and efficient form of NHEJ that is found in higher eukaryotes today was made possible by this evolutionary new protein. KU is a highly abundant protein in mammalian cells that binds with strong affinity to free DNA ends. Binding of KU to DNA ends results in the recruitment of DNA-PK_{cs} (Mladenov and Iliakis, 2011). This in turn leads to phosphorylation of multiple targets upon formation of the active holoenzyme, including

DNA-PKcs itself (Figure 9). These phosphorylations are an important step for the progression of the NHEJ process, and autophosphorylation of DNA-PKcs is believed to elicit conformational changes that allow for further steps to take place. Various factors like the polymerases μ and λ (Pol μ , Pol λ), the Artemis nuclease, terminal deoxynucleotidyl transferase (TdT) and polynucleotide kinase (PNK) are implicated in processing of DSB ends prior to rejoining by D-NHEJ (Mladenov and Iliakis, 2011). End processing by D-NHEJ usually stays limited as it only serves the cause of creating ligatable ends. Thus the extent of loss or addition of bases at junctions formed by D-NHEJ is usually relatively small (Lieber, 2010). The final ligation step is carried out by DNA Ligase IV (LIG4) aided by its interaction partners XRCC4 and XLF/Cernunnos (Figure 9).

Since D-NHEJ lacks a built-in mechanism to preserve the original sequence around the break site it is usually regarded as an error-prone repair process. Disregarding this error proneness, D-NHEJ is not an adverse process for the cell. On the contrary D-NHEJ is highly important for survival after irradiation and plays a crucial role in maintaining genome integrity and stability (Burma, 2006). Several arguments are conceivable to explain how it could have been advantageous for cells of higher eukaryotes to let an error prone repair pathway evolve to become the dominant mechanism of DSB repair. One might be that for large vertebrate genomes, which are rich in non-coding and repetitive sequences, there is a net-benefit in having an extremely fast pathway of DSB rejoining that quickly removes breaks before other accidents may occur, even if it comes at the cost of an elevated but manageable mutation rate. It is also possible that this beneficial role of D-NHEJ arises from suppression of other, more error prone pathways. Indeed, despite the conceptual capacity of D-NHEJ to rejoin unrelated ends it has been reported that components of the D-NHEJ pathway actively participate in suppressing chromosomal translocations (Simsek and Jasin, 2010).

Other nomenclature like “classical” or “canonical” NHEJ (cNHEJ) have been brought forward to name this repair pathway and discriminate it from alternative B-NHEJ pathways. In this work the term D-NHEJ will be used to refer to this pathway.

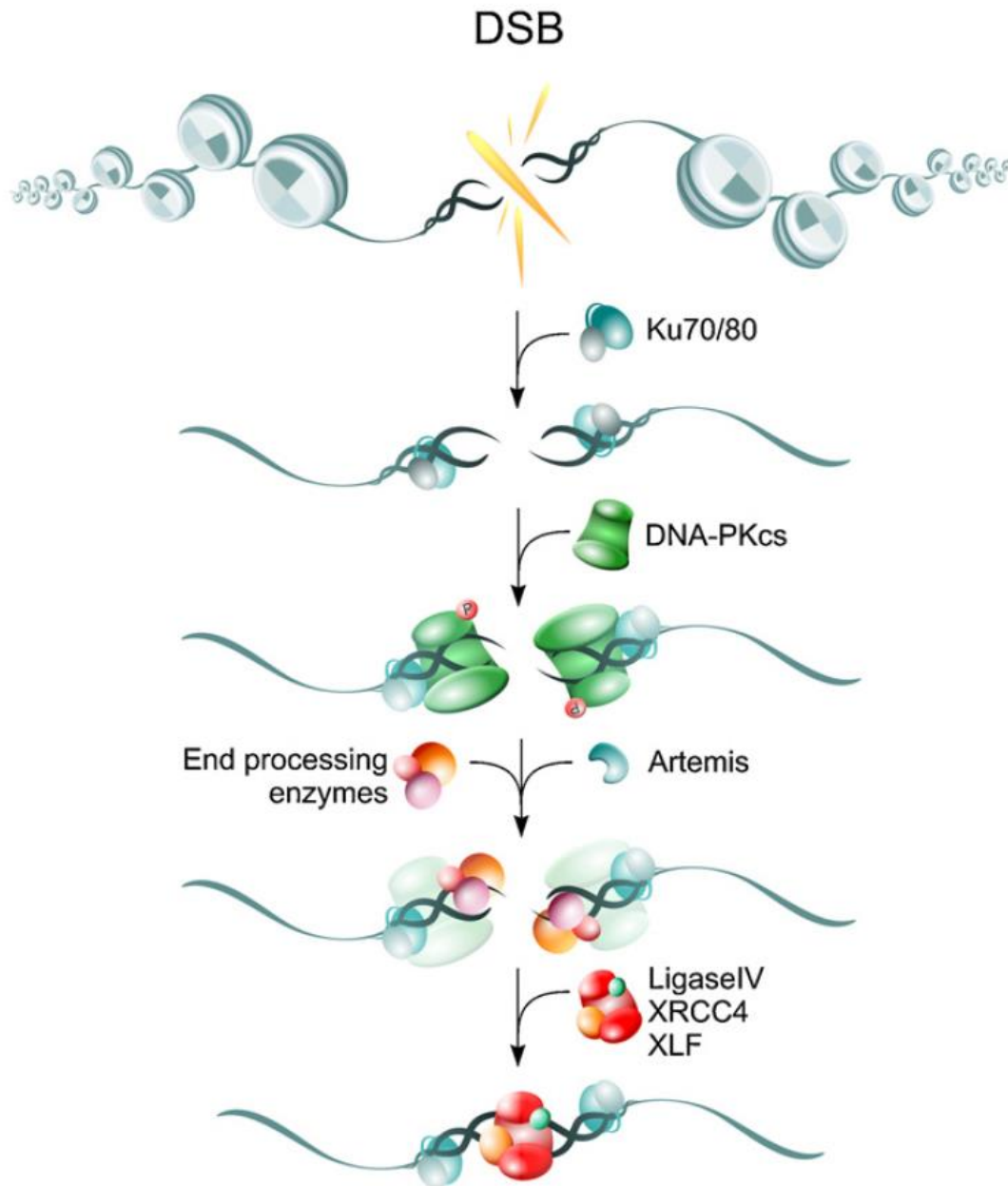


Figure 9 Schematic overview of key factors and steps of D-NHEJ D-NHEJ efficiently restores genomic integrity without ensuring sequence restoration. Association of Ku to DNA ends facilitates the recruitment of DNA-PKcs, a major kinase activated by DNA ends and contributing to the efficiency of this repair pathway. DNA-PKcs promotes end-processing by the Artemis nuclease and subsequent rejoining of broken DNA ends by the LigIV/XRCC4/XLF complex. (from (Mladenov and Iliakis, 2011))

1.4.2.3 HRR

HRR is the other main pathway of DSB repair in mammalian cells (Liang, 1998). In contrast to D-NHEJ, HRR by design faithfully restores the sequence to its original state. To achieve this goal it has to recover this information from an intact template molecule, which in the case of mitotic HRR is the sister chromatid. Intact sister chromatid sequences only start to become available with progression of DNA replication during S-phase. Thus, contrary to D-NHEJ HRR is a highly cell cycle dependent process. This dependence is not only determined by the presence of sister chromatids themselves, but is also tightly regulated through multiple PTMs that prevent crucial steps of HRR to occur outside its appropriate time window (Heyer, 2010; Mladenov, 2013). For HRR to commence an essential step is the creation of a long single-stranded 3'-overhang that can be used to find homology in an annealing based process. This 3'-overhang is created through nucleolytic resection of the 5'-end of the break (Symington and Gautier, 2011). Resection of DNA ends is tightly regulated in a cell cycle phase dependent manner and is restricted to the S and G2 phase (Huertas, 2010). Thereby the regulation of end-resection is likely to be one of the main determinants of the cell cycle specific constrain of HRR mentioned earlier (Ira, 2004). A key mechanism of the control of end resection is the balance between the actions of two proteins antagonizing each other: 53BP1 and BRCA1 (Bunting, 2010).

The opposing roles of these two proteins are impressively illustrated by a phenotype of “synthetic viability” in mice. Mice with a certain BRCA1 mutation display mid-gestational lethality. When these mice are placed in a 53BP1 deficient background this lethality is rescued (Cao, 2009). It has been shown that 53BP1 inhibits end resection, via its effector RIF1, thereby inhibiting HRR (Bunting, 2010; Escibano-Diaz, 2013). BRCA1 on the other hand promotes end resection, thereby favoring HRR over D-NHEJ (Bouwman, 2010; Bunting, 2010). This end resection promoting activity depends on interaction of BRCA1 with CtIP and the MRN complex (Chen, 2008). This interaction in turn is regulated by phosphorylation of CtIP on Serine 327, which is executed by CDKs in the S and G2 phase (Yu and Chen, 2004). Thus, in G1 53BP1 prevents end-resection, prohibiting HRR. However, when cells progress into S and G2 the phosphorylation of CtIP bestows BRCA1 with the power to alleviate the inhibition exerted by 53BP1 and to

stimulate end resection. Although important, the phosphorylation of CtIP is not the only mechanism that supports end-resection in S and G₂, but is complemented by a plethora of further cell cycle dependent PTMs of various proteins (Mladenov, 2013). Once a stretch of single-stranded DNA (ssDNA) has formed it will be coated with the heterotrimeric replication protein A complex (RPA). Coating with RPA prevents further degradation and formation of intramolecular secondary structures (Eggleter, 2002). However, for HRR to progress RPA has to be displaced by RAD51, the central recombinase protein in HRR. This process is mediated by the BRCA2 (breast cancer 2, early onset) protein (Yang, 2005; San Filippo, 2008). RAD51 forms a helical nucleoprotein filament with ssDNA that is capable of searching for homologous sequences and invasion of another double-stranded DNA (dsDNA) molecule (Raderschall, 1999; Aly and Ganesan, 2011). Besides core factors like RAD51 and BRCA2 many other factors participate in or facilitate these intricate reactions. These include the members of the RAD52 epistasis group (RAD50, RAD52, RAD54, MRE11), the RAD51 paralogs (RAD51B, C, D and XRCC2 and XRCC3) and CtIP the mammalian Sae2 homolog (San Filippo, 2008; Huertas and Jackson, 2009; Heyer, 2010). Strand invasion leads to formation of a structure called the displacement loop (D-loop). The 3'-end of the invading strand serves to prime DNA synthesis using the homologous sequence as template. Afterwards, depending on several factors, repair by homologous recombination can take several routes:

In the synthesis dependent strand annealing (SDSA) sub-pathway the invading strand is simply disengaged from the donor duplex after DNA synthesis is completed and re-anneals with the complementary strand on the opposing side of the break. Gaps are filled-in by another round of DNA synthesis and the remaining nicks are finally ligated (Figure 10).

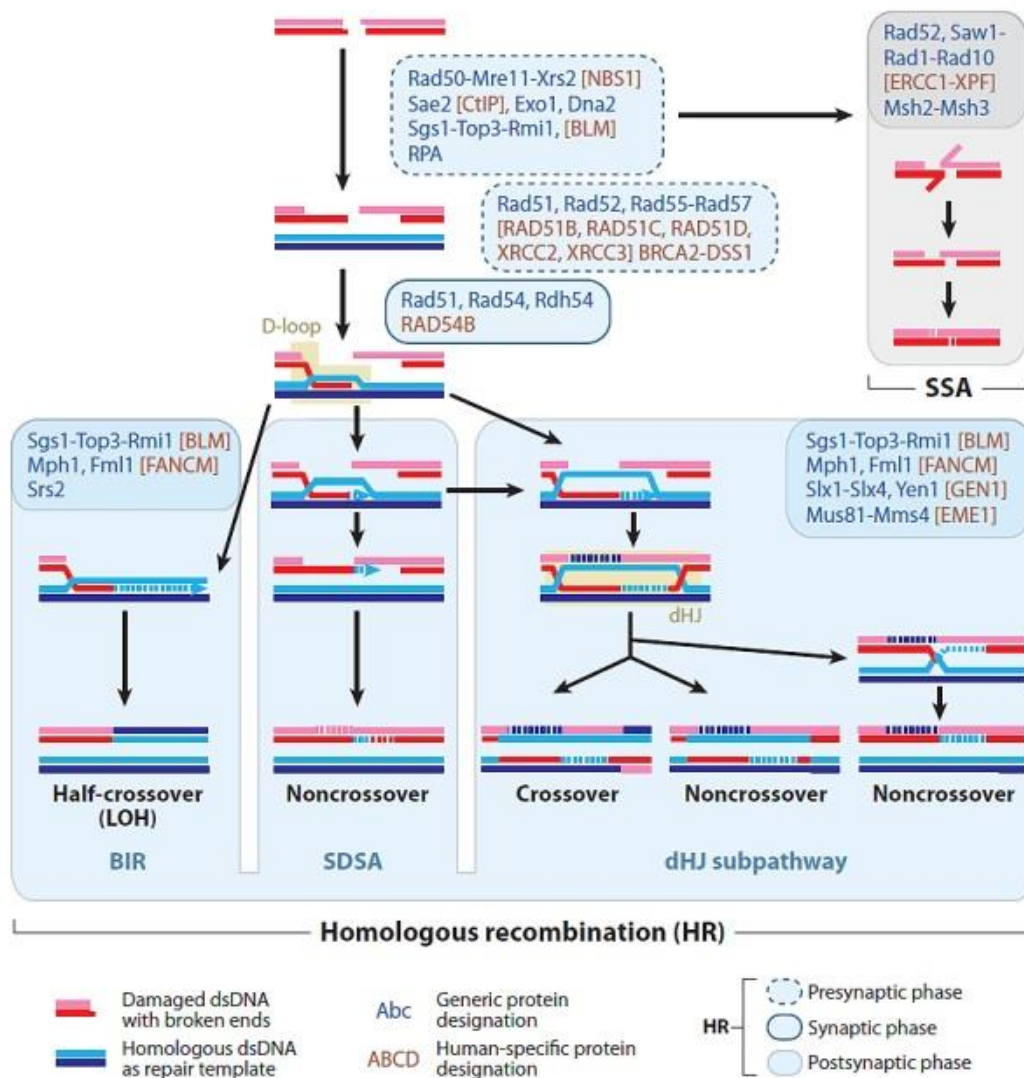


Figure 10 Steps and outcomes of homology directed repair pathways. Protein names refer to the budding yeast *Saccharomyces cerevisiae* (blue). Where different in human, names (brown) are given in brackets. For proteins without a yeast homolog, brackets for human proteins are omitted. Broken lines indicate new DNA synthesis and stretches of heteroduplex DNA. Abbreviations: BIR, break-induced replication; dHJ, double Holliday junction; LOH, loss of heterozygosity; SDSA, synthesis-dependent strand annealing; SSA, single-strand annealing. (modified from(Heyer, 2010))

In the double Holliday junction sub-pathway the second end of the DSB is captured by the displaced strand and elongated using the latter as a template. After DNA synthesis is

completed on the originally invading strand it is ligated with the 5'-prime end at the opposite side of the break. In this way a complex structure called a double Holliday junction (dHJ) is formed. Nucleolytic incision is required to resolve this structure and several enzymatic activities, like the Bloom's helicase (BLM) and the Mus81/Eme1 have been implicated in this process. Resolution of a dHJ can be achieved in several ways and can yield crossover or non-crossover products (Figure 10). DNA synthesis as it occurs during SDSA or dHJ HRR is limited to a few hundred bases, in contrast to BIR where much longer sequences are synthesized *de novo*.

Recently, in a collaborative effort of our laboratory with the group of Thanos Halazonetis, it could be demonstrated that the BIR pathway is important for genomic stability under conditions of DNA replication stress (Costantino, 2014). In yeast BIR has been characterized as the pathway that repairs one-ended DSB arising when replication forks collapse. This frequently occurs in cells that suffer from replication stress, as it is prevalent in cancer as well. A one-ended DSB cannot be repaired by a joining mechanism. Instead in BIR the break end is used to prime new long range DNA synthesis up to the end of the chromosome after strand invasion (Malkova, 2001; Davis and Symington, 2004; Malkova, 2005)(Figure 10). In this way sequences of 100 kB or more can be synthesized in yeast. BIR requires most essential replication factors as well as the non-essential Pol δ subunit Pol32/POLD3 (Wang, 2004c; Lydeard, 2007; Lydeard, 2010). Still, DNA synthesis during BIR does not seem to include assembly of a conventional replication fork. Instead, DNA is replicated in a conservative manner, by a migrating bubble mechanism accompanied by continuous lagging strand synthesis (Donnianni and Symington, 2013; Saini, 2013). In yeast this mechanism has been associated with extensive loss of heterozygosity (LOH), formation of non-reciprocal translocations, inversions and tandem duplications (Smith, 2007; Payen, 2008; Ruiz, 2009; Mizuno, 2013). We could show that in a human model of replication stress these rearrangements are induced and that their frequency is reduced after silencing of the essential BIR factor POLD3 (Costantino, 2014).

It is intriguing that HRR, while being the principal pathway in bacteria and lower eukaryotes and also the only truly faithful DSB repair process available, seems to have been pushed to the background by the emergence of D-NHEJ in higher eukaryotes. A

possible rationalization for this observation would be that HRR is not such an error-free process as it may appear at first glance. While it is true that HRR is the only process that can reliably accomplish the faithful restoration of sequence at complex DSB, there is also potential danger associated with this process. The human genome contains a high amount of shorter and longer repetitive sequences. These include so-called segmental duplications or low copy repeats, which can serve as targets for non-allelic homologous recombination (NAHR). The presence of such sequences may have made it favorable to exert a tighter control about homology directed repair. Indeed several syndromes exist that arise due to NAHR during meiosis (Liu, 2012a). NAHR is believed to be restricted to gametogenesis in mammals. However, this may be a consequence of the cell cycle specific regulation of HRR. If HRR was unleashed in G1/G0 cells, it would have to resort to the use of either the homologous chromosome or dispersed sequence duplications as recombination substrates. The first would result in LOH, the latter in NAHR (Carr and Lambert, 2013).

HRR has gained a lot of attention as a target for radiosensitization recently (Mladenov, 2013). A number of compounds that interact more or less directly with the DNA repair machinery or checkpoint and cell cycle control mechanisms (Asaad, 2000; Bohm, 2006; Morgan, 2010; Takagi, 2010; Meike, 2011; Prevo, 2012), as well as multiple treatments with less obvious connections to this repair pathway have been shown to elicit radiosensitization by inhibition of HRR (Chinnaiyan, 2005; Noguchi, 2006; Adimoolam, 2007; Murakawa, 2007; Li, 2008; Choudhury, 2009).

1.4.2.4 B-NHEJ

To date the description of back-up mechanisms of NHEJ remains incomplete, although an increasing number of proteins is emerging that may play roles in non-homologous DSB repair processes in the absence of D-NHEJ. Other nomenclature than B-NHEJ has been proposed to describe these processes, including alternative end-joining (A-EJ), alternative non-homologous end-joining (A-NHEJ) or microhomology mediated end-joining (MMEJ). B-NHEJ has been initially described based on the observation that mutant cell lines deficient in components of the main D-NHEJ machinery - although

severely impaired in the fast rejoining of DSB - are still capable of repairing DSB and eventually rejoin almost all breaks after prolonged repair times (Nevaldine, 1997; Kabotyanski, 1998; Wang, 2001b; Wang, 2003a; Iliakis, 2004). Defects in HRR did not influence residual repair suggesting that another mechanism of NHEJ, acting as a back-up for D-NHEJ, was at work (Wang, 2001a).

Later studies showed the participation of alternative pathways of NHEJ in physiological processes, like the generation of antibody diversity through V(D)J recombination (Verkaik, 2002; Corneo, 2007), or in class switch recombination (Soulas-Sprauel, 2007; Yan, 2007), when the classical DNA-PKcs dependent NHEJ was inactivated.

There is evidence that B-NHEJ has an increased preference for the usage of short sequence homologies (so called microhomologies) for the formation of joints (Roth and Wilson, 1986; Bogue, 1997; Kabotyanski, 1998), but it is not absolutely dependent on them (McVey and Lee, 2008; Fattah, 2010; Mansour, 2010). Typically, homologies <5bp sometimes <10bp are defined as microhomologies. It has been reported that microhomology mediated B-NHEJ events benefit from resection of DNA ends (Xie, 2009; Bothmer, 2010; Lee-Theilen, 2011; Symington and Gautier, 2011). This is not surprising considering that resection would be a prerequisite for detection and annealing of homologous sequences. Nevertheless, many B-NHEJ mediated junctions harbor large deletions without showing microhomology signature, even when microhomology would have been available. This suggests that end-resection plays a more general role in B-NHEJ than to purposefully reveal microhomologies. The presence and usage of microhomologies however could facilitate ligation of ends by holding them together.

It is possible that two or more B-NHEJ sub-pathways exist, microhomology dependent and independent ones, which fulfill end-joining tasks in the absence of other functional repair. Disregarding possible dependency on microhomology, repair by B-NHEJ has a characteristic tendency to cause large scale chromosomal alterations. Translocations and extensive deletions are found frequently when repair is carried out by B-NHEJ (Soulas-Sprauel, 2007; Yan, 2007; Robert, 2009; Boboila, 2010; Simsek and Jasin, 2010). Thus, B-NHEJ now is considered to be a major contributor to chromosome aberration formation and genomic instability (Mladenov and Iliakis, 2011; Symington and

Gautier, 2011; Mladenov, 2013). This places B-NHEJ not only in the center of cell killing during radiotherapy but also at the heart of carcinogenesis (Greaves and Wiemels, 2003; Edwards, 2008).

B-NHEJ can potentially act throughout the cell cycle, but does display remarkable variations in its efficiency depending on the position in the cycle. In G2 for example B-NHEJ is enhanced (Wu, 2008a; Wu, 2008b). This might be explainable with increased end-resection activities during G2 that facilitate B-NHEJ. In growth inhibited plateau phase or serum starved cells on the other hand B-NHEJ is strongly reduced (Windhofer, 2007; Singh, 2011). Although B-NHEJ is observable best on a D-NHEJ deficient background acting as a backup for this pathway, its association with end resection makes it easy to imagine that it also takes advantage of abortive HRR events (Symington and Gautier, 2011; Dueva and Iliakis, 2013).

B-NHEJ can be best observed when the major beneficial repair processes are impaired globally genetically or by chemical inhibition. Nevertheless it is likely that B-NHEJ can also occur in repair proficient background locally at sites of repair accidents, possibly also accounting for a majority of chromosomal translocations found in repair proficient cells. Candidates for proteins involved in B-NHEJ include LIG3 (Wang, 2005b; Simsek, 2011), LIG1 (Boboila, 2012), Histone 1 (Rosidi, 2008), PARP1 (Wang, 2006b; Robert, 2009; Wray, 2013), MRE11 (Xie, 2009) and CtIP (Zhang and Jasin, 2011).

1.4.2.5 SSA

Single-strand annealing (SSA) is another homology directed cellular DSB repair process besides HRR (Figure 10). In contrast to HRR, SSA does not favor homologous sequences on other DNA molecules, but preferentially on the same molecule where the DSB occurred (Ivanov, 1996; Symington, 2002). Similar to HRR it requires extensive resection to reveal those homologies, but unlike HRR the long 3'-ssDNA is not used for initiation of repair synthesis (Fishman-Lobell, 1992; Sugawara and Haber, 1992). Instead two homologous stretches of sequence are annealed, tails/flaps are removed and gaps are filled in (Symington, 2002). This inevitably leads to the loss of the intervening sequences, which may be hundreds of base pairs long. Thus SSA is a highly mutagenic process with the propensity to cause large deletions. Worse still, due to the

presence of vast numbers of dispersed repetitive elements like LINES and SINES in mammalian genomes SSA can also cause translocations (Elliott, 2005; Weinstock, 2006). SSA is strongly suppressed by HRR and if core components of this faithful homology directed repair pathway, like RAD51 or BRCA2, are inactivated the frequency of SSA event multiplies 4-8 fold (Tutt, 2001; Stark, 2004; Mansour, 2008; Manthey and Bailis, 2010). Similar to HRR, SSA shows strong cell cycle dependence, possibly due to the cell cycle regulated efficiency of end resection activities (Frankenberg-Schwager, 2009; Trovesi, 2011). Important proteins implicated in SSA in mammalian cells are RAD52, the ERCC4/XPF-ERCC1 endonuclease and RPA (Symington, 2002; Stark, 2004; Al-Minawi, 2008) .

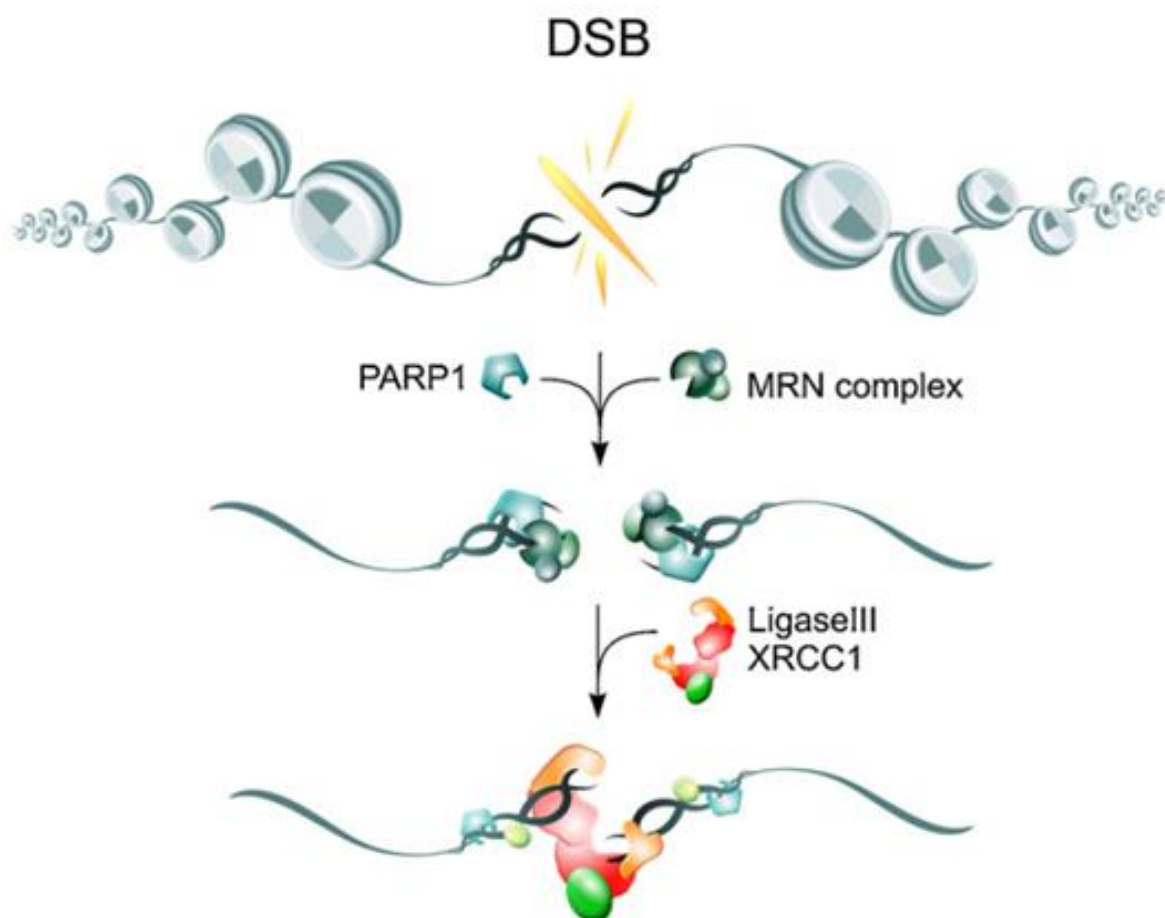


Figure 11 Schematic overview of key factors and steps of B-NHEJ. The enzymatic activities implicated in B-NHEJ are shown together with their possible contributions in the process. (modified from (Mladenov and Iliakis, 2011))

1.5 The role of DSB in cell killing and cancer induction by IR

1.5.1 The DSB as cancerogenic lesion

Only the breakage and rejoining of double-stranded DNA can eventually account for the gross chromosomal abnormalities that can be induced by ionizing radiation and which are also a common hallmark of cancer. There are certain chromosomal translocations that are known to be potent inducers of carcinogenesis, e.g. the t(9;22) translocation – also known as Philadelphia chromosome - that is found in >95% of patients with chronic myeloid leukemia (CML)(Greaves and Wiemels, 2003; Nambiar and Raghavan, 2011). This highlights the important role of DSB, not only for the killing of cells, but also for carcinogenesis. Still, although IR is a mutagenic agent that induces DSB, base damages and other lesions that can drive cancer development, it is the potentially lethal consequences of the DSB that make IR a valuable tool in cancer therapy.

1.5.2 The DSB as lethal lesion

Complex DSB as a product of IR are potent inducers of cell death. Although base damages and SSB are induced at a much higher frequency by IR than DSB, their contribution to the cytotoxicity of IR is far less than that of DSB (Iliakis, 1991; Foray, 1997a; Nikjoo, 1999). It has been shown that a single unrepaired DSB can be sufficient to kill an eukaryotic cell (Frankenberg, 1981). The importance of DSB in cell killing is also highlighted by the pronounced radiosensitivity of cells with defects in DSB processing that is found in several human syndromes or mutant cell lines (Jeggio and Kemp, 1983; Joubert, 2008; Mladenov, 2013). However, there is not a clear general correlation between DSB induction and rejoining (as measured by physical methods) and cell killing respectively survival. While cell lines that show defects in the rejoining of DSB are radiosensitive, not all radiosensitive cell lines have clear defects in the rate with which they rejoin DSB. A better correlation exists with the induction of chromosomal aberrations. So how can the particularly detrimental effects of the DSB be explained? DSB can result in the loss of vital genetic material in subsequent cell divisions if they remain un-rejoined, while rejoining of the wrong DNA ends can result in chromosomal

aberrations like translocations and chromosome or chromatid fusions that may cause cell death or lead to carcinogenesis (Bryant, 1988; Obe, 1992; Ferguson and Alt, 2001). Therefore the DSB can with high certainty be assumed to be the lesion underlying the formation of chromosomal aberrations and - via this route - cell killing (Bender, 1974; Natarajan, 1980; Radford, 1985; Iliakis, 2004).

1.6 Evidence connecting DSB repair to cellular radiosensitivity and PLD

It is known that the main genetic determinants of cellular sensitivity to IR are genes whose products are involved in the detection and repair of DSB, or those that participate in the signaling and control of cell cycle progression in response to DNA damage (checkpoints) (Jeggo and Lavin, 2009b). These genes include *ATM* (Foray, 1997b), *ATR* (Wang, 2004b), *CHK1* (Wang, 2005a), *BRCA1&2* (Foray, 1999), *LIG4* (Plowman, 1990; Badie, 1995), *MRE11* (Matsumoto, 2011), *NBS1* (Carney, 1998), *RAD50* (Waltes, 2009), *RAD51* (Liu, 2011), *RNF168* (Stewart, 2007; Stewart, 2009), *XRCC2&3* (Cui, 1999), Artemis (Moshous, 2001), *DNA-PKcs* (Hendrickson, 1991) and *KU* (Tzung and Runger, 1998) (reviewed in (Jeggo and Lavin, 2009a; Foray, 2012)). The presence of core components of both major DSB repair pathways in this list indicates that HRR, as well as NHEJ play important roles in conferring radioresistance to the cell. Thus, both pathways present as potentially promising targets for cell radiosensitization (Yoshihisa Matsumoto, 2013).

DSB are also the best candidate for the lesion constituting PLD due to their cytotoxic effects. Pathways of DSB repair can be envisioned to account for repair, as well as for fixation of PLD. The former occurring when the correct ends of DSB are rejoined with high fidelity, the latter when repair of DSB either entirely fails, or when misrejoining occurs that results in the formation of lethal chromosomal aberrations. These considerations are reinforced by observations that implicate NHEJ and HRR in PLD repair and the cell cycle dependent fluctuations in the sensitivity to IR.

XR-1 cells for example are deficient in XRCC4, a component of D-NHEJ. These cells are extremely sensitive to IR in G1, but only moderately sensitive in S/G2. Furthermore, they don't appear to repair PLD in G1/G0, but show substantial repair of PLD in S/G2 that operates with a halftime of approximately 5h (Stamato, 1988). In the parental cell line on the other hand, much of the PLD repair occurs in G1 and repair halftimes are about 1h (Stamato, 1988). The cell cycle dependence and kinetics of PLD repair in the mutant and parental cell line here reflect exactly what would be expected, if DSB constituted PLD and repair was carried out by NHEJ and HRR. In the mutant only the slow HRR pathway, which is restricted to S/G2, would be available for repair. In the parental cell line the fast NHEJ pathway, which dominates repair throughout the cell cycle would be capable of repairing most of the PLD.

Further evidence is provided by the hamster cell line *irs-1*, which is deficient for the RAD51 paralog XRCC2. In *irs-1*, the S-phase dependent increase in radiosensitivity usually observed in hamster-cells is abolished (Cheong, 1994). Similarly treatment with caffeine, which exerts an inhibitory effect on HRR, flattens the fluctuations of radiosensitivity throughout the cycle in cells that are proficient for this pathway (Beetham and Tolmach, 1984; Asaad, 2000). This list could be considerably extended with various other examples of mutant cell lines and treatments demonstrating the dependence of radiosensitivity during the cell cycle and PLD repair on the repair of DSB (Sonoda, 2006; Tamulevicius, 2007).

Taken together, a large body of evidence suggests that individual differences in cell-intrinsic sensitivity to IR, the fluctuations in radiosensitivity during the cell cycle and the repair of PLD depend largely on the ability of a cell to detect and repair DSB (Roberts, 1999; Joubert, 2008; West and Barnett, 2011). Thus, pathways of DSB repair present promising targets for the modulation of cellular radiosensitivity to killing for the optimization of radiotherapy (Yoshihisa Matsumoto, 2013).

1.7 Synergistic interactions between IR and nucleoside analogs

A number of NAs have been reported to show synergistic action with IR *in vitro* (Dewey and Humphrey, 1965; Iliakis, 1989a; Iliakis, 1989b; Gregoire, 1994; Shewach, 1994; Buchholz, 1995; Meike, 2011). Some of these drugs have been evaluated as radiosensitizers in clinical trials (Goffman, 1991; Miser, 1992; Bartelink, 1997; Aguilar-Ponce, 2004; Nitsche, 2008) and others already belong to the standard of care as concurrent treatments for some diseases (Vallerga, 2004; Gurka, 2013; Lee, 2013). Despite their great clinical promise the mechanisms of radiosensitization by many NAs remain poorly understood. In the following the NAs used in this study are described with respect to their potential radiosensitizing activities.

Early studies could show that ara-A is a particularly effective inhibitor of PLD repair (Iliakis, 1980; Iliakis and Bryant, 1983; Iliakis and Ngo, 1985; Chavaudra, 1989; Iliakis, 1989b; Little, 1989). In comparative studies with other inhibitors of replication and DNA synthesis ara-A consistently showed the strongest inhibitory effect on the repair of PLD (Iliakis and Bryant, 1983; Iliakis, 1989b). In the studies cited above plateau phase cultures were used for the generation of the results. Reports about radiosensitization by ara-A in actively cycling populations are scarcer (Iliakis and Nusse, 1983b; Chavaudra, 1989; Mustafi, 1994). Ara-A has also repeatedly been reported to inhibit the repair of chromosomal breaks (Bryant, 1983; Mozdarani and Bryant, 1987; Iliakis, 1988b; MacLeod and Bryant, 1992; Okayasu and Iliakis, 1993; Bryant, 2004). Intriguingly, the number of exchange type aberrations was observed to increase at the same time in some studies (Bryant, 1983; Mozdarani and Bryant, 1987). Taken together, this suggests that ara-A interferes with pathways of DSB repair that are involved in the repair of PLD and chromosomal breaks.

Radiosensitization by fludarabine has been demonstrated in numerous *in vitro* studies (Gregoire, 1994; Laurent, 1998; Nitsche, 2008) and also been tested in first clinical studies (Gregoire, 2002; Nitsche, 2012). Radiosensitization by fludarabine was found not to coincide with inhibition of DSB repair measured by pulsed field gel electrophoresis (PFGE) (Gregoire, 1998).

Ara-C is generally not recognized as a radiosensitizer and there are no clinical studies assessing such a potential. However, there are some reports that show a comparatively weak inhibition of PLD repair by ara-C (Iliakis and Bryant, 1983; Nakatsugawa, 1984; Iliakis, 1989b).

The *in vivo* radiosensitizing potential of Gemcitabine has been tested extensively in preclinical studies (Shewach, 1994; Lawrence, 1996; Latz, 1998; Rosier, 1999; Pauwels, 2003) and confirmed in numerous clinical trials (Eisbruch, 2001; Aguilar-Ponce, 2004; Evans, 2008). Concurrent chemo radiation with gemcitabine is currently considered as standard treatment for locally advanced pancreatic cancers in North America (Gurka, 2013). Like for fludarabine, radiosensitization by gemcitabine was found not to coincide with inhibition of DSB repair measured by (PFGE) (Gregoire, 1998).

Previous reports and preliminary data generated in the beginning of this study suggested that radiosensitization elicited by ara-A exceeds the effects of fludarabine, ara-C and gemcitabine. Thus, we chose to use ara-A as a model compound in most of our experiments to study NA mediated radiosensitization and to investigate the mechanisms that underlie its superior sensitization characteristics.

2 Aims and scope of this work

Improving the treatment of cancer belongs to the most important and most challenging tasks of modern medicine. The diversity of malignant entities and the variety of possible steps that can lead to carcinogenic transformation make solid cancers a highly heterogeneous group of diseases. The combination of different treatment modalities is one of the most promising current approaches to achieve improvements in cancer treatment for a broad range of patients. Radiotherapy is one of the most efficient means to eradicate cancer cells. However, some cancers are relatively radioresistant and even when tumors can be treated successfully, surviving cells are often responsible for relapses. Combining IR with drugs that sensitize targeted cancer cells to killing can significantly improve the outcome of radiotherapy.

NAs represent a large group of anticancer drugs, several members of which have been shown to possess radiosensitizing potential. Aim of the present study was to elucidate the mechanisms of radiosensitization by NAs using as a model compound ara-A, due to its superior radiosensitizing properties.

The DSB is the most detrimental IR-induced lesion, whose misrepair underlies cell killing and likely also ara-A radiosensitization. Therefore, we studied in detail the effects of ara-A on the main pathways of DSB repair: HRR, NHEJ and B-NHEJ, placing particular emphasis on cell cycle specific effects. To this end, we employed advanced methods of microscopy, flow cytometry and various cell biological and biophysical techniques. This approach led to the generation of a wealth of data that allowed the development of a mechanistic model of ara-A radiosensitization. This model invokes the selective inhibition of the error-free DSB repair pathway HRR and the parallel activation of the error-prone DSB repair pathway B-NHEJ by ara-A. This information also formed the basis for a comparative analysis of the mode of action of selected other NAs.

The efficiency of concurrent chemo-radiotherapy can greatly benefit from increased knowledge about mechanisms of action of radiosensitizers. We hope that the information generated as part of the present thesis will assist in the identification and selection of drugs able to maximize the radiation response of tumors and the optimization of treatment schedules.

3 Materials and Methods

3.1 Materials

Table 3.1: Laboratory Apparatuses

Laboratory Apparatus	Model	Manufacturer
Cell counter	Multisizer™ 3	Beckman Coulter Inc.

Cell Sorter	Epics Altra	Beckman Coulter Inc.
Centrifuge	Multifuge 3 S-R	Heraeus
Centrifuge	Avanti J-20XP	Beckman Coulter Inc.
Centrifuge	Tabletop GS-6R	Beckman Coulter Inc.
Elutriation Centrifuge	Beckman J2-21M centrifuge	Beckman Coulter Inc.
CO2- incubator	Hera Cell 240	Heraeus
Confocal Microscope	TCS-SP5	Leica Microsystems
Dry blotting system	iBlot	Invitrogen
Flow Cytometer	Coulter XL-MCL	Beckman Coulter Inc.
Flow Cytometer	Gallios	Beckman Coulter Inc.
Imaging scanner	Typhoon 9400	GE Healthcare
Infrared imaging system	Odissey	LI-COR
Laboratory microscope	Inverted phase contrast	Olympus
Laminar Flow Hood	Hera safe	Heraeus
Liquid Scintillation counter	TriCarb1900 TR	Packard
Magnetic stirrer	MR Hei-Mix L	Heidolph
Microtiter Pipettes	Rainin	
Mini centrifuge	Biofuge fresco	Heraeus

Molecular Imager	VersaDoc	Bio-Rad
Electroporation device	Nucleofector I	Lonza AG
pH-Meter	WTW	InoLab
Photometer	Nanodrop	Thermo Scientific
Photometer	UV-2401 PC	Shimadzu
Pipet Aid	Express	Falcon
Rocky Shaker	3D	Peter Oehmen
SDS PAGE equipment	Mini Protean	Bio-Rad
X-ray tube	Isovolt 320HS	General Electric- Pantak

Table 3.2: Chemicals

Chemical	Provider
1- β -D-arabinofuranosylcytosine	Sigma-Aldrich, Steinheim, Germany
2-Mercaptoethanol	Sigma-Aldrich, Steinheim, Germany
2'-deoxy-2',2'-difluorocytidine	LC Laboratories, USA
9- β -D-arabinofuranosyl-2-fluoro-adenine	Metkinen, Finland
9- β -D-arabinofuranosyladenosine	TCI America, USA
Aphidicolin	SERVA, Heidelberg
Boric acid	Roth, Karlsruhe, Germany
BSA [Bovine serum albumin fraction V]	Roth, Karlsruhe, Germany
Bromophenol blue	Sigma-Aldrich, Steinheim, Germany

Coomassie brilliant blue R 250	SERVA Electrophoresis GmbH, Heidelberg, Germany
Crystal violet	Merck, Darmstadt, Germany
DAPI	Sigma-Aldrich, Steinheim, Germany
Dichlorodimethylsilane	Merck, Darmstadt, Germany
DMSO [Dimethyl sulfoxide]	Sigma-Aldrich, Steinheim, Germany
DMEM [Dulbecco's Modified Eagle Medium]	Gibco™, Invitrogen, Karlsruhe, Germany
DTT [Dithiothreitol]	Roth, Karlsruhe, Germany
EtOH [Ethanol]	Sigma-Aldrich, Steinheim, Germany
EtBr [Ethidium bromide]	Roth, Karlsruhe, Germany
EDTA [Ethylenediaminetetraacetic acid]	Roth, Karlsruhe, Germany
FBS [Fetal bovine serum]	Biochrom, Berlin, Germany; Gibco™, Invitrogen, Karlsruhe, Germany
FBS [Fetal bovine serum]	PAA, Coelbe, Germany
FBS [Fetal bovine serum]	Gibco™, Invitrogen, Karlsruhe, Germany
HEPES	Roth, Karlsruhe, Germany
Hydroxyurea	Sigma-Aldrich, Steinheim, Germany
Isopropanol	Sigma-Aldrich, Steinheim, Germany
KCl	Roth, Karlsruhe, Germany
KH ₂ PO ₄	Roth, Karlsruhe, Germany
KOH	Roth, Karlsruhe, Germany
LMA [Low melting agarose]	Roth, Karlsruhe, Germany
Mc Coy's 5A medium	Sigma-Aldrich, Steinheim, Germany
Methanol	Sigma-Aldrich, Steinheim, Germany
MgCl ₂	Merck, Darmstadt, Germany
NaCl	Roth, Karlsruhe, Germany

NaHCO ₃	Roth, Karlsruhe, Germany
NaH ₂ PO ₄	Roth, Karlsruhe, Germany
Na ₂ HPO ₄	Roth, Karlsruhe, Germany
NLS [N-lauroyl sarcosine]	Merck, Heidelberg, Germany
Non-fat dry milk	Roth, Karlsruhe, Germany
NU7441	Tocris Bioscience, Ellisville, MO, USA
Paraformaldehyde	Honeywell Specialty Chemicals GmbH, Seelze, Germany
Penicillin	Sigma-Aldrich, Steinheim, Germany
Phenylmethanesulfonylfluoride	Roth, Karlsruhe, Germany
Phosphoric acid	Roth, Karlsruhe, Germany
Poly-L-lysine	Biochrom AG, Berlin, Germany
ProLong® Gold antifade reagent	Invitrogen, Karlsruhe, Germany
PI [Propidium iodide]	Sigma-Aldrich, Steinheim, Germany
Protease from <i>S. griseus</i>	Sigma-Aldrich, Steinheim, Germany
Protease inhibitor cocktail	Sigma-Aldrich, Steinheim, Germany
Puromycin	Sigma-Aldrich, Steinheim, Germany
RIPA buffer	Thermo Scientific, Schwerte, Germany
RNase A	Sigma-Aldrich, Steinheim, Germany
Scintillation Cocktail UniSafe1	(Zinsser Analytic)
SEAKEM LE® Agarose	Lonza
SeeBlue plus2 pre-stained protein ladder	Invitrogen, Karlsruhe, Germany
SDS [Sodium dodecyl sulfate]	Roth, Karlsruhe, Germany
Streptomycin	Calbiochem, Invitrogen, Karlsruhe, Germany
Tetramethylethylenediamine	Sigma-Aldrich, Steinheim, Germany

Trichloric acid	Roth, Karlsruhe, Germany
TRIS [Tris(hydroxymethyl)aminomethane]	Roth, Karlsruhe, Germany
Tris-HCl	Roth, Karlsruhe, Germany
Triton X-100	Sigma-Aldrich, Steinheim, Germany
Trypsin	Biochrom AG, Berlin, Germany
Tween 20	Roth, Karlsruhe, Germany

Table 3.3: Software

Software	Provider	Use
ImageQuant™ 5.0	GE Healthcare Life Sciences, USA	Quantification PFGE Gels
SigmaPlot® 11.0	Systat Software, USA	Graphic Presentation, Curve fitting
ImarisXT® 6.0	Bitplane Scientific Software, Switzerland	Immunofluorescence analysis (Foci)
Microsoft Excel 2010®	Microsoft Corp., USA	Data analysis and calculations
Wincycle™	Phoenix Flow Systems, USA	Cell cycle analysis
Kaluza 1.2	Beckman Coulter Inc., USA	Flow Cytometry analysis (Gallios)
EXPO32™ MultiComp V1.2	Beckman Coulter Inc., USA	Flow Cytometry analysis (XL-MCL/ALTRA)
Adobe® Creative Suite® 5.5	Adobe Systems Inc., USA	Illustrations, presentation, cropping

ApE A plasmid editor V1.17	Freeware, M.W. Davis	Sequence viewing/editing/alignments
EndNote X4	Thomson Reuters	Literature Bibliography

3.2 Methods

3.2.1 Cell culture

3.2.1.1 Cell lines and passage

A549 human non-small cell epithelial lung carcinoma cells (American Type Culture Collection; CCL-185TM; positive for p53) were maintained in McCoy's 5A medium. Stably transfected U2OS human Osteosarcoma cell lines (kindly provided by Jeremy Stark, Ph.D.; Beckman Research Institute of City of Hope, Duarte, CA) carrying different reporter substrates (279A/EJ2-GFP; 280A/EJ5-GFP; 282C/DR-GFP; 283C/SA-GFP) for the repair of I-SceI induced DSB were cultured in McCoy's 5A medium containing 2 µg/ml puromycin. HCT116 human colon carcinoma cell lines were cultured in McCoy's 5A medium. The following HCT116 cell lines were used in these studies: HCT116 (HCT116 WT), as well as HCT116 Lig4^{-/-} (HCT116 Lig4) (Fattah, 2010) and HCT116 DNA-PKcs^{-/-} (HCT116 DNA-PK) (Ruis, 2008) derivative knockout Mouse embryonic fibroblasts (MEF) were cultured in Dulbecco's modified Eagle medium DMEM. The following MEF cell lines were used in these studies: p53^{-/-}/Lig4^{+/+} (MEF Lig4^{+/+}), p53^{-/-}/Lig4^{-/-} (MEF Lig4^{-/-}) (kind gift of Dr. F. Alt; (Frank, 2000)). CHO cell lines were cultured in DMEM. All growth media were supplemented with 10% fetal bovine serum (FBS) as well as 100 µg/ml penicillin and 100 µg/ml streptomycin. All cell lines were grown as monolayer cultures and incubated at 37°C in a humidified atmosphere containing 5% CO₂ and 95% air. For passaging or collection of cells for experiments, dishes were washed with phosphate buffered saline (PBS) and trypsinized at 37°C for 3-5 min using a solution of 0.05% Trypsin. Human cell lines were passaged after 3 to 4 days, while the faster growing rodent cell lines were passaged every second day. Intervals between passages were kept regular and fixed cell numbers of cells were plated for a given cell

line and interval. Cell numbers were determined by counting in a Beckman Coulter Cell counter (Multisizer™ 3). Confluence was avoided during passage and all cells used in experiments were in the exponential phase of growth unless stated otherwise (experiments with plateau phase or serum deprived cells). Cell cycle distribution of cells in passage was regularly checked by flow cytometry after staining with propidium iodide.

Table 3.4: Cell lines

Cell line name	species	Cell type
A549	<i>Homo sapiens</i>	Alveolar adenocarcinoma
HCT116 WT	<i>Homo sapiens</i>	Colon carcinoma
HCT116 LIG4 ^{-/-}	<i>Homo sapiens</i>	Colon carcinoma
HCT116 DNA-PKcs ^{-/-}	<i>Homo sapiens</i>	Colon carcinoma
U2OS 280A	<i>Homo sapiens</i>	Osteosarcoma
U2OS 282C	<i>Homo sapiens</i>	Osteosarcoma
U2OS 283C	<i>Homo sapiens</i>	Osteosarcoma
U2OS EJ-DR	<i>Homo sapiens</i>	Osteosarcoma
MEF	<i>Mus musculus</i>	Embryonal fibroblasts
MEF Lig4 ^{-/-}	<i>Mus musculus</i>	Embryonal fibroblasts
DRaa40	<i>Cricetulus griseus</i>	Ovarian

3.2.1.2 Induction of a plateau-phase like growth state by serum deprivation

In a number of experiments we purposefully did not use cell cultures in the exponential phase of growth, but cultures that retained only very low levels of proliferative activity. In regular cultures this growth state is attained when cells are grown for a prolonged period of time without medium change. Growth factors that drive the entry of cells into the cell cycle are introduced into the culture medium by addition of FBS. Those factors become gradually depleted by cellular uptake. When growth factor levels become too low, cells exit the division cycle. This state is also referred to as G0 (in analogy to the gap phases of the cell cycle) or quiescence. It is not to be confused with terminal differentiation, as it is reversible upon stimulation with growth factors.

In many cell lines growing into a plateau phase is accompanied by a high accumulation of cells with G1 DNA content. This however is not a universal phenomenon, as especially cancer cell lines can be either relatively independent of growth factor regulation, or capable of their own growth factor production and secretion. Plateau phase cultures are preferable as model system over exponential cultures for a number of questions, as the vast majority of cells in an adult human body is in a resting, post-mitotic state. Also in tumor tissue usually not all cells are continuously, actively dividing (Moore and Lyle, 2011).

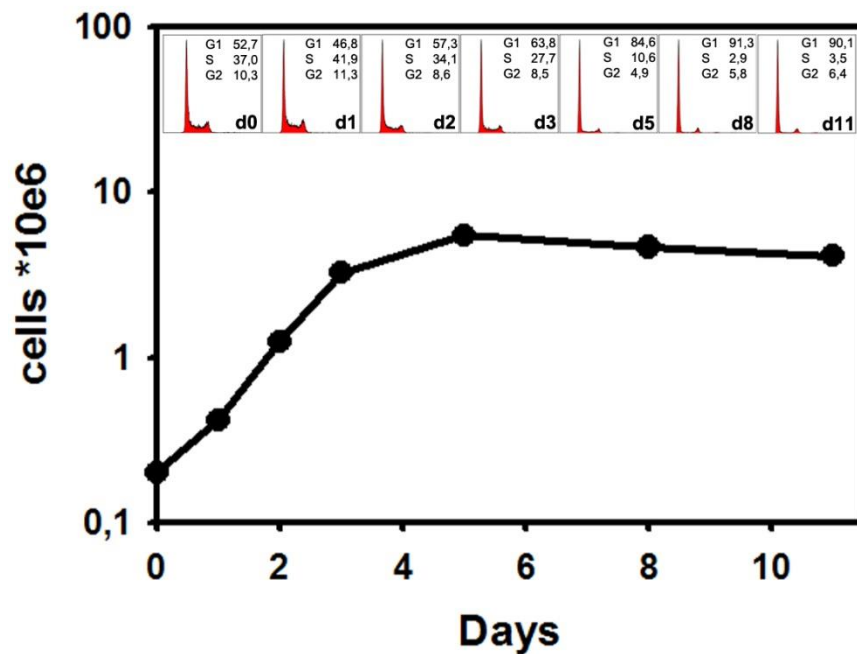


Figure 12 Growth curve of A549 cells. A549 cells were plated at a density of $0.2 \cdot 10^6$ in 5 ml per petri dish (60mm diameter) at day 0 (d0). Cells were counted every 24h and samples were fixed for later analysis of DNA content by PI staining. Red histograms show the result of PI flow cytometry. Black dots and line: Cell number/dish as determined by counting in a Beckmann Coulter cell counter.

When cells are grown into the plateau phase, small deviations in the initial cell number can cause substantial differences in the time when cells reach this phase. For reasons of accumulation of metabolic end products and dead cell remnants however, it is desirable to use cells that are in the early plateau phase. The variations mentioned above make it difficult to obtain cell populations with the same plateau state quality at a fixed time point (e.g. equal cell cycle distribution).

Since the plateau phase state derives from growth factor exhaustion, a plateau phase-like growth state can also be induced by depriving an exponentially growing culture from growth factors. Besides being time saving, such an approach creates defined conditions and ensures higher reproducibility. We employed a protocol that involved growing cells for 2 days under standard conditions for exponential culture. After 48h, medium containing serum was removed and replaced by medium without serum (i.e. free of growth factors). After 24h of serum deprivation cells were used in the respective experiments. Cells were continuously kept in serum free medium throughout the whole experiment. All experiments with non-cycling populations in this work were performed using this serum deprivation protocol. For this reason, the terms plateau phase cells and serum deprived cells are used interchangeably here.

3.2.1.3 Cell cycle analysis by Propidium iodide staining

Propidium iodide (PI) is a DNA intercalating dye that exhibits strongly increased fluorescence when bound to nucleic acids. It is not cell membrane permeable and binds to DNA as well as RNA. Thus, for measurements of DNA content, cells have to be permeabilized and treated with RNase. Cells are fixed and permeabilized by resuspension in cold EtOH 70% (4°C). After fixation cells can be stored at 4°C for a prolonged time. Before measurement cells are spun down, EtOH is aspirated and the pellet is resuspended in PI staining buffer (PBS, 40µg/ml PI, 62µg/ml RNase) and incubated for 15 min at 37°C in a water bath. For cell cycle determination routinely 1×10^4 cells were measured per sample.

3.2.2 Flow cytometry

Flow cytometry analysis of cells exhibiting a fluorescent signal, also known as fluorescence activated cell sorting or in short FACS, is a method to rapidly measure high numbers of cells in a single cell suspension. Sample cells are driven into a capillary, hydro-dynamically focused and transported within a sheath stream through the light path of an excitation laser. Emission light of excited fluorophores and scattered incident light

are collected by photomultiplier tubes (PMT) that amplify the signal. Scattered incident light provides information about size and granularity of cells (forward and side scatter). Incident light is selectively removed by a long pass filter (typically 488 nm LP) before reaching the PMTs assigned for fluorescence signal detection.

Flow cytometry analysis of cells was done using a Beckman Coulter XL-MCL flow cytometer equipped with an Argon ion laser (488 nm) and a Beckman-Coulter Gallios flow cytometer equipped with a solid state laser (488 nm). Analysis of experiment repeats was always performed with the same flow cytometer. Emission of green fluorescent protein (GFP) was measured using a 525 nm bandpass filter when measured alone, or a 510 nm bandpass filter when measured together with DsRed2. Emission of yellow fluorescent protein (YFP) was measured using a 550 nm bandpass filter and emission of dsRed2 was collected using a 610 nm bandpass filter. Propidium iodide (PI) was routinely measured with a 620 nm bandpass filter. Data acquired with the XL-MCL flow cytometer were analyzed in the EXPO32™ MultiComp V1.2 software. Data acquired with the Gallios flow cytometer were analyzed in the Kaluza 1.2 software. Detector settings (PMT gain) were chosen according to the application. Compensation was not required for most measurements. In experiments with multiple fluorochromes exhibiting emission overlap (GFP/YFP and GFP/dsRed2) compensation was done using monochrome control samples.

3.2.3 X-Irradiation

X-irradiation of cells was performed using an X-ray tube (General Electric-Pantak) operated at 320kV, 10 mA with a 1.65 mm aluminium filter. The distance of the X-ray tube to the irradiation table was adjusted according to the cell culture vessel format used in the experiment. This adjustment was done in order to achieve homogenous coverage of the target area by the radiation field. 60 mm and 30 mm diameter petri dishes were irradiated at a distance of 50 cm, while cells grown on 100 mm petri dishes were irradiated at a distance of 75 cm. Rotation of the irradiation table during exposure compensated for the intensity variations within the radiation field, ensuring homogenous

irradiation. The dose rate at 50 cm was ~ 2.7 Gy/min, and at 75 cm ~ 1.3 Gy/min. Radiation dose was confirmed at regular intervals using Fricke's chemical dosimetry.

3.2.4 Transfection of nucleic acids

The term transfection describes the introduction of nucleic acids into cells by non-viral methods. The most common approaches employed for the transfection of cells are usage of Lipid based transfection reagents (e.g. Lipofectamine), cationic Polymers (e.g. Polyethylenimin) or electroporation based methods (e.g. Nucleofection). In this work Nucleofection™ was exclusively used for the transfection of cells. Depending on the type of experiment 1×10^6 - 6×10^6 cells were used per transfection reaction. No differences in transfection efficiency could be observed for cell numbers up to 8×10^6 cells/reaction (highest cell number tested) with Plasmid DNA, or in knockdown efficiency up to 12×10^6 cells/reaction (highest cell number tested) for the transfection of siRNAs. Cells were collected for nucleofection by trypsinization and pelleted for 5 min at 1500 rpm. The supernatant was aspirated and the pellet resuspended in 100 μ l of custom nucleofection buffer (80 mM NaCl, 5 mM KCl, 12 mM Glucose, 25 mM HEPES, 20mM MgCl₂, 0.4 mM Ca(NO₃)₂, 40 mM Na₂HPO₄/NaH₂PO₄) and transferred in an electroporation cuvette. Nucleofection program was chosen according to the cell line (Table 3.5). After transfection cells were taken up in pre-warmed (37°C) growth medium, plated out and returned to the incubator. Measurements were taken, depending on the experimental system, after 24h, 48h or 72h hours using flow cytometry.

Table 3.5: Nucleofector Programs

Cell type	Nucleofector Program
A549	X-05
U2OS	X-01
CHO	U23

Table 3.6: siRNAs

siRNA	Target Sequence	Provider
GFP-22	CGG CAA GCT GAC CCT GAA GTT CAT	Qiagen
Luciferase GL2	AAC GTA CGC GGA ATA CTT CGA	Qiagen
Hs_BRCA2_7	TTG GAG GAA TAT CGT AGG TAA	Qiagen
Hs_RAD52_6	TGG GCC CAG AAT ACA TAA GTA	Qiagen
Hs_RAD51_7	AAG GGA ATT AGT GAA GCC AAA	Qiagen

3.2.5 Repair-outcome-specific chromosomal reporters

DRaa-40 were obtained from Maria Jasin, Ph.D. (Memorial Sloan Kettering Cancer Center, New York, USA). These cells were derived from the CHO cell line AA8 by stable integration of the DR-GFP reporter construct (Pierce, 1999).

A panel of four stably transfected human U2OS cell lines was obtained from Jeremy Stark, Ph.D. (Beckman Research Institute of City of Hope, Duarte, USA) and used to assay the influence of several drugs on the repair efficiency of distinct pathways of DSB repair (Pierce, 1999; Stark, 2004; Bennardo, 2008; Bennardo, 2009; Gunn and Stark, 2012). These assays are based on the reconstitution of a reporter gene by repair of an endonuclease induced chromosomal DSB. Each of the four U2OS cell lines used within this study carries a different reporter construct stably integrated into their genomes. Each of those constructs contains one or two recognition sites for the homing endonuclease I-SceI that has no naturally occurring target sites within mammalian genomes. None of those constructs generates a signal without having been processed for DSB repair resulting in a specific recombination outcome. Expression of I-SceI from a plasmid vector results in the creation of a DSB at its cutting site. Although this DSB may

be repaired by any pathway of DSB repair, only repair events that result in the restoration of a functional EGFP expression cassette are detected.

The DR-GFP construct (integrated into U2OS 282C, DRaa40 an EJ-DR) consists of two non-functional, direct repeat EGFP Sequences. The first consists of a modified eGFP gene with an I-SceI site containing a premature stop codon (SceGFP), the second is a 3'-truncated modified EGFP ORF (iGFP). Repair via HRR (more specifically short tract gene conversion) results in the generation of a functional EGFP-ORF from DR-GFP (Figure 17 A & Figure 20 A).

The SA-GFP construct (integrated into U2OS 283C) harbors two direct repeats of truncated EGFP-ORFs. The first of the two repeats is truncated at the 3'-end (5'-GFP) the second is truncated at the 5'-end (3'-GFP) and contains an I-SceI site. Signal generation through HRR repair of this construct is prevented by a premature stop codon at the 3'-end of the first ORF (5'-GFP). Upon repair by SSA a functional EGFP gene is reconstituted (Figure 21 A).

The EJ5- GFP construct consists of a CAG promoter (chicken beta-actin promoter with CMV enhancer) that is separated from a full length GFP open reading frame by a puromycin (Puro) gene (Figure 22 A). The Puro gene is flanked by two I-SceI sites in tandem orientation. DSBs induced by I-SceI in this construct can be directly repaired using the proximal ends, thus restoring the two original I-SceI sites. Alternatively, it is possible that the intervening DNA is lost and rejoining occurs between the distal ends, which results in the loss of the Puro gene and one or both of the I-SceI sites. GFP expression is only possible when distal ends are joined and the CAG promoter is brought into proximity of the GFP gene.

U2OS EJ-DR cells were obtained from the Lab of Ranjit S. Bindra, MD, Ph.D. (Smilow cancer hospital, Yale, USA) (Bindra, 2013). These cells were used to examine the influence of NAs on the general mutagenicity of DSB repair. The EJ-RFP system functions after a different principle than the three constructs described above. The EJ-RFP system consists of two integration cassettes that are randomly introduced at different locations in the genome (Figure 23 A). One cassette consists of a tetracycline repressor gene under the control of a constitutively active promoter. The TetR gene

contains a recognition site for the I-SceI endonuclease. The other cassette is a DsRed gene containing several TetR binding sites. Under non inducing conditions TetR is expressed and binds to its binding sites in the DsRed gene, resulting in suppression of gene expression. Upon expression of I-SceI a DSB can be induced in the TetR gene. If this DSB is repaired without any sequence alterations, TetR continues to be expressed. If repair of the DSB results in loss of sequence or a frame shift no functional TetR protein will be expressed. As a consequence, cells that have undergone mutagenic repair will eventually develop red fluorescence. EJ-DR cell also contained an integration of the DR-GFP construct. However, since measurements of the EJ-RFP signal had to be taken 4 days after transfection, data that concomitantly accrued from the DR-GFP integrate did not yield meaningful information with regard to short term NA treatment promptly after transfection (see Discussion 5.3.3 and Figure 37).

I-SceI expression in the U2OS cells was achieved by transient transfection of pCMV-3xNLS-I-SceI (Figure 17 A). Transfection was performed by nucleofection. After transfection, cells were allowed to re-attach for 1.5 h or 3h before drug treatment. Drug treatment lasted for 4 h unless indicated otherwise. Cells were collected and measured by flow cytometry 24 h after transfection unless indicated otherwise. FACS data was analyzed in the Kaluzaa 1.2 software and the percentage of GFP positive cells was determined. Results are expressed as percent repair efficiency of I-SceI transfected controls (no drug treatment). Variations in transfection efficiency could be excluded, as all cells used in one experiment were transfected together in a single reaction and subsequently distributed to several dishes before drug treatment.

3.2.6 Clonogenic survival assay

Clonogenic survival assays determine the reproductive integrity of cells. To allow the formation of isolated colonies arising from a single founder cell, test cells have to be plated at low density. To this end cells were plated from a single cell suspension aiming for 30-150 colonies/dish. With increasing expected cell killing (i.e. higher doses of IR or increasing drug concentrations) the number of plated cells was increased. In this work clonogenic survival assays were used to investigate the radiosensitizing effects of ara-A

and other drugs. A549 cells were grown for 2 days and collected in the exponential phase of growth at the day of the experiment. Survival data obtained at different doses of IR and drug treatment with different concentrations was always normalized to the survival of non-irradiated (0 Gy) cells treated with the same drug concentration. Two slightly different protocols were followed for these treatments:

Protocol I: Cells were plated with the respective concentrations of ara-A and immediately irradiated without significant pre-incubation with the drug (Figure 14 A).

Protocol II: Cells were plated and allowed to attach for 1.5-2 hours. Drugs were added and cells were pre-incubated for a defined period of time before irradiation (Figure 14 B, Figure 16 C, Figure 30 B). Length of pre-treatment was either 15 min (Figure 16 C) or 40 min (Figure 14 B and Figure 30 B), depending on the design and scale of the respective experiments. Within a set of experiments pre-treatment times were always identical.

There were no significant differences between results obtained with the two protocols or different length of pre-treatment. In all cases the medium containing ara-A was removed 4 h after irradiation, the cells were washed twice with medium and then supplied with fresh growth medium containing 10% FBS. The cells were kept at 37 °C, 5% CO₂ for 9-10 days and then stained for counting (1% crystal violet in 70% EtOH). Colonies that comprised 50 or more cells were scored. Curves were fitted to data using the linear-quadratic model.

3.2.7 Pulsed-field gel electrophoresis

Pulsed-field Gel electrophoresis (PFGE) is a method that allows the physical separation of large pieces of DNA within a gel matrix. Conventional constant field agarose gel electrophoresis allows the efficient separation of DNA fragments of 100-200 base pairs (bp) up to approximately 50 kbp. PFGE overcomes this size limit by applying an alternating electrical field and allows the resolution of DNA molecules up to 10 Mbp (Gardiner, 1991; Gurrieri, 1999). In this work asymmetric field inversion gel electrophoresis (AFIGE), a PFGE variation, was used to investigate the repair of DSB in irradiated cells. To this end, cells were embedded in low melting agarose (LMA), cut into

equally sized cylindrical pieces (plugs), lysed, loaded on a gel and subjected to the alternating electrical field for 40h. The amount of DNA that was able to escape the plug and migrate into the gel during the run provides a measure of DSB present in the assayed population.

DSB are induced in a linear fashion proportionally to the dose of IR. However, DNA release in PFGE can vary depending on cell line and cell cycle status of the used culture. To create a standard curve a dose response (DR) was determined within each experiment. Cells were collected, pelleted and resuspended in cold serum-free HEPES-buffered medium at a concentration of 6×10^6 cells/ml. This cell suspension was mixed with an equal volume of pre-warmed (50°C) serum-free medium containing 1% low melting agarose (LMA) to a final concentration of 3×10^6 cells/ml and poured into round glass capillaries for polymerization. The solidified agarose with the cell suspension was subsequently cut into plugs containing approximately 1.5×10^5 cells/plug. DR plugs were placed in 60 mm petri dishes containing 3.5 ml cold HEPES-buffered serum-free medium and X-irradiated on ice. X-ray doses used for DR curves were either from 5 Gy – 20 Gy in steps of 5 Gy, or from 10 Gy to 40 Gy in steps of 10 Gy. Irradiated plugs were immediately placed in cold lysis buffer (10 mM Tris, 50 mM NaCl, 100 mM EDTA, 2% N-lauryl sarcosine, pH 7.6, 0.2mg/ml protease), and incubated at 4°C for 30 min before placing them at 50°C for 18h.

For the evaluation of DSB repair kinetics after IR attached cells were irradiated on ice (unless stated otherwise) with 20 Gy of X-rays. After irradiation cold medium was replaced by fresh pre-warmed growth medium (42°C) to avoid time lag due to prolonged warm up of chilled medium. In drug treatment experiments the replacement medium contained the same concentrations as pre-treatment medium. After each repair time interval cells were collected by trypsinization, embedded in agarose plugs and lysed as described above. After lysis, plugs were washed for 1 h at 37°C in washing buffer (10 mM Tris, 100 mM EDTA, 50 mM NaCl, pH 7.6) and then treated with 0.1 mg/ml RNase A for 1 h in washing buffer at 37°C . For determination of the background-DNA-release, plugs were prepared from otherwise identically treated non-irradiated cells at different time points (typically 2h or 4h and 8h).

Plugs were loaded on 0.5% agarose gels (SeaKem® LE Agarose, Lonza) pre-stained with 0.7 µg/ml EtBr and gel slots were sealed with 1% Agarose. The gels were run in 0.5 x TBE (45 mM Tris, pH 8.2, 45 mM Boric Acid, 1 mM EDTA) in Horizon 20x25 gel boxes with circulating, continuously cooled buffer to ensure a stable temperature of approx. 10 °C during the whole run.

The opposing electrical fields for AFIGE were provided by two power supplies (Bio-Rad) connected to a custom build switching unit. Run parameters were set to cycles of 50 V (1.25 V/cm) for 900 s in the direction of DNA migration (forward) alternating with cycles of 200 V (5.0 V/cm) for 75 s in the reverse direction for a total of 40 hours. Afterwards gels were scanned with a Typhoon 9400 imaging device (GE Healthcare) and analyzed using the ImageQuant™ 5.0 software (GE Healthcare).

The fraction of DNA released (FDR) was calculated by dividing the signal of DNA released into the gel (lane) by the total signal (lane + plug). The FDR values of irradiated samples were corrected by the background values of non-irradiated control cells (see above). Using FDR values derived from the linear DR standard curves a dose equivalent (DEQ) in Gy was calculated for the repair kinetics (RK) data points. DEQ was plotted against repair time and curve fitting was performed in SigmaPlot 11.0 software using an exponential decay algorithm assuming a fast and slow component in the RK curves.

3.2.8 PFGE with sorted cell populations

Experiments with cell populations sorted by flow cytometry generally followed the protocol for PFGE described above with some adjustments as laid out below. Due to the large number of cells required per repair time point, sorting is a time consuming procedure that only allows the processing of a few samples per day. Thus the cells that were collected at each time point on the day of the experiment were frozen for later sorting. Freezing was done by resuspending washed, pelleted cells in cold freezing solution A (5mM KH₂PO₄, 25mM KOH, 30mM NaCl, 20mM L (+) lactic acid, 5mM Dextrose, 0.5mM MgCl₂, 200mM Sorbitol in Milli-Q H₂O) and gently mixing this suspension with an equal volume of freezing solution B (Freezing solution A with 20%

DMSO). Cells were then transferred to -150 °C for snap freezing and storage. Controls were prepared before freezing and every following step of the procedure. For sorting, aliquots of cells were quickly thawed and suspended in cold growth medium. The thawed cells were stained with propidium iodide (PI) in a permeabilizing solution (PI 40 µg/ml, Tris 0.1M, NaCl 0.1M, MgCl₂ 5mM, Triton X-100 0.05%) sorted according to DNA content in a Beckman-Coulter Epics Altra Flow Cytometer. Several measures had to be taken to optimize cell recovery. Cells were collected in tubes pre-coated with Dichlorodimethylsilane (Merck, 2% solution in 1,1,1-trichloroethane) into 0.5 ml of heat treated fetal bovine serum. Sheath fluid (phosphate-buffered saline, PBS) and collection tubes were continuously chilled (10 °C) during sorting. Numbers of deposited cells were reconfirmed with manual counting in a Rosenthal chamber. Plugs for PFGE were prepared as described above, with the exception that cell numbers of sorted populations were adjusted to contain 1 x 10⁵ cells/plug for G1 populations, and 0.5 x 10⁵ cells/plug for G2 populations - to ensure equal amounts of DNA per plug.

3.2.9 Immunofluorescence staining

For immunofluorescence detection of Rad51 foci in A549 cells were grown for two days on glass coverslips in 30 mm petri dishes aiming for a total number of 500.000 cells per dish. Prior to irradiation cells were subjected to a 15 min pulse of 10 µM 5-ethynyl-2'-deoxyuridine (EdU). This was done in order to enable identification of cells that were synthesizing DNA at the time of irradiation, i.e. S-Phase cells. Immediately before irradiation EdU was washed away and cells were supplied with fresh medium. Cells were irradiated with 4 Gy X-rays and kept at 37 °C for, 5% CO₂ for 3h. After incubation, cells were briefly washed with PBS and fixed with 2% PFA for 15 min. Fixed cells were washed with PBS again and permeabilized with 0.5% Triton X-100 in 100 mM Tris, 50 mM EDTA. After permeabilization cells were washed twice with 3% BSA. Incorporated EdU was stained with the Click-iT® EdU Alexa Fluor® 647 imaging kit according to manufacturer's instructions. Click chemistry allows the addition of a fluorophore to EdU incorporated in DNA without the need for denaturation. A Click reaction is a copper-catalyzed covalent reaction between an azide and an alkyne. In this application, the EdU

carries the alkyne and the Alexa Fluor® dye presents the azide (Salic and Mitchison, 2008; Invitrogen, 2011). Briefly, a reaction cocktail was prepared containing Copper sulfate (CuSO₄), Alexa Fluor® 647 azide and the buffer and additive provided in the kit. Cells grown on coverslips were placed on 100 µl drops of the reaction cocktail on Parafilm (Pechiney Plastic Packaging) for 30 min and protected from light. Afterwards cells were washed again in 3% BSA and then incubated for one hour in a blocking solution containing 0,2 % gelatin and 0,5 % BSA fraction V in PBS. Cells were then incubated with primary antibody (Ab) in blocking solution overnight, using mouse monoclonal IgG2b Rad51 14B4 (Genetex) and rabbit polyclonal IgG cyclin B1 H-433 (Santa Cruz). Incubation with secondary Ab for one hour was performed the next day after triple washing with PBS. Rad51 was detected using Alexa 488 polyclonal goat anti-mouse IgG and cyclin B1 was detected using a polyclonal Alexa 568 conjugated anti rabbit IgG antibody from goat (both Invitrogen). Finally the coverslips were incubated with 4',6-diamidino-2-phenylindole (DAPI) for staining of DNA and mounted on microscopic slides with ProLong® Gold antifade reagent (Invitrogen). Slides were stored in the dark for at least 24h before analysis by confocal laser scanning microscopy.

Immunofluorescence detection of various IRIF in serum deprived MEF Lig4^{-/-} was performed using the same antibody staining protocols using antibodies and dilutions as stated in Table 3.7, but without labeling with EdU.

Table 3.7: Antibodies Immunofluorescence

IF Primary Ab	Host/ type	specificity	Dilution	Provider
Cyclin B1	Rabbit polyclonal	Human	1:100	Santa Cruz
Rad51 (14B4)	Mouse monoclonal	Human	1:400	Genetex
gH2AX (pS139)	Mouse monoclonal	Human, mouse	1:200	Abcam
53BP1 (H-300)	Rabbit polyclonal	Human, mouse	1:200	Santa Cruz
pATM-S1981 (10H11.E12)	Mouse monoclonal	Human, mouse	1:400	Cell Signaling
IF Secondary AB	Host/ type	Specificity		Provider
Alexa488	goat polyclonal	Mouse IgG	1:400	Invitrogen
Alexa568	goat polyclonal	Rabbit IgG	1:400	Invitrogen
Alexa633	goat polyclonal	Rabbit IgG	1:400	Invitrogen

3.2.10 SDS-PAGE

Denaturing SDS-Polyacrylamide gel electrophoresis allows the separation of proteins according to their molecular weight in a unidirectional electrical field. Cellular protein extracts for SDS-PAGE were prepared using RIPA buffer with the addition of a protease inhibitor cocktail. SDS-PAGE gels consisted of a 5% stacking and a 10% resolving gel, which were cast into Bio-Rad mini gel stands. For loading 20-50 μ g (depending on the protein to be detected) cell extracts were mixed 1:1 with 2x Laemmli Buffer, denatured for 5 min at 96 °C and centrifuged briefly at 13000 rpm. For electrophoresis a constant voltage of 100 V was set for 2 h.

3.2.10.1 Western blot

During Western blotting proteins are transferred from a SDS-polyacrylamide gel onto a nitrocellulose membrane. Transfer was performed using an iBlot® dry blotting system (Invitrogen). For transfer pre-assembled blotting stacks (Invitrogen) containing a nitrocellulose membrane were used. After transfer the membrane was incubated for 2 h in 5% non-fat dry milk in 1 x TBS-T (0.05% Tween20 in 1 x PBS). For immunodetection the membranes were incubated overnight at 4 °C with primary Ab. After washing three times for 10 min in PBS-T the secondary Ab was incubated for 1.5 h and the membrane was again washed three times in PBS-T prior to detection. The Odyssey® Infrared Imaging System from LI-COR Biosciences was used for detection and analysis.

Table 3.8: Antibodies Western blot

WB Primary Ab	Host/ type	specificity	Dilution	Provider
BRCA2 (3E6)	Mouse monoclonal	Human	1:500	GeneTex
Rad51 (Ab-1)	Rabbit polyclonal	Human	1:2000	Calbiochem
Rad52 (F-7)	Mouse monoclonal	Human	1:500	SantaCruz
Ku80 (H-300)	Rabbit polyclonal	Human	1:400	SantaCruz
GAPDH (MAB374)	Mouse monoclonal	Human	1:10000	Millipore
WB Secondary Antibody	Host/ type	Specificity	Dilution	Provider
IRDye 800CW	Goat polyclonal	rabbit	1:10000	LI-COR
IRDye 800CW	Goat polyclonal	mouse	1:10000	LI-COR
IRDye 680LT	Goat polyclonal	mouse	1:10000	LI-COR
IRDye 680LT	Goat polyclonal	rabbit	1:10000	LI-COR

3.2.11 Confocal laser scanning microscopy (CLSM) and foci quantification

CLSM was performed on a LEICA TCS-SP5 confocal microscope to generate high resolution three dimensional image data of the stained cells. A key feature of a confocal microscope is the pinhole in front of the optical detector, a photo multiplier tube (PMT), that blocks out emission light that originates from all other points within the sample (out-of-focus light) but the points in the focal plane of the objective. Thus a considerable increase in optical resolution and contrast as compared to conventional fluorescence microscopy is achieved. In CLSM the sample is scanned by a focused laser beam that moves over the specimen in lines and only illuminates a small focal volume of the sample at any given time. Confocal scanning in steps of 0.5 μM along the Z-Axis through the whole specimen was performed to obtain a stack of optical sections (Z-stack). These pictures were used to create a three-dimensional image of the spatial structure of the investigated specimen, which was saved as LIF file and used for foci analysis. For data presentation, image stacks were merged into a single two-dimensional picture, the maximum intensity projection (MIP), and exported as TIFF files. For each slide at least 5 fields were analyzed, with an average of 120 S- and 20 G2-phase cells per sample. Parameters and settings used for CSLM and foci analysis are summarized in Table 3.9.

Foci were scored using the ImarisXT[®] 6.0 Software. For this purpose LIF files were loaded into the Imaris software and processed using embedded MatLab features. Fluorescent spots with a diameter above 0.5 μm and intensity above a set gray value threshold, which was kept constant within experiments, were identified as foci and grouped into object clouds within each nucleus. The threshold values were kept identical throughout all experiments. The number of foci within each single nucleus was recorded and average foci numbers were calculated. It was discriminated between cells in G1, S or G2 phase based on the staining of cyclin B1 and EdU incorporation.

Table 3.9: Microscope settings and parameters

Hardware	Type
Microscope	Leica TCS-SP5
Objective	HCX PL APO lambda blue; 63.0x1.4 OIL UV
Acquisition parameter	Mode
Scan direction	Bidirectional
Zoom	1
Speed	400 Hz
Resolution	1024x1024
Excitation laser	Intensity setting
405 nm	25 %
488 nm	10 %
561 nm	20 %
633 nm	20 %
Detector Range	PMT voltage / Offset
415 nm – 490 nm	700.8 / -4 %
505 nm – 547 nm	636.0 / -3.5 %
587 nm – 621 nm	750.2 / -4,9 %
657 nm – 684 nm	600.6 / -2 %

Imaris parameter	Value
Minimal spot size	0.5 μm

3.2.12 In vivo replication assay

Inhibition of cellular DNA synthesis by various drug treatments was assayed by incorporation of tritium labeled thymidine (^3H -thymidine). A549 Cells were grown in 25 cm^2 flasks under standard tissue culture conditions (37 $^{\circ}\text{C}$, 5% CO_2) with caps loosely screwed on for 24 h. One day before the experiment caps were fastened and flasks transferred to a warm room (37 $^{\circ}\text{C}$) with normal atmosphere for another 24 h. All further steps of the experiment were performed in the warm room, to avoid decrease of replicative activity caused by temperature fluctuations. Drugs were added 30 min prior addition of the ^3H -thymidine pulse. Controls were treated with the respective solvent. ^3H -thymidine was added to the drug containing medium to a concentration of 0,5 $\mu\text{Ci/ml}$. Radioactive medium was removed 20 min later, cells were washed with ice cold PBS and trypsinized. The collected cells were kept on ice until further processing. Cells were counted with the MultisizerTM 3 cell counter (Beckman coulter) for later normalization to allow comparisons between samples. Cells were sucked onto a glass microfibre filter (WhatmanTM, GF/A, 25 mm) using a vacuum manifold. Trichloroacetic acid was added to the filters and incubated for approximately 5 min before being sucked through. The filters were washed with Millipore water and sucked dry. Subsequently the filters were transferred to the bottom of scintillation vials. To each vial 0.5 ml of 0.5 N NaOH were added and incubated overnight at 65 $^{\circ}\text{C}$. On the following day 0.5 ml 0.5 N HCl were added to each vial. Lastly, 10 ml of a scintillation cocktail (Unisafe 1, Zinsser Analytic) was added and the vials were mixed thoroughly using a vortex mixer. Measurements were taken in a Tri-Carb Liquid Scintillation Counter 1900 TR (Packard) 6 h to 24 h later.

4 Results

4.1 Inhibition of DNA replication in A549 cells

One of the most prominent biological effects of ara-A in mammalian cells is inhibition of DNA replication. To determine the concentrations required to achieve effective inhibition at this endpoint we performed DNA replication assays with A549 lung carcinoma cells.

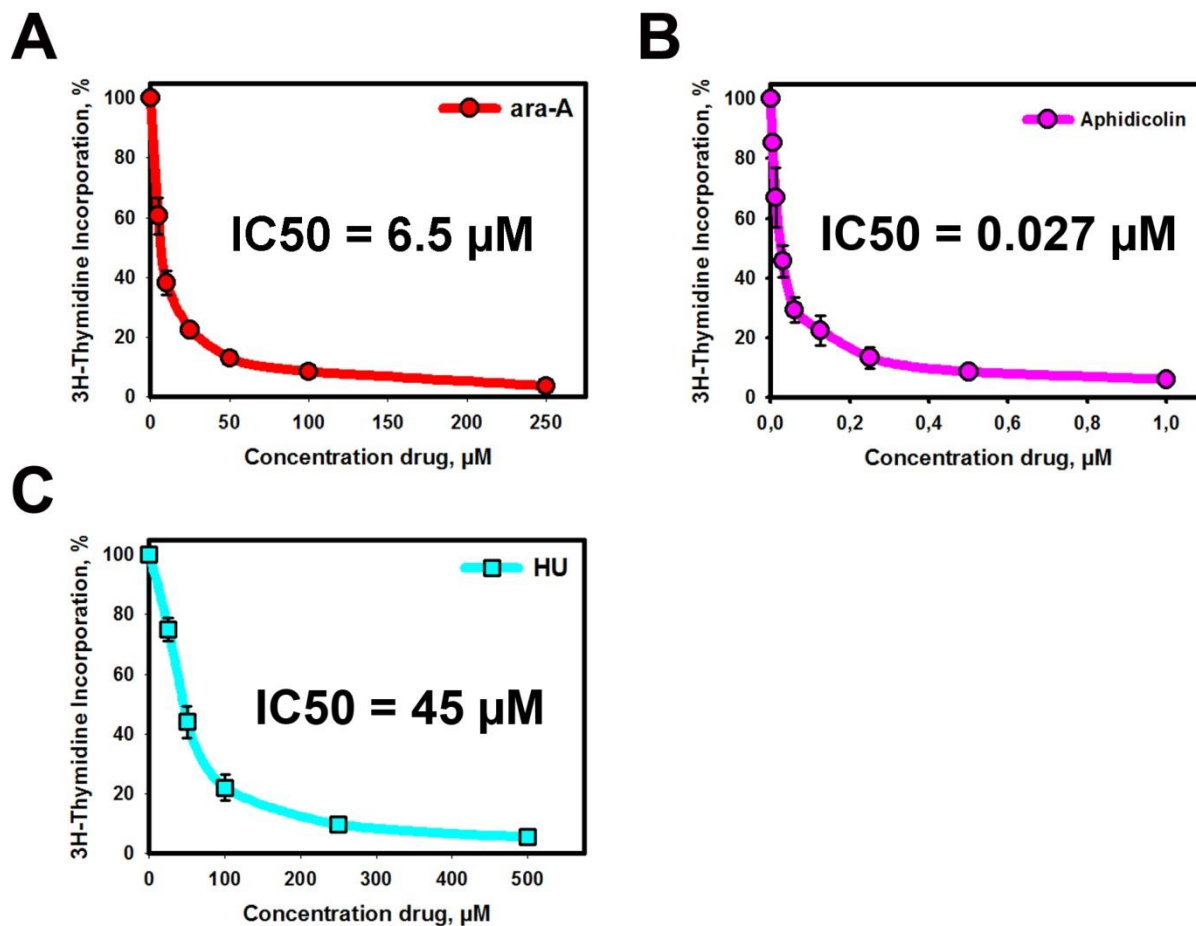


Figure 13 Measurement of DNA replication by ³H-thymidine incorporation in A549 cells. **A)** Effect of ara-A treatment on DNA replication. Data points show the mean and standard deviation (s.d.) of three independent experiments. **B)** Effect of aphidicolin treatment on DNA replication. Data points show the mean and standard deviation (s.d.) of three independent experiments. **C)** Effect of hydroxyurea (HU) treatment on DNA replication. Data points show the mean and standard deviation (s.d.) of three independent experiments. Bold text in each graph indicates the IC50 values for DNA replication inhibition.

We also compared the inhibition of replication exerted by ara-A in this assay to the inhibition by two non-NA replication inhibitors. Specifically, we used hydroxyurea (HU), a small molecule known to inhibit RnR, and aphidicolin, an inhibitor of DNA polymerases (α, δ & ϵ). Replication was assayed by incorporation of tritium labeled thymidine (3H-thymidine). Inhibitors were added 30 min prior to a 20 min pulse treatment with 3H-thymidine. Subsequently cells were lysed and incorporation of 3H-thymidine was measured in a liquid scintillation counter.

Figure 13 shows the results obtained with the replication inhibitors normalized to controls incubated without drug. The concentration at which 50% of the maximum inhibition of replication was achieved ($IC_{50_{repl}}$) was determined. Figure 13 A shows the inhibition of DNA replication by ara-A in A549 cells. An $IC_{50_{repl}}$ of 6.25 μ M was determined. Aphidicolin proved to be the most effective inhibitor of DNA replication in our experiments with an $IC_{50_{repl}}$ of 0.027 μ M (Figure 13 C). Much higher concentrations of HU were required to achieve comparable inhibition of replication ($IC_{50_{repl}} = 45$ μ M; Figure 13 D).

4.2 Radiosensitization of cycling A549 cells by ara-A

Having established the effectiveness of ara-A in our cell system, we next investigated the potential of ara-A to sensitize cycling A549 cells to IR. Cells were routinely maintained in the exponential phase of growth. For experiments, A549 cells were grown for 2 days and collected by trypsinization while still in the exponential phase of growth. Cells were plated at numbers (estimates from available survival data) aiming for 30-150 colonies/dish after exposure to pre-defined radiation doses. Two slightly different protocols for survival assays with drug treatment and irradiation were applied within this work (protocols I and II; see Materials and Methods), that vary with regard to cell attachment time and drug pre-incubation before irradiation. Both protocols yielded comparable results. Figure 14 A (protocol I) shows strong radiosensitization of A549 cells by 250 μ M, 500 μ M and 1000 μ M of ara-A that increased with increasing drug

concentration. At concentrations of 500 μM and above a shoulderless survival curve was obtained.

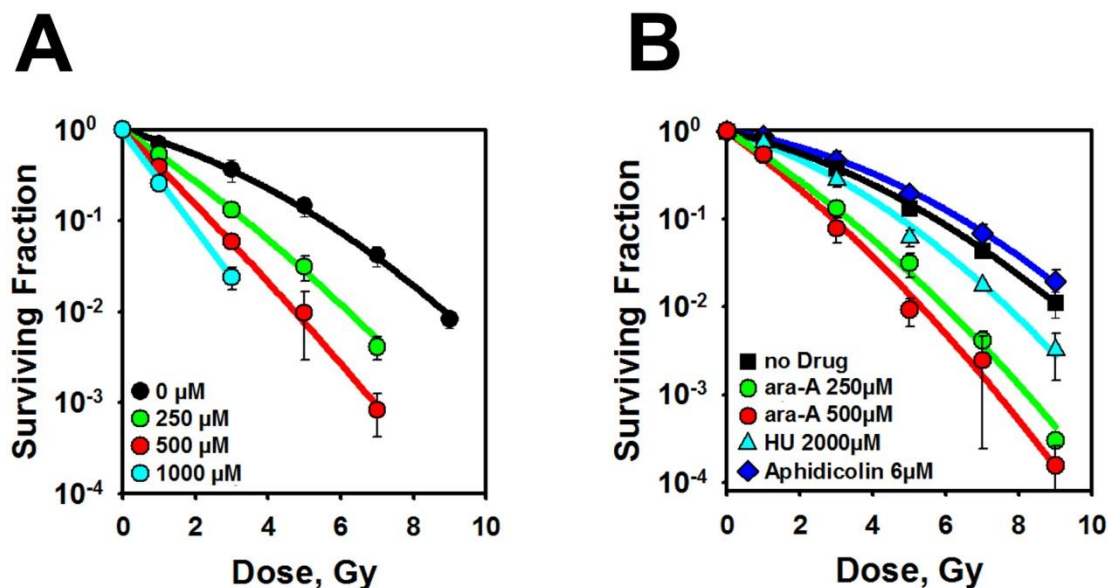


Figure 14 Effect of ara-A on the radiosensitivity to killing of A549 cells. **A)** Exponentially growing A549 cells were exposed to the indicated doses of ara-A for 4 h after IR. Plating efficiency (PE) was 0.68, 0.55, 0.42 and 0.29 for cells exposed to 0, 250, 500, and 1000 μM , respectively. Black circles represent cells treated with 0 μM ara-A, green circles cells treated with 250 μM ara-A, red circles cells treated with 500 μM ara-A and blue circles cells treated with 1000 μM ara-A. The results shown represent the mean and standard error calculated from three independent experiments, each including double determinations. **B)** Comparison of radiosensitization by 4h post-irradiation treatment with ara-A and other DNA replication inhibitors in exponentially growing A549 cells. Red circles, ara-A (500 μM); green circles ara-A (250 μM); light blue triangles, HU (2000 μM); dark blue diamonds, aphidicolin (6 μM); black squares, control (no drug treatment). The results shown represent the mean and standard error calculated from three independent experiments, each including double determinations.

Sensitizer enhancement ratios (SER) were calculated for radiosensitization by ara-A. Two different approaches were employed for this calculation: 1. SER was determined at a fixed dose of 2 Gy by dividing the fraction of surviving cells (SF2) without drug

treatment by that measured with ara-A treated cells. 2. SER was determined at a fixed cell survival of 37% (the survival fraction at which statistically each cell within a population has received on average one lethal hit) by dividing the corresponding radiation dose of untreated cells to that of treated cells. The SER calculated for 500 μM ara-A was 3.7 based on SF2 and 2.9 based on 37% survival (Table 1).

Table 4.1: Quantification of ara-A mediated radiosensitization. Sensitizer enhancement ratios (SER) were calculated for the survival of A549 cells at 2 Gy (SF2), as well as for the radiation dose where cell survival was 37% (37%sv).

Conc. Ara-A	SER (SF2)	SER (37%sv)
250 μM	2.0	1.9
500 μM	3.7	2.9
1000 μM	7.9	3.8

This observation was in agreement with earlier results showing radiosensitization of rodent and human cell lines (in the plateau and the exponential phases of growth, respectively) by treatment with ara-A. Since ara-A effectively inhibits DNA replication we inquired whether radiosensitization by ara-A may be attributable to inhibition of this cellular function alone. To answer this question we compared radiosensitization elicited by post-irradiation treatment with ara-A with the radiosensitizing effects of HU and aphidicolin (Figure 14 B; Protocol II, 40 min pre-incubation). Since these compounds inhibit DNA replication with widely different efficiencies we used the $\text{IC}_{50_{\text{repl}}}$ values as orientation for the comparison of the radiosensitizing effect. We observed that aphidicolin at 6 μM (~220-fold $\text{IC}_{50_{\text{repl}}}$) did not sensitize cells to IR at all. In contrast, ara-

A at 250 μM (40-fold $\text{IC}_{50_{\text{repl}}}$) and 500 μM (80-fold $\text{IC}_{50_{\text{repl}}}$) caused marked radiosensitization of A549 cells. HU at 2000 μM (\sim 45-fold $\text{IC}_{50_{\text{repl}}}$) did cause radiosensitization in these cycling cells, but the effect was only modest compared to the effect of ara-A. From this result we concluded that effects beyond DNA replication inhibition must underpin the radiosensitizing effect of ara-A, which should be more specific than global inhibition of DNA replication. We hypothesized that the drug somehow interferes with the repair of IR-induced DSB. Although inhibition of DNA synthesis alone appears not to be sufficient to explain the radiosensitizing effect of ara-A, it may well play a role in the interference with DSB repair. Pathways of HRR are the only DSB repair mechanisms known to involve extensive DNA synthesis. Thus, we decided to first investigate possible interactions of ara-A with HRR.

4.3 Impact of ara-A treatment on HRR

4.3.1 Inhibition of IR induced RAD51 foci formation by ara-A

Rad51 is the central recombinase in HRR that forms a nucleoprotein filament on the resected DNA ends during the repair process. Accumulation of Rad51 at sites of DSB can be visualized by immunofluorescence staining as discrete foci. These foci form and decay with characteristic kinetics upon exposure of cells to IR. Scoring of Rad51 foci is widely used as a surrogate marker of HRR function. We applied this method to investigate possible interference of ara-A with HRR.

We used exponentially growing A549 cells and selected a radiation dose (4 Gy) and time point of observation (3 h) known to produce maximum numbers of Rad51 foci (previous unpublished work from our group). In addition to Rad51 staining, we included additional staining protocols allowing the assignment of each cell in a particular phase of the cell cycle. Expression of cyclin B1 is regulated differentially throughout the cell cycle: Expression starts in S-phase and continues in G2. However, staining with cyclin B1 is not sufficient for a reliable assignment of cells in G1, G2 and S cells. Expression of cyclin B1 is weak in early- to mid-S phase cells, but remains high between late-S and G2 phase. Therefore, to improve the discriminatory power of our assay we also included

incorporation and staining of EdU. EdU is an analog of thymidine that was recently developed as an alternative for BrdU for the detection of S-phase cells in a proliferating cell population (Cappella, 2008). EdU like BrdU is incorporated into DNA without inhibiting DNA replication. However, for detection of BrdU, DNA must be denatured in order to grant the required antibodies access to the incorporated BrdU nucleotides. Detection of EdU on the other hand is based upon a chemical reaction whereby a fluorophore is coupled covalently to the incorporated nucleotide without the need for DNA denaturation. Together, EdU and Cyclin B1 staining allowed for an unambiguous assignment of each analyzed cell in a phase of the cell cycle. EdU positive cells were identified as being in S-phase at the time of irradiation and were analyzed either during S-phase or in the subsequent G2-phase of the cell cycle. Cells that were positive for cyclin B1 but negative for EdU were scored as being in G2 during the time of irradiation and remaining in G2 in the following repair time interval. Cyclin B1 and EdU negative cells were scored as being in G1 at the time of irradiation. G1 cells were not scored in the context of the present set of experiments, as G1 cells fail to develop Rad51 foci after IR (Figure 15 A).

Our labeling strategy allowed us to stringently discriminate G1, S and G2 phase cells from each other and allowed us to analyze a large number of S-phase cells (385 (+/-106); n= 3). However, the number of G2 cells that could be analyzed was relatively small (61 (+/-19); n= 3). This is mainly due to two factors: First, in an exponentially growing culture of A549 cells, the number of cells in G2 is typically only about a quarter of the number of cells in S. Second, in our experiments cells were fixed 3h after irradiation, a time during which a large proportion of cells that were in G2 could have entered mitosis without irradiation. However, irradiation with a dose of 4 Gy is expected to induce a G2 block that would prevent most G2 cells from progressing into mitosis. Nevertheless, more cells may have escaped the G2/M checkpoint activation than expected. This could explain why we did not only find 4 times more S-phase cells, but about 6 times more.

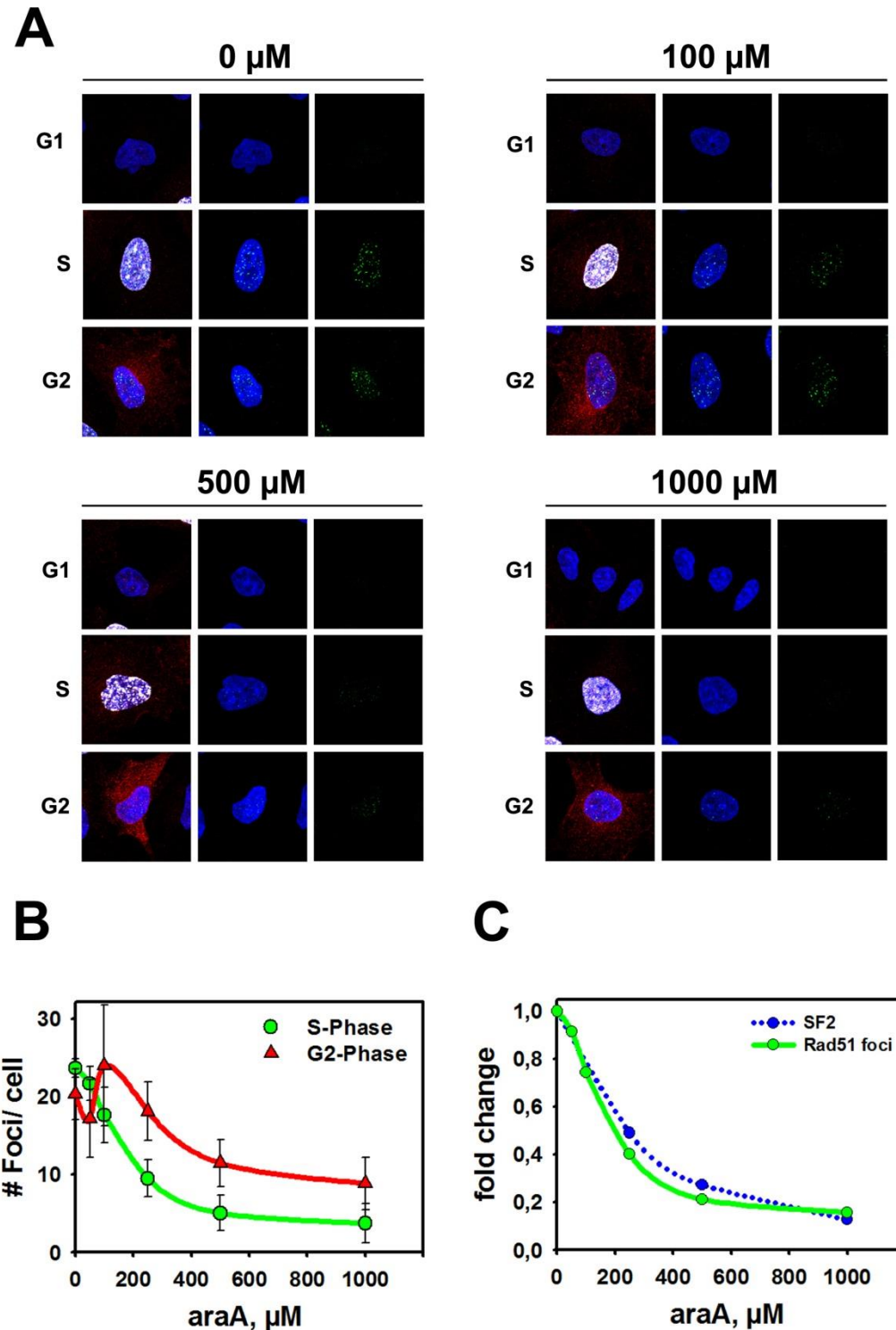


Figure 15 Inhibition of Rad51 foci formation in A549 cells by ara-A. Cells were fixed and stained 3 h after exposure of exponentially growing A549 cells to 4 Gy X-rays and treatment with different concentrations of ara-A. To label cells in S-phase, cultures were exposed to an EdU pulse (15 min) just before irradiation. Late-S and G2-cells were identified by staining for Cyclin B1. **A)** Split channel

representation of confocal microscopy immunofluorescence images. Micro molar indications above the individual blocks show the respective ara-A concentration. The left column of each block shows an overlay of DAPI (blue), EdU (white), Cyclin B1 (red) and Rad51 (green) staining. The middle column shows an overlay of DAPI (blue) and Rad51 (green) staining. The right column shows Rad51 staining alone (green). **B)** Number of Rad51 foci scored in S-phase (green circles and line) and G2-Phase cells (red circles and line) as a function of ara-A concentration. Mean foci number and s.e.m. from 3 independent experiments are shown. Each S-phase data point represents a total of 384 (± 105) cells (~130 S-phase cells were analyzed for each concentration in every experiment). Each G2 data point represents of 61 (± 19) cells on average in 3 independent experiments (~20 G2-phase cells were analyzed for each concentration in every experiment). **C)** Comparison of the concentration dependency of survival of A549 cells at 2 Gy (post-irradiation treatment with ara-A for 4 h) and Rad51 foci suppression in A549 by ara-A. Curves were derived from the data presented in Figure 14 and Figure 15 B.

Quantitative analysis of immunofluorescence images revealed a marked reduction in the number of Rad51 foci in ara-A treated cells irradiated during the S-phase (Figure 15 B; green circles). Half maximum inhibition of Rad51 foci formation was about 165 μM ara-A and Rad51 foci formation almost ceased above 500 μM . The ara-A concentration-Rad51 foci-effect relationship is very similar to that of radiosensitization to killing at 2 Gy, which implies a cause-effect relationship between these two endpoints (Figure 15 C).

Higher concentrations of ara-A appeared to be required in G2 to reduce the number of Rad51 foci to similar levels like in S-phase cells. Nevertheless, the reduction of Rad51 foci formation in ara-A treated G2-phase cells followed a similar trend. At concentrations above 250 μM a strong reduction was observed in the number of Rad51 foci and more than 50% inhibition was achieved at 1000 μM ara-A (Figure 15 B; red triangles and line). We concluded therefore that ara-A must exert a strong inhibitory effect on HRR. Figure 15 C shows the normalized number of Rad51 foci (S + G2) and the normalized survival at 2 Gy, both plotted against the ara-A concentration. The curves show an almost identical course in dependence of drug concentration, suggestive of an underlying cause-effect relationship.

4.3.2 Proficiency in HRR is a prerequisite for radiosensitization by ara-A

Results obtained by scoring Rad51 foci prompted us to hypothesize that inhibition of HRR may constitute an important mechanism of radiosensitization by ara-A. If inhibition of HRR was a major mechanism of radiosensitization, sensitization of cells already deficient for HRR should be reduced as compared to HRR proficient cells. Maximum suppression of HRR would theoretically be achieved in the absence of Rad51 (see also Figure 19). Since knockout of Rad51 is lethal in mice as well as in human cell lines, we attempted to induce a transient deficiency in HRR by RNAi mediated knockdown of Rad51. In order to enable direct comparisons with the already available cell survival measurements (see above), we used A549 cells to carry out these knockdown experiments. We used the same siRNA against Rad51 used in the DR-GFP experiments and as a negative control a siRNA against GFP. Cells were grown for 48 h before transfection with the respective siRNA. After transfection cells were cultured for another 24h before collection and processing for plating and irradiation for colony formation. Cells were left for 1.5h to attach before addition of ara-A. Cells were pre-incubated with the drug for 45 min before irradiation and the drug was washed away 4h later (Protocol II). Cellular levels of Rad51 protein were monitored by western blotting and proved to be reduced by more than 90% after transfection of the corresponding siRNA (Figure 16 A). Plating efficiency (PE) of cells transfected with siRNA targeting GFP was equal to that commonly found for untreated A549 cells. Furthermore, cells transfected with this control exhibited normal radiosensitivity to killing and were radiosensitized by ara-A to the same extend as untransfected cells in previous experiments.

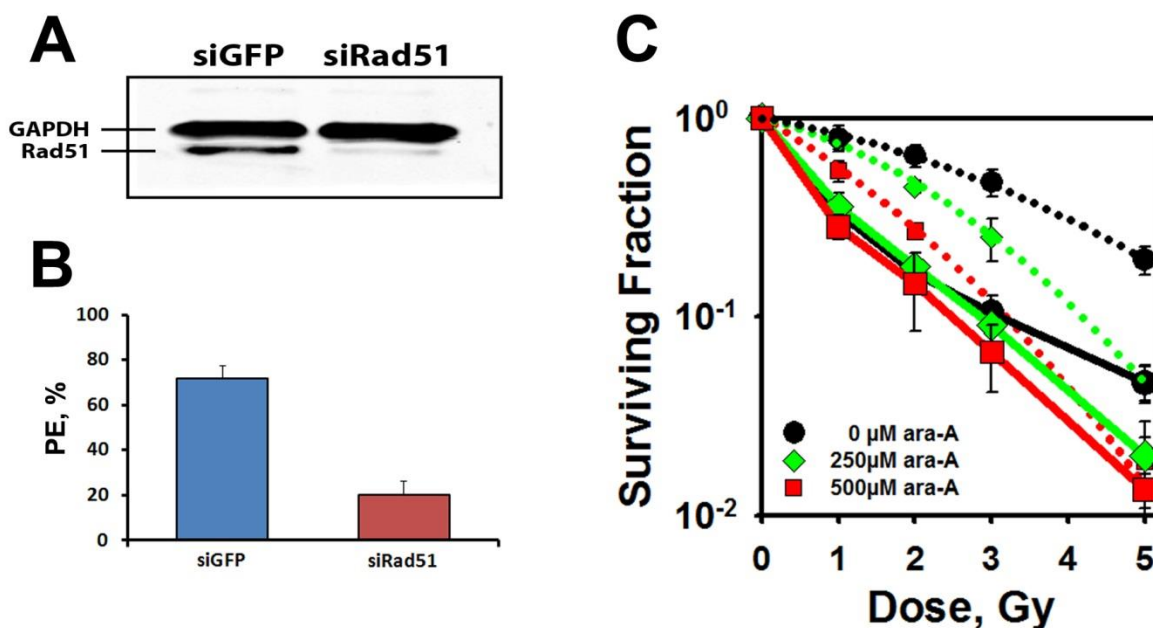


Figure 16 Requirement of HRR for the radiosensitization by ara-A. **A)** Detection of RAD51 protein in A549 cells 48h after transfection with either control (siGFP) or Rad51 (siRad51) siRNAs. GAPDH was used as a loading control. Detection of RAD51 and GAPDH was performed simultaneously using secondary antibodies with two different infrared dyes. Rad51 protein was reduced by more than 90% through RNAi. **B)** Plating efficiencies (PE) of siRNA transfected A549 cells. Cells transfected with the control siRNA exhibit the same PE typical for untransfected A549 cells. Cells transfected with siRad51 showed a decreased PE of about 20%. Bars show mean and s.d. from 3 independent experiments. **C)** Radiosensitivity of siRNA transfected cells treated with different concentrations of ara-A. *Dotted lines:* Cells transfected with siGFP. *Solid lines:* Cells transfected with siRad51. *Black circles and curves:* No ara-A treatment. *Green diamonds and curves:* Treatment with 250 μ M ara-A. *Red squares and curves:* Treatment with 500 μ M ara-A. Plots show mean and s.d. of 3 independent experiments.

This confirmed that the transfection procedure itself had no significant impact on the viability and radiosensitivity of cells. On the other hand, we found that the PE of cells transfected with siRNA against Rad51 was reduced (20% \pm 6% vs. 72% \pm 6) (Figure 16 B). This was not unexpected, as cells deprived of key HRR factors have been shown to display reduced PE (Feng, 2011; Liu, 2011; Short, 2011; Jensen, 2013). Importantly, cells treated with siRNA against Rad51 were significantly more radiosensitive than the corresponding controls. This is in agreement with the radiosensitive phenotype shown by others after Rad51 knockdown and confirms that cells retaining their ability to form

colonies after transfection of Rad51 siRNA do not represent an untransfected subpopulation (Liu, 2011; Short, 2011). In Rad51 depleted cells treatment with ara-A failed to further increase the radiosensitivity at most irradiation doses (Figure 16 C). Only at the highest radiation dose used in these experiments (5 Gy) we observed a significant ($p= 0.006$) radiosensitization by ara-A. However, the shape of the survival curve and the observed increase in radioresistance makes it likely that this radiosensitization derived from a small subpopulation that retained more HRR function than the bulk of cells. We concluded that HRR proficiency is a pre-requisite for efficient ara-A mediated radiosensitization.

4.3.3 Effects of ara-A on homology directed repair in reporter gene assays

4.3.3.1 Effects of ara-A on HRR

Several cellular reporter gene systems exist that claim to provide a measure for the activity of specific DSB repair pathways. To further investigate inhibition of HRR by ara-A we employed cell lines bearing stable integrations of a repair reporter construct that is designed to detect events that can arise due to the activity of the SDSA sub-pathway of HRR. This construct, DR-GFP, consists of two modified GFP gene sequences oriented as direct repeats (hence the name DR-GFP; see Figure 17 A). The first of the two sequences is a full length GFP gene (SceGFP), which is disrupted by an I-SceI site and a premature Stop-codon. It is followed by a 3' truncated inactive copy of GFP (iGFP). Functional GFP cannot be expressed from any of the two GFP gene sequences in the construct. Upon expression of the I-SceI endonuclease a DSB is introduced in the SceGFP gene. If this DSB is repaired by HRR using iGFP as donor sequence, the I-SceI site and the premature Stop-codon in the SceGFP gene will be replaced by functional GFP sequences. Such a gene conversion event results in the reconstitution of a functional GFP gene. Cells that have undergone this form of repair can be easily detected by flow cytometry due to the resulting GFP fluorescence.

A CHO cell line, Draa40, carrying the DR-GFP construct was immediately available to us. Initial experiments were carried out using the following experimental protocol: CHO cells were transfected with the I-SceI expression plasmid (pCMV3xNLSI-SceI; Figure 17 A) using electroporation (Nucleofector; Lonza), which requires cell trypsinization and the generation of a suspension with high cell concentration. After transfection cells were plated with normal growth medium and incubated for 3h at under standard culture conditions to allow for reattachment of cells and the expression of I-SceI. Three hours later, ara-A was added and the cells were maintained with the drug for an additional 4h. At the end of the treatment time interval, drug-containing medium was removed and cells were washed and supplemented with fresh growth medium. Cells were collected 24h after transfection for analysis by flow cytometry (Figure 17 B).

Using this protocol we first investigated the concentration-dependent effects of ara-A on HRR. Ara-A is significantly more toxic to CHO than to human cells. Therefore we chose 500 μ M ara-A to be the upper concentration limit. We found a strong correlation between increasing ara-A concentration and decreasing proportion of cells developing green fluorescence, indicating inhibition of HRR (Figure 17 C).

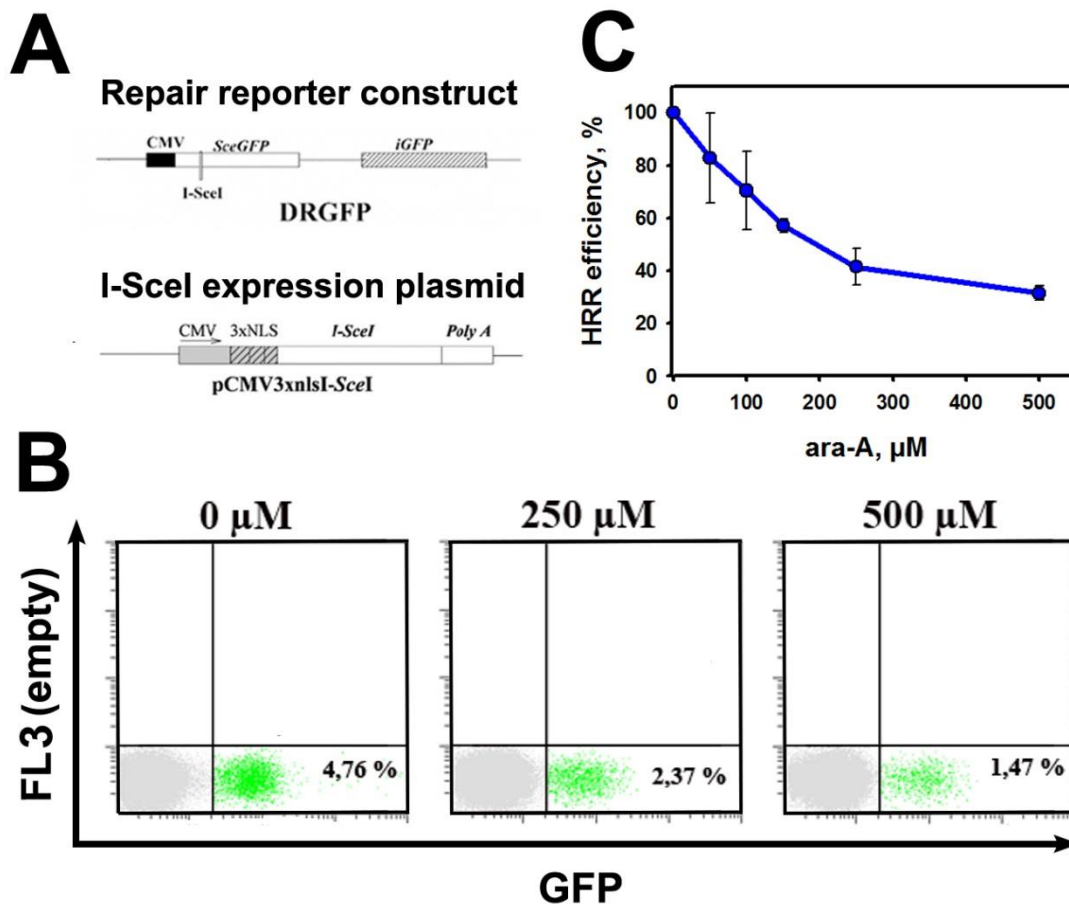


Figure 17 Suppression of HRR in DRaa40 cells harboring the DR-GFP reporter. **A)** Schematic of the stably integrated DR-GFP reporter construct and the I-SceI expression plasmid used to induce DSB in transfected cells. **B)** Representative flow cytometry dot plots of DRaa40 cells treated with different concentrations of ara-A. GFP was measured in fluorescence channel 1 (FL1). For better depiction of the positive populations, the GFP signal was plotted against signal recorded in FL3, for which no stain is included and in which cells showed very low autofluorescence. **C)** Graphical representation of HRR efficiency as a function of ara-A concentration (treatment 3h-7h after transfection) in DRaa40 cells. Data points show the mean and s.d. from 3 independent experiments.

At 500 μ M ara-A suppressed HRR by about 70% (Figure 17 B&C). We next sought to determine whether there is a temporal relationship between HRR inhibition and the position of the treatment time window. We performed experiments in which we compared the effect of the default 3-7h post-transfection treatment to equal duration treatments applied at later times after transfection. We found that inhibition was

significantly weaker ($p= 0.002$) when the treatment was initiated 7h after transfection, and not present when treatment started 20h post transfection (Figure 18).

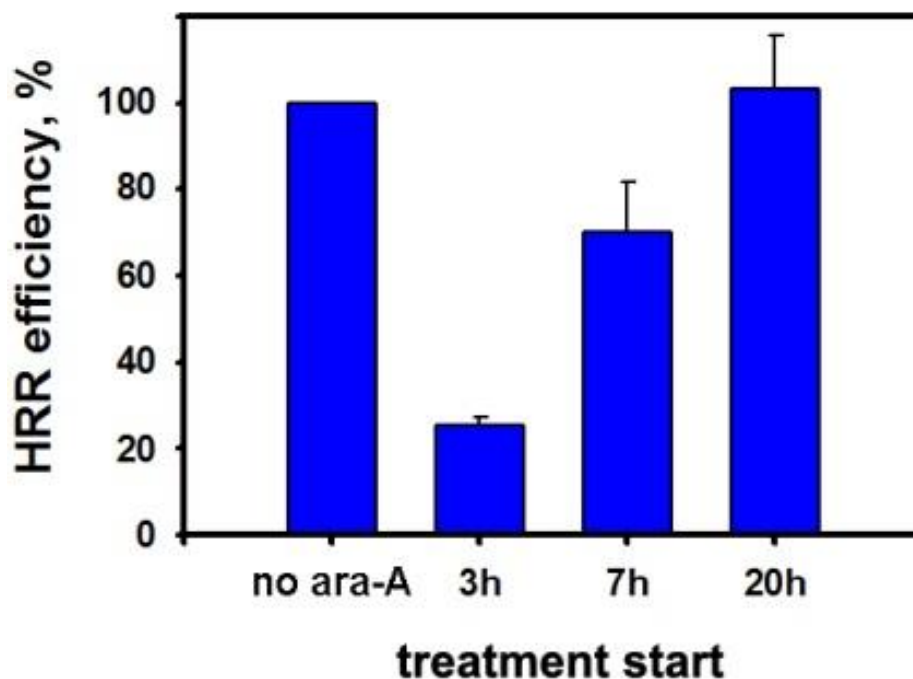


Figure 18 Time dependence of the effect of ara-A in DRaa40 cells (DR-GFP). A) Effect of a shift of the 4h treatment window to later times after transfection. Cells were treated with 500 μ M ara-A for 4h. X-axis categories indicate the time of treatment start after transfection of the I-SceI plasmid. Data shown represent the mean and s.d. from three independent experiments.

When the human osteosarcoma cell line U2OS 282C, which also carries the DR-GFP construct, became available to us, we switched to this more relevant human cell system. The switch to a human system also gave us the opportunity to validate the assay by silencing of various factors implicated in HRR with siRNAs designed to target human transcripts. As a negative control we used a siRNA against Luciferase (Ctrl). Cells were transfected with siRNA using nucleofection and incubated for 24h under standard culturing conditions before transfection with the I-SceI expression vector. Another 24h later (48h after siRNA transfection) cells were collected and analyzed by flow cytometry. The efficiency of the knockdowns was confirmed at the protein level by western blotting (Figure 19 and (Costantino, 2013)). Knockdown of both, BRCA2 and Rad51, lead to a

strong and highly significant reduction of HRR in this system (Figure 20 B). Silencing of Rad51, as expected, had the strongest effect reducing the frequency of gene conversion events by more than 98 % ($p= 0.00004$). Silencing of BRCA2, which is known to play an important role in loading Rad51 onto ssDNA, resulted in a decrease of HRR events by almost 80 % ($p= 0.017$). Rad52 is a crucial factor for HRR in yeast, but is not essential for this process in human cells, probably due to a functional redundancy with BRCA2 (Feng, 2011). Accordingly, Rad52 knockdown is associated with a reduction of HRR by only approximately 25 %, but which was still significant ($p= 0.049$) (Figure 19 B).

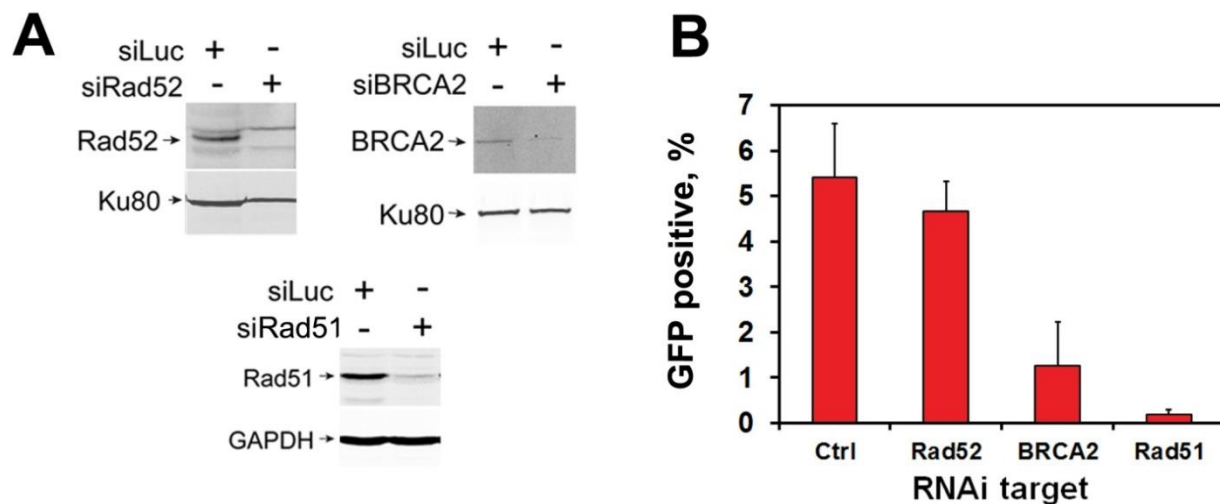


Figure 19 Knockdown of components of HRR in U2OS 282C cells (DR-GFP). **A)** Detection of protein levels by western blot. (Transfection and sampling were conducted by Simon Magin; gel runs, blotting and detection by Dr. Emil Mladenov). Upper left panel: RNAi of Rad52; knockdown>90%. Ku80 was used as loading control. Upper right panel: RNAi of BRCA2; knockdown~65%; loading control Ku80. Lower panel: RNAi of Rad51; knockdown 87%; loading control GAPDH. **B)** Quantification of GFP positive cells 24h after I-SceI-plasmid transfection and 48h after siRNA transfection. Bars show mean and s.d. of multiple experiments. Ctrl n=4; Rad52 n=5; BRCA2 n=3; Rad51 n=6.

Having confirmed the validity of U2OS 282C cells as a test system for HRR, we proceeded to test the effects of ara-A on HRR in human cells. Based on additional experimentation for optimization (Figure 35) we slightly modified the treatment protocol used in previous experiments and preponed drug-addition to 1.5h after transfection of

the I-SceI expression plasmid. After 4h of incubation with ara-A the medium was removed, cells were washed twice and supplied with fresh medium. Cells were analyzed by flow cytometry 24h after transfection.

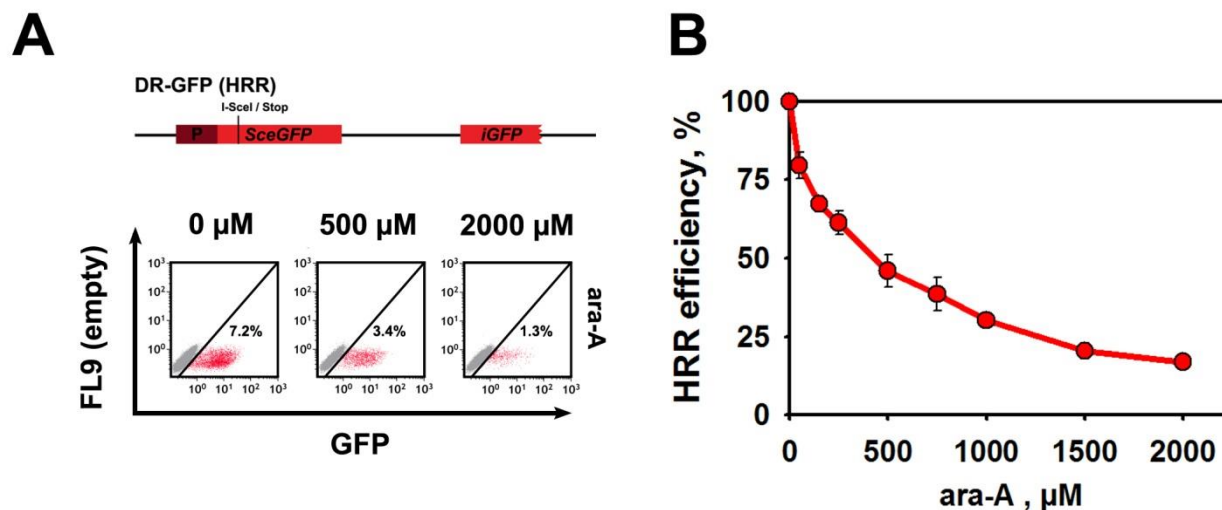


Figure 20 Inhibition of HRR by ara-A in U2OS 282C cells. **A)** *Top:* Schematic of DR-GFP construct present as single copy in this cell line. *Bottom:* representative flow cytometry dot plots of samples treated with different concentrations of ara-A. **B)** Titration of ara-A effect on HRR as measured 24h after transfection with the I-SceI expression plasmid. Data points represent mean and s.d. from 3-5 independent experiments.

Incubation of U2OS 282C with ara-A for 4h resulted in a clear, concentration dependent decrease of the frequency of gene conversion events (Figure 20 A&C). These results confirmed the observations made with immunofluorescence staining of IR induced Rad51 foci. We concluded that ara-A exerts a strong inhibitory effect on HRR.

4.3.3.2 Effects of ara-A on SSA

Besides HRR, SSA is the other homology directed process for the repair of DSB. SSA repairs DSB by the intramolecular annealing of homologous sequences (see Introduction). Thus, there is no conceptual requirement for the presence of a sister chromatid or *de novo* synthesis of DNA. SSA frequently leads to the creation of large deletions and must be considered a highly error prone rejoining process. To investigate potential effects of ara-A on SSA we employed another repair reporter system.

The SA-GFP construct consists of two consecutive truncated GFP-ORFs separated by 2,7kb (Figure 21 A). The two sequences share 266nt of homology (Gunn and Stark, 2012). The first ORF (5'-GFP) is truncated at its 3'-end the second (3'-GFP) is truncated at its 5'-end and harbors an I-SceI site. Signal generation after repair by HRR is hampered by a premature stop codon at the 3'-end of the first ORF (5'-GFP). Upon repair by SSA a functional GFP gene is reconstituted.

We obtained a U2OS cell line (283C) which carries this construct stably integrated into its genome. First we wanted to evaluate this system in a similar manner as we did for the DR-GFP cell line 282C. The protein repertoire required for SSA in mammalian cells has not been very well characterized, but it is known that a functional HRR pathway strongly suppresses SSA events (Tutt, 2001; Stark, 2002). Therefore we decided to knock down the same set of proteins involved in HRR that was used in the evaluation of DR-GFP in U2OS 282C. Efficiency of knockdowns was equivalent to those achieved in U2OS 282C cells (compare Figure 19 A).

Consistent with the reported suppression of SSA by HRR, knockdown of the key HRR factors BRCA2 and Rad51 resulted in an increase in the frequency of SSA events in our experiments by about 400% and 500% respectively (Figure 21 B). Knockdown of Rad52, which had only shown mild effects on HRR, resulted in a reduction of SSA by approximately 55%. This suggests a more important role for Rad52 in SSA than in HRR in human cells and is in line with findings by other groups (Stark, 2004). Together these results seemed to confirm the validity of the SA-GFP system in U2OS 283C cells. We investigated the effects of ara-A on SSA using the same treatment plan as in experiments with the DR-GFP construct in 282C cells.

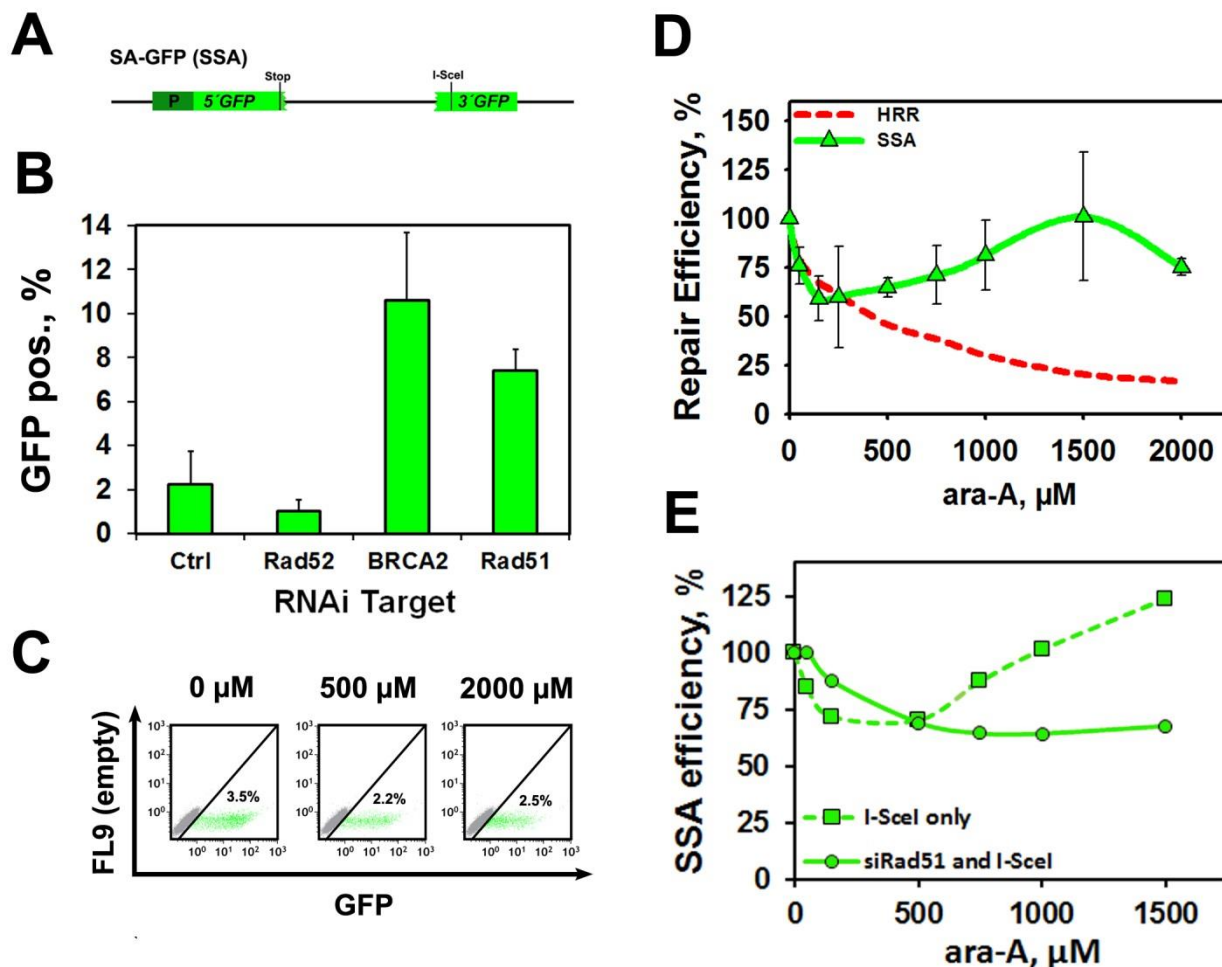


Figure 21 Effects of ara-A on SSA mediated repair in U2OS 283C cells (SA-GFP). **A)** Schematic of the SA-GFP construct. **B)** Effect of knockdown of several HRR factors on the SSA mediated repair of SA-GFP. Knockdown of BRCA2 and Rad51 lead to a dramatic increase in the proportion of GFP positive cells. **C)** Representative FACS plots of samples treated with different concentrations of ara-A measured 24h after transfection with the I-SceI expression plasmid. **D)** Titration of the effect of ara-A on SSA mediated repair, measured by flow cytometry 24h after transfection of the I-SceI expression plasmid. The dashed red line is a reproduction of the curve showing the effect of ara-A on HRR from Figure 20 C. Data points represent mean and s.d. from 3 independent experiments. **E)** Increase of SSA at higher concentrations of ara-A is dependent on inhibition of HRR. In cells that have been rendered deficient for HRR by RNAi of Rad51 no increase in SSA occurs at higher concentrations. Cells were transfected with siRNA for 48h and I-SceI was expressed for 24h prior to analysis. Data is normalized to the respective control without ara-A treatment. *Circles and solid line:* Cells silenced for Rad51. *Squares and dashed line:* Cells only transfected with I-SceI expression plasmid 24h prior to analysis. Plot represents data from one experiment.

Interestingly, we found that after an initial reduction of the efficiency of SSA at ara-A concentrations up to 150 μ M, the frequency of GFP positive cells increased again at higher concentrations of ara-A (Figure 21 C&D) leading to full recovery at around 1500 μ M ara-A. We speculated that this recovery of SSA at higher concentrations resulted from relieve of suppression mediated by Rad51 dependent HRR. We tested this hypothesis by silencing of Rad51 before subjecting U2OS 283C cells to ara-A treatment (Figure 21 E). As predicted, knockdown of Rad51 before induction of the DSB resulted again in a strong increase of repair by SSA compared to cells that were only transfected with the I-SceI expression plasmid (compare Figure 21 B). For better comparability values from Rad51 knockdown cells and cells left untreated before I-SceI expression were normalized to their respective controls (Figure 21 E). No recovery of SSA at higher concentrations was observed in cells deprived of Rad51, but SSA could still be reduced by about a third (Figure 21 E). This confirmed that the observed increase of SSA at higher concentrations of ara-A stemmed from the concomitant inhibition of HRR. Furthermore this result indicated that only a fraction of SSA events is sensitive to inhibition by ara-A, while about two thirds of SSA events are not.

4.4 Impact of ara-A treatment on NHEJ

4.4.1 Non-homologous rejoining of distal ends in paired DSB

Taken together the above results suggested an important role of HRR inhibition in the ara-A-mediated radiosensitization of cycling cells. However, a large amount of data from earlier studies showed strong inhibition of the repair of potentially lethal damage (PLD) by ara-A in non-cycling plateau phase cultures. Since the cell types used in most of these studies show extensive accumulation of cells with G1-DNA content in the plateau phase of growth, PLD inhibition in these populations cannot be explained by invoking inhibition of HRR. Therefore we inquired whether there may be other DSB repair pathways that are inhibited by ara-A.

The above results obtained with the SA-GFP construct indicated that mutagenic repair pathways may benefit from ara-A treatment under certain circumstances. SSA represents a homology dependent mode of mutagenic repair that results in the introduction of large deletions. Stark and colleagues have developed a reporter construct, EJ-5GFP, that also allows the measurement of non-homologous rejoining events associated with extensive deletions. The EJ5-GFP construct (integrated into U2OS 280A) consists of an intact EGFP ORF which is separated from its promoter by an interspersed puromycin resistance gene (Puro). In its uncut form only Puro is expressed. The Puro gene is flanked by two I-SceI sites. Upon cleavage at these sites rejoining can take place either between the proximal ends, leaving Puro in its place, or between the distal ends (distal end joining), resulting in excision of Puro and enabling expression of EGFP (Figure 22 A). This construct was stably integrated in U2OS cells resulting in the creation of the derivative cell line U2OS 280A.

The fidelity of the DNA-PK dependent pathway of NHEJ (D-NHEJ) is known to be higher than that of B-NHEJ, which is also frequently associated with large sequence losses. Therefore, we used chemical inhibition of DNA-PKcs to test if the EJ5-GFP can be used as an assay for the fidelity of NHEJ. NU7441 is a specific inhibitor of DNA-PKcs and induces a strong DSB repair defect in D-NHEJ proficient cells (Figure 38). Cells transfected with the I-SceI expression plasmid were treated with increasing concentrations of NU7441 for 6h after transfection. The proportion of GFP positive cells increased with increasing concentration reaching a plateau at approximately 5 μ M (Figure 22 B). Perturbation of D-NHEJ by inhibition of DNA-PKcs resulted in an increase from 12% GFP positive cells in the untreated control to more than 20% in cells treated with 5 μ M or more of Nu7441. We concluded that the use of distal over proximal ends in the repair of I-SceI induced tandem DSBs is indicative of compromised D-NHEJ, which is compensated for by B-NHEJ.

We proceeded to also perform experiments similar to those carried out with U2OS cells carrying the DR-GFP and SA-GFP constructs. We found that a 4h treatment with ara-A resulted, after a small decrease at lower concentrations (50 μ M and 150 μ M), in a concentration dependent increase in the proportion of GFP positive cells in the U2OS 280A cell line (Figure 22 C&D). This increase was found to be significant at all

concentrations above 250 μM ($p < 0.05$). At 2000 μM ara-A, joining of distal ends increased to 130% (+22%) of controls. Figure 22 D also shows the results obtained with the DR-GFP and SA-GFP constructs as dashed lines.

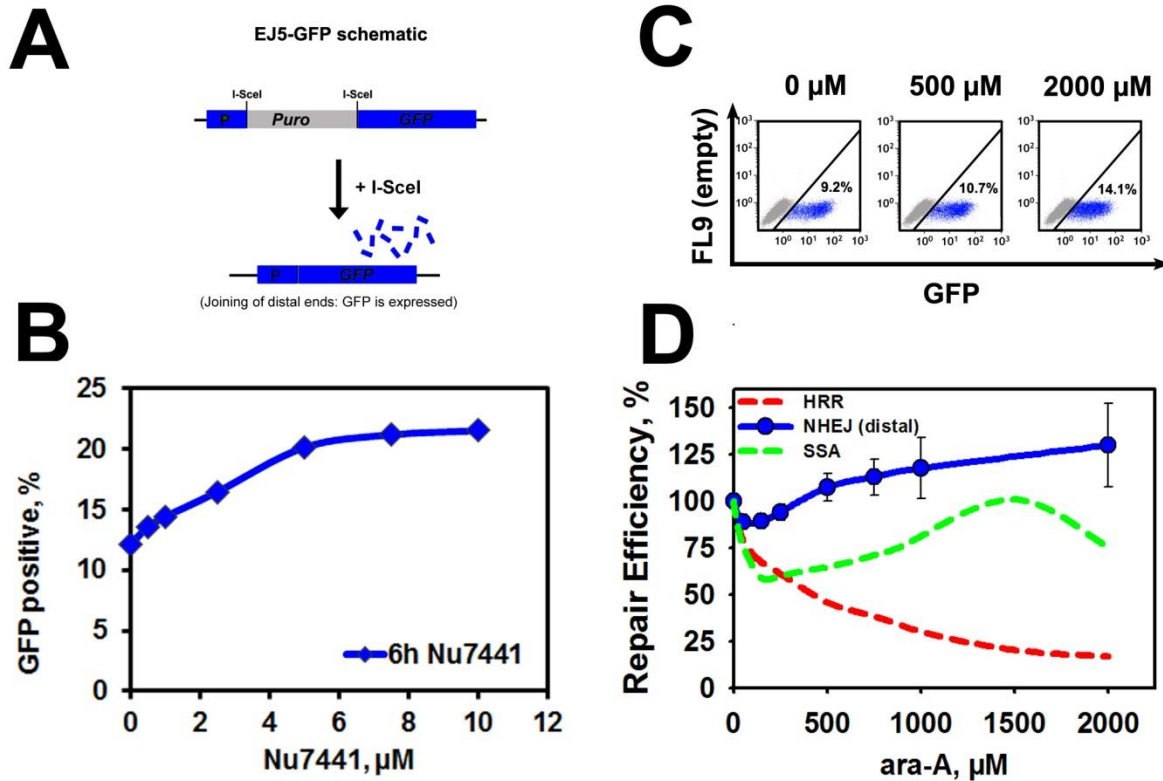


Figure 22 Effect of ara-A on the joining of distal ends in U2OS 280A (EJ5-GFP). **A**) Schematic of the EJ5-GFP construct. **B**) Effect of DNA-PKcs inhibition on the joining of distal ends. Cells were rendered deficient in D-NHEJ by treatment with the DNA-PKcs inhibitor Nu7441 for 6h. The inhibition resulted in a strong increase in the frequency of distal-end joining. Plot represents data from one experiment. An experiment with different treatment schedule yielding qualitatively equivalent results is presented in the appendix (Figure 39). **C**) Representative dot plots of U2OS 280A cells treated with different concentrations of ara-A. Flow cytometry was performed 24h after transfection of the I-SceI expression plasmid. **D**) Titration of the effect of ara-A on the use of distal ends for the repair of a DSB. Blue circles and line represent the mean and s.d. of three independent experiments with U2OS 280A cells and ara-A. The dashed red line shows the effect of ara-A on HRR and has been transferred from Figure 20 C. The dashed green line shows the effect of ara-A on SSA and has been transferred from Figure 21 D.

Taken together the results obtained with these DSB repair reporter constructs indicated that ara-A elicits a clear inhibition of the faithful HRR pathway, while mutagenic repair pathways like the rejoining of distal DSB ends or SSA appear to be favored and show enhancement.

4.4.2 The effect of ara-A on mutagenic repair in the EJ-RFP system

The EJ5-GFP construct allows the detection of a very specific repair event by NHEJ that results in the elimination of the intervening sequence between two I-SceI sites. This can be interpreted as an indicator for the tendency of a cell to perform mutagenic repair. However, the repair events that result in signal generation in this reporter system represent only a very small part of the spectrum of possible mutagenic NHEJ events.

A repair reporter system that allows the detection of the majority of mutagenic events was developed by Bindra et al. (Bindra, 2013) and stably integrated into U2OS cells. The resulting cell line was named U2OS EJ-DR. The EJ-RFP system consists of a tetracycline repressor gene and an independent DsRed gene containing several TetR binding sites (Figure 23 A). Expression of the DsRed gene is constitutively repressed. The TetR gene contains an I-SceI site that is cut upon expression of I-SceI in the cells. If the resulting DSB is repaired with mutagenic consequences the TetR gene is disrupted and a DsRed signal can develop. This requires clearance of the remaining TetR protein and subsequent expression of the DsRed gene. In addition maturation of DsRed protein requires more time than the maturation of GFP proteins (Magin, 2013). These factors are reflected by the slow kinetics of appearance of red fluorescent signal in the cell population (Figure 37 A&B). DsRed positive cells starts to appear 3 days after transfection of the I-SceI plasmid and after 4 days a robust population had built up (Figure 37 A&B). Thus, measurements using this system could not be performed after 24h as in the other reporter cell lines, but had to be carried out 96h after transfection.

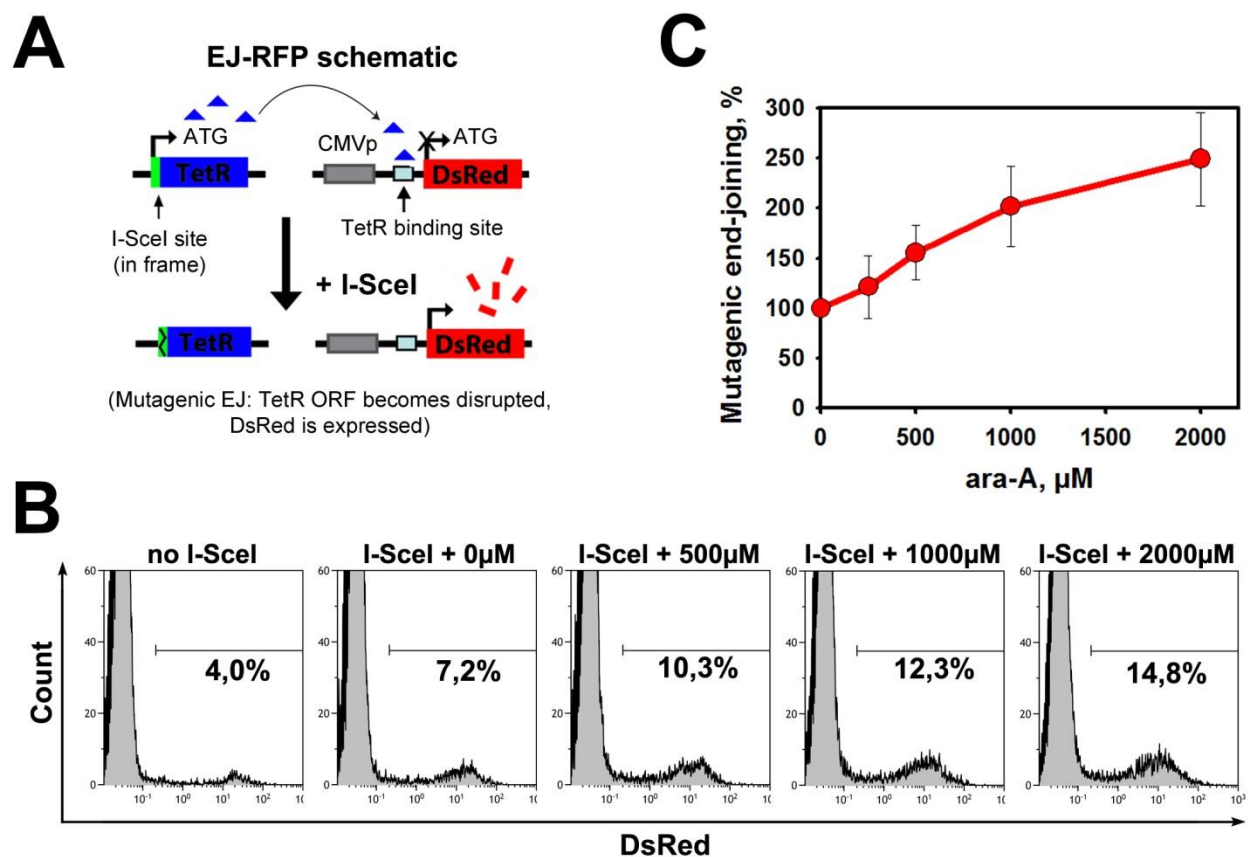


Figure 23 Effect of ara-A on mutagenic DSB repair pathways in U2OS EJ-DR cells. A) Schematic of the EJ-RFP system. **B)** DsRed expression in EJ-DR cells 96h after transfection. Non-transfected cells (no I-SceI) have a substantial background of DsRed positive cells. Transfection of I-SceI causes an increase in the portion of DsRed positive cells (I-SceI + 0 μM). Treatment with ara-A increased the fraction of DsRed positive cells significantly ($p < 0.05$) above 250 μM (I-SceI 500 μM -2000 μM). Y-Axis was limited to a fixed value to allow better comparison of the fraction of positive cells. Equal amounts of cells were measured for each sample ($1.5 \cdot 10^4$). **C)** Effect of ara-A treatment on mutagenic end-joining in EJ-DR cells 96h after transfection of the I-SceI expression plasmid. Measured values were corrected for background and normalized to the corrected control (0 μM). Data points represent mean and s.d. from three independent experiments.

Unlike the other reporter cell lines introduced so far the EJ-DR cells possessed a significant background, i.e. cells with fluorescent signal without induction of I-SceI (between 1.5%-5% of the total population; Figure 23 B). Therefore, measured values were corrected by the background detected in untransfected cells and normalized to the number of DsRed positive cells in the control (I-SceI transfected without drug treatment).

We observed that in cells that were treated with ara-A for a four hour period after transfection, the proportion of cells showing red fluorescence was elevated (Figure 23 C). With rising concentrations of ara-A the amount of mutagenic repair of the I-SceI induced DSB appeared to increase. At a concentration of 2000 μ M the corrected portion of DsRed positive cells was 250% of the control (Figure 23 C).

4.4.3 Effect of ara-A on DSB repair kinetics in D-NHEJ proficient cells

Results from experiments involving the SA-GFP, EJ5-GFP and EJ-RFP constructs suggested that treatment with ara-A induces a shift towards more mutagenic modes of DSB repair. While for SA-GFP the responsible repair pathway is clear (SSA), for EJ5-GFP and EJ-RFP interpretation is less unequivocal. However, results obtained with Nu7441 in U2OS 280A cells prompted us to hypothesize that signal generation in the EJ5-GFP construct is indicative of B-NHEJ activity. We asked whether this shift towards mutagenicity and putative promotion of B-NHEJ, as well as inhibition of HRR would be reflected in the kinetics of DSB repair in cells treated with ara-A.

PFGE is a method that allows the physical detection of DSB in DNA. The amount of DSB and the kinetics of their repair are measured in the pooled total DNA of irradiated cell populations. The method is described in detail under Materials and Methods. Briefly, cells are embedded in small agarose blocks (plugs), which are loaded onto agarose gels that are subjected to an alternating electrical field for long run times (40 hours). DSB reduce the molecular weight of DNA and generate DNA fragments that can migrate from the plug into the gel. Higher molecular weight chromosomal DNA remains trapped within the plug.

To obtain a measure for the amount of DSB present in a sample, the fluorescence signal generated by the stained DNA that leaves the plug and enters the lane is divided by the total signal of the same sample (plug + gel lane signal). This ratio is termed the fraction of DNA released (FDR). A linear relationship exists between FDR and radiation dose (Figure 24 B). Dose response curves (DR) are generated with samples that are irradiated with different doses of X-rays, but are not allowed to repair before processing. The DR data is used to express the FDR of cells that were allowed to repair as radiation

dose equivalents (DEQ). In this way repair kinetics (RK) are obtained that start (0 h) with a total DSB load equivalent to the initially delivered radiation dose (here 20 Gy). In repair proficient cells the kinetics of repair, as seen by the decline in DEQ, is biphasic. A fast component repairs ~80% of DSB within 0.5h-1h after irradiation and is followed by a second one that removes the remaining DSB within 4h-8h after IR.

It is well known that some pathways of DSB repair operate with varying efficiencies depending on the growth state and phase of the cell cycle. HRR for example can only operate during the S and G2 phase, while B-NHEJ is known to be inhibited in the plateau phase of growth but enhanced in G2 (Wu, 2008b; Singh, 2011) (see Introduction). Thus, it is possible that repair pathway specific effects of ara-A would be masked by the distribution of cells over all phases of the cell cycle when using asynchronous samples.

To overcome this complication we combined FACS with PFGE. In this way we could analyze populations highly enriched in G1 or G2 phase cells (Figure 24 A). Separate DR curves were prepared for asynchronous, G1 and G2 cells. G1 and G2 phase cells show a higher FDR per Gy than asynchronous cells (Figure 24 B). This is due to the S-phase cells present in the asynchronous population, which are known to display a lower FDR per Gy due to replication associated DNA structures (Latz, 1996; Dewey, 1997).

Treatment with 1 mM ara-A did not change the kinetics of DSB repair in asynchronous cells (Figure 24 C). Excellent purities were achieved for cells sorted in G1 and G2 from exponentially growing cultures. For G1 cells an enrichment of 95.8% +/- 2.0% and for G2 cells an enrichment of 81.1% +/- 6% was achieved. These purity levels were maintained for all populations sorted at the different repair time points; the cell cycle analysis is shown in the right panels of Figure 24 C, D and E. Neither G1 nor G2 cells showed inhibition of DSB repair after incubation with 1 mM ara-A.

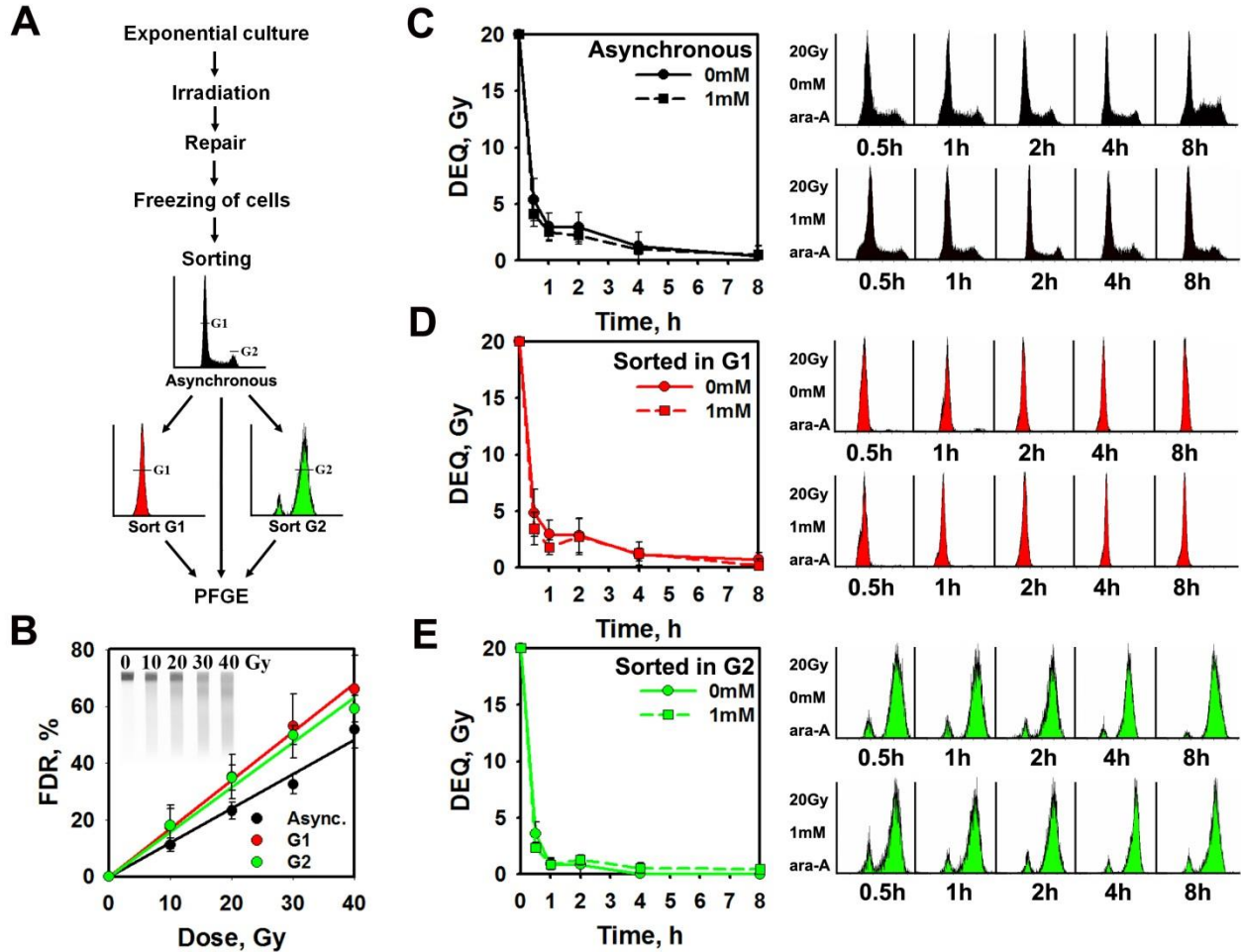


Figure 24 DSB repair by PFGE in sorted G1 and G2 A549 cells. A) Outline of the experimental workflow. **B)** Dose response (DR) curves for the induction of DSBs in sorted G1- and G2-phase cells, as well as in the asynchronous populations. Black circles, asynchronous cells; red circles, sorted G1 cells; green circles, sorted G2 cells. In the upper left corner an image of a typical DR on a PFGE gel is shown. **C)** Results for the asynchronous cell population. *Left panel:* DSB repair kinetics measured in the presence (1 mM; dashed line), or absence (0 mM; solid line) of ara-A. *Right panel:* Representative flow cytometry histograms of cell populations collected at different times after IR. **D)** As in C for cells sorted in G1-phase. **E)** As in C for cells sorted in the G2-phase. All graphs depict the mean and s.d. from 6-8 determinations from 2 independent experiments. FDR = fraction of DNA released; DEQ = Dose equivalent.

The careful approach and the accuracy of the obtained results allowed us to exclude confounding factors of PFGE technology as the reason why inhibition of DSB repair after incubation with ara-A could not be detected. D-NHEJ, unlike HRR and B-NHEJ, is

believed to operate with unaltered efficiency in G1, S and G2. Moreover, D-NHEJ is commonly regarded to be the dominant pathway of DSB repair throughout the cell cycle. If the great majority of DSB is repaired by D-NHEJ under the conditions employed for PFGE, interference of the drug with one of the remaining repair pathways or a partial shift to other pathways may be missed. This interpretation is supported by the observation that HRR mutants show in similar experiments no DSB repair defect, despite their increased radiosensitivity to killing (Wang, 2001a; Iliakis, 2004). Furthermore it is not clear if a shift to B-NHEJ in D-NHEJ proficient cells would necessitate a slowdown of repair.

4.4.4 Effect of ara-A on DSB repair in D-NHEJ deficient cells

Since we couldn't detect any effect of ara-A on the kinetics of DSB repair in D-NHEJ proficient cells we inquired if the same was true for D-NHEJ deficient cell lines. The activity of B-NHEJ becomes dominant in cells where core components of the classical, DNA-PKcs dependent pathway are dysfunctional or not present. Repair of DSB that is observable in these cells is chiefly carried out by B-NHEJ (Dibiase, 2000; Perrault, 2004). We reasoned that in these cells alterations of the activity of B-NHEJ may be more apparent.

For this purpose we utilized the human colorectal cancer cell line HCT116 (WT) and its two derivative knockout mutants HCT116 Lig4^{-/-} and HCT116 DNA-PKcs^{-/-}. We performed experiments with exponentially growing as well as with serum deprived cells. B-NHEJ is known to be suppressed under the latter condition (Singh, 2011) and we were curious to see if there might be differential effects. For serum deprivation we employed the protocol as described in Material and Methods (3.2.1.2). Briefly, cells were grown for 2 days. Then medium containing serum was removed and replaced by medium without serum. Another 24h later, cells were used in the experiment, during which they were continuously kept without serum. We used a treatment with 500 μ M of ara-A for all cell lines. Cells were treated until they were collected at the respective time points for further processing.

In exponentially growing cells ara-A treatment did not alter the repair kinetics of the WT, but enhanced the repair of DSB in Lig4 knockout cells (Figure 25 A). Repair in ara-A

treated $Lig4^{-/-}$ cells was increased by a dose equivalent of 5 Gy compared to the untreated $Lig4^{-/-}$ cells at 0.5h, but progressed with similar kinetics afterwards, keeping a constant gap (Δ DEQ= 4-5 Gy) (Figure 25 A). Ara-A treated DNA-PKcs knockout cells repaired quicker initially, but repair progressed faster in the untreated DNA-PKcs $^{-/-}$ cells between 1h and 4h (Figure 25 A). At 8h treated and untreated DNA-PKcs $^{-/-}$ cells had the same amount of residual DSB. Interestingly the curves of ara-A treated $Lig4^{-/-}$ and DNA-PKcs $^{-/-}$ cells were fully congruent (Figure 25 A).

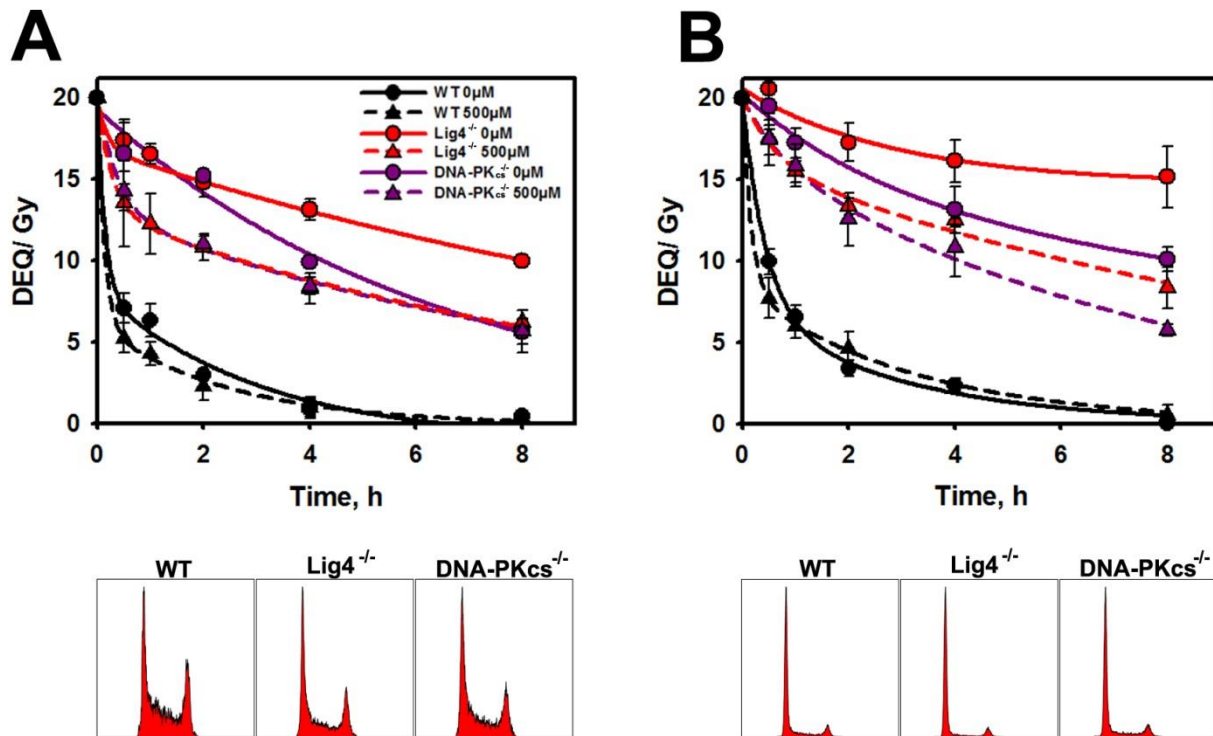


Figure 25 Enhancement of DSB repair in D-NHEJ deficient human cells. A) Top Panel: Exponentially growing HCT116 wild type (WT), Ligase 4 knockout ($Lig4^{-/-}$) and DNA-PKcs knockout (DNA-PKcs $^{-/-}$) cells were irradiated with 20 Gy X-rays and left to repair without or with 500 μ M ara-A. The amount of DSB was determined by PFGE. *Black circles and solid line:* HCT116 WT without ara-A. *Black triangles and dashed line:* HCT116 WT treated with 500 μ M ara-A. *Red circles and solid line:* HCT116 $Lig4^{-/-}$ without ara-A (0 μ M). *Red triangles and dashed line:* HCT116 $Lig4^{-/-}$ treated with 500 μ M ara-A. *Violet circles and solid line:* HCT116 DNA-PKcs $^{-/-}$ without ara-A (0 μ M). *Violet triangles and dashed line:* HCT116 DNA-PKcs $^{-/-}$ treated with 500 μ M ara-A. Data Points represent mean and s.d. from triple determination from one experiment. *Bottom Panel:* Cell cycle distributions of the starting populations of the three used cell lines. **B) As in (A),** but for serum deprived cells.

Under conditions of serum deprivation, DSB repair kinetics of WT cells were minimally slower than in exponentially growing cells, but were not altered by ara-A treatment (Figure 25 B). In line with the expectations the repair of DSB by the two knockout cell lines was substantially decreased in serum deprived cultures due to suppression of B-NHEJ (Figure 25 B). Treatment with 500 μ M ara-A clearly increased the efficiency of B-NHEJ in Lig4^{-/-} cells (Figure 25 B). After 8h, ara-A treated cells had repaired 52% of the initial DSB load. Untreated Lig4 on the other hand still retained more than 75% of the initial DSB (delta DEQ= 6.8). The difference was smaller in DNA-PKcs knockout cells (Figure 25 B), but present in contrast to exponentially growing cells. After 8h ara-A treated DNA-PK cells only retained DSB corresponding to a DEQ of 5.7 Gy. Untreated DNA-PK cells on the other hand retained DSB corresponding to a DEQ of 10.1 Gy (delta DEQ= 4.4).

PFGE experiments with HCT116 WT, Lig4^{-/-} and DNA-PKcs^{-/-} cells showed that ara-A modulates DSB repair in D-NHEJ deficient cells in the exponential phase of growth, as well as under serum deprivation. These results confirmed that ara-A treatment can positively regulate B-NHEJ. They also showed that promotion of B-NHEJ, compared to the untreated controls, was more pronounced when B-NHEJ was suppressed by serum deprivation.

4.4.5 Relieve of serum deprivation-induced inhibition of B-NHEJ by ara-A

In the light of the above results obtained with HCT116 cells we progressed to another system that reproducibly provides very strong inhibition of B-NHEJ under conditions of serum deprivation. MEF with a knockout for both alleles of Lig4 (MEF Lig4^{-/-}) have been extensively used in our institute. Under serum deprivation they frequently showed an almost full lack of DSB repair. To confirm that these standard could be met within this line of investigation we aimed to reproduce these PFGE results. We used exponentially growing, as well as serum-deprived cultures of MEF Lig4^{-/-} and the parental MEF Lig4^{+/+} for comparison. Exponentially growing Lig4^{-/-} MEFs showed a pronounced DSB repair defect while the parental cells repaired efficiently (Figure B). Still within 2h after

irradiation about 50% of the breaks were repaired in MEF Lig4^{-/-} cells, reflecting the activity of B-NHEJ.

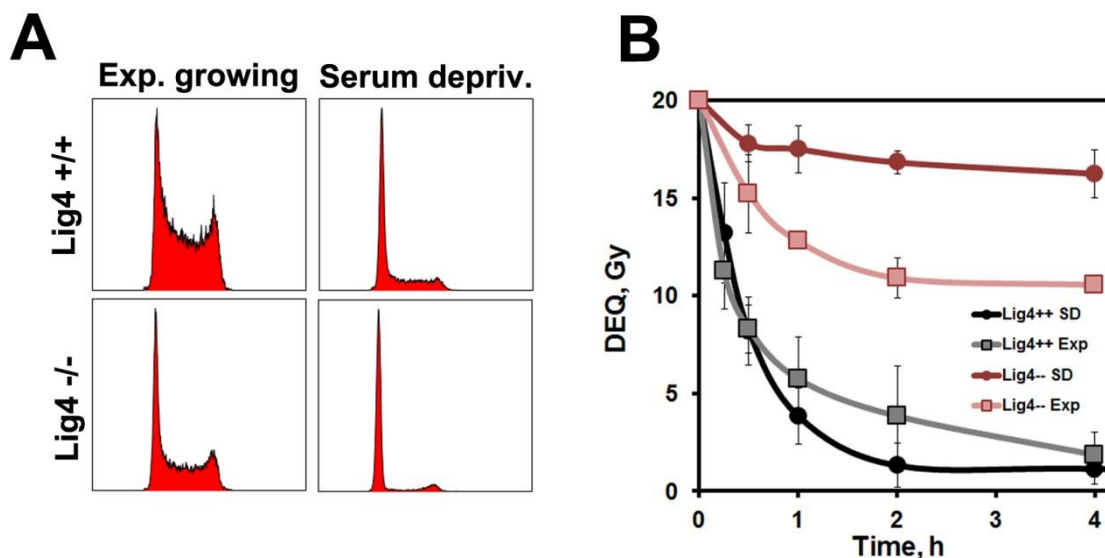


Figure 26 DSB repair by PFGE in exponentially growing and serum deprived MEF. A) Cell cycle distributions determined by FACS. **B)** DSB repair kinetics of MEF Lig4^{-/-} and MEF Lig4^{+/+} cells. *Grey squares and line:* Exponentially growing MEF Lig4^{+/+} cells. *Black circles and line:* Serum deprived MEF Lig4^{+/+} cells. *Light red squares and line:* Exponentially growing MEF Lig4^{-/-} cells. *Dark red circles and line:* Serum deprived MEF Lig4^{-/-} cells. Data points of MEF Lig4^{+/+} cells and exponentially growing MEF Lig4^{-/-} cells represent mean and s.d. of triple determinations from one experiment. Data points of serum deprived MEF Lig4^{-/-} represent mean and s.d. of 4 independent experiments with triple determinations each.

A plateau phase like state could be induced very efficiently in these cells by serum deprivation and resulted in accumulation of cells with G1 DNA content (Figure A). As a result of this, an almost complete inhibition of DSB repair was observed in serum deprived MEF Lig4^{-/-} cells (Figure 26 B). In contrast serum deprivation did not significantly alter DSB repair kinetics in MEF Lig4^{+/+} cells (Figure 26 B).

We found that exponentially growing MEF Lig4^{+/+} and MEF Lig4^{-/-} cells were very sensitive to ara-A treatment, which lead to extensive cell death and unacceptably high levels of background at longer treatment times in PFGE experiments (Data not shown). Therefore we decided to only use serum deprived Lig4^{-/-} cells for further experiments, where toxicity was not a problem (Figure 27 A; lower panel controls 4h). Cultures of serum deprived Lig4^{-/-} MEFs were irradiated with 20 Gy X-rays and treated with 250μM ara-A or solvent and left to repair for different time intervals. As expected the untreated

cells showed impaired DSB repair (Figure 27 A). Astoundingly cells treated with 250 μM ara-A showed repair kinetics almost equal to repair in MEF Lig4^{+/+} cells (compare Figure 27 A and Figure 26 B).

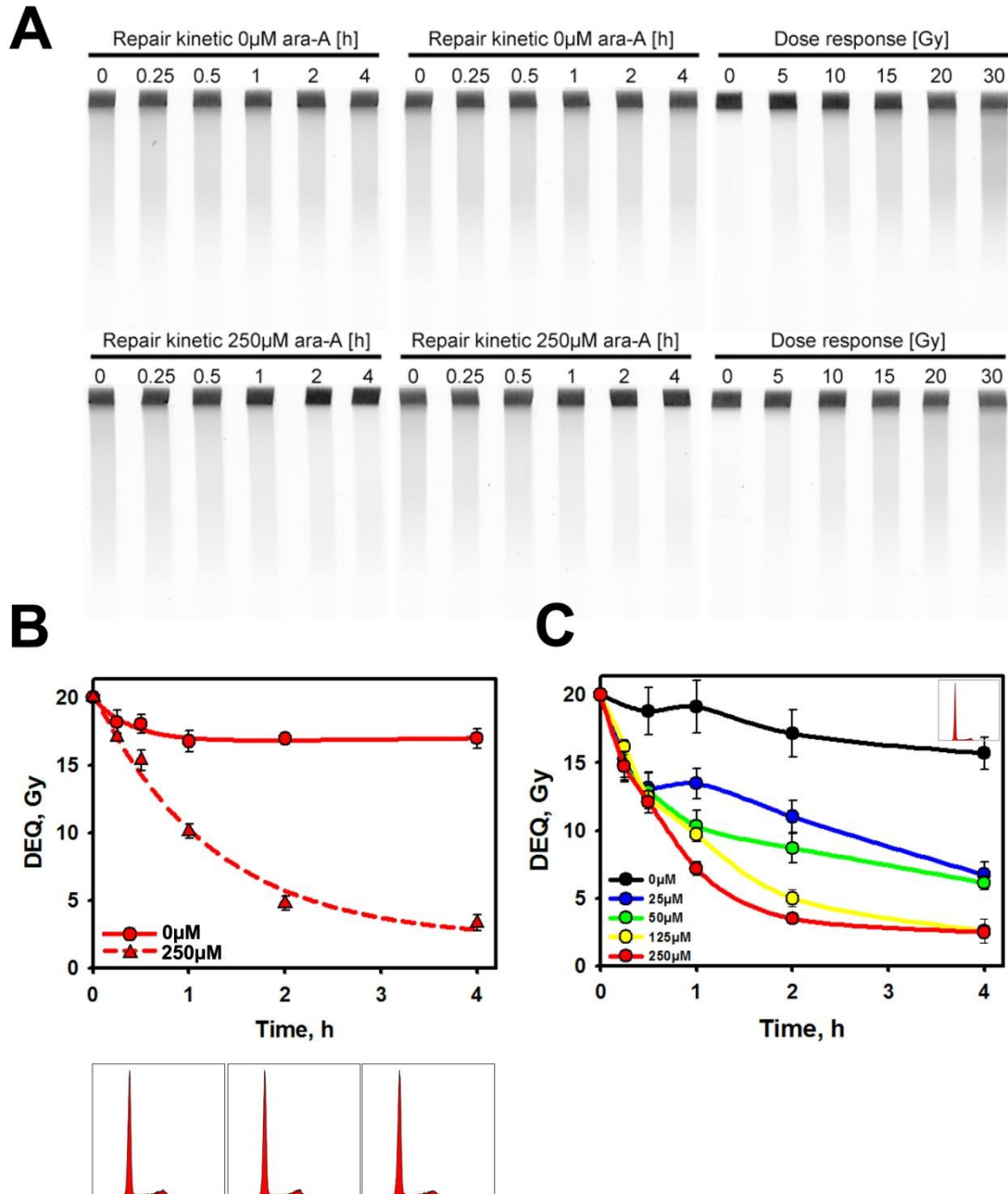


Figure 27 Ara-A treatment reactivates DSB repair in serum deprived Lig4^{-/-} cells. **A) Top:** DSB repair kinetics measured by PFGE in serum deprived Lig4^{-/-} cells. Cells were irradiated with 20 Gy and repair followed for 4h. Untreated cells hardly show any repair of DSB. Treatment with 250 μM enables efficient

repair which is almost complete after 4h. Data points represent mean and s.d. of triple determinations from one experiment. *Bottom*: Cell cycle distributions determined by FACS of cells stained for DNA content with PI. Treatment with ara-A did not cause any changes in the flow cytometry histograms. **B)** Titration of B-NHEJ enhancement by ara-A. DSB repair kinetics measured by PFGE in serum deprived MEF Lig4^{-/-} cells. Cells were irradiated with 20 Gy and repair followed for 4h. Cells were either left untreated (0 μM), or treated with 25 μM (blue symbols and line), 50 μM (green symbols and line), 125 μM (yellow symbols and line) or 250 μM (red symbols and line). *Upper right corner of the graph*: Cell cycle distribution of the starting population determined. Data points represent mean and s.d. of triple determinations from one experiment.

This effect surpassed our expectations by far. We inquired whether lower concentrations of ara-A elicit similar effects. We found that ara-A concentrations between 25 μM and 250 μM all strongly increased the efficiency of B-NHEJ (Figure 27 B). Interestingly all concentrations showed almost identical enhancement of DSB repair up to 30 min after irradiation. At later times, however, the effect clearly increased with rising concentrations (Figure 27 B). Yet, even 25 μM and 50 μM ara-A were sufficient to reduce residual DSB after 4h of repair by a factor of two compared to the untreated control (0 μM). After treatment with 125 and 250 μM respectively, cells had repaired 87.5% of the initial damage, while the untreated control had repaired only 23,5% (delta DEQ= 12,8).

These results strongly supported the notion that ara-A treatment enhances B-NHEJ efficiency. Furthermore they suggested that ara-A interferes with the mechanism that suppresses B-NHEJ in the plateau phase of growth respectively under serum deprivation.

4.4.6 Analysis of IR induced foci in serum deprived MEF Lig4^{-/-}

To further investigate the effect of B-NHEJ enhancement by ara-A we employed immunofluorescence combined with confocal microscopy to analyze DSB repair at low radiation doses. We selected proteins and modifications involved in the DNA damage response with the property of forming IRIF upon exposure to IR. One post-translational protein (PTM) modification we studied was the phosphorylation of Serine 139 (S139) of the histone variant H2AX. This PTM is commonly used as a surrogate marker for DSB

and is also known as γ H2AX. Foci of γ H2AX form in large chromatin domains around DSB.

Recruitment of the protein 53BP1 to the sites of DSB is another assay that has been regularly used to monitor the repair of DSB. Both of these markers can be used to assess the capability of a cell to repair DSB.

Another protein modification occurring after IR is the phosphorylation of Serine 1981 (S1981) of ATM (pATM). ATM is a central kinase in IR induced DNA damage signaling and requires this phosphorylation for activation. pATM accumulates at sites of DSB where it can also be detected as IRIF. We aimed to analyze the assembly and the kinetics of decay of foci formed by these proteins in serum deprived Lig4^{-/-} MEFs.

In cells that were not treated with ara-A, foci of γ H2AX persisted virtually unchanged from 1h (49.0 (+/- 13.7)) up to 24h (45.2 (+/- 8.4)) after exposure to 1 Gy (Figure 28 A). However, serum deprived MEF Lig4^{-/-} cells that were treated with 250 μ M ara-A developed a pan-nuclear γ H2AX staining that grew in intensity with time (Figure B). After 4h 90% of cells exhibited pan-nuclear staining and 8h and later 100% of cells showed this staining pattern (Figure 28 D), which made a meaningful quantitative analysis of γ H2AX foci impossible. Similarly, 98% of non-irradiated cells showed pan-nuclear staining for γ H2AX after 24h (Figure 28 C). However, the intensity of the staining in non-irradiated cells did not reach the glaring intensity found for irradiated cells treated with ara-A. Still, pan-nuclear γ H2AX staining was not exclusively observed in ara-A treated cells. In untreated cells with or without irradiation an average percentage of 16.3% (+/- 3.3%) of cells with pan-nuclear staining could be observed (Figure 28 A, C&D).

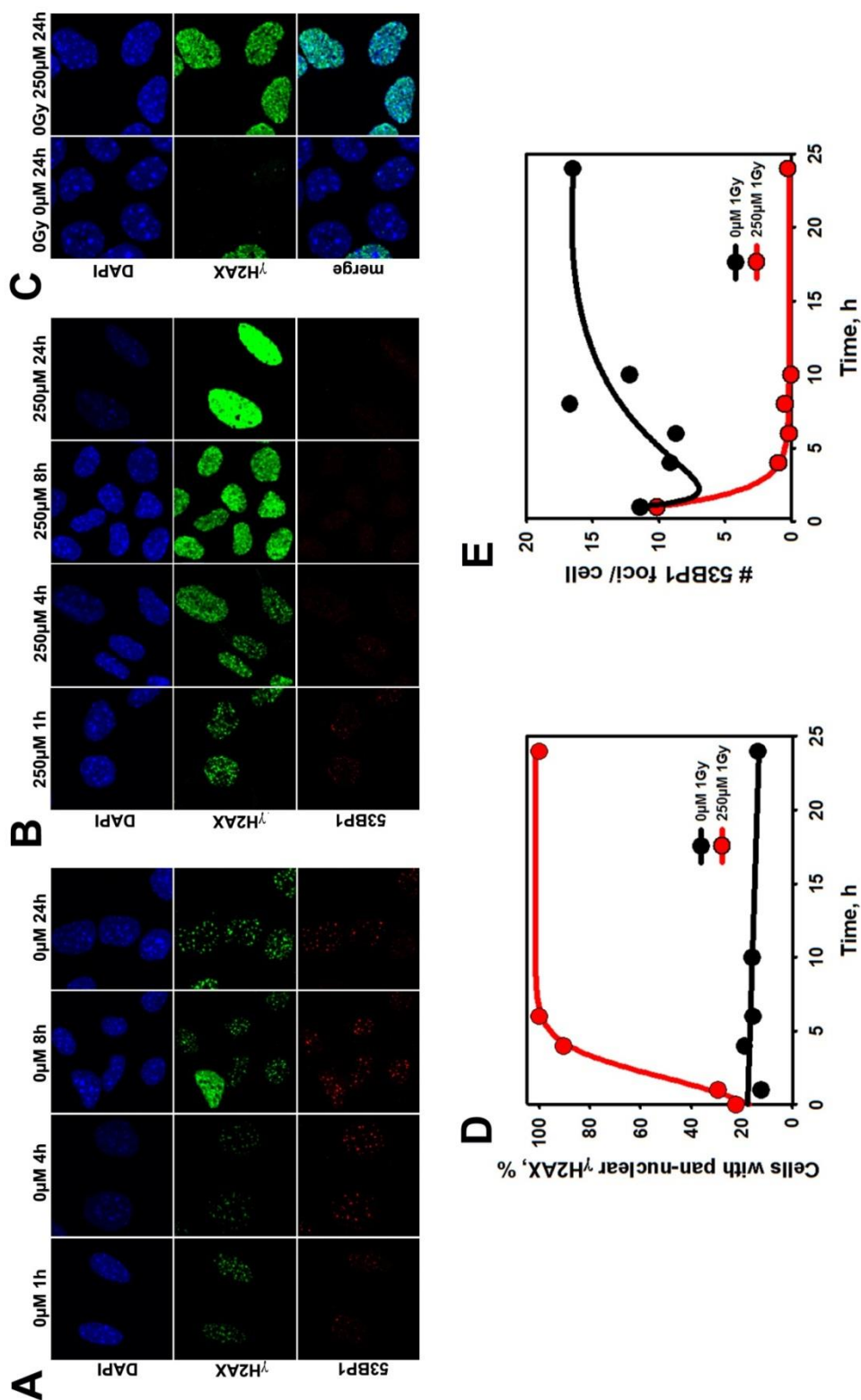


Figure 28 Quantification of γH2AX and 53BP1 foci in serum deprived $\text{Lig4}^{-/-}$ MEFs. **A)** Serum deprived $\text{Lig4}^{-/-}$ MEFs exposed to 1 Gy and left without further treatment until fixation. Maximum intensity projection (MIP) representations of Z-stacks recorded by confocal laser scanning microscopy (CLSM) of

immunofluorescent (IF) stained fixed cell samples. Cells were stained for DNA with DAPI (blue, top row), with an antibody against γ H2AX (green, middle row) and an antibody against 53BP1 (red, bottom row). Pictures of cells fixed after 1h (1st column), 4h (2nd column), 8h (3rd column) and 24h (4th column) are shown. **B)** Serum deprived Lig4^{-/-} MEFs exposed to 1 Gy X-rays and treated with 250 μ M ara-A until fixation. MIP representations of Z-stacks recorded by CLSM of IF stained fixed cell samples. Cells were stained for DNA with DAPI (blue, top row), with an antibody against γ H2AX (green, middle row) and an antibody against 53BP1 (red, bottom row). Pictures of cells fixed after 1h (1st column), 4h (2nd column), 8h (3rd column) and 24h (4th column) are shown. **C)** Non-irradiated serum deprived Lig4^{-/-} MEFs left without ara-A (left column) or treated with 250 μ M ara-A (right column) for 24h. Samples were fixed at the latest time point (24h) together with irradiated cells. MIP representations of Z-stacks recorded by CLSM. Cells were stained for DNA with DAPI (blue, top row) and with an antibody against γ H2AX (green, middle row). The bottom row shows an overlay of the DAPI and the γ H2AX stain. **D)** Quantification of the proportion of cells with pan-nuclear γ H2AX staining in cells left without ara-A after irradiation (0 μ M; black circles and line) and treated with 250 μ M ara-A (red circles and line). **E)** Quantification of 53BP1 foci per nucleus. *Black circles and line:* cells left without ara-A after irradiation (0 μ M). *Red circles and line:* Cells treated with 250 μ M ara-A after irradiation. Data points represent the mean of all cells (51 (+/-17) per time point) analyzed in one experiment.

Foci of 53BP1 on the other hand were, when detectable, always present in the form of distinct, quantifiable dots in ara-A treated and untreated cells (Figure 28 A&B). The initial number of average 53BP1 foci per cell was very similar (11.4 and 10.1 foci per cell) under both conditions. In cells without ara-A, 53BP1 foci persisted up to 24h after irradiation with a tendency to even slightly increase (Figure 28 A&E). In contrast, in cells treated with 250 μ M ara-A 53BP1 foci quickly disappeared (Figure 28 B&E). After 4h only about 1 focus per cell could be detected on average. After 24h the number had decreased to 0.25 foci per cell on average (Figure 28 E). Interestingly, pan-nuclear γ H2AX staining and the formation of 53BP1 foci seemed not to be mutually exclusive per se, at least in untreated cells (compare Figure 28 A; 0 μ M 8h: pan nuclear γ H2AX staining in cell with clear and bright 53BP1 foci). Still, most cells exhibiting pan-nuclear γ H2AX staining showed fewer or no 53BP1 foci.

Detection of pATM after irradiation with 1 Gy revealed bright, punctate nuclear foci (Figure 29 A&B). The initial number of pATM 1h after irradiation was virtually identical in ara-A treated (60.8 (+/-15.6)) and untreated cells (60.6(+/-12.7)) (Figure 29 C). In

untreated cells a slow decay of pATM foci was observable (Figure 29 C). After 24h cells retained approximately half of the initial foci (27.9 (+/-6.7)), which were still visible as clearly defined, bright spots (Figure 29 A&C). In cells that were treated with 250 μ M ara-A decay of pATM foci proceeded much faster, with approximately 50% of foci being lost after 8h (residual foci 8h: 27.3 (+/- 20.6)) (Figure 29 B&C). This resulted in complete disappearance of pATM foci 24h after irradiation (Figure 29 B&C). Cells that lost the discrete protein foci retained a weaker, diffuse nuclear staining (Figure 29 B).

We concluded that the complete disappearance of 53BP1 and pATM foci with time in serum deprived MEF Lig4^{-/-} cells, was indicative of complete repair of DSB. This supported data showing enhanced repair of those cells in PFGE experiments. Pan-nuclear staining with γ H2AX and to a lesser degree of pATM after treatment with ara-A require further investigation.

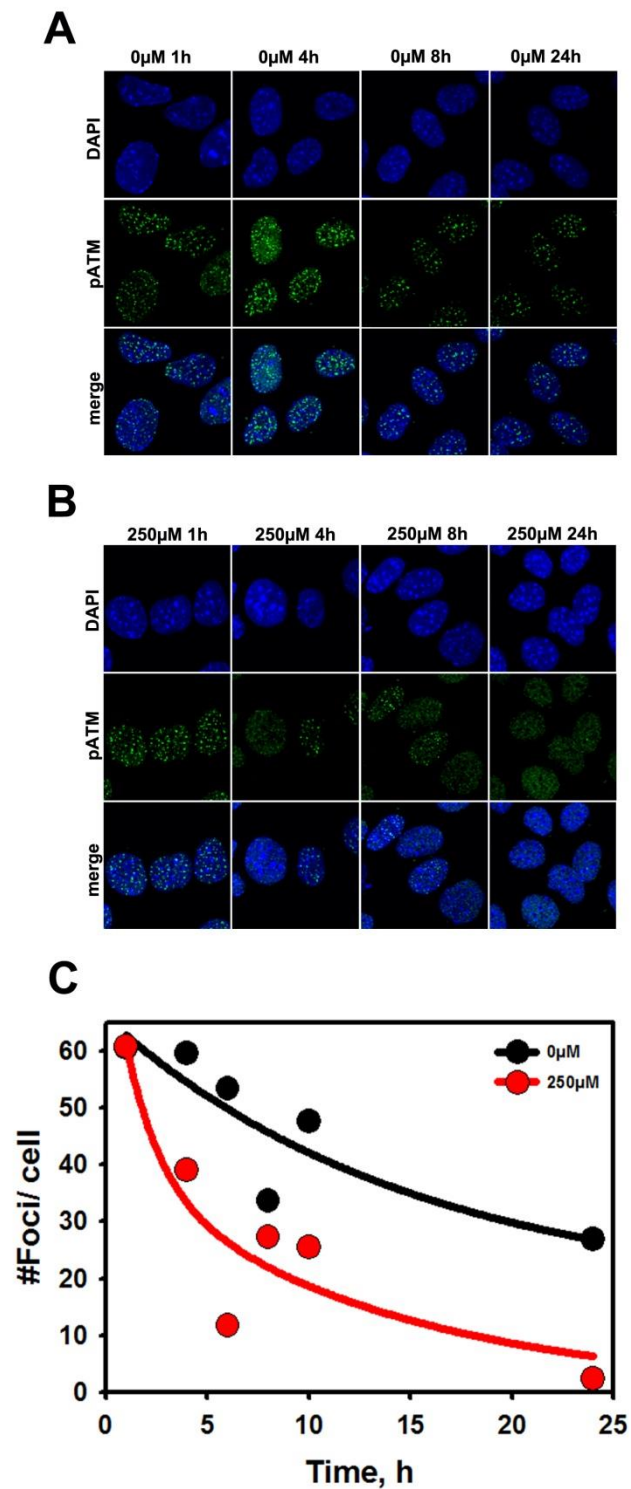


Figure 29 Quantification of pATM-S1981 Foci in serum deprived Lig4^{-/-} MEFs. **A)** Serum deprived Lig4^{-/-} MEFs exposed to 1 Gy X-rays. Maximum intensity projection (MIP) representations of Z-stacks recorded by confocal laser scanning microscopy (CLSM) of immunofluorescent (IF) stained fixed cell

samples. Cells were stained for DNA with DAPI (blue, top row) and with an antibody against pATM-S1981 (pATM; green, middle row). The bottom row shows a merged picture of the DNA and pATM stains. Pictures of cells fixed after 1h (1st column), 4h (2nd column), 8h (3rd column) and 24h (4th column) are shown. **B)** Serum deprived Lig4^{-/-} MEFs exposed to 1 Gy X-rays and treated with 250 μ M ara-A until fixation. MIP representations of Z-stacks recorded CLSM. Cells were stained for DNA with DAPI (blue, top row) and with an antibody against pATM-S1981 (pATM; green, middle row). The bottom row shows a merged picture of the DNA and pATM stains. Pictures of cells fixed after 1h (1st column), 4h (2nd column), 8h (3rd column) and 24h (4th column) are shown. **C)** Quantification of pATM foci in irradiated cells with or without ara-A. *Black circles and line:* cells left without ara-A after irradiation (0 μ M). *Red circles and line:* Cells treated with 250 μ M ara-A after irradiation. Data points represent the mean of all cells (43 (+/-8) per time point) analyzed in one experiment.

4.5 Effects of other NAs on radiosensitivity and DSB repair

4.5.1 Effects on the survival of A549 cells

The interesting results obtained with ara-A motivated us to expand our study to include other NAs. We decided to use fludarabine, ara-C and gemcitabine. Fludarabine, an adenosine analog, is a fluorinated derivative of ara-A. Ara-C is an analog of cytosine and gemcitabine the di-fluorinated derivative (Figure 1). Both of these compounds are significantly more cytotoxic than ara-A and fludarabine and effectively inhibit DNA replication at much lower concentrations (Figure 30 A and Figure 42). Fludarabine and gemcitabine have both been reported to possess radiosensitizing potential. Ara-C on the other hand is generally not regarded as a radiosensitizer.

We performed survival experiments in A549 cells as described above for ara-A using a 40 min pre-incubation and a 4h post-irradiation treatment (protocol II). From preliminary experiments we selected concentrations of the respective drug that yielded plating efficiencies no lower than 40% -50% of the control. This data had shown that in the case of ara-C, although only moderately toxic at doses below 100 μ M, toxicity increased drastically at concentrations above 250 μ M. Therefore concentrations below 100 μ M were used. Two concentrations were tested for ara-C (10 μ M and 50 μ M) and gemcitabine (1 μ M and 10 μ M). Fludarabine, which had shown toxicity very similar to

ara-A, was used at the same concentration as the latter (500 μM). Predictions for PE reduction were met well by the results obtained (Figure 30 A).

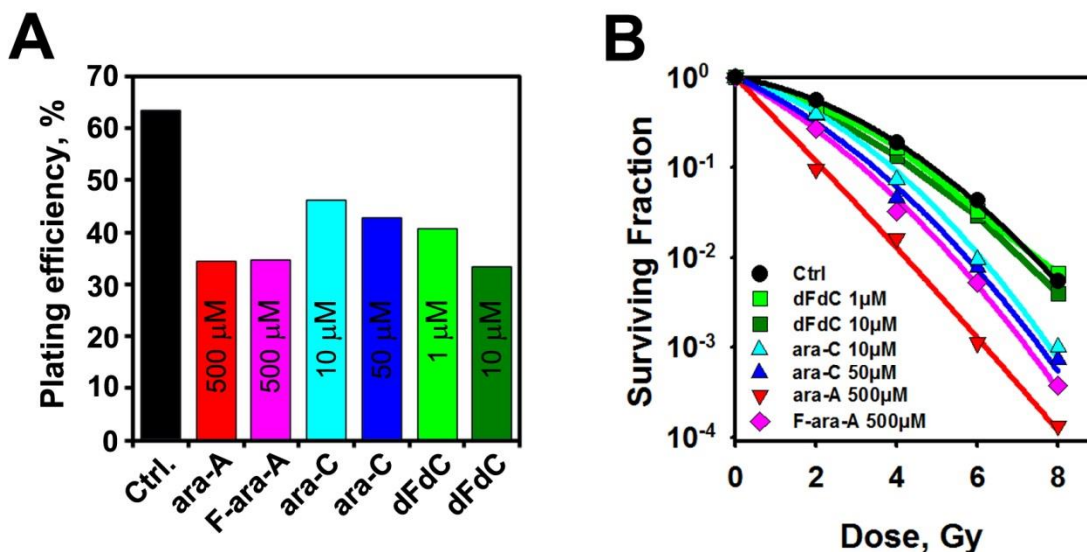


Figure 30 Comparison of radiosensitization by post-irradiation treatment with different NAs. A) Plating efficiencies for colony formation of exponentially growing A549 cells treated with different concentrations of NAs for 4h. Bars represent the mean of two independent experiments, each including double determinations. **B)** Survival of exponentially growing A549 cells after exposure to different doses of X-rays and the indicated concentrations of NA drugs for 4 h after IR. Red triangles, ara-A (500 μM); pink diamonds, fludarabine (F-ara-A; 500 μM); light blue triangles, ara-C (10 μM); dark blue triangles, ara-C (50 μM); light green squares, dFdC (1 μM); dark green squares, dFdC (10 μM); black circles, control (no drug treatment). Survival data is normalized to the corresponding unirradiated controls (compare panel A). The results shown represent the mean of two independent experiments, each including double determinations. A third experiment using different concentrations yielded similar results.

Treatment with 500 μM Ara-A resulted in a steep, shoulderless survival curve as expected (Figure 30 B). Fludarabine at the same concentration did sensitize the A549 cells, but to a lesser degree than ara-A (Figure 30 B). Unexpectedly, treatment with ara-C showed radiosensitization similar to fludarabine (Figure 30 B). There was only a very small increase in radiosensitization between treatment with 10 μM and 50 μM ara-C. We were surprised at first not to find radiosensitization by gemcitabine (Figure 30 B). However, an in-depth literature research revealed that results reporting

radiosensitization by gemcitabine generally use long pre-incubations (e.g. 16-32h) with the drug (Shewach, 1994; Rosier, 1999; Pauwels, 2003). On the other hand, studies that also test the effect of post-irradiation treatment don't find radiosensitization (Shewach, 1994). Thus, our finding is in accordance with the existing literature.

We concluded that post-irradiation treatment with gemcitabine is not sufficient to induce radiosensitization in A549 cells. Ara-C had some radiosensitizing potential in our hands, albeit distinctly weaker than ara-A. Fludarabine also proved to be a weaker radiosensitizer than ara-A in A549 cells.

4.5.2 Effects on ara-C and fludarabine on HRR, SSA and distal NHEJ

We decided to exploit the reporter assays, which we had used to measure the influence of ara-A on different pathways of DSB repair, to further evaluate the effects of ara-C and fludarabine, for which we had found radiosensitization as a post-treatment. We also included aphidicolin and HU as controls in these experiments.

Both compounds inhibit replication, but show no or only weak radiosensitizing potential (compare Figure 13 B&C and Figure 14 B). HU inhibits replication in a range comparable to ara-A ($IC_{50_{repl}} > 5 \mu M$), while aphidicolin inhibits DNA replication at much lower concentrations, in a range comparable to that of ara-C ($IC_{50_{repl}} < 0.3 \mu M$).

These controls were intended to confirm that transient inhibition of DNA replication alone was not sufficient to cause major changes in the read out of the reporter assays. Treatment conditions in these experiments were as described for ara-A above.

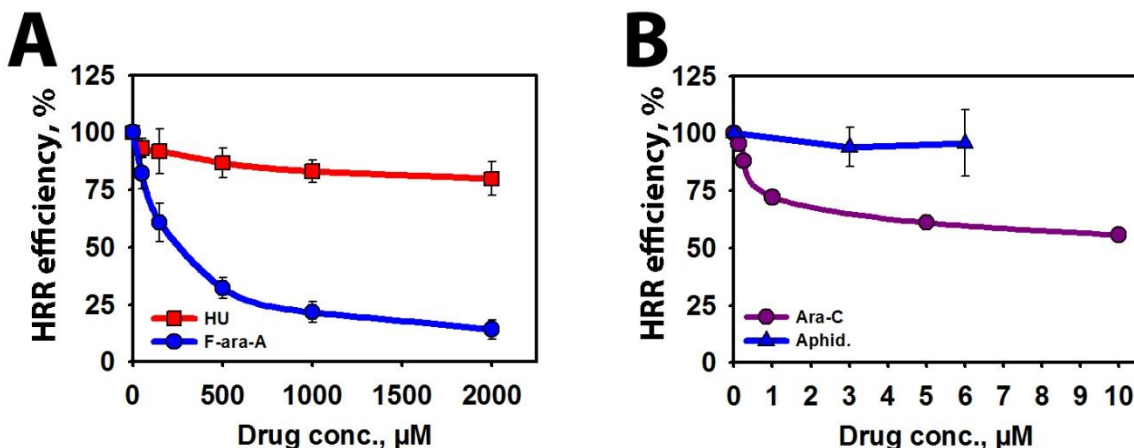


Figure 31 Effect of fludarabine and ara-C on HRR in U2OS 282C cells (DR-GFP).

A) Effects of fludarabine (F-ara-A) and hydroxyurea (HU) on HRR. *Blue circles and line:* F-ara-A. *Red squares and line:* HU. Data points represent mean and s.d. from three independent experiments. **B)** Effects of ara-C and aphidicolin on HRR. *Dark pink circles and line:* Ara-C. Plot shows the mean from two independent experiments *Blue triangles and line:* Aphidicolin. Data points represent mean and s.d. from three independent experiments.

We started by testing the effects of fludarabine and ara-C on HRR using the U2OS 282C cells, which carry the DR-GFP construct. Fludarabine proved to be an effective inhibitor of HRR with a concentration-effect relationship very similar to ara-A (Figure 31 A). Incubation with HU, even at 2000 μM , on the other hand, had only a very small effect on HRR (Figure 31 A). Aphidicolin also failed to inhibit HRR in U2OS 282C cells. Treatment with ara-C showed substantial but comparatively weak inhibition, reducing HRR by almost 45 % at a concentration of 10 μM (Figure 31 B). Since neither HU nor aphidicolin inhibited HRR despite their strong effects on DNA replication, we concluded that inhibition of replication per se was not sufficient to suppress HRR.

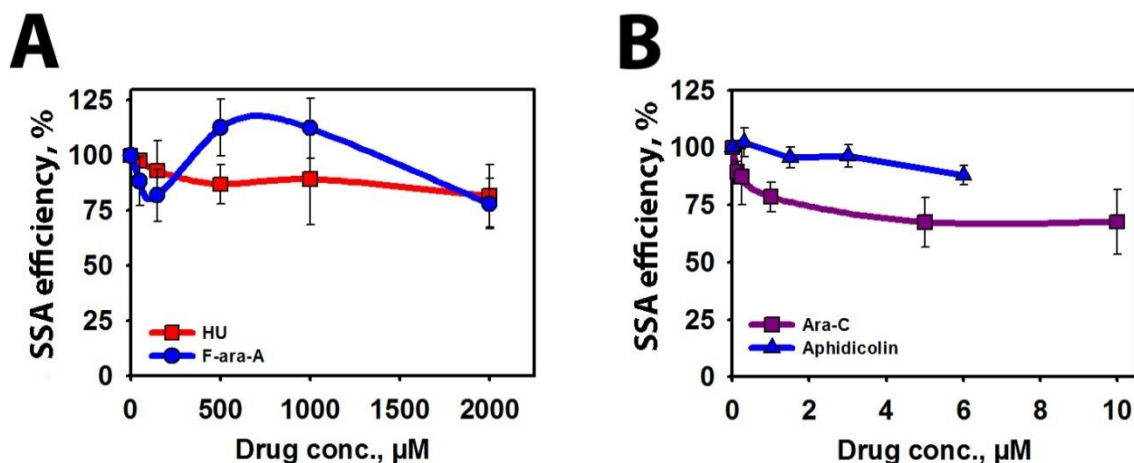


Figure 32 Effect of fludarabine and ara-C on SSA in U2OS 283C cells (SA-GFP).

A) Effects of fludarabine (F-ara-A) and hydroxyurea (HU) on SSA. Blue circles and line: F-ara-A. Red squares and line: HU. Data points represent mean and s.d. from three independent experiments. **B)** Effects of ara-C and aphidicolin on SSA. Dark pink squares and line: Ara-C. Blue triangles and line: Aphidicolin. Data points represent mean and s.d. from three independent experiments.

We proceeded to test fludarabine and ara-C in the U2OS 283C cells, to investigate their effect on the efficiency of SSA. Fludarabine treatment again resulted in a response similar to that of ara-A. After an initial decrease of SSA mediated repair, there was an increase at higher concentration, which was again abolished at very high concentrations (Figure 32; Figure 31 A). In contrast to ara-A, fludarabine lead to an effective net increase of SSA at concentrations between 500 and 1000 µM. HU again showed only little effect (Figure 32 A) and similar behavior was observed for aphidicolin. This drug only had a small impact on SSA, reducing its efficiency to 88% (+/- 4%) of control at 6 µM (Figure 32 B). Ara-C had a stronger effect, reducing SSA by more than 30% to 68% (+/- 11%) at 5 µM, but did not inhibit the pathway further at 10 µM (Figure 32 B).

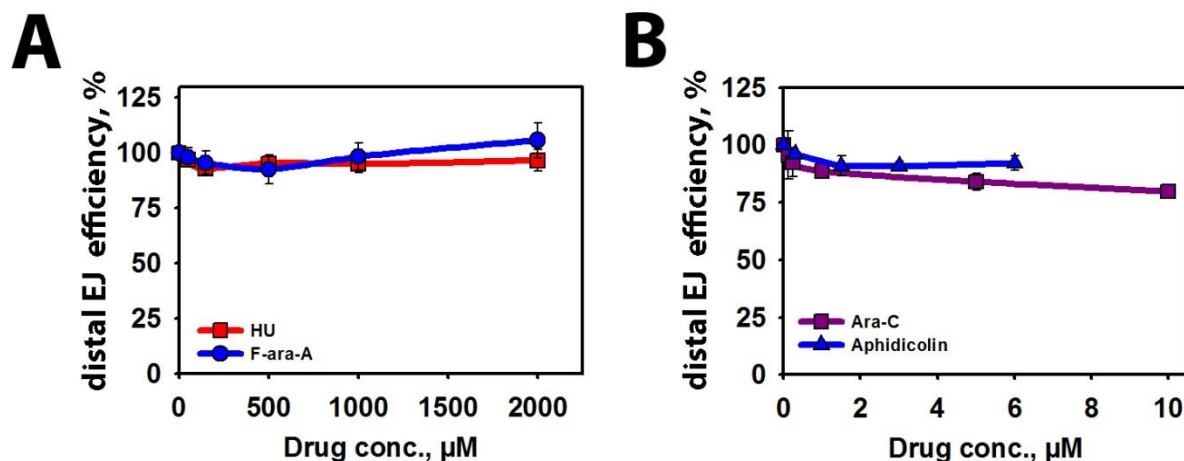


Figure 33 Effect of fludarabine and ara-C on the joining of distal ends of two DSB (EJ5-GFP). **A)** Effects of fludarabine (F-ara-A) and hydroxyurea (HU) on distal-end joining. *Blue circles and line:* F-ara-A. *Red squares and line:* HU. Data points represent mean and s.d. from three independent experiments. **B)** Effects of ara-C and aphidicolin on distal-end joining. *Dark pink squares and line:* Ara-C. *Blue triangles and line:* Aphidicolin. Data points represent mean and s.d. from three independent experiments.

We concluded this analysis with the EJ5-GFP construct in U2OS 280A to measure the joining of distal ends of DSB. The effects of HU and fludarabine on the joining of distal ends seemed negligible. However, there is a small trend for distal end-joining to increase at higher concentrations of fludarabine (Figure 33 A). Aphidicolin and ara-C also had only small effects on the readout of this assay. Aphidicolin caused a reduction of 8% in the rejoining of distal ends at 6 μM , while ara-C reduced the efficiency of this repair mode to 80% (+/- 1.8%) of the controls at 10 μM (Figure 31 B).

We concluded that inhibition of DNA synthesis by HU and aphidicolin had no important effects on the overall efficiency of any of the repair pathways or modes tested with this panel of cell lines. The profile of fludarabine for the modulation of repair pathway efficiencies was similar to that of ara-A, albeit with a much less pronounced effect on the joining of distal ends and a more pronounced effect on SSA. Ara-C was different from fludarabine and ara-A, as it uniformly reduced all types of repair events in these reporter

assays. The reductions elicited by ara-C were quiet moderate, ranging from 20% - 40%, but consistent.

4.5.3 Effects on mutagenic repair in EJ-DR cells

The differences in the action of fludarabine and ara-C on specific repair outcomes we had found were intriguing. We wondered how the individual drugs would influence the overall fidelity of DSB repair. To address this question we conducted experiments using the U2OS EJ-DR cell line. We used the same conditions as described for experiments with ara-A. In this series of experiments we increased the tested ara-C concentrations to 100 μM , to investigate if we would find more pronounced effects at higher concentrations. Fludarabine caused an increase of mutagenic end joining to about 150% of the controls at concentrations above 500 μM (Figure 34 A). Ara-C on the other hand caused a small reduction (about 20%) of mutagenic repair (Figure 34 B). However, this reduction was significant only at 1 μM ($p=0.001$).

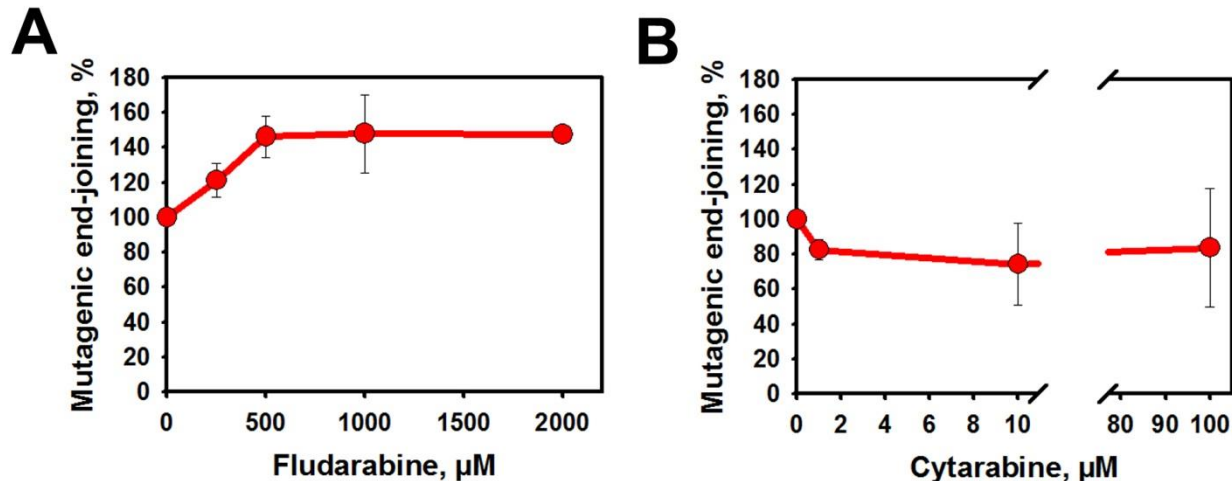


Figure 34 Effect of fludarabine and ara-C in U2OS EJ-DR cells (EJ-RFP).

A) Effect of treatment with fludarabine (4h starting 1.5h after transfection) on mutagenic end-joining. Flow cytometry analysis was performed four days after transfection with the I-SceI expression plasmid. Data points represent mean and s.d. from 3 independent experiments. **B)** As in (A) but with ara-C.

We concluded that Fludarabine behaved similar to ara-A in I-SceI reporter assays, but showed some differences in the strength of effects on individual repair pathways. Notably, fludarabine had lesser potential to increase distal-end joining and the overall mutagenicity of repair. Ara-C on the other hand did not have a positive influence on any of the examined repair pathways. Instead it showed small to moderate reduction of all repair outcomes.

5 Discussion

5.1 Design of this study and general considerations

It was our aim to investigate mechanisms of radiosensitization by NAs using ara-A as a model compound. We focused on possible interactions of ara-A with pathways of DSB repair. A well-known characteristic of this deoxyadenosine analog is its inhibitory effect on mammalian DNA replication (Plunkett, 1974; Muller, 1975; Kufe, 1983; Ohno, 1989). Most of the results previously reporting radiosensitization by ara-A were generated using cultures in the plateau phase of growth (Iliakis, 1980; Iliakis and Bryant, 1983; Iliakis and Ngo, 1985; Iliakis, 1989b; Little, 1989). Plateau-phase conditions conveniently circumvent complications frequently generated when treating an actively growing culture with substances that have cell cycle phase specific effects. In the case of an S-phase inhibitor these complications include S-phase specific cytotoxicity and changes in the cell cycle distribution that may modify the outcome of many types of experiments.

Despite the difficulties in experimentation and the interpretation of data that are associated with the usage of asynchronous cell populations, we decided to use exponentially growing cells for a large part of this work. One rationale for this decision was that also within a tumor, cells can be found distributed in all phases of the cell cycle. A second important reason was that we wanted to investigate the effects of this drug on all known pathways of DSB repair. Since the activity of some repair pathways, especially HRR, but also B-NHEJ, underlie cell cycle dependent control mechanisms the use of

proliferating cultures was without alternative (Shrivastav, 2008; Escribano-Diaz, 2013). However, it was essential for us to have controls that allowed us to differentiate between effects that were primarily due to inhibition of replication and other, not directly replication linked effects. For this reason we included two non-nucleoside replication inhibitors in our studies. Aphidicolin is a tetracyclic fungal metabolite that inhibits the DNA polymerases α , δ and ϵ by direct binding (Ikegami, 1978; Ohashi, 1978). Hydroxyurea (HU) is a hydroxylated analog of urea that acts by inhibiting the enzyme ribonucleotide reductase (RnR), which results in deregulation and depletion of deoxynucleotide pools (Chapman and Kinsella, 2011). Ara-A on the other hand can be incorporated into DNA and inhibits the DNA polymerases α and β , as well as the enzymes primase and RnR (Dicioccio and Srivastava, 1977; Chang and Cheng, 1980; Kuchta and Wilhelm, 1991).

5.2 Inhibition of replication and sensitization of cycling cells

The two control compounds and ara-A all have different, albeit partially overlapping, modes of action and are effective as replication inhibitors in different concentration ranges. We performed replication assays to assess their inhibitory activity. The results of these assays were used to calculate IC₅₀ values for replication (IC_{50_{repl}}), which enabled us to use the control compounds at equal-effect or higher concentrations than ara-A (Figure 13). Exponentially growing cells were sensitized very efficiently to IR by ara-A treatment (Figure 14 A). We compared the radiosensitizing effect of ara-A at 40 and 80 times IC_{50_{repl}} to the survival of cells that had been treated with HU at 45 times IC_{50_{repl}} or aphidicolin at 220 times IC_{50_{repl}} (Figure 14 B). Aphidicolin did not elicit any radiosensitization in treated cells. HU treatment caused some radiosensitization, which was much weaker than that caused by ara-A.

These experiments confirmed that radiosensitization by ara-A cannot solely be attributed to inhibition of replication during the treatment period. HU has been implicated as radiosensitizer and a number of clinical studies had been initiated in the 1960s and 70s, before interest declined again due to controversial results. The comparatively weak

sensitization that was caused by HU is likely to be related to the role of RnR in radiation response and possibly DNA repair (Chapman and Kinsella, 2011).

RnR is a tetrameric complex consisting of two subunits named R1 and R2. R1 is the larger, regulatory subunit, which is expressed constitutively throughout the cell cycle. The expression of the R2 subunit is cell cycle dependent, with highest levels reached in the S-phase (Kuo and Kinsella, 1998). Importantly, relatively recently an alternative R2 subunit, named p53R2, was discovered. This subunit is not cell cycle regulated, but becomes induced transcriptionally after exposure to IR (Tanaka, 2000). This finding suggests some replication independent functions of RnR in the response to IR. Ara-A is known to have an inhibitory effect on RnR as well (Moore and Cohen, 1967; Chang and Cheng, 1980). Thus, inhibition of RnR may also play a role in the radiosensitization by ara-A. However, the small radiosensitization elicited by HU suggests that the contribution of this mechanism to the overall radiosensitization by ara-A will be small.

The highly efficient radiosensitization by ara-A demonstrated in survival assays strongly suggested an interference of this drug with pathways of DSB repair. We applied various techniques for the detection of DSB and the measurement of their repair in this study. Each of these methods has its individual strength and weaknesses. These will be discussed comparatively in the next section, before proceeding to the discussion of the actual results.

5.3 Methods for the measurement of DSB repair

5.3.1 PFGE

PFGE is a physical method for the detection of DSB (Gardiner, 1991; Gurrieri, 1999). The amount of DSB and the kinetics of their repair are measured in the pooled total DNA of irradiated cell populations. For this end cells have to be exposed to high doses of IR and are incubated for different times afterwards. In this study 20 Gy were used as a standard induction dose. The clear advantage of PFGE is that it directly measures the actual physical presence of DSB within the genomes of cells and therefore can

accurately describe the kinetics with which they are rejoined. However, it cannot yield information about the repair pathways that conduct this repair. Switches in repair pathways that don't significantly change the overall rate of repair will go unnoticed in PFGE experiments. Evidence from genetic studies indicates that repair as it is measured by PFGE in repair proficient cells mostly represents D-NHEJ, while in D-NHEJ deficient cells the observed DSB repair can almost entirely be attributed to B-NHEJ (Dibiase, 2000; Perrault, 2004). HRR seems to play hardly any role in the repair that is detected by PFGE in D-NHEJ proficient as well as in D-NHEJ deficient cells (Wang, 2001a; Iliakis, 2004). This may also partly be due to a limitation of PFGE, which is the requirement for high doses of IR to allow sufficient resolution. Experiments with lower initial doses than 10 Gy become very difficult to analyze. This can be a problem, as radiation dose may also be a factor determining repair pathway choice (Sasaki, 2013). Finally, bulk analysis of cells in the standard application of this method means that distinct behavior of sub populations cannot be identified and distinguished. This includes cells from different phases of the cell cycle, which are known to show very different repair repertoires and potentials. However, in this study we could overcome the latter limitation by usage of a sophisticated combination of cell sorting and PFGE.

5.3.2 IRIF

The analysis of ionizing radiation induced protein foci (IRIF) by immunofluorescence microscopy offers a much higher sensitivity with regard to the required dose and number of DSB than PFGE. Foci analysis enables the use of doses as low as 0.01 Gy for the production of statistically significant results (Markova, 2007). It also allows analysis on a single cell level, including discrimination by cell cycle phase or other criteria. However it is not only advantageous, as it lacks the direct physical evidence for the presence of a DSB. While the number of γ H2AX foci for examples that is found after a given dose correlates very well with the theoretically predicted and with other methods verified numbers, it has become evident that there are substantial timely differences between the kinetics of the disappearance of physical DSB and the generation and decay of IRIF (Markova, 2007; Kinner, 2008). The number of γ H2AX foci for peaks about 1h after

irradiation in wild type cells, a time at which more than half of the DSB are already rejoined in repair proficient cells, as we know from physical methods like PFGE (see Figure 24, Figure 25 and Figure 26). Thus counting of foci may be used for the estimation of damage induction and residual damage, but caution must be exercised when drawing conclusions for the kinetics of repair, as the presence of a focus does not necessarily signify the presence of a physical break. Additionally it has been shown that phosphorylation of γ H2AX does not exclusively occur only after DSB induction, but can be induced by other factors as well (Tu, 2013). Nonetheless, analysis of IRIF is a valid approach for the investigation of some aspects of DSB repair, particularly because it offers the opportunity to gain mechanistic insights into how breaks become repaired.

5.3.3 The use of I-SceI reporter assays for the assessment of DSB repair pathway activities

Repair reporter constructs carrying recognition sites for rare cutting endonucleases that are stably integrated into the genome can be used to assay the frequency of specific repair events. In this type of reporter assay the expression of a site specific endonuclease (here I-SceI) leads to the introduction of a DSB in the reporter construct. The design of the construct is such, that only a special type of repair outcome, often specific to a single repair pathway, results in generation of a signal (Gunn and Stark, 2012). These I-SceI reporter assays are widely used to measure the efficiency of different pathways of DSB repair.

However, important differences to the repair of IR induced DSB have to be considered when working with these assays. These are mainly the different time frame of damage induction and the chemical composition of the breaks:

At the dose rates used in this study DSB are induced by IR in a manner of seconds or minutes. In the case of DSB induction by I-SceI, several steps precede the cutting: After transfection the I-SceI gene needs to be transcribed, the mRNA translated and the resulting enzyme has to translocate to the nucleus and find its cutting site. Moreover, once expressed I-SceI remains present and active within the cell. Additionally, more I-

Scel will continuously be expressed as long as the plasmid remains intact. Work from our group has shown that the levels of I-SceI protein in transfected cells remain constant up to 72h at least (Schipler, 2013). In the same study foci of 53BP1 were shown to be present for longer than 24h in repair proficient cells transfected with an I-SceI expression plasmid, indicating ongoing cutting of I-SceI sites (Schipler, 2013). Thus, DSB can be induced over a long period of time, possibly several days, in I-SceI inducible reporter assays.

The chemical nature of the ends of DSB induced by either IR or I-SceI is very different. While IR induced DSB usually harbor chemically modified ends that prohibit ligation without further processing (Figure 4 B&C), DSB introduced by I-SceI can readily be religated due to the presence of unaltered 3'-OH and 5'-phosphate groups and complementary overhangs (Figure 4 A) ((Magin, 2013; Schipler and Iliakis, 2013)). Simple religation of an I-SceI induced DSB will result in reconstitution of the I-SceI site without generation of a signal. This regenerated site is again susceptible to cutting by the restriction enzyme, which may result in cycles of repeated cutting and religation. These cycles will be ended only when either a signal generating event occurs or the I-SceI site is disrupted by another repair outcome. This can lead to under- or overestimation of the activity of different repair pathways and creates further uncertainty with regard to the time when damage induction and repair occur.

When conditions are tested that themselves last or can be sustained for prolonged times (e.g. knockdown or knockout of genes or treatments with low cytotoxicity), the continuous damage induction in I-SceI reporter assays does not present a major problem. However, treatment with many drugs, including NAs, is limited by cytotoxicity that increases with time. Furthermore, cell cycle phase specific drugs can elicit changes in the cell cycle distribution that could bias readings conducted at later times. Indeed we have found that such effects can lead to deceptive results when measurements are taken at 48h-72h after short term drug treatment (Figure 36 and Figure 37). Therefore, to avoid complications that would be associated with short term drug treatment and this inherent characteristic of the I-SceI system, we limited the observation time to 24h in this study where possible.

Taken together, I-SceI reporter assays allow the measurement of specific repair outcomes indicative of DSB repair pathway activity. These results can provide valuable information about the effect of various treatments on these pathways. However, due to the different kinetics of DSB induction and the distinct chemical characteristics of the breaks caution has to be exercised when interpreting results and drawing direct comparisons to the effect of IR.

In summary, each of the methods discussed above is able to provide a different kind of information about DSB repair. PFGE shows the actual presence of breaks, detection of IRIF by immunofluorescence sheds light on cellular responses to DSB and signaling, while I-SceI reporter assays provide information about how repair of some breaks has been completed. Each of these methods has its own limitations and peculiarities, knowledge about which is required for meaningful interpretation. Thus, data generated with each of those methods as individual piece of information has to be interpreted with care and under consideration of these limitations. Combination of information generated with multiple methods greatly strengthens the certainty with which conclusions can be drawn and broadens the scope of observations. Therefore we tried to address all question that arose in this study with a combination of methods.

5.4 Effects of ara-A on HRR

5.4.1 Effect of ara-A on IR induced Rad51 foci formation

Since ara-A is an efficient inhibitor of replication we wondered if it may also effect mechanisms of DSB repair that require substantial DNA synthesis. We used antibody staining and analysis by confocal microscopy to score Rad51 foci as a surrogate for ongoing HRR. We included cyclin B1 (CycB1) staining and labelling with EdU to enable the definitive discrimination of cells in G1, S and G2.

EdU incorporation itself had no influence on Rad51 foci formation. The maximum number of Rad51 foci and the time when the maximal number of foci is reached for a given dose are dependent on the applied dose of IR. Studies in our group have shown that the maximum number of Rad51 foci is reached at 4 Gy and that this maximum

occurs at about 3h after irradiation. Thus, we chose 4 Gy as the test dose, to induce a maximum number of Rad51 foci.

The results of these experiments clearly showed that the formation of Rad51 foci could efficiently be suppressed by ara-A treatment. Rad51 foci formation was almost fully abrogated at 1000 μ M ara-A in S-phase cells and showed strong reduction in G2 cells (Figure 15 B). The requirement of higher concentrations of ara-A in G2 to reduce the level of Rad51 foci to similar numbers as in S-phase cells may either indicate an initial resistance of HRR to ara-A in the G2 phase, or could be related to higher absolute numbers of DSB in G2-cells that are repaired by HRR. Induction of DSB is proportional to DNA amount and thus is expected to be higher in G2 than in S-phase cells. In any case, from 100 μ M onwards the curve for G2-cells followed an almost identical course as the curve for S-phase cells, suggesting a similar cause-effect relationship.

These results showing suppression of IR induced Rad51 foci formation by treatment with ara-A, strongly indicated that successful execution of HRR was directly inhibited by this drug. Furthermore, the suppression of Rad51 foci formation caused by ara-A correlated very well with the radiosensitization elicited by ara-A in cycling A549 cells (Figure 15 C). Therefore we decided to test the importance of HRR inhibition in ara-A mediated radiosensitization in clonogenic survival assays.

5.4.2 Survival with Rad51 silenced cells

If inhibition of HRR was a major mechanism of radiosensitization, the sensitization of cells already deficient for HRR should be reduced as compared to HRR proficient cells. Knockout of Rad51 is embryonic lethal in mice and Rad51 knockout cell lines are not viable. However, work by others indicated that transient silencing of Rad51 allows cells to remain viable (Liu, 2011; Short, 2011). Therefore we decided to induce HRR deficiency in A549 cells via knock down of Rad51 by RNAi. As control population we used cells that were transfected with a siRNA against GFP. We found that Rad51 silenced cells retained a PE of 20% (Figure 16 B). This represented a considerable reduction compared to the control, but was expected and similar to reductions in PE after Rad51 knockdown reported by others (Liu, 2011; Short, 2011). This reduction in

viability is likely due to functions of Rad51 in replication (Sonoda, 1998; Daboussi, 2008; Petermann, 2010).

Rad51 knockdown cells were much more radiosensitive than the controls. This as well was in accordance with results reported by others and confirmed that cells that retained viability still represented successfully transfected cells (Liu, 2011; Short, 2011). Importantly, treatment with ara-A did not further increase the radiosensitivity of those cells. Only at 5 Gy, which was the highest dose used in these experiments, some sensitization seemed to occur. It is important to note though, that the curve of the Rad51 knockdown cells flattens out at this dose, displaying a resistance tail (Figure 16 C). This type of curvature occurs typically when radioresistant subpopulations start to dominate the shape of the survival curve. The higher the radiation dose, the smaller is the number of cells that survive. Sensitive cells become inactivated first, while more radioresistant cells may remain clonogenic at higher doses. A very small subpopulation of resistant cells will have hardly any impact on the course of the survival curve at lower doses, but will determine its shape almost entirely at higher doses (Iliakis and Okayasu, 1990). It is likely that the resistance tail of the survival curve of Rad51 knockdown cells is largely due to cells in which silencing was less efficient than in the bulk of the population. Those cells would still be at least partially proficient for HRR and thus also susceptible to sensitization by an HRR inhibitor. We concluded that inhibition of HRR indeed is an important factor in ara-A mediated radiosensitization in cycling cells.

5.4.3 Effect of ara-A on HRR of the DR-GFP reporter construct

Initially only a CHO cell line, DRaa40, carrying a reporter for HRR (DR-GFP) was available to us. Development of a GFP signal in this system is indicative of successfully completed HRR (Figure 17 B) (Pierce, 1999). For experiments cells were transfected with an expression plasmid for the I-SceI endonuclease and were exposed to different concentrations of ara-A three hours later. After a four hour treatment the drug was removed. 24h after transfection the cells were collected and analyzed by flow cytometry. Treatment with ara-A strongly suppressed HRR in this system, showing 70% inhibition at a concentration of 500 μ M (Figure 17 C).

At a later time we were able to obtain human cell lines (U2OS) carrying DR-GFP and other reporter constructs. Knockdown of several proteins implicated in HRR in the cell line harboring DR-GFP (U2OS 282C) confirmed the validity of this reporter as test system for HRR (Figure 19). Ara-A proved to be a very effective inhibitor of HRR of the DR-GFP construct in these human cells as well. The concentrations that were required to achieve equal suppression were higher than in DRaa40 cells (1000 μ M vs. 500 μ M for 70% inhibition), which is in accordance with the higher toxicity this compound is known to show in rodent cells (Juranka and Chan, 1980).

Taken together, suppression of Rad51 foci formation, lack of radiosensitization after knockdown of Rad51 in human A549 cells and inhibition of HRR measured by the DR-GFP reporter in CHO and human U2OS cells confirm strong inhibition of HRR by ara-A. So far the exact molecular mechanisms that cause this inhibition remain unknown. The multistep process of HRR can be envisioned to be inhibited at several stages. This includes the resection of DSB ends that creates the ssDNA intermediate, formation of the Rad51 nucleoprotein filament, search for homology, elongation of the invading strand upon synapsis or resolution of recombinational structures and final ligation (Li and Heyer, 2008). Considering the effects of ara-A as an inhibitor of replication, inhibition of repair synthesis seems like an obvious mechanism for inhibition of this repair pathway. For ara-A inhibition of polymerase alpha/primase and polymerase beta has been reported (Dicioccio and Srivastava, 1977; Kuchta and Willhelm, 1991). A main mechanism of replication inhibition by ara-A is inhibition of RNA primer synthesis for lagging strand synthesis by the primase enzyme (Kuchta and Willhelm, 1991). However, primer synthesis is not required in HRR as the invading strand serves to prime DNA synthesis. Furthermore, multiple polymerases have been implicated to promote HRR, including the Polymerases beta, delta, eta, zeta and REV1 (Canitrot, 2004; Maloisel, 2008; Kane, 2012; Sharma, 2012). Moreover the Polymerase delta subunit POLD3 (POL32 in yeast) has been shown to play an important role in the BIR pathway of HRR (Costantino, 2014). Except for Polymerase beta for none of the other polymerases listed an inhibition by ara-A has been reported. Additionally, the presence of several translesion synthesis polymerases (zeta, eta and REV1) in this list suggests that HRR may possess the flexibility to bypass disturbances, like incorporated NAs, in template DNA.

Incorporation of ara-A during repair synthesis itself may hamper completion of HRR. However, the amount of DNA synthesis required during most HRR events is limited (several hundred bases) and it is unclear if incorporation of ara-A could be sufficient to obviate its completion, since it does not act as a chain terminator (Plunkett, 1974; Muller, 1975; Kufe, 1983; Ohno, 1989). Therefore inhibition of DNA synthesis cannot readily be assumed to underlie inhibition of HRR. The strong suppression of Rad51 foci formation observed under ara-A treatment may indicate that suppression of HRR takes place at an even earlier stage, like the resection of break ends or loading of Rad51 on ssDNA. Further studies are required to clearly identify the molecular mechanisms of the inhibition of HRR by ara-A. However, first evidence helping to eliminate one candidate process came from the usage of another reporter cell line.

5.4.4 Effect of ara-A on SSA

Using the SA-GFP construct integrated into U2OS 283C cells, we examined the effect of ara-A on the mutagenic SSA pathway. Silencing of HRR factors in the SA-GFP system resulted in a massive increase of SSA events. This impressively demonstrated the suppression of SSA that is mediated by HRR and has also been reported previously (Tutt, 2001; Stark, 2004; Mansour, 2008). We found that SSA could be partially inhibited by ara-A, but also benefited from inhibition of HRR at higher concentrations of ara-A. We showed that this recovery of SSA derived from an ara-A mediated release of SSA from the suppression exerted by HRR. This result gave further indirect evidence for inhibition of HRR by ara-A. It is interesting that ara-A could reduce SSA efficiency only by around 30%. This means that the majority of SSA events is resistant to ara-A. Since all SSA events are dependent on extensive end-resection, this indicates that end resection is not inhibited by ara-A. Thus inhibition of end-resection can likely be excluded as a potential mechanism for the inhibition of HRR.

5.5 Effects of ara-A on NHEJ

5.5.1 Effect of ara-A on distal end-joining

Another repair reporter system, the EJ5-GFP construct integrated into U2OS 280A cells, allowed the analysis of the effect of ara-A on a specific subtype of NHEJ events. This construct does not simply measure the repair of a single I-SceI-induced DSB, but involves induction and misrepair of two DSB. Each of these DSB can either be repaired by rejoining of the proximate ends, or by rejoining of one end from the first and one from the second DSB (distal ends). Rejoining of distal ends results in the loss of the large (~1.8kb) intervening fragment, but enables expression of a GFP gene. Thus, signal generating events in this system have to be considered as a highly mutagenic form of NHEJ. Therefore, this assay should be expected not to measure the activity of the classical DNA-PK dependent pathway of NHEJ (D-NHEJ), but rather that of backup pathways of NHEJ (B-NHEJ). To confirm this interpretation we inhibited DNA-PKcs, a central component of D-NHEJ, with the specific inhibitor NU7441. Measurements by PFGE (Figure 38) or the phosphorylation of H2AX (Shaheen, 2011) show that treatment with this inhibitor induces a substantial defect in the repair of DSB, clearly demonstrating an inhibition of D-NHEJ. In U2OS cells harboring the EJ5-GFP construct on the other hand, treatment with NU7441 almost doubled the usage of distal ends (Figure 22 and Figure 39). This finding is in accordance with similar reports from others (Gunn, 2011).

Treatment with ara-A caused distal-end joining events to increase by 30%. We interpreted this finding as an indication for increased activity of backup NHEJ. Taken together, the results obtained with this set of reporter cell lines indicated that HRR is inhibited by ara-A, while mutagenic pathways of homology directed (SSA) or NHEJ benefit from ara-A treatment.

5.5.2 Effect of ara-A on mutagenic DSB repair in the EJ-RFP system

To further investigate whether repair by B-NHEJ is really promoted by ara-A, we employed another reporter cell system. The EJ-RFP system was recently developed in the group of Dr. Simon Powell (Bindra, 2013). In contrast to the previously used

reporters, in this system the expression of a signal is not based on the generation of a functional gene by one certain, predefined repair event. Instead, the disruption of a gene by any kind of mutagenic repair leads to generation of a signal. The different way of signal generation is mirrored in delayed appearance of the signal as compared to the I-SceI reporter assays above. This necessitated measurement after 96h instead of 24h after transfection of the I-SceI plasmid. Treatment with ara-A resulted in a 2.5-fold increase of the DsRed signal compared to untreated controls. This showed that ara-A greatly promotes the mutagenic repair of DSB. In contrast to NU7441 there is no evidence so far for any impairment of D-NHEJ by ara-A. To address the question if ara-A may have an inhibitory effect on D-NHEJ we examined its influence on the kinetics of DSB repair in D-NHEJ proficient A549 cells by PFGE. Furthermore, we were interested to see if the inhibition of HRR that is mediated by ara-A may be detectable in this assay.

5.5.3 PFGE of sorted G1 and G2 cells from an exponentially growing culture

We used pulsed field gel electrophoresis (PFGE) to measure the repair of DSB in the genome of X-irradiated A549 cells. As discussed above (5.3.1) DSB repair as it can be observed by PFGE in repair proficient asynchronous cell populations is mainly due to the activity of D-NHEJ, which is generally assumed to be the dominant pathway of DSB repair throughout the cell cycle (Dibiase, 2000; Wang, 2001a; Iliakis, 2004; Perrault, 2004; Mladenov and Iliakis, 2011). However, since HRR as well as B-NHEJ show strong cell cycle dependence in their activity, which is absent or lower in G1 and higher in G2, we reasoned that it might be possible to see their influence when G1 and S/G2 cells were analyzed separately (San Filippo, 2008; Wu, 2008a; Wu, 2008b; Heyer, 2010).

Thus, we decided to irradiate and treat cells as exponentially growing cultures, but sort cells by FACS in different phases of the cell cycle for later analysis by PFGE. DNA from cells in the S-phase of the cell cycle has different characteristics of release migration in a gel, than G1 and G2 cells. This differential DNA release is related to S-phase specific DNA structures (Latz, 1996; Dewey, 1997). Thus, it was necessary to prepare separate dose response curves for each category.

Since S-phase cells are themselves a heterogeneous population with regard to their progress in DNA replication and the related potential to perform HRR, we decided to concentrate on G1 and G2 cells. These represent two extremes of the cell cycle with G1 cells putatively having 0% potential and G2 cells theoretically having 100% potential to perform HRR. Cell sorting gave us the best possible purity (Figure 24). G1 cells could be enriched >95% and G2>80%. It is not possible to achieve the same purity for G2 as for G1, because the broader distribution of the G2 peak partially overlaps with cells in late S-phase (and vice versa). Additionally, the smaller number of G2 cells precludes overly restrictive gating, due to the large cell numbers that were required for the analysis. A purity of >80% G2 cells however is a better enrichment than can be achieved with any other non-chemical method in this cell system. The cleanliness of those preparations is also reflected by the dose response curves of the G1 and G2 fractions (Figure 24 B). Both G1 and G2 cell dose responses are steeper than the curve of the asynchronous cells, due to the absence of S-phase cells. G1 and G2 cell dose responses are almost superimposable, only the G2 is minimally lower due to the slightly higher S-phase contamination.

The results of this experiment clearly showed that neither in the asynchronous population, nor in G1 or G2 cells from the same exponentially growing culture, the kinetics of DSB repair were altered by ara-A in any way. This suggested that the inability to detect defects in HRR in asynchronous cell populations by PFGE (Wang, 2001a; Iliakis, 2004), which we had hoped to overcome by our sorting strategy, was not only due to masking effects of cells in other phases of the cell cycle. Importantly, novel, thus far unpublished findings from our group demonstrate that the contribution of HRR to the total load of repair is diminished with increasing radiation dose. These results indicate that the contribution of HRR drops from as much as 70% at 0.25 Gy to about 15% at 2 Gy. This ratio is further reduced at a slower rate at even higher doses. At the dose of 20 Gy applied in our PFGE experiments, the fraction of DSB that remains destined for repair by HRR can be expected to be minuscule. Thus, the high doses required to achieve satisfying resolution in PFGE experiments reduce the contribution of HRR to the overall repair of DSB and thus render PFGE inappropriate for the investigation of the role of this pathway in DSB repair.

However, an important motivation to conduct these experiments had also been to observe potential signs of a shift from relatively accurate D-NHEJ to more error-prone B-NHEJ as it had been indicated by I-SceI reporter assays. B-NHEJ as it can be observed in D-NHEJ deficient cells operates with slower kinetics than D-NHEJ. The repair kinetics in our experiments yielded no indication for a shift from a fast to a slower process. We concluded, that if B-NHEJ took a greater part in the repair of DSB in those cells when treated with ara-A, this form of B-NHEJ could not be characterized by a slower rate of repair. We speculated that if a fast form of B-NHEJ was enhanced by ara-A treatment, which was not distinguishable from D-NHEJ in A549 cells, it may be observable in D-NHEJ deficient cells.

5.5.4 Ara-A enhances B-NHEJ in D-NHEJ deficient HCT116 cells

We used a panel of human HCT116 colon carcinoma cells including two knockout mutants for core components of D-NHEJ. We performed experiments with exponentially growing and serum deprived cells. We found that for the D-NHEJ deficient HCT116 *LIG4^{-/-}* and HCT116 *DNA-PKcs^{-/-}* cells DSB repair was enhanced by treatment with ara-A in the exponential phase of growth as well as after serum deprivation. On the other hand, in agreement with results previously obtained for A549 cells, the DSB repair kinetics of HCT116 WT cells were not altered by ara-A treatment. Previous work from our group has demonstrated that B-NHEJ is suppressed in the plateau phase of growth respectively under conditions of serum deprivation (Singh, 2011). Our results obtained with serum deprived D-NHEJ deficient HCT116 cells had also shown this inhibition and concomitantly an even greater repair enhancement after treatment with ara-A.

5.5.5 Relieve of B-NHEJ suppression in plateau phase MEF *Lig4^{-/-}* cells by ara-A

This indicated that ara-A treatment could not only promote B-NHEJ, but also relieve the suppression of DSB repair observed in the plateau phase of growth (Singh, 2012). In MEF *Lig4^{-/-}* cells, repair is essentially absent in the plateau phase of growth (Figure 26 B). Therefore we chose this cell system to conduct further experiments. Indeed we found

that DSB repair was promoted when those cells were treated with ara-A. Treatment with ara-A did not only restore B-NHEJ to nearly normal efficiency (25 μ M-50 μ M), but could also improve it beyond that point (125 μ M- 250 μ M). In fact, after 4h treatment of serum deprived Lig4^{-/-} MEFs with 125 μ M or 250 μ M ara-A, the repair of DSBs observed was closer to the repair usually observed in wild type cells than to the repair in exponentially growing Lig4^{-/-} MEFs.

These impressive results clearly demonstrated that backup pathways of NHEJ can be promoted by treatment with ara-A. This strongly suggests that ara-A treatment creates conditions that are generally favorable or even required for B-NHEJ, but which are usually prevented in G1/G0 cells. A candidate process could be 5' - 3' resection of DSB ends. End resection is highly cell cycle regulated. While end resection mechanisms are active in the S and G2 phases of the cycle, in G1/G0 only very limited nucleolytic processing takes place (Jazayeri, 2006). B-NHEJ on the other hand, has been shown to be associated with and benefit from end-resection (Bennardo, 2008; Rass, 2009; Xie, 2009; Bothmer, 2010; Lee-Theilen, 2011; Symington and Gautier, 2011; Grabarz, 2013). In accordance with this, B-NHEJ has been found to be enhanced in the G2 phase of the cell cycle (Wu, 2008a; Wu, 2008b), where end resection is active. Thus, end-resection may be enhanced under ara-A treatment, thereby facilitating repair by B-NHEJ in plateau phase Lig4^{-/-} MEFs.

5.5.6 Promotion of B-NHEJ is not productive for survival

The improved DSB repair capacity induced in plateau phase Lig4^{-/-} MEFs by ara-A treatment, could have been possible to be associated with an increase of survival of these cells after irradiation. To verify this we performed preliminary survival experiments with serum deprived MEF Lig4^{-/-} cells with or without ara-A treatment. We found no increase in the survival of ara-A treated cells. On the contrary we observed radiosensitization of treated cells, demonstrating that enhanced B-NHEJ function is not associated with improved chances for cell survival (Figure 40).

Cells that show DSB repair defects are usually more radiosensitive than their repair proficient counter parts. However, some very radiosensitive cell lines also show only a mild or no DSB repair defect at all, indicating that removal of breaks as measured by

physical methods alone is not predictive of survival (Iliakis, 2009). It follows that not only the capacity for and rate of DSB repair are important for cell survival, but also the type and outcome of the repair. Thus over-activation of erroneous repair pathways may even negatively affect survival.

B-NHEJ has been implicated in the formation of translocations and other chromosomal aberrations (Bunting and Nussenzweig, 2013). Formation of chromosomal aberrations is adverse to survival and thus increased repair by B-NHEJ may not support survival, but even contribute to sensitization of cells to IR.

5.5.7 Detection of IRIF in plateau phase MEF cells

We sought to confirm and extend the observations we had made in the MEF Lig4^{-/-} cells with a complementary method. We decided to use immunofluorescence microscopy to investigate formation and decay of radiation induced foci of γ H2AX, 53BP1 and phosphorylated ATM. From this combination we hoped not only to gain information about the rate of DSB repair, but to gather some mechanistic information on DSB processing and signaling as well.

The phosphorylation of H2AX on Serine 139 (S139), also known as γ H2AX, is one of the first events in the response to DSB and has been frequently used as a surrogate marker for DSB (Rogakou, 1998; Nakamura, 2010). Formation and decay of 53BP1 foci also has been used to quantify induction and repair of DSB (Asaithamby and Chen, 2009). 53BP1 is a protein that acts early in the response to DSB and forms foci that colocalize with γ H2AX (Schultz, 2000; Polo and Jackson, 2011). Importantly, 53BP1 is not only a general component of the DDR, but is also known to play an important role in the regulation of DNA end-resection as well. It has been shown that 53BP1 and BRCA1 act antagonistically on end-resection and thereby influence pathway choice (Cao, 2009; Bouwman, 2010; Bunting, 2010; Escribano-Diaz, 2013). ATM is a central kinase in IR induced damage signaling. Phosphorylation of ATM at Serine 1981 (pATM) occurs in response to DSB and is required for its activation (Bakkenist and Kastan, 2003). pATM accumulates at sites of DSB where it can be detected as nuclear protein foci.

Phosphorylations mediated by ATM in response to DSB enable the analysis of key interactions during DSB repair. Thus, the presence or absence of pATM foci may provide important information about activation and maintenance of DDR signaling.

Lig4^{-/-} MEFs had developed a large number (~50/cell) of bright, distinct γ H2AX foci after 1h and untreated cells retained the same level of γ H2AX foci until 24h (Figure 28). This finding was in full accordance with the almost complete defect in DSB repair observed with PFGE. In contrast, when cells were treated with 250 μ M ara-A, they developed a pan-nuclear γ H2AX staining, which intensified with time. After 8h of ara-A treatment no cells with scorable foci were left, but the total phosphorylation of H2AX was increased enormously. Pan-nuclear γ H2AX staining can also be observed in cells that become apoptotic. However, hyperphosphorylation of γ H2AX related to apoptosis has been reported to be preceded by a ring shaped staining of the nuclear periphery and to be closely correlated with apoptotic DNA fragmentation (Talasza, 2002) (Solier and Pommier, 2009). Furthermore, pan-nuclear γ H2AX staining is ensued by the development of the characteristic pyknotic nuclear morphology of apoptotic cells.

Among many thousands of cells observed we did not find any of those earlier or later apoptotic signs at any time point. Importantly, if the ara-A induced pan-nuclear γ H2AX staining was due to apoptosis induced DNA fragmentation, massive DNA release into the gel should have been detected in PFGE experiments. Strikingly the exact opposite was what we had found: Reduced DNA release indicating improved repair (see above).

In the literature a variety of reports can be found that describe pan-nuclear phosphorylation of H2AX, which is not related to apoptosis and can be caused by different stimuli or stressors. Ewald et al. found that checkpoint abrogation by a CHK1 inhibitor in previously gemcitabine treated cells elicited pan-nuclear phosphorylation of H2AX, which was not related to apoptosis (Ewald, 2007). Similarly, Gagou et al. reported pan-nuclear staining in CHK1 depleted cells in response to prolonged treatment with thymidine and also excluded apoptosis as a cause (Gagou, 2010). Ewald et al., as well as Gagou et al., both performed their experiments in cycling cells and link the effects they observe to replication stress, collapsed replication forks, or the inappropriate firing of replication origins. Interestingly Gagou et al. report that depletion of the helicase

co-factor CDC45 greatly reduced pan-nuclear γ H2AX staining. Pan-nuclear staining can also be elicited by transfection of small DNA molecules mimicking DSB, which results in DNA-PK hyperactivation (Quanz, 2009). Pan-nuclear H2AX phosphorylation in response to adeno-associated virus infection is also coordinated by DNA-PK (Schwartz, 2009). Furthermore, pan-nuclear γ H2AX staining can be caused by UV-C radiation in G1 cells (Marti, 2006) or hypotonic treatment that induces chromatin changes (Baure, 2009). Finally, induction of pan-nuclear γ H2AX has been reported to occur in cells that received clustered DNA damage from traversing heavy ions (Meyer, 2013).

Taken together, our observations and the reports from others strongly suggest that pan-nuclear H2AX phosphorylation does not have to be associated with apoptosis and that other factors and mechanisms are capable of inducing γ H2AX in a nuclear wide manner. It is noteworthy, that pan-nuclear γ H2AX was not only caused by the combination of irradiation and ara-A treatment. In unirradiated cells not treated with ara-A around 15% of cells exhibited pan-nuclear γ H2AX staining (Figure 28 A, C&D). In irradiated cells without ara-A the frequency was similar. Unirradiated cells treated with ara-A for 24h also developed pan-nuclear γ H2AX staining in 100% of the cases (Figure 28 C).

We found high numbers of pATM foci (~60/cell), similar to the amount of γ H2AX foci, in ara-A treated and untreated cells 1h after irradiation. Slow decay of pATM foci was observed in cells without ara-A treatment, but after 24h still about 50% of initial foci were present (~30/cell). In contrast, in cells treated with 250 μ M ara-A, repair appeared to progress much faster and 24h after irradiation no foci were detectable. This observation was again in accordance with the repair defect and reactivation of B-NHEJ observed in PFGE experiments. However, we did also notice that the cells which lost their foci under ara-A treatment exhibited a diffuse, homogenous nuclear staining that appeared to be a little higher than background. Thus, it is possible that decline of pATM-foci number was not only due to completion of DSB repair, but to redistribution of pATM by the genome wide generation of γ H2AX. It was apparent that in serum deprived Lig4^{-/-} MEFs without ara-A treatment, DDR signaling remains active up to 24h and probably longer. This was evidenced by the persistence of bright pATM foci and was likely due to the persistence of DSB as also observed in PFGE. So far it is unclear if dissolution of pATM foci under

ara-A treatment is a consequence of ongoing DSB repair or whether loss of pATM foci is part of the mechanistic basis for the observed enhancement of rejoining.

The numbers of initial 53BP1 foci we found 1h after irradiation (~12/cell) were 4-5 fold lower than the numbers of γ H2AX or pATM foci. The initial number of foci was almost equal in ara-A treated and untreated cells. However, in untreated cells foci became brighter and appeared to increase in size over time, while in cells treated with 250 μ M 53BP1 foci formation was almost completely abolished after 4h and additional foci could not be detected up to 24h. This finding was again in accordance with increased repair in ara-A treated cells, although DSB repair-unrelated processes cannot be excluded at this time.

Furthermore, the rapid disappearance of 53BP1 foci may also offer first insights for a mechanistic explanation as to how B-NHEJ may be reactivated in serum deprived MEF Lig4^{-/-} cells. As mentioned above, 53BP1 is known to play an important role in the regulation of end-resection (Cao, 2009; Bouwman, 2010; Bunting, 2010; Escribano-Diaz, 2013). 53BP1 is antagonized by BRCA1 which forms, together with its interaction partner CtIP, a module that promotes resection of DSB ends (Yun and Hiom, 2009). The balance between those two counteracting forces is shifted towards 53BP1 dependent end-protection in G1 and towards BRCA1-CtIP dependent promotion of end resection in S and G2 by cell cycle regulatory mechanisms. These shifts reflect the potential and requirement of a cell to perform HRR at different stages during the cell cycle. In G1/G0 a sister chromatid is not available and end resection is suppressed in favor of D-NHEJ mediated repair, while in S and G2 DNA ends become frequently resected to allow for repair by HRR. The fact that CtIP has also been shown to be required for the repair by alternative or backup pathways of NHEJ in G1 (Yun and Hiom, 2009) together with other reports strengthen the notion that B-NHEJ is more active in G2 than in G1 because it benefits from resection of DNA ends (Bennardo, 2008; Wu, 2008a; Wu, 2008b; Rass, 2009; Xie, 2009; Yun and Hiom, 2009; Bothmer, 2010; Lee-Theilen, 2011; Symington and Gautier, 2011; Grabarz, 2013).

Decay of 53BP1 foci may therefore indicate that the protection of DSB ends from resection typical in G1/0 cells is reverted by ara-A. B-NHEJ and possibly also SSA are

the only known DSB repair processes expected to benefit from resection in serum deprived Lig4^{-/-} MEFs. Thus, enhancement of DNA end-resection in ara-A treated G1/G0 cells may be an important contributor of the observed B-NHEJ reactivation.

5.6 Radiosensitization by other NAs

5.6.1 Clonogenic survival after exposure to IR

The interesting results obtained for ara-A prompted us to test additional NAs and compare to the effects found for ara-A. First, we performed survival experiments in which we tested the NAs ara-C, gemcitabine and fludarabine for their radiosensitizing potential, and compared the results obtained to those of ara-A. Both, gemcitabine and fludarabine have been reported to act as radiosensitizers (Gregoire, 1994; Shewach, 1994; Lawrence, 1996; Latz, 1998; Pauwels, 2006; Nitsche, 2008). In fact, these observations have led to the initiation of a number of clinical trials to assess the therapeutic potential of these NAs in combination with radiation therapy (Gregoire, 2002; Aguilar-Ponce, 2004; Nitsche, 2012; Gurka, 2013). Ara-C on the other hand is not regarded as a radiosensitizer in the medical literature, but there are primary reports that show some inhibition of PLD repair by ara-C (Iliakis and Bryant, 1983; Nakatsugawa, 1984; Iliakis, 1989b).

We used a 4h post-irradiation treatment protocol like in previous survival experiments and concentrations that generated similar cytotoxicity as 500 μ M ara-A.

For fludarabine, we observed that treatment with 500 μ M was able to generate significant radiosensitization in cycling A549 cells. However, the observed sensitization was weaker than after treatment with ara-A at the same concentration. Furthermore, we found that ara-C was able to sensitize A549 cells to a similar extent as fludarabine. This finding was not in agreement with the general tenor of the literature (D'Angio, 2005), but was not entirely surprising considering previous reports about inhibition of PLD repair by ara-C.

We were surprised not to find any radiosensitization by gemcitabine despite the large amount of publications that report radiosensitization by this drug. This is most likely due

to the different treatment schedule we applied. The vast majority of studies reporting radiosensitization by gemcitabine use long pretreatments (usually 24h) at drug concentrations generating low cytotoxicity (Shewach, 1994; Rosier, 1999; Pauwels, 2003). In our study, on the other hand, and as a result of its focus on the analysis of NAs effects on DSB repair processes, treatment was post-irradiation, relatively short (4h), and included only a 40 min pre-treatment allowed mainly for drug entry into cells before DNA damage induction.

In a pilot study by Shewach et al. that assessed the dependence of treatment schedule on radiosensitization by gemcitabine, significant sensitization was only found for pre-irradiation, but not post-irradiation incubation with gemcitabine (Shewach, 1994). The radiation enhancement ratios found in this study increased with the duration of pre-treatment. It should be noted, however, that relatively low drug concentrations (10nM-30nM) were used to produce these results, whereas in our study 100-fold higher concentrations were applied (1 μ M-10 μ M).

Our results and the findings by Shewach et al. suggest that the effects of gemcitabine on cells when given before irradiation, seem to be indispensable for radiosensitization. Accumulation of cells in S-phase as well as depletion of intracellular dATP pools for example have been correlated with radiosensitization by gemcitabine (Shewach, 1994; McGinn, 1996)

Collectively, these observations allowed us to conclude that post-irradiation treatment is sufficient to induce radiosensitization in the case of ara-A, fludarabine and ara-C but not in the case of gemcitabine. The great dependence of gemcitabine on a pre-irradiation treatment schedule suggests that other effects than direct inhibition of DSB repair pathways play the major role in radiosensitization by this NA. Therefore we did not include it in further test, but continued to analyze the effects of ara-C and fludarabine.

5.6.2 Effect of other NAs in reporter cell assays

We started investigating the effects of ara-C and fludarabine on HRR, SSA and the joining of distal ends with U2OS reporter cell lines. For fludarabine we found inhibition of

HRR with efficiency similar to ara-A. Ara-C showed some, but comparatively weak inhibition of HRR.

Investigation of the effects of the same NAs on SSA showed that fludarabine induced a biphasic response similar to that seen with ara-A. This is in accordance with the model discussed above, in which SSA benefits from HRR inhibition at higher drug concentrations. The net benefit for SSA appeared to be larger in the case of fludarabine than for ara-A. Ara-C showed moderate suppression of the SSA repair pathway that did not increase further above 5 μ M.

We also investigated effects of NAs on the joining of distal ends in U2OS cells carrying the EJ5-GFP construct. Fludarabine, in contrast to ara-A, showed almost no effect on the rejoining of distal ends. However, a very small trend for increase was observed from 500 μ M onwards. Ara-C slightly reduced distal-end joining.

Neither nor HU showed a substantial reduction of the repair efficiency of any of the examined DSB repair pathways, confirming that inhibition of S-phase related DNA synthesis does not play a role for the effects observed with the nucleoside analogs.

It is interesting to note that ara-A remained the only drug that caused a substantial increase in the rejoining of distal ends. The EJ5-GFP construct differs from all other reporter constructs used in this study, in that it contains two sites for the induction of a DSB. Only if the distal ends of these DSB interact a signal is generated. Such an event is highly mutagenic, as it is accompanied by a large deletion. Such sequence loss is by itself dangerous and highly undesirable for the cell, but may also pose larger threats to chromatin stability and genome integrity. Selection of distal ends over the very proximal ends may be the result of rare endonucleolytic cleavage of the intervening DNA segment and other chromatin destabilizing activities. Similar processes of misrepair are most likely also responsible for the generation of translocations and other chromosomal aberrations frequently observed in irradiated cells and implicated in cell killing and transformation {Nambiar, 2011 #266}{Bunting, 2013 #524}.

By inhibiting DNA-PKcs we have shown that this reporter provides a measure for the activity of a form of B-NHEJ. As mentioned before, B-NHEJ has been heavily implicated in translocation formation. In addition, work from our Institute shows that a single DSB

introduced by I-SceI in a chromosome has a far lower toxicity than multiple (two or more) DSBs induced in close proximity (Schieler, 2013). The corresponding project was devised based on the assumption that increased complexity resulting from multiple breaks may lead to loss of whole nucleosomes or even larger chromatin units (Figure 4 D). In conclusion: Although the repair event that is detected by the EJ5-GFP reporter cannot easily be assigned to a single, well defined repair pathway, it is tempting to speculate that it is indicative of a type of repair that can have particularly lethal outcomes.

Finally, we investigated the effects of fludarabine and ara-C in EJ-DR cells. Those cells carried the EJ-RFP system for the measurement of the general mutagenicity of DSB repair. We found increased mutagenic repair when cells were treated with fludarabine. However, the increase was substantially smaller than in the case of ara-A. In cells treated with ara-C no increase in mutagenic repair could be observed. On the contrary, overall repair appeared to be even somewhat more accurate.

Taken together fludarabine and ara-C exhibited a very different profile of effects on DSB repair pathways, when assayed with I-SceI inducible reporter systems. Fludarabine performed similar to ara-A with respect to the homology directed repair pathways HRR and SSA, but showed lower potency for increasing mutagenic repair related to NHEJ. Ara-C on the other hand did neither show strong inhibitory effects nor a promotional effect on any of the modes of repair analyzed. Nevertheless, both drugs showed similar radiosensitizing potential in clonogenic survival assays. In the case of ara-C this strongly suggests that other mechanisms than inhibition of DSB repair pathways play an important role for radiosensitization, as it also appears to be the case for gemcitabine, although ara-C was effective as a post-irradiation treatment. On the other hand, it appears likely that radiosensitization by fludarabine for a good part is related to its inhibitory effect on HRR.

Ara-A distinguished itself from fludarabine and ara-C mostly by its superior capability to enhance mutagenic end-joining and was the only drug that caused a significant increase in the usage of distal ends. Together with the PFGE data from D-NHEJ deficient cells and the results of immunofluorescence detection of IRIF in plateau phase MEFs, we

could conclusively show that ara-A effectively promotes the activity of B-NHEJ. Furthermore, lack of additional radiosensitization after silencing of Rad51 and suppression of Rad51 foci formation by ara-A convincingly confirmed inhibition of HRR observed with the DR-GFP construct. We conclude that ara-A exerts its superior radiosensitizing effects through a shift in the balance from DSB repair that helps to maintain genomic stability and promotes survival, represented by HRR and D-NHEJ, to error-prone mechanisms that threaten genomic integrity and are adverse to survival, represented by B-NHEJ and SSA.

It will be important to investigate the effects of ara-C and fludarabine with complementary methods as well. Future work will also focus on the This, together with the results obtained for distal end-joining may indicate that fludarabine has a lesser propensity to promote mutagenic NHEJ than ara-A.

6 Summary and Conclusions

Achieving improvements in cancer therapy is one of the major challenges of contemporary medicine. Combining drug treatment and radiotherapy to achieve synergistic killing of cancer cells is one of the most promising current approaches towards this goal. Aim of this thesis was to elucidate mechanisms of radiosensitization by nucleoside analogs (NAs), a highly promising class of chemotherapeutics, using 9- β -D-arabinofuranosyladenosine (ara-A) as a model compound.

Towards this goal, we investigated in detail the effect of ara-A on the repair of DSB. We established that ara-A inhibits homologous recombination repair (HRR) and showed that this inhibition plays an important role in the radiosensitization of exponentially growing human tumor cells.

We also examined the effect of ara-A on pathways of non-homologous end-joining (NHEJ). We found an increase in the frequency of erroneous DSB repair events in two cellular reporter assays. However, we could not detect a decrease by ara-A in the overall DSB repair efficiency in repair proficient cancer cells exposed to high doses of IR, when tested in the G1 or G2 phase of the cell cycle by pulsed-field gel

electrophoresis (PFGE). This result implied a switch between DSB repair pathways, rather than an overall inhibition of DSB repair.

Through examination of DSB repair by PFGE in repair deficient cells we could show for the first time promotion of error prone backup pathways of non-homologous end-joining (B-NHEJ) by a NA. Ara-A enhanced the repair of DSB by B-NHEJ in human tumor cells. Furthermore, ara-A treatment completely abrogated the plateau-phase-dependent inhibition of B-NHEJ in mouse cells, causing a dramatic restoration of DSB repair.

Investigation of IR induced damage foci by immunofluorescence microscopy confirmed the above observations and implicated end-resection and deregulation of DSB signaling as underlying mechanisms. We conclude that in cycling cells treatment with ara-A causes direct inhibition of HRR resulting in radiosensitization. At the same time the balance of NHEJ is shifted towards the more error prone B-NHEJ. Over-activation of mutagenic B-NHEJ is likely to make an important contribution to radiosensitization by ara-A, especially in G1 and plateau phase cells, but also in G2 and S-phase cells.

Our findings reveal a novel mechanism of radiosensitization by nucleoside analogs. That opens new avenues in the investigation of interactions of these drugs with IR and may have important implications for the clinical application of NAs as radiosensitizers.

7 Bibliography

Adimoolam, S., M. Sirisawad, J. Chen, P. Thiemann, J. M. Ford and J. J. Buggy (2007). "HDAC inhibitor PCI-24781 decreases RAD51 expression and inhibits homologous recombination." Proceedings of the National Academy of Sciences of the United States of America **104**(49): 19482-19487.

Aguilar-Ponce, J., M. Granados-Garcia, V. Villavicencio, A. Poitevin-Chacon, D. Green, A. Duenas-Gonzalez, A. Herrera-Gomez, K. Luna-Ortiz, A. Alvarado, H. Martinez-Said, C. Castillo-Henkel, B. Segura-Pacheco and J. De la Garza (2004). "Phase II trial of gemcitabine concurrent with radiation for locally advanced squamous cell carcinoma of the head and neck." Ann Oncol **15**(2): 301-306.

Ahmad, S. S., S. Duke, R. Jena, M. V. Williams and N. G. Burnet (2012). "Advances in radiotherapy." BMJ **345**: e7765.

Al-Minawi, A. Z., N. Saleh-Gohari and T. Helleday (2008). "The ERCC1/XPF endonuclease is required for efficient single-strand annealing and gene conversion in mammalian cells." Nucleic acids research **36**(1): 1-9.

Alberts, B., J. H. Wilson and T. Hunt (2008). Molecular biology of the cell. New York, Garland Science.

Aly, A. and S. Ganesan (2011). "BRCA1, PARP, and 53BP1: conditional synthetic lethality and synthetic viability." Journal of molecular cell biology **3**(1): 66-74.

Arner, E. S. J. and S. Eriksson (1995). "Mammalian Deoxyribonucleoside Kinases." Pharmacology & Therapeutics **67**(2): 155-186.

Asaad, N. A., Z. C. Zeng, J. Guan, J. Thacker and G. Iliakis (2000). "Homologous recombination as a potential target for caffeine radiosensitization in mammalian cells: reduced caffeine radiosensitization in XRCC2 and XRCC3 mutants." Oncogene **19**(50): 5788-5800.

Asaithamby, A. and D. J. Chen (2009). "Cellular responses to DNA double-strand breaks after low-dose gamma-irradiation." Nucleic Acids Research **37**(12): 3912-3923.

Badie, C., G. Iliakis, N. Foray, G. Alsbeih, B. Cedervall, N. Chavaudra, G. Pantelias, C. Arlett and E. P. Malaise (1995). "Induction and rejoining of DNA double-strand breaks and interphase chromosome breaks after exposure to X rays in one normal and two hypersensitive human fibroblast cell lines." Radiation Research **144**: 26-35.

Bakkenist, C. J. and M. B. Kastan (2003). "DNA damage activates ATM through intermolecular autophosphorylation and dimer dissociation." Nature **421**(6922): 499-506.

Balcer-Kubiczek, E. K. (2012). "Apoptosis in radiation therapy: a double-edged sword." Exp Oncol **34**(3): 277-285.

Bartelink, H., F. Roelofsen, F. Eschwege, P. Rougier, J. F. Bosset, D. G. Gonzalez, D. Peiffert, M. vanGlabbeke and M. Pierart (1997). "Concomitant radiotherapy and chemotherapy is superior to radiotherapy alone in the treatment of locally advanced anal cancer: Results of a phase III randomized trial of the European organization for research and treatment of cancer radiotherapy and gastrointestinal cooperative groups." Journal of Clinical Oncology **15**(5): 2040-2049.

Baure, J., A. Izadi, V. Suarez, E. Giedzinski, J. E. Cleaver, J. R. Fike and C. L. Limoli (2009). "Histone H2AX phosphorylation in response to changes in chromatin structure induced by altered osmolarity." Mutagenesis **24**(2): 161-167.

Beetham, K. L. and L. J. Tolmach (1984). "The Action of Caffeine on X-Irradiated Hela-Cells .7. Evidence That Caffeine Enhances Expression of Potentially Lethal Radiation-Damage." Radiation Research **100**(3): 585-593.

Begonie, J. T., L. (1906). "L'interpretation de quelques resultats de la radiotherapie et essai de fixation d'une technique rationelle." C.R. Seances. Acad. Sci. **143**: 983-985.

Bekker-Jensen, S. and N. Mailand (2010). "Assembly and function of DNA double-strand break repair foci in mammalian cells." DNA Repair (Amst) **9**(12): 1219-1228.

Bender, M. A., H. G. Griggs and J. S. Bedford (1974). "Mechanisms of Chromosomal Aberration Production .3. Chemicals and Ionizing-Radiation." Mutation Research **23**(2): 197-212.

Bennardo, N., A. Cheng, N. Huang and J. M. Stark (2008). "Alternative-NHEJ is a mechanistically distinct pathway of mammalian chromosome break repair." PLoS genetics **4**(6): e1000110.

Bennardo, N., A. Gunn, A. Cheng, P. Hasty and J. M. Stark (2009). "Limiting the persistence of a chromosome break diminishes its mutagenic potential." PLoS genetics **5**(10): e1000683.

Bertout, J. A., S. A. Patel and M. C. Simon (2008). "The impact of O₂ availability on human cancer." Nature reviews. Cancer **8**(12): 967-975.

Bindra, R. S., A. G. Goglia, M. Jasin and S. N. Powell (2013). "Development of an assay to measure mutagenic non-homologous end-joining repair activity in mammalian cells." Nucleic acids research **41**(11): e115.

Boboila, C., M. Jankovic, C. T. Yan, J. H. Wang, D. R. Wesemann, T. Zhang, A. Fazeli, L. Feldman, A. Nussenzweig, M. Nussenzweig and F. W. Alt (2010). "Alternative end-joining catalyzes robust IgH locus deletions and translocations in the combined absence

of ligase 4 and Ku70." Proceedings of the National Academy of Sciences of the United States of America **107**(7): 3034-3039.

Boboila, C., V. Oksenysh, M. Gostissa, J. H. Wang, S. Zha, Y. Zhang, H. Chai, C. S. Lee, M. Jankovic, L. M. Saez, M. C. Nussenzweig, P. J. McKinnon, F. W. Alt and B. Schwer (2012). "Robust chromosomal DNA repair via alternative end-joining in the absence of X-ray repair cross-complementing protein 1 (XRCC1)." Proceedings of the National Academy of Sciences of the United States of America **109**(7): 2473-2478.

Bogue, M. A., C. Wang, C. Zhu and D. B. Roth (1997). "V(D)J recombination in Ku86-deficient mice: distinct effects on coding, signal, and hybrid joint formation." Immunity **7**(1): 37-47.

Bohgaki, T., M. Bohgaki and R. Hakem (2010). "DNA double-strand break signaling and human disorders." Genome Integr **1**(1): 15.

Bohm, L. (2006). "Inhibition of homologous recombination repair with Pentoxifylline targets G2 cells generated by radiotherapy and induces major enhancements of the toxicity of cisplatin and melphalan given after irradiation." Radiation oncology **1**(1): 12.

Bothmer, A., D. F. Robbiani, N. Feldhahn, A. Gazumyan, A. Nussenzweig and M. C. Nussenzweig (2010). "53BP1 regulates DNA resection and the choice between classical and alternative end joining during class switch recombination." The Journal of experimental medicine **207**(4): 855-865.

Bouwman, P., A. Aly, J. M. Escandell, M. Pieterse, J. Bartkova, H. van der Gulden, S. Hiddingh, M. Thanasoula, A. Kulkarni, Q. Yang, B. G. Haffty, J. Tommiska, C. Blomqvist, R. Drapkin, D. J. Adams, H. Nevanlinna, J. Bartek, M. Tarsounas, S. Ganesan and J. Jonkers (2010). "53BP1 loss rescues BRCA1 deficiency and is associated with triple-negative and BRCA-mutated breast cancers." Nature structural & molecular biology **17**(6): 688-695.

Brockman, R. W., F. M. Schabel and J. A. Montgomery (1977). "Biologic Activity of 9-Beta-D-Arabinofuranosyl-2-Fluoroadenine - Metabolically Stable Analog of 9-Beta-D-Arabinofuranosyladenine." Biochemical Pharmacology **26**(22): 2193-2196.

Bruso, C. E., D. S. Shewach and T. S. Lawrence (1990). "Fluorodeoxyuridine-induced radiosensitization and inhibition of DNA double strand break repair in human colon cancer cells." Int J Radiat Oncol Biol Phys **19**(6): 1411-1417.

Bryant, P. E. (1983). "9-beta-D-arabinofuranosyladenine increases the frequency of X-ray induced chromosome abnormalities in mammalian cells." Int J Radiat Biol Relat Stud Phys Chem Med **43**(4): 459-464.

Bryant, P. E. (1988). "Use of restriction endonucleases to study relationships between DNA double-strand breaks, chromosomal aberrations and other end-points in mammalian cells." International journal of radiation biology **54**(6): 869-890.

- Bryant, P. E., L. J. Gray and N. Peresse (2004). "Progress towards understanding the nature of chromatid breakage." Cytogenet Genome Res **104**(1-4): 65-71.
- Buchholz, D. J., K. J. Lepek, T. A. Rich and D. Murray (1995). "5-Fluorouracil-radiation interactions in human colon adenocarcinoma cells." Int J Radiat Oncol Biol Phys **32**(4): 1053-1058.
- Bunting, S. F., E. Callén, N. Wong, H.-T. Chen, F. Polato, A. Gunn, A. Bothmer, N. Feldhahn, O. Fernandez-Capetillo, L. Cao, X. Xu, C.-X. Deng, T. Finkel, M. Nussenzweig, J. M. Stark and A. Nussenzweig (2010). "53BP1 Inhibits Homologous Recombination in Brca1-Deficient Cells by Blocking Resection of DNA Breaks." Cell **141**: 243-254.
- Bunting, S. F. and A. Nussenzweig (2013). "End-joining, translocations and cancer." Nat Rev Cancer **13**(7): 443-454.
- Burma, S., B. P. Chen and D. J. Chen (2006). "Role of non-homologous end joining (NHEJ) in maintaining genomic integrity." DNA repair **5**(9-10): 1042-1048.
- Canitrot, Y., J. P. Capp, N. Puget, A. Bieth, B. Lopez, J. S. Hoffmann and C. Cazaux (2004). "DNA polymerase beta overexpression stimulates the Rad51-dependent homologous recombination in mammalian cells." Nucleic Acids Research **32**(17): 5104-5112.
- Cao, L., X. L. Xu, S. F. Bunting, J. Liu, R. H. Wang, L. Y. L. Cao, J. J. Wu, T. N. Peng, J. J. Chen, A. Nussenzweig, C. X. Deng and T. Finkel (2009). "A Selective Requirement for 53BP1 in the Biological Response to Genomic Instability Induced by Brca1 Deficiency." Molecular Cell **35**(4): 534-541.
- Cappella, P., F. Gasparri, M. Pulici and J. Moll (2008). "A novel method based on click chemistry, which overcomes limitations of cell cycle analysis by classical determination of BrdU incorporation, allowing multiplex antibody staining." Cytometry A **73**(7): 626-636.
- Carney, J. P., R. S. Maser, H. Olivares, E. M. Davis, M. Le Beau, I. Yates, J.R., L. Hays, W. F. Morgan and J. H. J. Petrini (1998). "The hMre 11/hRad50 protein complex and Nijmegen breakage syndrome: Linkage of double-strand break repair." Cell **93**: 477-486.
- Carr, A. M. and S. Lambert (2013). "Replication Stress-Induced Genome Instability: The Dark Side of Replication Maintenance by Homologous Recombination." J Mol Biol.
- Carrano, A. V. (1973). "Chromosome Aberrations and Radiation-Induced Cell Death .2. Predicted and Observed Cell Survival." Mutation Research **17**(3): 355-366.
- Carrico, C. K. and R. I. Glazer (1979). "Effect of 5-fluorouracil on the synthesis and translation of polyadenylic acid-containing RNA from regenerating rat liver." Cancer Res **39**(9): 3694-3701.

- Cass, C. E., M. Selner and J. R. Phillips (1983). "Resistance to 9-Beta-D-Arabinofuranosyladenine in Cultured Leukemia L 1210 Cells." Cancer Research **43**(10): 4791-4798.
- Catapano, C. V., F. W. Perrino and D. J. Fernandes (1993). "Primer RNA chain termination induced by 9-beta-D-arabinofuranosyl-2-fluoroadenine 5'-triphosphate. A mechanism of DNA synthesis inhibition." J Biol Chem **268**(10): 7179-7185.
- Catton, C., M. Milosevic, P. Warde, A. Bayley, J. Crook, R. Bristow and M. Gospodarowicz (2003). "Recurrent prostate cancer following external beam radiotherapy: follow-up strategies and management." Urol Clin North Am **30**(4): 751-763.
- Cavanagh, B. L., T. Walker, A. Norazit and A. C. Meedeniya (2011). "Thymidine analogues for tracking DNA synthesis." Molecules **16**(9): 7980-7993.
- Chan, V. L. and P. Juranka (1981). "Isolation and preliminary characterization of 9-beta-d-arabinofuranosyladenine-resistant mutants of baby hamster cells." Somatic Cell Genet **7**(2): 147-160.
- Chang, A. E., J. M. Collins, P. A. Speth, R. Smith, J. B. Rowland, L. Walton, M. G. Begley, E. Glatstein and T. J. Kinsella (1989). "A phase I study of intraarterial iododeoxyuridine in patients with colorectal liver metastases." J Clin Oncol **7**(5): 662-668.
- Chang, C. H. and Y. C. Cheng (1980). "Effects of deoxyadenosine triphosphate and 9-beta-D-arabinofuranosyl-adenine 5'-triphosphate on human ribonucleotide reductase from Molt-4F cells and the concept of "self-potential"." Cancer Res **40**(10): 3555-3558.
- Chapman, T. R. and T. J. Kinsella (2011). "Ribonucleotide reductase inhibitors: a new look at an old target for radiosensitization." Front Oncol **1**: 56.
- Chavaudra, N., M. Halimi, C. Parmentier, N. Gaillard, S. Grinfeld and E. P. Malaise (1989). "The initial slope of human tumor cell survival curves: its modification by the oxycell sensitizer beta-arabinofuranosyladenine." Int J Radiat Oncol Biol Phys **16**(5): 1267-1271.
- Chehab, N. H., A. Malikzay, M. Appel and T. D. Halazonetis (2000). "Chk2/hCds1 functions as a DNA damage checkpoint in G(1) by stabilizing p53." Genes Dev **14**(3): 278-288.
- Chen, L. C., C. J. Nievera, A. Y. L. Lee and X. H. Wu (2008). "Cell cycle-dependent complex formation of BRCA1.CtIP.MRN is important for DNA double-strand break repair." Journal of Biological Chemistry **283**(12): 7713-7720.

Cheong, N., X. M. Wang, Y. Wang and G. Iliakis (1994). "Loss of S-Phase-Dependent Radioresistance in Irs-1 Cells Exposed to X-Rays." Mutation Research **314**(1): 77-85.

Chinnaiyan, P., S. Huang, G. Vallabhaneni, E. Armstrong, S. Varambally, S. A. Tomlins, A. M. Chinnaiyan and P. M. Harari (2005). "Mechanisms of enhanced radiation response following epidermal growth factor receptor signaling inhibition by erlotinib (Tarceva)." Cancer research **65**(8): 3328-3335.

Choudhury, A., H. Zhao, F. Jalali, S. Al Rashid, J. Ran, S. Supiot, A. E. Kiltie and R. G. Bristow (2009). "Targeting homologous recombination using imatinib results in enhanced tumor cell chemosensitivity and radiosensitivity." Molecular Cancer Therapeutics **8**(1): 203-213.

Chuang, R. Y. and L. F. Chuang (1976). "Inhibition of RNA polymerase as a possible anti-leukaemic action of cytosine arabinoside." Nature **260**(5551): 549-550.

Chun, H. G., B. Leyland-Jones and B. D. Cheson (1991). "Fludarabine phosphate: a synthetic purine antimetabolite with significant activity against lymphoid malignancies." J Clin Oncol **9**(1): 175-188.

Connell, P. P. and S. Hellman (2009). "Advances in radiotherapy and implications for the next century: a historical perspective." Cancer research **69**(2): 383-392.

Consoli, U., I. El-Tounsi, A. Sandoval, V. Snell, H. D. Kleine, W. Brown, J. R. Robinson, F. DiRaimondo, W. Plunkett and M. Andreeff (1998). "Differential induction of apoptosis by fludarabine monophosphate in leukemic B and normal T cells in chronic lymphocytic leukemia." Blood **91**(5): 1742-1748.

Corneo, B., R. L. Wendland, L. Deriano, X. Cui, I. A. Klein, S. Y. Wong, S. Arnal, A. J. Holub, G. R. Weller, B. A. Pancake, S. Shah, V. L. Brandt, K. Meek and D. B. Roth (2007). "Rag mutations reveal robust alternative end joining." Nature **449**(7161): 483-486.

Cornforth, M. N. and J. S. Bedford (1987). "A Quantitative Comparison of Potentially Lethal Damage Repair and the Rejoining of Interphase Chromosome Breaks in Low Passage Normal Human-Fibroblasts." Radiation Research **111**(3): 385-405.

Cory, A. H. and J. G. Cory (1994). "Use of Nucleoside Kinase-Deficient Mouse Leukemia-L1210 Cell-Lines to Determine Metabolic Routes of Activation of Antitumor Nucleoside Analogs." Advances in Enzyme Regulation, Vol 34 **34**: 1-12.

Costantino, L., S. K. Sotiriou, J. K. Rantala, S. Magin, E. Mladenov, T. Helleday, J. E. Haber, G. Iliakis, O. Kallioniemi and T. D. Halazonetis (2013). "Break-Induced Replication Repair of Damaged Forks Induces Genomic Duplications in Human Cells." Science.

Costantino, L., S. K. Sotiriou, J. K. Rantala, S. Magin, E. Mladenov, T. Helleday, J. E. Haber, G. Iliakis, O. P. Kallioniemi and T. D. Halazonetis (2014). "Break-Induced Replication Repair of Damaged Forks Induces Genomic Duplications in Human Cells." Science **343**(6166): 88-91.

Cui, X., M. Brenneman, J. Meyne, M. Oshimura, E. H. Goodwin and D. J. Chen (1999). "The *XRCC2* and *XRCC3* repair genes are required for chromosome stability in mammalian cells." Mutation Research **434**: 75-88.

D'Angio, G. J. (2005). "Regarding the alleged radiosensitization of intrathecal cytarabine." Journal of Pediatric Hematology Oncology **27**(7): 349-350.

D'Silva, I., J. D. Pelletier, J. Lagueux, D. D'Amours, M. A. Chaudhry, M. Weinfeld, S. P. Lees-Miller and G. G. Poirier (1999). "Relative affinities of poly(ADP-ribose) polymerase and DNA-dependent protein kinase for DNA strand interruptions." Biochim Biophys Acta **1430**(1): 119-126.

Daboussi, F., S. Courbet, S. Benhamou, P. Kannouche, M. Z. Zdzienicka, M. Debatisse and B. S. Lopez (2008). "A homologous recombination defect affects replication-fork progression in mammalian cells." J Cell Sci **121**(Pt 2): 162-166.

Davis, A. P. and L. S. Symington (2004). "RAD51-dependent break-induced replication in yeast." Mol Cell Biol **24**(6): 2344-2351.

Davis, M. A., H. Y. Tang, J. Maybaum and T. S. Lawrence (1995). "Dependence of fluorodeoxyuridine-mediated radiosensitization on S phase progression." Int J Radiat Biol **67**(5): 509-517.

de Vries, J. F., J. H. Falkenburg, R. Willemze and R. M. Barge (2006). "The mechanisms of Ara-C-induced apoptosis of resting B-chronic lymphocytic leukemia cells." Haematologica **91**(7): 912-919.

Deacon, J., M. J. Peckham and G. G. Steel (1984). "The radioresponsiveness of human tumours and the initial slope of the cell survival curve." Radiotherapy and oncology : journal of the European Society for Therapeutic Radiology and Oncology **2**(4): 317-323.

Delaney, G., S. Jacob, C. Featherstone and M. Barton (2005). "The role of radiotherapy in cancer treatment: estimating optimal utilization from a review of evidence-based clinical guidelines." Cancer **104**(6): 1129-1137.

Dewey, W. C. and R. M. Humphrey (1965). "Increase in radiosensitivity to ionizing radiation related to replacement of thymidine in mammalian cells with 5-bromodeoxyuridine." Radiat Res **26**(4): 538-553.

Dewey, W. C., R. S. L. Wong and N. Albright (1997). "Pulsed-field gel electrophoretic migration of DNA broken by X irradiation during DNA synthesis: Experimental results compared with Monte Carlo calculations." Radiation Research **148**(5): 413-420.

Dibiase, S. J., Z. C. Zeng, R. Chen, T. Hyslop, W. J. Curran and G. Iliakis (2000). "DNA-dependent protein kinase stimulates an independently active, nonhomologous, end-joining apparatus." Cancer Research **60**(5): 1245-1253.

Dicioccio, R. A. and B. I. Srivastava (1977). "Kinetics of inhibition of deoxynucleotide-polymerizing enzyme activities from normal and leukemic human cells by 9-beta-D-arabinofuranosyladenine 5'-triphosphate and 1-beta-D-arabinofuranosylcytosine 5'-triphosphate." Eur J Biochem **79**(2): 411-418.

Djordjevic, B. and W. Szybalski (1960). "Genetics of human cell lines. III. Incorporation of 5-bromo- and 5-iododeoxyuridine into the deoxyribonucleic acid of human cells and its effect on radiation sensitivity." J Exp Med **112**: 509-531.

Donnianni, R. A. and L. S. Symington (2013). "Break-induced replication occurs by conservative DNA synthesis." Proc Natl Acad Sci U S A **110**(33): 13475-13480.

Dow, L. W., D. E. Bell, L. Poulakos and A. Fridland (1980). "Differences in Metabolism and Cyto-Toxicity between 9-Beta-D Arabinofuranosyladenine and 9-Beta-D-Arabinofuranosyl-2-Fluoroadenine in Human-Leukemic Lymphoblasts." Cancer Research **40**(5): 1405-1410.

Dueva, R. and G. Iliakis (2013). "Alternative pathways of non-homologous end joining (NHEJ) in genomic instability and cancer." 2013 **2**(3).

Early, A. P., H. D. Preisler, H. Slocum and Y. M. Rustum (1982). "A pilot study of high-dose 1-beta-D-arabinofuranosylcytosine for acute leukemia and refractory lymphoma: clinical response and pharmacology." Cancer Res **42**(4): 1587-1594.

Edwards, S. L., R. Brough, C. J. Lord, R. Natrajan, R. Vatcheva, D. A. Levine, J. Boyd, J. S. Reis-Filho and A. Ashworth (2008). "Resistance to therapy caused by intragenic deletion in BRCA2." Nature **451**(7182): 1111-1115.

Eggler, A. L., R. B. Inman and M. M. Cox (2002). "The Rad51-dependent pairing of long DNA substrates is stabilized by replication protein A." Journal of Biological Chemistry **277**(42): 39280-39288.

Eisbruch, A., D. S. Shewach, C. R. Bradford, J. F. Little, T. N. Teknos, D. B. Chepeha, L. J. Marentette, J. E. Terrell, N. D. Hogikyan, L. A. Dawson, S. Urba, G. T. Wolf and T. S. Lawrence (2001). "Radiation concurrent with gemcitabine for locally advanced head and neck cancer: a phase I trial and intracellular drug incorporation study." J Clin Oncol **19**(3): 792-799.

Elliott, B., C. Richardson and M. Jasin (2005). "Chromosomal translocation mechanisms at intronic alu elements in mammalian cells." Molecular cell **17**(6): 885-894.

Eriksson, D., P. O. Lofroth, L. Johansson, K. A. Riklund and T. Stigbrand (2007). "Cell cycle disturbances and mitotic catastrophes in HeLa Hep2 cells following 2.5 to 10 Gy of ionizing radiation." Clinical cancer research : an official journal of the American Association for Cancer Research **13**(18 Pt 2): 5501s-5508s.

Escribano-Diaz, C., A. Orthwein, A. Fradet-Turcotte, M. Xing, J. T. Young, J. Tkac, M. A. Cook, A. P. Rosebrock, M. Munro, M. D. Canny, D. Xu and D. Durocher (2013). "A Cell Cycle-Dependent Regulatory Circuit Composed of 53BP1-RIF1 and BRCA1-CtIP Controls DNA Repair Pathway Choice." Molecular cell.

Evans, D. B., G. R. Varadhachary, C. H. Crane, C. C. Sun, J. E. Lee, P. W. Pisters, J. N. Vauthey, H. Wang, K. R. Cleary, G. A. Staerke, C. Charnsangavej, E. A. Lano, L. Ho, R. Lenzi, J. L. Abbruzzese and R. A. Wolff (2008). "Preoperative gemcitabine-based chemoradiation for patients with resectable adenocarcinoma of the pancreatic head." J Clin Oncol **26**(21): 3496-3502.

Ewald, B., D. Sampath and W. Plunkett (2007). "H2AX phosphorylation marks gemcitabine-induced stalled replication forks and their collapse upon S-phase checkpoint abrogation." Molecular Cancer Therapeutics **6**(4): 1239-1248.

Ewald, B., D. Sampath and W. Plunkett (2008). "Nucleoside analogs: molecular mechanisms signaling cell death." Oncogene **27**(50): 6522-6537.

Ewing, D. (1998). "The oxygen fixation hypothesis: a reevaluation." American journal of clinical oncology **21**(4): 355-361.

Fattah, F., E. H. Lee, N. Weisensel, Y. Wang, N. Lichter and E. A. Hendrickson (2010). "Ku regulates the non-homologous end joining pathway choice of DNA double-strand break repair in human somatic cells." PLoS genetics **6**(2): e1000855.

Feng, Z., S. P. Scott, W. Bussen, G. G. Sharma, G. Guo, T. K. Pandita and S. N. Powell (2011). "Rad52 inactivation is synthetically lethal with BRCA2 deficiency." Proceedings of the National Academy of Sciences of the United States of America **108**(2): 686-691.

Ferguson, D. O. and F. W. Alt (2001). "DNA double strand break repair and chromosomal translocation: lessons from animal models." Oncogene **20**(40): 5572-5579.

Ferlay, J., P. Autier, M. Boniol, M. Heanue, M. Colombet and P. Boyle (2007). "Estimates of the cancer incidence and mortality in Europe in 2006." Ann Oncol **18**(3): 581-592.

Fertil, B. and E. P. Malaise (1981). "Inherent cellular radiosensitivity as a basic concept for human tumor radiotherapy." International journal of radiation oncology, biology, physics **7**(5): 621-629.

Fietkau, R. (2012). "[Concurrent radiochemotherapy for the treatment of solid tumors]." Strahlentherapie und Onkologie : Organ der Deutschen Rontgengesellschaft ... [et al] **188 Suppl 3**: 263-271.

Fishman-Lobell, J., N. Rudin and J. E. Haber (1992). "Two alternative pathways of double-strand break repair that are kinetically separable and independently modulated." Molecular and cellular biology **12**(3): 1292-1303.

Foray, N., C. F. Arlett and E. P. Malaise (1997a). "Radiation-induced DNA double-strand breaks and the radiosensitivity of human cells: a closer look." Biochimie **79**(9-10): 567-575.

Foray, N., C. Colin and M. Bourguignon (2012). "100 Years of Individual Radiosensitivity: How We Have Forgotten the Evidence." Radiology **264**(3): 627-631.

Foray, N., A. Priestley, G. Alsbeih, C. Badie, E. P. Capulas, C. F. Arlett and E. P. Malaise (1997b). "Hypersensitivity of ataxia telangiectasia fibroblasts to ionizing radiation is associated with a repair deficiency of DNA double-strand breaks." International Journal of Radiation Biology **72**(3): 271-283.

Foray, N., V. Randrianarison, D. Marot, M. Perricaudet, G. Lenoir and J. Feunteun (1999). "Gamma-rays-induced death of human cells carrying mutations of BRCA1 or BRCA2." Oncogene **18**(51): 7334-7342.

Frank, K. M., N. E. Sharpless, Y. Gao, J. M. Sekiguchi, D. O. Ferguson, C. Zhu, J. P. Manis, J. Horner, R. A. DePinho and F. W. Alt (2000). "DNA ligase IV deficiency in mice leads to defective neurogenesis and embryonic lethality via the p53 pathway." Mol Cell **5**(6): 993-1002.

Frankenberg-Schwager, M., A. Gebauer, C. Koppe, H. Wolf, E. Pralle and D. Frankenberg (2009). "Single-strand annealing, conservative homologous recombination, nonhomologous DNA end joining, and the cell cycle-dependent repair of DNA double-strand breaks induced by sparsely or densely ionizing radiation." Radiation research **171**(3): 265-273.

Frankenberg, D., M. Frankenberg-Schwager, D. Blocher and R. Harbich (1981). "Evidence for DNA double-strand breaks as the critical lesions in yeast cells irradiated with sparsely or densely ionizing radiation under oxic or anoxic conditions." Radiat Res **88**(3): 524-532.

Friedland, W., P. Kundrat and P. Jacob (2012). "Stochastic modelling of DSB repair after photon and ion irradiation." International journal of radiation biology **88**(1-2): 129-136.

Gagou, M. E., P. Zuazua-Villar and M. Meuth (2010). "Enhanced H2AX Phosphorylation, DNA Replication Fork Arrest, and Cell Death in the Absence of Chk1." Molecular Biology of the Cell **21**(5): 739-752.

Galluzzi, L., I. Vitale, J. M. Abrams, E. S. Alnemri, E. H. Baehrecke, M. V. Blagosklonny, T. M. Dawson, V. L. Dawson, W. S. El-Deiry, S. Fulda, E. Gottlieb, D. R. Green, M. O. Hengartner, O. Kepp, R. A. Knight, S. Kumar, S. A. Lipton, X. Lu, F. Madeo, W. Malorni, P. Mehlen, G. Nunez, M. E. Peter, M. Piacentini, D. C. Rubinsztein, Y. Shi, H. U. Simon, P. Vandenabeele, E. White, J. Yuan, B. Zhivotovsky, G. Melino and G. Kroemer (2012). "Molecular definitions of cell death subroutines: recommendations of the Nomenclature Committee on Cell Death 2012." Cell Death Differ **19**(1): 107-120.

Galmarini, C. M., J. R. Mackey and C. Dumontet (2002). "Nucleoside analogues and nucleobases in cancer treatment." Lancet Oncol **3**(7): 415-424.

Gardiner, K. (1991). "Pulsed field gel electrophoresis." Analytical chemistry **63**(7): 658-665.

Gerweck, L. E., S. Vijayappa, A. Kurimasa, K. Ogawa and D. J. Chen (2006). "Tumor cell radiosensitivity is a major determinant of tumor response to radiation." Cancer research **66**(17): 8352-8355.

Goffman, T., Z. Tochner and E. Glatstein (1991). "Primary treatment of large and massive adult sarcomas with iododeoxyuridine and aggressive hyperfractionated irradiation." Cancer **67**(3): 572-576.

Goodhead, D. T. (1994). "Initial events in the cellular effects of ionizing radiations: clustered damage in DNA." International journal of radiation biology **65**(1): 7-17.

Grabarz, A., A. Barascu, J. Guirouilh-Barbat and B. S. Lopez (2012). "Initiation of DNA double strand break repair: signaling and single-stranded resection dictate the choice between homologous recombination, non-homologous end-joining and alternative end-joining." American Journal of Cancer Research **2**(3): 249-268.

Grabarz, A., J. Guirouilh-Barbat, A. Barascu, G. Pennarun, D. Genet, E. Rass, S. M. Germann, P. Bertrand, I. D. Hickson and B. S. Lopez (2013). "A Role for BLM in Double-Strand Break Repair Pathway Choice: Prevention of CtIP/Mre11-Mediated Alternative Nonhomologous End-Joining." Cell Reports **5**(1): 21-28.

Graham, F. L. and G. F. Whitmore (1970). "Studies in mouse L-cells on the incorporation of 1-beta-D-arabinofuranosylcytosine into DNA and on inhibition of DNA polymerase by 1-beta-D-arabinofuranosylcytosine 5'-triphosphate." Cancer Res **30**(11): 2636-2644.

Greaves, M. F. and J. Wiemels (2003). "Origins of chromosome translocations in childhood leukaemia." Nature reviews. Cancer **3**(9): 639-649.

Gregoire, V., K. K. Ang, J. F. Rosier, M. Beauduin, A. S. Garden, M. Hamoir, W. N. Hittelman, Y. Humblet, F. R. Khuri, L. Milas, C. Mitine and P. Scalliet (2002). "A phase I study of fludarabine combined with radiotherapy in patients with intermediate to locally advanced head and neck squamous cell carcinoma." Radiother Oncol **63**(2): 187-193.

Gregoire, V., M. Beauduin, M. Bruniaux, B. De Coster, M. O. Prignot and P. Scalliet (1998). "Radiosensitization of mouse sarcoma cells by fludarabine (F-ara-A) or gemcitabine (dFdC), two nucleoside analogues, is not mediated by an increased induction or a repair inhibition of DNA double-strand breaks as measured by pulsed-field gel electrophoresis." International Journal of Radiation Biology **73**(5): 511-520.

Gregoire, V., N. Hunter, W. A. Brock, L. Milas, W. Plunkett and W. N. Hittelman (1994). "Fludarabine Improves the Therapeutic Ratio of Radiotherapy in Mouse-Tumors after Single-Dose Irradiation." International Journal of Radiation Oncology Biology Physics **30**(2): 363-371.

Group, G. T. S. (1985). "Radiation therapy combined with Adriamycin or 5-fluorouracil for the treatment of locally unresectable pancreatic carcinoma." Cancer **56**(11): 2563-2568.

Gunn, A., N. Bennardo, A. Cheng and J. M. Stark (2011). "Correct end use during end joining of multiple chromosomal double strand breaks is influenced by repair protein RAD50, DNA-dependent protein kinase DNA-PKcs, and transcription context." The Journal of biological chemistry **286**(49): 42470-42482.

Gunn, A. and J. M. Stark (2012). "I-SceI-based assays to examine distinct repair outcomes of mammalian chromosomal double strand breaks." Methods in molecular biology **920**: 379-391.

Gurka, M. K., S. P. Collins, R. Slack, G. Tse, A. Charabaty, L. Ley, L. Berzcel, S. Lei, S. Suy, N. Haddad, R. Jha, C. D. Johnson, P. Jackson, J. L. Marshall and M. J. Pishvaian (2013). "Stereotactic body radiation therapy with concurrent full-dose gemcitabine for locally advanced pancreatic cancer: a pilot trial demonstrating safety." Radiat Oncol **8**: 44.

Gurrieri, S., S. B. Smith and C. Bustamante (1999). "Trapping of megabase-sized DNA molecules during agarose gel electrophoresis." Proceedings of the National Academy of Sciences of the United States of America **96**(2): 453-458.

Haince, J. F., D. McDonald, A. Rodrigue, U. Dery, J. Y. Masson, M. J. Hendzel and G. G. Poirier (2008). "PARP1-dependent kinetics of recruitment of MRE11 and NBS1 proteins to multiple DNA damage sites." J Biol Chem **283**(2): 1197-1208.

Hajdo, L., A. B. Szulc, B. Klajnert and M. Bryszewska (2010). "Metabolic Limitations of the Use of Nucleoside Analogs in Cancer Therapy May Be Overcome by Application of Nanoparticles as Drug Carriers: A Review." Drug Development Research **71**(7): 383-394.

Hall, E. J. and A. J. Giaccia (2006). Radiobiology for the radiologist. Philadelphia, Lippincott Williams & Wilkins.

Harrigan, J. A., R. Belotserkovskaya, J. Coates, D. S. Dimitrova, S. E. Polo, C. R. Bradshaw, P. Fraser and S. P. Jackson (2011). "Replication stress induces 53BP1-containing OPT domains in G1 cells." J Cell Biol **193**(1): 97-108.

Heidelberger, C., L. Griesbach, B. J. Montag, D. Mooren, O. Cruz, R. J. Schnitzer and E. Grunberg (1958). "Studies on fluorinated pyrimidines. II. Effects on transplanted tumors." Cancer Res **18**(3): 305-317.

Heinemann, V., Y. Z. Xu, S. Chubb, A. Sen, L. W. Hertel, G. B. Grindey and W. Plunkett (1990). "Inhibition of ribonucleotide reduction in CCRF-CEM cells by 2',2'-difluorodeoxycytidine." Molecular pharmacology **38**(4): 567-572.

Heinemann, V., Y. Z. Xu, S. Chubb, A. Sen, L. W. Hertel, G. B. Grindey and W. Plunkett (1992). "Cellular Elimination of 2',2'-Difluorodeoxycytidine 5'-Triphosphate - a Mechanism of Self-Potentialion." Cancer Research **52**(3): 533-539.

Held, K. D. (1997). "Radiation-induced apoptosis and its relationship to loss of clonogenic survival." Apoptosis **2**(3): 265-282.

Hendrickson, E. A., X.-Q. Qin, E. A. Bump, D. G. Schatz, M. Oettinger and D. T. Weaver (1991). "A link between double-strand break-related repair and V(D)J recombination: The *scid* mutation." Proceedings of the National Academy of Sciences of the United States of America **88**: 4061-4065.

Hershfield, M. S., J. E. Fetter, W. C. Small, A. S. Bagnara, S. R. Williams, B. Ullman, D. W. Martin, D. B. Wasson and D. A. Carson (1982). "Effects of Mutational Loss of Adenosine Kinase and Deoxycytidine Kinase on Deoxy-Atp Accumulation and Deoxyadenosine Toxicity in Cultured CEM Human T-Lymphoblastoid Cells." Journal of Biological Chemistry **257**(11): 6380-6386.

Hertel, L. W., G. B. Boder, J. S. Kroin, S. M. Rinzel, G. A. Poore, G. C. Todd and G. B. Grindey (1990). "Evaluation of the Antitumor-Activity of Gemcitabine (2',2'-Difluoro-2'-Deoxycytidine)." Cancer Research **50**(14): 4417-4422.

Hertel, L. W., J. S. Kroin, J. W. Misner and J. M. Tustin (1988). "Synthesis of 2-Deoxy-2,2-Difluoro-D-Ribose and 2-Deoxy-2,2-Difluoro-D-Ribofuranosyl Nucleosides." Journal of Organic Chemistry **53**(11): 2406-2409.

Heyer, W. D., K. T. Ehmsen and J. Liu (2010). "Regulation of homologous recombination in eukaryotes." Annu Rev Genet **44**: 113-139.

Huang, P., S. Chubb, L. W. Hertel, G. B. Grindey and W. Plunkett (1991). "Action of 2',2'-Difluorodeoxycytidine on DNA-Synthesis." Cancer Research **51**(22): 6110-6117.

Huang, P., S. Chubb and W. Plunkett (1990). "Termination of DNA-Synthesis by 9-Beta-D-Arabinofuranosyl-2-Fluoroadenine - a Mechanism for Cytotoxicity." Journal of Biological Chemistry **265**(27): 16617-16625.

Huang, P. and W. Plunkett (1991). "Action of 9-beta-D-arabinofuranosyl-2-fluoroadenine on RNA metabolism." Mol Pharmacol **39**(4): 449-455.

Hubeek I, K. G., Ossenkuppele GJ, Peters GJ (2006). Cytosine arabinoside Deoxynucleoside Analogs in Cancer Therapy. . P. GJ. Totowa, NJ, Humana Press: pp 289-329

Huertas, P. (2010). "DNA resection in eukaryotes: deciding how to fix the break." Nature structural & molecular biology **17**(1): 11-16.

Huertas, P. and S. P. Jackson (2009). "Human CtIP Mediates Cell Cycle Control of DNA End Resection and Double Strand Break Repair." Journal of Biological Chemistry **284**(14): 9558-9565.

Ikegami, S., T. Taguchi and M. Ohashi (1978). "Aphidicolin Prevents Mitotic Cell-Division by Interfering with Activity of DNA Polymerase-Alpha." Nature **275**(5679): 458-460.

Iliakis, G. (1980). "Effects of beta-arabinofuranosyladenine on the growth and repair of potentially lethal damage in Ehrlich ascites tumor cells." Radiat Res **83**(3): 537-552.

Iliakis, G. (1988a). "Radiation-induced potentially lethal damage: DNA lesions susceptible to fixation." Int J Radiat Biol Relat Stud Phys Chem Med **53**(4): 541-584.

Iliakis, G. (1991). "The role of DNA double strand breaks in ionizing radiation-induced killing of eukaryotic cells." Bioessays **13**(12): 641-648.

Iliakis, G. (2009). "Backup pathways of NHEJ in cells of higher eukaryotes: cell cycle dependence." Radiother Oncol **92**(3): 310-315.

Iliakis, G. and P. E. Bryant (1983). "Effects of the nucleoside analogues alpha-ara A, beta-ara A and beta-ara C on cell growth and repair of both potentially lethal damage and DNA double strand breaks in mammalian cells in culture." Anticancer Res **3**(2): 143-149.

Iliakis, G., S. Kurtzman, G. Pantelias and R. Okayasu (1989a). "Mechanism of radiosensitization by halogenated pyrimidines: effect of BrdU on radiation induction of DNA and chromosome damage and its correlation with cell killing." Radiat Res **119**(2): 286-304.

Iliakis, G. and F. Q. Ngo (1985). "Effects of adenosine deaminase inhibitor 2'-deoxycoformycin on the repair and expression of potentially lethal damage sensitive to beta-araA." Radiat Environ Biophys **24**(2): 81-88.

Iliakis, G. and M. Nusse (1983a). "Effects of caffeine on X-irradiated synchronous, asynchronous and plateau phase mouse ascites cells: the importance of progression

through the cell cycle for caffeine enhancement of killing." Int J Radiat Biol Relat Stud Phys Chem Med **43**(6): 649-663.

Iliakis, G. and M. Nusse (1983b). "Evidence that repair and expression of potentially lethal damage cause the variations in cell survival after X irradiation observed through the cell cycle in Ehrlich ascites tumor cells." Radiat Res **95**(1): 87-107.

Iliakis, G., G. Pantelias, R. Okayasu and R. Seaner (1989b). "Comparative studies on repair inhibition by araA, araC and aphidicolin of radiation induced DNA and chromosome damage in rodent cells: comparison with fixation of PLD." Int J Radiat Oncol Biol Phys **16**(5): 1261-1265.

Iliakis, G., G. E. Pantelias and R. Seaner (1988b). "Effect of arabinofuranosyladenine on radiation-induced chromosome damage in plateau-phase CHO cells measured by premature chromosome condensation: implications for repair and fixation of alpha-PLD." Radiation research **114**(2): 361-378.

Iliakis, G., H. Wang, A. R. Perrault, W. Boecker, B. Rosidi, F. Windhofer, W. Wu, J. Guan, G. Terzoudi and G. Pantelias (2004). "Mechanisms of DNA double strand break repair and chromosome aberration formation." Cytogenetic and genome research **104**(1-4): 14-20.

Iliakis, G. E. and R. Okayasu (1990). "Radiosensitivity Throughout the Cell-Cycle and Repair of Potentially Lethal Damage and DNA Double-Strand Breaks in an X-Ray-Sensitive Cho Mutant." International Journal of Radiation Biology **57**(6): 1195-1211.

IMPACT (1995). "Efficacy of adjuvant fluorouracil and folinic acid in colon cancer. International Multicentre Pooled Analysis of Colon Cancer Trials (IMPACT) investigators." Lancet **345**(8955): 939-944.

Ingraham, H. A., L. Dickey and M. Goulian (1986). "DNA fragmentation and cytotoxicity from increased cellular deoxyuridylate." Biochemistry **25**(11): 3225-3230.

Invitrogen (2011). Click-iT® EdU Imaging Kits Application Manual. **MP 10338**.

Ira, G., A. Pelliccioli, A. Balijja, X. Wang, S. Fiorani, W. Carotenuto, G. Liberi, D. Bressan, L. H. Wan, N. M. Hollingsworth, J. E. Haber and M. Foiani (2004). "DNA end resection, homologous recombination and DNA damage checkpoint activation require CDK1." Nature **431**(7011): 1011-1017.

Ivanov, E. L., N. Sugawara, J. Fishman-Lobell and J. E. Haber (1996). "Genetic requirements for the single-strand annealing pathway of double-strand break repair in *Saccharomyces cerevisiae*." Genetics **142**(3): 693-704.

Jazayeri, A., J. Falck, C. Lukas, J. Bartek, G. C. M. Smith, J. Lukas and S. P. Jackson (2006). "ATM- and cell cycle-dependent regulation of ATR in response to DNA double-strand breaks." Nature Cell Biology **8**(1): 37-U13.

Jeggo, P. and M. F. Lavin (2009a). "Cellular radiosensitivity: How much better do we understand it?" International Journal of Radiation Biology **85**(12): 1061-1081.

Jeggo, P. and M. F. Lavin (2009b). "Cellular radiosensitivity: how much better do we understand it?" International journal of radiation biology **85**(12): 1061-1081.

Jeggo, P. A. and L. M. Kemp (1983). "X-Ray-Sensitive Mutants of Chinese-Hamster Ovary Cell-Line - Isolation and Cross-Sensitivity to Other DNA-Damaging Agents." Mutation Research **112**(6): 313-327.

Jemal, A., F. Bray, M. M. Center, J. Ferlay, E. Ward and D. Forman (2011). "Global cancer statistics." CA Cancer J Clin **61**(2): 69-90.

Jensen, R. B., A. Ozes, T. Kim, A. Estep and S. C. Kowalczykowski (2013). "BRCA2 is epistatic to the RAD51 paralogs in response to DNA damage." DNA Repair **12**(4): 306-311.

Jordheim, L. P., D. Durantel, F. Zoulim and C. Dumontet (2013). "Advances in the development of nucleoside and nucleotide analogues for cancer and viral diseases." Nat Rev Drug Discov **12**(6): 447-464.

Joubert, A., K. M. Zimmerman, Z. Bencokova, J. Gastaldo, N. Chavaudra, V. Favaudon, C. F. Arlett and N. Foray (2008). "DNA double-strand break repair defects in syndromes associated with acute radiation response: at least two different assays to predict intrinsic radiosensitivity?" International journal of radiation biology **84**(2): 107-125.

Juranka, P. and V. L. Chan (1980). "Relative cytotoxicity of 9-beta-D-arabinofuranosyladenine and 9-beta-D-arabinofuranosyladenine 5'-monophosphate." Cancer Res **40**(11): 4123-4126.

Kabotyanski, E. B., L. Gomelsky, J. O. Han, T. D. Stamato and D. B. Roth (1998). "Double-strand break repair in Ku86- and XRCC4-deficient cells." Nucleic acids research **26**(23): 5333-5342.

Kanamaru, R., H. Kakuta, T. Sato, C. Ishioka and A. Wakui (1986). "The inhibitory effects of 5-fluorouracil on the metabolism of preribosomal and ribosomal RNA in L-1210 cells in vitro." Cancer Chemother Pharmacol **17**(1): 43-46.

Kane, D. P., M. Shusterman, Y. Rong and M. McVey (2012). "Competition between replicative and translesion polymerases during homologous recombination repair in *Drosophila*." PLoS Genet **8**(4): e1002659.

Kinner, A., W. Wu, C. Staudt and G. Iliakis (2008). "Gamma-H2AX in recognition and signaling of DNA double-strand breaks in the context of chromatin." Nucleic Acids Res **36**(17): 5678-5694.

- Kuchta, R. D. and L. Willhelm (1991). "Inhibition of DNA primase by 9-beta-D-arabinofuranosyladenosine triphosphate." Biochemistry **30**(3): 797-803.
- Kufe, D. W., P. P. Major, E. M. Egan and G. P. Beardsley (1980). "Correlation of cytotoxicity with incorporation of ara-C into DNA." J Biol Chem **255**(19): 8997-8900.
- Kufe, D. W., P. P. Major, D. Munroe, M. Egan and D. Herrick (1983). "Relationship between Incorporation of 9-Beta-D-Arabinofuranosyladenine in L1210 DNA and Cytotoxicity." Cancer Research **43**(5): 2000-2004.
- Kun, E., E. Kirsten and C. P. Ordahl (2002). "Coenzymatic activity of randomly broken or intact double-stranded DNAs in auto and histone H1 trans-poly(ADP-ribosylation), catalyzed by poly(ADP-ribose) polymerase (PARP I)." J Biol Chem **277**(42): 39066-39069.
- Kuo, M. L. and T. J. Kinsella (1998). "Expression of ribonucleotide reductase after ionizing radiation in human cervical carcinoma cells." Cancer Res **58**(10): 2245-2252.
- Latz, D., W. C. Dewey, M. Flentje, F. Lohr, F. Wenz and K. J. Weber (1996). "Migration patterns in pulsed-field electrophoresis of DNA restriction fragments from log-phase mammalian cells after irradiation and incubation for repair." International Journal of Radiation Biology **70**(6): 637-646.
- Latz, D., K. Fleckenstein, M. Eble, J. Blatter, M. Wannemacher and K. J. Weber (1998). "Radiosensitizing potential of gemcitabine (2',2'-difluoro-2'-deoxycytidine) within the cell cycle in vitro." International Journal of Radiation Oncology Biology Physics **41**(4): 875-882.
- Laurent, D., O. Pradier, H. Schmidberger, M. Rave-Frank, D. Frankenberg and C. F. Hess (1998). "Radiation rendered more cytotoxic by fludarabine monophosphate in a human oropharynx carcinoma cell line than in fetal lung fibroblasts." Journal of Cancer Research and Clinical Oncology **124**(9): 485-492.
- Lavin, M. F. (2007). "ATM and the Mre11 complex combine to recognize and signal DNA double-strand breaks." Oncogene **26**(56): 7749-7758.
- Lawrence, T. S., E. Y. Chang, T. M. Hahn, L. W. Hertel and D. S. Shewach (1996). "Radiosensitization of pancreatic cancer cells by 2',2'-difluoro-2'-deoxycytidine." Int J Radiat Oncol Biol Phys **34**(4): 867-872.
- Lawrence, T. S., M. A. Davis, J. Maybaum, P. L. Stetson and W. D. Ensminger (1990). "The effect of single versus double-strand substitution on halogenated pyrimidine-induced radiosensitization and DNA strand breakage in human tumor cells." Radiat Res **123**(2): 192-198.

- Lawrence, T. S., M. A. Davis and D. P. Normolle (1995). "Effect of bromodeoxyuridine on radiation-induced DNA damage and repair based on DNA fragment size using pulsed-field gel electrophoresis." Radiat Res **144**(3): 282-287.
- Lee-Theilen, M., A. J. Matthews, D. Kelly, S. Zheng and J. Chaudhuri (2011). "CtIP promotes microhomology-mediated alternative end joining during class-switch recombination." Nature structural & molecular biology **18**(1): 75-79.
- Lee, M. W., W. B. Parker and B. Xu (2013). "New insights into the synergism of nucleoside analogs with radiotherapy." Radiation Oncology **8**.
- Lepage, G. A., S. R. Naik, S. B. Katakhar and A. Khaliq (1975). "9-Beta-D-Arabinofuranosyladenine 5'-Phosphate Metabolism and Excretion in Humans." Cancer Research **35**(11): 3036-3040.
- Levin, V. A., M. R. Prados, W. M. Wara, R. L. Davis, P. H. Gutin, T. L. Phillips, K. Lamborn and C. B. Wilson (1995). "Radiation therapy and bromodeoxyuridine chemotherapy followed by procarbazine, lomustine, and vincristine for the treatment of anaplastic gliomas." Int J Radiat Oncol Biol Phys **32**(1): 75-83.
- Li, L., H. Wang, E. S. Yang, C. L. Arteaga and F. Xia (2008). "Erlotinib attenuates homologous recombinational repair of chromosomal breaks in human breast cancer cells." Cancer research **68**(22): 9141-9146.
- Li, X. and W. D. Heyer (2008). "Homologous recombination in DNA repair and DNA damage tolerance." Cell Res **18**(1): 99-113.
- Liang, F., M. G. Han, P. J. Romanienko and M. Jasin (1998). "Homology-directed repair is a major double-strand break repair pathway in mammalian cells." Proceedings of the National Academy of Sciences of the United States of America **95**(9): 5172-5177.
- Lieber, M. R. (2010). "The mechanism of double-strand DNA break repair by the nonhomologous DNA end-joining pathway." Annual review of biochemistry **79**: 181-211.
- Liliemark, J. O., W. Plunkett and D. O. Dixon (1985). "Relationship of 1-beta-D-arabinofuranosylcytosine in plasma to 1-beta-D-arabinofuranosylcytosine 5'-triphosphate levels in leukemic cells during treatment with high-dose 1-beta-D-arabinofuranosylcytosine." Cancer Res **45**(11 Pt 2): 5952-5957.
- Little, J. B. (1969). "Repair of sub-lethal and potentially lethal radiation damage in plateau phase cultures of human cells." Nature **224**(5221): 804-806.
- Little, J. B., A. M. Ueno and W. K. Dahlberg (1989). "Differential response of human and rodent cell lines to chemical inhibition of the repair of potentially lethal damage." Radiat Environ Biophys **28**(3): 193-202.

Liu, P. F., C. M. B. Carvalho, P. J. Hastings and J. R. Lupski (2012a). "Mechanisms for recurrent and complex human genomic rearrangements." Current Opinion in Genetics & Development **22**(3): 211-220.

Liu, Q., H. Jiang, Z. Liu, Y. Wang, M. Zhao, C. Hao, S. Feng, H. Guo, B. Xu, Q. Yang, Y. Gong and C. Shao (2011). "Berberine radiosensitizes human esophageal cancer cells by downregulating homologous recombination repair protein RAD51." PLoS One **6**(8): e23427.

Liu, X. J., H. Kantarjian and W. Plunkett (2012b). "Sapacitabine for cancer." Expert Opinion on Investigational Drugs **21**(4): 541-555.

Longley, D. B., D. P. Harkin and P. G. Johnston (2003). "5-fluorouracil: mechanisms of action and clinical strategies." Nat Rev Cancer **3**(5): 330-338.

Lydeard, J. R., S. Jain, M. Yamaguchi and J. E. Haber (2007). "Break-induced replication and telomerase-independent telomere maintenance require Pol32." Nature **448**(7155): 820-823.

Lydeard, J. R., Z. Lipkin-Moore, Y. J. Sheu, B. Stillman, P. M. Burgers and J. E. Haber (2010). "Break-induced replication requires all essential DNA replication factors except those specific for pre-RC assembly." Genes Dev **24**(11): 1133-1144.

MacLeod, R. A. and P. E. Bryant (1992). "Effects of adenine arabinoside and cofomycin on the kinetics of G2 chromatid aberrations in X-irradiated human lymphocytes." Mutagenesis **7**(4): 285-290.

Magin, S., J. Saha, M. Wang, V. Mladenova, N. Coym and G. Iliakis (2013). "Lipofection and nucleofection of substrate plasmid can generate widely different readings of DNA end-joining efficiency in different cell lines." DNA repair **12**(2): 148-160.

Malkova, A., M. L. Naylor, M. Yamauchi, G. Ira and J. E. Haber (2005). "RAD51-dependent break-induced replication differs in kinetics and checkpoint responses from RAD51-mediated gene conversion." Molecular and Cellular Biology **25**(3): 933-944.

Malkova, A., L. Signon, C. B. Schaefer, M. L. Naylor, J. F. Theis, C. S. Newlon and J. E. Haber (2001). "RAD51-independent break-induced replication to repair a broken chromosome depends on a distant enhancer site." Genes Dev **15**(9): 1055-1060.

Maloisel, L., F. Fabre and S. Gangloff (2008). "DNA polymerase delta is preferentially recruited during homologous recombination to promote heteroduplex DNA extension." Molecular and Cellular Biology **28**(4): 1373-1382.

Mansour, W. Y., T. Rhein and J. Dahm-Daphi (2010). "The alternative end-joining pathway for repair of DNA double-strand breaks requires PARP1 but is not dependent upon microhomologies." Nucleic acids research **38**(18): 6065-6077.

Mansour, W. Y., S. Schumacher, R. Roskopf, T. Rhein, F. Schmidt-Petersen, F. Gatzemeier, F. Haag, K. Borgmann, H. Willers and J. Dahm-Daphi (2008). "Hierarchy of nonhomologous end-joining, single-strand annealing and gene conversion at site-directed DNA double-strand breaks." Nucleic Acids Research **36**(12): 4088-4098.

Manthey, G. M. and A. M. Bailis (2010). "Rad51 inhibits translocation formation by non-conservative homologous recombination in *Saccharomyces cerevisiae*." PloS one **5**(7): e11889.

Mao, Z., M. Bozzella, A. Seluanov and V. Gorbunova (2008). "Comparison of nonhomologous end joining and homologous recombination in human cells." DNA repair **7**(10): 1765-1771.

Markova, E., N. Schultz and I. Y. Belyaev (2007). "Kinetics and dose-response of residual 53BP1/gamma-H2AX foci: co-localization, relationship with DSB repair and clonogenic survival." Int J Radiat Biol **83**(5): 319-329.

Marti, T. M., E. Hefner, L. Feeney, V. Natale and J. E. Cleaver (2006). "H2AX phosphorylation within the G(1) phase after UV irradiation depends on nucleotide excision repair and not DNA double-strand breaks." Proceedings of the National Academy of Sciences of the United States of America **103**(26): 9891-9896.

Matsukage, A., T. Takahashi, C. Nakayama and M. Saneyoshi (1978). "Inhibition of Mouse Myeloma DNA Polymerase-Alpha by 5'-Triphosphates of 1-Beta-D-Arabinofuranosylthymine and 1-Beta-D-Arabinofuranosylcytosine." Journal of Biochemistry **83**(5): 1511-1515.

Matsumoto, Y., T. Miyamoto, H. Sakamoto, H. Izumi, Y. Nakazawa, T. Ogi, H. Tahara, S. Oku, A. Hiramoto, T. Shiiki, Y. Fujisawa, H. Ohashi, Y. Sakemi and S. Matsuura (2011). "Two unrelated patients with MRE11A mutations and Nijmegen breakage syndrome-like severe microcephaly." DNA repair **10**(3): 314-321.

McGinn, C. J. and T. S. Lawrence (2001). "Recent advances in the use of radiosensitizing nucleosides." Semin Radiat Oncol **11**(4): 270-280.

McGinn, C. J., D. S. Shewach and T. S. Lawrence (1996). "Radiosensitizing nucleosides." J Natl Cancer Inst **88**(17): 1193-1203.

McVey, M. and S. E. Lee (2008). "MMEJ repair of double-strand breaks (director's cut): deleted sequences and alternative endings." Trends in genetics : TIG **24**(11): 529-538.

Meike, S., T. Yamamori, H. Yasui, M. Eitaki, A. Matsuda, M. Morimatsu, M. Fukushima, Y. Yamasaki and O. Inanami (2011). "A nucleoside anticancer drug, 1-(3-C-ethynyl-beta-D-ribo-pentofuranosyl)cytosine (TAS106), sensitizes cells to radiation by suppressing BRCA2 expression." Molecular cancer **10**: 92.

Merlano, M., M. Benasso, R. Corvo, R. Rosso, V. Vitale, F. Blengio, G. Numico, G. Margarino, L. Bonelli and L. Santi (1996). "Five-year update of a randomized trial of alternating radiotherapy and chemotherapy compared with radiotherapy alone in treatment of unresectable squamous cell carcinoma of the head and neck." J Natl Cancer Inst **88**(9): 583-589.

Meyer, B., K. O. Voss, F. Tobias, B. Jakob, M. Durante and G. Taucher-Scholz (2013). "Clustered DNA damage induces pan-nuclear H2AX phosphorylation mediated by ATM and DNA-PK." Nucleic Acids Research **41**(12): 6109-6118.

Miller, M. R. and D. N. Chinault (1982). "Evidence that DNA polymerases alpha and beta participate differentially in DNA repair synthesis induced by different agents." J Biol Chem **257**(1): 46-49.

Miser, J. S., J. Roloff, J. Blatt, G. H. Reaman, M. D. Krailo and G. D. Hammond (1992). "Lack of significant activity of 2'-deoxycoformycin alone or in combination with adenine arabinoside in relapsed childhood acute lymphoblastic leukemia. A randomized phase II trial from the Childrens Cancer Study Group." Am J Clin Oncol **15**(6): 490-493.

Mizuno, K., I. Miyabe, S. A. Schalbetter, A. M. Carr and J. M. Murray (2013). "Recombination-restarted replication makes inverted chromosome fusions at inverted repeats." Nature **493**(7431): 246-249.

Mladenov, E. and G. Iliakis (2011). "Induction and repair of DNA double strand breaks: The increasing spectrum of non-homologous end joining pathways." Mutat Res.

Mladenov, E., S. Magin, A. Soni and G. Iliakis (2013). "DNA double-strand break repair as determinant of cellular radiosensitivity to killing and target in radiation therapy." Frontiers in oncology **3**: 113.

Montgomery, J. A. and K. Hewson (1969). "Nucleosides of 2-Fluoroadenine." Journal of Medicinal Chemistry **12**(3): 498-&.

Moore, E. C. and S. S. Cohen (1967). "Effects of arabinonucleotides on ribonucleotide reduction by an enzyme system from rat tumor." The Journal of biological chemistry **242**(9): 2116-2118.

Moore, N. and S. Lyle (2011). "Quiescent, slow-cycling stem cell populations in cancer: a review of the evidence and discussion of significance." J Oncol **2011**.

Morgan, M. A., L. A. Parsels, L. Zhao, J. D. Parsels, M. A. Davis, M. C. Hassan, S. Arumugarajah, L. Hylander-Gans, D. Morosini, D. M. Simeone, C. E. Canman, D. P. Normolle, S. D. Zabludoff, J. Maybaum and T. S. Lawrence (2010). "Mechanism of Radiosensitization by the Chk1/2 Inhibitor AZD7762 Involves Abrogation of the G2 Checkpoint and Inhibition of Homologous Recombinational DNA Repair." Cancer research **70**(12): 4972-4981.

Moshous, D., I. Callebaut, R. de Chasseval, B. Corneo, M. Cavazzana-Calvo, F. Le Deist, I. Tezcan, O. Sanal, Y. Bertrand, N. Philippe, A. Fischer and J. de Villartay (2001). "Artemis, a novel dna double-strand break repair/v(d)j recombination protein, is mutated in human severe combined immune deficiency." Cell **105**: 177-186.

Mozdarani, H. and P. E. Bryant (1987). "The effect of 9-beta-D-arabinofuranosyladenine on the formation of X-ray induced chromatid aberrations in X-irradiated G2 human cells." Mutagenesis **2**(5): 371-374.

Muller, W. E., H. J. Rohde, R. Beyer, A. Maidhof, M. Lachmann, H. Taschner and R. K. Kahn (1975). "Mode of action of 9-beta-D-arabinofuranosyladenine on the synthesis of DNA, RNA, and protein in vivo and in vitro." Cancer Res **35**(8): 2160-2168.

Murakawa, Y., E. Sonoda, L. J. Barber, W. Zeng, K. Yokomori, H. Kimura, A. Niimi, A. Lehmann, G. Y. Zhao, H. Hochegger, S. J. Boulton and S. Takeda (2007). "Inhibitors of the Proteasome Suppress Homologous DNA Recombination in Mammalian Cells." Cancer research **67**(18): 8536-8543.

Mustafi, R., D. Heaton, W. Brinkman and J. L. Schwartz (1994). "Enhancement of X-ray toxicity in squamous cell carcinoma cell lines by DNA polymerase inhibitors." Int J Radiat Biol **65**(6): 675-681.

Nakamura, A. J., V. A. Rao, Y. Pommier and W. M. Bonner (2010). "The complexity of phosphorylated H2AX foci formation and DNA repair assembly at DNA double-strand breaks." Cell Cycle **9**(2): 389-397.

Nakatsugawa, S., T. Kada, O. Nikaido, Y. Tanaka and T. Sugahara (1984). "PLDR inhibitors: their biological and clinical implications." Br J Cancer Suppl **6**: 43-47.

Nambiar, M. and S. C. Raghavan (2011). "How does DNA break during chromosomal translocations?" Nucleic acids research **39**(14): 5813-5825.

Natarajan, A. T., G. Obe, A. A. Vanzeeland, F. Palitti, M. Meijers and E. A. M. Verdegaalimmerzeel (1980). "Molecular Mechanisms Involved in the Production of Chromosomal-Aberrations .2. Utilization of Neurospora Endonuclease for the Study of Aberration Production by X-Rays in G1 and G2 Stages of the Cell-Cycle." Mutation Research **69**(2): 293-305.

Nevaldine, B., J. A. Longo and P. J. Hahn (1997). "The scid defect results in much slower repair of DNA double-strand breaks but not high levels of residual breaks." Radiation research **147**(5): 535-540.

Nikjoo, H., P. O'Neill, M. Terrissol and D. T. Goodhead (1999). "Quantitative modelling of DNA damage using Monte Carlo track structure method." Radiation and environmental biophysics **38**(1): 31-38.

Nitsche, M., H. Christiansen, R. M. Hermann, E. M. Lucke, K. Peters, M. Rave-Frank, H. Schmidberger and O. Pradier (2008). "The combined effect of fludarabine monophosphate and radiation as well as gemcitabine and radiation on squamous carcinoma tumor cell lines in vitro." International Journal of Radiation Biology **84**(8): 643-657.

Nitsche, M., H. Christiansen, K. Lederer, F. Griesinger, H. Schmidberger and O. Pradier (2012). "Fludarabine combined with radiotherapy in patients with locally advanced NSCLC lung carcinoma: a phase I study." Journal of Cancer Research and Clinical Oncology **138**(7): 1113-1120.

Noguchi, M., D. Yu, R. Hirayama, Y. Ninomiya, E. Sekine, N. Kubota, K. Ando and R. Okayasu (2006). "Inhibition of homologous recombination repair in irradiated tumor cells pretreated with Hsp90 inhibitor 17-allylamino-17-demethoxygeldanamycin." Biochemical and Biophysical Research Communications **351**(3): 658-663.

Obe, G., C. Johannes and D. Schulte-Frohlinde (1992). "DNA double-strand breaks induced by sparsely ionizing radiation and endonucleases as critical lesions for cell death, chromosomal aberrations, mutations and oncogenic transformation." Mutagenesis **7**(1): 3-12.

Ohashi, M., T. Taguchi and S. Ikegami (1978). "Aphidicolin - Specific Inhibitor of DNA-Polymerases in Cytosol of Rat-Liver." Biochemical and Biophysical Research Communications **82**(4): 1084-1090.

Ohno, Y., D. Spriggs, A. Matsukage, T. Ohno and D. Kufe (1988). "Effects of 1-beta-D-arabinofuranosylcytosine incorporation on elongation of specific DNA sequences by DNA polymerase beta." Cancer Res **48**(6): 1494-1498.

Ohno, Y., D. Spriggs, A. Matsukage, T. Ohno and D. Kufe (1989). "Sequence-specific inhibition of DNA strand elongation by incorporation of 9-beta-D-arabinofuranosyladenine." Cancer Res **49**(8): 2077-2081.

Okayasu, R. and G. Iliakis (1993). "Ionizing radiation induces two forms of interphase chromosome breaks in Chinese hamster ovary cells that rejoin with different kinetics and show different sensitivity to treatment in hypertonic medium or beta-araA." Radiat Res **136**(2): 262-270.

Pardee, T. S., E. Gomes, J. Jennings-Gee, D. Caudell and W. H. Gmeiner (2012). "Unique dual targeting of thymidylate synthase and topoisomerase1 by FdUMP[10] results in high efficacy against AML and low toxicity." Blood **119**(15): 3561-3570.

Parker, W. B. (2009). "Enzymology of purine and pyrimidine antimetabolites used in the treatment of cancer." Chemical reviews **109**(7): 2880-2893.

Pauwels, B., A. E. Korst, G. G. Pattyn, H. A. Lambrechts, D. R. Van Bockstaele, K. Vermeulen, M. Lenjou, C. M. de Pooter, J. B. Vermorken and F. Lardon (2003). "Cell

cycle effect of gemcitabine and its role in the radiosensitizing mechanism in vitro." Int J Radiat Oncol Biol Phys **57**(4): 1075-1083.

Pauwels, B., A. E. C. Korst, G. G. O. Pattyn, H. A. J. Lambrechts, J. A. E. Kamphuis, C. M. J. De Pooter, G. J. Peters, F. Lardon and J. B. Vermorcken (2006). "The relation between deoxycytidine kinase activity and the radiosensitising effect of gemcitabine in eight different human tumour cell lines." Bmc Cancer **6**.

Payen, C., R. Koszul, B. Dujon and G. Fischer (2008). "Segmental Duplications Arise from Pol32-Dependent Repair of Broken Forks through Two Alternative Replication-Based Mechanisms." Plos Genetics **4**(9).

Perrault, R., H. Wang, M. Wang, B. Rosidi and G. Iliakis (2004). "Backup pathways of NHEJ are suppressed by DNA-PK." J Cell Biochem **92**(4): 781-794.

Petermann, E., M. L. Orta, N. Issaeva, N. Schultz and T. Helleday (2010). "Hydroxyurea-Stalled Replication Forks Become Progressively Inactivated and Require Two Different RAD51-Mediated Pathways for Restart and Repair." Molecular Cell **37**(4): 492-502.

Phillips, R. A. and L. J. Tolmach (1966). "Repair of potentially lethal damage in x-irradiated HeLa cells." Radiat Res **29**(3): 413-432.

Pierce, A. J., R. D. Johnson, L. H. Thompson and M. Jasin (1999). "XRCC3 promotes homology-directed repair of DNA damage in mammalian cells." Genes Dev **13**(20): 2633-2638.

Plowman, P. N., B. A. Bridges, C. F. Arlett, A. Hinney and J. E. Kingston (1990). "An instance of clinical radiation morbidity and cellular radiosensitivity, not associated with ataxia-telangiectasia." British Journal of Radiology **63**: 624-628.

Plunkett, W., P. Huang and V. Gandhi (1995). "Preclinical characteristics of gemcitabine." Anti-Cancer Drugs **6**: 7-13.

Plunkett, W., L. Lapi, P. J. Ortiz and S. S. Cohen (1974). "Penetration of mouse fibroblasts by the 5'-phosphate of 9-beta-D-arabinofuranosyladenine and incorporation of the nucleotide into DNA." Proc Natl Acad Sci U S A **71**(1): 73-77.

Polo, S. E. and S. P. Jackson (2011). "Dynamics of DNA damage response proteins at DNA breaks: a focus on protein modifications." Genes Dev **25**(5): 409-433.

Prados, M. D., C. Scott, H. Sandler, J. C. Buckner, T. Phillips, C. Schultz, R. Urtasun, R. Davis, P. Gutin, T. L. Cascino, H. S. Greenberg and W. J. Curran (1999). "A phase 3 randomized study of radiotherapy plus procarbazine, CCNU, and vincristine (PCV) with or without BUdR for the treatment of anaplastic astrocytoma: A preliminary report of RTOG 9404." International Journal of Radiation Oncology Biology Physics **45**(5): 1109-1115.

Prevo, R., E. Fokas, P. M. Reaper, P. A. Charlton, J. R. Pollard, W. G. McKenna, R. J. Muschel and T. B. Brunner (2012). "The novel ATR inhibitor VE-821 increases sensitivity of pancreatic cancer cells to radiation and chemotherapy." Cancer Biology & Therapy **13**(11): 1072-1081.

Puck, T. T. and P. I. Marcus (1956). "Action of x-rays on mammalian cells." The Journal of experimental medicine **103**(5): 653-666.

Quanz, M., D. Chassoux, N. Berthault, C. Agrario, J. S. Sun and M. Dutreix (2009). "Hyperactivation of DNA-PK by Double-Strand Break Mimicking Molecules Disorganizes DNA Damage Response." Plos One **4**(7).

Raderschall, E., E. I. Golub and T. Haaf (1999). "Nuclear foci of mammalian recombination proteins are located at single-stranded DNA regions formed after DNA damage." Proceedings of the National Academy of Sciences of the United States of America **96**(5): 1921-1926.

Radford, I. R. (1985). "The Level of Induced DNA Double-Strand Breakage Correlates with Cell Killing after X-Irradiation." International Journal of Radiation Biology **48**(1): 45-54.

Rass, E., A. Grabarz, I. Plo, J. Gautier, P. Bertrand and B. S. Lopez (2009). "Role of Mre11 in chromosomal nonhomologous end joining in mammalian cells." Nature Structural & Molecular Biology **16**(8): 819-U838.

Reinhardt, H. C. and M. B. Yaffe (2009). "Kinases that control the cell cycle in response to DNA damage: Chk1, Chk2, and MK2." Curr Opin Cell Biol **21**(2): 245-255.

Robert, I., F. Dantzer and B. Reina-San-Martin (2009). "Parp1 facilitates alternative NHEJ, whereas Parp2 suppresses IgH/c-myc translocations during immunoglobulin class switch recombination." The Journal of experimental medicine **206**(5): 1047-1056.

Roberts, S. A., A. R. Spreadborough, B. Bulman, J. B. Barber, D. G. Evans and D. Scott (1999). "Heritability of cellular radiosensitivity: a marker of low-penetrance predisposition genes in breast cancer?" American journal of human genetics **65**(3): 784-794.

Rogakou, E. P., D. R. Pilch, A. H. Orr, V. S. Ivanova and W. M. Bonner (1998). "DNA double-stranded breaks induce histone H2AX phosphorylation on serine 139." J Biol Chem **273**(10): 5858-5868.

Rosidi, B., M. Wang, W. Wu, A. Sharma, H. Wang and G. Iliakis (2008). "Histone H1 functions as a stimulatory factor in backup pathways of NHEJ." Nucleic acids research **36**(5): 1610-1623.

Rosier, J. F., M. Beauduin, M. Bruniaux, M. De Bast, B. De Coster, M. Octave-Prignot, P. Scalliet and V. Gregoire (1999). "The effect of 2'-2'-difluorodeoxycytidine (dFdC, gemcitabine) on radiation-induced cell lethality in two human head and neck squamous

carcinoma cell lines differing in intrinsic radiosensitivity." International Journal of Radiation Biology **75**(2): 245-251.

Ross, G. M. (1999). "Induction of cell death by radiotherapy." Endocr Relat Cancer **6**(1): 41-44.

Roth, D. B. and J. H. Wilson (1986). "Nonhomologous recombination in mammalian cells: role for short sequence homologies in the joining reaction." Molecular and cellular biology **6**(12): 4295-4304.

Rothkamm, K., I. Kruger, L. H. Thompson and M. Lobrich (2003). "Pathways of DNA double-strand break repair during the mammalian cell cycle." Molecular and cellular biology **23**(16): 5706-5715.

Ruis, B. L., K. R. Fattah and E. A. Hendrickson (2008). "The catalytic subunit of DNA-dependent protein kinase regulates proliferation, telomere length, and genomic stability in human somatic cells." Molecular and cellular biology **28**(20): 6182-6195.

Ruiz, J. F., B. Gomez-Gonzalez and A. Aguilera (2009). "Chromosomal Translocations Caused by Either Pol32-Dependent or Pol32-Independent Triparental Break-Induced Replication." Molecular and Cellular Biology **29**(20): 5441-5454.

Saini, N., S. Ramakrishnan, R. Elango, S. Ayyar, Y. Zhang, A. Deem, G. Ira, J. E. Haber, K. S. Lobachev and A. Malkova (2013). "Migrating bubble during break-induced replication drives conservative DNA synthesis." Nature **502**(7471): 389-+.

Salic, A. and T. J. Mitchison (2008). "A chemical method for fast and sensitive detection of DNA synthesis in vivo." Proceedings of the National Academy of Sciences of the United States of America **105**(7): 2415-2420.

San Filippo, J., P. Sung and H. Klein (2008). "Mechanism of eukaryotic homologous recombination." Annu Rev Biochem **77**: 229-257.

Santi, D. V. and L. W. Hardy (1987). "Catalytic mechanism and inhibition of tRNA (uracil-5-)methyltransferase: evidence for covalent catalysis." Biochemistry **26**(26): 8599-8606.

Sasaki, M. S., A. Tachibana and S. Takeda (2013). "Cancer risk at low doses of ionizing radiation: artificial neural networks inference from atomic bomb survivors." J Radiat Res.

Schipler, A. (2013). "Homing endonuclease-based model systems for the study of DNA double strand break induced cell signaling and repair." Inaugural-Dissertation zur Erlangung des Doktorgrades Dr. rer. nat.: Fakultät für Biologie an der Universität Duisburg-Essen.

Schipler, A. and G. Iliakis (2013). "DNA double-strand-break complexity levels and their possible contributions to the probability for error-prone processing and repair pathway choice." Nucleic acids research.

Schultz, L. B., N. H. Chehab, A. Malikzay and T. D. Halazonetis (2000). "p53 Binding protein 1 (53BP1) is an early participant in the cellular response to DNA double-strand breaks." Journal of Cell Biology **151**(7): 1381-1390.

Schwartz, R. A., C. T. Carson, C. Schuberth and M. D. Weitzman (2009). "Adeno-Associated Virus Replication Induces a DNA Damage Response Coordinated by DNA-Dependent Protein Kinase." Journal of Virology **83**(12): 6269-6278.

Seiwert, T. Y., J. K. Salama and E. E. Vokes (2007). "The concurrent chemoradiation paradigm--general principles." Nature clinical practice. Oncology **4**(2): 86-100.

Shaheen, F. S., P. Znojek, A. Fisher, M. Webster, R. Plummer, L. Gaughan, G. C. Smith, H. Y. Leung, N. J. Curtin and C. N. Robson (2011). "Targeting the DNA double strand break repair machinery in prostate cancer." PLoS One **6**(5): e20311.

Sharma, S., J. K. Hicks, C. L. Chute, J. R. Brennan, J. Y. Ahn, T. W. Glover and C. E. Canman (2012). "REV1 and polymerase zeta facilitate homologous recombination repair." Nucleic Acids Res **40**(2): 682-691.

Shewach, D. S., T. M. Hahn, E. Chang, L. W. Hertel and T. S. Lawrence (1994). "Metabolism of 2',2'-difluoro-2'-deoxycytidine and radiation sensitization of human colon carcinoma cells." Cancer Res **54**(12): 3218-3223.

Shewach DS, L. T. (2006). Nucleoside radiosensitizers
Deoxynucleoside Analogs in Cancer Therapy. . P. GJ. Totowa, NJ, Humana Press: pp 289-329

Shewach, D. S. and W. Plunkett (1979). "Effect of 2'-Deoxycoformycin on the Biologic Half-Life of 9-Beta-D-Arabinofuranosyladenine 5'-Triphosphate in Cho Cells." Biochemical Pharmacology **28**(15): 2401-2404.

Short, S. C., S. Giampieri, M. Worku, M. Alcaide-German, G. Sioftanos, S. Bourne, K. I. Lio, M. Shaked-Rabi and C. Martindale (2011). "Rad51 inhibition is an effective means of targeting DNA repair in glioma models and CD133+tumor-derived cells." Neuro-Oncology **13**(5): 487-499.

Shrivastav, M., L. P. De Haro and J. A. Nickoloff (2008). "Regulation of DNA double-strand break repair pathway choice." Cell Research **18**(1): 134-147.

Siegel, R., C. DeSantis, K. Virgo, K. Stein, A. Mariotto, T. Smith, D. Cooper, T. Gansler, C. Lerro, S. Fedewa, C. Lin, C. Leach, R. S. Cannady, H. Cho, S. Scoppa, M. Hachey, R. Kirch, A. Jemal and E. Ward (2012). "Cancer treatment and survivorship statistics, 2012." CA: a cancer journal for clinicians **62**(4): 220-241.

Siglin, J., C. E. Champ, Y. Vakhnenko, P. R. Anne and N. L. Simone (2012). "Radiation therapy for locally recurrent breast cancer." Int J Breast Cancer **2012**: 571946.

Simsek, D., E. Brunet, S. Y. Wong, S. Katyal, Y. Gao, P. J. McKinnon, J. Lou, L. Zhang, J. Li, E. J. Rebar, P. D. Gregory, M. C. Holmes and M. Jasin (2011). "DNA ligase III promotes alternative nonhomologous end-joining during chromosomal translocation formation." PLoS genetics **7**(6): e1002080.

Simsek, D. and M. Jasin (2010). "Alternative end-joining is suppressed by the canonical NHEJ component Xrcc4-ligase IV during chromosomal translocation formation." Nature structural & molecular biology **17**(4): 410-416.

Singh, S. K., T. Bednar, L. H. Zhang, W. Q. Wu, E. Mladenov and G. Iliakis (2012). "Inhibition of B-NHEJ in Plateau-Phase Cells Is Not a Direct Consequence of Suppressed Growth Factor Signaling." International Journal of Radiation Oncology Biology Physics **84**(2): E237-E243.

Singh, S. K., A. Bencsik-Theilen, E. Mladenov, B. Jakob, G. Taucher-Scholz and G. Iliakis (2013). "Reduced contribution of thermally labile sugar lesions to DNA double strand break formation after exposure to heavy ions." Radiat Oncol **8**: 77.

Singh, S. K., W. Wu, L. Zhang, H. Klammer, M. Wang and G. Iliakis (2011). "Widespread dependence of backup NHEJ on growth state: ramifications for the use of DNA-PK inhibitors." International journal of radiation oncology, biology, physics **79**(2): 540-548.

Singh, S. K., W. Z. Wu, W. Q. Wu, M. L. Wang and G. Iliakis (2009). "Extensive Repair of DNA Double-Strand Breaks in Cells Deficient in the DNA-PK-Dependent Pathway of NHEJ after Exclusion of Heat-Labile Sites." Radiation Research **172**(2): 152-164.

Smith, C. E., B. Llorente and L. S. Symington (2007). "Template switching during break-induced replication." Nature **447**(7140): 102-105.

Solier, S. and Y. Pommier (2009). "The apoptotic ring A novel entity with phosphorylated histones H2AX and H2B and activated DNA damage response kinases." Cell Cycle **8**(12): 1853-1859.

Sonoda, E., H. Hochegger, A. Saberi, Y. Taniguchi and S. Takeda (2006). "Differential usage of non-homologous end-joining and homologous recombination in double strand break repair." DNA Repair **5**(9-10): 1021-1029.

Sonoda, E., M. S. Sasaki, J. M. Buerstedde, O. Bezzubova, A. Shinohara, H. Ogawa, M. Takata, Y. Yamaguchi-Iwai and S. Takeda (1998). "Rad51-deficient vertebrate cells accumulate chromosomal breaks prior to cell death." Embo Journal **17**(2): 598-608.

Soulas-Sprauel, P., G. Le Guyader, P. Rivera-Munoz, V. Abramowski, C. Olivier-Martin, C. Goujet-Zalc, P. Charneau and J. P. de Villartay (2007). "Role for DNA repair factor XRCC4 in immunoglobulin class switch recombination." The Journal of experimental medicine **204**(7): 1717-1727.

Spycher, C., E. S. Miller, K. Townsend, L. Pavic, N. A. Morrice, P. Janscak, G. S. Stewart and M. Stucki (2008). "Constitutive phosphorylation of MDC1 physically links the MRE11-RAD50-NBS1 complex to damaged chromatin." J Cell Biol **181**(2): 227-240.

Stamato, T. D., A. Dipatri and A. Giaccia (1988). "Cell-cycle-dependent repair of potentially lethal damage in the XR-1 gamma-ray-sensitive Chinese hamster ovary cell." Radiat Res **115**(2): 325-333.

Stark, J. M., P. Hu, A. J. Pierce, M. E. Moynahan, N. Ellis and M. Jasin (2002). "ATP hydrolysis by mammalian RAD51 has a key role during homology-directed DNA repair." Journal of Biological Chemistry **277**(23): 20185-20194.

Stark, J. M., A. J. Pierce, J. Oh, A. Pastink and M. Jasin (2004). "Genetic steps of mammalian homologous repair with distinct mutagenic consequences." Molecular and cellular biology **24**(21): 9305-9316.

Steel, G. G., T. J. McMillan and J. H. Peacock (1989). "The 5Rs of radiobiology." International journal of radiation biology **56**(6): 1045-1048.

Stewart, G. S., S. Panier, K. Townsend, A. K. Al-Hakim, N. K. Kolas, E. S. Miller, S. Nakada, J. Ylanko, S. Olivarius, M. Mendez, C. Oldreive, J. Wildenhain, A. Tagliaferro, L. Pelletier, N. Taubenheim, A. Durandy, P. J. Byrd, T. Stankovic, A. M. Taylor and D. Durocher (2009). "The RIDDLE syndrome protein mediates a ubiquitin-dependent signaling cascade at sites of DNA damage." Cell **136**(3): 420-434.

Stewart, G. S., T. Stankovic, P. J. Byrd, T. Wechsler, E. S. Miller, A. Huissoon, M. T. Drayson, S. C. West, S. J. Elledge and A. M. Taylor (2007). "RIDDLE immunodeficiency syndrome is linked to defects in 53BP1-mediated DNA damage signaling." Proc Natl Acad Sci U S A **104**(43): 16910-16915.

Stiff, T., M. O'Driscoll, N. Rief, K. Iwabuchi, M. Lobrich and P. A. Jeggo (2004). "ATM and DNA-PK function redundantly to phosphorylate H2AX after exposure to ionizing radiation." Cancer Res **64**(7): 2390-2396.

Stucki, M., J. A. Clapperton, D. Mohammad, M. B. Yaffe, S. J. Smerdon and S. P. Jackson (2005). "MDC1 directly binds phosphorylated histone H2AX to regulate cellular responses to DNA double-strand breaks." Cell **123**(7): 1213-1226.

Sugawara, N. and J. E. Haber (1992). "Characterization of double-strand break-induced recombination: homology requirements and single-stranded DNA formation." Molecular and cellular biology **12**(2): 563-575.

Symington, L. S. (2002). "Role of RAD52 epistasis group genes in homologous recombination and double-strand break repair." Microbiology and molecular biology reviews : MMBR **66**(4): 630-670, table of contents.

Symington, L. S. and J. Gautier (2011). "Double-strand break end resection and repair pathway choice." Annual review of genetics **45**: 247-271.

Szafraniec, S. I., K. J. Stachnik and J. S. Skierski (2004). "New nucleoside analogs in the treatment of solid tumors." Acta Pol Pharm **61**(4): 297-305.

Takagi, M., K.-i. Sakata, M. Someya, H. Tauchi, K. Iijima, Y. Matsumoto, T. Torigoe, A. Takahashi, M. Hareyama and M. Fukushima (2010). "Gimeracil sensitizes cells to radiation via inhibition of homologous recombination." Radiotherapy and Oncology **96**(2): 259-266.

Talasz, H., W. Helliger, B. Sarg, P. L. Debbage, B. Puschendorf and H. Lindner (2002). "Hyperphosphorylation of histone H2A.X and dephosphorylation of histone H1 subtypes in the course of apoptosis." Cell Death and Differentiation **9**(1): 27-39.

Tamulevicius, P., M. Wang and G. Iliakis (2007). "Homology-directed repair is required for the development of radioresistance during S phase: interplay between double-strand break repair and checkpoint response." Radiat Res **167**(1): 1-11.

Tanaka, H., H. Arakawa, T. Yamaguchi, K. Shiraishi, S. Fukuda, K. Matsui, Y. Takei and Y. Nakamura (2000). "A ribonucleotide reductase gene involved in a p53-dependent cell-cycle checkpoint for DNA damage." Nature **404**(6773): 42-49.

Tanaka, Y., K. Akagi, K. Sokawa and T. Sugahara (1984). "Pld Repair Inhibitors as Radiosensitizer and Clinical-Trials." International Journal of Radiation Oncology Biology Physics **10**(9): 1803-1803.

Thariat, J., J. M. Hannoun-Levi, A. Sun Myint, T. Vuong and J. P. Gerard (2013). "Past, present, and future of radiotherapy for the benefit of patients." Nat Rev Clin Oncol **10**(1): 52-60.

Tomimatsu, N., B. Mukherjee and S. Burma (2009). "Distinct roles of ATR and DNA-PKcs in triggering DNA damage responses in ATM-deficient cells." EMBO Rep **10**(6): 629-635.

Trovesi, C., M. Falcettoni, G. Lucchini, M. Clerici and M. P. Longhese (2011). "Distinct Cdk1 requirements during single-strand annealing, noncrossover, and crossover recombination." PLoS genetics **7**(8): e1002263.

Tu, W. Z., B. Li, B. Huang, Y. Wang, X. D. Liu, H. Guan, S. M. Zhang, Y. Tang, W. Q. Rang and P. K. Zhou (2013). "gammaH2AX foci formation in the absence of DNA damage: mitotic H2AX phosphorylation is mediated by the DNA-PKcs/CHK2 pathway." FEBS Lett **587**(21): 3437-3443.

Tucker, S. L. and H. D. Thames, Jr. (1989). "The effect of patient-to-patient variability on the accuracy of predictive assays of tumor response to radiotherapy: a theoretical evaluation." International journal of radiation oncology, biology, physics **17**(1): 145-157.

Tutt, A., D. Bertwistle, J. Valentine, A. Gabriel, S. Swift, G. Ross, C. Griffin, J. Thacker and A. Ashworth (2001). "Mutation in Brca2 stimulates error-prone homology-directed repair of DNA double-strand breaks occurring between repeated sequences." The EMBO journal **20**(17): 4704-4716.

Tzung, T.-Y. and T. M. Runger (1998). "Reduced joining of DNA double strand breaks with an abnormal mutation spectrum in rodent mutants of DNA-PKcs and Ku80." International Journal of Radiation Biology **73**: 469-474.

Uziel, T., Y. Lerenthal, L. Moyal, Y. Andegeko, L. Mittelman and Y. Shiloh (2003). "Requirement of the MRN complex for ATM activation by DNA damage." EMBO J **22**(20): 5612-5621.

Vallerga, A. K., D. A. Zarling and T. J. Kinsella (2004). "New radiosensitizing regimens, drugs, prodrugs, and candidates." Clin Adv Hematol Oncol **2**(12): 793-805.

Vanhaperen, V. W. T. R., G. Veerman, J. B. Vermorcken and G. J. Peters (1993). "2',2'-Difluoro-Deoxycytidine (Gemcitabine) Incorporation into Rna and DNA of Tumor-Cell Lines." Biochemical Pharmacology **46**(4): 762-766.

Verkaik, N. S., R. E. Esveldt-van Lange, D. van Heemst, H. T. Bruggenwirth, J. H. Hoeijmakers, M. Z. Zdzienicka and D. C. van Gent (2002). "Different types of V(D)J recombination and end-joining defects in DNA double-strand break repair mutant mammalian cells." European journal of immunology **32**(3): 701-709.

Virsik, R. P. and D. Harder (1980). "Numerical Relationship between Cells with Radiation-Induced Chromosome-Aberrations and Cells Lethally Injured by Radiation." Radiation and Environmental Biophysics **18**(1): 73-77.

Waltes, R., R. Kalb, M. Gatei, A. W. Kijas, M. Stumm, A. Soback, B. Wieland, R. Varon, Y. Lerenthal, M. F. Lavin, D. Schindler and T. Dork (2009). "Human RAD50 deficiency in a Nijmegen breakage syndrome-like disorder." American journal of human genetics **84**(5): 605-616.

Wang, C. R., A. Hu and Q. B. Lu (2006a). "Direct observation of the transition state of ultrafast electron transfer reaction of a radiosensitizing drug bromodeoxyuridine." J Chem Phys **124**(24): 241102.

Wang, H., W. Boecker, H. Wang, X. Wang, J. Guan, L. H. Thompson, J. A. Nickoloff and G. Iliakis (2004a). "Caffeine inhibits homology-directed repair of I-SceI-induced DNA double-strand breaks." Oncogene **23**(3): 824-834.

Wang, H., B. Hu, R. Liu and Y. Wang (2005a). "CHK1 affecting cell radiosensitivity is independent of non-homologous end joining." Cell cycle **4**(2): 300-303.

- Wang, H., A. R. Perrault, Y. Takeda, W. Qin and G. Iliakis (2003a). "Biochemical evidence for Ku-independent backup pathways of NHEJ." Nucleic acids research **31**(18): 5377-5388.
- Wang, H., S. N. Powell, G. Iliakis and Y. Wang (2004b). "ATR affecting cell radiosensitivity is dependent on homologous recombination repair but independent of nonhomologous end joining." Cancer research **64**(19): 7139-7143.
- Wang, H., B. Rosidi, R. Perrault, M. Wang, L. Zhang, F. Windhofer and G. Iliakis (2005b). "DNA ligase III as a candidate component of backup pathways of nonhomologous end joining." Cancer research **65**(10): 4020-4030.
- Wang, H., X. Wang, G. Iliakis and Y. Wang (2003b). "Caffeine could not efficiently sensitize homologous recombination repair-deficient cells to ionizing radiation-induced killing." Radiat Res **159**(3): 420-425.
- Wang, H., Z. C. Zeng, T. A. Bui, E. Sonoda, M. Takata, S. Takeda and G. Iliakis (2001a). "Efficient rejoining of radiation-induced DNA double-strand breaks in vertebrate cells deficient in genes of the RAD52 epistasis group." Oncogene **20**(18): 2212-2224.
- Wang, H., Z. C. Zeng, A. R. Perrault, X. Cheng, W. Qin and G. Iliakis (2001b). "Genetic evidence for the involvement of DNA ligase IV in the DNA-PK-dependent pathway of non-homologous end joining in mammalian cells." Nucleic acids research **29**(8): 1653-1660.
- Wang, H. Y., M. L. Wang, H. C. Wang, W. Bocker and G. Iliakis (2005c). "Complex H2AX phosphorylation patterns by multiple kinases including ATM and DNA-PK in human cells exposed to ionizing radiation and treated with kinase inhibitors." Journal of Cellular Physiology **202**(2): 492-502.
- Wang, M., W. Wu, B. Rosidi, L. Zhang, H. Wang and G. Iliakis (2006b). "PARP-1 and Ku compete for repair of DNA double strand breaks by distinct NHEJ pathways." Nucleic acids research **34**(21): 6170-6182.
- Wang, X., G. Ira, J. A. Tercero, A. M. Holmes, J. F. X. Diffley and J. E. Haber (2004c). "Role of DNA replication proteins in double-strand break-induced recombination in *Saccharomyces cerevisiae*." Molecular and Cellular Biology **24**(16): 6891-6899.
- Ward, I. M., K. Minn and J. J. Chen (2004). "UV-induced ataxia-telangiectasia-mutated and Rad3-related (ATR) activation requires replication stress." Journal of Biological Chemistry **279**(11): 9677-9680.
- Weinstock, D. M., B. Elliott and M. Jasin (2006). "A model of oncogenic rearrangements: differences between chromosomal translocation mechanisms and simple double-strand break repair." Blood **107**(2): 777-780.

- West, C. M. and G. C. Barnett (2011). "Genetics and genomics of radiotherapy toxicity: towards prediction." Genome medicine **3**(8): 52.
- Weterings, E. and D. J. Chen (2008). "The endless tale of non-homologous end-joining." Cell Research **18**(1): 114-124.
- White, E. L., S. C. Shaddix, R. W. Brockman and L. L. Bennett, Jr. (1982). "Comparison of the actions of 9-beta-D-arabinofuranosyl-2-fluoroadenine and 9-beta-D-arabinofuranosyladenine on target enzymes from mouse tumor cells." Cancer research **42**(6): 2260-2264.
- Williams, R. S., G. Moncalian, J. S. Williams, Y. Yamada, O. Limbo, D. S. Shin, L. M. Grocock, D. Cahill, C. Hitomi, G. Guenther, D. Moiani, J. P. Carney, P. Russell and J. A. Tainer (2008). "Mre11 dimers coordinate DNA end bridging and nuclease processing in double-strand-break repair." Cell **135**(1): 97-109.
- Windhofer, F., W. Wu, M. Wang, S. K. Singh, J. Saha, B. Rosidi and G. Iliakis (2007). "Marked dependence on growth state of backup pathways of NHEJ." International journal of radiation oncology, biology, physics **68**(5): 1462-1470.
- Withers, H., editor (1975). Advances in radiation biology. The four R's of radiotherapy. New York, Academic Press.
- Wray, J., E. A. Williamson, S. B. Singh, Y. Wu, C. R. Cogle, D. M. Weinstock, Y. Zhang, S. H. Lee, D. Zhou, L. Shao, M. Hauer-Jensen, R. Pathak, V. Klimek, J. A. Nickoloff and R. Hromas (2013). "PARP1 is required for chromosomal translocations." Blood **121**(21): 4359-4365.
- Wu, W., M. Wang, T. Mussfeldt and G. Iliakis (2008a). "Enhanced use of backup pathways of NHEJ in G2 in Chinese hamster mutant cells with defects in the classical pathway of NHEJ." Radiation research **170**(4): 512-520.
- Wu, W., M. Wang, S. K. Singh, T. Mussfeldt and G. Iliakis (2008b). "Repair of radiation induced DNA double strand breaks by backup NHEJ is enhanced in G2." DNA repair **7**(2): 329-338.
- Xie, A., A. Kwok and R. Scully (2009). "Role of mammalian Mre11 in classical and alternative nonhomologous end joining." Nature structural & molecular biology **16**(8): 814-818.
- Yan, C. T., C. Boboila, E. K. Souza, S. Franco, T. R. Hickernell, M. Murphy, S. Gumaste, M. Geyer, A. A. Zarrin, J. P. Manis, K. Rajewsky and F. W. Alt (2007). "IgH class switching and translocations use a robust non-classical end-joining pathway." Nature **449**(7161): 478-482.

Yang, H. J., Q. B. Li, J. Fan, W. K. Holloman and N. P. Pavletich (2005). "The BRCA2 homologue Brh2 nucleates RAD51 filament formation at a dsDNA-ssDNA junction." Nature **433**(7026): 653-657.

Yang, S. W., P. Huang, W. Plunkett, F. F. Becker and J. Y. Chan (1992). "Dual mode of inhibition of purified DNA ligase I from human cells by 9-beta-D-arabinofuranosyl-2-fluoroadenine triphosphate." J Biol Chem **267**(4): 2345-2349.

Yoshihisa Matsumoto, S. I., Mikoto Fukuchi, Sicheng Liu,, S. K. Wanotayan Rujira, Kazuki Yoshida, Yasuhiro Mae and a. M. K. Sharma (2013). Radiosensitization Strategies Through Modification of DNA Double-Strand Break Repair.

Yu, X. and J. Chen (2004). "DNA Damage-Induced Cell Cycle Checkpoint Control Requires CtIP, a Phosphorylation-Dependent Binding Partner of BRCA1 C-Terminal Domains." Molecular and cellular biology **24**(21): 9478-9486.

Yun, M. H. and K. Hiom (2009). "CtIP-BRCA1 modulates the choice of DNA double-strand-break repair pathway throughout the cell cycle." Nature **459**(7245): 460-U184.

Zhang, Y. and M. Jasin (2011). "An essential role for CtIP in chromosomal translocation formation through an alternative end-joining pathway." Nature structural & molecular biology **18**(1): 80-84.

Zimbrick, J. D., J. F. Ward and L. S. Myers, Jr. (1969). "Studies on the chemical basis of cellular radiosensitization by 5-bromouracil substitution in DNA. II. Pulse- and steady-state radiolysis of bromouracil-substituted and unsubstituted DNA." Int J Radiat Biol Relat Stud Phys Chem Med **16**(6): 525-534.

8 Appendix

8.1 Part A: Supplementary data

8.1.1 Effect of earlier start of ara-A treatment in DRaa40 cells

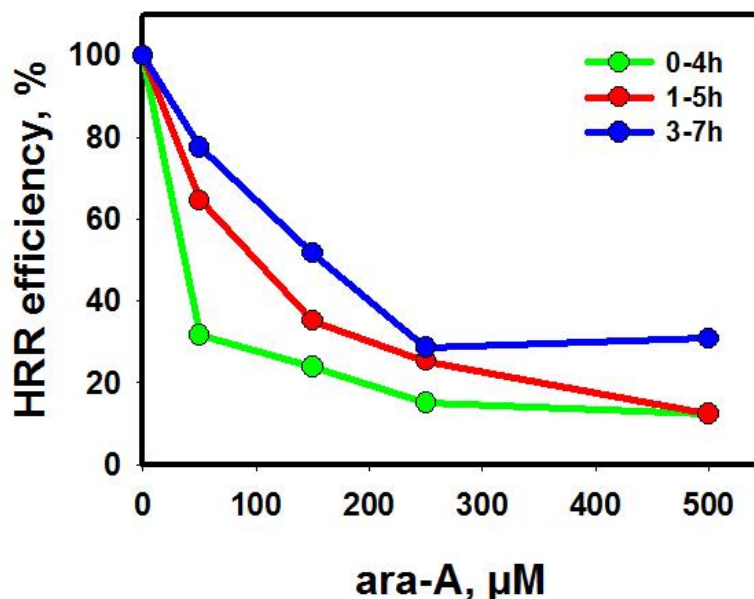


Figure 35 Effect of earlier start of ara-A treatment in DRaa40 cells Effect of a shift of the 4h treatment window to earlier times. Cells were treated with different concentrations of ara-A for 4h. Green circles and line represent treatment for 4h beginning immediately after transfection. Red circles and line represent treatment starting 1h after transfection and blue circles and line represent treatment starting 3h after transfection. Graph shows data from one experiment. The strong correlation between HRR suppression and the onset of ara-A treatment shown in Figure 18 prompted us to inquire whether an earlier ara-A treatment start would influence the outcome of the experiments. We found that treatment of cells with ara-A immediately after transfection, including a medium change after 4h, resulted in 70% inhibition already at 50 μM (Figure 35). This effect was equivalent to the maximum effect that was obtained at 500 μM when ara-A was given 3-7h after transfection (Figure 18 and Figure 35). Using the immediate treatment protocol, 88% inhibition was observed at 500 μM ara-A (Figure 35). When ara-A treatment was initiated 1h after transfection, inhibition was also stronger than in 3-7h hour treatments, but allowed for a larger effect-range of approximately 53% (Figure 35). The results obtained with delayed treatment start as opposed to the immediate

treatment start, clearly indicated a strong concentration dependence of the effect, which we wanted to follow-up. Furthermore, results from another line of investigation showed that ara-A reduced the transfection efficiency when added immediately after transfection. Also we could not rule out direct toxicity of immediate drug treatment after electroporation stress. These complications and the interpretation difficulties they generated made us decide to use the delayed treatment schedules in further experiments, but initiate treatment 1.5h after transfection.

8.1.2 Inherent problems with the interpretation of data obtained at later times in I-SceI inducible reporter systems

8.1.2.1 Analysis of GFP signal after 24h or 48h in U2OS 282C cells (DR-GFP) treated with ara-A

As laid out in the discussion (5.3.3) it is a characteristic of I-SceI reporter assays, that DSB are induced over a long time span that may last several days (Schipler, 2013). With regard to short term drug treatment this can create complications when it is attempted to collect data at later times, e.g. 48h or 72h after transfection of the I-SceI plasmid. At this time most drugs will have been fully metabolized. Ara-A which is rapidly inactivated by deamination through ADA has an intracellular half-life of 1.5h-2h (Shewach and Plunkett, 1979; Cass, 1983), meaning that 18h after the end of treatment the cell has been qualitatively cleared of ara-A. Repair of DSB that are induced by cutting at this time will not any longer underlie any potential inhibitory or beneficial effects of the drug, which will likely have waned already earlier due to declining concentrations. The situation is further complicated by the fact that 18h after the end of ara-A treatment, a dramatic redistribution in the cell cycle can be observed with about 70-80% of cells accumulating in the S-phase (Figure 36). That means a massive concentration of cells in a phase of the cell cycle where HRR may occur as opposed to the normal situation in an exponentially growing culture, where 40% of cells or more are in the G1 phase and cannot perform HRR. This creates conditions in which the likelihood for HRR is

increased, but inhibition by the drug is no longer present. At the same time, DSB continue to be induced by I-SceI (Schipler, 2013). As the appearance of fluorescence after a signal generating event requires several hours to develop, this leads to an increase of the portion of GFP positive cells in ara-A treated cells that can be detected when cells are measured 48h or later after transfection of the I-SceI plasmid (i.e. ~42h after the end of ara-A treatment). This translates into an ostensible recovery of HRR efficiency that can be calculated at 48h. However, this increase does not represent a characteristic of the interaction of ara-A with HRR, but is a consequence of the continuous induction of DSB by I-SceI, rapid deactivation of ara-A and reassortment of cells in the cycle.

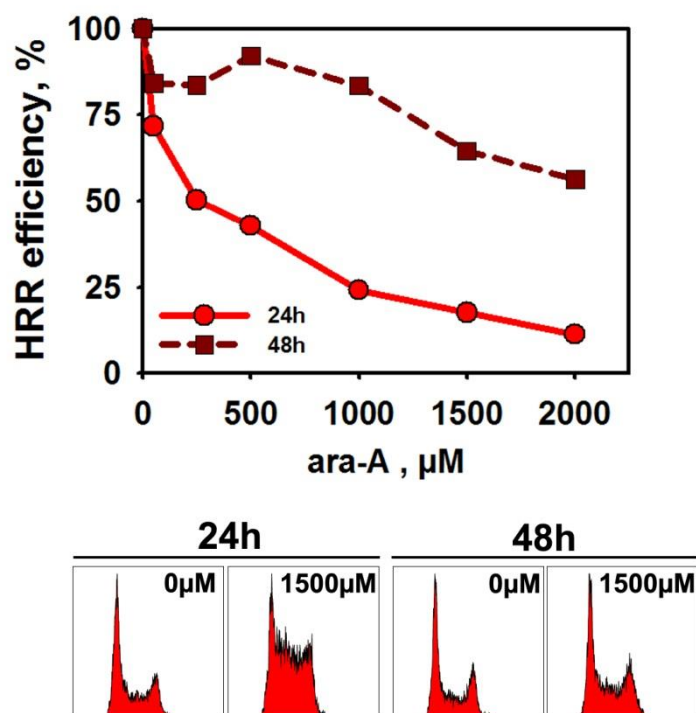


Figure 36 Continuous damage induction and shifts in cell cycle distribution lead to deceptive signal generation in late measurements in I-SceI reporter assays. Upper panel: Calculated HRR efficiency. A pool of cells was transfected and distributed in several dishes that were treated accordingly. One dish from each concentration was analyzed at the indicated time point. Light red circles and solid line, 24h after transfection. Dark red squares and dashed line, 48h after transfection. Data from one experiment is shown. Lower panel: PI Histograms for U2OS 282C cells 24h and 48h after transfection of the I-SceI plasmid. Ara-A treated cells are highly enriched in S-phase cells at 24h. At 48h Cell cycle distribution of treated cells is almost back to normal.

8.1.2.2 Development of fluorescence signals over time in EJ-DR cells (EJ-RFP & DR-GFP)

The EJ-DR cell line was generated by introduction of the EJ-RFP into a U2OS cell line that also already harbored a DR-GFP insertion. The DsRed signal originating from the EJ-RFP system started to appear only 3 days after transfection and still showed strong increase up to 96h (Figure 37 A&B). Due to the kinetics of signal development of the EJ-RFP system, the information provided by which was our primary interest in this series of experiments, measurements had to be taken 4 days after transfection. For the signal originating from the DR-GFP construct this meant that it was subjected to the same problematic described for U2OS 282C cells above (8.1.2.1). Consequently, measurements taken 96h after I-SceI transfection (i.e. ~90h after the end of ara-A treatment) showed only little effect of ara-A on the proportion of GFP positive cells in the EJ-DR system. To confirm that inhibition of HRR takes place in EJ-DR cells, we performed a time course experiment. We transfected EJ-DR cells with I-SceI and treated them for 4h with 1000 μ M ara-A. Cells were split on 4 different dishes and analyzed at 24h, 48h, 72h and 96h after transfection to measure the proportion of cells positive for GFP. We observed strong suppression in the development of a GFP signal up to 48h after transfection (Figure 37 C). This confirmed that ara-A had an inhibitory effect on the HRR mediated repair in the DR-GFP construct in the EJ-DR cells as well. As expected and in agreement with the findings for U2OS 282C cells, at later times GFP positive cells started to appear in the population, as a consequence of continuous induction of DSB by I-SceI and metabolic inactivation of ara-A.

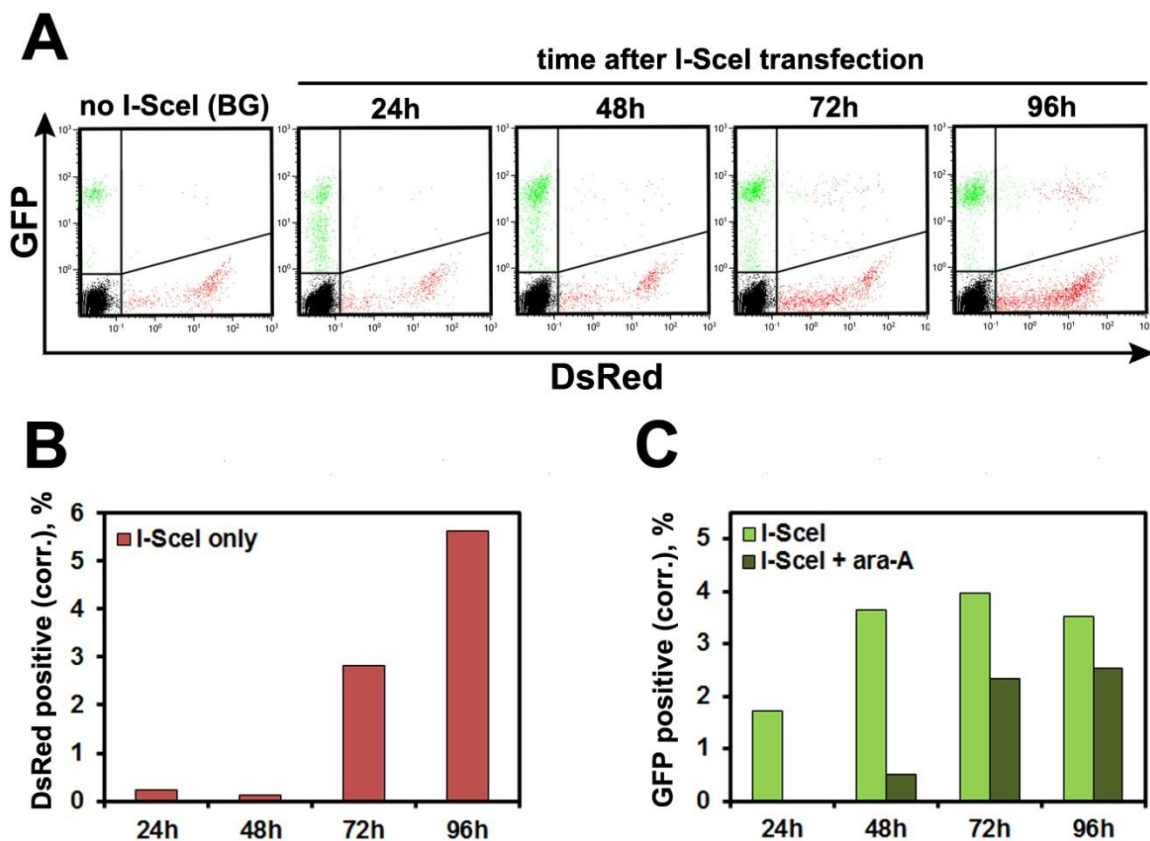


Figure 37 Kinetics of reporter gene expression in EJ-DR cells. A) Development of the signals from the DR-GFP construct (GFP) and the EJ-RFP system (DsRed) over time within a population of EJ-DR cells transfected with I-SceI (no ara-A treatment). Significant increase of DsRed positive cells above the background occurs only 72h after transfection. The GFP signal begins to develop already 24h after transfection and has almost reached maximum after 48h already. **B)** Graphical depiction of the DsRed Data shown in (A). Measured values were corrected by the background (BG) of untransfected cells. **C)** Graphical depiction of the GFP Data shown in (A) (light green bars) together with data for the development of GFP expression in cells treated with 1000 μ M ara-A (dark green bars) collected in the same experiment. Measured values were corrected by the background (BG) of untransfected cells. Cells that were treated with 1000 μ M ara-A for 4h show almost complete inhibition of HRR at 24h and 48h, but a robust signal starts to appear after 72h.

8.1.3 Effects of Nu7441 on DSB repair

8.1.3.1 Effect of Nu7441 on kinetics of DSB repair in A549 cells measured by PFGE

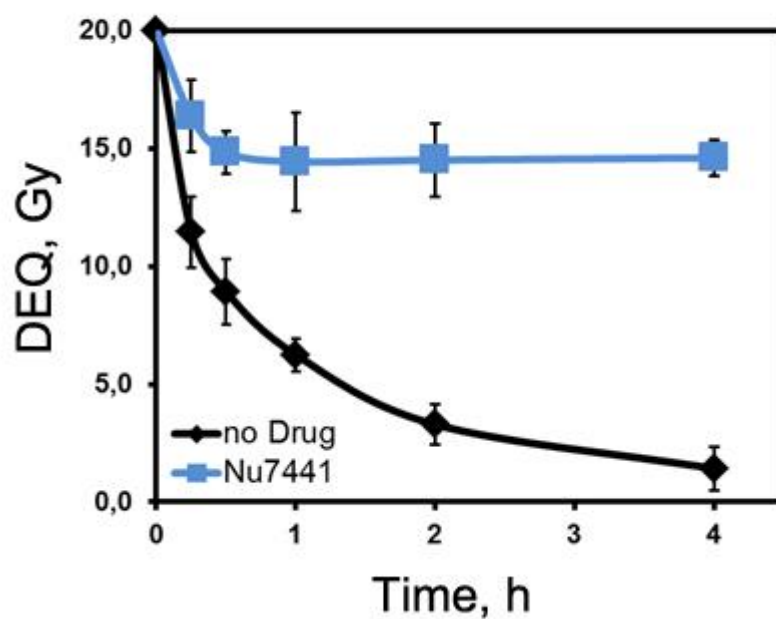


Figure 38 A549 exponentially growing with or without 5 μM Nu7441. PFGE data from an experiment performed with exponentially growing A549 cells irradiated with 20Gy X-rays. Incubation with 5 μM of the DNA-PKcs inhibitor Nu7441 induces a strong DSB repair defect in D-NHEJ proficient cells.

8.1.3.2 Effects of different treatment durations with Nu7441 on distal end-joining

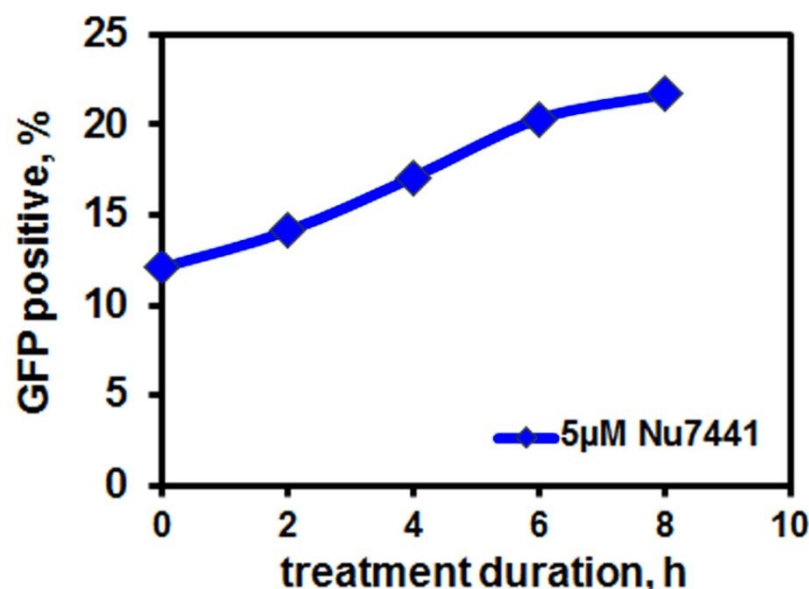


Figure 39 Treatment of U2OS 280A (EJ5-GFP) with 5µM Nu7441 for different length of time. U2OS 280A cells were transfected with an I-SceI expression plasmid and treated with 5µM Nu7441 for different length of time before the drug was washed away. The portion of GFP positive cells increases with time indicating increased usage of distal ends for re-joining. After 6h a plateau is reached.

8.1.4 Enhancement of B-NHEJ by ara-A does not confer radioresistance

It was reasonable to assume that the improvement of DSB rejoining upon treatment with ara-A we observed in serum deprived Lig4^{-/-} MEFs may allow cells to repair PLD, which would result in increased cell survival after irradiation. Therefore we inquired whether the enhancement of B-NHEJ was accompanied by an increase in radioresistance. To address this question we performed delayed plating survival experiments with serum deprived MEF Lig4^{-/-} cells. We followed the serum deprivation protocol as described before. Since these cells are extremely radiosensitive, especially in G1/G0, we only applied up to 2 Gy in steps of 0.5 Gy. Different concentrations of ara-A or solvent were added 15 min before irradiation. Cells were irradiated in the plateau-phase like state and incubated under these conditions in the presence or absence of ara-A for 2h after

irradiation. After 2h, cells were collected and plated as single cell suspensions at appropriate dilutions. Colonies were fixed and stained after 7 days.

We observed no improvement of survival in ara-A treated cells (Figure 40). On the contrary, ara-A treatment further sensitized cells. Plating efficiency values indicated that ara-A treatment had no strong cytotoxic effect on non-cycling MEFs. In fact we noticed, that the PE of cells treated with 25 μM (PE= 55%) was substantially higher than that of untreated cells (PE= 39%). When the ara-A concentration was further increased the PE declined again to 51% at 50 μM and 43% at 125 μM , which was still slightly higher than that for untreated cells.

We concluded that the enhancement of B-NHEJ we had observed in serum deprived MEF Lig4^{-/-} cells after treatment with ara-A had no positive effect on the repair of PLD and thus could not confer radioresistance. On the contrary, it appears to enhance PLD fixation, probably due to misrepair of DSB.

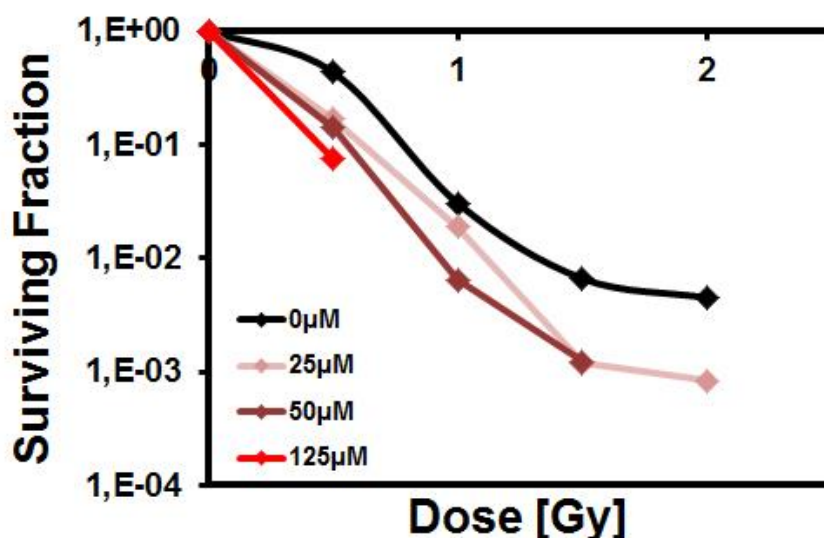


Figure 40 Ara-A does not improve survival in serum deprived MEF Lig4^{-/-} cells Serum deprived Lig4^{-/-} cells were irradiated in the plateau phase and incubated for 2h after irradiation in the presence or absence of ara-A before plating. The means of double determinations from one experiment are shown. Black symbols and curve, no ara-A treatment (PE=0.39). Pink symbols and curve, 25 μM ara-A (PE=0.55). Dark red symbols and curve, 50 μM ara-A (PE=0.51). Light red symbols and curve, 125 μM ara-A (PE=0.43).

8.1.5 53BP1 bodies in serum deprived MEF Lig4^{-/-}

In addition to the observations described under 4.4.6 we noticed that a large portion of MEF Lig4^{-/-} cells contained one large, very bright focus of 53BP1 after 24h of serum deprivation in the absence of any further treatment (Figure 41). These foci always colocalized with γ H2AX and were too big and distributed too regularly as it would be expected from background foci. Literature research revealed that such a phenomenon has already been described to arise in G0/G1 cells and has been linked to replication stress and common fragile sites (Harrigan, 2011). Common fragile sites are chromosome areas that show a higher incidence of spontaneous chromosome breakage than the average of genomic sequences. These 53BP1 bodies or domains were hypothesized to form after replication problems in these areas in the subsequent G1 phase to protect common fragile sites against erosion.

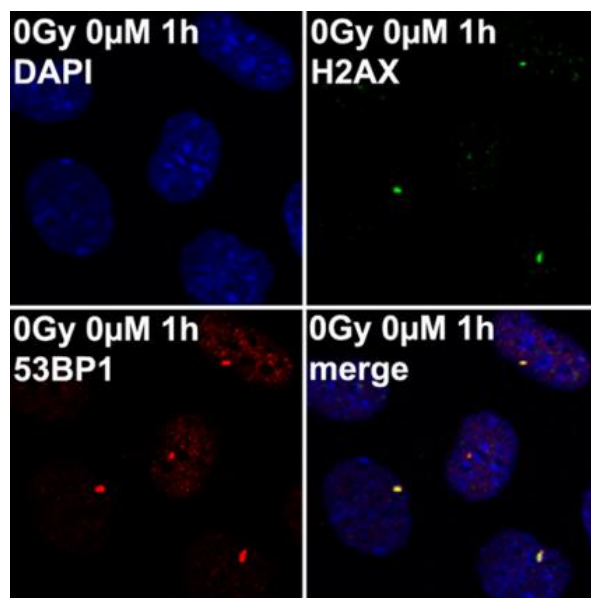


Figure 41 53BP1 bodies in serum deprived MEF Lig4^{-/-} Depiction of 53BP1 nuclear bodies in unirradiated, serum deprived MEF Lig4^{-/-} cells. Blue = DNA; red=53BP1; green= γ H2AX; yellow= Colocalization of 53BP1 and γ H2AX.

8.1.6 Inhibition of DNA replication by ara-C and gemcitabine

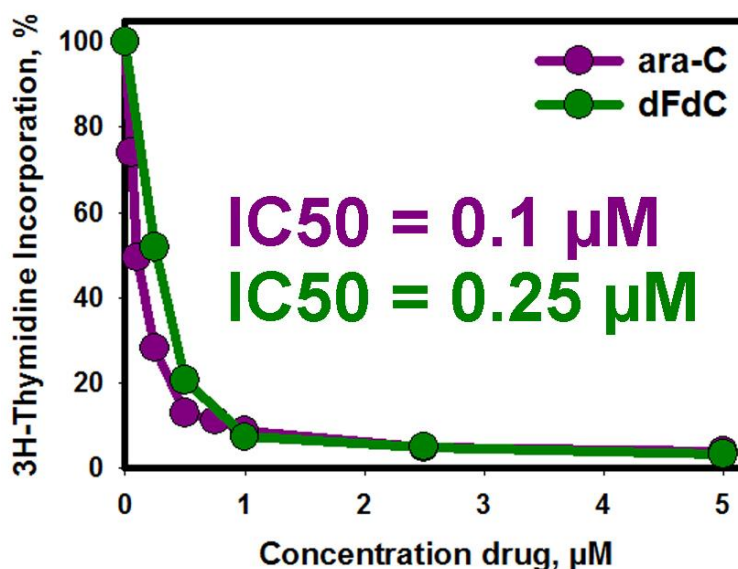


Figure 42 Inhibition of replication by ara-C and gemcitabine. Effects of ara-C (ara-C; violet curve) or gemcitabine (dFdC; green curve) treatment on DNA replication. Data points show the results of one experiment (Data generated by Dr. Maria Papaioannou).

We performed preliminary experiments with ara-C and gemcitabine (dFdC) to evaluate their effectiveness as replication inhibitors. Replication was assayed by incorporation of tritium labeled thymidine (³H-thymidine). Inhibitors were added prior to a 20 min pulse treatment with ³H-thymidine. Subsequently cells were lysed and incorporation of ³H-thymidine was measured in a liquid scintillation counter.

Figure 42 shows the results obtained with the replication inhibitors normalized to controls incubated without drug. The concentration at which 50% of the maximum inhibition of replication was achieved (IC_{50_{repl}}) was determined. Gemcitabine and ara-C both inhibited replication very effectively with IC_{50_{repl}} values of 0.25 μM and 0.1 μM, respectively.

8.2 Part B: Supplementary information on NAs

In this section the intracellular metabolism and mechanisms of cytotoxicity and radiosensitization of some NAs that are considered to be of clinical and/or historical importance are described. This overview is intended as a complementary reference for the interested reader.

8.2.1 BrdU and IdU

The first results showing radiosensitization by NAs were reported in the late 1950s, only a few years after it became clear that DNA is the hereditary material and its structure was resolved. They were obtained with the halogenated deoxythymidine analogs 5-bromo-2'-deoxyuridine (BrdU) and 5-iodo-2'-deoxyuridine (IdU) (Djordjevic and Szybalski, 1960). The van-der-Waals-radius of Bromine and Iodine is comparable to the size of a methyl-group, thus BrdU and IdU act mainly as competitors of thymidine in the cell. BrdU and IdU were shown to synergistically enhance radiation induced cell killing when administered before irradiation and radiosensitization correlated with the degree of incorporation into the DNA (Dewey and Humphrey, 1965; Iliakis, 1989a; Lawrence, 1990).

In contrast to most NAs used in chemotherapy, these C-5 halogenated thymidine analogs don't markedly interfere with replication. Many types of cells can be cultured in the presence of BrdU at micro molar concentrations for prolonged times without significant cytotoxic effects. In this way high rates of substitution for thymidine by BrdU can be achieved in both strands of the DNA. A specific radiochemical mechanism was described as an important factor for the radiosensitization elicited by these halogenated thymidine analogs. It has been shown that the presence of the halogenated pyrimidine bases in DNA during irradiation leads to the generation of uracyl radicals by radiolysis that can extract hydrogen atoms from the sugar residues of nucleotides (Wang, 2006a). This results in the formation of strand breaks and also increases the yield of DSB per Gy IR (Zimbrick, 1969; Lawrence, 1995; Shewach DS, 2006).

Despite very promising results *in vitro* and some clinical phase I-II studies (Chang, 1989; Goffman, 1991; Levin, 1995) neither BrdU nor IdU ever achieved approval for medical use as radiosensitizers, because the results of phase III clinical trials did not yield satisfactory results (Prados, 1999). The special properties of BrdU and IdU are exploited in diverse labeling strategies for research purposes, e.g. for the detection of S-Phase cells, progression of replication forks, sister chromatid exchanges or DNA resection (Cavanagh, 2011).

8.2.2 5-FU

In contrast, the fluorinated base analog 5-fluorouracil (5-FU) developed into a great clinical success. 5-FU is utilized in the treatment of breast, lung, head and neck cancers and has proven to be particularly effective in colorectal cancers (IMPACT, 1995). Several prodrugs of 5-FU exist to date (e.g. Capecitabine, Floxuridine) that have different pharmacokinetics but share similar or identical mechanisms of action. Upon entry into the cell 5-FU is converted to three major metabolites: fluorodeoxyuridine monophosphate (FdUMP), fluorodeoxyuridine triphosphate (FdUTP) and fluorouridine triphosphate (FUTP) (Longley, 2003). The majority of the cytotoxic effect of 5-FU is usually ascribed to the inhibition of thymidilate synthase (TS) it exerts through FdUMP. Inhibition of TS results in depletion of dTTP pools and consequently leads to disruption of DNA synthesis.

Due to the smaller van-der-Waals radius of the fluorine atom as compared to bromine or iodine, the nucleotides derived from 5-FU have more similarity with uridine than thymidine (Shewach DS, 2006). Consequently FUTP can be incorporated into RNA. This can lead to toxicity through disturbance on several levels, including mRNA polyadenylation, rRNA maturation and posttranscriptional modification of tRNAs (Carrico and Glazer, 1979; Kanamaru, 1986; Santi and Hardy, 1987). Another metabolite of 5-FU, FdUTP, is also misincorporated into DNA, where it can lead to DNA strand break formation (Ingraham, 1986). The enzyme uracil-DNA-glycosylase excises the faulty base, which in the presence of high concentrations of FdUTP leads to futile cycles of

excision and re-incorporation (Longley, 2003). Radiosensitizing effects of 5-FU on transplanted tumors were recognized as early as 1958 (Heidelberger, 1958).

Radiosensitization by 5-FU has been demonstrated *in vitro* for administration before and after irradiation (Bruso, 1990; Buchholz, 1995). For pre-incubation with 5-FU redistribution in the cell cycle apparently plays a significant role (Davis, 1995). An inhibition of DSB repair has been described as well, that may contribute to the radiosensitization achieved when 5-FU is administered after irradiation (Bruso, 1990). A number of clinical trials have shown a clear benefit in a number of tumors when radiotherapy was combined with 5-FU (Group, 1985; Merlano, 1996; Bartelink, 1997). Consequently concurrent chemoradiotherapy with 5-FU has become the standard of care for several solid tumor entities (Vallerga, 2004).

9 Acknowledgements

I thank the BMBF for funding (Grant: 03NUK005C) as part of the Projektverbund: "Biodosimetrie: Ein systembiologischer Ansatz für die Strahlenbiodosimetrie und der Analyse der individuellen Strahlensensitivität: ATM/ATR Signaltransduktionswege und Strahlenempfindlichkeit in Normal- und Tumor-Zellen". Many thanks also to the initiative for the preservation of radiation biology expertise in Germany (KVSV) for their commitment to the interests of the German radiobiological community.

I would like to thank my supervisor Prof. Dr. George Iliakis for his trust, support and the many enjoyable and lively scientific discussions. Your ceaseless energy is a great motivation. Thanks also for the introduction to the fascinating realm of radiobiology and for providing such an excellent working environment.

Jenny und Rafi für die Geduld mit der ihr meine fortwährende Abwesenheit ertragen habt und dafür, dass mich das zu Euch nach Hause-Kommen immer sofort in gute Laune versetzen kann. Auch wenn die zeitliche Aufteilung es vielleicht nicht immer hat erkennen lassen, Ihr seid für mich das Wichtigste auf der Welt.

Thanks to all colleagues in the lab, present and past, who were always very helpful.

Special thanks go to Tamara Mußfeldt for her help in cell sorting and the long days spent together at the Altra.

Many thanks to Emil Mladenov for his expertise in everything, and here in particular for Western Blotting. I hope we will participate together in many more excellent collaborations and I'm looking forward to many more jam sessions outside the lab as well!

Thanks to Veronika Mladenova, for her contributions to the plasmid work and joining in with her voice to our house music.

Thanks to Nadine Coym, for the good teamwork and helping to speed things up a bit.

Thanks also to Malihe Mesbah for her fundamental contributions in keeping the lab running.

Thanks to Fr. Lander, the good spirit of the basement.

Thanks a lot to Marcel Thissen for shuttle navigation on the last meters. Live long and prosper!

Thanks to all those who accompanied me on parts or all along my scientific education.

Vielen Dank Andre für die moralische Unterstützung und gelegentliche Ablenkung. Bald können wir mal wieder ein paar triumphale Bälle schlagen.

Simon Gengler für die gegenseitige Bestätigung unserer Ansichten.

Steffen, Uli und Simon für viele schöne Erinnerungen an die Uni-Zeit. Hoffentlich können wir bald die letzte Promotion zusammen feiern.

Bernd Giebel für den soliden Drill der Grundausbildung.

Allen anderen Essener rund um die Transfusionsmedizin.

Und natürlich meinen Eltern und Geschwistern, für alle Unterstützung und schönen Zeiten über die Jahre.

Vielen Dank auch an den ganzen Rest meiner Familie, ob angeheiratet oder angeboren. Vielen Dank vor allem auch an Tante Anni, Oma Ulla und Opa Udo für das gelegentliche Entlasten wenn sonst gar nichts gegangen wäre.

10 Curriculum vitae

**Der Lebenslauf ist
in der
veröffentlichten
Version aus
Gründen des
Datenschutzes nicht
enthalten.**

**Der Lebenslauf ist
in der
veröffentlichten
Version aus
Gründen des
Datenschutzes nicht
enthalten.**

**Der Lebenslauf ist
in der
veröffentlichten
Version aus
Gründen des
Datenschutzes nicht
enthalten.**

11 Publications

Research papers

Magin, S., J. Saha, M. Wang, V. Mladenova, N. Coym and G. Iliakis. "Lipofection and Nucleofection of Substrate Plasmid Can Generate Widely Different Readings of DNA End-Joining Efficiency in Different Cell Lines." *DNA repair* 12, no. 2 (2013): 148-60.

Costantino, L., S. K. Sotiriou, J. K. Rantala, S. Magin, E. Mladenov, T. Helleday, J. E. Haber, G. Iliakis, O. P. Kallioniemi and T. D. Halazonetis. "Break-Induced Replication Repair of Damaged Forks Induces Genomic Duplications in Human Cells." *Science* 343, no. 6166 (2014): 88-91.

Review articles

Mladenov, E., S. Magin, A. Soni and G. Iliakis. "DNA Double-Strand Break Repair as Determinant of Cellular Radiosensitivity to Killing and Target in Radiation Therapy." *Frontiers in oncology* 3, (2013): 113.

Manuscripts in preparation

Magin, S., M. Papaioannou, J. Saha, C. Staudt and G. Iliakis. "Inhibition of homologous recombination repair by the nucleoside analog 9-b-D-arabinofuranosyladenosine."

12 Declaration

Erklärung:

Hiermit erkläre ich, gem. § 6 Abs. 2, g der Promotionsordnung der Fakultät für Biologie zur Erlangung der Dr. rer. nat., dass ich das Arbeitsgebiet, dem das Thema „A balance shift between error-free and error-prone DNA double-strand break repair pathways as a novel mechanism of radiosensitization by nucleoside analogs.“ zuzuordnen ist, in Forschung und Lehre vertrete und den Antrag von Herrn Simon Magin befürworte.

Essen, _____

Name d. wissenschaftl. Betreuers/ Mitglieds der Universität Duisburg-Essen	Unterschrift d. wissenschaftl. Betreuers/ Mitglieds der Universität Duisburg-Essen
----------------------------------------------------------------------------------	---------------------------------------------------------------------------------------

Erklärung:

Hiermit erkläre ich, gem. § 7 Abs. 2, d und f der Promotionsordnung Fakultät für Biologie zur Erlangung des Dr. rer. nat., dass ich die vorliegende Dissertation selbständig verfasst und mich keiner anderen als der angegebenen Hilfsmittel bedient habe und alle wörtlich oder inhaltlich übernommenen Stellen als solche gekennzeichnet habe.

Essen, _____

Unterschrift des Doktoranden

Erklärung:

Hiermit erkläre ich, gem. § 7 Abs. 2, e und g der Promotionsordnung der Fakultät für Biologie zur Erlangung des Dr. rer. nat., dass ich keine anderen Promotionen bzw. Promotionsversuche in der Vergangenheit durchgeführt habe, dass diese Arbeit von keiner anderen Fakultät abgelehnt worden ist, und dass ich die Dissertation nur in diesem Verfahren einreiche.

Essen, _____

Unterschrift des Doktoranden

Appendices 6, 7 und 8 vertraulich

[Veröffentlichung steht noch aus]

Berichtsblatt

1. ISBN oder ISSN Noch nicht bekannt	2. Berichtsart (Schlussbericht oder Veröffentlichung) Schlussbericht	
3. Titel Verbundprojekt: „Biodosimetrie: Ein systembiologischer Ansatz für die Strahlenbiodosimetrie und der Analyse der individuellen Strahlensensitivität: ATM/ATR Signaltransduktionswege und Strahlenempfindlichkeit in Normal- und Tumor-Zellen“		
4. Autor(en) [Name(n), Vorname(n)] Iliakis, George Magin, Simon Sak, Ali	5. Abschlussdatum des Vorhabens 31.10.2013	6. Veröffentlichungsdatum
	7. Form der Publikation	
	8. Durchführende Institution(en) (Name, Adresse) Universitätsklinikum Essen Institut für Med. Strahlenbiologie Hufelandstraße 55 45147 Essen	
12. Fördernde Institution (Name, Adresse) Bundesministerium für Bildung und Forschung (BMBF) 53170 Bonn		9. Ber. Nr. Durchführende Institution
		10. Förderkennzeichen 02NUK005C
		11. Seitenzahl 597
16. Zusätzliche Angaben		13. Literaturangaben 1085
		14. Tabellen 24
		15. Abbildungen 144
17. Vorgelegt bei (Titel, Ort, Datum) Prof. Dr. George Iliakis, Essen, 05.09.2014		
18. Kurzfassung Ziel des Projektes war es Grundlagen der Zellabtötung durch ionisierende Strahlung unter Aspekten der Schadenskomplexität, der Kombinationstherapie mit Nukleosidanalogen, sowie der individuellen Strahlensensitivität und der Aktivierung von intrazellulären Signalkaskaden zu untersuchen. Dabei konnte: - Erstmalig ein neuer Mechanismus der Strahlensensibilisierung durch Nukleosidanaloge beschrieben werden. Nukleosidanaloge können Zellen gegenüber IR sensibilisieren indem die HRR gehemmt und gleichzeitig die alternative B-NHEJ gefördert wird. - Ein neuartiges Modellsystem zur Testung der biologischen Effekte von geclusterten DSBs etabliert werden. Damit konnte erstmalig gezeigt werden, dass mit steigender Komplexität von DSBs deren Toxizität zunimmt, sowie auch die Signalentwicklung und die Entstehung von Chromosomenaberrationen beeinflusst werden. - Gezeigt werden, dass Unterschiede in dem Anteil residueller DNA Schäden, treten nach fraktionierter Bestrahlung von Fibroblasten und auch von Gliomlinien deutlicher hervor. In strahlensensitiven Gliomlinien konnte eine höhere Anreicherung von DSB nach fraktionierter Bestrahlung als in strahlenresistenten Linien festgestellt werden. Inhibition von ATM Signalwegen der DNA-Schadensreparatur verstärkt die Fraktionierungsempfindlichkeit von Gliomlinien. - Gezeigt werden, dass epigenetische Modulation über zentrale Trithorax- und Polycombproteinen, eine Möglichkeit ist die Strahlensensitivität von Gliomzelllinien zu beeinflussen.		
19. Schlagwörter Strahlensensitivität, DNA Doppelstrangbruchreparatur, Nukleosidanaloge, komplexe Schäden, B-NHEJ, Chromatinstruktur, ATM/ATR		
20. Verlag	21. Preis	

Document Control Sheet

1. ISBN or ISSN Not known yet	2. type of document (e.g. report, publication) Report
3. title Joint Project: Biodosimetry: "A systems biology approach for radiobiosimetry and analysis of individual radiosensitivity: ATM/ATR signal transduction and radiosensitivity in normal and tumor cells"	
4. author(s) (family name, first name(s)) Iliakis, George Magin, Simon Sak, Ali	5. end of project 31.10.2013
	6. publication date
	7. form of publication
8. performing organization(s) (name, address) University of Duisburg-Essen University Hospital Institute for Medical Radiation Biology Hufelandstraße 55 45147 Essen	9. originator's report no.
	10. reference no. 02NUK005C
	11. no. of pages 597
12. sponsoring agency (name, address) Bundesministerium für Bildung und Forschung (BMBF) 53170 Bonn	13. no. of references 1085
	14. no. of tables 24
	15. no. of figures 144
16. supplementary notes	
17. presented at (title, place, date) Prof. Dr. George Iliakis, Essen, 05.09.2014	
18. Abstract Aim of this study was to investigate basic mechanisms of cell killing by ionizing radiation with regard to damage complexity, combined treatment with nucleoside analogs as well as individual radiosensitivity and the activation of intracellular signal transduction pathways. - For the first time a new mechanism of radiosensitization by nucleoside analogs could be described. Nucleoside analogs can sensitize cells to IR by inhibiting HRR and promotion of B-NHEJ. - A novel model system for testing of the biological effects of clustered DSB was established. With this system it could be showed for the first time that the toxicity of clustered DSBs increases with their complexity. Signal transduction after DSB induction and the induction of chromosome aberrations was also influenced by the complexity of the induced DSB. - It was demonstrated that differences in residual DNA damage were more distinct in glioma cells and normal fibroblast after fractionated irradiation. In radioresistant glioma cell lines a higher accumulation of DSB was found in radiosensitive cell lines compared to resistant cell lines. Inhibition of ATM signal transduction reinforced fractionation sensitivity of glioma cells. - It was shown that epigenetic modulation via manipulation of trithorax- and polycomb proteins is an option to influence the radiosensitivity of glioma cells.	
19. keywords Radiosensitivity, DNA double-strand break repair, nucleoside analogs, complex damage, B-NHEJ, chromatin structure, ATM/ATR	
20. publisher	21. price